UNIVERSITY OF SOUTHAMPTON
FACULTY OF ENGINEERING AND APPLIED SCIENCE
Department of Ship Science

AN INVESTIGATION INTO THE RESISTANCE COMPONENTS OF HIGH SPEED DISPLACEMENT CATAMARANS

by
Mustafa Insel

A thesis submitted for
the degree of
Doctor of Philosophy
1990

To the three perfect persons :
My wife, my daughter and my father

CONTENTS

UNIVERSITY OF SOUTHAMPTON

ABSTRACT

FACULTY OF ENGINEERING AND APPLIED SCIENCE

SHIP SCIENCE

Doctor of Philosophy

AN INVESTIGATION INTO THE RESISTANCE COMPONENTS OF HIGH SPEED DISPLACEMENT CATAMARANS

by

Mustafa Insel

High speed displacement and semi-displacement catamarans have received considerable attention during the last two decades and a number of such vessels, mainly passenger ferries, have been built. This thesis describes an experimental and theoretical investigation into the resistance components in calm water of these types of craft with symmetric demihulls.

Total resistance, running trim, sinkage measurements and wave pattern analysis based on multiple longitudinal cut techniques were carried out for five hull forms : a conventional hull form, a mathematically defined hull form (Wigley hull) both in fixed and free to trim and sink conditions and three round bilge hulls derived from the NPL round bilge series. The tests were conducted over a Froude number range of Ø.2 to 1.Ø and separation to length ratio range of Ø.2, to Ø.6 as well as ∞, resulting in 31 catamaran configurations. Wake traverse analysis was also carried out for the Wigley model and one round bilge model. Interference resistance effects for both the wave pattern and the viscous components were derived.

A theoretical method based on linearised wave resistance theory was developed, and a prediction method for the wave pattern resistance of the catamaran using the wave pattern analysis of the demihull was investigated. Both methods were applied to the models and compared with the experimental results.

The results of the investigation provide a better understanding of the components of catamaran resistance including the influence of hull separation and length to beam ratio over a wide range of Froude numbers. Conclusions are drawn from the results of the interference effects on both wave resistance and viscous resistance. Comparisons between the experimental results and theoretical predictions are used to assess the suitability of the theoretical methods. Finally, overall observations are made on the components of catamaran resistance, on suitable scaling procedures and on practical prediction methods.

ACKNOWLEDGEMENTS

The author wishes to acknowledge the support and assistance given by following :

Dr. A.F. Molland, who supervised this project, for his continuous encouragement, advice, patience and friendship

Dr. J.F. Wellicome for his guidance in the theoretical field

Professor G.J. Goodrich for his generous support

Mr. A. Tang for his long and creative discussions

The Wolfson Unit for Marine Technology and Industrial Aerodynamics at Southampton University and Southampton Institute of Higher Education for providing test facilities

Mr. S.Ryan of Southampton Institute of Higher Education and the personnel of the workshops at Southampton University for their help in the construction of the experimental equipment and conducting the experiments

The Turkish Ministry of Education for their financial support throughout the project

Finally, my family and in-laws for their patience, love and understanding

NOMENCLATURE

Nomenclature, as listed below, follows the terms given by "ITTC Dictionary of Ship Hydrodynamics" [94], except for some additional terms which are described as follows ;

"CATAMARAN" refers to any ship with two hulls, side by side, joined to each other by means of a bridge structure above the free-surface.

A "DEMIHULL" is one of the hulls which make up the catamaran vessel.

"SEPARATION", (S), is the distance between the centrelines of the demihulls of a catamaran ship.

C_T	: Total Resistance Coefficient	
C_F	: Frictional Resistance Coefficient	
C_{FO}	: Form Resistance Coefficient	: kC_F
C_V	: Viscous Resistance Coefficient	: $(1+k)C_F$
C_{WT}	: Wake Traverse Resistance Coefficient	
C_R	: Residuary Resistance Coefficient	: $C_T - C_F$
C_W	: Wave Resistance Coefficient	: $C_T - C_V$
C_{WP}	: Wave Pattern Resistance Coefficient	
C_I	: Induced Drag Coefficient	
C_{WTHE}	: Theoretical Wave Resistance Coefficient	
C_{TS}	: Transom Stern Resistance Coefficient	
$(1+k)$	: Form Factor	: C_V / C_F
$(1+k_{WP})$	: Form factor	: $(C_T - C_{WP}) / C_F$
L, L_{WL}	: Length on Waterline	
L_{OA}	: Length overall	
L_{BP}	: Length Between Perpendiculars	
B	: Beam	
T	: Draught	
D	: Depth	

S	: Separation Distance Between the Centrelines of a Catamaran
G	: Gap Between the Demihulls of a Catamaran
W	: Width of a Catamaran
C_B	: Block Coefficient
C_P	: Prismatic Coefficient
C_{WL}	: Waterline Coefficient
C_M	: Midship Section Coefficient
∇	: Displacement Volume
$\mathcal{f}$	: Wave height
V	: Ship Speed
V_{SER}	: Service Speed
V_{MAX}	: Maximum Speed
Fn	: Froude Number
Re	: Reynolds Number
K_o	: g/U^2
U	: Free Stream Velocity
u,v,w	: Perturbation Velocities
σ	: Frictional Resistance Interference Factor
Ω	: Residuary Resistance Interference Factor
β	: Form Resistance Interference Factor
τ	: Wave Resistance Interference Factor
α	: Wake Traverse Resistance Interference Factor
μ	: Wave Pattern Resistance Interference Factor

CHAPTER 1 : INTRODUCTION

The demand for high speed small ships has increased during the last two decades, especially in the passenger ferry boat market. Various hull forms have therefore been developed to satisfy the design criteria of these vessels. Among them, the catamaran ship concept has received considerable attention for such vessels due to its large deck area and its unusual resistance characteristics.

High power requirements for these fast ships entails a thorough investigation into the resistance characteristics in order to achieve a feasible design. However, catamaran resistance presents a complex phenomenon for the ship designer as the interference effects between the demihulls must be considered in addition to the resistance of the demihulls in isolation.

The dependency of the interference on speed, hull separation and hull form restricts the practical use of model series, as such a series has to cover a wide range of models. Hence previous experimental studies of catamaran resistance have been confined to a small number of isolated resistance experiments. The data obtained from these tests, although useful, are not sufficient to establish a prediction method for the design stage. This necessitates basic research into the resistance components for a better understanding of the interference phenomena.

Two types of interference resistance specific to catamarans have been identified : Body interference, or viscous resistance interference, is caused by the asymmetric flow around a demihull and its effects on the

viscous flow such as boundary layer formation and longitudinal vortices. The second interference resistance, wave interference, originates from the interactions between the wave systems of the demihulls.

Although a number of experimental and theoretical investigations of catamaran resistance have been conducted in the past, there is a lack of understanding of the interference resistance components, especially at higher speeds.

Because the wave interference drag varies with speed, these components cannot be determined independently with standard resistance tests. Therefore, wave pattern analysis and wake surveys are required to be used to determine them.

The present study is concerned with the resistance components in calm water of high speed displacement and semi-displacement catamarans with symmetric demihulls. The study covers a wide range of hull separations and a speed range of up to Froude number of unity. An approach comprising total resistance measurements together with wave pattern analysis and wake surveys is utilised.

The main objectives of the work presented in this thesis are

i) To conduct a review of the state of art in catamaran resistance.

ii) To identify the interference effects on catamarans, describe the effects of these on resistance components and observe their effect on scaling methods.

iii) To improve the understanding of the interference resistance by conducting experiments and theoretical analysis on both mathematically simplified and practical catamaran hull forms over a practical hull separation range.

iv) To obtain experimental data for a small series of practical hull forms over a wide speed range which could

be used for the validation of the theoretical analysis used and would be useful for preliminary design purposes in their own right.

v) To suggest practical methods for resistance prediction including experimental, empirical and theoretical approaches.

In chapter 2, a survey of built catamarans and a review of the published literature on catamaran resistance is conducted. This allows required research in this field to be defined by comparing the available data with the practical needs derived from the survey of built ships. In view of this evaluation and facilities available, the detailed methods and scope of this work are derived.

In chapter 3, the conventional methods used in tank testing, for the division of resistance into components, are described to identify the basic assumptions involved in such methods. Adaptations of these methods for catamarans are discussed.

Chapter 4 is concerned with the determination of wave resistance of a ship model from linearised wave resistance theory. The wave interference between two symmetrical demihulls is investigated by the same method and interference factors are derived.

Chapter 5 describes the experimental methods for the determination of total resistance, trim, sinkage and wave elevation along the hull.

Chapter 6 covers the description of wave pattern experiments with use of a new analysis method based on multiple longitudinal cuts. A method for the prediction of wave pattern resistance of catamarans using the wave coefficients of the monohull is presented.

In Chapter 7, the wake traverse experiments are described. The newly developed experimental rig is described in detail.

Chapter 8 gives the results of experimental and theoretical analysis for five models. Comparisons are made for the resistance components, interference effects and hull form behaviour such as trim and sinkage.

In Chapter 9 conclusions drawn from the various aspects of the work are presented. The recommendations for further work are given.

CHAPTER 2 : A REVIEW OF THE FEATURES OF CATAMARANS

2.1 INTRODUCTION

Increasing the speed of a conventional displacement ship is possible only to a certain extent as the wave resistance increases at a relatively high rate above a Froude number of about Ø.4. Because the wave resistance is related to the square of the free surface disturbance, wave resistance can be minimised only if most of the displacement volume is positioned either above the water surface, such as with planing hulls, hydrofoils and hovercraft or below the water surface such as with submarines and semisubmerged ships. However these hull forms have additional complexities and limitations on design such as weight sensitivity, stability and low payload.

Meanwhile twin hull vessels can achieve higher speeds in four different ways; by achieving a favourable wave interaction between the hulls, by having very slender hulls causing minimum disturbance on the free surface which is not possible with monohull configurations due to stability requirements, by locating the hull displacement volume above the water surface such as with planing catamarans, hydrofoil catamarans and SECAT or by locating it under the water surface such as with SWATH ships.

This variety of hull forms for twinhull vessels exhibits different kinds of resistance features for each type. Therefore, a classification of hull forms with an emphasis on resistance characteristics has been made in

order to define the hull forms used in this research. The features of the catamaran concept are described for these hull forms.

A survey of built catamarans is made in order to find the main hull parameters used in practice. The results of the survey are presented by charts to show the current application range of the concept.

A review of the literature on the resistance of catamarans is made in order to define the required research in this field. The experimental resistance data found from the review are summarized.

Finally, a summary is made for the application range of both the built vessel survey and the resistance review. Scope for further research is derived.

2.2 CLASSIFICATION OF CATAMARAN HULL FORMS

Catamarans offer great freedom in the design of the hull shape and the dimensions of demihulls due to the high transverse stability which is effectively independent of the hull shape. Hence, the volume of the demihulls can be distributed more freely than the monohull both transversely and longitudinally in order to optimise resistance, seakeeping, manoeuvrability and stability characteristics. This flexible design aspect enables catamaran demihulls to be designed asymmetrical relative to their centreplane. In this sense three basic hull shapes are adopted: symmetric, asymmetric, and fully asymmetric.

a) Symmetric demihulls (Fig.1) are a direct adaptation of various conventional monohull forms. However the absence of stability restrictions enables the catamaran demihull to be designed with a much bigger range of L/B, B/T, C_B, C_{WP} than

the monohulls as well as with revolutionary hull forms such as the SWATH.

b) Asymmetric demihulls (Fig.2) are developed by shifting the displacement volume inwards or outwards asymmetricaly to the centerline of the demihull in order to reduce the adverse interference effects between the demihulls.

c) Fully asymmetric demihulls (Fig.3) are obtained by shifting all the displacement volume of a symmetric demihull to one side of the centerline, i.e. by separating a monohull with twice the beam into two pieces from the centerline. This form is also called a half monohull, or split hull.

Comparisons between the performance of these hull types are difficult to make as the characteristics of a catamaran hull depend on the operating Froude number, separation, and hull form itself. In general, symmetric demihulled catamarans have the smallest total resistance in infinite separation, i.e. demihulls in isolation.

However the success or failure of symmetric demihulls is governed by the interference effects between the demihulls which change across the speed range resulting in adverse effects at certain speeds even in a well designed hull. Asymmetric hulls, in contrast to symmetric hulls, show higher resistance in isolation and less pronounced interference effects across the Froude number range. This may be used to design a minimum resistance catamaran for the nonbeneficial speed range for the equivalent symmetric demihull. Asymmetric demihulls and fully asymmetric demihulls can also be utilised to minimise the wave formation and the spray in the tunnel.

Although there is no widely accepted criterion that classifies hull forms according to resistance features the following categorisation has been made :

2.2.1 DISPLACEMENT CATAMARANS

These ships usually operate under Froude number of about Fn:Ø.7, and are called displacement catamarans as their buoyancy is the major lift force. Displacement hulls can be divided into four sections according to speed range, and their distinctive resistance characteristics belong to these speed ranges.

a) Ships operating under Fn:Ø.2 can be called slow ships such as tankers, which usually have full hull forms for carrying weight important goods.

The catamaran does not show any benefits in this speed range due to its bigger wetted surface resulting in a power disadvantage as well as a payload smaller than the monohull vessel.

b) Medium speed displacement vessels can operate at Froude numbers between Ø.2 and Ø.4. In this range displacement hulls are finer than in the low speed range in order to minimise wave resistance.

Experiments with displacement catamarans show that very favourable interference on wave resistance can be achieved for symmetric hulls at about Fn:Ø.3Ø-Ø.36. Most displacement catamarans are designed to operate in this speed range.

c) A prehump region can be described between Fn:Ø.4 to Ø.5 where displacement ships experience significant wave resistance.

Although catamarans can operate in this speed range due to their thin hulls, reducing wave resistance, they also show unfavourable wave resistance interference

resulting in an increase of up to 70% of the wave resistance of the demihulls in isolation. Asymmetric and fully asymmetric hulls may be introduced in order to reduce this interference resistance in the main hump region.

d) In the posthump region for the monohulls between Froude numbers 0.5 and 0.7,the wave resistance starts to loose its dominance relative to the prehump region. Catamarans in this region still suffer from unfavourable interference, and asymmetric hulls may be used to minimise the wave effects.

2.2.2 SEMI-DISPLACEMENT CATAMARANS

Vessels operating between froude numbers 0.7 and 1.0 are termed semi-displacement or semi-planing hulls, because 20 to 30 % of the displacement is balanced by dynamic lift generated by the flat buttocks of the hull. This results in a reduction in wetted surface, and less frictional resistance. Additionally, as some part of the displacement volume is above the water surface, the wave making is also reduced. Monohull semi-displacement vessels usually have round bilge sections, U or V shaped fore sections and transom sterns.

Semi-displacement catamarans follow the design practices of monohulls. As the interference effects on wave resistance is less pronounced than displacement catamarans, the demihulls may be designed to prevent wave formation and spray formation in the tunnel by the use of asymmetric and fully asymmetric hulls.

The symmetric hulls are used in order to minimise the wetted surface of the hulls and the wave resistance of catamarans.

There is a lack of information on the hull forms of semi-displacement catamaran hulls. Resistance data for this type of catamaran is also very scarce.

2.2.3 OTHER CATAMARAN TYPES

As the predominance of built catamarans is in the displacement and semi-displacement range, the current research concentrates on these vessel types. The literature search did however cover other catamaran types

The Small-Waterplane-Area-Twin-Hull (SWATH) Ship concept, is distinguished from the displacement catamaran by its small waterplane area which reduces the wavemaking of the demihulls, and submerged displacement volume which reduces the motions and perfects the seakeeping of this hull form [92,93].

Planing catamarans which operate above Froude number 1.0 have dynamic lift features balancing more than 50 % of the hull weight. Due to high transverse stability, the catamarans are superior to the monohull in this speed range.

The catamaran concept has also the potential to be applied to hybrid type advanced marine vehicles. Most of the hybrid catamaran designs use a combination of the buoyancy force and either aerostatic lift or dynamic lift obtained either from the hull or hydrofoils attached between the demihulls [6,50].

The catamaran as a sailing boat is superior to the monohull sailing boat in many aspects for high speed sailing. The high transverse stability, caused by the separation between the demihulls, enables the catamaran to sail without a heavy keel ballast, i.e. the catamaran sail boat can be much lighter than the monohull for the same

sail area, hence has a smaller wavemaking resistance and faster speed [57,87,90].

2.3 FEATURES OF CATAMARANS

The decision to design and build a catamaran ship for a particular operation is made on the basis of the capabilities of the catamaran concept being superior to conventional monohulls or any other advanced marine craft, such as hydrofoil, SES etc., operating in the same conditions. The features implicit in the catamaran concept can be summarised as :

From the point view of utilization, the most outstanding feature of the catamaran is the large usable area for its length, by converting the gap between the hulls into considerable amount of usable deck space. This allows the catamaran to be applied to deck area intensive applications such as fishing boats, passenger ferries and research vessels.

Good low speed manoeuvrability is an exclusive feature of catamarans because of the wide separation between propulsors. The long and thin hulls also provide good directional stability and course keeping.

The large inertia moment of the two hulls due to separation makes the catamaran extremely stable resulting in small angular accelerations in roll motion. However due to the wide beam, very high vertical accelerations on the deckside may be encountered. Additionally the natural roll frequency may be in a similar area to natural pitch frequency resulting in corkscrew motion and severe seasickness. Pitching in catamarans presents the most dangerous motion as it may cause slamming of the cross deck structure.

Propulsion efficiency is likely to be less compared with a monohull but more than a twin screw ship. Considering the speed range at which catamarans operate, where the equivalent monohull must be twin or even triple screw, propulsive efficiency is likely to be superior to the monohull.

The catamaran has a better freedom in choice of principal dimensions. e.g. very shallow draught can be very advantageous in shallow waters such as rivers.

The cost of catamaran may however be greater than the equivalent monohull due to the need for cross structure, twin hulls and engines.

The major problem in the structural design of catamarans appears to be the design of the cross structure which may suffer from severe slamming in heavy seas. Transverse bending in beam seas and twisting in quartering seas of the cross structure must also be considered in the design stage.

The weight penalty associated with catamaran bridging structure and construction of two shells and engines prohibits the use of catamaran for high payload operations such as cargo ships and tankers.

Any catamaran design has to balance these advantageous and disadvantageous features of the concept in the detailed design. These features are discussed in detail for various conceptual designs and built ships in Refs.[4,13,22,47,58, 80,81,88].

2.4 SURVEY OF BUILT CATAMARANS

In view of the wide range of catamarans now being designed and constructed, a survey of the main

characteristics of 314 catamaran ships has been conducted in order to explore the trends in catamaran design. The data were collected from various published sources, mainly from Refs. [91,95,96,99]. Over 90 % of the sample ships have been built since 1970 (Fig.4). Further statistics of these characteristics are given in Figs.5 to 28.

It must be emphasised that these characteristics only show the trends of built catamarans, and must not be taken as optimum in catamaran design as they were designed mainly for specific purposes. Furthermore, most of these catamarans were designed by four companies; Fjellstrand and Westamarin of Norway, Marinteknik of Sweden and International Catamarans of Australia. Therefore they have been determined by the design practice of these four companies. Lastly, some variables, such as C_B, could not be obtained for most of the ships, therefore deriving the optimum trends with such small numbers of data can be very misleading.

For the ships where the service speed (Vser) is not given, a regression analysis has been carried out from all the data between Vser and Vmax (Fig.5). Similar regressions have been carried between L_{WL} and L_{OA}, L_{OA} and L_{BP} (Figs.6,7).

Passenger ferries provide the main application of catamarans with over 64 % of the ships in the survey (Fig.8), as the catamaran concept provides these vessels with a large deck area for a compact, stable ship. The number of passengers per length varies between 5 and 20 per metre (Fig.9).

The length and speed of these ships are given in Figs.10 to 13. Over 95 % of the ships has length between 10 and 40 metres (Fig.10). Meanwhile the service speed shows two distinctive peaks around 10 knots and 25 knots (Fig.11) which correspond to Froude number of 0.35 and 0.9

respectively (Fig.12). Fig.13 shows the relation between the speed and ship length.

The dimensionless coefficients for the demihull forms from this survey of ships are given in Figs.14 to 23 from which the following range are mainly used : L/B: 6-12 (Fig.14), B/T: Ø.8-2.4 (Fig.16), D/T: 1.5-3.5 (Fig.18), C_B: Ø.3Ø-Ø.66 (Fig.2Ø), $L/\nabla^{1/3}$: 4.5-9 (Fig.22). The effect of speed on form parameters is apparent as seen for L/B (Fig.15), B/T (Fig.17), C_B (Fig.21), $L/\nabla^{1/3}$ (Fig.23).

The figures for the hull separation, probably the most important variable for the catamaran design, are given in Figs. 24 to 27, in which (W-B)/L and (W-B)/B (which correspond to S/L and S/B in symmetric catamarans) vary between Ø.2 and Ø.45, 1.4 and 2.4 respectively.

Fig. 28 shows the speed-power diagram for these vessels with favourable Froude numbers of Ø.3 and Ø.9.

2.5 REVIEW OF PUBLISHED LITERATURE ON CATAMARAN RESISTANCE

The wetted surface, and hence frictional resistance of catamarans is accepted as being higher than that of the equivalent monohull, because of splitting the displacement into two halves. However the base of comparison such as displacement, deck area etc. is the prime factor deciding the magnitude of the penalty. This effect may be minimised by choosing optimum B/T ratio for a particular hull form [66].

The resistance of catamarans differs from that of monohull vessels due to interference effects. Two types of interference were reported by Pien [6Ø]; Firstly the flow about a symmetric demihull becomes asymmetrical due to the influence of the other hull, which was called body interference by Pien. It was assumed to exist even in the

absence of the free surface. This asymmetric flow may cause a cross flow under the keel resulting in induced drag which may be prevented by introducing a camber on each hull. Secondly, a wave interaction between the demihulls is created which may be positive or negative depending on the hull form, speed and separation between the hulls.

Body interference introduces an increase in the viscous resistance of catamarans. The velocity augmentation between the hulls increases the frictional drag even at low speeds. Miyazawa [51] reported that this interference is more important than the cross flow under the keel by presenting the velocity measurements about a symmetric catamaran.

Wake traverse experiments on a symmetrical catamaran were carried out by Miyazawa [51] for two separation ratios, Ø.177 and ∞, and two Froude numbers, Ø.156 and Ø.319. These experiments showed that the viscous resistance of the catamaran was higher than twice the viscous resistance of the demihull. Thus unfavourable viscous resistance interference effects can occur. By investigating the interactions theoretically on a pair of cylinders the following formulae were given for viscous and wave interferences.

$$E = B/S \tag{1.1}$$

$$(C_{WT})_{CAT} = (1+ E^2)\ (C_{WT})_{DEMIHULL} \tag{1.2}$$

$$(C_{WP})_{CAT} = (1+3/2\ E^2)\ (C_{WP})_{DEMIHULL} \tag{1.3}$$

The wake traverse experiments conducted by Volheim [82] at three speeds for S/L:Ø.3 displayed wake contours skewed inwards in the lower half of draught suggesting cross flow. Meanwhile outward flow near to free surface may occur at some speeds.

The wave resistance has possibly been the most investigated feature in this type of craft, as it is the major resistance component which can be optimised by the

designer. There are two factors in achieving favourable wave resistance for a catamaran compared with an equivalent monohull. Firstly, the demihulls can be designed with low wave resistance in various ways, e.g. thin hulls. Secondly a favourable wave interference resistance can be established by a careful design of the hulls and the choice of separation between the hulls.

A theoretical approach for the wave resistance of a catamaran in unbounded water was given by Lunde [43] in his well known article in which he suggested that the wave resistance of a catamaran is identical to the wave resistance of a demihull moving alongside an infinitely deep wall. By using the classical Michell [48] and Srettensky [71] formulations, the following formulae were given;

$$R_W = 2 \left(R_O + R_I \right) \tag{1.4}$$

$$R_O = 16 \pi \rho K_O^2 \int_{\emptyset}^{\pi/2} (P^2+Q^2) \, Sec^3\Theta \, d\Theta \tag{1.5}$$

$$R_I = 16 \pi \rho K_O^2 \int_{\emptyset}^{\pi/2} (P^2+Q^2) \, Cos(K_O \, S \, Sec^2\Theta \, Sin\Theta) \, Sec^3\Theta \, d\Theta \tag{1.6}$$

$$\begin{matrix} P \\ Q \end{matrix} = \iint_{WS} \mu \begin{matrix} Cos \\ Sin \end{matrix} (K_O \, x \, Sec\Theta) \exp(K_O \, z \, Sec^2\Theta) \, dx \, dz \tag{1.7}$$

Where $K_O = g/U^2$

R_O : Wave resistance of a demihull in isolation

R_I : Wave interaction resistance for one demihull

Eggers [15] used this method and extended it to shallow water. He also compared numerical results with experimental ones for a mathematically defined hull form in both deep and shallow water. Two models with length to beam ratios of 8 and 16 were investigated over an S/L range of Ø to Ø.65 for Froude Numbers of Ø.316 and Ø.5. A satisfactory

agreement between the theory and experiment was obtained for S/L over Ø.4. The experiments demonstrated that a negative interaction resistance can be achieved for a favourable separation range, i.e. S/L=Ø.4 to Ø.5 for Fn=Ø.316.

Yokoo and Tasaki [85,86] used the same method and made a comparison with experimental results for an Inuid model over a Fn range of Ø.2 to Ø.45 for S/L values of Ø.2,Ø.3,Ø.4,Ø.5 and ∞. Although the numerical and experimental results are similar, a phase shift on Fn base for humps and hollows in the interaction resistance was apparent [86]. They also presented experiments on a fully asymmetric hull with four separations for both flat inboard and outboard configurations [85].

Theoretical work on the effects of a bulbous bow on catamaran wave resistance was carried out by Michalski [46]. The optimum bulbous bow was calculated by using the method described above and by representing the hulls with source-sink and dipole distributions. Experiments with a hull form with two different bulbous bow forms were conducted. A reduction about 48 % in residuary resistance was obtained for a bulbous bow design.

In another approach, Lin [4Ø] suggested that a catamaran demihull should be represented by source-sink and transverse doublet distributions simultaneously on the centreplane in order to define the asymmetric flow about each hull. Furthermore he concluded that the doublet distribution can be ignored if the demihulls have a camber designed to stop asymmetric flow. However he did not present any numerical examples for conventional catamarans.

Rich et al [63] calculated the resistance of a high speed round bilge model moving along a vertical wall in shallow water and compared the results with experiments.

Recently, Min and Kim [49] applied theoretical formulae to 25 mathematically generated hull forms in search of hull form effects on the interference resistance. These results were compared with experimental results for 5 models with sufficient correlation to be used at the design stage.

Hsiung [33] expressed the wave resistance of a catamaran in a quadric form in terms of hull offsets. The resistance was subjected to a number of geometric constraints such as C_B and waterline slopes. Then solving this quadric problem, the optimal form and separation for given constraints was obtained.

In an experimental approach to the wave resistance of catamarans, Everest carried out wave pattern experiments by the transverse cut method [18], and developed a prediction method for the wave resistance of catamarans by superimposing the wave patterns obtained from demihull wave pattern measurements in isolation. This method aimed to understand the distribution of resistance across the wave spectrum. Although the predictions were similar to experimental results, a phase shift in Froude number base was observed similar to the one from theoretical calculation by use of thin ship theory.

Experiments on a mathematically defined model showed that a favourable interaction between the demihulls was possible in divergent waves, while the transverse wave system of each demihull reinforces the other causing adverse interactions. This interference resulted in resistance reduction in the Fn range of Ø.32-Ø.37 where divergent waves were significant, and an increase in Fn range of Ø.4 to Ø.6 in which transverse waves were dominant. The experiments with a conventional catamaran supported the conclusions with a favourable resistance between Fn=Ø.3Ø to Ø.34.

Everest also carried out some experiments on symmetric and asymmetric catamarans for trawlers. Experiments showed that the total resistance of the symmetric hull and the asymmetric hull are almost the same. It was also found that infinite separation had lower resistance than the other separations [19].

Pien [60] developed a design procedure to take account of body interference in catamarans. The first part entails designing an effective hull form which is similar to a monohull design, but differing from the monohull design in the freedom of choice of beam, buoyancy distribution, and afterbody form. In the design, both good wave cancellation and high propulsive efficiency may be obtained by means of a suitable afterbody form.

The second task is the conversion of the effective hull to a demihull in order to prevent the asymmetric flow and induced drag. The method uses streamline tracing for the singularities in a free stream. The demihull obtained from this method is slightly asymmetric.

Some experiments on models of two ships ,a 700 ft. cargo catamaran and the ASR-21 Pigeon naval catamaran , were carried out by Turner and Taplin [78]. For the 700 ft. catamaran three different hull forms were used : symmetric, asymmetric, fully asymmetric. For the 700 ft catamaran, models were investigated at Froude numbers 0.17 to 0.33, at four separation ratios 0.164, 0.221, 0.297 and ∞ and for two draughts. Experiments for ASR-21 were conducted with one symmetric and four asymmetric models. The ship was built with slightly asymmetric demihulls in 1961.

The effects of U and S* forms on the resistance were investigated by Schimke [67,68]. Two U form and three S forms were used in the Froude number range 0.24-0.36 with five S/B ratios 2.05, 2.43, 2.73, 3.02, and infinite separation. Experimental results show that U forms have

* See Fig. 398.

less resistance than S forms due to their smaller wetted surface area. Infinite separation is the most favourable position for U shaped forms. In S forms infinite separation causes higher resistance than other separation ratios in certain Froude number ranges, i.e. Ø.29-Ø.33 for model S-65 and Ø.32-Ø.37 for model S-71.

The optimum separation ratios for Froude number range of Ø.3 to 1.Ø were given for a symmetric demihulled catamaran by Ralf [62]. It shows an increasing tendency from S/L=Ø.3 for Fn=Ø.3 to S/L=Ø.8 for Fn=Ø.45 and decreasing tendency from S/L=Ø.7 for Fn=Ø.6 to S/L=Ø.42 for Fn=1.Ø. For a Fn range of Ø.45 to Ø.55, infinite separation was found to be smallest resistance solution.

Model tests for a 7ØØ ft catamaran (also described in Ref.[78]) and LHA catamaran models were carried out by General Dynamics [88]. The LHA catamarans were tested in about 48 configurations which included symmetric, asymmetric hulls, different bow and stern forms, and bulbous bows.

Data for high speed catamarans is more scarce, especially concerning the interaction terms.

Spray drag and the interference of spray drag may result in a wetted tunnel increasing the wetted surface [55]. It was stated that the power prediction of fast catamarans on the basis of model tests was not as reliable as that for monohulls when Froude's method is used. There were a number of reasons suggested such as : Wetted area could not be determined exactly due to spray in the tunnel region. Additionally, the scale effects on the interference are not known.

Clement [10] extended the empirical equations derived from high speed monohull model tests into catamaran configurations by presenting design charts for practical

trim angles and aspect ratios. But the interference effects on both resistance and lift were not included.

Resistance experiments with three high speed catamaran hull forms, one round bilge, one hard chine, and asymmetric hull form, were given by Chengyi [9] with five separation ratios over the Froude number range of Ø.4 to 1.Ø. A formula for demihull spacing which does not introduce interference was given.

Rutgersson [64] compared the resistance interference between a symmetrical and asymmetrical catamaran for four speeds of Fn:Ø.38, Ø.51, Ø.64 and Ø.76 for four gap ratios. The symmetrical catamaran has smaller drag than the asymmetrical one except at the smallest gap ratio.

Total resistance and wave pattern experiments for a fully asymmetrical catamaran were conducted by Ozawa [59] as a first step of an air cushion vehicle research. Test were made from Fn:Ø.2 to 1.Ø for four separations.

Fry & Graul [22] tested three hard chine planing hulls, one symmetric, one asymmetric and one fully asymmetric, over a Fn range of Ø.3 to 1.2 with three separations. Results from both symmetric and asymmetric hulls were favourable when compared with a parent monohull design from Fn=Ø.5 to Fn=Ø.95, while fully asymmetric hulls did not have any advantage. There was little difference in the results due to changing separation for Fn>Ø.75. The experiments for these models were also described by Moss [54] with details of total resistance data, LCG rise and running trim.

Model tests with fully asymmetric hulls, flat sides outboard, were conducted by Guohua et al [27] in order to improve the low wash hull form. The effect of hull spacing, foils and spray rails were investigated experimentally over

the speed range of Ø.2 to 1.6. Reductions were achieved in high speeds by the use of spray rails and foils.

Three hard chine planing catamaran hulls, one symmetric one asymmetric and one fully asymmetric , were tested in three separations over Froude number of Ø.3 to 1.8 by Sherman [7Ø]. The fully asymmetric hull had the best resistance features whilst symmetric hulls were the worst of all.

Planing catamarans with fully asymmetric demihulls, both flat side inboard and flat side outboard were tested by Yermotayev et al [84]. Resistance ratio and dynamic trim of the hulls were given for a F_n range of Ø.5 to 3.5. The authors also gave optimum operating separation ratios based on speed by conducting further experiments.

Experiments with high speed flat surfaces indicated that there is a lift interference at small separations [65]. The lift interference is about 47 % when the surfaces are adjacent to each other and becomes negligible when Gap/B ratio is over 4. The wetted length of the plates is also increased by decreasing the gap.

Liu and Wang [42] developed two sets of empirical equations based on Savitsky's equations for planing hulls by using an interaction factor which lies between 1 and $\sqrt{2}$. A fit for interaction factor based on separation distance was derived from the experiments conducted.

The resistance of hydrofoil assisted catamarans was investigated by Calkins [6] and Miyata [5Ø] independently.

Resistance data found in the review is summarised in Appendix A by specifying hull form parameters and Froude number range.

2.6 SUMMARY

The statistics of built catamaran ships are presented to discover the hull form parameters. A wide range of scatter on form ratios was found as the mission of the vessels varies.

The survey of built catamarans has indicated that two speed ranges at about Fn:Ø.3 and Ø.9 are used for most of the vessels. Although the slow speed range is well investigated and quite a substantial amount of resistance data is published in the literature, there is a lack of data and fundamental knowledge for the higher speed range. For speeds higher than Fn:1.Ø, there is some data available, although not conclusive.

The demihull forms of catamaran can be one of three types : symmetric, asymmetric, fully asymmetric. Symmetric catamarans show the best resistance characteristics up to Fn=1.Ø except in the main wave hump where asymmetric hulls are beneficial. Favourable resistance interference effects were found at about Fn=Ø.33 while adverse effects occurred at about Fn=Ø.5 for symmetric catamarans.

Asymmetrical hulls are believed to be less influenced by the interactions due to separation changes. However asymmetric hull resistance data is rather disappointing as it is almost always higher than for symmetrical equivalents. Fundamental research into the understanding of asymmetrical hulls is required.

Two types of interference, body interference and wave interference were reported for catamarans. Body interference affects the viscous resistance for which the data is extremely limited, and only for slow speeds. More data on velocity measurements and wake traverse experiments would improve our knowledge of the nature of this component.

Theoretical wave resistance prediction for catamarans has been applied to several hulls and compared with experimental results. A satisfactory degree of correlation was obtained for the wave interference factor with change of separation. More data on the suitability of the theory for hull form changes, such as variation in L/B, B/T, C_B etc., are required in order to gain confidence and test the reliability of the method. This is particularly true if the method is to be used in the design stages to find optimum hull form factors.

Experimental determination of wave resistance by wave pattern analysis is the only available method to obtain wave interference resistance, as residuary drag may also include viscous interaction resistance. Wave pattern analysis data on catamarans is also very limited, and available only below Fn:Ø.5. Further work is required to understand the nature of this component, especially at higher speeds.

Scaling of catamaran resistance is reported to be not as good as monohulls, if Froude's method is used. Better scaling may be obtained by the determination of components, such as form resistance, wave interference resistance, and viscous interference resistance, which are included in the residuary resistance in Froude's method. There is also need for full scale measurements to assess the suitability of any scaling procedure.

The effects of hull form variations such as L/B, B/T, and C_B were not investigated systematically as most of the available data were one off designs with variation of separation only. Drawing conclusions from this available data would not be accurate. Model experiments with these variations are needed, although a catamaran series is much more costly than a monohull series because of the variation of separation.

Although there are some data on the effects of local hull changes such as bulbous bows and foils between the hulls, the results are not conclusive as the effects on individual components were not measured.

2.7 THE SCOPE OF THE INVESTIGATION

Following the conclusions derived from the survey of existing vessels and the review of literature, and by considering the facilities at Southampton University, the scope of the current programme of work was developed as follows ;

Experiments in calm water on high speed displacement and semi-displacement catamarans were planned to investigate the effect of hull parameters and separation. Planing catamarans are not considered in the current work, as their tests are beyond the available facilities. The measurement of sinkage and trim was included in order to complement the total resistance measurements. Wave pattern experiments for all the models were planned in order to improve the understanding of wave resistance interactions. Wake traverse experiments were also planned to investigate viscous interactions. The wake traverse experiments would however be limited, as this method is very time consuming.

Asymmetric hulls are beyond the scope of the current work, as it was felt that the fundamentals of symmetric catamarans must be explained before introducing more complexities into the hydrodynamic problem. However investigation of the resistance of asymmetric hulls is recommended as a subject of further work.

The survey indicates that interference effects are typically presented for various separation ratios such as S/L, G/L, S/B, G/B, W/B. Although there is an indication

from linearised theory that S/L has a major influence on wave resistance interaction, S/B or G/B may be dominant in viscous interactions. Further work on models having constant S/L ratio and variable S/B ratio would help to clarify the dominant ratios.

In the view of these proposals, it was decided to test three round bilge semi-displacement models, with varying length to beam ratio in order to include the influence of both separation and the gap between the hulls. The main parameters for these models were determined from the survey of built vessels, resulting in : B/T=2, C_B=Ø.4, L/B=7,9,11 and S/L=Ø.2,Ø.3,Ø.4,Ø.5,∞.

As the direct measurements of resistance components are very sensitive to various conditions such as temperature and turbulence simulation, it was planned to test a standard ITTC Model, the Wigley parabolic hull. This would prove the accuracy of the measurements and improve the confidence in the results by comparing with other results available in the literature.

An assessment of linearised wave resistance theory would be made by comparing it with the experimental results. Prediction of the wave pattern resistance of the catamaran from the wave pattern analysis of the demihull was also planned in order to investigate the error due to representation of the hulls with source and sink distributions using thin ship theory.

The experimental and theoretical approach to the components would help to explain the characteristics of the interference effects and therefore may provide a reliable method for use in the design stages and for scaling to ship. This investigation was intentionally limited to hull forms used in practice as a good starting point in order to provide a better understanding of the problem.

CHAPTER 3 : RESISTANCE COMPONENTS OF A CATAMARAN

3.1 INTRODUCTION

The assumption of treating catamaran resistance as a summation of a number of independent components can be made in order to facilitate the understanding of catamaran resistance and the influence of hull separation on the resistance. Such a division allows one not only to carry out systematic model experiments for comparative purposes but also to provide better scaling to full scale. For this purpose, a brief review of the available methods for conventional vessels is made, and modifications of these methods for catamaran resistance are suggested.

The methods used in conventional hull testing by dividing resistance into components are based on either the measurement of total resistance from model experiments with the estimation of frictional resistance from empirical formulae, or direct measurements of the components. Both methods are considered in order to identify the components and the assumptions involved in such a division.

The separation of resistance into components from consideration of the momentum principle for a ship model in a tank is formulated to obtain the expressions for wave pattern and wake traverse resistance.

The interference effects between the demihulls which modify the resistance components in catamaran configurations are described.

Modified ITTC-1957, ITTC-1978 and direct measurement methods for the determination of catamaran resistance are introduced by defining interference factors. Although these methods have not yet been proven, it is considered that such an approach would provide a better understanding of the components and interference effects.

3.2 RESISTANCE COMPONENTS OF A SHIP MODEL

A ship model, moving on the undisturbed free surface of a fluid with a constant speed experiences a force, known as the total resistance, in such a way that it opposes its motion and acts parallel to the motion of the model. This total resistance can be split into a number of components. Although these components interact with each other in a very complicated way, they may be assumed to be independent of each other for practical purposes. This allows one not only to conduct the experiments on scaled models for the prediction of resistance of the full scale ship, but also to carry out systematical model experiments to optimise a particular resistance characteristic of a hull form. Discussions on the justification of such a division of resistance into components and on the interdependence of these components can be found in Refs. [12,39,69,72].

It is possible to present these components in a diagrammatic breakdown as shown in Fig. 29. Although several methods can be deduced from this figure for use in a towing tank, two main methods are in common use by experimental tanks:

i) By measuring total resistance and employing an empirical formula for frictional resistance, a practical method for the determination of the components can be established, such as Froude's, or Hughes' Methods.

ii) By measuring the components directly using advanced experimental techniques, a laborious but physically justifiable method can be achieved.

3.3 ESTIMATION OF RESISTANCE COMPONENTS

The methods based on the measurement of total resistance from towing tank experiments and the estimation of skin friction resistance by an empirical formula are very practical for extrapolating the model results to ship scale, as it is fairly easy to measure the total resistance. However the division into components is hypothetical.

3.3.1 FROUDE'S APPROACH

W. Froude was the first person to present a breakdown of total resistance into components [20,21].

$$R_{TM} = R_{FM} + R_{RM} \qquad (3.1)$$

where

R_{TM}= Total resistance of model measured from experiments

R_{FM}= Frictional resistance for a flat surface having the same wetted surface as the model which can be obtained from

$R_{FM} = f\ S\ V^n$

f,n : Constants which are functions of length and nature of the surface

R_{RM}= Residuary resistance of model calculated from (3.1)

Furthermore, Froude assumed that residuary resistance of a model is correlated to the ship by the ratios of the displacements, i.e. $(R_{RM}/\Delta_M)=(R_{RS}/\Delta_S)$ for corresponding speeds which can be obtained from $(V_M/\sqrt{gL_M})=(V_S/\sqrt{gL_S})$ for which the wave patterns of model and ship are similar.

Using Froude's method, results can be extrapolated to ship by using a resistance coefficient presentation :

$$C_{TS} = C_{FS} + (C_{TM} - C_{FM}) \tag{3.2}$$

3.3.2 IMPROVEMENTS ON FROUDE'S APPROACH

Following Froude's method, series of experiments with planks were conducted by several researchers resulting in improved friction resistance formulations for flat surfaces among which the following are the most used ones [28]:

ATTC - SCHOENHERR

$$\frac{0.242}{\sqrt{C_F}} = \log(Re\ C_F) \tag{3.3}$$

HUGHES

$$C_F = \frac{0.067}{(\log(Re) - 2.03)^2} \tag{3.4}$$

ITTC studied these formulations and in 1957 suggested a new formula for skin friction " ITTC 1957 model-ship correlation line " and implying this line was only an interim solution to the problem for practical purposes.

ITTC 1957

$$C_F = \frac{0.075}{(\log(Re) - 2)^2} \tag{3.5}$$

It must be emphasised that all these methods are based solely on Froude's assumption that total resistance is the summation of the frictional resistance calculated from formula and residuary resistance obtained from experiments. In this assumption scale effects for surface tension, spray, wave breaking, and form effect on the frictional

resistance are neglected. The interactions between the viscous and gravitational forces are not taken into account, i.e.

$$R_T\ (Re = \frac{VL}{\nu},\ Fn = \frac{V}{\sqrt{gL}}) = R_F\,(Re) + R_R\,(Fn) \qquad (3.6)$$

3.3.3 FORM FACTOR METHODS

In 1954, Hughes [34,35] proposed a method for use in model ship correlation which regards total resistance as a sum of three components :

i) Frictional resistance as the resistance of a plane surface of the same area and the same length as model.

ii) Form resistance as the excess over item (i) in the case of the deeply submerged body. Hughes assumed that for a streamlined body in turbulent flow it can be expressed as a proportion of the frictional resistance.

iii) The free surface resistance, wave resistance, is the excess of total resistance for the surface model from the summation of the frictional resistance and the form resistance of the model.

i.e. $C_T = C_F + C_{Fo} + C_W$ where $C_{Fo} = k\,C_F$

Hence $C_T = (1+k)\,C_F + C_W$ (3.7)

(1+k) is called the form factor and can be found from very low speed experiments where C_W can be neglected.

In 1978, the 15th ITTC Resistance committee proposed a new method called " 1978 ITTC Performance Prediction Method for Single Screw Ships " [41]. In this method total resistance for a ship is divided into four components:

$$C_T = (1+k)\ C_F + C_R + \Delta C_F + C_{AA} \qquad (3.8)$$

where

$(1+k)$ = form factor

C_F = Frictional resistance from ITTC-1957 Line

C_R = Residuary resistance from model experiments

ΔC_F = Roughness allowance (Ø for a smooth model)

C_{AA} = Air resistance (assumed Ø for a model without superstructures)

The recommended method to find k is by low speed measurements where C_R approximates to zero and $(1+k)=C_T/C_F$. In practice low speed experiments are often not accurate enough due to instrumentation inaccuracy. Therefore another method due to Prohaska is recommended :

Assuming $C_{RM} = a\ Fn^n$ for low speeds (generally $Fn<Ø.2$)

$$C_T = (1+k)\ C_F + a\ Fn^n \qquad (3.9)$$

$(1+k)$, a, n can be solved from a least squares analysis of low speed measurements.

In the form factor methods, form effect on frictional resistance is taken into account, hence scaling between the model and ship can be done more accurately. But $(1+k)$ is assumed to be independent of speed, hence Reynolds number and Froude number. In the case of models where flow separation, transom stern vortices and bilge vortices may occur, Reynolds number effects on the form factor may have to be considered.

3.4 DIRECT MEASUREMENT OF RESISTANCE COMPONENTS

A number of physically identifiable resistance components can be measured directly from towing tank experiments by utilising advanced experimental techniques. There are two well known methods in use :

i) Total resistance can be interpreted as a summation of the forces acting, namely the skin friction resistance obtained from the measurements of tangential stresses on the hull surface and pressure resistance derived from the measurement of pressures on the hull surface. i.e. $C_T = C_F + C_P$*. This method is relatively straightforward but is also very laborious and very sensitive to measurement errors, since the shear stress and pressures of relatively small magnitude have to be measured over the whole hull surface. It is therefore not commonly used in practice.

ii) Alternatively, total resistance can be deduced from an energy approach as the summation of wave pattern resistance derived from the energy loss in created waves, and the viscous wake traverse resistance measured from the total head loss in the wake of the model. i.e. $C_T = C_{WP} + C_{WT}$. The assumption of negligible induced drag is acceptable for most conventional craft.

This method requires more sophisticated techniques to derive the components than the first one, but the experimental set up is easier and quicker to conduct. Experimental errors are also less pronounced. Wave pattern analysis is now used extensively whilst the wake traverse is less preferred due to the long experimental time needed.

This method is chosen for direct measurements of the resistance components in the current work. Derivation of these components may be made for a ship model (Fig.3Ø) in a tank from considerations of momentum changes as given in Appendix B. This leads to representation of resistance as:

$$R_T = \int_{-W/2}^{W/2} \int_{-H}^{y_B} \Delta P \, dz dy + \rho/2 \int_{-W/2}^{W/2} \int_{-H}^{y_B} (u^2 - u^2) \, dz dy$$

* e.g. see Ref. 69, Steele B.N. Pearce G.B. Experimental Determination of the Distribution of Skin Friction on a Model of a High Speed Liner TRINA 1968 Vol:11Ø and Townsin R.L. The Frictional and Pressure Resistance of Two "Lucy Ashton" Geosims TRINA 1967 Vol:1Ø9

$$+ \rho g/2 \int_{-W/2}^{W/2} \zeta_B^2 \, dy + \rho/2 \int_{-W/2}^{W/2} \int_{-H}^{\zeta_B} (\underline{v}^2 + \underline{w}^2 - \underline{u}^2) \, dzdy$$

$$+ \rho/2 \int_{-W/2}^{W/2} \int_{-H}^{\zeta_B} [(v^2 - \underline{v}^2) + (w^2 - \underline{w}^2) - (u^2 - \underline{u}^2)] \, dzdy \qquad (3.10)$$

where

u, v, w : perturbation velocities at B

$\underline{u}$, $\underline{v}$, $\underline{w}$: wave orbital velocities at B

ζ_B : wave height at B

ΔP : head loss between A and B

u : fictitious velocity at B corresponding to no head loss case

The first line in the resistance equation (3.10) represents the viscous resistance which can be derived from wake traverse surveys. The second line is the wave resistance which can be defined from an analysis of the model wave pattern. The velocity components $\underline{u}$,$\underline{v}$,$\underline{w}$ are determined from this wave pattern by utilising linear wave theory. The third line is the induced drag. Unlike the first two it can not be easily measured unless all the velocity components are measured in plane B. It may be neglected for most ship types.

3.5 RESISTANCE COMPONENTS OF A CATAMARAN

The resistance components of a catamaran present much more complicated phenomena than those of monohulls due to the interference effects between the hulls. The interaction effects can be divided into two distinct groups.

1) Body interference : The flow around a symmetric demihull is asymmetric due to the influence of other demihull. i.e.

the pressure field is not symmetric relative to the centreline of the demihulls. This has following outcomes:

a) The perturbation velocity around the demihull increases, especially on the inside, tunnel side, of the hull due to the venturi effect. This velocity augmentation causes an increase in skin friction resistance and modifies the form factor. Experiments of Miyazawa [51] and Schimke [68] indicate an increase in perturbation velocity of up to 10 % in the x direction compared with that of the demihull in isolation.

b) A cross flow may occur under the keel which can lead into an induced drag component which is normally neglected in monohulls. Although this component is reported to be important in symmetric catamarans by Pien [60], Miyazawa [51] has suggested that this component is relatively small compared with (a) in his experimental results. In these experiments the cross flow velocity in the y direction is about 5-7 % of the model speed. Crossflow in the entrance is outwards, while in the run it is inwards.

c) Because the wave heights at the stern inside and outside of the demihull are different, the flow at the stern can show inwards or outwards flow. This causes vortices and spray at the stern resulting in an induced drag component.

d) The velocity increase on the tunnel side may change the structure of the boundary layer.

e) As the waves of one demihull reach the other hull, the wetted surface, and therefore the skin friction resistance, can change.

2) Wave interference : As a result of two hulls running side by side, interference effects on wave resistance may also be observed.

a) Due to the change in the pressure field, wavemaking of the demihulls may change. In other words the wave formation of a demihull may be different than from the assumed case of the demihull in isolation.

b) A favourable or unfavourable interaction between the waves of the demihulls may occur. The transverse wave of a demihull is always reinforced by the other hull while divergent bow wave of the one hull can be cancelled by the divergent stern wave of the other hull or by the reflection of the same bow wave from the other hull.

c) The reflections of divergent waves from the other demihull complicate the interference phenomena.

d) The bow wave of a demihull in the tunnel meets the bow waves of the other demihull on the centerline, and superposition of these two waves can become very high resulting in an unstable wave, even in breaking waves and spray at high speeds.

e) Inward or outward flow at the stern changes the wave formation at the stern.

Taking the interference effects into account, the methods for monohulls described earlier can be adapted for catamarans as follows :

ITTC 1957 Method

$$(C_T)_{CAT} = (C_F)_{CAT} + (C_R)_{CAT}$$
$$= \sigma C_F + \Omega C_R \qquad (3.11)$$

where

σ : Frictional resistance interference factor
Ω : Residuary resistance interference factor
subscript $_{CAT}$ denotes catamaran

The velocity augmentation between the hulls may be taken into account by introducing an interference factor σ which would be calculated from the integration of local frictional resistance over the wetted surface. It is mainly dependent on the separation. The residuary resistance interference factor Ω can be investigated from experimental results. The tendency of this factor due to variation of separation and speed is given in Refs.55 and 78.

ITTC 1978 Method

$$(C_T)_{CAT} = (1+k_{CAT})\ (C_F)_{CAT} + (C_W)_{CAT}$$
$$= (1+\phi\ k)\ \sigma\ C_F + \tau\ C_W \qquad (3.12)$$

where
σ : Frictional resistance interference factor as in ITTC 1957 method.
ϕ : Form resistance interference factor
τ : Wave resistance interference factor

ϕ is introduced to take into account the effects of pressure field change around a demihull. For practical purposes, ϕ and σ can be combined into a viscous resistance interference factor β where $(1+\phi k)\ \sigma = (1+\beta k)$. The wave resistance interference factor can be determined from experimental results.

Direct Measurement Method

$$(C_T)_{CAT} = (C_{WT})_{CAT} + (C_{WP})_{CAT} + (C_I)_{CAT}$$
$$= \alpha\ C_{WT} + \mu\ C_{WP} + (C_I)_{CAT} \qquad (3.13)$$

where
α : Wake traverse interference factor
μ : Wave pattern resistance interference factor
C_I : Coefficient of induced drag (e.g. due to cross flow, vortices etc.)

The wake traverse interference factor, α, will include wave breaking interference as well as viscous interference. Miyazawa suggested that α can be taken as $(1+(B/S)^2)$. μ differs from τ and Ω as it can be defined directly from wave pattern experiments. Although data are sparse, $(C_I)_{CAT}$ may be of importance in the catamaran case due to cross flow, induced vortices and spray.

3.6 SUMMARY

From the methods described above, three main methods are utilised in order to explore the resistance components of catamarans in the current work :

i) The ITTC 1957 approach was used as the simplest method of separating the resistance into components

For Monohulls :

$C_T = C_F + C_R$

For Catamarans

$(C_T)_{CAT} = \sigma C_F + \Omega C_R$

where $C_F = \dfrac{0.075}{(\text{Log}(Re)-2)^2}$

ii) The ITTC 1978 method for the ship model without any correction for surface roughness or air drag.

For Monohulls :

$C_T = C_V + C_W$

$= (1+k) C_F + C_W$

For Catamarans :

$(C_T)_{CAT} = (1+ \beta k) C_F + \tau C_W$

where C_F is calculated from the ITTC 1957 Model ship correlation line.

iii) Direct measurements of wave pattern resistance and wake traverse resistance.

For Monohulls :

$C_T = C_{WT} + C_{WP}$

For Catamarans :

$(C_T)_{CAT} = \alpha C_{WT} + \mu C_{WP} + (C_I)_{CAT}$

where C_{WT} and C_{WP} are derived from experiments.

CHAPTER 4 : DETERMINATION OF THEORETICAL WAVE RESISTANCE FOR A SHIP MODEL IN A SHALLOW WATER CANAL

4.1 INTRODUCTION

Linearised wave resistance theory has been applied to several hull forms to obtain the pure theoretical prediction of wave resistance since Michell [48] first introduced the method. Although the quantitative results of the method have not been successful for most hull forms, qualitative results have proved to very valuable for most cases. This prediction method has also been applied to catamarans as reviewed in Chapter 2.

In the current work, the far field wave system for a Kelvin source in a shallow water canal has been developed by the author. In order to establish an analytical approach to the wave resistance, wave coefficients for a ship model are obtained by using this method and the assumption of thin ship theory, and wave resistance is derived from these coefficients. The method is also applied to the catamaran hull forms to obtain the wave interference resistance. Modifications to the theory are made in order to take account of transom sterns, sinkage and trim.

In order to analyse the theory numerically, a computer program has been developed. The results of the program for two standard models, the Wigley hull and the Athena hull form, are compared with available theoretical and experimental results in order to assess the effectiveness of the current implementation of the method.

The prediction program has also been used to conduct a parametric study of hull form effects on catamaran wave resistance interaction. The effects of speed, separation distance, length to beam ratio, beam to draught ratio, prismatic coefficient, and entrance angle have been investigated.

4.2 BASIC ASSUMPTIONS AND BOUNDARY CONDITIONS

Throughout the theoretical approach to the wave making resistance of ship models, the following assumptions are made :

a) The fluid is inviscid, incompressible and homogeneous.
b) The fluid motion is steady and irrotational.
c) The surface tension can be neglected.
d) There is no sinkage or trim for the model while advancing with a constant velocity.
e) The wave height at the free surface is small compared with the wave length.

A cartesian coordinate system moving with the model and having its origin on the free surface at the model centre is used. Ox is in the direction of the motion, Oy and Oz are to the starboard and vertical upwards respectively (Fig. 31).

As the model advances in the positive direction of the x-axis at a constant speed U, the velocity potential can be expressed as a summation of the free stream and flow disturbance potentials.

$$\Phi = Ux + \phi(x,y,z) \qquad (4.1)$$

Assuming the free surface is expressed as $z=\zeta(x,y)$ and the underwater geometry of the model as $y=f(x,z)$, then the following linearised boundary conditions must be satisfied:

i) Continuity equation for potential flow

$$\nabla^2 \phi = \frac{\delta^2 \phi}{\delta x^2} + \frac{\delta^2 \phi}{\delta y^2} + \frac{\delta^2 \phi}{\delta z^2} = 0 \qquad (4.2)$$

ii) Free surface conditions

a) Dynamic free surface condition

$$g\zeta + U\phi_x + 1/2\ (\phi_x^2 + \phi_y^2 + \phi_z^2) = 0$$

or by linearising

$$g\zeta + U\phi_x = 0 \qquad \text{at } z=0 \qquad (4.3)$$

b) Kinematic free surface condition

$$\frac{d\zeta}{dt} = (U+\phi_x)\ \zeta_x + \phi_y\ \zeta_y + \phi_z = 0$$

or by linearising

$$U\ \zeta_x - \phi_z = 0 \qquad \text{at } z=0 \qquad (4.4)$$

or by combining both conditions, the linearised free surface condition can be written as

$$\phi_{xx} + K_o\ \phi_z = 0 \text{ at } z=0 \qquad (4.5)$$

where

$K_o = g/U^2$

iii) Bottom condition

$$\phi_z = 0 \qquad \text{at } z=-H \qquad (4.6)$$

iv) Hull surface condition

$$\frac{df}{dt} = (U+\phi_x)\ f_x + \phi_y f_y + \phi_z\ f_z = 0$$

or by linearising

$$U\ f_x + \phi_y = 0 \qquad \text{at } y=f(x,z) \qquad (4.7)$$

iv) Radiation condition

$$\lim_{(x^2+y^2)\to\infty} \phi = O(1) \qquad \text{for } x<0$$

$$\lim_{(x^2+y^2)\to\infty} \phi = 0 \qquad \text{for } x>0$$

(4.8)

4.3 VELOCITY POTENTIAL OF A SOURCE IN SHALLOW CANAL

The velocity potential of a source with density μ located at $(0,0,z_o)$ (Fig.32) in shallow unbounded water with the depth of H is given as [83] :

$$\phi = -\frac{\mu}{r_1} - \frac{\mu}{r_2} + \frac{4\mu}{\pi} \int_0^\infty \int_0^{\pi/2} F(\theta,k,z)\, \cos(kx\cos\theta)\, \cos(ky\sin\theta)\, d\theta dk + 4\mu \int_0^{\pi/2} G(\theta,K,z)\, \sin(Kx\cos\theta)\, \cos(Ky\sin\theta)\, d\theta$$

(4.9)

For $K_o H>1$

where

$K_o = g/U^2$

$$r_1^2 = (x)^2+(y)^2+(z-z_o)^2$$
$$r_2^2 = (x)^2+(y)^2+(z+(2H+z_o))^2$$

$$F(\theta,k,z) = \frac{e^{-kH}\, \cosh(k(H+z_o))\, (k+K_o \sec^2\theta)}{\cosh(kH)\, (k-K_o \sec^2\theta \tanh(kH))} \cosh(k(z+H))$$

(4.10)

$$G(\Theta,K,z) = \frac{e^{-KH}\ \mathrm{Cosh}(K(H+z_o))\ (K+K_o\,\mathrm{Sec}^2\Theta)}{\mathrm{Cosh}(KH)\ (1-K_o H\ \mathrm{Sec}^2\Theta\ \mathrm{Sech}^2(KH))}\ \mathrm{Cosh}(K(z+H)) \tag{4.11}$$

k in (4.1Ø) is the integration variable

meanwhile K in (4.11) is the wave number obtained from

$$K - K_o\ \mathrm{Sec}^2\Theta\ \mathrm{Tanh}(KH) = Ø \tag{4.12}$$

H = Depth of water

U = Free stream velocity

$\int\!\!\!\!\!\!-$ = Represents the Cauchy principal value integral

Equation (4.9) can also be written as :

$$\phi = -\mu I_1 + 4/\pi\ \mu I_2 + 4\mu I_3 \tag{4.13}$$

In equation (4.13), the I_1 term represents a unit source located at $(Ø,Ø,z_o)$ and its image at $(Ø,Ø,-(2H+z_o))$. The I_2 term shows the effect of the free surface due to this source and its image. And finally, the I_3 term exists in order to satisfy the radiation condition.

The velocity potential of a source in a shallow canal of width W (Fig.33), can be found by application of the method of images to Equation (4.13). If the source is located at (x_o, y_o, z_o), the images of the source with the same strength and located at (x_o, y_o', z_o) and (x_o, y_o'', z_o) must be taken into account.

$$\text{Where}\quad y_o' = y_o + 2nW \qquad \text{for } n=-\infty..\infty$$
$$y_o'' = -y_o + (2n+1)W \qquad \text{for } n=-\infty..\infty \tag{4.14}$$

Hence Equation (4.13) becomes :

$$\phi = -\mu \sum_{n=-\infty}^{\infty} [I_1' + I_1''] + 4/\pi \, \mu \sum_{n=-\infty}^{\infty} [I_2' + I_2''] + 4\mu \sum_{n=-\infty}^{\infty} [I_3' + I_3''] \tag{4.15}$$

By simplifying this equation

$$\phi = -\mu J_1 + 4/\pi \, \mu J_2 + 4\mu J_3 \tag{4.16}$$

By using the derivation described in Appendix C

$$J_1 = \sum_{n=-\infty}^{\infty} \left[\frac{1}{r_1'} + \frac{1}{r_1''} + \frac{1}{r_2'} + \frac{1}{r_2''}\right] \tag{4.17}$$

where

$$r_1'^2 = (x-x_o)^2 + (y-y_o')^2 + (z-z_o)^2$$

$$r_1''^2 = (x-x_o)^2 + (y-y_o'')^2 + (z-z_o)^2$$

$$r_2'^2 = (x-x_o)^2 + (y-y_o')^2 + (z+(2H+z_o))^2$$

$$r_2''^2 = (x-x_o)^2 + (y-y_o'')^2 + (z+(2H+z_o))^2$$

$$J_2 = \frac{2\pi}{W} \int_{\emptyset}^{\infty} \sum_{m=\emptyset}' \frac{e^{-kH} \, \mathrm{Cosh}(k(H+z_o)) \, (k+K_o \, \mathrm{Sec}^2\theta_m)}{\mathrm{Cosh}(kH) \, (k-K_o \, \mathrm{Sec}^2\theta_m \, \mathrm{Tanh}(kH))} \, \mathrm{Cosh}(k(z+H))$$

$$\frac{\mathrm{Cos}(k(x-x_o)\mathrm{Cos}\theta_m)}{k \, \mathrm{Cos}\theta_m} \quad \begin{matrix} \mathrm{Cos}(ky\mathrm{Sin}\theta_m) & \mathrm{Cos}(ky_o \mathrm{Sin}\theta_m) \\ \mathrm{Sin}(ky\mathrm{Sin}\theta_m) & \mathrm{Sin}(ky_o \mathrm{Sin}\theta_m) \end{matrix} \tag{4.18}$$

$$J_3 = \frac{2\pi}{W} \sum_{m=\emptyset}^{\infty}{}' \frac{e^{-K_m H} \, \mathrm{Cosh}(K_m(H+z_o)) \, (K_o + K_m \mathrm{Cos}^2\theta_m)}{\mathrm{Cosh}(K_m H) \, (1-K_o H \, \mathrm{Sech}^2(K_m H) + \mathrm{Sin}^2\theta_m)} \, \mathrm{Cosh}(K_m(z+H))$$

$$\frac{\mathrm{Sin}(K_m(x-x_o)\mathrm{Cos}\theta_m)}{K_m \mathrm{Cos}\theta_m} \quad \begin{matrix} \mathrm{Cos}(K_m y \mathrm{Sin}\theta_m) & \mathrm{Cos}(K_m y_o \mathrm{Sin}\theta_m) \\ \mathrm{Sin}(K_m y \mathrm{Sin}\theta_m) & \mathrm{Sin}(K_m y_o \mathrm{Sin}\theta_m) \end{matrix} \tag{4.19}$$

where

Σ' denotes that $m=\emptyset$ term is halved

Cos terms apply to even m and Sin terms apply to odd m

4.4 FAR FIELD WAVE SYSTEM OF A SHIP MODEL IN A SHALLOW WATER CANAL

The far field velocity potential of a source located at (x_o, y_o, z_o) in a shallow canal can be found from equation (4.16) by allowing x to go to $-\infty$.

$$\phi_{FF} = \lim_{x\to-\infty} \phi$$

$$= [-\mu \lim_{x\to-\infty} J_1 + 4\mu/\pi \lim_{x\to-\infty} J_2 + 4\mu \lim_{x\to-\infty} J_3] \qquad (4.20)$$

By using the analysis described in appendix D

$$\lim_{x\to-\infty} J_1 = \lim_{x\to-\infty} \{ \sum_{n=-\infty}^{\infty} [\frac{1}{r_1'} + \frac{1}{r_1''} + \frac{1}{r_2'} + \frac{1}{r_2''}] \} = \emptyset \qquad (4.21)$$

$$\lim_{x\to-\infty} J_2 = \frac{2\pi^2}{W} \sum_{m=\emptyset}' \frac{e^{-K_m H} \cosh(K_m(H+z_o))\ (K_o + K_m \cos^2\theta_m)}{(1 - K_o H \operatorname{Sech}^2(K_m H) + \sin^2\theta_m)} \frac{1}{K_m \cos\theta_m}$$

$$\frac{\cosh(k(z+H)}{\cosh(kH)} \sin(K_m(x-x_o)\cos\theta_m) \begin{matrix} \cos(K_m y \sin\theta_m)\ \cos(K_m y_o \sin\theta_m) \\ \sin(K_m y \sin\theta_m)\ \sin(K_m y_o \sin\theta_m) \end{matrix} \qquad (4.22)$$

$$\lim_{x\to-\infty} J_3 = \frac{2\pi}{W} \sum_{m=\emptyset}' \frac{e^{-K_m H} \cosh(K_m(H+z_o))\ (K_o + K_m \cos^2\theta_m)}{(1 - K_o H \operatorname{Sech}^2(K_m H) + \sin^2\theta_m)} \frac{1}{K_m \cos\theta_m}$$

$$\frac{\text{Cosh}(k(z+H)}{\text{Cosh}(kH)} \begin{matrix} \text{Cos}(K_m y \text{Sin}\theta_m) \\ \text{Sin}(K_m y \text{Sin}\theta_m) \end{matrix} \text{Sin}(K_m(x-x_o)\text{Cos}\theta_m) \begin{matrix} \text{Cos}(K_m y_o \text{Sin}\theta_m) \\ \text{Sin}(K_m y_o \text{Sin}\theta_m) \end{matrix} \quad (4.23)$$

where

Σ' denotes that m=Ø term is halved

Cos terms apply to even m and Sin terms apply to odd m

By substituting (4.21), (4.22) and (4.23) into (4.2Ø) the far field velocity potential can be found as

$$\phi_{FF} = \frac{16\pi\mu}{W} \sum_{m=\emptyset}^{\infty}{}' \frac{e^{-K_m H}\ \text{Cosh}(K_m(H+z_o))\ (K_o + K_m \text{Cos}^2\theta_m)}{(1-K_o H\text{Sech}^2(K_m H)+\text{Sin}^2\theta_m)} \frac{1}{K_m \text{Cos}\theta_m}$$

$$\frac{\text{Cosh}(k(z+H)}{\text{Cosh}(kH)} \begin{matrix} \text{Cos}(K_m y \text{Sin}\theta_m) \\ \text{Sin}(K_m y \text{Sin}\theta_m) \end{matrix} \text{Sin}(K_m(x-x_o)\text{Cos}\theta_m) \begin{matrix} \text{Cos}(K_m y_o \text{Sin}\theta_m) \\ \text{Sin}(K_m y_o \text{Sin}\theta_m) \end{matrix} \quad (4.24)$$

Now the dynamic free surface condition (4.3) can be used to derive the wave system in the far field:

$$\zeta = \frac{U}{g}\phi_x \qquad \text{at } z=\emptyset$$

By defining the derivative of the far field potential and substituting z=Ø

$$\zeta = \frac{16\pi U}{Wg} \sum_{m=\emptyset}^{\infty}{}' \frac{e^{-K_m H}\ \text{Cosh}(K_m(H+z_o))\ (K_o + K_m \text{Cos}^2\theta_m)}{(1-K_o H\ \text{Sech}^2(K_m H)+\text{Sin}^2\theta_m)} \text{Cos}(K_m(x-x_o)\text{Cos}\theta_m) \begin{matrix} \text{Cos}(K_m y \text{Sin}\theta_m) \\ \text{Sin}(K_m y \text{Sin}\theta_m) \end{matrix} \begin{matrix} \text{Cos}(K_m y_o \text{Sin}\theta_m) \\ \text{Sin}(K_m y_o \text{Sin}\theta_m) \end{matrix} \quad (4.25)$$

The following equations are also satisfied

$$K_m \operatorname{Sin}\theta_m = m\pi/W$$

$$K_m - K_o \operatorname{Sec}^2\theta_m \operatorname{Tanh}(KH) = \emptyset \qquad (4.26)$$

Equation (4.25) can be simplified for a ship model represented by an assembly of sources :

$$\varphi = \sum_{m=\emptyset}^{\infty} \left\{ \begin{bmatrix} \xi_m \\ \alpha_m \end{bmatrix} \operatorname{Cos}(w_m x) + \begin{bmatrix} \eta_m \\ \beta_m \end{bmatrix} \operatorname{Sin}(w_m x) \right\} \begin{matrix} \operatorname{Cos}(m\pi y/W) \\ \operatorname{Sin}(m\pi y/W) \end{matrix} \qquad (4.27)$$

where cos term applies to even m and sin term applies to odd m

$$w_m = K_m \operatorname{Cos}\theta_m \qquad (4.28)$$

$$\tau_m = \frac{16\pi U}{Wg} \; \frac{e^{-K_m H} \operatorname{Cosh}(K_m(H+z_o))}{(1-K_o H \operatorname{Sech}^2(K_m H)+\operatorname{Sin}^2\theta_m)} \qquad (4.29)$$

where the m=∅ term must be halved

$$\begin{bmatrix} \xi_m \\ \eta_m \end{bmatrix} = \sum \frac{\mu_o \tau_m}{WS} \operatorname{Cos}(m\pi y_o/W) \begin{matrix} \operatorname{Cos}(w_m x_o) \\ \operatorname{Sin}(w_m x_o) \end{matrix} \qquad (4.30)$$

$$\begin{bmatrix} \alpha_m \\ \beta_m \end{bmatrix} = \sum \frac{\mu_o \tau_m}{WS} \operatorname{Sin}(m\pi y_o/W) \begin{matrix} \operatorname{Cos}(w_m x_o) \\ \operatorname{Sin}(w_m x_o) \end{matrix} \qquad (4.31)$$

By substituting

$$\varphi_m^2 = \begin{cases} (\xi_m^2+\eta_m^2) & \text{for even } m \\ (\alpha_m^2+\beta_m^2) & \text{for odd } m \end{cases} \qquad (4.32)$$

$$\zeta = \sum_{m=0}^{\infty} \zeta_m \cos(w_m x+\varepsilon) \begin{matrix} \cos(m\pi y/W) \\ \sin(m\pi y/W) \end{matrix} \tag{4.33}$$

If $\zeta_m, \eta_m, \alpha_m, \beta_m$ terms are substituted

$$\phi_{FF} = \frac{g}{U} \sum_{m=0}^{\infty}{}' \begin{bmatrix} -\eta_m \\ -\beta_m \end{bmatrix} \cos(w_m x) + \begin{bmatrix} \zeta_m \\ \alpha_m \end{bmatrix} \sin(w_m x) \frac{1}{K_m \cos\theta_m} * \frac{\cosh(K_m(z+H))}{\cosh(K_m H)} \begin{matrix} \cos(m\pi y/W) \\ \sin(m\pi y/W) \end{matrix} \tag{4.34}$$

If the ship model is symmetric relative to the tank centerline, then equations (4.27) and (4.33) can be expressed by taking the even terms only and substituting n=2m as

$$\zeta = \sum_{n=0}^{\infty} [\zeta_n \cos(w_n x) + \eta_n \sin(w_n x)] \cos(2n\pi y/W) \tag{4.35}$$

$$\zeta = \sum_{n=0}^{\infty} \zeta_n \cos(w_n x+\varepsilon) \cos(2n\pi y/W) \tag{4.36}$$

where

$w_n = K_n \cos\theta_n$

$K_n \sin\theta_n = 2\pi n/W$

$K_n - K_o \sec^2\theta_n \tanh(K_n H) = 0$

Hence the far field wave potential can be expressed as

$$\phi_{FF} = \frac{g}{U} \sum_{n=0}^{\infty}{}' [-\eta_n \cos(w_n x) + \zeta_n \sin(w_n x)] \frac{1}{K_n \cos\theta_n} *$$

$$\frac{\text{Cosh}(K_n(z+H))}{\text{Cosh}(K_n H)} \quad \text{Cos}(2n\pi y/W) \tag{4.37}$$

4.5 REPRESENTATION OF A SHIP MODEL BY A SOURCE ASSEMBLY

There are a number of methods for representing a body with a source-sink distribution among which the centreplane and surface distributions are the most used. The centreplane source distribution can model only thin, slender hull forms satisfactorily. As the catamaran demihulls are fairly thin, the centreplane source distribution is used throughout the numerical calculations.

Equation (4.7) was determined as

$$U f_x + \phi_y = 0 \tag{4.7}$$

The flow from a source in the y direction will be

$$\phi_y = 2\pi\mu$$

By substituting this into (4.7)

$$\mu = -\frac{U}{2\pi} f_x \tag{4.38}$$

4.6 WAVE RESISTANCE OF A SHIP MODEL IN A SHALLOW WATER CANAL

The wave resistance of a ship model advancing with constant speed U can be determined from considerations of momentum changes as described in Chapter 3. If the terms in the second line of equation 3.10 are derived and substituted, the wave resistance equation can be determined.

By assuming small wave height (ζ_B) from (3.10)

$$R_w = 1/2\ \rho g \int_{-W/2}^{W/2} \zeta^2\ dy + 1/2\ \rho \int_{-W/2}^{W/2} \int_{-H}^{0} (\phi_y^2 + \phi_z^2 - \phi_x^2)\ dz dy \tag{4.39}$$

By using the analysis described in Appendix E

$$R_w = \frac{W\rho g}{4} \{ (\xi_0^2 + \eta_0^2)\ (1 - \frac{2K_0 H}{\mathrm{Sinh}(2K_0 H)}) + \sum_{m=1}^{\infty} \left[\frac{\xi_m^2 + \eta_m^2}{\alpha_m^2 + \beta_m^2}\right] [1 - 0.5\ \mathrm{Cos}^2\Theta_m (1 + \frac{2K_m H}{\mathrm{Sinh}(2K_m H)}]\} \tag{4.40}$$

where ξ, η are applied for even m, α, β are applied for odd m

For a ship model symmetric to the tank centerline the wave resistance will correspond to

$$R_w = \frac{W\rho g}{4} \{ (\xi_0^2 + \eta_0^2)\ (1 - \frac{2K_0 H}{\mathrm{Sinh}(2K_0 H)}) + \sum_{n=1}^{\infty} (\xi_n^2 + \eta_n^2)\ [1 - 0.5\ \mathrm{Cos}^2\Theta_n (1 + \frac{2K_n H}{\mathrm{Sinh}(2K_n H)}]\} \tag{4.41}$$

In practice m or n may be truncated at a finite number as the contribution to the resistance decreases with increasing m or n when approaching high wave angles.

4.7 FAR FIELD WAVE SYSTEM OF A CATAMARAN

The far field wave system of a catamaran can be found from equation (4.27) by utilizing a source distribution for

each hull and calculating (4.3Ø) and (4.31) over both distributions. This method can be used for any number and combination of sources representing any shape of hull form including catamarans and trimarans, staggered hulls and tandem combinations.

Alternatively the far field wave system of the catamaran, symmetric to the tank centerline, can be formulated from a simple analysis of equation (4.25) for two demihull wave systems. The sources representing the hulls will be located at $y_1 = y_H + S/2$ and $y_2 = -(y_H + S/2)$ where y_H is the lateral distance from the centreplane of the demihull for each source, i.e. $y_H = \emptyset$ for symmetric demihulls, and S is the separation between the centrelines of the demihulls.

$$\zeta = \zeta_1 + \zeta_2$$

$$\zeta = \frac{16\pi U}{Wg} \sum_{m=\emptyset}^{\infty}{}' \frac{e^{-K_m H}\ \mathrm{Cosh}(K_m(H+z_o))\ (K_o + K_m \mathrm{Cos}^2\theta_m)}{(1 - K_o H\ \mathrm{Sech}^2(K_m H) + \mathrm{Sin}^2\theta_m)} \cdot \mathrm{Cos}(K_m(x-x_o)\mathrm{Cos}\theta_m) \cdot \begin{matrix} \mathrm{Cos}(K_m y \mathrm{Sin}\theta_m)\ \mathrm{Cos}(K_m(y_H+S/2)\mathrm{Sin}\theta_m) \\ \mathrm{Sin}(K_m y \mathrm{Sin}\theta_m)\ \mathrm{Sin}(K_m(y_H+S/2)\mathrm{Sin}\theta_m) \end{matrix}$$

$$+ \frac{16\pi U}{Wg} \sum_{m=\emptyset}^{\infty}{}' \frac{e^{-K_m H}\ \mathrm{Cosh}(K_m(H+z_o))\ (K_o + K_m \mathrm{Cos}^2\theta_m)}{(1 - K_o H\ \mathrm{Sech}^2(K_m H) + \mathrm{Sin}^2\theta_m)} \cdot \mathrm{Cos}(K_m(x-x_o)\mathrm{Cos}\theta_m) \cdot \begin{matrix} \mathrm{Cos}(K_m y \mathrm{Sin}\theta_m)\ \mathrm{Cos}(-K_m(y_H+S/2)\mathrm{Sin}\theta_m) \\ \mathrm{Sin}(K_m y \mathrm{Sin}\theta_m)\ \mathrm{Sin}(-K_m(y_H+S/2)\mathrm{Sin}\theta_m) \end{matrix} \qquad (4.42)$$

Where
Cos terms apply to even m
Sin terms apply to odd m

The following equations are satisfied

$$K_m \mathrm{Sin}\theta_m = m\pi/W$$

$$K_m - K_o \, Sec\theta^2{}_m \, Tanh(KH) = \emptyset \tag{4.43}$$

by substituting $C_s = Cos(K_m \; S/2 \; Sin\theta_m) = Cos(m\pi S/2W)$

$$S_s = Sin(K_m \; S/2 \; Sin\theta_m) = Sin(m\pi S/2W) \tag{4.44}$$

$$\zeta = \sum_{m=\emptyset}^{\infty} \left\{ \begin{bmatrix} \mathcal{F}_m C_s - \alpha_m S_s & \eta_m C_s - \beta_m S_s \\ \alpha_m C_s + \mathcal{F}_m S_s & \beta_m C_s + \eta_m S_s \end{bmatrix} \begin{matrix} Cos(w_m x) + \\ Sin(w_m x) \end{matrix} \begin{matrix} Cos(m\pi y/W) \\ Sin(m\pi y/W) \end{matrix} \right\}$$

$$+ \sum_{m=\emptyset}^{\infty} \left\{ \begin{bmatrix} \mathcal{F}_m C_s - \alpha_m S_s & \eta_m C_s - \beta_m S_s \\ -\alpha_m C_s - \mathcal{F}_m S_s & -\beta_m C_s - \eta_m S_s \end{bmatrix} \begin{matrix} Cos(w_m x) + \\ Sin(w_m x) \end{matrix} \begin{matrix} Cos(m\pi y/W) \\ Sin(m\pi y/W) \end{matrix} \right\} \tag{4.45}$$

$$= \sum_{m=\emptyset}^{\infty} \left\{ \begin{bmatrix} 2(\mathcal{F}_m C_s - \alpha_m S_s) & 2(\eta_m C_s - \beta_m S_s) \\ \emptyset & \emptyset \end{bmatrix} \begin{matrix} Cos(w_m x) + \\ Sin(w_m x) \end{matrix} \begin{matrix} Cos(m\pi y/W) \\ Sin(m\pi y/W) \end{matrix} \right\} \tag{4.46}$$

by substituting n=2m

$$= 2\sum_{n=\emptyset}^{\infty} \left[(\mathcal{F}_n C_s - \alpha_n S_s) Cos(w_n x) + (\eta_n C_s - \beta_n S_s) Sin(w_n x) \right] Cos(2n\pi y/W) \tag{4.47}$$

For a catamaran made up two symmetric demihulls, (4.47) can be simplified to

$$\zeta = \sum_{n=\emptyset}^{\infty} \left[(2\mathcal{F}_n C_s) \; Cos(w_n x) + (2\eta_n C_s) \; Sin(w_n x) \right] Cos(2n\pi y/W) \tag{4.48}$$

4.8 WAVE RESISTANCE OF A CATAMARAN

The wave resistance of a catamaran can be calculated from (4.40) by using the wave coefficients found in equation (4.46) :

$$R_w = \frac{W\mathcal{F}g}{4} \left\{ \left[(2\mathcal{F}_o)^2 + (2\eta_o)^2 \right] \left(1 - \frac{2K_o H}{Sinh(2K_o H)} \right) \right.$$

$$+\sum_{n=1}^{\infty} [4(\mathcal{F}_n C_s - \alpha_n S_s)^2 + 4(\gamma_n C_s - \beta_n S_s)^2] \left[1 - \frac{\cos^2\theta_n}{2}\left(1 + \frac{2K_n H}{\sinh(2K_n H)}\right)\right]\}$$

(4.49)

For the catamaran with symmetric demihulls

$$R_w = \frac{W\mathcal{F}g}{4}\{ [(2\mathcal{F}_o)^2 + (2\gamma_o)^2] \left(1 - \frac{2K_o H}{\sinh(2K_o H)}\right)$$

$$+\sum_{n=1}^{\infty} [(2\mathcal{F}_n C_s)^2 + (2\gamma_n C_s)^2] \left[1 - \frac{\cos^2\theta_n}{2}\left(1 + \frac{2K_n H}{\sinh(2K_n H)}\right)\right]\}$$

(4.50)

where

$$C_s = \cos(\pi n S/W) = \sqrt{(1+\cos(2\pi n S/W))/2}$$

hence $(2C_s)^2 = 2\,(1+\cos(2\pi n S/W))$

$\cos(2\pi n S/W)$, or $\cos(K_n \sin\theta_n S)$, is the interference factor which can be positive or negative depending on the harmonic. However for the first harmonic, it is equal to 2. Hence the transverse wave is always magnified by a factor of 2, resulting in an increase of the wave resistance.

4.9 MODIFICATIONS TO THE METHOD

In order to provide a practical use of the method two modifications to the theory were made for determining the correlation with experimental results. Firstly, the method uses a fixed model approach by not allowing the model to sink or to trim. To overcome this assumption, model offsets for a particular trim and sinkage were input to the method. The sinkage and trim were obtained from the experimental results. Secondly the method does not take a transom stern into account, and leaves an open transom stern to infinity.

A method is suggested in Ref.8 in which the hydrostatic force on the transom is added to the wave resistance :

$$R_{TS} = \rho g \int_{TS} \int z \, dy \, dz \tag{4.51}$$

Hence

$$C_{TS} = \frac{2g \int_{TS} \int z \, dy \, dz}{S_w \, U^2} \tag{4.52}$$

For the models with a transom stern this component is added to the wave resistance obtained from the sources. As can be seen from (4.52), the hydrostatic resistance coefficient gets smaller as the speed increases. Hence the low speeds are the most affected range.

4.10 DEVELOPMENT OF A COMPUTER PROGRAM FOR THE DETERMINATION OF THEORETICAL WAVE RESISTANCE

Based on the results of the theoretical investigation detailed above, a computer program for the determination of theoretical wave resistance for a ship model in a shallow water canal has been developed. The program WAVERES has been written in FORTRAN 77 with the capability of running on both an IBM 3090 Mainframe and MSDOS Microcomputers.

The program can calculate the far field wave system and wave resistance for a hull or a combination of up to three hulls. As the wave coefficients are calculated from the superimposition of sources, the hulls can be positioned in any combination and the hull forms and dimensions can be different for each hull.

Firstly, the hull offsets in still water are read by the program. These offsets are then changed into the

calculation hull by taking the trim and sinkage into account.

The source strengths are calculated from the hull offsets by the use of thin ship theory, i.e equation (4.38). The centreplane is divided into rectangular elements (Fig.35). The contribution of each element is calculated by replacing the continuous source distribution of the element with a point source located at the centre of the element with density :

$$\mu = -\frac{U}{2\pi}\,\frac{[(y_{I+1,J}+y_{I+1,J+1}) - (y_{I,J}+y_{I,J+1})]}{2\,(x_{I+1}-x_I)}\,dA \qquad (4.53)$$

The wave coefficients are calculated by applying (4.30) and (4.31) to these sources. The wave resistance is calculated from equation (4.40) using the coefficients obtained. A transom stern correction is applied to all the hulls. A flow diagram of the program is given in Fig.36.

In order to test the program, calculation of wave resistance has been carried out for two models : One parabolic hull (Wigley Hull) (Fig.132) and a transom stern semi-displacement hull (Athena hull) (Fig.34). The results of the calculations have been compared with available theoretical calculations for these hulls (Figs.37,38). Although there is a scatter in the available theoretical results due to implementation of different numerical schemes, the results of the current analysis are generally in good agreement with these calculations for both hulls.

For the Wigley hull, the results confirm the accuracy of the current numerical method across the speed range. For the Athena hull, wave resistance and transom correction are calculated. The hydrostatic resistance, i.e. transom correction, is very important at low speeds. The results for wave resistance are consistent with Hong's results as

he did not use any correction for a transom stern. The corrected wave resistance curve agrees with Gadd's results.

The results for the Wigley hull are also compared with experimental measurements of wave pattern and residuary resistance for both fixed and free to sink and trim conditions to investigate the correlation between them (Figs.39,40). The theoretical wave resistance is higher than the wave pattern resistance across the speed range, while it is in better agreement with the residuary resistance below Fn:0.45. An overestimation between Fn:0.47 and 0.7 is also visible. By considering the similarity of the results for both the fixed and free conditions (Fig.41), it can be concluded that the correction for the sinkage and trim is very successful. The theoretical results oscillate much more than the experimental curves which is a characteristic of the linearised theory approach. This may be attributed to neglecting viscous effects. The positions of the humps and hollows are accurately predicted in both cases.

The calculations for the Athena hull were only conducted in the fixed condition (Fig.42), as the sinkage and trim data were not available. The wave resistance is in satisfactory agreement with the wave pattern results up to Fn:0.4. Above this speed overprediction is visible. The same trends are apparent in the corrected wave resistance and residuary drag measurements. The correction for transom stern compensates the large difference between the wave resistance and residuary resistance.

In general the theoretical prediction for the wave resistance overestimates the wave pattern resistance, although it predicts the places of humps and hollows accurately. The corrections for transom stern, sinkage and trim improves the correlation with the experimental results.

4.11 A PARAMETRIC STUDY OF HULL FORM EFFECTS ON THE CATAMARAN WAVE RESISTANCE INTERFERENCE

In order to investigate the effect of hull form changes on the theoretical wave resistance features of catamarans, a parametric study was conducted using the Wigley hull form. By varying length to beam ratio (L/B), beam to draught ratio (B/T), prismatic coefficient (C_P) and entrance angle (α_E)*, wave resistance interference factors have been calculated for separation length ratios of Ø.2, Ø.3, Ø.4 and Ø.5. The results are presented in Figs.43 to 62.

The variation of hull form changes are applied to the parent hull form with L/B:1Ø, B/T:1.6, C_P:Ø.666, α_E:11.31. During the variation of a particular hull form factor all the other factors were kept constant, i.e. the factors L/B:1Ø, B/T:1.6, C_P:Ø.666 were constant while α_E was varied as shown in Figs.59 to 62.

Figs.43 to 46 display the change of theoretical wave resistance per unit displacement ($R_W/\rho U^2 \nabla$) for monohulls without any interaction effects. The wave resistance interference factor, wave resistance for catamaran divided by twice wave resistance of a monohull i.e. $(R_W)_{CAT}/2(R_W)_{MONO}$, are given in Figs.47 to 62. However it must be emphasised that these figures show the interference only, and the lowest interference does not mean the lowest wave resistance.

Length to beam ratio is important mainly in the region of Fn:Ø.35 to Fn:Ø.9. The higher the length to beam ratio, the lower the interaction is. Over L/B:1Ø there is not much difference between the results.

Beam to draught ratio influences the interference ratio only above Fn:Ø.35. Higher B/T ratios give smaller

* C_P and α_E by changing order of polinomial per WIGLEY W.C.S. Calculated and Measured Wave Resistance of a Series of Forms Defined Algebraically, the Prismatic and Angle of Entrance being Varied Independently TRINA 1942 Vol:84

interference resistance. However the change above B/T=1.2 is very small.

The effect of prismatic coefficient on the interference factor displays an influence which is different from the other factors. High prismatic coefficients show a favourable interference between Fn:Ø.3 and Ø.4, and the maximum interference occurs at decreasing Fn as Cp is increased for this speed range. above this speed smaller prismatic coefficients are favourable.

The entrance angle at the load water line has an oscillatory effect on the interference resistance, higher entrance angles causing smaller resistance up to hump speed, and higher resistance above this speed.

In general it can be seen that speed and separation change are the main factors affecting interference. The hull form changes have a secondary effect compared with these. The main interference region for L/B and B/T variation is above the main hump speed, whilst prismatic coefficient and entrance angle have more effect on the last hollow before the main hump speed, at about Fn:Ø.35.

4.12 SUMMARY

Theoretical wave resistance and the far field wave system of a ship model in a shallow tank independent of its symmetry have been developed from linearised theory. This method can be applied to any hull shape and any number of hulls in the tank, provided that the source strengths can be found. The thin ship approach is used as, whilst it is the simplest, it is a very powerful and satisfactory method for slender hulls.

The far field wave pattern and the wave resistance of a catamaran with symmetric or asymmetric demihulls were

derived from the demihull analysis. The wave reflections and venturi effects between the hulls were neglected.* The interference factor is found to be $1+\cos(K_n \sin\theta_n S)$. It oscillates with the change of harmonics resulting in an increase or reduction in the wave resistance.

The modification for models free to trim and sink is established by changing hull input data. Hydrostatic resistance which may be very important below the hump speed is presented for transom stern models.

The numerical results of the developed program are compared with existing calculations and experimental results. The comparison with existing calculations is very good considering the scatter in the available data. The theoretical results are higher than the experimental ones ruling out at present quantitative use of the method. However the positions of the humps and hollows are predicted accurately, providing a qualitative use for the linearised theory.

A parametric study of the effects of hull form changes on the catamaran wave resistance interactions has been conducted using the Wigley model. Separation distance, and speed were found to be the primary factors. Length to beam and beam to draught ratios are the secondary factors at higher speeds, whilst entrance angle and prismatic coefficient are important at lower speeds.

During the theoretical analysis of catamaran wave resistance, the lack of available experimental data prevented clear conclusions to be drawn on the adequacy of the method. It was therefore decided to conduct comparisons with the various resistance components measured during the current work. The results of this comparative work together with the conclusions on the potential applications of the theoretical method are presented in Chapter 8.

* due to the use of linear theory and thin ship method, although they will be present in practice.

CHAPTER 5 : EXPERIMENTAL DETERMINATION OF TOTAL RESISTANCE, RUNNING TRIM, SINKAGE, AND WAVE ELEVATION ALONG THE HULL

5.1 INTRODUCTION

A series of resistance tests were conducted to explore the resistance components of catamarans. The tests included the measurements of total resistance, sideforce, sinkage, running trim and wave elevation along the hull. Wave pattern experiments, described in Chapter 6, were carried out concurrent with these tests in order to save time and to simulate the same conditions, such as temperature, ballast and speed.

A microcomputer controlled data acquisition system was used to acquire the analogue signals from the total resistance and side force dynamometer, running trim and sinkage potentiometers, while wave elevation was digitised from the photographs taken.

The resistance tests were conducted with five model forms. An existing model was used to assess the feasibility of the experimental set-up in the low speed range, Fn:Ø.2 to Ø.5. A mathematical hull, tested both in fixed and free to trim and sink conditions was used to validate the experimental techniques against other published data over a large speed range, Fn:Ø.1 to Ø.95. A series of three round bilge high speed hulls were tested to establish a database for the displacement and semi-displacement speed range up to Fn:1.ØØ and to investigate the influence of gap ratio. Details of the five models, denoted C1 to C5, are given in Tables 1 and 2. The results of the experiments are given in Chapter 8.

5.2 GENERAL SET-UP

All the model experiments were carried out in the Southampton Institute of Higher Education (SIHE) towing tank, the dimensions of which are as follows :

Length : 60.0 m
Width : 3.7 m
Depth : 1.85 m
Max Speed : 4.6 m/s.

This tank has a rectangular section with constant width and depth along its length. A wave suppression beach is installed at one end of the tank, and a wavemaker at the other end. There are a number of wooden beaches for wave damping along one side of the tank. These were lifted out of the water during wave pattern experiments in order to get near perfect wave reflections from the tank walls. In the wake traverse experiments the beaches were kept in the water in order to reduce the time between the tests.

The tank is equipped with a manned carriage and is rigged with a microcomputer based data acquisition system, two component dynamometer and a heavy model dynamometer. Acceleration distance in the tank is about 20 m which was sufficient to achieve the max speed used in the experiments, i.e. 4.2 m/s. The stationary test distance is about 20 m. A section of 15.24 m long was used during the measurements. Total resistance readings in this section were satisfactorily steady. The tests were carried out at up to 4.2 m/s as the measuring time becomes unacceptably short above this speed.

The microcomputer controlled data acquisition system used in the experiments is described in detail in Appendix G. The total resistance, side force, sinkage, and running

trim were acquired simultaneously. The averages for each channel were recorded as test results. The set up for the total resistance system is shown in Fig.63.

Viscous blockage effects were neglected for the models as the biggest cross section area of the models was less than Ø.5 % of tank cross section. The application of a tank wall interference correction to the catamarans with wide separations was investigated due to possible wave interference from the tank walls. Theoretical calculations on the Wigley model indicated that the maximum interference would be less than 1 % for all tested catamarans in the tank used (Fig.64). Hence, no correction was applied to the results.

Shallow water effects were also neglected as the tank depth was bigger than the model length and all the models were tested only in the subcritical speed zone of Fnh<Ø.95 which corresponds to Fn=Ø.95 for model C2 and Fn=1.Ø2 for models C1,C3,C4,C5. Furthermore, theoretical calculations on shallow water effects in the SIHE tank were conducted for the Wigley model (Fig.65). In this case, the wave resistance increase is less than 2 % and 4 % for the monohull and catamaran models respectively except in the region of Ø.95<Fnh<1.Ø2. Therefore shallow water effects are not pronounced except at the top end of the speed range. Differences in the resistance increase for the different catamaran combinations is found to be negligible. It is however noted that special care should be taken when comparing the catamaran hulls with the demihull in isolation at high speeds.

The experiments were conducted over a three year time period. The temperature of the tank water was found to vary between 13 °C and 18.5 °C during the experiments. A temperature correction was therefore applied to all the

models, and the results presented at a standard temperature of 15 °C in such a way that

$$C_T = C_T^{TC} - C_F^{TC} + C_F^{15}$$

where
TC : measurement temperature
C_F^{TC}: ITTC 1957 ship model correlation line for temperature TC

5.3 TOTAL RESISTANCE AND SIDEFORCE MEASUREMENTS

The total resistance and sideforce measurements were made using the Wolfson Unit dynamometer (Fig.66) which is fully described in Ref [7]. Total resistance was recorded for all the speeds tested while the sideforce was monitored at all speeds to ensure that the model yaw degree was negligible. The accuracy of the total resistance was found to be in the range of ±0.02 N which was satisfactory for speeds above 1.0 m/s. Total resistance results were nondimensionalised using $\rho S_W U^2/2$ in the usual way.

All the models were tested in the free to trim and sink condition. Additionally the Wigley hull was tested in the fixed trim and sink condition. In all tests, the models were restrained in surge, sway, yaw and roll. The model was fixed in sink by restraining the towing post in vertical motion (Fig.67), and to trim by the use of specially designed tow fittings. Four tow fitting were developed and used in the catamaran tests :

a) Fixed monohull tow fitting (Fig.68)
b) Free monohull tow fitting (Fig.69)
c) Fixed catamaran tow fitting (Fig.70)
d) Free catamaran tow fitting (Fig.71)

In order to validate the total resistance results, comparisons with available data in the literature were

carried out for the Wigley monohull model and are shown in Figs.72 and 73. The results for a catamaran made up of Wigley hulls was also compared with available data in Fig.74. A close fit in the fixed condition indicates a satisfactory validation of the data. The results for the free to trim and sink case are at the high side of the result envelope. This may be justified by considering the current model to have a higher form drag due to its smaller size, as the other data were collected from models between 2m and 6m long. In both fixed and free conditions the total resistance is higher than the existing data at the lower speeds. This is probably caused by the very small drag, typically less than 1N, which is not possible to measure accurately with the dynamometer. The same trends are apparent in Fig. 74 for the catamaran experiments.

5.4 MEASUREMENT OF RUNNING TRIM AND SINKAGE

The running trim of the models was measured by potentiometers mounted on the tow fittings. For the catamaran models, one potentiometer in each hull was used, and an average of these two was recorded as running trim. The accuracy of the potentiometers was in the range of ±Ø.Ø5 degree. Trim was measured as angle in degrees and taken positive for bow up.

The sinkage of the models was measured by a linear displacement potentiometer mounted on the tow post bearing unit and connected to the tow post guide arm which moves vertically with the model. This potentiometer was only used for models which were free to trim and sink. The accuracy of the linear potentiometer was found to be ±Ø.1 mm whilst sensitivity is ±Ø.Ø5 mm. The vertical motion downwards, sinkage, is taken positive and nondimensionalised using the draught of the model.

5.5 MEASUREMENT OF WAVE ELEVATIONS ALONG THE HULL

The wave elevation along the hull at various speeds was digitised from photographs. The models were marked with lines at every longitudinal half section, and waterlines spaced at 5 mm intervals above and below the load waterline. The wave elevation was nondimensionalised by draught.

For the monohull models one photograph was taken for each speed. For the catamaran models, two photographs were necessary in order to measure the elevations along the inside and the outside of the demihulls as they were substantially different from each other. However the wave elevation inside the demihulls was not visible for small separations.

5.6 MODELS

Five different models were used in the investigation and their details are given in Tables 1 and 2.

The first model, C1 (Fig.111), was built from an existing frigate model, constructed from GRP, and used in previous work at Southampton University [5]. It was tested in order to assess the feasibility of the experimental methods. Only the low speed region , Fn:Ø.2 to Ø.5 was chosen for the model in the free to trim and sink configuration both as a monohull and a catamaran. Catamarans with separation ratios of Ø.25, Ø.3, Ø.4, Ø.5, Ø.6 were tested.

The second model, C2 (Fig.132), was built in GRP in a mathematical form with parabolic waterlines and cross sections (known as a Wigley Model). This model was used to validate the experimental approach taken, as there is a substantial amount of experimental data on the resistance

components of this form from several towing tanks [44]. This model was tested from Fn:Ø.1 to Fn:Ø.95 both free and fixed to trim and sink as a monohull and in catamaran configurations.

The last three models, C3, C4, C5 (Fig.217) were constructed from dense foam by utilising the numerically controlled model cutting machine described in Ref. [52]. They were derived from the NPL round bilge series [2] parent form by changing Length to Beam ratio (L/B) systematically. These models were tested free to trim and sink for a speed range of Fn:Ø.1 to 1.ØØ.

The models were ballasted to a given displacement and checked for their draught marks. Models were towed from their longitudinal centre of buoyancy. Towing height was taken at an assumed thrust line which was at a third of draught above the keel.

For models C1 and C2 the towing height was approximately the same as the assumed thrust line. For C3, C4, C5, it was not possible to position the tow fittings on the thrust line. Therefore a bow up trimming moment was applied by shifting a required amount of weight in the stern direction in order to compensate the moment caused by the difference between the towing and thrust lines. i.e. a moment equal to R_T * (Tow height-Thrust height) for every test.

To stimulate turbulent flow conditions the models were fitted with turbulence studs with 3.2 mm diameter and 2.5 mm height. These were located 25 mm and 9Ø mm behind the stem for models C1 and C2 respectively, and 37.5 mm behind the stem for models C3,C4 and C5. The distance between the studs was taken as 25 mm. The results given in this report were not corrected for the resistance of the studs or for the laminar flow ahead of the studs, as it was assumed that they will approximately cancel each other. However if the

results are to be extrapolated to ship scale a correction for the studs may be applied to the total resistance results.

5.7 SUMMARY

Five model forms were tested in 31 combinations to measure the total resistance, running trim, sinkage and wave elevation. The tank used in the experiments was found to be satisfactory for these tests across the model and speed range.

The data acquisition system coupled to the dynamometer and potentiometers was found to be very efficient. The towing moment due to the difference between the towing and thrust lines was compensated by use of shifting weights and special tow fittings developed for these experiments..

Corrections for water temperature were carried out. The effects of tank walls and shallow water were found to be small, hence were neglected.

The total resistance results were validated by comparing them with available data in the literature for model C2. Good agreement was obtained except at low speeds.

CHAPTER 6 : EXPERIMENTAL DETERMINATION OF WAVE PATTERN RESISTANCE OF A MODEL

6.1 INTRODUCTION

The determination of ship wave resistance directly from measurements of the wave pattern during model tests has received considerable attention over the last three decades in order to improve the understanding of the nature of wave resistance. Several wave pattern analysis methods have been developed in order to improve the effectiveness of model experiments as a tool for the hull form development process. Comprehensive reviews of wave analysis methods were conducted by Eggers et al [16] and Gadd[24].

The wave resistance of a catamaran represents a big challenge for the designer, as it is probably the most complex wave pattern for a practical ship form and includes not only the wave generation of the hulls but also the wave interaction between the hulls. Whilst the former has been investigated reasonably thoroughly for the monohull, the interaction phenomena associated with the catamaran are not yet fully understood.

A comprehensive wave pattern analysis programme was conducted on all the six models of the current work in order to improve the understanding of wave interference of catamarans. An analysis method based on multiple longitudinal cuts was developed and applied to the models.

A fully automated acquisition-analysis system consisting of four wave probes, a microcomputer based data

acquisition system and data analysis software program was used for the experiments.

In order to validate the experimental set-up and the analysis method, the results for model C2 (Wigley hull) were compared with available data in the literature both for fixed and free to trim and sink conditions. Examples of standard outputs of the analysis are given, namely the resistance distribution across the wave angle and the fit of the calculated wave trace over the measured wave trace.

A method for the prediction of catamaran wave pattern resistance from the wave pattern experimental results for a demihull was developed and tested on all the models.

6.2 WAVE PATTERN ANALYSIS METHOD

The wave pattern of a ship model, symmetric relative to the tank centerline, can be expressed as a summation of a number free waves, as shown in Chapter 4.

$$\zeta = \sum_{n=0}^{\infty} [f_n \cos(x w_n) + \eta_n \sin(x w_n)] \cos(2\pi n y / W) \qquad (6.1)$$

The wave pattern analysis aims to derive the wave coefficients f_n and η_n from the wave traces taken either across the tank or along the tank by employing one of the four main analysis methods developed and used by several experimental tanks. These methods were investigated as a first step in the wave pattern analysis programme for the understanding of catamaran wave resistance characteristics.

A) Transverse cut method, by measuring the wave elevation in two lateral positions (Fig.75). This was used successfully in several investigations of wave analysis

[16,23]. However this method was found not to be feasible for the current work due to the difficulties in measurement techniques. The common method, using pointers mounted on the carriage, was not possible because of the very short run time, e.g. 3.5 seconds for the top speed. Additionally, the need for an extra person to adjust the pointers was not acceptable. The possibility of using other carriage mounted wave probes was investigated. This included laser and ultrasonic techniques as well as capacitance and resistance probes. In no case could a simple and sufficiently accurate technique be achieved, as flow disturbance would make speed dependent calibrations necessary.

B) NPL matrix method developed at NPL by Hogben [29,31]. This is based on a least squares solution of the wave coefficients from the matrix of measurement points (Fig. 75). Although the method shows practical advantages as it can be fully automated, the results are very dependent on the choice of measurement points which requires skills developed by long experience. This method was therefore not pursued further.

C) XY Method based on the force measurements taken on a long vertical cylinder [16]. The method is very simple to analyse. However It was decided not to use this method due to the difficulties in the calibration of the forces [16] and extra instrumentation for the force measurement .

D) Longitudinal cut method. This is used as a standard test in several tanks due to its practicality and suitability for short tanks. Therefore it was chosen to be used in the wave pattern experiments.

In this method, the wave elevation is measured along the tank in one or more longitudinal cuts as shown in Fig.75 for which the wave elevation can be expressed as :

$$\gamma_P = \sum_{n=0}^{\infty} [\, P_n \cos(x w_n) + Q_n \sin(x w_n) \,] \qquad (6.2)$$

where

$P_n = \xi_n \cos(2\pi n y_P / W)$

$Q_n = \eta_n \cos(2\pi n y_P / W)$

y_P = probe distance from the centreline

Two main analysis techniques are in current use ;

i) Direct Fourier Transform Method

This method is based on the direct Fourier transform of equation 6.2 resulting in :

$$P_n = \frac{2}{L_{CUT}} \int_0^{L_{CUT}} \gamma_P \cos(x w_n)\, dx \qquad Q_n = \frac{2}{L_{CUT}} \int_0^{L_{CUT}} \gamma_P \sin(x w_n)\, dx \qquad (6.3)$$

hence

$$\xi_n = \frac{P_n}{\cos(2\pi n y_P / W)} \qquad \eta_n = \frac{Q_n}{\cos(2\pi n y_P / W)} \qquad (6.4)$$

There are two assumptions made in this method :

1) The wave trace is infinitely long
2) The wave trace is continuous

The assumption of an infinitely long wave trace is never satisfied, hence the application of a truncation correction is necessary for small tanks [16].

Additionally, the value of $\cos(2\pi n y_P / W)$ causes numerical problems when it is small or zero. $y_P = 1/3\ W$ is usually the recommended parameter for higher cosine terms as $|\cos(2\pi n y/W)|$ is always equal or higher than 0.5

ii) Matrix Solution Method

The errors due to truncation of the wave trace length and due to a non periodic wave trace can be prevented by applying a matrix solution method. This method was applied to model experiments by Iowa University [53] and by Southampton University [5,11] with different implementations. The latter will be described as it formed the basis for the method developed and used in the analysis.

By defining a wave trace for a longitudinal cut taken at $y=y_P$, and sampled in equally distanced points such that $x=\Delta k$ $k=k_1..k_2$ and by substituting $W_n=w_n\Delta$, the wave pattern can be expressed as :

$$\zeta_k = \sum_{n=\emptyset}^{\infty} [P_n \cos(W_n k) + Q_n \sin(W_n k)] \qquad (6.5)$$

where

$$P_n = \xi_n \cos(2\pi n y_P / W)$$
$$Q_n = \eta_n \cos(2\pi n y_P / W)$$

By multiplying both sides by $\exp(iW_m k)$ for $m=\emptyset..\infty$ and summing over k

$$\sum_{k=k_1}^{k_2} \zeta_k \exp(iW_m k) = \sum_{k=k_1}^{k_2} \sum_{n=\emptyset}^{\infty} \exp(iW_m k) [P_n \cos(W_n k) + Q_n \sin(W_n k)] \qquad (6.6)$$

In equation (6.6) real and imaginary parts can be written as

$$\sum_{k=k_1}^{k_2} \zeta_k \cos(W_m k) = \sum_{k=k_1}^{k_2} \sum_{n=\emptyset}^{\infty} [P_n \cos(W_n k) \cos(W_m k) + Q_n \sin(W_n k) \cos(W_m k)] \qquad (6.7a)$$

$$\sum_{k=k_1}^{k_2} \mathcal{Y}_k \sin(W_m k) = \sum_{k=k_1}^{k_2} \sum_{n=\emptyset}^{\infty} [\, P_n \cos(W_n k) \sin(W_m k) + Q_n \sin(W_n k) \sin(W_m k) \,] \qquad (6.7b)$$

By performing cos sin multiplications and substituting

$W_- = W_n - W_m$

$W_+ = W_n + W_m$

$W_2 = 2W_m$

$$\sum_{k=k_1}^{k_2} \mathcal{Y}_k \cos(W_m k) = \underline{\sum}_{n=\emptyset}^{\infty} \sum_{k=k_1}^{k_2} [\, P_n/2 \{\cos(W_+ k) + \cos(W_- k)\} + Q_n/2 \{\sin(W_+ k) + \sin(W_- k)\}] + P_m/2 \{1 + \cos(W_2 k)\} + Q_m/2 \{\sin(W_2 k)\} \qquad (6.8a)$$

$$\sum_{k=k_1}^{k_2} \mathcal{Y}_k \sin(W_m k) = \underline{\sum}_{n=\emptyset}^{\infty} \sum_{k=k_1}^{k_2} [\, P_n/2 \{\sin(W_+ k) - \sin(W_- k)\} - Q_n/2 \{\cos(W_+ k) + \cos(W_- k)\}] + P_m/2 \{\sin(W_2 k)\} + Q_m/2 \{1 + \cos(W_2 k)\} \qquad (6.8b)$$

$\underline{\Sigma}$ denotes that the term n=m is excluded

By summing over k as described in appendix A and substituting

$k_- = k_2 - k_1 + 1$

$k_+ = k_2 + k_1$

$$\sum_{k=k_1}^{k_2} \mathcal{Y}_k \cos(W_m k) = \underline{\sum}_{n=\emptyset}^{\infty} [P_n/2 \{ \frac{\cos(W_+ k_+) \sin(W_- k_-)}{\sin(W_+)} + \frac{\cos(W_+ k_+) \sin(W_- k_-)}{\sin(W_-)} \}$$

$$+Q_n/2\{\frac{\sin(W_+k_+)\sin(W_-k_-)}{\sin(W_+)}+\frac{\sin(W_+k_+)\sin(W_-k_-)}{\sin(W_-)}\}]$$

$$+P_m/2\{\quad k_2-k_1+1\quad+\frac{\cos(W_+k_+)\sin(W_-k_-)}{\sin(W_2)}\}$$

$$+Q_m/2\{\qquad\qquad+\frac{\sin(W_+k_+)\sin(W_-k_-)}{\sin(W_2)}\}$$

(6.9a)

$$\sum_{k=k_1}^{k_2}\mathcal{J}_k\sin(W_mk)=\sum_{n=\emptyset}^{\infty}[P_n/2\{\frac{\sin(W_+k_+)\sin(W_-k_-)}{\sin(W_+)}-\frac{\sin(W_+k_+)\sin(W_-k_-)}{\sin(W_-)}\}$$

$$-Q_n/2\{\frac{\cos(W_+k_+)\sin(W_-k_-)}{\sin(W_+)}-\frac{\cos(W_+k_+)\sin(W_-k_-)}{\sin(W_-)}\}]$$

$$+P_m/2\{\qquad\qquad+\frac{\sin(W_+k_+)\sin(W_-k_-)}{\sin(W_2)}\}$$

$$+Q_m/2\{\ k_2-k_1+1\qquad-\frac{\cos(W_+k_+)\sin(W_-k_-)}{\sin(W_2)}\}$$

(6.9b)

Equations (6.9a) and (6.9b) lead to a simultaneous linear equation system if n is truncated at a finite N.

$$\sum_{k=k_1}^{k_2}\mathcal{J}_k\cos(W_mk)=\mathcal{J}_{\cos(m)k}=\sum_{n=\emptyset}^{N}[P_nA_{mn}+Q_nB_{mn}]\qquad\text{for } m=1..N$$

(6.10a)

$$\sum_{k=k_1}^{k_2}\mathcal{J}_k\sin(W_mk)=\mathcal{J}_{\sin(m)k}=\sum_{n=\emptyset}^{N}[P_nC_{mn}+Q_nD_{mn}]\qquad\text{for } m=1..N$$

(6.10b)

which can be written in matrix form as

$$\begin{bmatrix}\mathcal{J}_{\cos(m)k}\\ \mathcal{J}_{\sin(m)k}\end{bmatrix}_{2m*1}=\begin{bmatrix}A_{mn} & B_{mn}\\ C_{mn} & D_{mn}\end{bmatrix}_{2m*2n}\begin{bmatrix}P_n\\ Q_n\end{bmatrix}_{2n*1}$$

(6.11)

The wave coefficients can be obtained from the solution of eq (6.11) as

$$\mathcal{F}_n = P_n / \cos(2\pi n y_P / W) \tag{6.12a}$$

$$\eta_n = Q_n / \cos(2\pi n y_P / W) \tag{6.12b}$$

Although this method is an improvement over direct Fourier analysis, because of not assuming an infinite cut length, the results are very much dependant on the probe position y_P. The wave coefficients, $\mathcal{F}_n$ and η_n, are overestimated when $\cos(2\pi n y_P / W)$ is small. An alternative method is given by Tsai[77] which involves fitting a least squares solution with the weighting factor of $\cos(2\pi n y_P / W)$ for a number of probes. This method is however also dependant on the probe positions.

The problem was investigated further and a new method based on measurements of multiple longitudinal cuts has been developed by the author in order to establish a method which is effectively independent of probe positions. By using P number of longitudinal cuts, equation (6.11) can be satisfied for each probe in such a way that

$$\begin{bmatrix} \mathcal{G}_{\cos(m)k,P} \\ \mathcal{G}_{\sin(m)k,P} \end{bmatrix}_{2m*1} = \begin{bmatrix} A_{mn} & B_{mn} \\ C_{mn} & D_{mn} \end{bmatrix}_{2m*2n} \begin{bmatrix} \mathcal{F}_n * C_{nP} \\ \eta_n * C_{nP} \end{bmatrix}_{2n*1} \tag{6.13}$$

where

$C_{nP} = \cos(2\pi n y_P / W)$

hence 2n*P equations with 2n unknown wave coefficients must be solved.

By using a probe which gives maximum C_{nP} value for a particular n, a simultaneous equation system with 2n equations can be chosen i.e.

$$\begin{bmatrix} \mathcal{J}_{\cos(m)k,Pn} \\ \mathcal{J}_{\sin(m)k,Pn} \end{bmatrix}_{2m*1} = \begin{bmatrix} A_{mn} & B_{mn} \\ C_{mn} & D_{mn} \end{bmatrix}_{2m*2n} \begin{bmatrix} \mathcal{f}_n * C_{nPn} \\ \mathcal{\eta}_n * C_{nPn} \end{bmatrix}_{2n*1} \quad (6.14)$$

where C_{nPn} = Max (Cos($2\pi n y_P/W$)) for p=1..P

The solution for this system is very stable, and it is not very dependant on the probe positions as long as there is one y_P which results in a sufficiently high Cos($2\pi n y_P/W$) for every n.

6.3 DETERMINATION OF WAVE PATTERN RESISTANCE

The wave pattern resistance of a ship model symmetric to the centerline of the tank is given by equation (4.41) as

$$R_W = \frac{W\rho g}{4}\left\{ (\mathcal{f}_0^2+\mathcal{\eta}_0^2)\left(1-\frac{2K_0H}{\mathrm{Sinh}(2K_0H)}\right) + \sum_{n=1}^{\infty} (\mathcal{f}_n^2+\mathcal{\eta}_n^2)\left[1-\emptyset.5\,\mathrm{Cos}^2\Theta_n\left(1+\frac{2K_nH}{\mathrm{Sinh}(2K_nH)}\right)\right]\right\} \quad (4.41)$$

where $\mathcal{f}_n$, $\mathcal{\eta}_n$ are wave coefficients which can be determined from the wave pattern analysis described earlier. The main advantage of the method is that it can be applied to any model independent of hull form and number of physical bodies. There is no modification required for catamaran resistance. In practice n can be truncated at a finite number N, as the resistance contribution of high harmonics to the resistance becomes small. e.g. Table 3 indicates the results for a mathematical hull form in which N=28 is sufficient at Fn=Ø.33.

6.4 EXPERIMENTAL SET-UP

The wave pattern analysis for all the six models (Table 1) were conducted in the SIHE towing tank. Resistance wave probes connected to a microcomputer controlled data acquisition system were used to measure the longitudinal wave traces. These traces were analysed during tests using the wave pattern analysis program, LMCUT, for instant monitoring of the results.

6.4.1 WAVE PROBES

Four resistance type wave probes (Fig.76) were used in order to conduct the multiple longitudinal cut wave pattern analysis. The probes, which had been successfully used previously at Southampton University [5], were positioned at one side of the tank in the same longitudinal position. The probes (Fig.77) consist of two isolated stainless steel rods, 1.5 mm in diameter and 12.5 mm apart. These probes were connected to a Churchill wave monitor, described in Ref.89, from which the output was fed into the data acquisition system (Fig.78). The accuracy of the probes was found to be within ±Ø.Ø5 mm. The wave probe output was satisfactorily stable with a typical maximum 1.5 mm drift over 12 hours. It was observed that if the wave amplitude is higher than 3 mm, a sufficiently defined wave trace can be obtained.

A calibration of the wave probes was made after every ten runs to ensure that the effects of calibration change were minimised. The static calibration of the probes was conducted by moving the probes vertically to two known immersions and acquiring the voltages for these immersions.

6.4.2 TRANSVERSE POSITIONING OF WAVE PROBES

N, the truncation harmonic number is a function of tank width and speed. For the tank used, which is 3.7m wide, and for speeds higher than 1.0 m/s, N=40 is found to be sufficient. At speeds faster than 2.0 m/s the analysis method requires a lower N value for a stable result. N is as low as 10 for 4.0 m/s.

In order to find accurate results for the wave coefficients, the $|\cos(2\pi n y_P/W)|$ term must be sufficiently large for at least one probe and for every n value for n=0..N. Additionally, y_P/W has to be chosen in such a way that the wave trace taken is outside the near field effect, i.e. $y_P/W>0.2$

All values of y_P/W except $y_P/W=1/3$ will result in $|\cos(2\pi n y_P/W)|<0.5$ for some n=0..40. It was also found that a combination of $y_P/W=$ 3/10, 1/3, 2/5, 4/9 for the four probes will yield a value of $|\cos(2\pi n y_P/W)|\geq 0.809$ for n=0..40 and will be outside the nearfield effects.

6.4.3 LONGITUDINAL POSITIONING OF WAVE PROBES

It is convenient to place the probes in a longitudinal position which enables the length of the recorded wave trace to be optimised. Colman [11] gave a simple method for this purpose :

Let A be the plane in which the model reaches steady state (i.e. at the end of acceleration), C be the plane in which the model leaves the steady state (i.e. at the start of deceleration), and B is the plane in which the probes are situated (Fig.79).

While the model is moving with velocity U the group velocity of the waves generated by the model will be U/2 :

$$C_g = \frac{U}{2}\left[1 + \frac{2K_o H}{\text{Sinh}\ (K_o H)}\right] = \frac{U}{2} \text{ for deep water} \qquad (6.15)$$

where $K_o = g/U^2$, and H=depth

If it is assumed that the model passes plane A at time $t_o = \emptyset$, then the waves due to acceleration reach plane B at time:

$$t_{AB} = \frac{(L_{AB} - l_1)}{C_g} = \frac{2(L_{AB} - l_1)}{U} \qquad (6.16)$$

where
l_1 is the distance between the stem of the model and the longitudinal towing position

and waves due to deceleration reach plane B at time
$t_{BC} = t_{AC} + t_{CB}$

$$t_{BC} = \frac{L_{AC}}{U} + \frac{(L_{BC} - l_2)}{C_g}$$

$$= \frac{L_{AC}}{U} + \frac{2(L_{BC} - l_2)}{U} \qquad (6.17)$$

where l_2 is the distance between the longitudinal towing position and transom of the model.

In order to optimise the probe positions t_{AB} must be equal to t_{BC}.

hence $2(L_{AB} - l_1) = 2(L_{BC} - l_2) + L_{AC}$ (6.18)

Assuming $l_1 = l_2$, and substituting $L_{AC} = L_{AB} + L_{BC}$

$L_{AB} = 3/4\ L_{AC}$ $L_{BC} = 1/4\ L_{AC}$

In the SIHE towing tank, the stationary test distance is about 20 m long. Hence L_{AB}=15 m, L_{BC}=5 m is obtained, and the probes were positioned according to these parameters. The maximum wave trace length was thus determined as 15m.

6.4.4 DATA ACQUISITION SYSTEM

A microcomputer controlled data acquisition system (Fig.78) was developed for the wave pattern analysis. It was positioned at the side of the tank in addition to the system on the carriage.

Wave height signals from the Churchill wave monitor were fed to the data acquisition system. These traces were acquired with the SSDAP data acquisition program. The acquisition of the wave traces was started when the stem of the model reached the longitudinal position of the probes. Wave traces with a total length of 25m were recorded using a time signal, and saved on floppy disks to enable further analysis. A graphical check of these traces was also made after each test.

6.4.5 ANALYSIS

The wave pattern analysis was based on multiple longitudinal cuts and a matrix analysis as described in Section 6.2. A new analysis program was written to integrate with the data acquisition system and software in order to establish a fully automated wave pattern analysis system employing the multiple cut method.

The wave traces were edited to exclude the acceleration and deceleration effects in the data acquisition and manipulation program. These traces were analysed in the wave pattern analysis program LMCUT for the multiple longitudinal cut method described earlier.

The program LMCUT, written in Fortran by the author, is completely menu driven for MSDOS microcomputers. It calculates the wave coefficients from the longitudinal wave traces derived by solving equation (6.14). The Gauss-Siedel iteration method was employed to solve the equation as matrices A and D are strongly diagonal matrices.

The wave coefficients calculated were checked by calculating the wave traces and comparing them with the experimental traces, e.g. Fig.8Ø. Additionally, the stability of the analysis was verified by plotting the wave resistance distribution across the wave angle (Fig.81).

A wave analysis of the Wigley model was conducted and the results were compared with other available data in Figs.82 and 83. The results of the current analysis are in good agreement with existing data, validating the experimental set-up and analysis method. The results of the catamaran configuration for the Wigley model with S/L:Ø.3 were compared with the results of Everest [18] in Fig.84. The correlation is satisfactory except at low speeds. This may be caused by the inability to measure wave height accurately enough at low speeds where it can be very small, e.g. less than 3 mm.

6.5 PREDICTION OF THE CATAMARAN WAVE PATTERN FROM THE DEMIHULL WAVE PATTERN ANALYSIS

The far field wave pattern of a catamaran with symmetric demihulls was given by equation (4.48) as

$$\mathcal{Y}= \sum_{n=0}^{\infty} [(2\mathcal{F}_n C_s) \cos(w_n x) + (2\mathcal{Y}_n C_s) \sin(w_n x)] \cos(2n\pi y/W) \quad (4.48)$$

where $C_s = \cos(K_n S/2 \sin\Theta_n) = \cos(n\pi S/W)$

This results in a wave resistance given by equation (4.50)

$$R_w = \frac{W\rho g}{4} \{ [(2\mathcal{F}_0)^2 + (2\mathcal{Y}_0)^2] \left(1 - \frac{2K_0 H}{\sinh(2K_0 H)}\right) + \sum_{n=1}^{\infty} [(2\mathcal{F}_n C_s)^2 + (2\mathcal{Y}_n C_s)^2] \left[1 - \frac{\cos^2\Theta_n}{2} \left(1 + \frac{2K_n H}{\sinh(2K_n H)}\right)\right]\} \quad (4.50)$$

In these equations $\mathcal{F}_n$, $\mathcal{Y}_n$ are determined from wave pattern analysis of a demihull alone. This prediction method eliminates the assumptions used in thin ship theory given by equation (4.38). However the wave reflection effect between the demihulls and the venturi effect on the hulls can not be taken into account. The method was applied to all the models and the results are presented in Chapter 8.

6.6 SUMMARY

A preliminary investigation of the wave pattern analysis for ship models was carried out. The longitudinal cut technique with a matrix solution was found to be the most suitable method. A multiple longitudinal cut method was developed based on this approach.

An automated system using this method of analysis was developed to investigate the wave pattern resistance of catamarans. The rig consisted of four wave probes, amplifiers, filters and data acquisition system and was utilised in the experiments conducted with all six models.

The lateral and longitudinal positioning of the wave probes was optimised. The system was found to be very efficient for a series of experiments as the wave traces could be acquired and analysed very quickly during the experiments.

The results of experiments with the Wigley model in the monohull condition showed close agreement with available data for both fixed and free to trim and sink conditions. The results for a catamaran model were also compared with existing data. They also show a satisfactory validation of the method. Although some underprediction was observed at low speeds for both the monohull and catamaran, this may have resulted from inaccurate definition of the wave traces due to very small wave heights at low speeds.

A prediction method for the wave pattern resistance of a catamaran from the wave pattern analysis of a demihull in isolation was given, analogous to the theoretical approach given in Chapter 4.

The results of the wave pattern analysis are presented in Chapter 8.

CHAPTER 7 : EXPERIMENTAL DETERMINATION OF VISCOUS RESISTANCE

7.1 INTRODUCTION

Experiments for the determination of viscous resistance from direct measurements have been conducted in the past for a limited number of hull forms in order to investigate the validity of Froude's and Hughes' assumptions [44,69].

Although wind tunnel experiments with duplex models have been utilised to derive viscous resistance [69], wake traverse surveys in towing tanks have been accepted as being more accurate because of the absence of the free surface in the wind tunnel experiments. Two methods of wake traverse analysis due to Betz and Melvill-Jones have been applied to ship models with successful results and have been reported in Refs.[37,79] and [69,73,74,75,76] respectively. In the current work a series of wake traverse experiments were made in order to investigate the viscous resistance of the models used.

An alternative method of obtaining viscous resistance is by subtracting the wave pattern resistance from the total resistance, if such an assumption is justified by some experimental data. Although this would lead to a more convenient method, the effect of wave breaking can only be determined from wake traverse experiments. During the current work, wake survey experiments have served to check the validity of this assumption for the models used.

There is some evidence [18,51] that the viscous resistance of a catamaran differs from twice that of a demihull in isolation because of interference effects such as cross flow under the keel and velocity augmentation between the hulls. However the experimental data is extremely limited, i.e. wake traverse results for two speeds and one separation and the demihulls in isolation in Ref.51, and some wave pattern analysis results in Ref.18. Therefore wake traverse experiments with two hull forms and variation of separation have been included in the present work to investigate these interference effects and to validate the results of wave pattern experiments on catamarans.

A wake traverse rig consisting of a wake rake with 24 pitot tubes, 12 2-way solenoid valves and 12 pressure transducers and a microcomputer based data acquisition system have been developed for use in the wake surveys of catamaran models. A suite of computer programs to automate the analysis by using the Melvill-Jones method have been developed. The validation of the current setup was made by comparing the wake survey results with available data in the literature for the Wigley model. Further comparisons were made by checking the correlation between the total resistance and the summation of wave pattern resistance and wake traverse resistance.

The Wigley hull (C2) and a Round Bilge hull (C3) were tested in the wake survey at three speeds at separation ratios of 0.2, 0.3, 0.4 as well as with the demihulls (Table 4). The results are presented and compared with other experimental results in chapter 8.

7.2 WAKE TRAVERSE ANALYSIS METHOD

The viscous resistance for a ship model in a tank (Fig.30) has been given in equation (3.10) as

$$R_V = \int_{-W/2}^{W/2} \int_{-H}^{y_B} [\Delta P + \rho/2 \, (u^2 - u^2)] \, dydz \tag{7.1}$$

or otherwise it can be expressed by velocity terms as

$$R_V = \rho \int_{-W/2}^{W/2} \int_{-H}^{y_B} (U_A - U_B) \, U_B \, dydz \tag{7.2}$$

Although the wake traverse resistance can be determined from (7.2), measuring velocities in very far downstream is impractical if not impossible. Two main methods due to Melvill Jones [45], and Betz [26] were developed to calculate (7.2) by measuring velocities in a plane near to the model. Both methods have generally been found to result in the same drag value except when the measurements are very close to the model [26]. The method due to Melvill-Jones was chosen for the current work, as the Betz method is less convenient.

By taking plane C near to the model (Fig.3Ø), and making the following assumptions.

A) Along a stream tube between B and C there is no head loss

$$H_B = H_C \tag{7.3}$$

B) The static pressure at B is equal to the static pressure at A.

Hence

$$H_B = 1/2 \, \rho \, U_B^2 + P_B = 1/2 \, \rho \, U_C^2 + P_C$$
$$= 1/2 \, \rho \, U_B^2 + P_A \tag{7.4}$$

Additionally the conservation of mass between C and B

$$\int_{-W/2}^{W/2}\int_{-H}^{y_B} U_B \, dydz = \int_{-W/2}^{W/2}\int_{-H}^{y_C} U_C \, dydz \tag{7.5}$$

By defining

$$G_o = 1/2 \, \rho \, U^2 \tag{7.6}$$

$$\left[\frac{U_B}{U}\right]^2 = g \tag{7.7}$$

$$p = \frac{P_C - P_B}{G_o} = \frac{P_C - P_A}{G_o} \tag{7.8}$$

$$\left[\frac{U_C}{U}\right]^2 = \left[\frac{U_B}{U}\right]^2 - \frac{P_C - P_B}{1/2 \, \rho U^2} = \left[\frac{U_B}{U}\right]^2 - \frac{P_C - P_B}{G_o}$$
$$= g - p \tag{7.9}$$

$$\frac{U - U_B}{U} = 1 - \left[\frac{U_B}{U}\right] = 1 - \sqrt{g} \tag{7.10}$$

By substituting (7.5) into (7.2)

$$R_V = \rho \int_{-W/2}^{W/2}\int_{-H}^{y_B} U_B \, (U-U_B) \, dydz = \rho \int_{-W/2}^{W/2}\int_{-H}^{y_C} U_C \, (U-U_B) \, dydz \tag{7.11}$$

By substituting (7.6), (7.9) and (7.10) into (7.11)

$$R_V = \rho \, U^2 \int_{-W/2}^{W/2}\int_{-H}^{y_C} \sqrt{g-p} \, (1-\sqrt{g}) \, dydz \tag{7.12}$$

or

$$R_V = G_o \int_{-W/2}^{W/2} \int_{-H}^{\zeta_c} 2\sqrt{g-p}\,(1-\sqrt{g})\,dydz \tag{7.13}$$

and local drag function can be defined as

$$d = 2\sqrt{g-p}\,(1-\sqrt{g}) \tag{7.14}$$

In practice, (7.13) only needs to be investigated over the wake as outside the wake $U_B = U$ hence $(1-\sqrt{g}) = \emptyset$.

Horizontal and vertical velocity components , i.e v and w, are assumed to be negligible compared with the longitudinal velocity (U+u) in plane C. This assumption is not always true, specially near the model stern. Nevertheless experiments with variation of traverse distance from the model have indicated that this assumption will be justified if the traverse is further than $\emptyset.15$ L behind the stem [69]. Additionally the vortices caused by the bilge pressure field and transom stern are possible causes of errors in this analysis. However the results of wake surveys on several hull forms are encouraging as the summation of wake traverse and wave pattern resistance is equal to total resistance, at least at low speeds [25].

The measurement of total and static pressures on the plane C relative to the still water is the only requirement for the determination of wake traverse resistance as

$$g = \left[\frac{1/2\ \rho\ U_c^2 + P_c}{1/2\ \rho\ U^2} \right] = \frac{H_c}{1/2\ \rho\ U^2} \tag{7.15}$$

$$p = \frac{P_c}{1/2\ \rho\ U^2} \tag{7.16}$$

where P_c : Static Head

H_c : Total Head

The measurement of total head on plane C is straightforward, while static pressure measurement is more difficult, due to very low pressure involved. As an alternative, the static pressure term can be derived from surface wave elevations taken above the tube positions. The simplest way is to assume that the static change is related to surface wave height :

$$p = \frac{\rho g \eta}{\rho U^2 / 2} = 2 K_0 \eta \qquad (7.17)$$

where η is wave height

Alternatively the static term can be derived by taking the two dimensional sub-surface wave profiles into account as shown by Townsin [74].

The surface and sub-surface wave profiles are shown with η and η_s in Fig.85. z_T is the immersion of the tube in still water.

The static pressure along a sub-surface wave profile is constant and the same as the corresponding still water level. Hence the static pressure change will be :

$$p = \frac{2 g \eta_s}{U^2} = 2 K_0 \eta_s \qquad (7.18)$$

The sub-surface wave profile coordinates will experience an exponential decay with the depth so that :

$$\eta_s = \eta e^{-K_0 z}$$

$$= \eta e^{-K_0 (z_T + \eta_s)} \qquad (7.19)$$

by substituting (7.18) into (7.19)

$$\frac{p}{2K_0} = \gamma\, e^{-K_0\,(z_T + p/2K_0)}$$

$$\frac{p}{2} - e^{p/2} = \gamma\, K_0\, e^{-K_0 z_T} \qquad (7.20)$$

This nonlinear equation can be solved by the Newton-Raphson method for a given tube immersion, wave height and speed. At high speeds, the wave elevation above the rake exhibits a three dimensional feature. However a comparison of the experimental results from a pitot tube and wave height measurements (Fig.86) indicated that the assumption of this analysis is reasonable.

7.3 ERROR ANALYSIS OF PRESSURE AND WAVE ELEVATION MEASUREMENTS

The effects of measurement errors on the wake traverse resistance must be investigated as the pressure measurement and integration over the section is open to errors. The following error analysis has been derived from Refs. [73,76].

7.3.1 EFFECT OF ERRORS IN TOTAL PRESSURE MEASUREMENTS

Drag function given by equation (7.14)

$$d = 2\sqrt{g-p}\,(1-\sqrt{g}) \qquad (7.14)$$

By differentiating (7.11) with respect to g

$$\frac{\delta d}{\delta g} = \frac{(1-\sqrt{g})}{\sqrt{g-p}} - \frac{\sqrt{g-p}}{\sqrt{g}}$$

$$\frac{\delta d}{\delta g} = \frac{\sqrt{g}-2g+p}{\sqrt{g-p}\ \sqrt{g}} \qquad (7.21)$$

Hence the maximum error in δd will occur for the greatest p and g. For the current experiments the maximum p is Ø.25 while the greatest g is 1.25. By substituting these values

$\delta d = -1.Ø125\ \delta g$ or

$$\frac{\delta d}{d} = 5.36\ \frac{\delta g}{g}$$

Hence the effect of an error in g is very important e.g. 1 % error in g will create a maximum 5.36 % error in d and care must be taken in achieving an accurate measurement of total pressure.

7.3.2 EFFECT OF ERRORS IN STATIC PRESSURE MEASUREMENTS

$$d=2\sqrt{g-p}\ (1-\sqrt{g}) \qquad (7.14)$$

$$\frac{\delta d}{\delta p} = 2\ (1-\sqrt{g})\ \frac{-1/2}{\sqrt{g-p}}$$

By differentiating with respect to p

$$\frac{\delta d}{\delta p} = (1-\sqrt{g})\ \frac{\sqrt{g-p}}{(g-p)}$$

$$\frac{\delta d}{d} = -\frac{\delta p}{2(g-p)} \qquad (7.22)$$

Hence the maximum error occurs at the greatest p and smallest g. By substituting p=Ø.25 and g=Ø.6

$$\frac{\delta d}{d} = 0.357 \frac{\delta p}{p}$$

i.e for a 10 % error in p, a 3.57 % error in d will follow. Hence a small inaccuracy in p readings is more acceptable than errors in g.

7.3.3 EFFECT OF ERRORS IN WAVE ELEVATION MEASUREMENTS

From equation (7.20)

$$\frac{p}{2} e^{p/2} = \gamma K_0 e^{-K_0 z_T} \qquad (7.20)$$

By differentiating with respect to γ

$$\delta p \left[1/2\, e^{p/2} + p/4\, e^{p/2}\right] = \delta\gamma\, K_0\, e^{-K_0 z_T}$$

$$\delta p = \delta\gamma\, K_0\, e^{-K_0 z_T} \frac{2}{p+2} \frac{2}{e^{p/2}}$$

$$\frac{\delta p}{p} = \frac{\delta\gamma}{\gamma} \frac{2}{(p+2)}$$

by using p=-.18 to find the maximum error

$$\frac{\delta p}{p} = 1.1 \frac{\delta\gamma}{\gamma} \qquad (7.23)$$

In other words, 10 % error in wave elevation will lead to a 11 % error in p. By taking the max wave elevation in the range of 10 mm to 50 mm, and assuming the wave elevation readings have an average error of ± 1 mm, 11 % to 2.2 % maximum error in p will be recorded.

This investigation further justifies the acceptability of the method of deriving static pressures from wave elevation measurements.

7.4 EXPERIMENTAL SETUP

The wake traverse experiments were conducted in the SIHE towing tank. The tank has a 15.24 m long measured steady run length which was used in the experiments for the speeds of Fn=Ø.35, Ø.5, Ø.7. The repeatibility of the carriage speed is found to be within ± Ø.Ø1 m/s.

The wide wake area of catamarans to be covered by the traverse experiments necessitated the development of an automated experimental rig (Fig.88) and analysis system. The rig consists of a rake housing the pitot tubes, a vertical and horizontal movement table to position the pitot tubes accurately and a horizontal plate housing the solenoid valves and the pressure transducers. An attachment to the rake was made for the wave elevation measurements above the traverse plane. The data acquisition and analysis system consists of bridge balance and amplifier units, CED 1401 A/D converters, a 16 bit microcomputer and software.

7.4.1 PRESSURE MEASUREMENT METHOD

A number of possible methods for the pressure measurements were considered in the early stages of the current work. The use of laser velocitimeters and hot wire anemometers were ruled out, as these devices need extra attention during calibration, suffer from complex setups, in addition to their fragility and high expense. The use of vane wheels was also investigated as these devices give an output which is linear with speed rather than pressure. However vane wheels were found not to be suitable for the current work due to small model size. Therefore, pitot tubes were selected as the most practical approach to the problem.

The water manometer as a measurement system was investigated. Because a water manometer response time is rather slow, and it is not easy to automate the system for a digital conversion for a series of experiments, pressure transducers were found to be more suitable.

The size of the expected wake to measure was about 150 mm deep and 600 mm wide. A large number of pitot tubes, about 50 tubes for each depth, were required to cover this wide wake area with satisfactory resolution. If every tube were connected to a pressure transducer, the pressure transducer costs would be unacceptably high. To reduce the cost, scanivalve systems were evaluated. However it was reported that the settling time for a scanivalve can take about one second for a switch of input [37]. This would lead to very short measurement time since the run time is limited. Additionally the cost of the scanivalve is also very high.

The use of 2 way electrically actuated solenoid valves was considered as a low cost alternative, and it was found that a 2 way valve connected to a pressure transducer could measure two pressures in one run with a satisfactory length of measuring time at minimum cost. The settling time for the investigated pressure range was found to be less than 1.5 second in the preliminary investigations. (Fig.87)

7.4.2 WAKE TRAVERSE RAKE

A rake comb was designed and built in order to house and support the pitot tubes. It consists of two streamlined aluminium alloy side struts, a streamlined GRP bottom strut and aluminium alloy top bar resulting in a rigid frame (Fig.89).

The horizontal bottom strut (Fig.90) with a 127 mm chord length and 15 mm thickness was built from GRP. The

strut was reinforced by two brass bars running along its length. The pitot tubes were placed in the strut in such a way that they could be changed between runs, as they were attached by a push fit system into the strut. The stainless tubes were soldered to the brass bar, and were carried vertically inside wooden struts and attached to clear plastic tubes at the top of the rake.

The rake was found to be satisfactorily rigid during the experiments.

7.4.3 PITOT TUBES

During the preliminary design stages of the rake, interactions between the tubes and with the supporting strut were investigated in order to find the best parameters to minimise errors on the pressure measurements [36]. The following conclusions were drawn from this work.

a) The tip to static orifice distance in the static tubes must be more than 6 diameters to achieve an error less than 0.005 in p (Fig.91).

b) The separation between the two adjacent tubes must be more than 6 diameters to obtain an error of less than 0.002 in p. If the separation is higher than about 7 diameters, the interference can be neglected (Fig.92).

c) The distance between the static orifices and supporting strut must be more than 4 strut thicknesses if the error is to be less than 0.05 in p (Fig.93).

Taking these conclusions into account, the total and static pitot tubes were manufactured from stainless steel tubes with 2.2 mm outside diameter and 1.8 mm inside diameter. The static pitot tubes were formed by soldering the tip and deriving a hemi-spherical shape and drilling four static orifices with 0.5 mm diameter. The distance between the tip and static orifices was taken as 20 mm (9.1

tube diameters) to minimise error (a). The total head tubes tubes were tapered to ensure the minimum flow disturbance.

In order to cover all the wake, about 50 pitot tubes would be needed. Due to a shortage of pressure transducers, the decision was taken to conduct two runs, or three where required, at each depth. Two different techniques were considered. Firstly, shifting the rake, designed with distance x between the pitot tubes a full rake width (Fig.95) was considered. The second option was to design a rake with distance 2x between the pitot tubes and to shift the rake with x distance to obtain the same number pressure readings. The second option was chosen as with this system the discrepancies between the two runs can be observed easily. Additionally the higher separation distance between the pitot tubes would minimise the interference effects from neighbouring tubes, i.e. error (b).

A tube separation of 28 mm (12.7 diameters) was decided upon resulting in a rake comb width of 658 mm with 24 pitot tubes. Hence the interference between the tubes would be negligible.

The static pressure tube length was taken as 110 mm, 20 mm of which was located inside the strut giving 70 mm (4.67 strut thickness) distance between static orifice and strut (Fig.90). This would result in an error of less than about 0.04 in p value, i.e. error (c). Lengthening of the tubes was not attempted since this could lead to vibration of the tubes. However this was taken into account by conducting the dynamic calibrations for each depth. It was also assumed that this process will minimise the errors due to the proximity of the support to the free surface (Fig 102).

In order to maximise the number of total pressure readings and to obtain a reasonable number of static pressures, a distribution of two total tubes and one static

tube distribution was decided upon as shown in Fig.96. This resulted in 8 static pitot tubes and 16 total pressure tubes across the rake.

7.4.4 MOVEMENT TABLE

The positioning of pitot tubes relative to still water level is very important for accurate results. In order to reduce any errors due to this process a two way movement table was designed and built (Fig.97). It has the facilities for 280 mm lateral and 300 mm vertical adjustment. All the movements were measured by verniers mounted on the system giving an accuracy of within 0.1 mm. The rake is attached to the table by use of two brackets which allow the distance from the model to be adjusted. The compactness and weight of the table were prime factors in the design as it had to be mounted on the carriage by two persons before every set of experiments.

The weight of the table is about 50 kg. allowing it to be mounted easily by two persons. The table was found to be very rigid during the experiments.

7.4.5 HORIZONTAL PLATE

In order to utilise the full range of the pressure transducers, the pressures were offset by a 110 mm water column which was obtained by applying a vacuum to the transducers.

A horizontal plate (Figs.98,99) housing the solenoid valves and pressure transducers was mounted on the carriage, 110 mm above the still water level outside the wave system of the models. A valve system was connected to every tube before the solenoid valve connection(Fig.100). A vacuum was applied to every tube by sucking air out of the

tube through these valves. The water level was at the plate level and due to the horizontal layout of the tubes stayed at the same level independent of the pressure applied during the experiments. The horizontal position of water level was checked before every run and corrected if there was any leakage.

There were two problems arising with this arrangement: Firstly the carriage moves up and down along the tank effectively changing the vacuum level. However the averaging of the pressure signals along the tank should prevent this error from being significant during the experiments. Secondly, special care was needed during the sucking of the air out of the tubes not to pass a marked position and flood the solenoid valves. However such a system provides some very important advantages: Firstly any leakage or blockage in the system can be identified easily during the course of the experiments. Secondly, the complete pressure range of transducers can be used, i.e. increasing the sensitivity of the measurements. Thirdly, due to the applied vacuum the rake comb can be positioned above the water level to measure the pressures above still water level without allowing air into the system. Fourthly, by using water for the pressure transmission instead of air much shorter response times can be achieved. And lastly, due to horizontal layout there is no change of vertical water level following pressure changes. The distance between the valves and transducers is kept as short as possible.

The solenoid valves (Martonair M49/A) were operated from a 24 volt power supply. A switch mechanism was developed for switching the solenoid valves on and off automatically along the tank by two trigger switches (Fig.94).

Two types of pressure transducers were utilized during the experiments :

a) Low pressure transducers : 11 large diaphragm type pressure transducers with ±0.2 psi range (Maywood P402) were available in the University.
b) High pressure range transducers : At speeds in excess of 2.0 m/s, the low pressure transducers were being overloaded. Therefore 13 differential piezoelectric sensors (Sensym SCX01DN) with ±1 psi range were purchased at a relatively low cost. These sensors were boxed and cabled to connect to the bridge balance system.

The Main characteristics of the transducers are given in Table5.

7.4.6 WAVE ELEVATION MEASUREMENT

Wave elevation measurements were required in order to calculate static pressures as well as to define the limit of the drag function integration. It was measured by pointers attached to the rake (Fig.101). They were adjusted manually in the vertical direction during the run. Two possible sources of errors in the measurements were identified : Firstly, the carriage moves up and down along the tank changing the effective wave height, Secondly, instability of the wave elevation over the traverse section was observed at high speeds. The accuracy of the measurements was found to be within ± 1 mm.

7.4.7 DATA ACQUISITION

An automated data acquisition system was developed for use in the wake traverse experiments as one man operation was necessary. The pressure signals from the pressure transducers were amplified using two six channel bridge balance and amplifier units. Amplified signals were fed into CED 1401 A/D Conversion ports (Fig.103).

The acquisition was started by trigger signals which were also used in the total resistance experiments. Three more triggers were positioned along the tank to switch the solenoid valves on and off automatically (Fig.94). The signal from the solenoid valve trigger was acquired on channel Ø to identify when the valves were actuated. the acquired signals were transferred to a microcomputer and saved for later analysis.

7.4.8 CALIBRATION AND EXPERIMENTAL PROCEDURE

During the wake traverse experiments the following method was followed.

A) All the tubes and transducers were connected.

B) The static pitot tubes were calibrated by immersing the rake comb to several depths, h, and calculating the pressure from ρgh.

C) Vacuum was applied to all the tubes by sucking water into the tubes.

D) The carriage was run at several speeds and rake comb immersions in the free stream, typically at three depths and four speeds.

E) The error term in static pressure from these runs was calculated for each depth and speed.

F) Total head calibration was conducted using these runs.

G) The model was connected

H) The depth and offset of the rake comb was set.

I) The static and total heads were acquired in the stationary position to find zero values.

J) The carriage was run at a constant speed and static and total head values recorded.

K) The corrected total and static head values were calculated by taking into account zero values and carriage speed. A correction for the carriage speed change was applied in such a way that

$$P = P_{MEASURED} \frac{U^2}{U^2_{CARRIAGE}}$$

L) The wave elevation over the wake traverse plane was measured.
M) Analysis of the data was performed to find the wake traverse drag.

Steps H to L were repeated for every depth and offset until a satisfactory matrix of points was established. This procedure takes about a day for each speed. It resulted in 3 tank days for the preliminary experiments and 23 days for the traverse experiments.

The rake comb was positioned at 150 mm depth from the still water line and raised in 10 mm steps. Near the free surface the steps were reduced to 5 mm. When all the tubes were out of the water, the experiments were stopped. Due to the use of a vacuum, the tubes could be positioned above the still water level.

All the wake of the monohull was measured whilst only half of the catamaran wake was covered. An overlap of 100 mm was allowed for all the catamaran experiments. The wake traverses were positioned 0.583 L and 0.719 L behind the aft ends of models C2 and C3 respectively.

7.4.9 ANALYSIS

In order to analyse the acquired data a program suite consisting of three individual programs was developed. The first program reads several runs which were made at several depths and speeds over the range in the free stream, makes a least square fit for each depth and stores these fits. The second program reads the calibrations and a run, calculates pressures for each tube and stores them in a file. The third program reads the pressure data for each tube found by the second program and together with the wave

height, interpolates these data where necessary and integrates the drag over the wake. The static pressures can be taken from static tube readings or can be calculated from wave elevations. Due to errors arising from the static head measurements, the static pressures used in the results presented in Chapter 8 were calculated from wave elevations. The program includes plotting facilities for static, dynamic and total pressures, drag function, speed distribution in the shape of contours, and 2 D distributions for both on display and plotter. Examples of these plots are given in Figs 104, 105, 106, 399, 400 and 401.

Validation of the experimental setup and analysis techniques was made by comparing the results for the Wigley hull with available data in the literature. Values of C_{WT}/C_F are plotted in Fig.107. The current results are inside the range given by several other experiments. Assuming the form factor is 0.1 for the Wigley model the results are within a 5% error level. As there are no other available data at Fn:0.75, a conclusion could not be drawn for this speed. A second method of validation is to compare wake traverse results with total resistance minus wave pattern results. This is presented in Fig.108 for the Wigley model. Again, the correlation is satisfactory.

7.5 WAKE TRAVERSE RESISTANCE OF CATAMARANS

There is some evidence that the wake traverse resistance of a catamaran differs from twice that of a monohull. Wake traverse experiments on catamarans have been conducted by Volheim [82] and Miyazawa [51]. The experiments [51] indicated that there is an increase in the wake traverse resistance of catamarans even at low speeds. Miyazawa gave an interference factor for the wake traverse factor derived from theoretical analysis of two cylinders.

$$(C_{WT})_{CAT} = (1+(B/S)^2)\ C_{WT}$$

Application of this approach is discussed further in Chapter 8.

In the current work, a series of wake traverse experiments on both catamarans and monohulls have been conducted as shown in Table 4. The interaction factors were derived. Results of all these experiments are presented in Chapter 8 in order that the correlation with other components may be examined.

7.6 SUMMARY

Conducting wake surveys with a fully automated system is highly recommended for a large number of measurements. The current instrumentation and analysis technique is found to be satisfactory for these experiments.

Pitot tubes coupled to pressure transducers is an efficient way of making pressure measurements provided the transducers are accurate in the investigated pressure range. For bigger models and higher speeds, the high pressure range piezoelectric transducers (e.g. ±1 psi) can be employed at a relatively low cost. A rake with a large number of pitot tubes and these transducers can be built at a commercially affordable cost. The use of solenoid valves doubled the measurements in a run hence halving the required run time. In a longer tank these valves could be connected in series making four or five reading possible at a relatively small cost.

The use of a horizontal plate with horizontal water tubes has provided important advantages and its use is highly recommended.

Although the pressure measurements are likely to be the main error source in the experiments, other standard

testing factors are found to be possible causes of errors, such as vertical movement of the carriage along the tank, velocity fluctuations, vibrations on the carriage, size of the model and alignment of the model to fixed yaw motion. Although these factors may not be so important in standard tank testing, they have a big share in producing errors in wake surveys.

In general, for the current setup and analysis, it is estimated that an accuracy within ±5 % was achieved for most of the wake survey.

Although the wake traverse results are crucial for the investigation of viscous interactions, they are laborious. For practical purposes, the viscous resistance can be derived by subtracting the wave pattern resistance from the total resistance. This method of deriving viscous resistance has been justified by the wake traverse surveys.

The results for viscous interactions on catamarans, investigated by the wake surveys for two models, are given in Chapter 8.

CHAPTER 8 : EXPERIMENTAL AND THEORETICAL RESULTS

8.1 INTRODUCTION

The experimental techniques investigated in Chapters 5, 6, 7 and theoretical calculations outlined in Chapter 4 were applied to the five hull forms described in Chapter 5.

The tests and calculations were conducted over a range of Froude numbers between Ø.1 and 1.Ø using monohull and four catamaran separations of Ø.2, Ø.3, Ø.4 and Ø.5 with the exception of model C1. Separation ratios of Ø.25, Ø.3, Ø.4, Ø.5 and Ø.6 in addition to the monohull were utilised from Fn:Ø.15 to Fn:Ø.5Ø for this model.

Suitable prediction methods by regression analysis and by interpolating experimental series data were applied to the models in the monohull configuration for comparative purposes. The Holtrop-Mennen [32] regression method was applied to models C1, C3, C4 and C5, and the Chinese regression method [61] was utilised for models C3, C4 and C5. The resistance of model C3 was also interpolated from the NPL Round Bilge Series [2] resistance data. Preliminary calculations for C4 and C5 using this method proved unsatisfactory as this series was tested only up to L/B:7.5. In the case of model C2 (Wigley Hull), the comparisons are confined to available experimental data in the literature.

Three methods for the division of total resistance into components , described in chapter 3, are investigated in order to identify the interference components namely:

$C_T = C_F + \Omega C_R$

$C_T = (1+\beta k) C_F + \tau C_W$

$C_T = \alpha C_{WT} + \mu C_{WP} + C_I$

where β varies with hull form and separation but is assumed constant across the speed range. Ω, τ, μ and α are all speed, separation and hull form dependent. $\beta,\Omega,\tau,\mu,\alpha=1$ for the monohull.

Three groups of experiments, namely total resistance / sinkage / trim measurements, wave pattern analysis and wake traverse surveys were conducted for 31 hull combinations. Table 2 outlines these experiments. A discussion of the results of these experiments is given below for each model and overall observations on these results are made.

The frictional resistance is calculated from the ITTC 1957 line. Viscous resistance is obtained from $(1+\beta k)C_F$ ($\beta=1$ for the monohulls) where the constant form factor $(1+\beta k)$ for each monohull and catamaran configuration is estimated for each hull by choosing the smallest $(1+\beta k)$ value satisfying $C_T=(1+\beta k)C_F+C_{WP}$. Additionally a form factor varying with Froude number $(1+k_{WP})=(C_T-C_{WP})/C_F$ is plotted for each hull to investigate the speed dependence of viscous interactions.

Theoretical wave resistance calculations were conducted for all the models. For the models for which trim and sinkage were measured, i.e. C2, C3, C4 and C5, a correction for trim and sinkage is applied. A correction for the transom stern is also applied to models C3, C4 and C5. The results of these calculations are compared with the measured components.

Predictions of catamaran wave pattern resistance from the monohull wave pattern analysis, C_{WP} (PREDICTED), have been calculated for all the models tested, the results of

which are given for each model and compared with the other components.

The experimental and theoretical results are presented as complete as possible in order to enable the reader to conduct cross comparisons.

By taking the experimental and theoretical results into account, conclusions on the accuracy of each method are derived. The effects of hull form and separation distance on the resistance components and interference components are discussed. Overall conclusions on the catamaran resistance are made by making cross comparisons between different models. Suitability of the methods for the division of catamaran resistance into components as described in Section 3 are discussed and their effect on extrapolation to ship scale are observed.

8.2 MODEL C1

An existing model tested previously at Southampton University [5] was utilised in order to asses the feasibility of the experimental techniques concerned in the preliminary stages of the current work. The hull form denoted C1 is shown in Figs. 109, 110, and 111.

Predictions using the Holtrop-Mennen regression method were made and are compared with the experimental measurements for the monohull case in Fig. 112. Good agreement is obtained up to Fn:0.42. A form factor of 1.193 is calculated with this method.

Due to the low freeboard of the model, it was tested in a low speed range only, i.e. from Fn:0.15 to Fn:0.5. The experimental measurements were also restricted to total resistance and wave pattern resistance. Monohull and catamarans with five separation ratios : 0.25, 0.3, 0.4,

Ø.5, Ø.6 were utilised. The results of these experiments are given in Figs. 113 to 131. Both total resistance and wave pattern resistance follow well defined curves, showing little scatter.

Although C1 does not represent a popular catamaran hull form, beneficial interference effects are evident in the speed range of Fn:Ø.31 to Fn:Ø.35 for a catamaran with S/L:Ø.5 and S/L:Ø.6. Adverse effects are found in the same speed range but for separation ratios of S/L:Ø.2, Ø.3 and Ø.4 (Figs. 125,126). However the results for wave pattern resistance (Fig. 127) indicate that these separations have lower resistance than the monohull. This difference between wave resistance and wave pattern resistance may be accepted as the wave breaking resistance caused by the interaction of the demihull waves. Although different in magnitude , wave resistance, C_W (Fig.126), and wave pattern resistance, C_{WP} (Fig.127) show broad agreement.

The agreement between the estimated viscous resistance, $(1+\beta k)C_F$, and total resistance minus wave pattern resistance, C_T-C_{WP}, is generally poor (Figs. 113,115,117,119,121,123). For the monohull and high separation catamarans, S/L:Ø.5 and S/L:Ø.6, $(C_T-C_{WP})/C_F$ follows more or less a constant value below Fn:Ø.3 (Fig.13Ø). Above this speed a gradual increase is evident. This is probably due to wave breaking phenomenon as suggested by Hogben [3Ø]. This feature is more pronounced for small separations suggesting more wave breaking due to the interference of bow waves in the tunnel for small separations.

The predicted wave pattern resistance (Fig.128), C_{WP} (PREDICTED), is close to the wave pattern resistance (Fig.127) results but the prediction of the humps and hollows is poor.

Theoretical wave resistance is also calculated for the monohull and all the catamaran derivations. No correction is applied to the results as trim and sinkage were not measured. The quantitative and qualitative results of the theoretical calculations (Fig.131) are very poor compared with wave resistance (Fig.126) and wave pattern resistance (Fig.127).

8.3 MODEL C2

Due to some questionable results from the theoretical calculations and experimental methods applied to model C1, validation of the techniques used was decided upon. Therefore a mathematically defined model (Figs. 132, 133, 134) with parabolic waterlines (known as the Wigley hull) was utilised, as a substantial amount of experimental and theoretical results are available [44]. In order to define the effects of trim and sinkage, hence change of mean wetted surface, experiments with both fixed and free to trim and sink were utilised.

Firstly validation of the experiments and theoretical calculations for the total resistance and wave pattern experiments was made by comparing the results with available data in the literature for the monohull case (Figs.39,72,82 for the fixed condition and Figs. 40,73,83,107 when free to trim and sink) .

The total resistance, wave pattern resistance and calculated resistance components are illustrated in Figs. 135 to 158 for fixed and Figs.161 to 192 for the free to trim and sink conditions. Although the experiments were conducted from Fn:0.1 to 0.9, some of the experiments had to be curtailed at Froude numbers below 0.9 due to excessive wave height or spray in the tunnel.

As with C1, the total resistance curve is well defined. However the wave pattern resistance curve has a considerable scatter above Fn:Ø.5 as compared with a well defined region below Fn:Ø.5 (Figs.135 to 144 and Figs. 161 to 179).

Wave Resistance

Although the fixed and free conditions have different residuary and wave resistance, the interference between the demihulls is very similar (Figs. 343 to 35Ø) except at the higher speeds i.e. Fn>Ø.5. This is not so surprising as the hulls have maximum trim and sinkage above this speed (Fig.193,194).

Beneficial wave resistance interactions are observed at about Fn:Ø.3 to Ø.4Ø depending on the separation of the demihulls (Figs.146,147,182,183). There is a phase shift for this hollow with separation change, i.e. the higher the separation distance, the lower is the position of the hollow. The best interference is found to be at S/L:Ø.3 for Fn:Ø.37 which leads to up to 45 % reduction in wave resistance (Figs.156,19Ø). However two humps at about Fn:Ø.3 and Fn:Ø.45 are also found in the resistance curves. These humps have a particular importance because the designer not only has to avoid designing a vessel at these speeds, but the humps must also be taken into account for vessels operating above these speeds in order to confirm that enough power is installed. Above Fn:Ø.8, the wave interactions can practically be neglected (Figs.189 to 192, 155 to 158).

The wave pattern experiment results (Fig.147,183) for this model are good in both conditions when compared with wave resistance (Fig.146,182). The positions of humps and hollows of wave resistance are accurately measured. The amplitude is also in very good correlation except at some speeds where wave breaking is suspected to take place. This

accuracy of the method verified the reliability of the analysis technique and experimental setup.

The wave pattern predictions from wave pattern analysis of the monohull (Fig.148,184) have very similar features to C_W (Fig.146,182). However there is a phase shift between the predicted interference and measured one (Figs.155 to 158, 189 to 192). This is believed to be caused by the asymmetric flow effect about each demihull which is not taken into account in the prediction method.

Theoretical predictions (Figs.151,187,188) have similar interference to the predicted ones with the same misprediction of the positions of humps and hollows. Again the same explanation applies due to flow asymmetry which can not be predicted as the positions and densities of the sources are not affected by the separation.

The resistance distribution across the wave angle are illustrated in Figs. 159 to 160 and Figs. 195 to 196 at Fn:Ø.5 and Fn:Ø.75 respectively. The adverse effects of transverse waves are demonstrated while it is seen that beneficial interference can only be achieved in the divergent wave system. As the transverse wave system is of prime importance at Fn:Ø.5, catamarans can not achieve beneficial interference at this speed unless transverse wave damping devices are added such as bulbous bows, or horizontal submerged hydrofoils. Meanwhile at Fn:.75 the adverse effects up to Θ=5Ø degrees are cancelled by the beneficial effects for Θ>5Ø, resulting in small interference drag.

Viscous Resistance

The correlation between $(1+k)C_F$ and $(C_T - C_{WP})$ is very satisfactory for the monohull both in the fixed and free conditions (Figs.135, 161) except where the total resistance increases steeply, i.e. about Fn:32 and Fn:Ø.44.

(1+k) is found to be 1.Ø8 for the fixed and 1.1Ø for the free to trim and sink models which are similar to published results. The undulations in the ($C_T - C_{WP}$) curve are believed to be the result of wave breaking which can not be determined by wave pattern analysis, but only by wake traverse surveys. These undulations are more pronounced in the catamaran configurations for both conditions (Figs. 137 to 144, 165 to 179). The amplitude decreased with increasing separation, which would suggest that the undulations depend on the wave breaking between the demihulls.

Additionally, different (1+βk) values are determined for each separation which decrease with increasing separation. This leads to the assumption that the difference between (1+βk) is a result of viscous interactions while undulations are caused by wave breaking. The errors in such an assumption are not known, but it is believed that this assumption will be sufficient for practical purposes as the ($1+k_{WP}$) curves are fairly constant across the speed range (Figs.15Ø,186). There is a slight difference in the variation of (1+βk) across the separation and it is higher for the free condition than the fixed condition for a given separation (Fig.378). This is probably due to trim angle difference.

Wake survey experiments were conducted for the free to trim and sink condition. Figs 2Ø3 to 211 display the wake contours obtained during these surveys. Additionally, integrations of the drag function with respect to z for the wake surveys are given in Figs. 197 to 2Ø2. The Wigley hull has a thin well defined wake behind the monohull (Figs.2Ø3 to 2Ø5). At the higher speeds, i.e. Fn: Ø.5 and Ø.75, there is a turbulent wake near the surface. It is noted that there are not any wake survey data available in the literature at these high speeds to support these results.

The wake contours for a catamaran with S/L:Ø.2Ø display distinct features due to asymmetric flow behind each demihull (Fig.2Ø6,2Ø7). There is a substantial inward flow due probably to the cross flow under the keel. It is evident that flow under each demihull keel is outwards in the entrance and inwards in the run part of the demihulls [51].

The monohull wake contours show the speed effect as being wider and with a smaller peak to the drag distribution (Fig.2ØØ) suggesting stern wave breaking at the high speeds. This has also been supported by visual observations during the experiments.

As the separation increases, this asymmetric wake loses its dominance. At S/L:Ø.4 the wake is nearly symmetric (Fig.211). The asymmetry results in a wider and smaller peak shape of drag distribution across the traverse (Fig.197). Although there is some evidence of wave breaking in the centre of the tunnel, the accuracy of the experiments prevents clear conclusions on the magnitude of this turbulent flow.

The summation of wave pattern resistance and wake traverse drag is nearly equal to total drag (Figs.185,186) which is very satisfactory considering the possible experimental errors involved in such methods.

Wave Elevation, Trim and Sinkage

The interference effects on running trim and sinkage of the hulls are given in Figs. 193 and 194. Trim interference is important between Fn:Ø.3 and Fn:Ø.7 where the catamaran displays higher trim angles than the monohull and approximates to the monohull trim angle as separation distance is increased. Outside this region there are no significant trim interactions.

Sinkage of the catamarans is higher than the monohull up to Fn:Ø.5 and less above this speed (Fig.194). As the separation distance gets larger the interactions are less pronounced.

The wave elevations along the hull are given in Figs. 152 to 154 for the fixed hull and in Figs 212 to 214 for the free to trim and sink condition. As these data were digitised from photographs, the accuracy of the results are not very good, especially at low separations where the wave elevation inboard was not clearly visible due to spray and the angle at which the photographs were taken.

8.4. MODELS C3, C4 AND C5

The three round bilge transom stern models are illustrated in Figs.215, 216 and 217 and described in Table 1. As described in Table 2 all the hulls were tested for total resistance, wave pattern analysis, sinkage and running trim. The tests were conducted over a speed range of Fn:Ø.1 to 1.Ø with the exception of S/L:Ø.2 for models C3 and C4 which were tested only up to Fn:Ø.6 and Ø.8 respectively due to the creation of excessive wave heights. Wake traverse surveys were carried out for model C3.

Measured residuary resistance for the monohulls is compared with empirical predictions from the Holtrop-Mennen and Chinese regression methods, as well as interpolations from the NPL Round Bilge Series. These are illustrated in Fig.218, 219, 22Ø for C3, C4 and C5 respectively. A sufficient degree of correlation is obtained with the NPL Series interpolation and Chinese regression method whilst the Holtrop-Mennen regression method always underpredicted the main hump. Errors of up to 3Ø % were found from these predictions. Form factors of 1.317, 1.193, 1.174 were calculated by the Holtrop-Mennen method for models C3, C4 and C5 respectively.

The results of the resistance experiments, wave pattern analysis and wake survey results, as well as theoretical results and predictions from the wave pattern analysis, are presented in Figs.221 to 270 for Model C3, Figs.271 to 304 for model C4 and Figs.305 to 338 for model C5.

Wave drag estimates ($C_T-(1+\beta k)C_F$) are given in Figs. 242,292 and 326, The main interference occurs as an adverse effect at about Fn:0.48 to 0.60 depending on separation and L/B ratio. There is a substantial increase in interference when the separation is decreased.

Wave resistance interference ratios are given in Fig.249 to 252, 299 to 304 and 333 to 336. The wave resistance interference ratio, τ, is considerably smaller than the wave pattern interference ratio, μ. This is due to the inclusion of the transom stern resistance in the wave resistance whilst it is not included in the wave pattern resistance. The wave pattern resistance interference is similar to the interference obtained for the Wigley model, C2. The higher separations result in smaller wave interference with humps and hollows located at lower Froude numbers. Additionally, larger interference effects are obtained with smaller L/B ratios as well as the positioning of humps and hollows at higher Froude numbers.

Beneficial wave interference is found at about Fn:0.35 to 0.42 while adverse effects are found both sides of this speed range. The wave interference can be neglected above a particular speed which is both separation and L/B ratio dependent.

Figs. 244, 294, 328 indicate that the wave pattern resistance predicted from monohull experiments is very successful when compared with measured catamaran wave pattern resistance (Figs.243, 293, 327), although the

locations of humps and hollows are mispredicted by a phase shift up to Ø.Ø5 (Fn). As this change follows a consistent pattern (Figs. 249 to 252, 299 to 3Ø4 and 333 to 336) it is believed that an empirical correction would be sufficient for practical purposes. The prediction of amplitude is very satisfactory except model C5 above Fn:Ø.5, the reasons for which are not fully understood.

The theoretical predictions are satisfactory compared with wave resistance above Fn:Ø.4 if the trim and sink correction is applied (Figs.247,248,297,298,331,332). The calculations without this correction are underestimating the interference ratio considerably (Figs. 249 to 252, 299 to 3Ø4 and 333 to 336). This is quite expected when noting the trim and sinkage changes of these hull forms.

Viscous Resistance

The correlation between $(1+\beta k)\ C_F$ and $(C_T - C_{WP})$ is poor at low speeds, i.e. Fn<Ø.6 for all the models (Figs. 221 to 239, 271 to 289, 3Ø5 to 323). This is due to the hydrostatic resistance component of the transom stern, the share of this component in the resistance budget for the monohulls increasing with increasing L/B ratio. Although the prediction of the transom component at high speeds is possible by the method described in Chapter 4, the low speed results are not reliable as the transom stern does not clear the water. Hence $(1+\beta k)$ must be derived from high speed experiments.

The curves of $(1+k_{WP})$ for change in separation are given in Figs. 246, 296 and 33Ø. $(1+k_{WP})$ follow almost a horizontal pattern at about Fn:Ø.7 where $(1+\beta k)$ is derived. There is an indication of the effect of hull separation, $(1+k_{WP})$ decreasing with increasing separation.

Wake traverse experiments were conducted for model C3 in the monohull and catamaran configurations with S/L:Ø.2,

Ø.3 and Ø.4. The wake contours are given in Figs.261 to 27Ø. This model, contrary to model C2, has a wide shallow wake with very turbulent flow near the free surface.

The integrations of the drag function with respect to z for various separations and speeds are given in Figs.255 to 26Ø. Due to the wide shallow wake, there is no apparent hump in the distributions except at S/L:Ø.2.

For the monohull at Fn:Ø.35, the drag is located around the centreline (Fig.261), but side lobes begin to gain importance at the higher speeds (Fig.262, 263). This feature is believed to be caused by the transom stern, as at the lowest speed the transom is not clear of the water. At the higher speeds longitudinal vortices occur at the sides of the transom stern. Additionally the rooster tail wave system breaks causing turbulence on both sides. Hence the flow is highly turbulent near the free surface particularly outboard of the transom. This also tends to cause the wave elevation at the stern to be unstable.

The agreement between C_{WT} and $C_T - C_{WP}$ (Fig.245,246) varies with speed. At the lowest speed, Fn:Ø.35, the change of C_{WT} across the separation range is similar to $C_T - C_{WP}$. But underprediction of $C_T - C_{WP}$ is observed for all the separations. This may be caused by the very wide wake which is not fully covered. For the mid speed, the agreement between C_{WT} and $C_T - C_{WP}$ is very good with the exception of S/L:Ø.2. However for the top speed, Fn:Ø.75, the results do not show a good correlation. It is believed that this is caused by a short dwell time, unstable wave height and highly turbulent flow.

In general, the wake traverse experiments are of sufficient accuracy to reinforce the total resistance and wave pattern results, and to support the derivation of viscous resistance through $C_T - C_{WP}$. They are not considered accurate enough to derive the viscous interactions for this

kind of hull form. It is believed that substantial improvements could be achieved by using bigger models, which was not possible with the available test facilities.

Trim and Sinkage

The highest trim and sinkage was observed for model C3 as it is the widest of the three models tending to behave more like a planing surface (Figs. 253,254,303,304,337,338). The trim and sink interference is similar to the trends found for model C2. Trim interference is only important between Fn:0.3 and Fn:0.7 while the sinkage interaction is effective over all the speed range.

8.5 OVERALL OBSERVATIONS AND CONCLUSIONS

Wave Breaking

During the experiments, wave breaking between the demihulls was observed in addition to the bow and stern wave breaking components found in monohulls. As the bow waves of each hull meet on the centerline of the catamaran, they form two or three wave cusps which move aft with increasing speed and increasing hull separation. At speeds in excess of a critical speed, the first cusp reaches a very high wave height becoming unstable. Therefore wave breaking and turbulence are created (Fig.339). By increasing the speed, the wave breaking includes a water jet causing spray. In the case of a cross structure between the hulls, which has not been implemented in the current work, this spray may wet the structure and increase the frictional drag. The wave breaking feature was observed for separations ratios of less than 0.4 independent of hull shape (Figs.393 to 396) .

The second type of wave breaking phenomenon for catamarans was observed near to the stern of the hulls. The

transom stern creates a very turbulent stern flow (Fig.341). This wave breaking, although also existing in monohulls [1], is highly affected by the hull separation. The stern wave of the demihull collapses to one side due to differences in pressures and wave height and due to cross flow under the keel just behind the stern of a demihull (Fig.342). These effects result in turbulent flow near the surface. Additionally another wave breaking component associated with these stern flow occurs on the centerline of the catamaran where the stern waves of the demihulls meet each other (Fig.340). This component is similar to the one observed for the bow waves. These stern wave breaking features were also observed for model C2 which has no transom stern.

The wavebreaking specific to catamarans across the separation range is demonstrated in Figs. 385 to 388 for model C2 and Figs.389 to 392 for model C3.

These wavebreaking components are believed to create turbulence which changes the wave pattern of the hulls hence causing the experimental wave pattern analysis to be unstable. Additionally some of this turbulence is on the free surface which is very difficult to measure by a wake traverse survey. Therefore the resistance budget can not be fully balanced.

Wave Resistance

The experimental accuracy of the results for total resistance and wave pattern resistance is satisfactory above Fn:0.25 and below Fn:0.9. Below Fn:0.25, the total resistance is very small due to very fine hull forms and high L/B ratio, e.g. typically below 2 Newtons. Wave elevations are also very small causing wave pattern measurements to be inaccurate. At the top end of the speed range, i.e. Fn>0.9 some inaccuracy was also observed in the

total resistance results due to acceleration effects and shallow water, although these are not drastically high.

Above Fn:Ø.45, there is some scatter in the measured wave pattern resistance, similar to some other available data for high speeds [17] . Various problems concerning wave pattern analysis were identified for high speeds: Firstly, the waves from one demihull cross the highly turbulent wake of the other demihull and hence they are modified by the wake. Secondly, the wavebreaking in the tunnel and in the stern are other possible sources of errors. Additionally, some turbulence on the surface of the bow waves further away from the model was observed. This could be measured neither by the wave pattern analysis nor the wake traverse experiments.

The wave pattern analysis employs linear theory. As the radiated waves are not likely to satisfy the assumptions of this theory because either they are too steep (hence nonlinear) or because of the interference from the viscous flow [26], the results obtained can not be exact.

Prediction of wave pattern resistance from monohull wave pattern analysis [355 to 358] has advantages over the fully theoretical approach since the limitations of expressing the basic form by sources and viscous effects on these sources are overcome. However, the effects of the reflections of bow waves of a demihull from the other hull, and perturbation velocity change around a demihull are ignored. Additionally, the change of boundary layer due to asymmetric flow, and wave breaking effects, can not be taken into account. Nevertheless, the simplicity of the method enables one to use it whenever wave pattern analysis is conducted for a monohull design in order to investigate its suitability for a catamaran application.

The theoretical prediction of wave resistance (Fig.359 to 362) has a reasonable degree of accuracy for the catamaran compared with experiments, especially if the corrections for transom stern, trim and sinkage are applied. This approach gives better results than some of the available prediction methods. It also has the advantage of predicting the interference resistance. The simple and fast execution of computer code provides designers with a satisfactory preliminary design tool.

Viscous Resistance

Wake traverse experiments have shown two levels of accuracy. For the Wigley model C2, the contours of the wake are well defined, the drag function is smooth and the main drag humps across the wake are easily distinguished, although the wave breaking can not be measured quantitavely. However the results for round bilge model C3 are not as good as C2. This is probably due to the highly turbulent and unstable nature of the transom stern wake. Drawing other than broad conclusions from this model might be misleading, and it would be advisable to conduct similar experiments with a bigger model where wake can be defined more precisely.

A rooster tail stern wave, whose peak moves progressively down stream of the stern at the higher speeds [25], occurs in the transom models. This feature adds complexity to the wake traverse experiments.

Wave pattern measurements require only one run for each speed under investigation while wake survey measurements require an average of 30 runs per speed. It is thus applicable to academic investigation unless an advanced traverse design is available [76].

Ideally the sum of the wave pattern resistance and wake survey resistance be should equal to total resistance.

However experimental errors can sometimes easily occur as a large number of data must be measured and processed. The second component is more likely to be affected by measurement errors than the first one. Additionally, induced drag from the asymmetric flow of the catamarans may have influence at the small separations.

Direct determination of resistance components from the momentum deficit principle is the only practical experimental technique available to derive the interference resistance components of catamarans independently. However, such a method to determine the detailed variation of interference factors assumes a standard of experimental accuracy which is almost impossible to attain. On the other hand, the measurement of such components does provide the ability to successfully conduct a comparative study of these interferences across a separation and hull form variation.

Comparison of suggested viscous interference factor $(1+(B/S)^2)$ [51] and experimental curves of $(1+\beta k)/(1+k)$ is given in Fig. 397. Although the results are in the same order, the experimental results have smaller change with variation of S/B, and the effect of L/B ratio is important. This is probably because the current experimental results are obtained in high speeds where free surface has an important effect on viscous resistance, whilst $(1+(B/S)^2)$ was compared with low speeds in Ref.51. $(1+(B/S)^2)$ is also in agreement with wind tunnel experiments [3].

Interference Factors

The interference factor Ω for residuary resistance ,i.e. $(C_R)_{CAT}/(C_R)_{MONO}$, obtained from total resistance measurements is given in Figs. 343 to 346. At the lower end of the speed range ,i.e. less than Fn:Ø.3Ø, very oscillatory results are obtained partly due to very small values of C_R. Hence no attempts were made to draw conclusions for this speed range. Two humps and a hollow

are apparent for all the hulls and separations. The positions of the hollow at about Fn:Ø.37 and humps at about Fn:Ø.3Ø and Fn:Ø.45 are dependent on separation distance and L/B. The smaller separation leads to a higher Froude number for the humps and hollows. E.g. for model C2, the hollow occurs at about Fn:Ø.38 for S/L:Ø.2 and Fn:Ø.33 for S/L:Ø.5. A similar tendency is observed for change in L/B ratio, i.e. a smaller L/B ratio results in a higher Froude number for the position of humps and hollows. The positions of humps and hollows for the current models are given in Figs.375 to 378. It is suggested that the designer should avoid designing a catamaran working in the shaded areas. The amplitude of the interference depends on the hull form as well as separation.

Figs. 347 to 35Ø show the interference factor τ, i.e. $(C_T-(1+\beta k)C_F)_{CAT}/(C_T-(1+k)C_F)_{MONO}$. The same tendencies for the positions of humps and hollows are observed. The effect of L/B ratio on the interference amplitude is pronounced for the small separations, i.e. S/L:Ø.2 and S/L:Ø.3 where higher L/B ratio leads to smaller wave interference. At S/L:Ø.5 the interference is practically the same for L/B:9 and L/B:11. The interference effects can be neglected above a critical Froude number which is separation dependant. The higher the separation, the lower the critical Froude number becomes. E.g. Fn:Ø.8 for S/L:Ø.2 and Fn:Ø.55 for S/L:Ø.5.

The change in wave pattern interference factor, μ, across the model range is given in Figs.351 to 354. Similar tendencies to Ω, and τ are observed across the separation and L/B range tested. The critical Froude number change above which the wave pattern interference can be practically neglected is found to be similar and is given in Fig.375. This has an important outcome giving the designer freedom to optimise other characteristics of the ship such as seakeeping, stability and strength of cross structure.

Predicted wave pattern interference factor using the monohull wave pattern are given in Figs.355 to 358. Unlike the previous wave interference factors it is mainly dependent on the separation ratio rather than hull shape. A small phase shift was observed for a change of L/B. This suggests that the effect of the asymmetric flow is of an important nature which may not be predicted by the current method.

It is found that theoretical calculations and predictions from the monohull wave pattern analysis may predict wave resistance with a phase shift. This shift may be corrected by using the experimental results obtained in this work. Firstly, the main hump position of wave resistance can be found from Figs. 375-377 for a given separation and L/B ratio. Secondly the wave resistance curve can be shifted to match to this hump.

The effect of dividing resistance into components by different methods for extrapolating to ship scale can result in significantly different results. e.g. the results of the experiments for model C4-Monohull and C4-S/L:Ø.3 are extrapolated to a 4Ø m ship, using the ITTC 1957 method, the ITTC 1978 method with a constant $(1+\beta k)$ over the speed range but varying with the separation, and by direct measurement method with a varying $(1+k_{WP})$ across the speed range. The difference between the extrapolated results are given in Figs.383, 384.

The main difference between the methods is seen in the low speed range, i.e. Fn<Ø.6. Above Fn:Ø.6 the ITTC 1978 and direct determination methods lead to the same result whilst the ITTC 1957 method results in a higher drag value. Due to the influence of wavebreaking on the direct method, the ITTC 1978 method is believed to be the most suitable of these three methods for the extrapolation to full scale, although there is not any available full scale resistance data to confirm this.

Trim and Sinkage

The interactions on the running trim of catamarans are of importance between Fn:Ø.3 to Fn:Ø.7Ø as shown in Figs.367 to 37Ø (In these figures. the trim angles were increased by 18Ø to suppress the inaccuracies of the measurements in small trim angles encountered at low speeds). The catamarans showed a steeper increase in trim than the monohull which has already shown a rapid increase in the speed range up to Fn:Ø.5. Above this speed, the trim of catamarans drops down reaching the monohull trim at about Fn:Ø.7Ø. Although the interference is effective across the separation range, the trim increase in catamarans is more pronounced with a decrease in the separation . E.g. for S/L:Ø.5 and L/B:11, the running trim is very similar to the monohulls. The catamarans with higher L/B ratio have smaller trim interactions for all separations tested. Outside this speed range, both monohull and catamaran configurations have similar running trim characteristics. The Wigley hull has a similar trim interference to the round bilge hulls except that the interference occurs at slightly lower speeds. It is also noteworthy that the interference occurs where catamaran wave resistance shows severe adverse interference. This follows the link between the wave resistance and running trim [56].

The dynamic vertical position of LCG, i.e. sinkage of the hull, was also effected by the interference between the demihulls (Figs. 371 to 374). In other words, the dynamic lift generated by the hulls is related to the separation distance. Up to about Fn:Ø.5, the catamaran has higher sinkage than the monohull. This increase gets smaller with increasing separation distance. The main interference is observed above this speed, as the catamaran rises more than the monohull at the higher speeds at which these ships normally operate. A lift of up to 2.5 times the lift

generated by the monohulls can be observed i.e. is up to 5 %.of draught.

The catamarans with lower L/B ratio have more interference both on increase and decrease of the sinkage. The Wigley hull, although its hull form is very different from the round bilge hulls, also shows good agreement with these trends.

A Preliminary Prediction Method

The experimental time needed to cover necessary separation and speed variations can be very lengthy. A regression analysis of all available experimental data is a possible approach. However due to the lack of data at high speeds, this method can not be utilised satisfactorily. A preliminary design procedure utilising both theoretical and empirical methods may be adopted. Taking into account all the information gathered in the current investigation a practical method based on the ITTC 1978 proposal is outlined for the prediction of catamaran resistance, suitable for use at the preliminary design stage:

A) The frictional resistance is calculated from the ITTC 1957 formula.

B) A form factor (1+k) for the monohull is determined by an available method which can be from published model data, from empirical formulae or from tests of a similar model.

C) Factor β is calculated from Fig.378 or from a cross plot in Fig.379 and viscous resistance $(C_V)_{CAT}$ can be derived from $(1+\beta k)\ C_F$.

D) Wave resistance of the monohull can be calculated from specific model experiments, regression formulae or suitable model series. In the absence of all these methods theoretical wave resistance can be used.

E) Using the current results, if the design is similar to the models, the wave interference ratio can be obtained

from Figs.347 to 350 for a given separation and L/B ratio. For the designs which are not similar to the current hull forms, theoretical predictions from linearised theory can be utilised.

F) The wave resistance $(C_W)_{CAT}$ is calculated by τC_W. If theoretical predictions are utilised for the interference ratio, a phase shift should be applied to these results as described earlier.

G) Total resistance is calculated by
$(C_T)_{CAT} = (C_V)_{CAT} + (C_W)_{CAT}$.

This method is suggested for use at the preliminary design stage. It allows some investigation of hull form, separation and speed to be made. However model tests would be recommended to determine the resistance of the final design.

Using this method with theoretical wave interference factor for τ, calculations of errors in total resistance prediction for models C2, C3, C4, C5 are presented in Figs. 380 to 382. It is observed that estimates at lower speeds, particularly with small separations, should to be treated with caution. At higher speeds, particularly above Fn:0.5, the results are promising and should prove satisfactory for preliminary design.

CHAPTER 9 : CONCLUSIONS AND RECOMMENDATIONS

The investigation has demonstrated that the resistance of catamarans can be treated as a summation of the principal resistance components, analogous to monohull resistance, and interference resistance components which can be obtained by the application of interference factors to the principal components. Experimental and theoretical results have revealed a number of the characteristics of these interference effects, particularly at high speeds, and have contributed to a better understanding of catamaran resistance.

The principal findings and conclusions drawn from this investigation are outlined as follows:

The survey of built catamarans revealed the main application range of catamaran hull form parameters. The hull forms are invariably long and thin and with small block coefficients. The vessels are grouped around two speed ranges at about Fn:Ø.3Ø and Fn:Ø.9. The main thrust of this investigation was therefore focused around these characteristics, together with extensions beyond them where possible.

The literature review indicated that two types of interaction, namely wave and viscous interaction, must be taken into account. Whilst a number of investigations into the wave resistance of catamarans had been carried out, there is very little published information on viscous interactions. More importantly, there was effectively no published information available for catamarans at speeds

higher than about Fn:0.5, i.e. the range specifically applicable to modern high speed catamarans.

Total resistance experiments were conducted for five hull forms and provide useful data over a wide range of separations and Froude numbers. These data were used for the validation of the techniques developed in the investigation, but they can also be used directly in the practical prediction of catamaran resistance, as the hull forms represent catamaran forms in common use.

The automated wave pattern analysis system, developed for the investigation, proved to be successful over a wide range of speeds, providing very valuable information on the wave interference of catamarans as well as achieving a direct method for the determination of form factor. This is probably the first set of data obtained for high speed catamarans with symmetric demihulls. Additionally, these data improve the knowledge of wave pattern resistance for monohulls at high speeds.

The experimental observations revealed wave breaking phenomena specific to catamarans, due to bow and stern wave interactions between the demihulls. This wave breaking is likely to cause some underprediction of wave resistance by the wave pattern analysis over certain speed ranges.

It was demonstrated that theoretical prediction of catamaran wave resistance by the use of linearised theory and a thin ship approximation has a reasonable degree of accuracy, especially when corrections for transom stern, trim and sinkage are applied. The phase shift due to asymmetric flow does require to be corrected by empirical methods. The simple and fast execution of this computer code provides the designer with a satisfactory preliminary design tool for parametric concept models. It may be possible to predict the positions of humps and hollows more accurately by the use of a full three dimensional source

panel method such as Neuman-Kelvin, as the asymmetric features of flow can be included. Such a method would however require excessive computing time for parametric studies and is unlikely to be cost effective. It would therefore be confined to checking certain applications only. As a further comment on the use of theoretical methods, it should be noted that the derivation and use of wave interference factors, rather than direct wave resistance prediction, has led to much better accuracy. The simplified theory developed in this investigation provides a satisfactory basis for predicting these interference factors.

A parametric study of catamaran wave resistance using the theory, indicated that speed and S/L are of prime importance in the wave resistance interaction. The hull form parameters L/B and B/T have an influence at higher speeds whilst entrance angle and prismatic coefficient are of more importance at lower speeds. The effect of L/B ratio, i.e. higher interference with decreasing L/B ratio, was confirmed by the experiments. This increased the reliability of the method.

The wave resistance interference factor exhibits two humps and a hollow in the speed range up to Fn:1.Ø. The exact positions of the humps and hollows are influenced by separation and L/B ratio. Smaller separation and L/B ratios result in higher speeds for the locations of the humps and hollows. The amplitude of interference also follows a similar pattern, i.e. a smaller separation and L/B ratio leads to higher interference. This correlates well with theoretical estimations.

Above a critical speed, which is separation dependent, the wave resistance interference can be neglected. The higher the separation, the lower the critical Froude number becomes. It changes from Fn:Ø.55 for S/L:Ø.5 to Fn:Ø.8 for S/L:Ø.2.

The prediction of the catamaran wave pattern from the wave pattern analysis of a monohull presents a simple but powerful method of prediction, as it predicts the amplitude of the interference fairly well. However, a correction for the positions of humps and hollows must be applied in order to compensate the phase shift created by the asymmetric flow around a demihull. This approach has advantages over a fully theoretical approach since there are limitations in expressing the hull form by sources and sinks, and viscous effects on these sources are taken into account. It is suggested that this prediction method could be applied to existing monohulls tested for wave pattern analysis. This would lead to the identification of those hull forms which have potential applications for catamarans.

The viscous wake traverse system provided a satisfactory method of obtaining the viscous drag of catamarans. Shortcomings with this analysis method were identified, in particular, the method is found to be limited due its long, tedious test procedure for practical applications. Nevertheless, the method proved that the sum of the viscous and wave pattern resistance achieved a budget close to total resistance. It thus confirmed the alternative method for the derivation of viscous resistance, that is from the difference between total and wave pattern resistance. Additionally this method displayed the effect of asymmetric flow on the shape of viscous wake behind the stern which is highly affected by the separation.

Small separations are likely to create cross flow under the keel. An asymmetric wake skewed inside at the lower body and outside near to the surface was observed in this condition. It was not possible to quantify the likely induced drag resulting from these cross flows.

Viscous interactions were investigated by wake traverse experiments and by total resistance and wave pattern analysis. These investigations indicated that application of a form factor varying with separation and L/B ratio, but not with speed, is sufficient for the practical prediction of viscous interactions. The interference factor β has been presented in graphs for various L/B ratios and separations.

It was found that the values of trim and sinkage for the catamaran can be substantially different from the monohull and need to be borne in mind when freeboard and clearance of cross structure are being considered.

The effect of interference on the running trim of catamarans is pronounced between about Fn:0.3 and Fn:0.7. The catamaran has a higher running trim angle showing a steep increase up to Fn:0.5 and a gradual decrease approximating to the monohull trim at about Fn:0.7. Increasing the separation decreases this interference. For separations over S/L:0.5 the trim is likely to be equal to that of monohull. L/B ratio also has an influence on the trim interference; a lower L/B ratio results in an increased trim angle interaction.

Sinkage of the catamaran is also influenced by the separation distance between the demihulls. Decreasing the separation results in higher sinkage below Fn:0.5. Above this speed the catamaran has higher lift than the monohull which increases with decrease in the separation. By increasing the separation above S/L:0.5, the sinkage becomes similar to that of the monohull. The interference effects are increased by decreasing L/B ratio.

The choice of a suitable parameter for the interference components is not fully conclusive. S/L is the principal parameter for the wave interference. However S/B, which is equivalent to L/B for the current models., has

importance on the positions of humps and hollows. The viscous interactions are mainly affected by L/B. Further work involving various parameters is needed.

In summary, the investigation achieved its goal in identifying the interference components by both experimental and theoretical methods, and their influence on the resistance of catamarans at higher speeds. The effect of variation of separation and L/B ratio on interference resistance components and hull behaviour were also discovered. These lead to a better understanding of the resistance features of high speed catamarans.

Following the experience gained during this work the following recommendations are made for further research on catamaran powering:

Research on asymmetric demihulled catamarans would be beneficial, especially if such vessels are required to operate near the main hump speed. Additionally, hull form changes such as bulbous bows and submerged nonlifting hydrofoils between the demihulls may increase the efficiency of catamarans near the main hump speed by cancellation of transverse waves.

The experimental and theoretical approaches described have identified the effects of separation and L/B ratio on the resistance interference factors. Similar investigations for the effects of B/T ratio and C_P are recommended in order to completely understand hull form effects.

Hull form modifications, especially at the bow, to reduce the wave breaking at the centerline of the catamaran may have an influence on the overall performance of these craft, and deserves further investigation.

A complete powering prediction of these vessels requires the propulsion efficiency to be determined.

However, there are few data on wake fractions and thrust deductions for catamarans, which will be influenced by asymmetric flow behind the stern. Research on this topic would be very valuable.

The current investigation has been concerned entirely with model scale. The detailed investigation of resistance components has indicated the likely suitable breakdown of the components for the extrapolation to full scale. Confirmation of this aspect would depend on full scale trial results which are currently not available. Such a model-ship correlation exercise is necessary if the extrapolation methods for this particular ship type are to be validated.

REFERENCES

1) BABA E.
Wave Breaking Resistance of Ships
International Seminar on Wave Resistance, Tokyo, Japan
The Society of Naval Architects of japan
1976

2) BAILEY D.
The NPL High Speed Round Bilge Displacement Hull Series
Marine Technology Monograph, No:4, RINA
1976

3) BIERMAN D., HERRNSTEIN W.H.
The Interference between Struts in Various Combinations
NACA Report No:468
1933

4) BOND J.R.
Catamarans - Dream or Reality
Naval Engineers Journal, Vol:82, No:3
June, 1970

5) BRICKWOOD J.
An Investigation of the Components of Resistance Using Wave Resistance Measurements and a Predicted Form Factor
BSc Honours Report No:SS-207
Department of Ship Science, Southampton University
1986

6) CALKINS D.E.
HYCAT : Hybrid Hydrofoil Catamaran Concept
Ocean Engineering, Vol:11, No:1
1984

7) CAMPBELL I., CLAUGHTON A.
The Interpretation of Results from Tank Test on 12m Yachts
The Eight Chesapeake Sailing Yacht Symposium, SNAME
1987

8) CHANG M.S.
Wave Resistance Predictions Using a singularity Method
The Proceedings of the Workshop on Ship Wave Resistance Computations, Maryland, USA, Vol II
1979

9) CHENGYI W.
On the Resistance and Interference of Wave Systems of High-Speed Catamaran
(In Chinese)
Shipbuilding of China, Vol:106
1989

10) CLEMENT E.P.
Graphs for predicting the Ideal High-Speed Resistance of Planing Catamarans
International Shipbuilding Progress, Vol:9, No:99
November
1962

11) COLMAN D.A.
Measurement of the Wave Pattern Resistance of Asymmetric Hull Forms the Longitudinal Cut Method
MPhil Thesis
Department of Ship Science, University of Southampton
1975

12) CONN J.F.C.
Ship Resistance - Retrospect and Prospect
Transaction of NECIES, Vol:91, No:3
1975

13) CORLETT E.C.B.
Twin Hull Ships
Transactions of RINA, Vol:111
1969

14) CORTELLINI L., LAURO G., ALLIERI E., CARRERA G.
Hull Resistance Components direct Measurement
La Marina Italiana, Vol:83
May-June 1985

15) EGGERS K.
Resistance Conditions of Two-Body Ships
BSRA Translation No: 1860
(Translated from Jahrbuch der Schiffbautech. Gesellschaft), Vol:49
1955

16) EGGERS K.W.H., SHARMA S.D., WARD L.W.
An Assessment of Some Experimental Methods for Determining the Wavemaking Characteristics of a Ship Form
Transactions of SNAME, Vol:75
1967

17) EVEREST J.T., BAILEY D.
The Wave Resistance of High Speed Semi-Displacement Type Hulls and Its Influence in the Design of Unconventional High Speed Craft
NPL Ship Division, TM 177
1967

18) EVEREST J.T.
Some Research on the Hydrodynamics of Catamarans and Multi-Hulled Vessels in Calm Water
Transaction of NECIES, Vol:84
1967-1968

19) EVEREST J.T.
Some Comments on the Performance in Calm Water of a Single-Hull Trawler Form and Corresponding Catamaran Ship Made up from Symmetrical and Asymmetrical Hulls
NPL Ship Division, Ship Report: 129
1969

20) FROUDE W.
Observations and Suggestions of Determining by Experiment the Resistance of Ships
Correspondence with Admiralty
1868
Reprinted in "The Papers of William Froude", INA
1955

21) FROUDE W.
Experiments for the Determination of the Frictional Resistance of Water on a Surface Under Various Conditions
Report to Admiralty and British Association for the Advancement of Science
1874
Reprinted in "The Papers of William Froude", INA
1955

22) FRY E.D., GRAUL T.
Design and Application of Modern High-Speed Catamarans
Marine Technology, Vol:9, No:3
July, 1972

23) GADD G.E., HOGBEN N.
The Determination of Wave Resistance from Measurements of the Wave Pattern
NPL Ship Report No: 70
1965

24) GADD G.E.
Wave Pattern Measurement
Appendix 3, 14th ITTC
1975

25) GADD G.E.
The Use of Resistance Component Measurement as Diagnostic Tools in assessing the resistance qualities of Ship Models
NMI Report No:R153
1983

26) GOLDSTEIN S.
Modern Developments in Fluid Dynamics
New York, Dover Publications
1965

27) GUOHUA S., SHAOQIU D., DANGGUANG C.
The Research of Wave-Element for a High Speed Catamaran in the Inland River
International High-Performance Vehicle Conference, China
1988

28) HARVALD Sv. Aa.
Resistance and Propulsion of Ships
Wiley Publications
1983

29) HOGBEN N.
The Computing of Wave Resistance from a Wave patter by a Matrix Method
NPL Ship Report No: 56
1964

30) HOGBEN N.
A Summary of the Results from Automated Wave Pattern Analysis
NPL Ship Report No:157
1971

31) HOGBEN N.
Automated Recording and Analysis of Wave Patterns Behind Towed Models
Transactions of RINA, Vol:114
1972

32) HOLTROP J.
A Statistical Re-Analysis of Resistance and Propulsion Data
International Shipbuilding Progress, Vol:31, No:363
November, 1984

33) HSIUNG C.C.
Theoretical Investigation of Optimal Forms for Mono-Hull and Twin-Hull Ships
Canadian Maritime Industries Association
Fortieth Annual Conference, Section 6

34) HUGHES G.
Friction and Form Resistance in Turbulent Flow, and a Proposed Formulation for use in Model and Ship Correlation
Transactions of RINA, Vol:96
1954

35) HUGHES G.
An Analysis of Ship Model Resistance into Viscous and Wave Components
Transaction of RINA, Vol:108
1966

36) INSEL M.
Interactions in a Wake Traverse Rake
Progress Report:2
Department of Ship Science, Southampton University
1986

37) JU S.
Study of Total and Viscous Resistance for Wigley Parabolic Ship Form
Iowa Institute of Hydraulic Research, Report:IIHR-261
1983

38) KAJITANI H., MIYATA H., IKEHATA M., TANAKA H., ADACHI H., NAMIMATSU M., OGIWERA S.
The Summary of the Cooperative Experiments on Wigley Parabolic Model in Japan
Proceedings of The second DTNSRDC Workshop on Ship Wave Resistance Computations, Maryland, USA
1983

39) LACKENBY H.
An Investigation into the Nature and Interdependence of the Components of Ship Resistance
Transaction of RINA, Vol:107
1965

40) LIN W.C.
The Force and Moment on a Twin-Hull Ship in a Steady Potential Flow
Tenth Naval Hydrodynamics Symposium, MIT, USA
1974

41) LINDGREN H., DYNE G.
Ship Performance Prediction
Publications of the Swedish Maritime Research Centre (SSPA), No:85
1980

42) LIU C.Y., WANG C.T.
Interference Effect of Catamaran Planing Hulls
Journal of Hydronautics, Vol:13, No:1
January, 1979

43) LUNDE J.K.
On the Linearized Theory of Wave Resistance for Displacement Ships in Steady and Accelerated Motion
Transaction of SNAME, Vol:59
1951

44) MCCARTHY J.H.
Collected Experimental Resistance Component and Flow Data for Three Surface Ship Model Hulls
DTNSRDC Report:85/011
1985

45) MELVILL JONES B.
The Measurement of Profile Drag by the Pitot-Traverse Method
The Cambridge University Aeronautics Laboratory
ARC Reports and Memoranda No:1688
1935-1936

46) MICHALSKI J.P.
Analytical Bulbous Bow for a Catamaran Ship
Budownictwo Okretowe, Vol:24, No:12
1979

47) MICHEL W.H.
The Sea-Going Catamaran Ship its Features and Its Feasibility
International Shipbuilding Progress, Vol:8, No:85
September, 1961

48) MICHELL J.H.
The Wave Resistance of a Ship
Philosophical Magazine and Journal of Science, Vol:5-45
1898

49) MIN K.S., KIM K.J.
Catamaran Design from the View Point of Wave Resistance
Workshop on evelopments in Hull Form Design, Wageningen, The Netherlands
1985

50) MIYATA H.
Development of a New-Type Hydrofoil Catamaran
Journal of Ship Research, Vol:3 No:2
June, 1989

51) MIYAZAWA M.
A Study on the Flow around a Catamaran
Journal of Society of Naval Architects of Japan, No:145
1979

52) MOLLAND A.F.
A New NC-Controlled Three-Axis Model Cutting Machine
The Naval Architect
October, 1989

53) MORAN D.D., LANDWEBER L.
A Longitudinal-Cut method for Determining Wavemaking Resistance
Journal of Ship Research, Vol:16, No:1
March, 1972

54) MOSS J.L.
Resistance Tests for 1/12 Scale Models of Three Catamarans
University of Michigan, Department of Naval Architecture and Marine Engineering
Ship Hydrodynamics Laboratory
1969

55) MÜLLER-GRAF B.
General Resistance and Propulsion Aspects of Different Vehicle Types
Thirteenth WEGEMT School, Delft, The Netherlands, Lecture 7
1989

56) NAMIMATSU M., OGIWARA S., TANAKA H., HINATSU M., KAJITANI H.
An Evaluation of Resistance Components on Wigley Geosim Models
Journal of the Kansai Society of Naval Architects, Japan, No: 197
June 1985

57) NORWOOD J.
High Speed Sailing
Granada Publishing, London
1979

58) OZAWA H.
The Design and Operation of Catamaran Vessels
Transactions of NECIES, Vol:103, No:4
1987

59) OZAWA H, SHIMADA K., SAITO T., KOBAYASHI M., NOJIRI T., YAMASHITA S., DAIMAON Y.
Experimental Study on the Resistance of Twin-hulled Air Cushion Vehicle
Japan Shipbuilding & Marine Engineering, Vol: 11, No:11
1977

60) PIEN P.C.
Catamaran Hull-Form Design
International Seminar on Wave Resistance, Tokyo, Japan
1976

61) PING-ZHONG J., BA-YING S., ZHANG-KAI T.
A Parametric Study on High Speed Round Bilge Displacement Hulls
High Speed Surface Craft, Vol:19, No:12
September, 1980

62) RALF A.I.
Discussion to MANDEL P.
A Comparative Evaluation of Novel Ship Types
Transactions of SNAME, Vol:70
1962

63) RICH A.J., SPROSTON J.L., MILLWARD A.
A Theoretical Prediction of the Effect of a Wall on the Resistance of a Fast Ship Shape in Water of Uniform Depth
International Shipbuilding Progress, Vol:32, No:376
December, 1985

64) RUTGERSSON O.
Catamarans versus Single-Hull Concepts, a Study of Stability, Powering and Seakeeping Qualities for Small Warships
International Symposium on Coastal Defence and Assault Vessels and Systems, RINA
1986

65) SAVITSKY D., DINGEE D.A.
Some Interference Effects Between Two Flat Surfaces Planing Parallel to Each Other at High Speed
Journal of the Aeronautical Sciences, Vol:21, No:1
January, 1954

66) SCHIMKE A.
Zur Wajl des B/T Verhältnisses für zwei Katamaranspantformen
(In German)
Schiffbautechnik, Vol:16, No:6
1966

67) SCHIMKE A., PUCHSTEIN K.
Widerstandsschleppversuche mit Katamaran-Modellen
(In German)
Schiffbautechnik, No:8
1966

68) SCHIMKE A., PUCHSTEIN K.
Ein Beitrag zum Problem des Katamaranwiderstandes
(In German)
Schiffbauforschung, No:6
1967

69) SHEARER J.R., CROSS J.J.
The Experimental Determination of the Components of Ship Resistance for a Mathematical Model
Transaction of RINA, Vol:107
1965

70) SHERMAN T.J., FISHER P., COUCH R.B.
A Study of Planing Catamaran Hull and Tunnel Interactions
University of Michigan, Department of Naval Architecture and Marine Engineering
Ship Hydrodynamics Laboratory
1975

71) SRETTENSKY L.N.
On the Wave-making Resistance of a Ship Moving Along in a Canal
Philosophical Magazine and Journal of Science
Vol: 22 - Seventh Series
December, 1936

72) TODD F.H.
Resistance and Propulsion
Principles of Naval Architecture, SNAME
1967

73) TOWNSIN R.L.
Viscous Drag from a Wake Survey Measurements in the Wake of a Lucy Ashton Model
Transactions of RINA, Vol:110
1967

74) TOWNSIN R.L.
The Viscous Drag from a Victory Model. Results from Wake and Wave Pattern Measurements
Transactions of RINA, Vol: 113
1971

75) TOWNSIN R.L.
Ship resistance Components Revealed by Wake Momentum and Wave Pattern Measurements in the Presence of Breaking Ship Waves
Transactions of NECIES, Vol: 89
1972-1973

76) TOWNSIN R.L., WYNNE J.B.
Viscous Drag Measurement of Ship Models: The Design and Use of an Automated System
Transactions of NECIES, Vol:96
1979-1980

77) TSAI C.E., LANDWEBER L.
Further Development of a Procedure for Determination of Wave Resistance from Longitudinal Surface-Profile Measurements
Journal of Ship Research, Vol:19, No:2
June, 1975

78) TURNER H., TAPLIN A.
The Resistance of Large Powered Catamarans
Transactions of SNAME, Vol:76
1968

79) TZOU K.T.S., LANDWEBER L.
Determination of the Viscous Drag of a Ship Model
Journal of Ship Research, Vol:12, No:2
June, 1980

80) UNOZAWA M., SHIMUZU K.
The Design of Catamarans
PRADS - International Symposium on Practical Design in Shipbuilding, Tokyo, Japan
1977

81) VERCOE H.J.
Catamarans
BSRA Technical Momerandum No:527
1977

82) VOLHEIM R.
Über Formgebung und Widerstand von Katamaranen
Schiffbauforschung, 7
1968

83) WEHAUSEN J.V.
The Wave Resistance of Ships
Advances in applied Mechanics, Vol:13
1973

84) YERMOTAYEV S.G., AFRAMEYEV E.A., TEDER L.A., RABINOWICH Y.S.
Hydrodynamic Features of High Speed Catamarans
Hovering Craft & Hydrofoil, Vol:16, No:9-10
June/July, 1977

85) YOKOO K., TASAKI R.
On the Twin-Hull Ship (No:1)
Dept. of Naval Architecture and Marine Engineering
University of Michigan, Publication No:33
1969

86) YOKOO K., TASAKI R.
On the Twin-Hull Ship (No:2)
Dept. of Naval Architecture and Marine Engineering
University of Michigan, Publication No:34
1969

87) ———
Catamarans 1969
Amateur Yacht Research Society, Publication No:67
1969

88) ———
Catamaran Study Volume I-V
General Dynamics
1969

89) ———
Churchill Wave Monitor : Technical Manual
Churchill Controls Ltd.

90) ———
Cruising Catamaran
Amateur Yacht Research Society
1977

91) _____
High Speed Surface Craft
Various Issues
1980-1990

92) _____
International Conference on SWATH Ships and Advanced Multi-Hulled Vessels
London, RINA
1985

93) _____
International Conference on SWATH Ships and Advanced Multi-Hulled Vessels II
London, RINA
1988

94) _____
ITTC Dictionary of Ship Hydrodynamics
Maritime Technology Monograph No:6, RINA
1978

95) _____
Janes High Speed Craft and Air Cushion Vehicles
1986

96) _____
Janes Surface Skimmers
1986

97) _____
Proceedings of the Workshop on Ship Wave Resistance Computations
Maryland, USA
Vol I,II
1979

98) _____
Proceedings of the Second DTNSRDC Workshop on Ship Wave Resistance Computations
Maryland, USA
1983

99) _____
Ship & Boat International
Various Issues
1980-1990

APPENDIX A : SUMMARY OF AVAILABLE DATA ON CATAMARAN RESISTANCE

Author & Hull	Ref	Sym	Fn	S	L/B	B/T	C_B	C_P	Type
Schimke U55	67	S	.24- .36	S/B= ∞, 2.05,2.43 2.73,3.02	6.484	1.092	.550	.577	R_T
Schimke S65	67	S	.24- .36	S/B= ∞, 2.00,2.39 2.67,3.00	7.668	0.910	.654	.682	R_T
Schimke S71	67	S	.24- .36	S/B= ∞, 2.00,2.40 2.70,3.00	7.668	0.910	.706	.730	R_T
Everest Parabolic	18	S	.23- .48	S/L= ∞,.3	10.000	1.600	.444	.667	R_T ,R_{WP}
Everest Conventional	18	S	.29- .37	S/L= ∞,.3	8.800	1.670	.548	.574	R_T ,R_{WP}
Everest 4890 (Trawler)	19	S	.26- .38	S/L= ∞,.2 0.25,0.30	9.25	1.2	.52	.58	R_T/∇
Everest 4918 (Trawler)	19	A	.26- .38	S/L= ∞,.2 0.25,0.30	9.25	1.2	.52	.58	R_T/∇
Miyazawa	51	S	.07- .35	S/L= ∞, 0.177	11.542	1.359	.554		C_T ,C_{WP} C_{WT}
Michalski Original Form	46	S	.22- .35	S/L=.287	8.0	1.36	.594		C_R
Michalski Bulb A	46	S	.22- .35	S/L=.287	8.0	1.36			C_R
Michalski Bulb B	46	S	.22- .35	S/L=.287	8.0	1.36			C_R
Turner et al 1A-25 FT	78	S	.18- .34	W/L= ∞, .257,.314 .386	10.77	2.6	.584	.598	EHP
Turner et al 1C-25 FT	78	FA	.18- .34	W/L= ∞, .257,.314 .386	10.77	2.6	.584	.598	EHP
Turner et al 1A-30 FT	78	S	.18- .34	W/L= ∞, .257,.314 .386	10.77	2.163	.6	.615	EHP

Author & Hull	Ref	Sym	Fn	S	L/B	B/T	C_B	C_P	Type
Turner et al 1B-30 FT	78	A	.18- .34	W/L= ∞, .257,.314 .386	10.77	2.163	.6	.615	EHP
Turner et al 1C-30 FT	78	FA	.18- .34	W/L= ∞, .257,.314 .386	10.77	2.163	.6	.615	EHP
Turner et al ASR-5060	78	S	.18- .36	G/L=.181	8.75	1.333	.531		R_T/∇
Turner et al ASR-5061 (Sym AftBody)	78	A	.18- .36	G/L=.181	8.75	1.333	.531		R_T/∇
Turner et al ASR-5093	78	A	.164-.39	G/L=.162	8.077	1.368	.539	.551	EHP
Turner et al ASR-5094 (Bulbous Bow)	78	A	.164-.39	G/L=.162	7.88	1.45	.585	.601	EHP
Turner et al ASR-5116	78	A	.196-.37	G/L=.148	8.846	1.969	.537		EHP
Fry & Graul 1175 (Hard Chine)	22	S	.3 -1.2	G/L=.067, .133,.383	6.67	3.0	.43	.753	R_T/∇
Fry & Graul 1177 (Hard Chine)	22	A	.3 -1.2	G/L= ∞ .067,.133 .383	6.67	3.0	.43	.753	R_T/∇
Fry & Graul 1179 (Hard Chine)	22	FA	.3 -1.2	G/L= 0 .067,.133 .383	6.67	3.0	.43	.753	R_T/∇
Moss 1175 (Hard Chine)	54	S	.3 -1.2	G/L=.067 .133,.383	6.67	3.0	.43	.753	R_T/∇ Sinka. Trim
Moss 1177 (Hard Chine)	54	A	.3 -1.2	G/L= ∞ .067,.133 .383	6.67	3.0	.43	.753	R_T/∇ Sinka. Trim
Moss 1179 (Hard Chine)	54	FA	.3 -1.2	G/L= 0 .067,.133 .383	6.67	3.0	.43	.753	R_T/∇ Sinka Trim
Volheim 488	82	S	.26 -.36	S/L= ∞ .2,.25,.3 .35	8.118	1.624	.597	.58	R_T/∇

Author & Hull	Ref	Sym	Fn	S	L/B	B/T	C_B	C_P	Type
Guohua et al (Round Bilge, Spray strip, Foils)	27	FA -FA	.2 -1.0	G/B= 0,2 2.6,3.2, 5.0,6.0, 8.0	16.889	1.875	.508	.646	C_R
Chengyi (Round Bilge)	9	S	.4 -1.1	G/B=1.6 2,2.6,3.2 6.0	10.526	2.375	.5		C_R, R_T/∇
Chengyi (Hard Chine)	9	S	.4 -1.1	G/B=1.6 2,2.6,3.2 6.0	10.526	2.375	.5		C_R, R_T/∇
Chengyi (Round Bilge)	9	FA	.4 -1.1	G/B=1.6 2,2.6,3.2 6.0	10.526	2.375	.5		C_R, R_T/∇
Yermotayev (Hard Chine)	84	FA	F∇ .5 -3.7	G/2B= 0 .25,.5, .75					R_T/∇ Trim
Yermotayev (Hard Chine)	84	-FA	F∇ .5 -3.7	G/2B=.25 .5,.75, 1.5					R_T/∇ Trim
Min & Kim Mathematical	49	S	.1 -1.2	S/L=0.3 .5	8.0	1.333			C_R
Yokoo (Inuid)	85	S	.2 -.48	S/L= ∞,.2 .3,.4,.5	13.46	.922	.54		R_T, C_T
Yokoo	85	FA -FA	.1 -.42	G/L=0,.04 .087,.347	5.77	2.17	.545		C_R
Eggers Mathematical	15	S	.316,0.5	S/L= ∞ .125-.75	16.00	1.25	.6		$R_T/R_{T\infty}$
Eggers Mathematical	15	S	.316,0.5	S/L= ∞ .125-.75	8.00	2.5	.6		$R_T/R_{T\infty}$
Ozawa	58	A	.6 -.97						BHP
Miyata (HC-200A)	50	A	F∇=.2-3.	S/L=.162	21.47	.67			C_T, Trim Sinka.
Miyata (HC-200B)	50	A	F∇=.2-3.	S/L=.21	21.96	.425			C_T, Trim Sinka.
Michell	47	S	.26-.39	S/L= ∞ .246,.277 .339	8.125	2.0	.528	.572	EHP

Author & Hull	Ref	Sym	Fn	S	L/B	B/T	C_B	C_P	Type
Pien	60	A	.15-.34	S/L= ∞ .076,.117 .171,.244	8.45	2.661	.545	.568	C_R
Calkins HYCAT	6	A	.2 -1.7	S/L=.37					R_T/∇ Trim Sinka.
Corrlett Castalia	13	A	.14-0.24	G/L=.1875	17.1	2.429	.655	.69	EHP
Corrlett Waterbus	13	S	.25-0.45	W/L=∞,.14 .162,.182	12.4	1.81	.375	.678	EHP
Corrlett River Cargo	13	A	.16- .24	W/L=.214	11.67	4.00	.716		EHP
General Dyna. MIT-26	88	S	.1 - .39	S/L= ∞ .206,.238 .27,.302	12.6	1.923		.436	Rt
General Dyna. MIT-30	88	S	.1 - .39	S/L= ∞ .206,.238 .27,.302	12.6	1.667		.536	Rt
General Dyna. MIT-34	88	S	.1 - .39	S/L= ∞ .206,.238 .27,.302	12.6	1.47		.647	Rt
Rutgersson	64	S	.38,.51, .64,.76	G/L= ∞ .048,.095 .143,.19	10.5	2.105	.6	.	EHP/ EHP∞
Rutgersson	64	A	.38,.51, .64,.76	G/L= ∞ .048,.095 .143,.19	10.5	2.105	.6		EHP/ EHP∞
Ozawa et al	59	FA	.2 - 1.2	G/L=.133, .185,.290 .395	9.18	2.32	.461	.57	C_T Trim Sinka.
Sherman	70	FA		G/L=0.0, .166,.333	6.0	1.067			R_T/∇

APPENDIX B: DERIVATION OF COMPONENTS OF TOTAL RESISTANCE FROM CONSIDERATIONS OF MOMENTUM CHANGES

The resistance components of a model can be derived from considerations of momentum changes.

The cartesian coordinate system (x,y,z) has its origin on the free surface at the model centre, and moves with the model. X-axis, y-axis and z-axis are positive in the direction of motion, starboard and upwards respectively (Fig.3Ø). u, v, w are corresponding perturbation velocities in the directions of x, y, z.

It is assumed that flow about model, wake, and wave pattern are steady and symmetrical relative to the towing tank centerline during a run, and the model is free only to sink and trim.

A and B are two planes perpendicular to the x-axis such that A is sufficiently upstream i.e. in undisturbed water, and B is sufficiently far downstream i.e. outside of nonlinear disturbance of the model.

Planes A and B, the tank walls, tank floor, and model surface are taken as a control box. There are two conditions to be applied to the motion.

Condition 1: Conservation of Mass
Flow through A and B planes must be equal to each other ;

$$\int_{-W/2}^{W/2}\int_{-H}^{\emptyset} U\,dzdy = \int_{-W/2}^{W/2}\int_{-H}^{\zeta_B} (U+u)\,dzdy \qquad (B.1)$$

Condition 2 : Conservation of Momentum

The total force on the control surface must be equal to the momentum flux on the control surface. By neglecting the frictional forces on the tank walls and bottom.

$$M_B - M_A = F_A - F_B - R_T \tag{B.2}$$

Momentum in plane A :

$$M_A = \rho \int_{-W/2}^{W/2} \int_{-H}^{\emptyset} U^2 \, dzdy = U \rho \int_{-W/2}^{W/2} \int_{-H}^{\emptyset} U \, dzdy \tag{B.3}$$

by substituting (B.1) into (B.3)

$$M_A = \rho \int_{-W/2}^{W/2} \int_{-H}^{y_B} U \, (U+u) \, dzdy \tag{B.4}$$

Momentum in plane B :

$$M_B = \rho \int_{-W/2}^{W/2} \int_{-H}^{y_B} (U+u)^2 \, dzdy = \rho \int_{-W/2}^{W/2} \int_{-H}^{y_B} (U^2+2Uu+u^2) \, dzdy \tag{B.5}$$

F_A and F_B are the forces which are caused by pressures on the A and B planes respectively.

Assuming flow is in streamlined form, Bernoulli equation between A and B can be set as

$$\rho/2 \, U^2 = P_A + \rho/2 \, U^2 + \rho g z \tag{B.6}$$

$$= P_B + \rho/2 \, [(U+u)^2+v^2+w^2] + \rho g z + \Delta P \tag{B.7}$$

where ΔP is head loss between A and B

using (B.6)

$$F_A = \int_{-W/2}^{W/2} \int_{-H}^{\emptyset} P_A \, dzdy = -\rho \int_{-W/2}^{W/2} \int_{-H}^{\emptyset} gz \, dzdy$$

$$= \rho/2 \; gWH^2 \tag{B.8}$$

$$F_B = \int_{-W/2}^{W/2} \int_{-H}^{y_B} P_B \, dzdy = -\int_{-W/2}^{W/2} \int_{-H}^{y_B} [-\rho gz - \rho/2 \; (2Uu+u^2+v^2+w^2) - \Delta P] dzdy \tag{B.9}$$

substituting (B.4),(B.5),(B.8),(B.9) into (B.2)

$$\rho \int_{-W/2}^{W/2} \int_{-H}^{y_B} (U^2+2Uu+u^2) \, dzdy - \rho \int_{-W/2}^{W/2} \int_{-H}^{y_B} U \, (U+u) \, dzdy = -\rho/2 \; gWH^2$$

$$- R_T + \int_{-W/2}^{W/2} \int_{-H}^{y_B} [\rho gz + \rho/2 \; (2Uu+u^2+v^2+w^2) + \Delta P] \, dzdy \tag{B.10}$$

by arranging terms

$$R_T = \rho g/2 \int_{-W/2}^{W/2} y_B^{\,2} \, dy + \rho/2 \int_{-W/2}^{W/2} \int_{-H}^{y_B} (v^2+w^2-u^2) \, dzdy + \int_{-W/2}^{W/2} \int_{-H}^{y_B} \Delta P dzdy \tag{B.11}$$

The second integral includes the term u which is affected by the wake. By introducing a fictious velocity u

at plane B which would be the velocity if viscous head losses were neglected, i.e.

$$P_B + \rho g z_B + \rho/2\,[(U+u)^2+v^2+w^2] + \Delta P = P_B + \rho g z_B + \rho/2\,[(U+\underline{u})^2+v^2+w^2] \tag{B.12}$$

by substituting $u^2 = \underline{u}^2 + (u^2-\underline{u}^2)$

$$R_T = \int_{-W/2}^{W/2}\int_{-H}^{y_B} \Delta P\, dz dy + \rho/2 \int_{-W/2}^{W/2}\int_{-H}^{y_B} (\underline{u}^2-u^2)\, dz dy$$

$$+ \rho g/2 \int_{-W/2}^{W/2} y_B^2\, dy + \rho/2 \int_{-W/2}^{W/2}\int_{-H}^{y_B} (v^2+w^2-\underline{u}^2)\, dz dy \tag{B.13}$$

The equation (B.13) represents the total resistance as a summation of two groups. The first two terms are viscous resistance terms due to head loss and kinetic energy loss. These terms can be determined by a viscous wake traverse experiment. It must be noted that these integrals are significant only in the wake region and are zero outside the wake. The last two terms represent the wave resistance due to the potential energy loss because of the waves, and the kinetic energy loss due to perturbation velocities. The latter component would be very tedious to measure as all velocities below the free surface have to be measured. Therefore an alternative method is used :

By introducing $\underline{u}$, $\underline{v}$, $\underline{w}$ as wave orbital velocities obtained from the measured wave pattern at B and employing linearised wave theory.

By substituting

$$u^2 = \underline{u}^2 + (u^2 - \underline{u}^2)$$
$$v^2 = \underline{v}^2 + (v^2 - \underline{v}^2)$$
$$w^2 = \underline{w}^2 + (w^2 - \underline{w}^2)$$

$$R_t = \int_{-W/2}^{W/2} \int_{-H}^{\zeta_B} \Delta P \, dzdy + \rho/2 \int_{-W/2}^{W/2} \int_{-H}^{\zeta_B} (u^2 - u^2) \, dzdy$$

$$+ \rho g/2 \int_{-W/2}^{W/2} \zeta_B^2 \, dy + \rho/2 \int_{-W/2}^{W/2} \int_{-H}^{\zeta_B} (\underline{v}^2 + \underline{w}^2 - \underline{u}^2) \, dzdy$$

$$+ \rho/2 \int_{-W/2}^{W/2} \int_{-H}^{\zeta_B} [(v^2 - \underline{v}^2) + (w^2 - \underline{w}^2) - (u^2 - \underline{u}^2)] \, dzdy \qquad \text{(B.14)}$$

The first line in the resistance equation (B.14) represents the viscous resistance. The second line is the wave resistance which can be defined from an analysis of the model wave pattern. The velocity components $\underline{u}, \underline{v}, \underline{w}$ are determined from this wave pattern by utilising linear wave theory. The third line is the induced drag. Unlike the first two it can not be easily measured unless all the velocity components are measured in plane B. It may be neglected for most ship types.

APPENDIX C : DERIVATION OF VELOCITY POTENTIAL OF A SOURCE IN A SHALLOW WATER CANAL

The equation (4.16)

$$\phi = -\mu J_1 + 4/\pi\, \mu J_2 + 4\mu J_3 \tag{C.1}$$

$$J_1 = \sum_{n=-\infty}^{\infty} \left[\frac{1}{r_1'} + \frac{1}{r_1''} + \frac{1}{r_2'} + \frac{1}{r_2''}\right] \tag{C.2}$$

where

$$r_1'^2 = (x-x_o)^2+(y-y_o')^2+(z-z_o)^2$$

$$r_1''^2 = (x-x_o)^2+(y-y_o'')^2+(z-z_o)^2$$

$$r_2'^2 = (x-x_o)^2+(y-y_o')^2+(z+(2H+z_o))^2$$

$$r_2''^2 = (x-x_o)^2+(y-y_o'')^2+(z+(2H+z_o))^2$$

$$J_2 = \sum_{n=-\infty}^{\infty}\{ \int_0^{\infty} \int_0^{\pi/2} F(\Theta,k,z)\ \mathrm{Cos}(kx\mathrm{Cos}\Theta)\ \mathrm{Cos}(k[y-y_o+2nW]\mathrm{Sin}\Theta)\ dk\ d\Theta$$

$$+ \int_0^{\infty} \int_0^{\pi/2} F(\Theta,k,z)\ \mathrm{Cos}(kx\mathrm{Cos}\Theta)\ \mathrm{Cos}(k[y+y_o+W+2nW]\mathrm{Sin}\Theta)\ dk d\Theta\} \tag{C.3}$$

$$= \mathrm{Re}\{ \sum_{n=-\infty}^{\infty} \int_0^{\infty} dk \int_0^{\pi/2} F(\Theta,k,z)\ \mathrm{Cos}(kx\mathrm{Cos}\Theta)$$

$$[e^{ik[y-y_o+2nW]\mathrm{Sin}\Theta} + e^{ik[y+y_o+W+2nW]\mathrm{Sin}\Theta}]\ d\Theta\ \} \tag{C.4}$$

$$=\mathrm{Re}\left\{\int_{\emptyset}^{\infty} dk \sum_{n=-\infty}^{\infty} \int_{\emptyset}^{\pi/2} [F_1(\Theta,k,x,y,z)+ F_2(\Theta,k,x,y,z)]\, e^{ik2nW\mathrm{Sin}\Theta}\, d\Theta\right\} \tag{C.5}$$

where

$$F_1(\Theta,k,x,y,z)=F(\Theta,k,z)\ \mathrm{Cos}(kx\mathrm{Cos}\Theta)\ e^{ik[y-y_o]\mathrm{Sin}\Theta}$$

$$F_2(\Theta,k,x,y,z)=F(\Theta,k,z)\ \mathrm{Cos}(kx\mathrm{Cos}\Theta)\ e^{ik[y+y_o+W]\mathrm{Sin}\Theta} \tag{C.6}$$

By using Poisson summation formula (Appendix E)

$$J_2=\mathrm{Re}\left\{\int_{\emptyset}^{\infty} dk\ 2\pi \sum_{m=\emptyset}^{\infty}{}' \left[\frac{F_1(\Theta_m,k,x,y,z)+ F_2(\Theta_m,k,x,y,z)}{f'(\Theta_m)}\right]\right\} \tag{C.7}$$

where

Σ' denotes that $m=\emptyset$ is halved

$$f(\Theta_m)=2kW\mathrm{Sin}\Theta_m=2m\pi$$

$$k\mathrm{Sin}\Theta_m = m\pi/W \tag{C.8}$$

$$f'(\Theta)=2kW\mathrm{Cos}\Theta$$

$$J_2=\mathrm{Re}\left\{\int_{\emptyset}^{\infty} dk\ \frac{\pi}{W} \sum_{m=\emptyset}^{\infty}{}' \frac{F(\Theta_m,k,z)}{k\ \mathrm{Cos}\Theta_m}\ \mathrm{Cos}(kx\mathrm{Cos}\Theta_m)\right.$$

$$\left. e^{iky\mathrm{Sin}\Theta_m}\left[e^{-iky_o\mathrm{Sin}\Theta_m}+(-1)^m\, e^{iky_o\mathrm{Sin}\Theta_m}\right]\right\} \tag{C.9}$$

$$J_2 = \frac{2\pi}{W} \int_{\emptyset}^{\infty} dk \sum_{m=\emptyset}^{\infty}{}' \frac{F(\Theta_m, k, z)}{k \cos\Theta_m} \cos(kx\cos\Theta_m) \begin{matrix} \cos(ky\sin\Theta_m)\ \cos(ky_o \sin\Theta_m) \\ \sin(ky\sin\Theta_m)\ \sin(ky_o \sin\Theta_m) \end{matrix} \tag{C.10}$$

where Cos terms applies for even m and Sin terms applies for odd m

by substituting the other terms and $x = x - x_o$

$$J_2 = \frac{2\pi}{W} \int_{\emptyset}^{\infty} dk \sum_{m=\emptyset}^{\infty}{}' \frac{e^{-kH} \cosh(k(H+z_o))\ (k + K_o \sec^2\Theta_m)}{\cosh(kH)\ (k - K_o \sec^2\Theta_m \tanh(kH))} \cosh(k(z+H))$$

$$\frac{\cos(k(x-x_o)\cos\Theta_m)}{k \cos\Theta_m} \begin{matrix} \cos(ky\sin\Theta_m)\ \cos(ky_o \sin\Theta_m) \\ \sin(ky\sin\Theta_m)\ \sin(ky_o \sin\Theta_m) \end{matrix} \tag{C.11}$$

And the last term

$$J_3 = \sum_{n=-\infty}^{\infty} \{ \int_{\emptyset}^{\pi/2} G(\Theta, K, z) \sin(Kx\cos\Theta) \cos(K[y - y_o + 2nW]\sin\Theta)\, d\Theta$$

$$+ \int_{\emptyset}^{\pi/2} G(\Theta, K, z) \sin(Kx\cos\Theta) \cos(K[y + y_o + W + 2nW]\sin\Theta)\, d\Theta \}$$

(C.12)

$$= \mathrm{Re}\{ \sum_{n=-\infty}^{\infty} \int_{\emptyset}^{\pi/2} G(\Theta, K, z) \sin(Kx\cos\Theta)$$

$$[e^{iK[y - y_o + 2nW]\sin\Theta} + e^{iK[y + y_o + W + 2nW]\sin\Theta}]\, d\Theta \} \tag{C.13}$$

$$= \mathrm{Re}\left[\sum_{n=-\infty}^{\infty} \int_{\emptyset}^{\pi/2} [G_1(\theta,K,x,y,z) + G_2(\theta,K,x,y,z)]\, e^{iK2nW\mathrm{Sin}\theta}\, d\theta\right] \tag{C.14}$$

where

$$G_1(\theta,K,x,y,z) = G(\theta,K,z)\ \mathrm{Sin}(Kx\mathrm{Cos}\theta)\ e^{iK[y-y_o]\mathrm{Sin}\theta}$$

$$G_2(\theta,K,x,y,z) = G(\theta,K,z)\ \mathrm{Sin}(Kx\mathrm{Cos}\theta)\ e^{iK[y+y_o+W]\mathrm{Sin}\theta} \tag{C.15}$$

By using Poisson integration formula (Appendix E)

$$J_3 = \mathrm{Re}\left[2\pi \sum_{m=\emptyset}^{\infty}{}' \left[\frac{F_1(\theta_m,K_m,x,y,z) + F_2(\theta_m,K_m,x,y,z)}{f'(\theta_m)}\right]\right] \tag{C.16}$$

where $f(\theta_m) = 2K_m W\mathrm{Sin}\theta_m = 2m\pi$

$$K_m \mathrm{Sin}\theta_m = m\pi/W \tag{C.17}$$

as $\emptyset \le \theta \le \pi/2 \quad \emptyset \le m \le \infty$

$$f'(\theta) = 2KW\mathrm{Cos}\theta + 2W\mathrm{Sin}\theta \frac{dK}{d\theta}$$

at the same time $K - K_o\, \mathrm{Sec}^2\theta\, \mathrm{Tanh}(KH) = \emptyset$ from equation (4.12)

$$\frac{dK}{d\theta} - K_o H \mathrm{Sec}^2\theta\, \mathrm{Sech}^2(KH) \frac{dK}{d\theta} - 2K_o \mathrm{Sec}^2\theta\, \mathrm{Tan}\theta\, \mathrm{Tanh}(KH) = \emptyset$$

$$\frac{dK}{d\Theta} = \frac{2K_o \ Sec^2\Theta \ Tan\Theta \ Tanh(KH)}{1-K_o H \ Sec^2\Theta \ Sech^2(KH)} = \frac{2K \ Tan\Theta}{1-K_o H \ Sec^2\Theta \ Sech^2(KH)}$$

Hence

$$f'(\Theta)=2WK \ Sec\Theta \ \frac{Cos^2\Theta \ (1-K_o H \ Sec^2\Theta \ Sech^2(KH))+2 \ Sin^2\Theta}{1-K_o H \ Sec^2\Theta \ Sech^2(KH)}$$

$$f'(\Theta)=2WK \ Sec\Theta \ \frac{1-K_o H \ Sech^2(KH)+Sin^2\Theta}{1-K_o H \ Sec^2\Theta \ Sech^2(KH)} \qquad (C.18)$$

$$J_3 = \frac{\pi}{W} \sum_{m=\emptyset}^{\infty}{}' \ [G_1(\Theta_m, K_m, x, y, z)+G_2(\Theta_m, K_m, x, y, z)] \ * \ \frac{1-K_o H \ Sec^2\Theta_m Sech^2(K_m H)}{(K_m Sec\Theta_m)\ (1-K_o H \ Sech^2(K_m H)+Sin^2\Theta_m)} \qquad (C.19)$$

$$J_3 = Re\{\frac{\pi}{W} \sum_{m=\emptyset}^{\infty}{}' \frac{G(\Theta_m, K_m, z)}{K_m Sec\Theta_m} \ \frac{1-K_o H \ Sec^2\Theta_m \ Sech^2(K_m H)}{1-K_o H \ Sech^2(K_m H)+Sin^2\Theta_m} \ Sin(K_m x Cos\Theta_m) \ e^{iK_m y Sin\Theta_m} \ [e^{-iK_m Sin\Theta_m} + (-1)^m \ e^{iK_m y_o Sin\Theta_m}] \} \qquad (C.2\emptyset)$$

$$J_3 = \frac{2\pi}{W} \sum_{m=\emptyset}^{\infty}{}' \frac{G(\Theta_m, K_m, z)}{K_m Sec\Theta_m} \ \frac{1-K_o H \ Sec^2\Theta_m \ Sech^2(K_m H)}{1-K_o H \ Sech^2(K_m H)+Sin^2\Theta_m} \ Sin(K_m x Cos\Theta_m) \ \begin{matrix} Cos(K_m y Sin\Theta_m) & Cos(K_m y_o Sin\Theta_m) \\ Sin(K_m y Sin\Theta_m) & Sin(K_m y_o Sin\Theta_m) \end{matrix} \qquad (C.21)$$

where Cos terms applies for even m and Sin terms applies for odd m

by substituting the other terms and $x=x-x_o$

$$J_3 = \frac{2\pi}{W} \sum_{m=0}^{\infty}{}' \frac{e^{-K_m H}\ \mathrm{Cosh}(K_m(H+z_o))\ (K_o + K_m \mathrm{Cos}^2\Theta_m)}{\mathrm{Cosh}(K_m H)\ (1 - K_o H\ \mathrm{Sech}^2(K_m H) + \mathrm{Sin}^2\Theta_m)} \mathrm{Cosh}(K_m(z+H))$$

$$\frac{\mathrm{Sin}(K_m(x-x_o)\mathrm{Cos}\Theta_m)}{K_m \mathrm{Cos}\Theta_m} \quad \begin{matrix} \mathrm{Cos}(K_m y \mathrm{Sin}\Theta_m) \\ \mathrm{Sin}(K_m y \mathrm{Sin}\Theta_m) \end{matrix} \quad \begin{matrix} \mathrm{Cos}(K_m y_o \mathrm{Sin}\Theta_m) \\ \mathrm{Sin}(K_m y_o \mathrm{Sin}\Theta_m) \end{matrix} \qquad \text{(C.22)}$$

APPENDIX D : DERIVATION OF FAR FIELD WAVE SYSTEM

From equation (4.20)

$$\phi_{FF} = [-\mu \lim_{x\to-\infty} J_1 + 4\mu/\pi \lim_{x\to-\infty} J_2 + 4\mu \lim_{x\to-\infty} J_3] \tag{D.1}$$

By evaluating each term separately

$$\lim_{x\to-\infty} J_1 = \lim_{x\to-\infty} \{ \sum_{n=-\infty}^{\infty} [\frac{1}{r_1'} + \frac{1}{r_1''} + \frac{1}{r_2'} + \frac{1}{r_2''}] \} = \emptyset \tag{D.2}$$

$$\lim_{x\to-\infty} J_2 = \lim_{x\to-\infty} \{ \frac{2\pi}{W} \int_{\emptyset}^{\infty} \sum_{m=\emptyset}^{\infty}{}' \frac{e^{-kH} \cosh(k(H+z_o)) (k+K_o \sec^2\theta_m)}{(k-K_o \sec^2\theta_m \tanh(kH))} \frac{1}{k\cos\theta_m}$$

$$\frac{\cosh(k(z+H)}{\cosh(kH)} \cos(k(x-x_o)\cos\theta_m) \begin{matrix} \cos(ky\sin\theta_m)\ \cos(ky_o\sin\theta_m) \\ \sin(ky\sin\theta_m)\ \sin(ky_o\sin\theta_m) \end{matrix} \} \tag{D.3}$$

now using equality

$$I = \lim_{|x|\to\infty} \int_a^b \frac{D(k)}{k-K} e^{id(k)x} dk = \pm \pi i D(K) e^{id(K)x}$$

where - for $x<\emptyset$, + for $x>\emptyset$ (D.4)

But first defining a function

$$g(k) = k - K_o \sec^2\theta_m \tanh(kH) = \emptyset \tag{D.5}$$

$$g'(K) = 1 - K_o H \sec^2\theta_m \operatorname{sech}^2(KH) - K_o \tanh(kH) \frac{d(\sec^2\theta_m)}{dk}$$

Using equation (C.8) $\sin\theta_m = m\pi/Wk$

$$\frac{d(\mathrm{Sec}^2\Theta_m)}{dk} = -2\ \mathrm{Tan}^2\Theta_m\ \mathrm{Sec}^2\Theta_m\ /K \qquad (D.6)$$

and substituting this result in

$$\begin{aligned} g(K) &= g'(K)\ (k-K) \\ &= (1-K_o H\mathrm{Sec}^2\Theta_m \mathrm{Sech}^2(KH)+2K_o \mathrm{Tan}^2\Theta_m \mathrm{Sec}^2\Theta_m \mathrm{Tanh}(KH)/K)\ (k-K) \\ &= \mathrm{Sec}^2\Theta_m\ (1-K_o H\mathrm{Sech}^2(KH)+\mathrm{Sin}^2\Theta_m)\ (k-K)\ \text{as}\ k\to K \end{aligned} \qquad (D.7)$$

If equations (C.8) and (D.7) are combined $K=K_m$ can be determined from

$$\begin{aligned} &K_m - K_o\,\mathrm{Sec}^2\Theta_m \mathrm{Tanh}(K_m H)=\emptyset \\ &K_m \mathrm{Sin}\Theta_m = m\pi/W \end{aligned} \qquad (D.8)$$

by substituting (D.7) into J_2 and by defining

$$D(K_m) = \frac{e^{-KH}\ \mathrm{Cosh}(K_m(H+z_o))\ (K_o+K_m\mathrm{Cos}^2\Theta_m)}{(1-K_o H\mathrm{Sech}^2(K_m H)+\mathrm{Sin}^2\Theta_m)}\ \frac{1}{K_m\mathrm{Cos}\Theta_m}$$

$$\frac{\mathrm{Cosh}(k(z+H)}{\mathrm{Cosh}(kH)}\quad \begin{matrix}\mathrm{Cos}(K_m y \mathrm{Sin}\Theta_m) \\ \mathrm{Sin}(K_m y \mathrm{Sin}\Theta_m)\end{matrix}\quad \begin{matrix}\mathrm{Cos}(K_m y_o \mathrm{Sin}\Theta_m) \\ \mathrm{Sin}(K_m y_o \mathrm{Sin}\Theta_m)\end{matrix} \qquad (D.9)$$

and $d(K_m)=K_m\mathrm{Cos}\Theta_m$

$$\begin{aligned} J_2 &= \frac{2\pi}{W} \sum_{m=\emptyset}^{\infty}{}' \{\ \mathrm{Real}(I)\ \} \\ &= \frac{2\pi}{W} \sum_{m=\emptyset}^{\infty}{}' \{\ \pi D(K_m)\ \mathrm{Cos}(K_m(x-x_o)\mathrm{Cos}\Theta_m)\ \} \end{aligned} \qquad (D.10)$$

$$\lim_{x\to-\infty} J_2 = \frac{2\pi^2}{W} \sum_{m=\emptyset}^{\infty}{}' \frac{e^{-K_m H}\,\mathrm{Cosh}(K_m(H+z_o))\,(K_o+K_m\mathrm{Cos}^2\Theta_m)}{(1-K_o H\mathrm{Sech}^2(K_m H)+\mathrm{Sin}^2\Theta_m)} \frac{1}{K_m\mathrm{Cos}\Theta_m}$$

$$\frac{\mathrm{Cosh}(k(z+H)}{\mathrm{Cosh}(kH)} \mathrm{Sin}(K_m(x-x_o)\mathrm{Cos}\Theta_m) \begin{matrix}\mathrm{Cos}(K_m y \mathrm{Sin}\Theta_m) \\ \mathrm{Sin}(K_m y \mathrm{Sin}\Theta_m)\end{matrix} \begin{matrix}\mathrm{Cos}(K_m y_o \mathrm{Sin}\Theta_m) \\ \mathrm{Sin}(K_m y_o \mathrm{Sin}\Theta_m)\end{matrix}$$

$$\lim_{x\to-\infty} J_3 = \frac{2\pi}{W} \sum_{m=\emptyset}^{\infty}{}' \frac{e^{-K_m H}\,\mathrm{Cosh}(K_m(H+z_o))\,(K_o+K_m\mathrm{Cos}^2\Theta_m)}{(1-K_o H\mathrm{Sech}^2(K_m H)+\mathrm{Sin}^2\Theta_m)} \frac{1}{K_m\mathrm{Cos}\Theta_m}$$

$$\frac{\mathrm{Cosh}(k(z+H)}{\mathrm{Cosh}(kH)} \mathrm{Sin}(K_m(x-x_o)\mathrm{Cos}\Theta_m) \begin{matrix}\mathrm{Cos}(K_m y \mathrm{Sin}\Theta_m) \\ \mathrm{Sin}(K_m y \mathrm{Sin}\Theta_m)\end{matrix} \begin{matrix}\mathrm{Cos}(K_m y_o \mathrm{Sin}\Theta_m) \\ \mathrm{Sin}(K_m y_o \mathrm{Sin}\Theta_m)\end{matrix} \quad (D.11)$$

APPENDIX E : DERIVATION OF WAVE RESISTANCE

Wave resistance can be obtained from (3.10)

$$R_w = 1/2\ \rho g \int_{-W/2}^{W/2} \zeta^2\ dy + 1/2\ \rho \int_{-W/2}^{W/2} \int_{-H}^{0} (\phi_y^2 + \phi_z^2 - \phi_x^2)\ dz dy \tag{E.1}$$

where

$$\phi_{FF} = \frac{g}{U} \sum_{n=0}^{\infty}{}' \left[-\eta_n \cos(w_n x) + \xi_n \sin(w_n x)\right] \frac{1}{K_n \cos\Theta_n} * \frac{\cosh(K_n (z+H))}{\cosh(K_n H)} \cos(2n\pi y/W) \tag{E.2}$$

$$\zeta = \sum_{m=0}^{\infty} \left[\frac{\xi_m}{\alpha_m} \cos(w_m x) + \frac{\eta_m}{\beta_m} \sin(w_m x)\right] \begin{matrix} \cos(m\pi y/W) \\ \sin(m\pi y/W) \end{matrix} \tag{E.3}$$

by taking derivatives of (E.2)

$$\phi_x = \frac{g}{U} \sum_{m=0}^{\infty} \frac{\cosh(K_m (z+H))}{\cosh(K_m H)} * \left[\frac{\xi_m}{\alpha_m} \cos(w_m x) + \frac{\eta_m}{\beta_m} \sin(w_m x)\right] \begin{matrix} \cos(m\pi y/W) \\ \sin(my\pi/W) \end{matrix} \tag{E.4}$$

$$\phi_y = \frac{g}{U} \sum_{m=0}^{\infty} \frac{\cosh(K_m (z+H))}{\cosh(K_m H)} \frac{\sin(K_m \Theta_m)}{\cos(K_m \Theta_m)} * \left[\frac{-\eta_m}{-\beta_m} \cos(w_m x) + \frac{\xi_m}{\alpha_m} \sin(w_m x)\right] \begin{matrix} -\sin(m\pi y/W) \\ \cos(m\pi y/W) \end{matrix} \tag{E.5}$$

$$\phi_z = \frac{g}{U}\sum_{m=0}^{\infty} \frac{\mathrm{Sinh}(K_m(z+H))}{\mathrm{Cosh}(K_m H)} \frac{1}{\mathrm{Cos}(K_m \Theta_m)} *$$

$$\begin{bmatrix} -\eta_m \\ -\beta_m \end{bmatrix} \mathrm{Cos}(w_m x) + \begin{bmatrix} \xi_m \\ \alpha_m \end{bmatrix} \mathrm{Sin}(w_m x) \Bigg] \begin{matrix} \mathrm{Cos}(m\pi y/W) \\ \mathrm{Sin}(m\pi y/W) \end{matrix} \qquad \text{(E.6)}$$

By calculating the necessary integrals

$$\int_{-W/2}^{W/2} \zeta^2 \, dy = \sum_{m=0}^{\infty} \left[\begin{bmatrix} \xi_m \\ \alpha_m \end{bmatrix} \mathrm{Cos}(w_m x) + \begin{bmatrix} \eta_m \\ \beta_m \end{bmatrix} \mathrm{Sin}(w_m x) \right] * \int_{-W/2}^{W/2} \begin{matrix} \mathrm{Cos}^2(m\pi y/W) \\ \mathrm{Sin}^2(m\pi y/W) \end{matrix} dy$$

$$= \frac{W}{2} \sum_{m=0}^{\infty}{}^{\circ} \left[\begin{bmatrix} \xi_m \\ \alpha_m \end{bmatrix} \mathrm{Cos}(w_m x) + \begin{bmatrix} \eta_m \\ \beta_m \end{bmatrix} \mathrm{Sin}(w_m x) \right]^2 \qquad \text{(E.7)}$$

where Σ° denotes that m=0 term must be doubled

$$\int_{-W/2}^{W/2} \int_{-H}^{0} \phi_x{}^2 \, dz dy = \frac{g^2}{U^2} \sum_{m=0}^{\infty} \left[\begin{bmatrix} \xi_m \\ \alpha_m \end{bmatrix} \mathrm{Cos}(w_m x) + \begin{bmatrix} \eta_m \\ \beta_m \end{bmatrix} \mathrm{Sin}(w_m x) \right]^2 * \int_{-W/2}^{W/2} \int_{-H}^{0} \frac{\mathrm{Cosh}^2(K_m(z+H))}{\mathrm{Cosh}^2(K_m H)} \begin{matrix} \mathrm{Cos}^2(m\pi y/W) \\ \mathrm{Sin}^2(m\pi/W) \end{matrix}$$

$$= \frac{gW}{4} \sum_{m=0}^{\infty}{}^{\circ} \left[\begin{bmatrix} \xi_m \\ \alpha_m \end{bmatrix} \mathrm{Cos}(w_m x) + \begin{bmatrix} \eta_m \\ \beta_m \end{bmatrix} \mathrm{Sin}(w_m x) \right]^2 \mathrm{Cos}^2 \Theta_m \left[1 + \frac{2K_m H}{\mathrm{Sinh}(2K_m H)} \right] \qquad \text{(E.8)}$$

$$\int_{-W/2}^{W/2}\int_{-H}^{\emptyset}\phi_y{}^2\,dzdy=\frac{g^2}{U^2}\sum_{m=\emptyset}^{\infty}\left[\frac{-\eta_m}{-\beta_m}\cos(w_m x)+\frac{\digamma_m}{\alpha_m}\sin(w_m x)\right]^2 * \frac{\sin^2\Theta_m}{\cos^2\Theta_m}$$

$$\int_{-W/2}^{W/2}\int_{-H}^{\emptyset}\frac{\cosh^2(K_m(z+H))}{\cosh^2(K_m H)}\quad\begin{matrix}\sin^2(m\pi y/W)\\ \cos^2(my\pi/W)\end{matrix}$$

$$=\frac{gW}{4}\sum_{m=\emptyset}^{\infty}{}^{\circ}\left[\frac{-\eta_m}{-\beta_m}\cos(w_m x)+\frac{\digamma_m}{\alpha_m}\sin(w_m x)\right]^2\sin^2\Theta_m\left[1+\frac{2K_m H}{\sinh(2K_m H)}\right] \qquad (E.9)$$

$$\int_{-W/2}^{W/2}\int_{-H}^{\emptyset}\phi_z{}^2\,dzdy=\frac{g^2}{U^2}\sum_{m=\emptyset}^{\infty}\left[\frac{-\eta_m}{-\beta_m}\cos(w_m x)+\frac{\digamma_m}{\alpha_m}\sin(w_m x)\right]^2 * \frac{1}{\cos^2\Theta_m}$$

$$\int_{-W/2}^{W/2}\int_{-H}^{\emptyset}\frac{\sinh^2(K_m(z+H))}{\cosh^2(K_m H)}\quad\begin{matrix}\sin^2(m\pi y/W)\\ \cos^2(my\pi/W)\end{matrix}$$

$$=\frac{gW}{4}\sum_{m=\emptyset}^{\infty}{}^{\circ}\left[\frac{-\eta_m}{-\beta_m}\cos(w_m x)+\frac{\digamma_m}{\alpha_m}\sin(w_m x)\right]^2\left[1-\frac{2K_m H}{\sinh(2K_m H)}\right] \qquad (E.10)$$

And by substituting (E.3),(E.6),(E.8),(E.10) into (E.1)

$$R_w=\frac{W\rho g}{4}\left\{(\digamma_o{}^2+\eta_o{}^2)\left(1-\frac{2K_o H}{\sinh(2K_o H)}\right)+\sum_{m=1}^{\infty}\left[\frac{\digamma_m{}^2+\eta_m{}^2}{\alpha_m{}^2+\beta_m{}^2}\right]\left[1-\emptyset.5\cos^2\Theta_m\left(1+\frac{2K_m H}{\sinh(2K_m H)}\right]\right\}\right. \qquad (E.11)$$

where $\digamma,\eta$ are applied for even m, α,β are applied for odd m

APPENDIX F : POISSON SUMMATION FORMULA

$$S_N = \sum_{n=-\infty}^{\infty} \int_a^b E(\Theta)\, e^{i n f(\theta)}\, d\Theta \qquad (F.1)$$

$$= \int_a^b E(\Theta) \sum_{n=-\infty}^{\infty} e^{i n f(\theta)}\, d\Theta \qquad (F.2)$$

for which the summation formula for geometric series :

$$\sum_{n=-N}^{N-1} e^n = \frac{e^N - e^{-N}}{e - 1} \qquad (F.3)$$

By substuting the summation formula for geometric series

$$= \int_a^b F(\Theta) \frac{[e^{iNf(\theta)} - e^{-iNf(\theta)}]}{e^{if(\theta)}-1}\, d\Theta \qquad N \to \infty \qquad (F.4)$$

This integral has poles at $\Theta_m = \pm 2m\pi$ assuming there are a number of such poles in [a,b] the limit $N \to \infty$ is obtained as the sum of the pole contributions:

for $\Theta = \Theta_m + p$ by applying Taylor expansion

$$f(\Theta) = f(\Theta_m) + p\, f'(\Theta_m) + p^{2/2}\, f''(\Theta_m) \ldots \approx 2m\pi + p\, f'(\Theta_m)$$

$$e^{if(\theta)} - 1 = e^{ipf'(\theta m)} \approx ip\, f'(\Theta_m) \quad \text{as } p \to \emptyset \qquad (F.5)$$

$$S_N = \sum_m \int_{-\varepsilon}^{\varepsilon} F(\Theta_m) \frac{[e^{iNpf'(\theta m)} - e^{-iNpf'(\theta m)}]}{ip\, f'(\Theta_m)}\, dp \qquad (F.6)$$

by substituting

$u = Npf'(\Theta_m)$

$du = Nf'(\Theta_m)\, dp$

$R = N\varepsilon f'(\Theta_m)$

$$= \sum_m{}' \pm \frac{F(\Theta_m)}{if'(\Theta_m)} \int_{-R}^{R} \frac{[e^{iu} - e^{-iu}]}{u}\, du \qquad \begin{matrix} \text{as } + & f'(\Theta_m) > \emptyset \\ - & f'(\Theta_m) < \emptyset \end{matrix} \tag{F.7}$$

$$S_N = \sum_m{}' \frac{2\pi\, F(\Theta_m)}{|f'(\Theta_m)|} \tag{F.8}$$

Σ' denotes if $\Theta=a$ or $\Theta=b$ the term must be halved

APPENDIX G : DATA ACQUISITION SYSTEM

A microcomputer based data acquisition system has been developed to be used in the experiments. The system consists of CED1401, a microcomputer and peripherals such as plotter, printer and the software.

CED1401 is an intelligent peripheral with its processor and 64 kb ram in capability of

i) 16 channel analog to digital conversion with 12 bit accuracy.

ii) 4 Channel digital to analog conversion with 12 bit

iii) 4 real time clocks

iv) 16 Channel digital input-output

For the current use only ADC channels and real time clocks are utilised.

A 16 bit microcomputer is connected to drive CED1401. During the experiments a RM-NIMBUS and Compaq-286 were utilised. The software to control data acquisition , SSDAP, has been developed in Pascal and it is fully menu driven. It has been designed to be as flexible as possible to be used in all the experiments described in this thesis. The program has provided the routines for setup, calibration, data acquisition, storing, loading, printing and plotting the data. Some editing routines have also been provided such as cutting the start and end of the trace, reducing sampling frequency. Data acquisition can be started and stopped automatically by a trigger pulse or manually by a key pressing.

Three sets of experiments were conducted using this system.

A) Resistance experiments : Total resistance, sideforce, running trim and sinkage were measured using the system described in Fig. 63. Acquisition started and stopped by trigger signals. The speed was calculated from these signals

for 50 ft distance. Sampling frequency of 50 Hz to 100 Hz was used.

B) Wave pattern experiments : Four wave traces were acquired using system given in Fig.78. The acquisition started by a trigger signal as the carriage approaches, and it was stopped after a preset time passed. The signals from wave probes were edited where required. The low pass filters were set for 250 Hz. Sampling frequency was between 100 Hz and 200 Hz depending on speed.

C) Wake traverse experiments : Twelve pressure transducer signals and valve actuating signal were acquired at 50 Hz. (Fig. 103). The signals from transducers were amplified by 500 to 1000 times. The acquisition started and stopped by trigger signals for 50 ft measured distance. Additionally two more triggers were installed to actuate the valves, the valve actuating was recorded to define exact position of valve actuating.

APPENDIX H : SUMMATION OF HARMONIC FUNCTIONS

The summation of the trigonometric function from k_1 to k_2 can be done as follows ;
ts

$$\sum_{k=k_1}^{k_2} a^k = T_N = a^{k_1} + a^{k_1+1} + a^{k_1+2} \ldots\ldots\ldots + a^{k_2} \tag{H.1}$$

$$a\,T_N = a^{k_1+1} + a^{k_1+2} \ldots\ldots\ldots + a^{k_2} + a^{k_2+1} \tag{H.2}$$

Hence

$$(1-a)T_N = \frac{a^{k_2+1} - a^{k_1}}{a-1} \tag{H.3}$$

$$\sum_{k=k_1}^{k_2} \mathrm{Cos}(ck) = \tfrac{1}{2} \sum_{k=k_1}^{k_2} e^{ick} + e^{-ick}$$

$$= \tfrac{1}{2} \left[\frac{e^{ic(k_2+1)} - e^{ick_1}}{e^{ic}-1} + \frac{e^{-ic(k_2+1)} - e^{-ick_1}}{e^{-ic}-1}\right]$$

$$= \frac{\mathrm{Cos}\,[c(k_2+k_1)/2]\ \mathrm{Sin}[c(k_2-k_1+1)/2]}{\mathrm{Sin}(c/2)} \tag{H.4}$$

$$\sum_{k=k_1}^{k_2} \mathrm{Sin}(ck) = \tfrac{1}{2} \sum_{k=k_1}^{k_2} e^{ick} - e^{-ick}$$

$$= \tfrac{1}{2} \left[\frac{e^{ic(k_2+1)} - e^{ick_1}}{e^{ic}-1} - \frac{e^{-ic(k_2+1)} - e^{-ick_1}}{e^{-ic}-1}\right]$$

$$= \frac{\mathrm{Sin}\,[c(k_2+k_1)/2]\ \mathrm{Sin}[c(k_2-k_1+1)/2]}{\mathrm{sin}(c/2)} \tag{H.5}$$

MODEL	C1	C2	C2-FX	C3	C4	C5
L	1.536	1.800	1.800	1.600	1.600	1.600
L/B	6.219	10.000	10.000	7.000	9.000	11.000
B/T	2.515	1.600	1.600	2.000	2.000	2.000
$L/\nabla^{1/3}$	5.678	7.116	7.116	6.273	7.417	8.479
C_B	0.528	0.444	0.444	0.397	0.397	0.397
C_P	0.619	0.667	0.667	0.693	0.693	0.693
C_M	0.852	0.667	0.667	0.565	0.565	0.565
WS	0.471	0.482	0.482	0.434	0.338	0.276
MATERIAL	GRP	GRP	GRP	FOAM	FOAM	FOAM
HULL	ROUND BILGE	PARABOLIC	PARABOLIC	ROUND BILGE	ROUND BILGE	ROUND BILGE

Table 1 : Details of the models

MODEL	C1	C2	C2-FX	C3	C4	C5
Fn	.1-.5	.2-.95	.2-.8	.2-1.1	.2-1.1	.2-1.1
	S/L S/B	S/L S/B	S/L S/B	S/L S/B	S/L S/B	S/L S/B
	.25 1.55	.2 2.0	.2 2.0	.2 1.4	.2 1.8	.2 2.2
	.3 1.87	.3 3.0	.3 3.0	.3 2.1	.3 2.7	.3 3.3
	.4 2.49	.4 4.0	.4 4.0	.4 2.8	.4 3.6	.4 4.4
	.5 3.11	.5 5.0	.5 5.0	.5 3.5	.5 4.5	.5 5.5
	.6 3.73					
	D23456	D2345	D2345	D2345	D2345	D2345
TotRes	√√√√√√	√√√√√	√√√√√	√√√√√	√√√√√	√√√√√
SideF	√√√√√√	√√√√√	√√√√√	√√√√√	√√√√√	√√√√√
Trim		√√√√√	——	√√√√√	√√√√√	√√√√√
Sink		√√√√√	——	√√√√√	√√√√√	√√√√√
WaveP	√√√√√√	√√√√√	√√√√√	√√√√√	√√√√√	√√√√√
WakeT		√√√√		√√√√		
WaveEl		√√√√√	√√√√√			

Table 2 : Test conditions for the models

RESULTS

MODEL : C2
Fn : 0.33097
Rwp : 0.62437 N
Cwp : 0.00134
Cut Start : 0.49122 m
Cut End : 13.48537 m
Theta : 71.45804
N : 28
NO. OF PROBE: 4

n	θ_n	w_n	f_n	η_n	R_{WPn}	% R_{WPn}
0	0.000	5.072	-.000736	.000453	.00677	1.08486
1	17.693	5.323	-.002407	.000259	.02906	4.65375
2	30.090	5.861	-.004586	-.000071	.11944	19.12991
3	38.264	6.459	-.004760	-.000057	.14226	22.78514
4	43.955	7.045	-.003743	-.000440	.09549	15.29299
5	48.159	7.603	-.002352	-.000171	.03922	6.28214
6	51.410	8.131	-.001137	.000541	.01160	1.85716
7	54.016	8.631	.000263	.000812	.00547	0.87637
8	56.162	9.108	.001361	.001367	.02853	4.56926
9	57.968	9.562	.001763	.001314	.03769	6.03659
10	59.515	9.997	.002120	.000862	.04140	6.63138
11	60.859	10.415	.001303	.000457	.01524	2.44102
12	62.040	10.817	.001444	.000066	.01687	2.70160
13	63.089	11.205	.000670	-.000578	.00637	1.02096
14	64.028	11.581	-.000091	.000515	.00224	0.35943
15	64.876	11.945	-.000645	-.000332	.00434	0.69562
16	65.646	12.299	-.000931	-.000180	.00747	1.19631
17	66.350	12.642	-.000838	-.000298	.00659	1.05616
18	66.996	12.977	-.000501	.000108	.00220	0.35292
19	67.592	13.304	-.000545	.000224	.00292	0.46753
20	68.144	13.623	-.000245	-.000128	.00065	0.10369
21	68.657	13.935	-.000248	-.000163	.00075	0.11945
22	69.136	14.240	-.000115	-.000128	.00025	0.04024
23	69.584	14.538	.000089	-.000288	.00078	0.12427
24	70.004	14.831	.000144	-.000111	.00028	0.04544
25	70.399	15.118	-.000048	-.000045	.00004	0.00597
26	70.772	15.400	.000148	-.000104	.00028	0.04486
27	71.124	15.676	.000105	-.000019	.00010	0.01575
28	71.458	15.948	-.000070	-.000042	.00006	0.00925

Table 3 : Typical results for a wave pattern analysis

HULL / FN	0.25	0.35	0.50	0.70
C2-S/L:0.0	√	√	√	√
0.2		√	√	
0.3		√	√	√
0.4		√		
C3-S/L:0.0		√	√	√
0.2		√	√	
0.3		√	√	
0.4		√	√	√

Table 4 : Summary of wake traverse experiments

Transducer	Low Pressure	High Pressure
Range	± 0.2 psi	± 1 psi
Linearity	± 0.20 %	± 0.5 %
Repeatibilty	± 0.15 %	±0.5 %
Supply voltage	10 volts	12 volts
Response Time		100 ms
Output	300 mv	18 mV/psi

Table 5 : Main characteristics of the pressure transducers

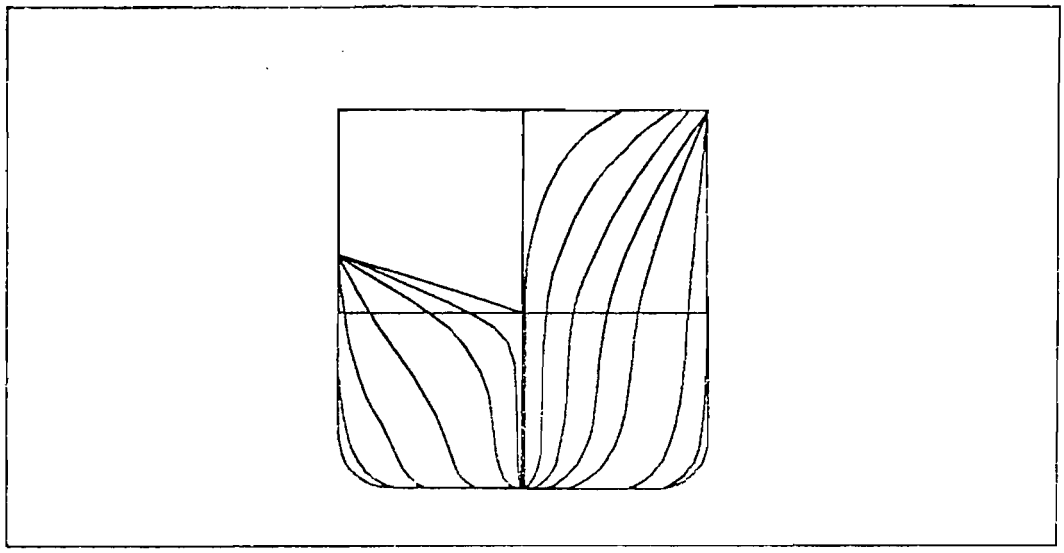

Fig. 1: Typical symmetric catamaran hull form [78]

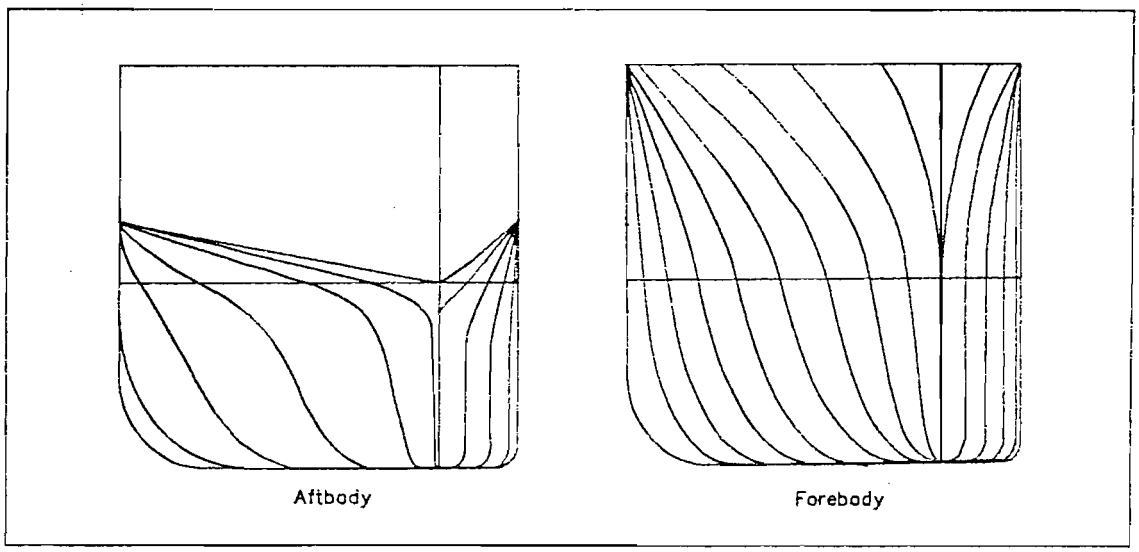

Fig. 2: Typical asymmetric catamaran hull form [78]

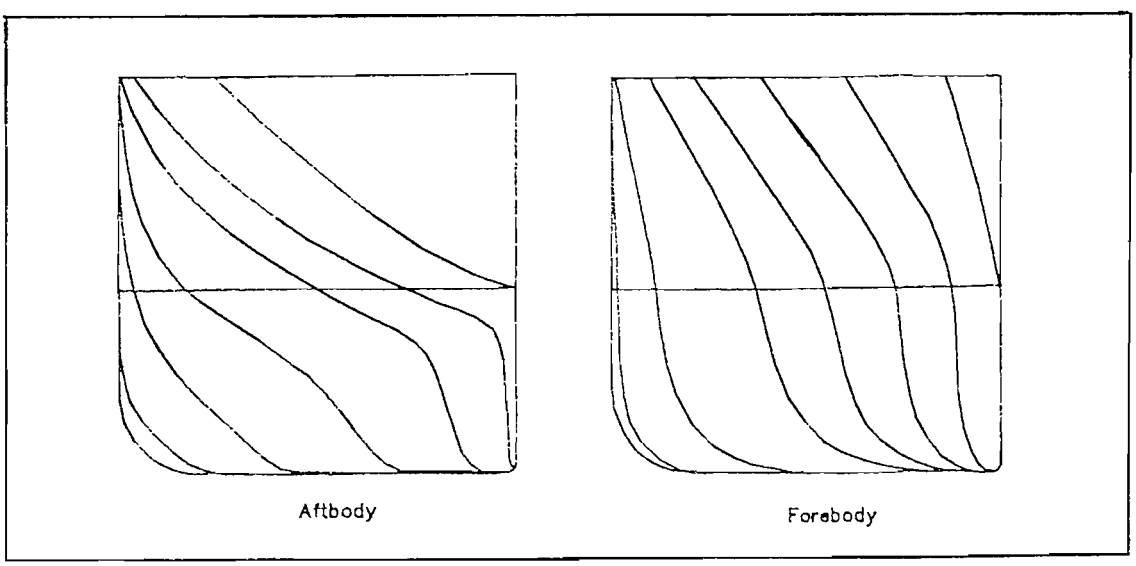

Fig. 3: Typical fully asymmetric catamaran hull form [78]

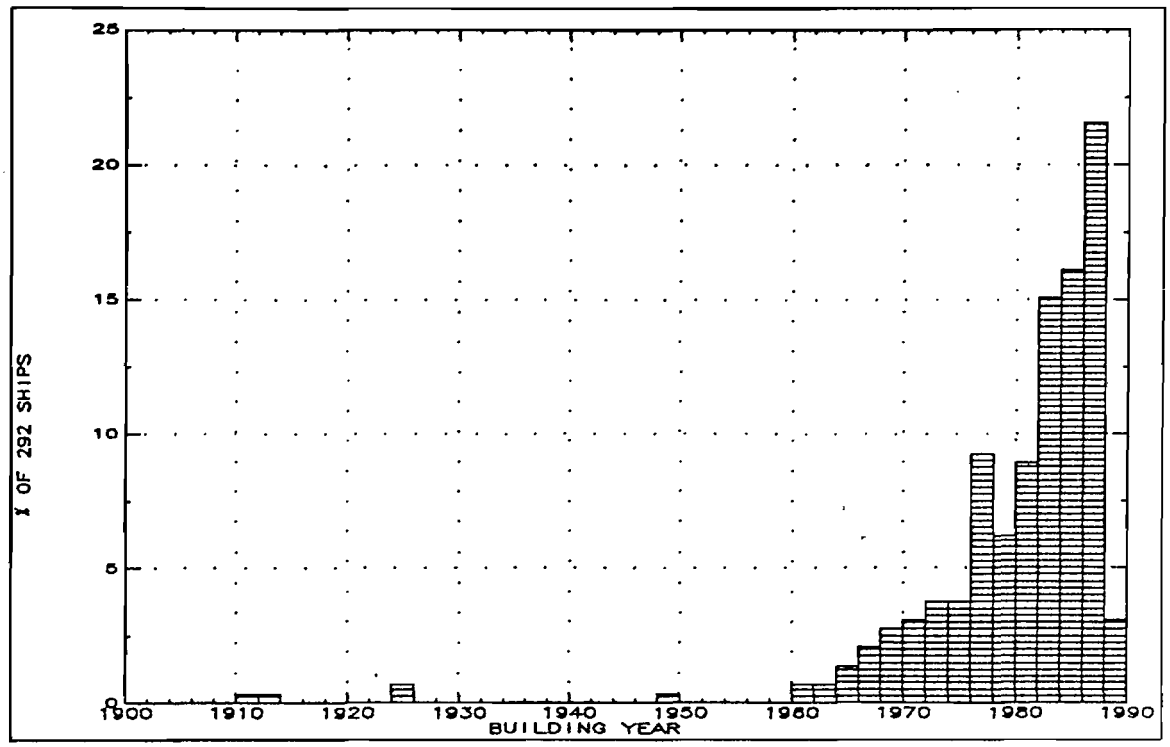

Fig.4: Survey of catamarans built since 1900

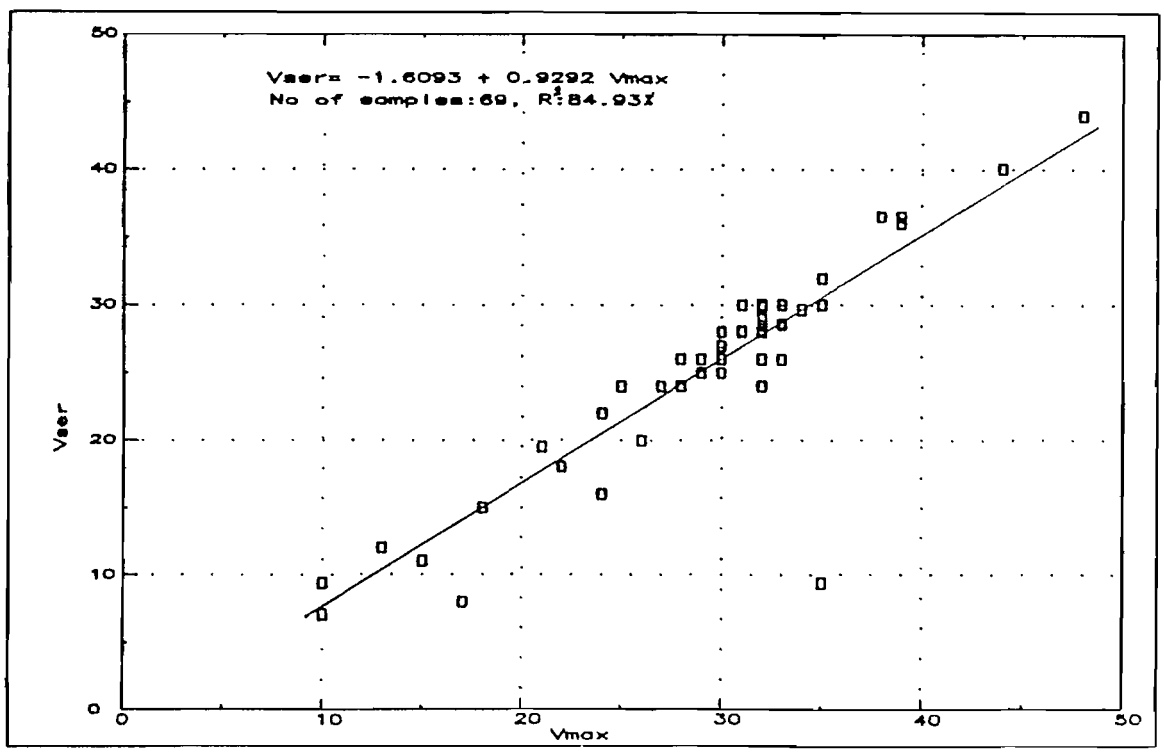

Fig.5: Regression between Vmax and Vser

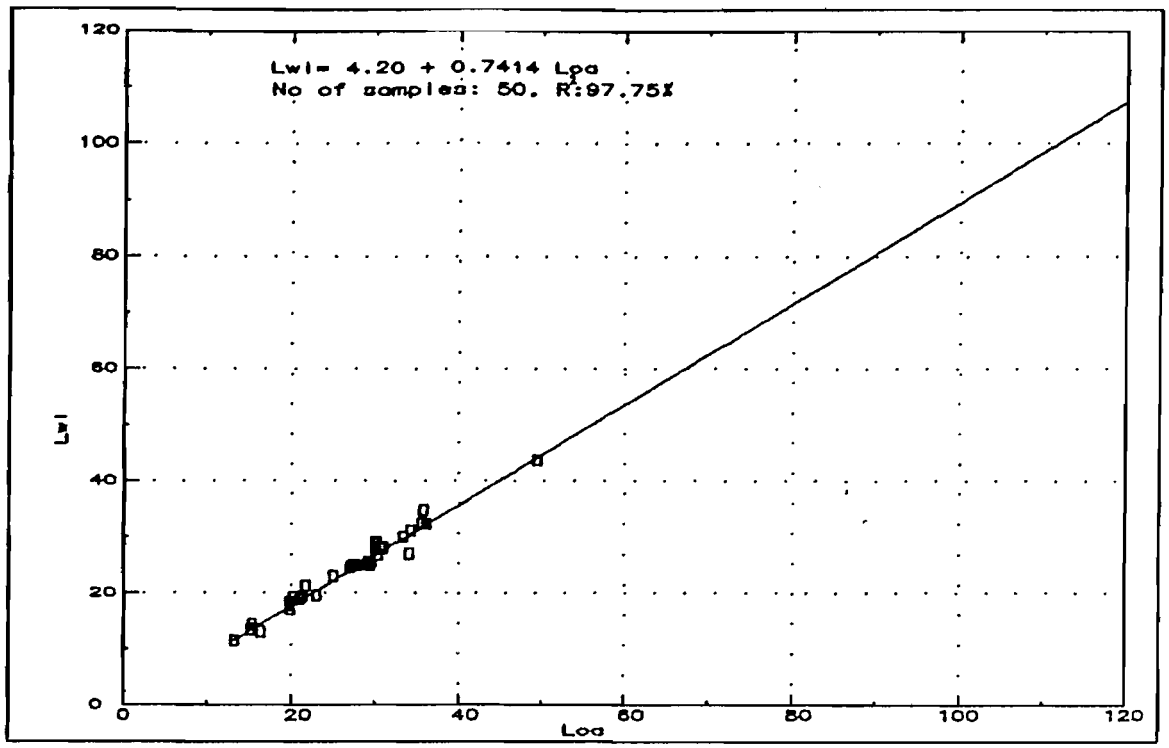

Fig.6: Regression between Loa and Lwl

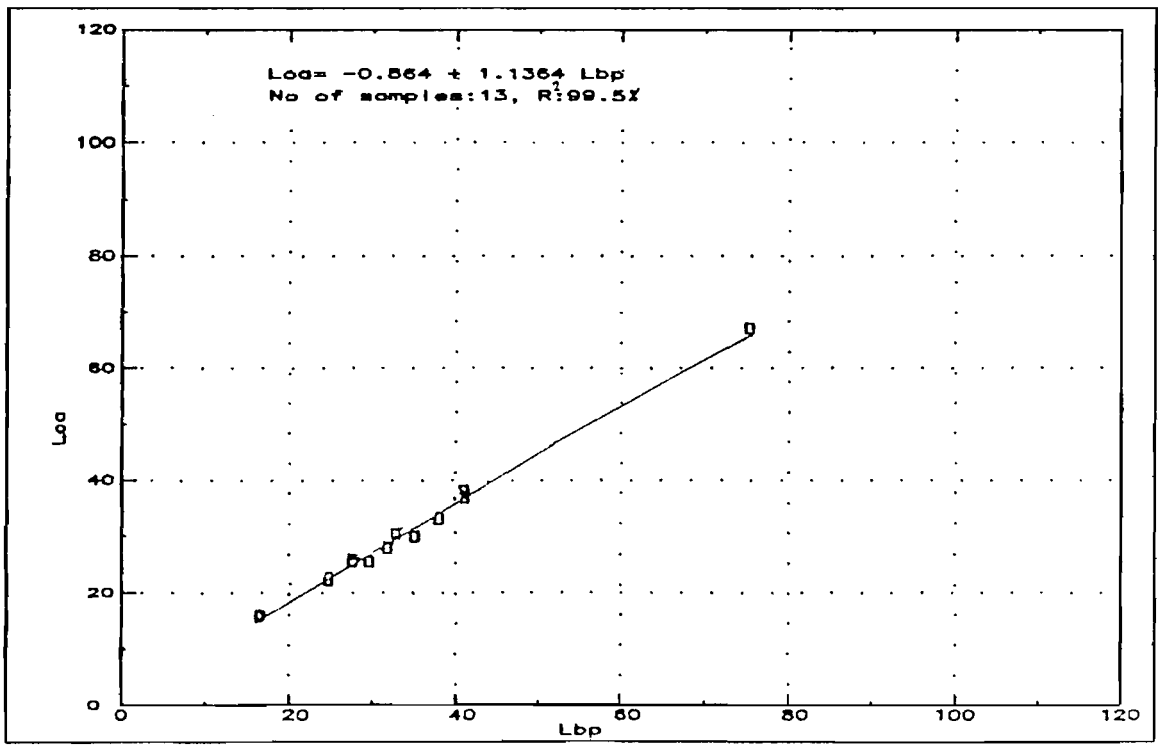

Fig.7: Regression between Lbp and Loa

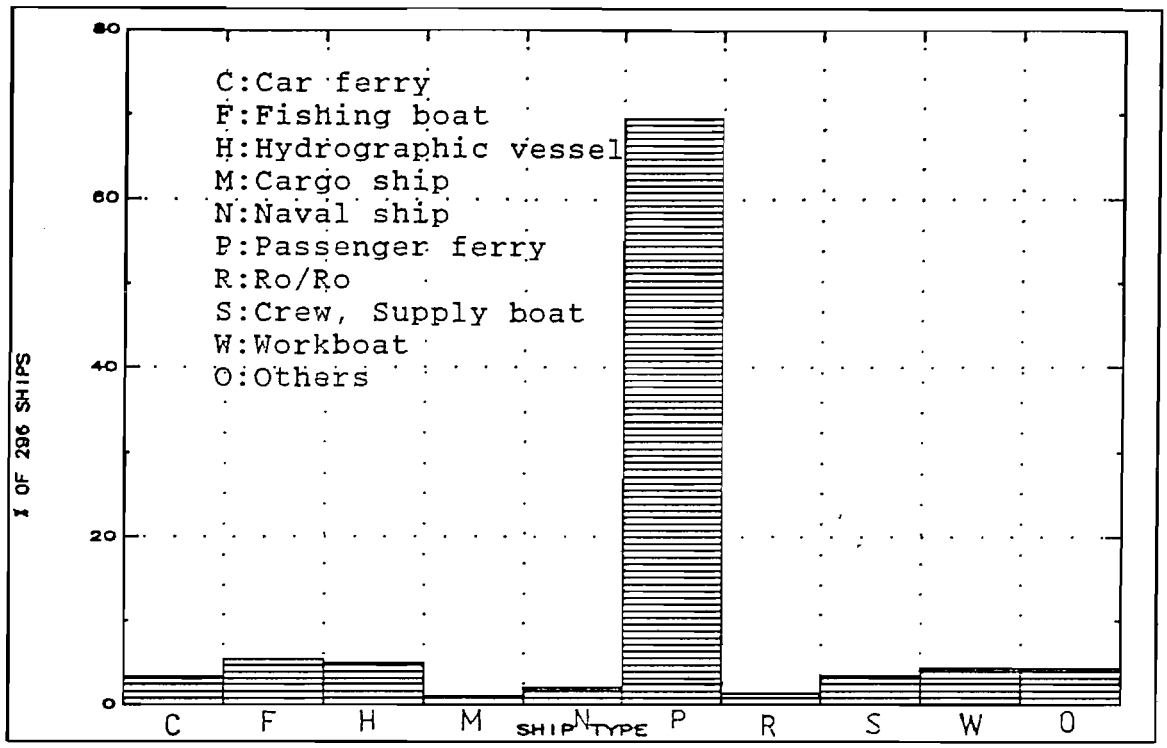

Fig.8: Survey of ship type

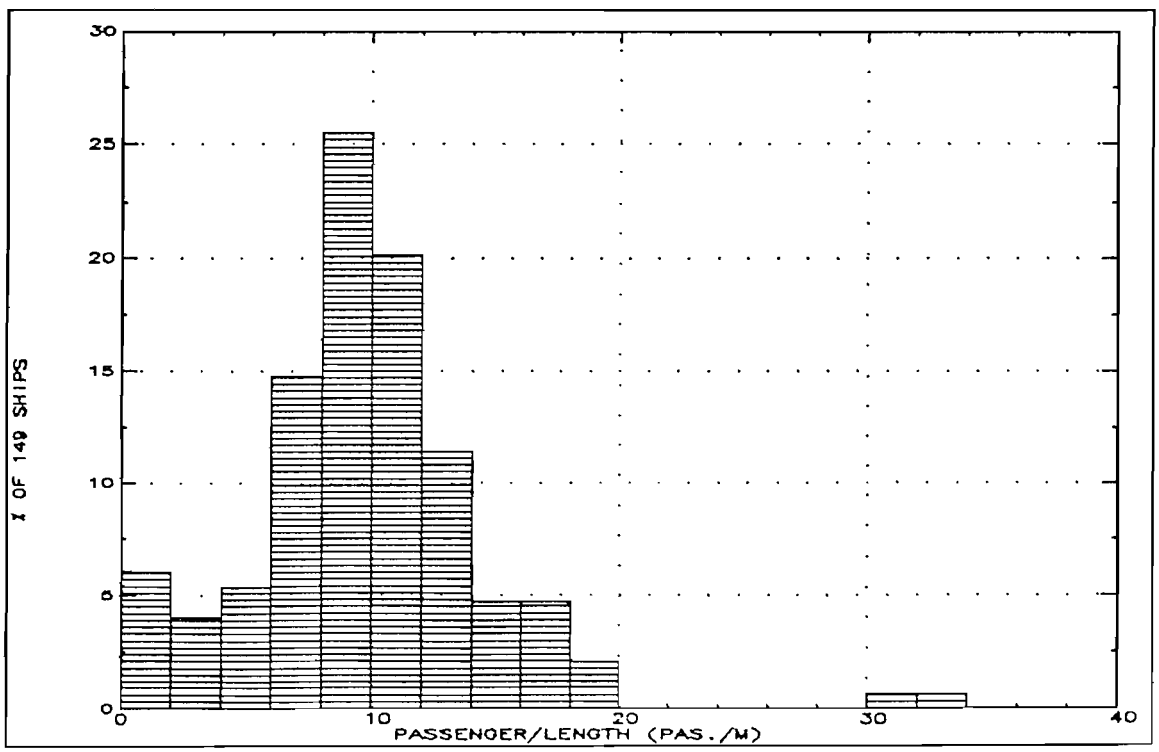

Fig.9: Survey of number of passengers per unit length

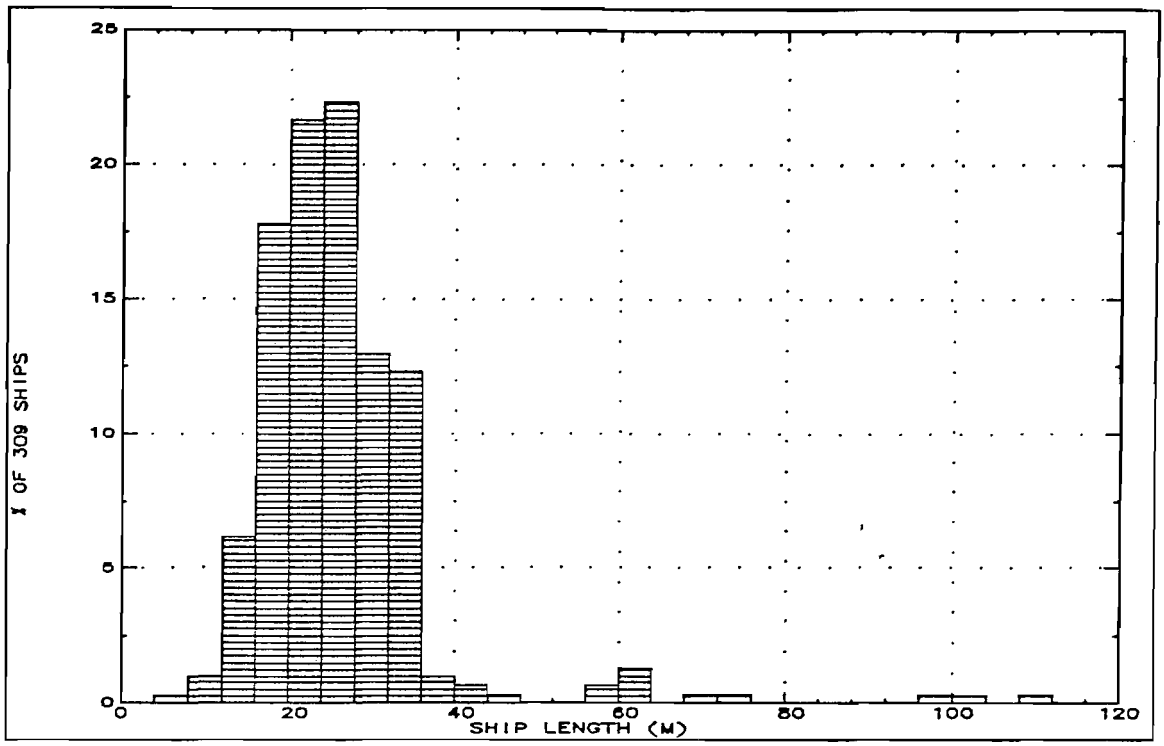

Fig.10: Survey of ship length

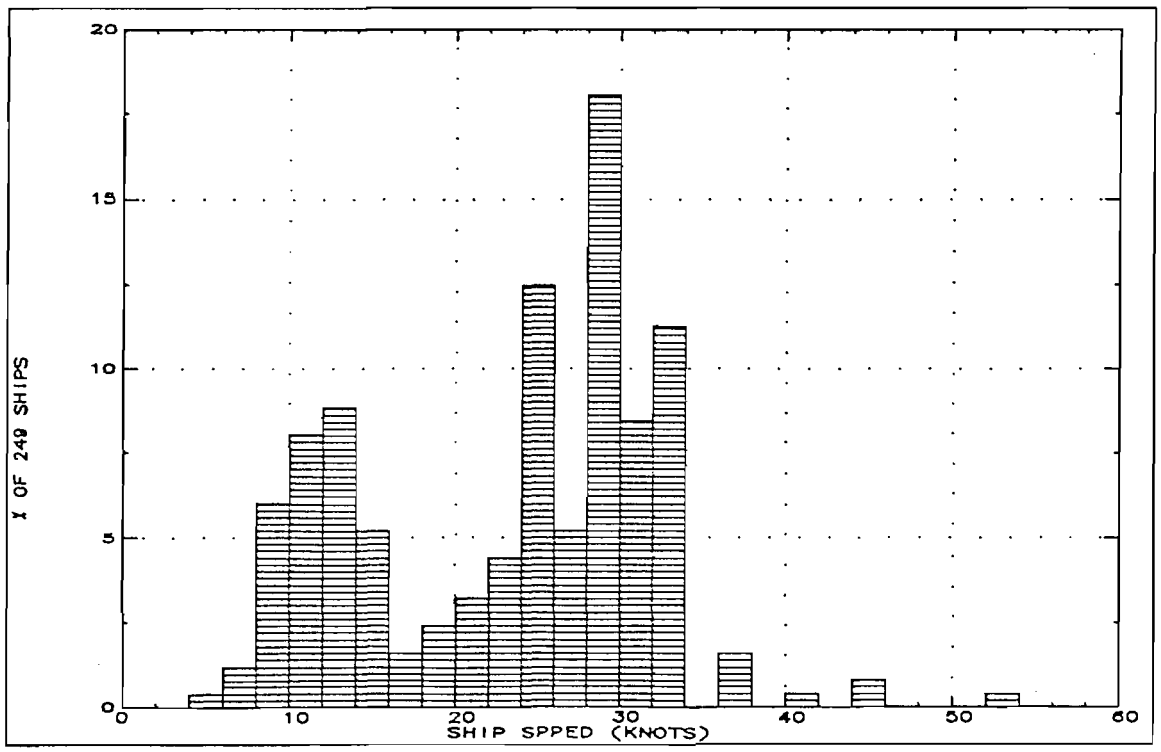

Fig.11: Survey of ship speed

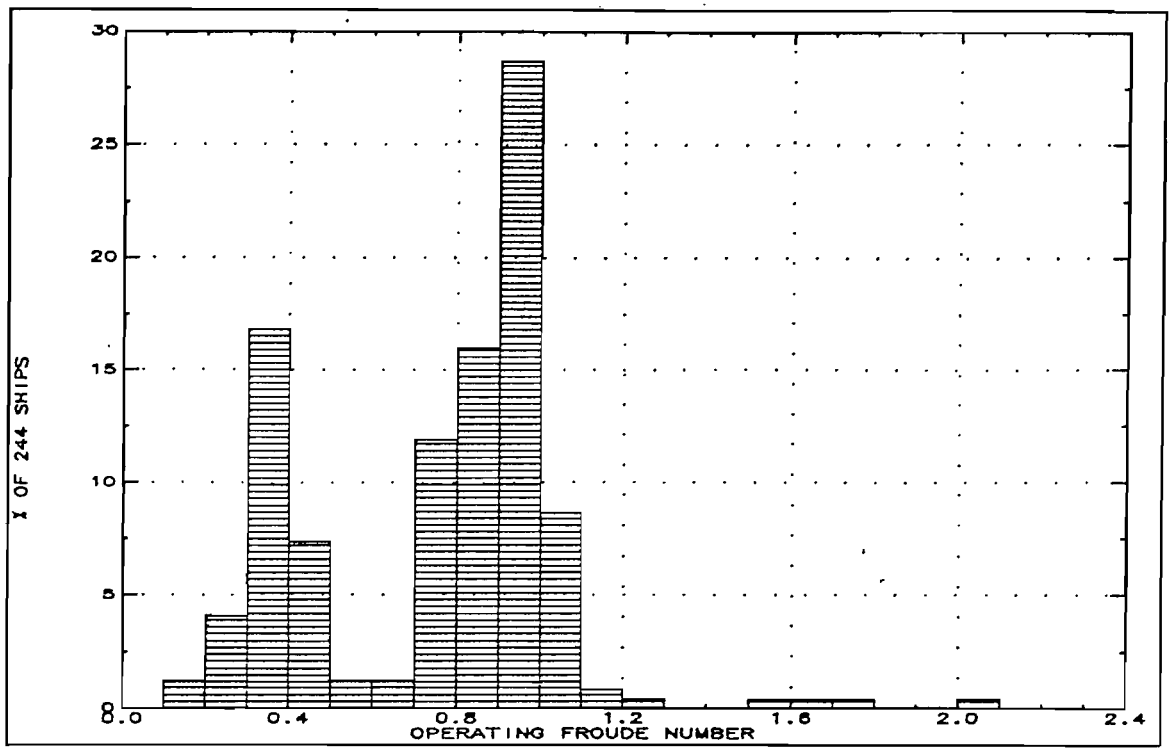

Fig.12: Survey of operating Froude number

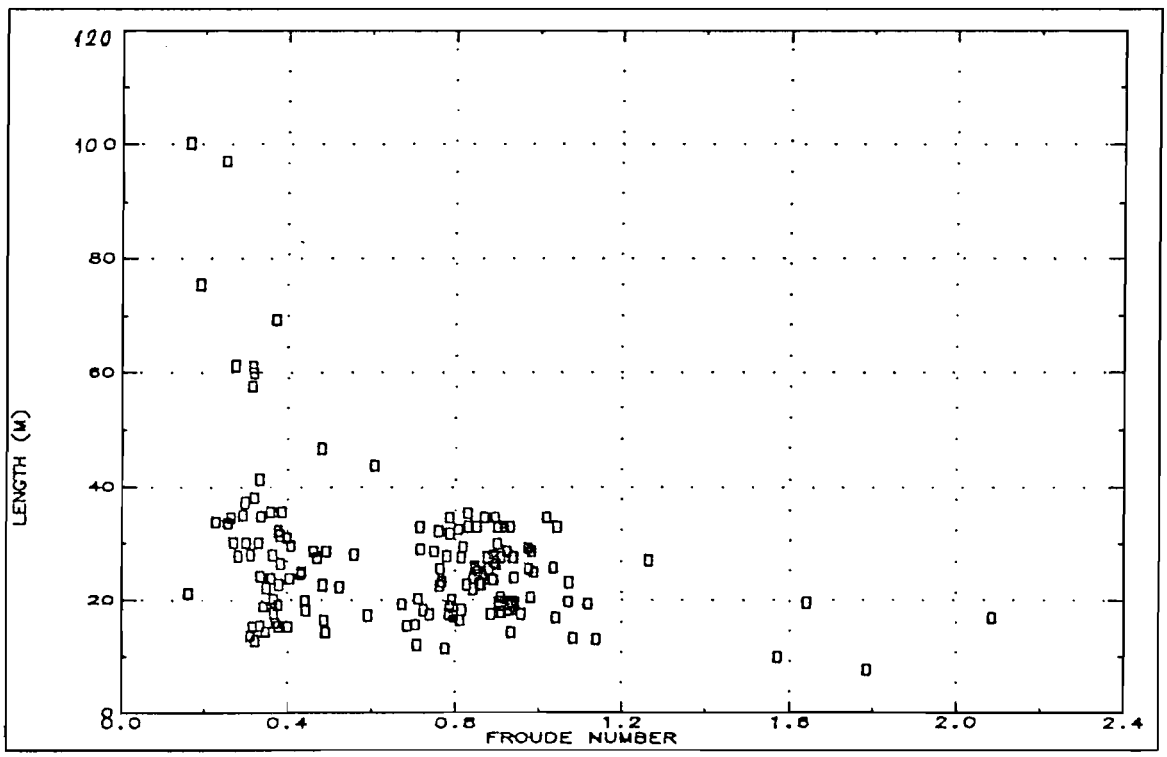

Fig.13: Relationship between ship speed and ship length

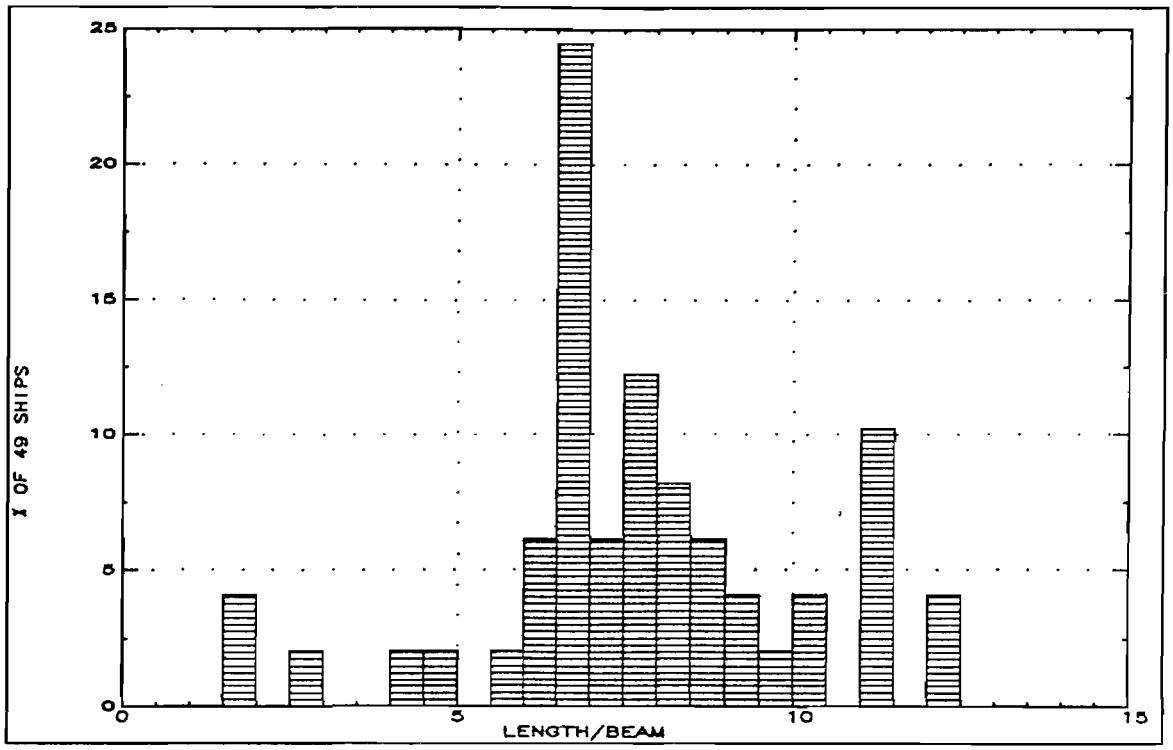

Fig.14: Survey of length to beam ratio (L/B)

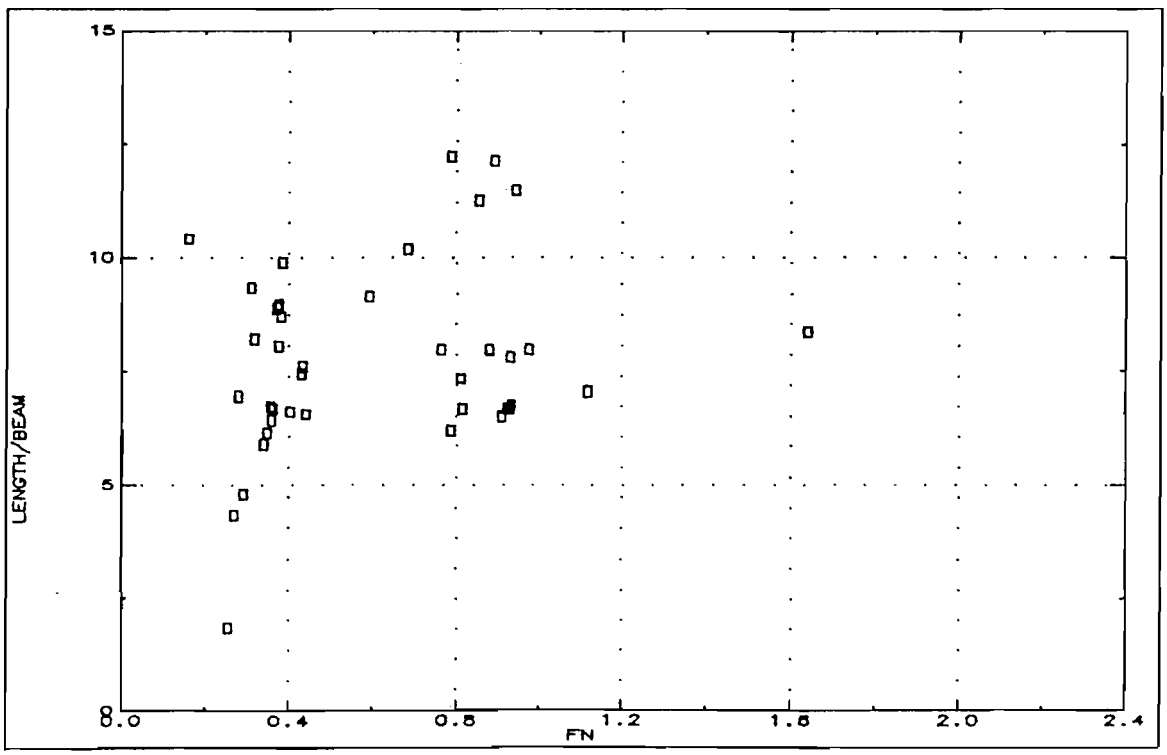

Fig.15: Survey of length to beam ratio (L/B) across Froude number range

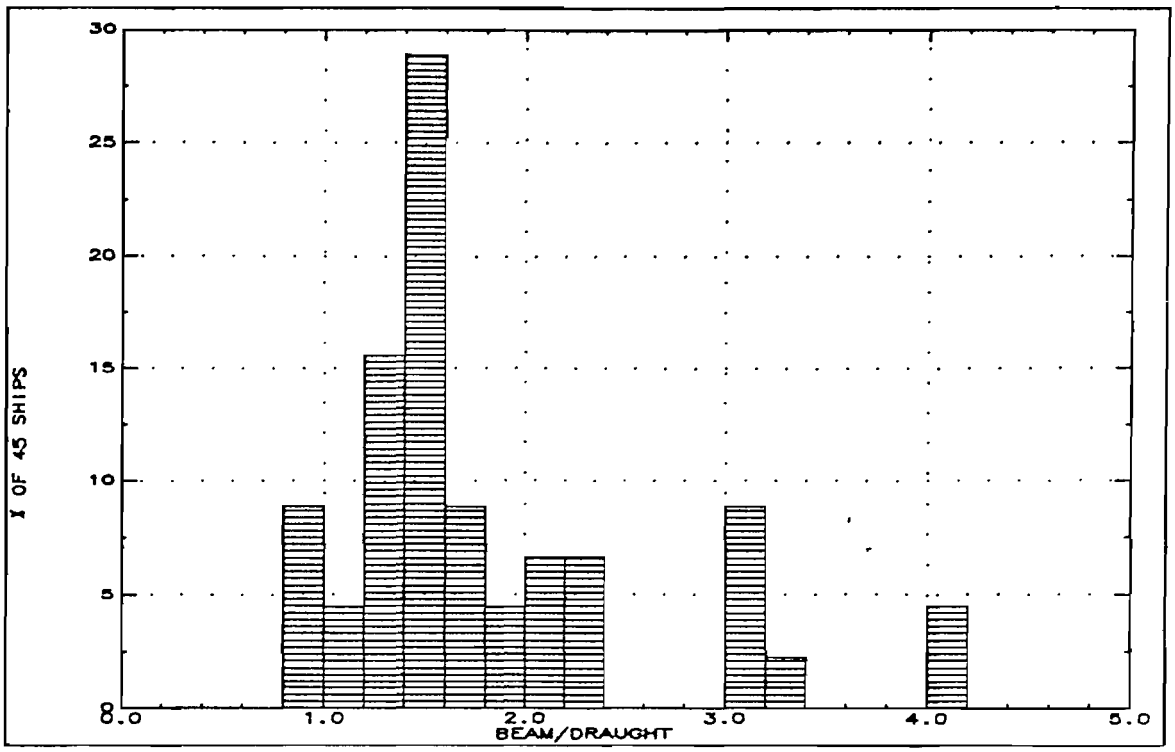

Fig.16: Survey of beam to draught ratio (B/T)

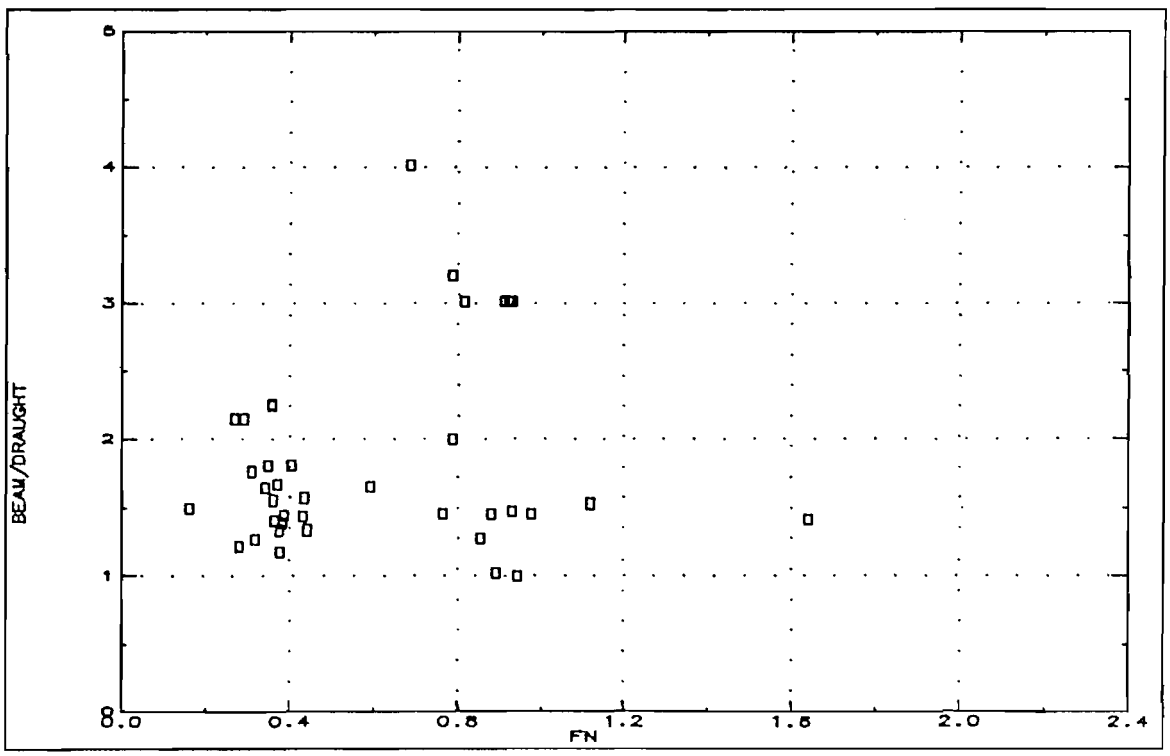

Fig.17: Survey of beam to draught ratio (B/T) across Froude number range

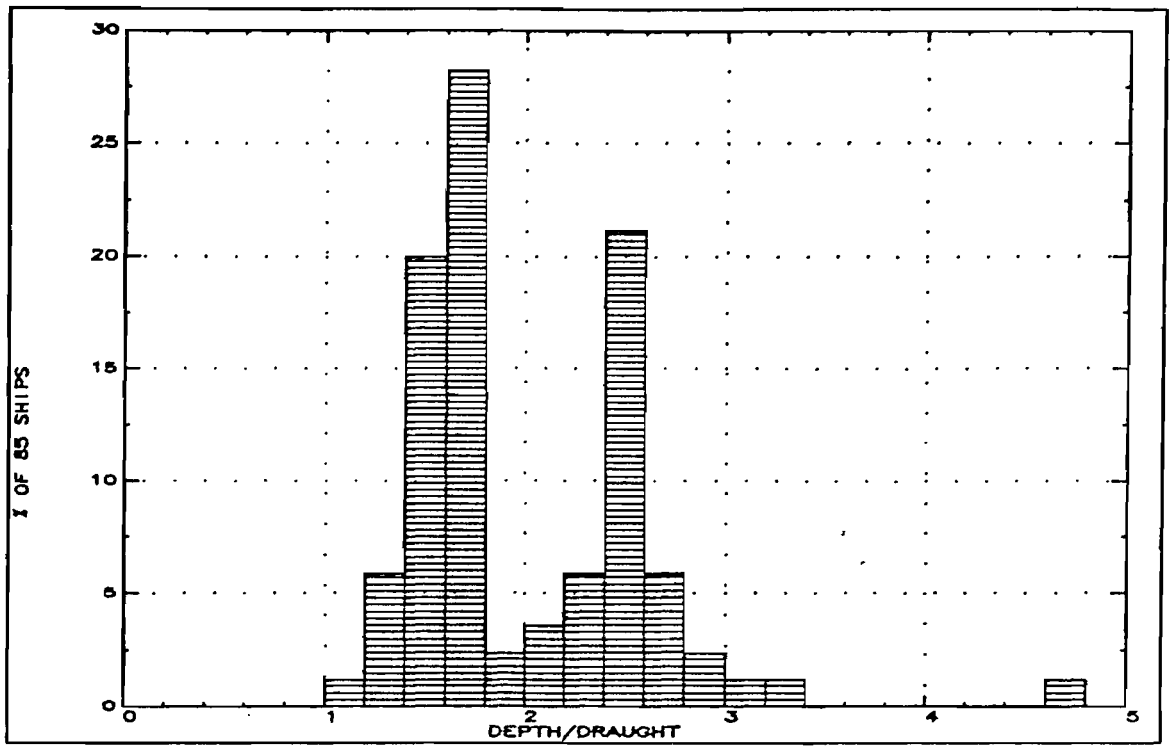

Fig.18: Survey of depth to draught ratio (D/T)

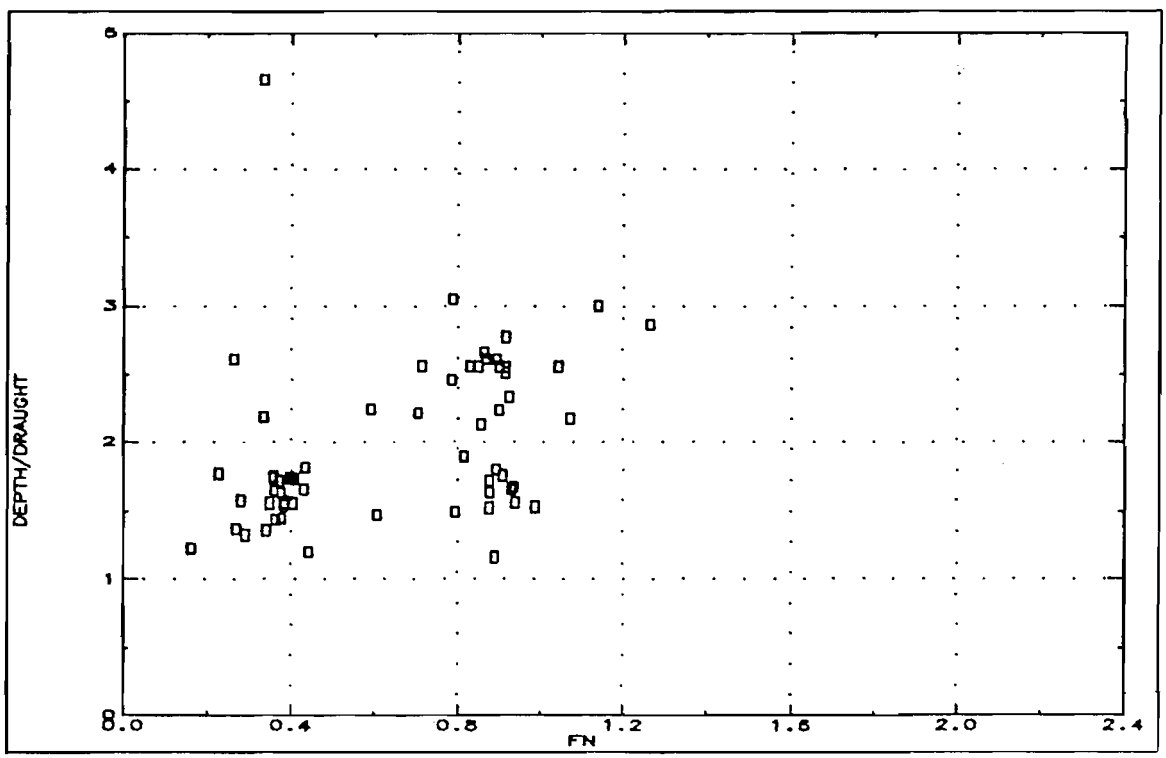

Fig.19: Survey of depth to draught ratio (D/T) across Froude number range

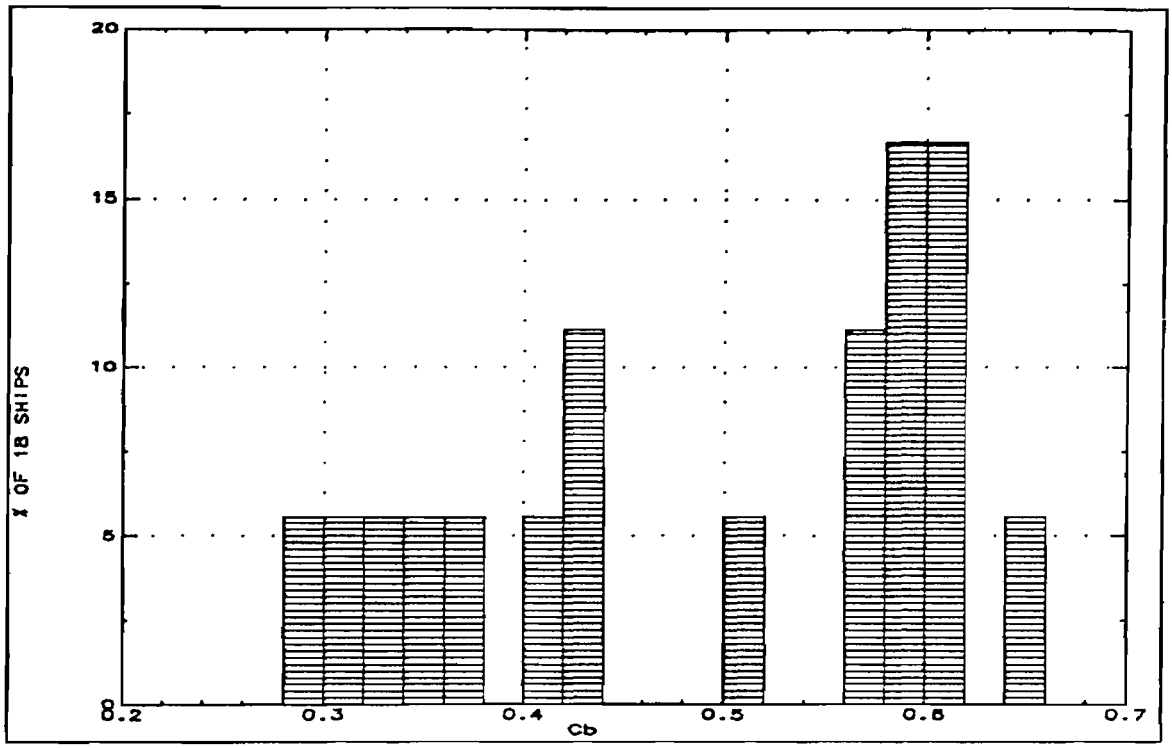

Fig.20: Survey of block coefficient (C_B)

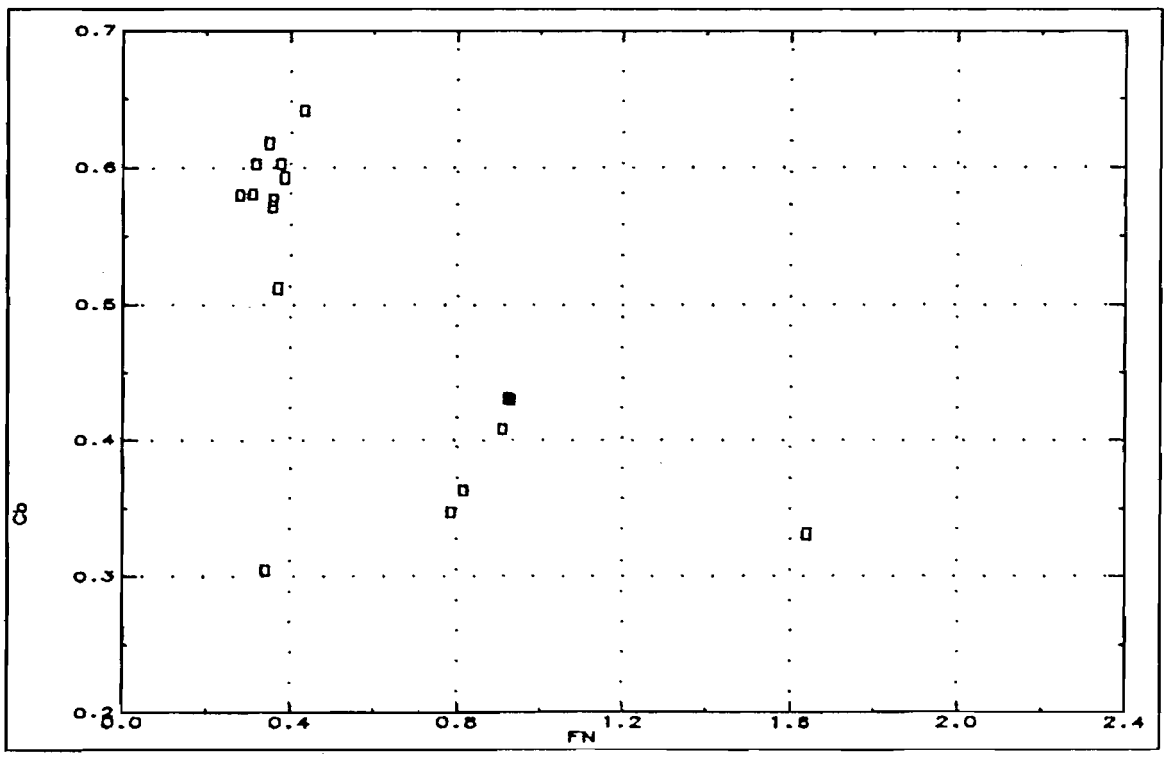

Fig.21: Survey of block coefficient (C_B) across Froude number range

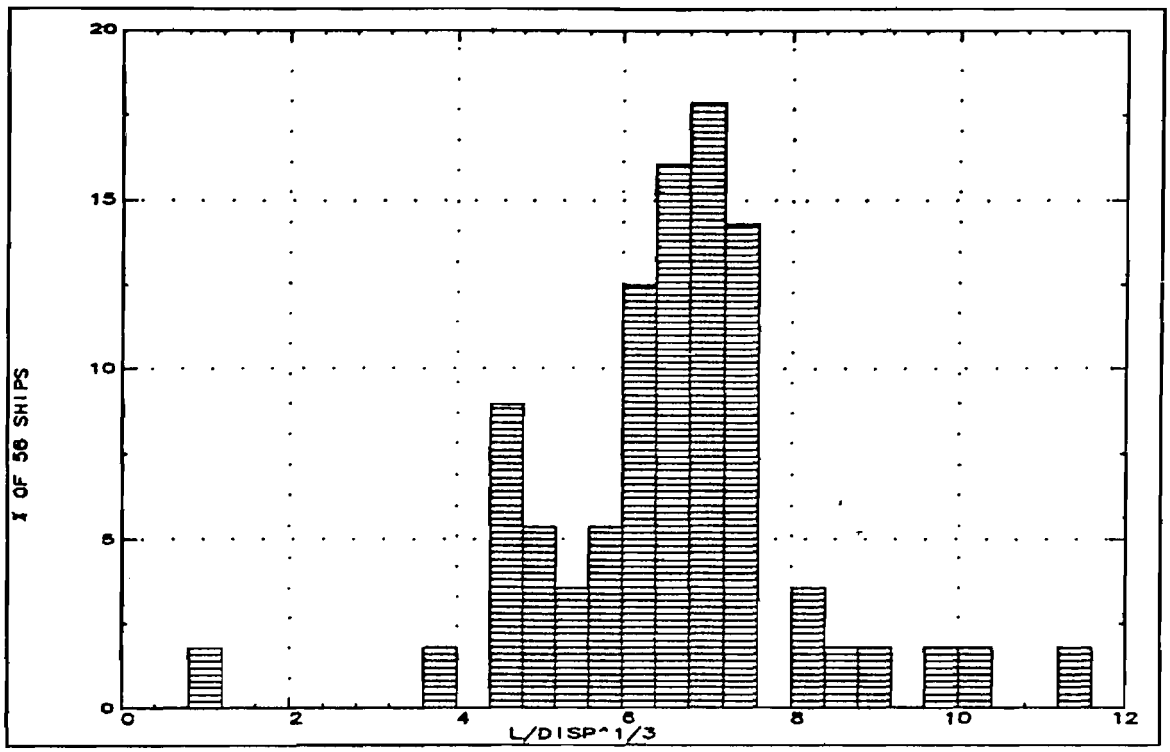

Fig.22: Survey of length to displacement ratio ($L/\nabla^{1/3}$)

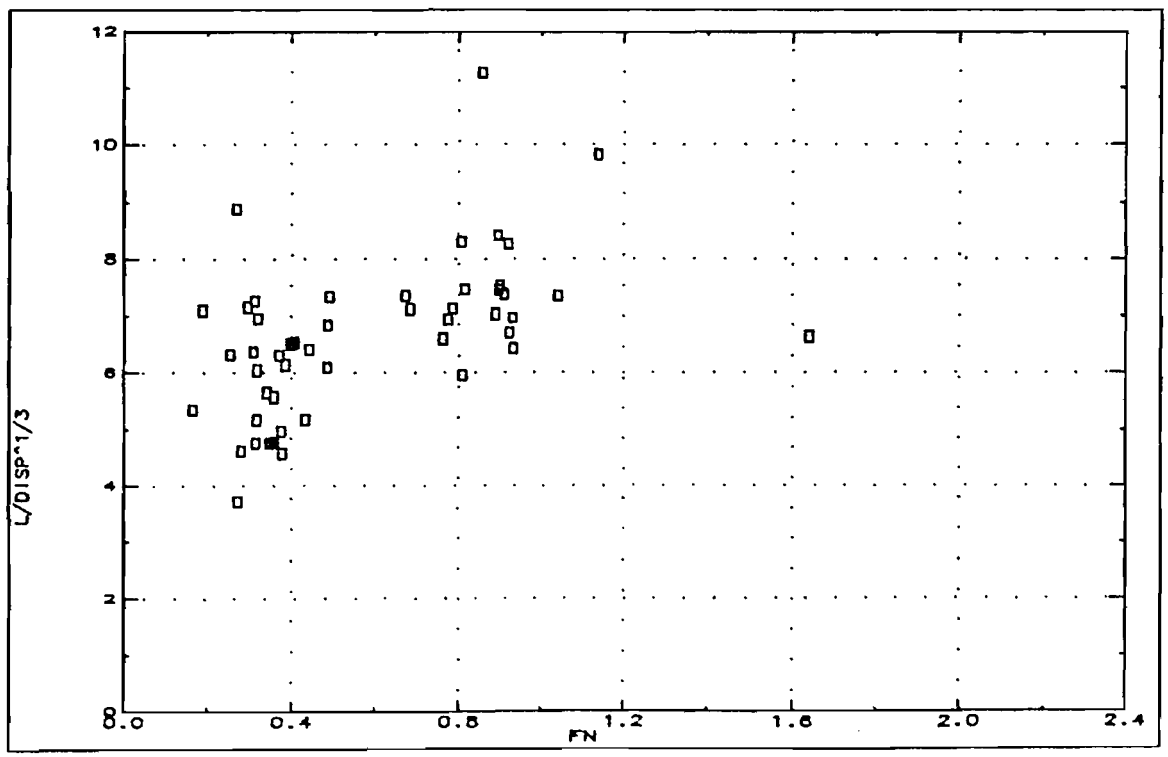

Fig.23: Survey of length to displacement ratio ($L/\nabla^{1/3}$) across Froude number range

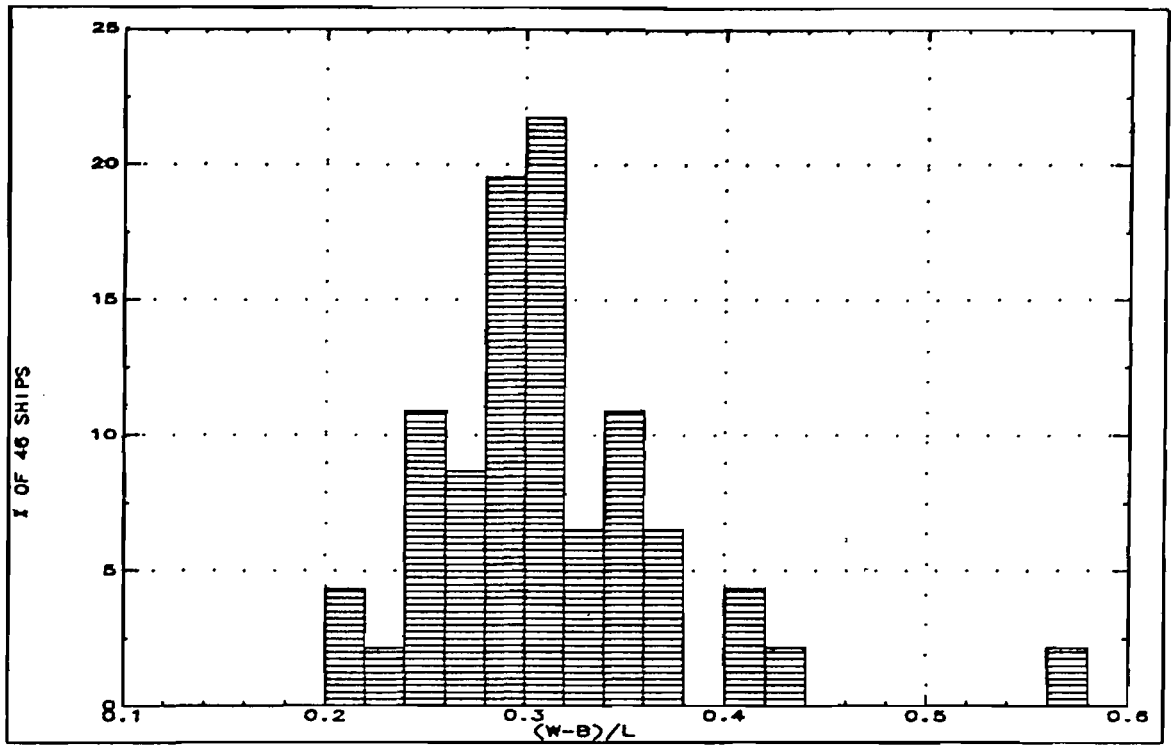

Fig.24: Survey of separation to length ratio ((W-B)/L)

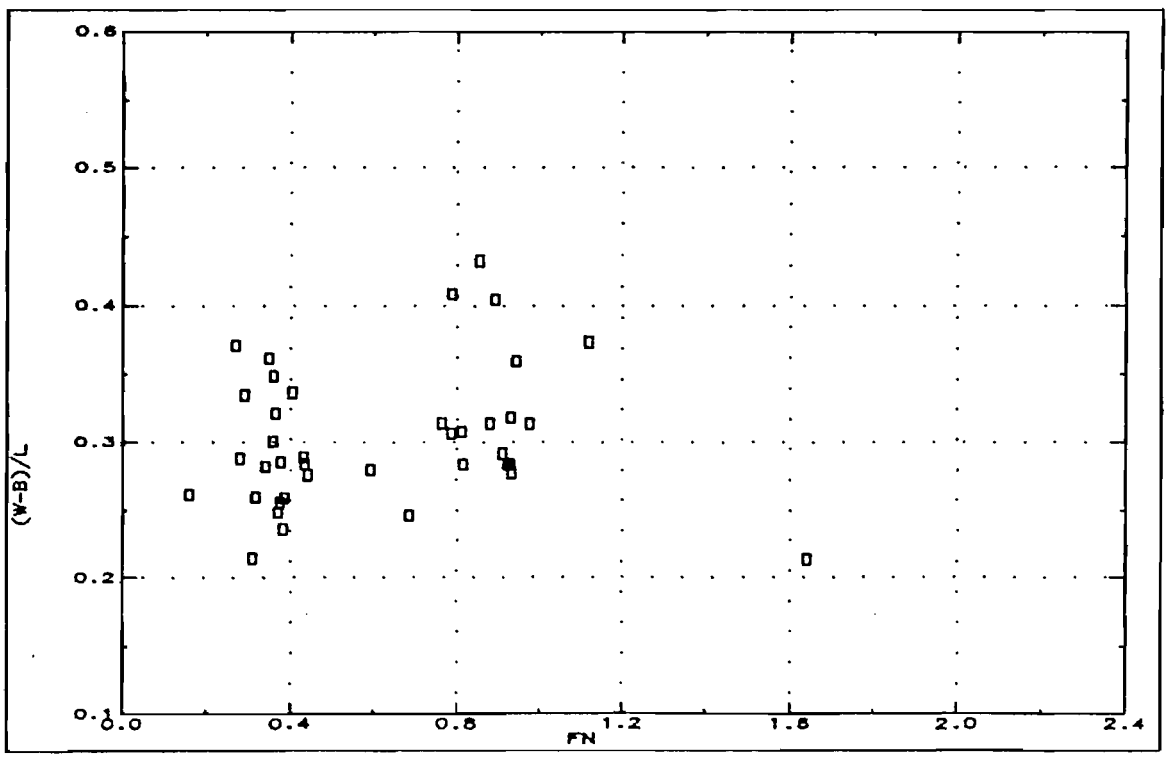

Fig.25: Survey of separation to length ratio ((W-B)/L) across Froude number range

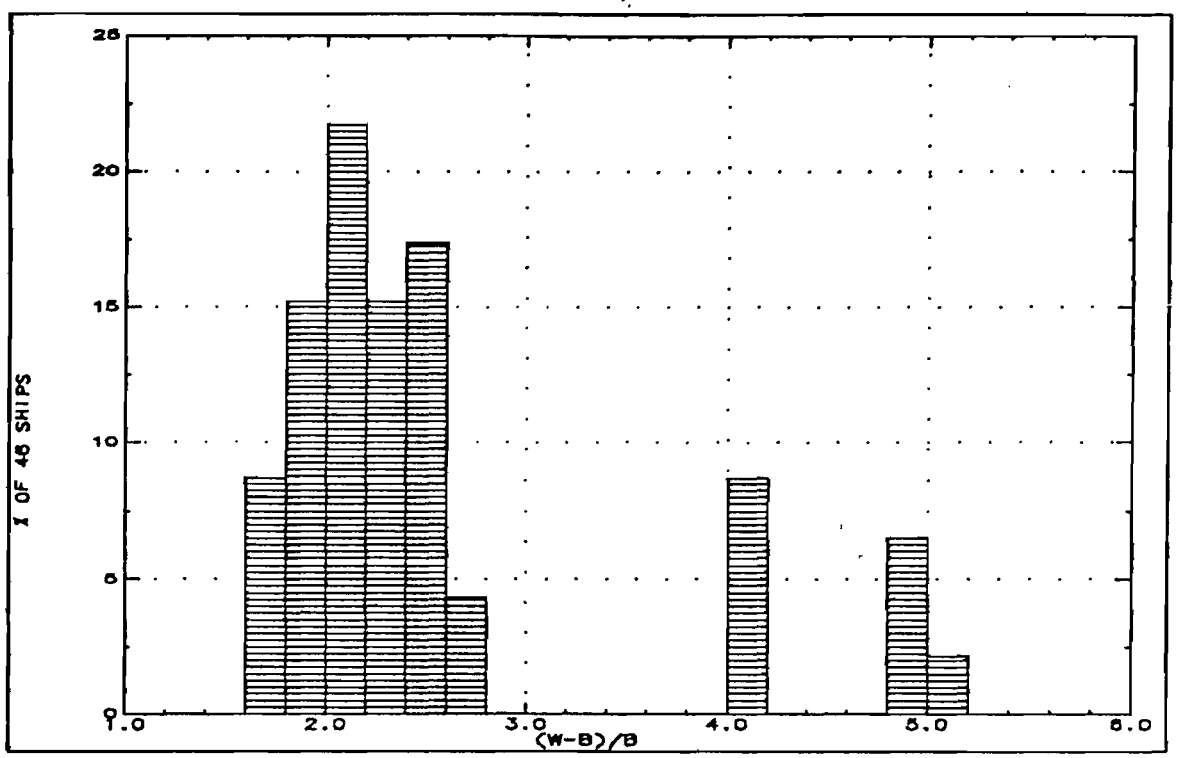

Fig.26: Survey of separation to beam ratio ((W-B)/B)

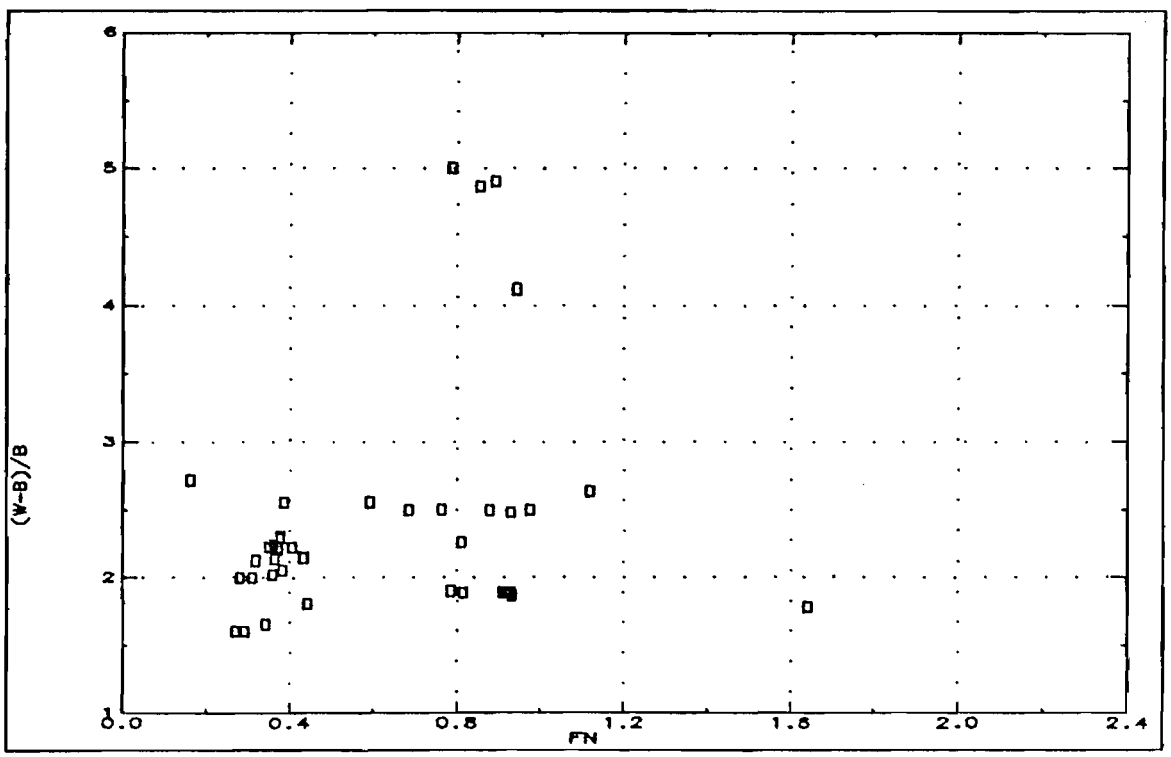

Fig.27: Survey of separation to beam ratio ((W-B)/B) across Froude number range

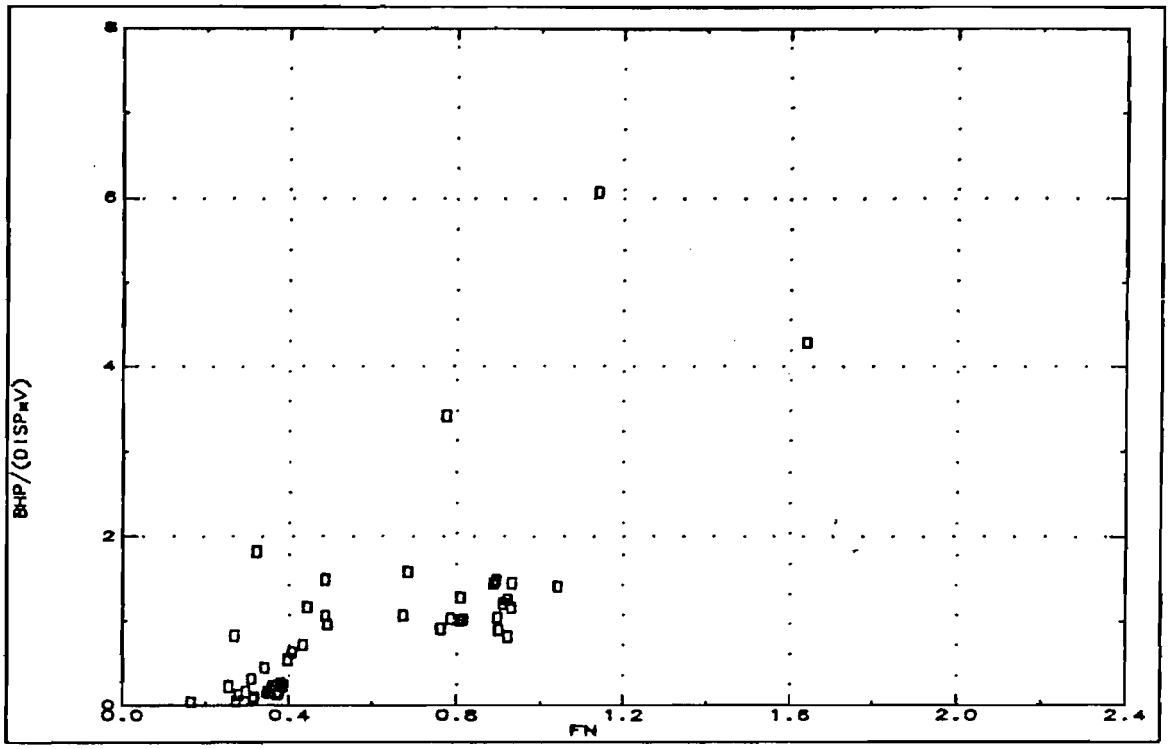

Fig.28: Survey of Power to displacement-speed ratio (BHP/∇V)

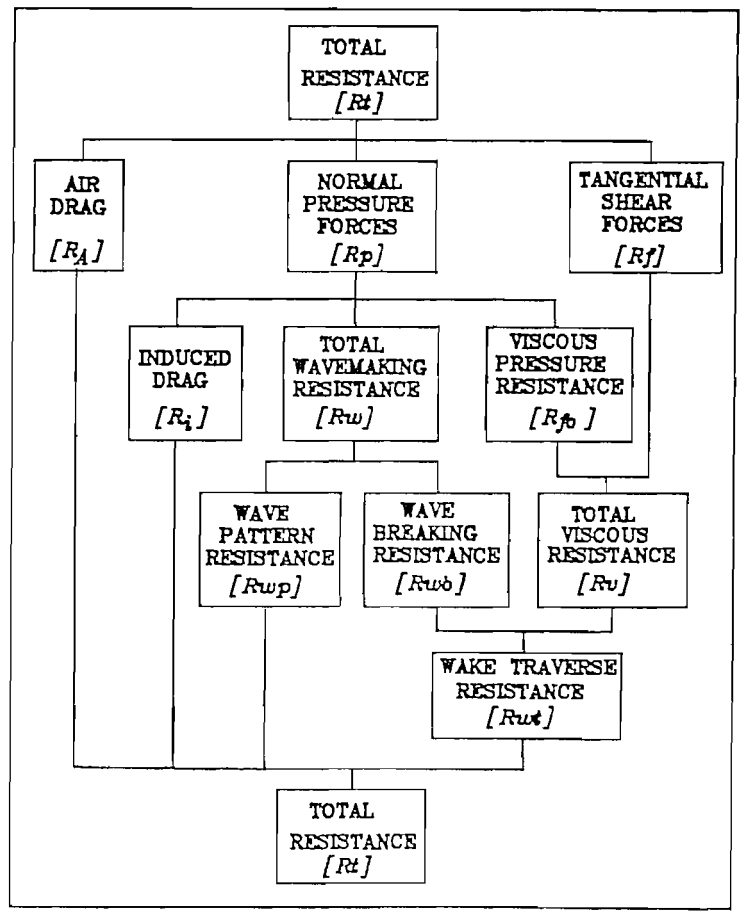

Fig.29: Resistance components of a ship model

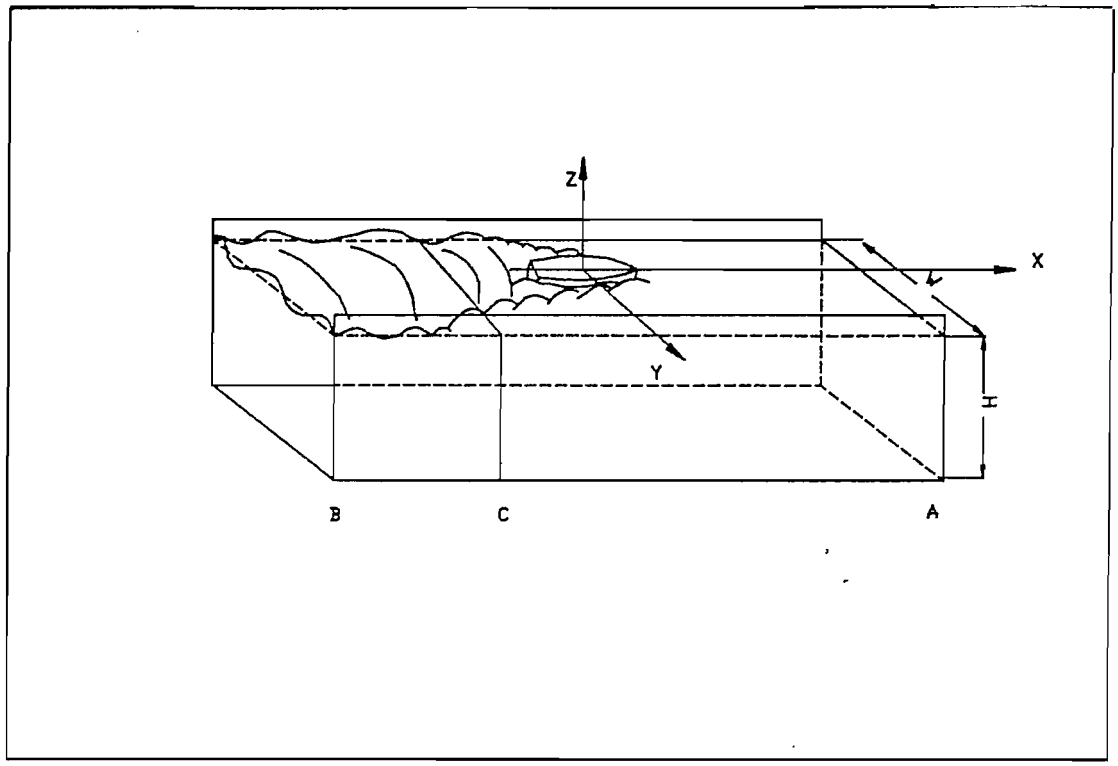

Fig.30: A ship model in towing tank

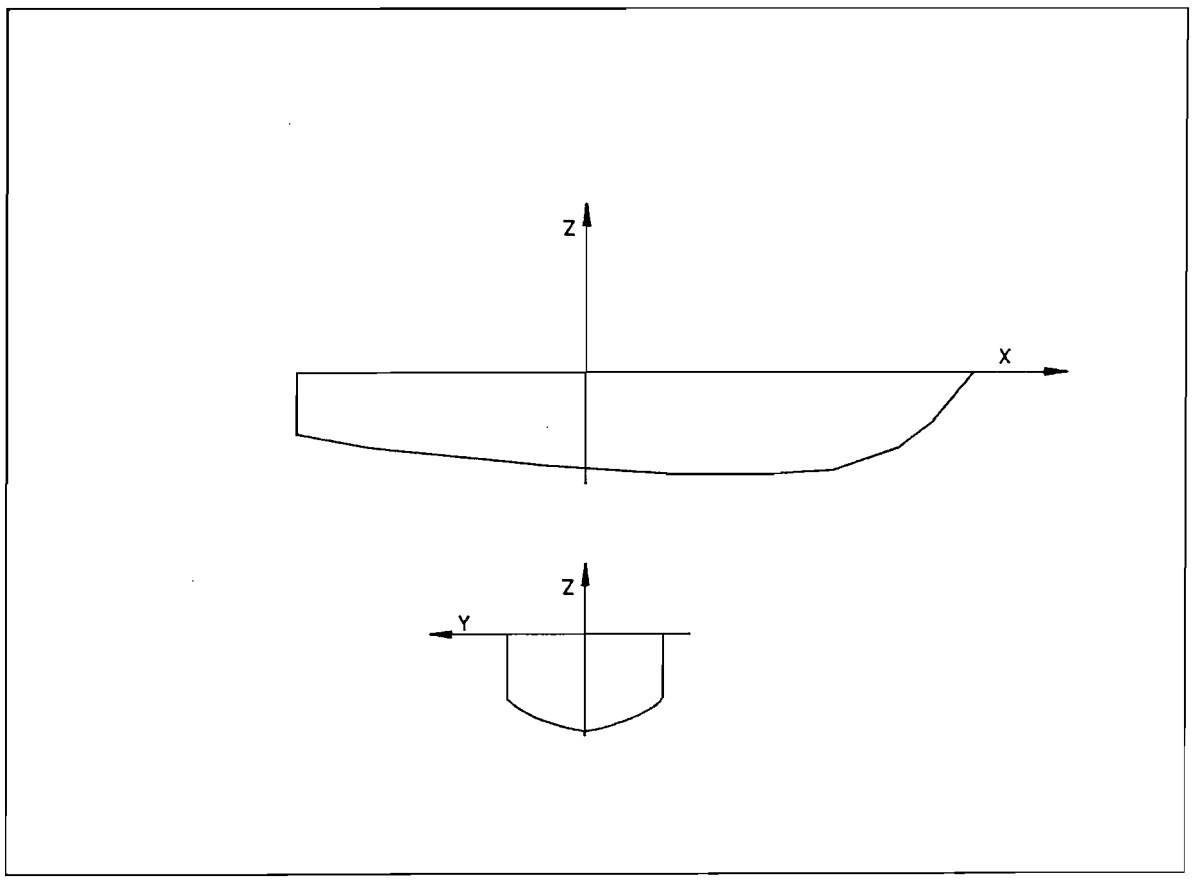

Fig.31: Coordinate system

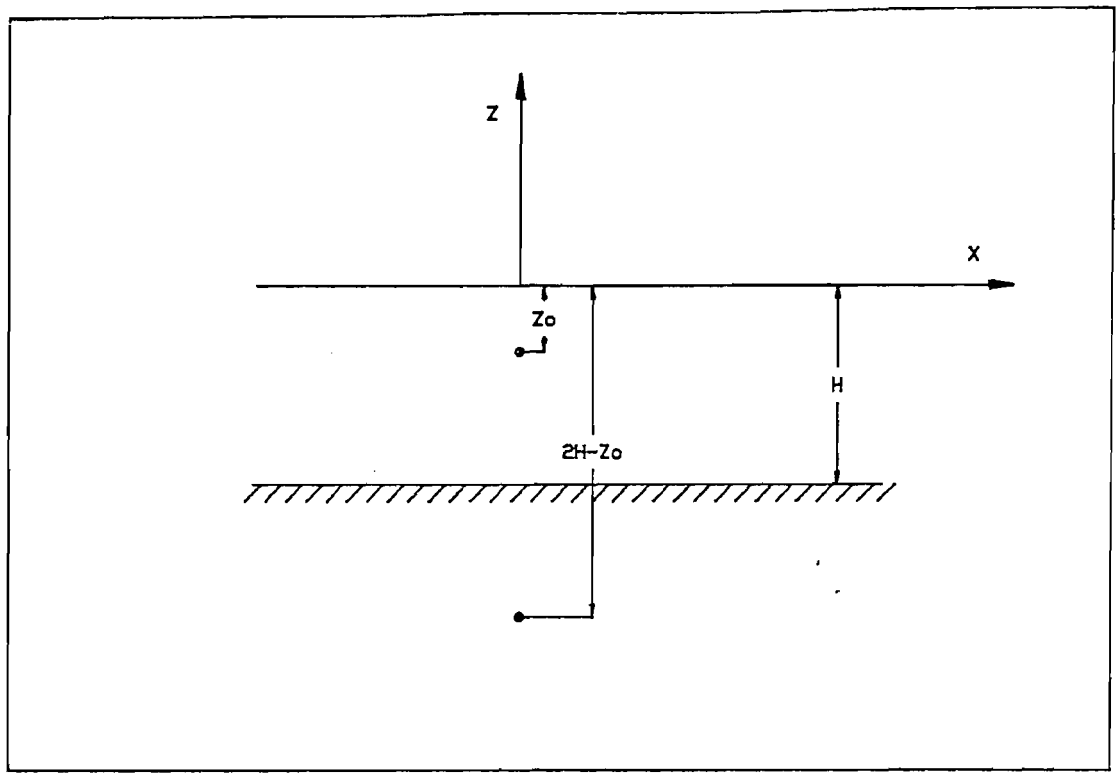

Fig.32: A source in shallow water

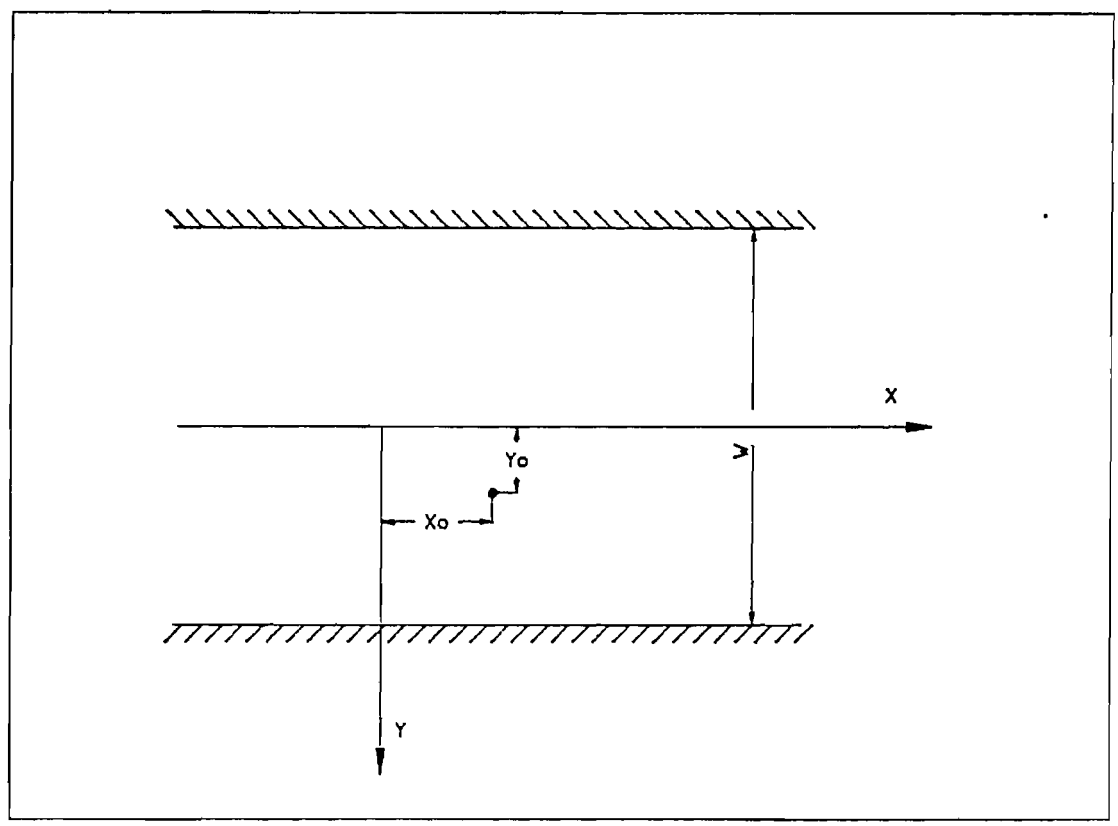

Fig.33: A source in a canal

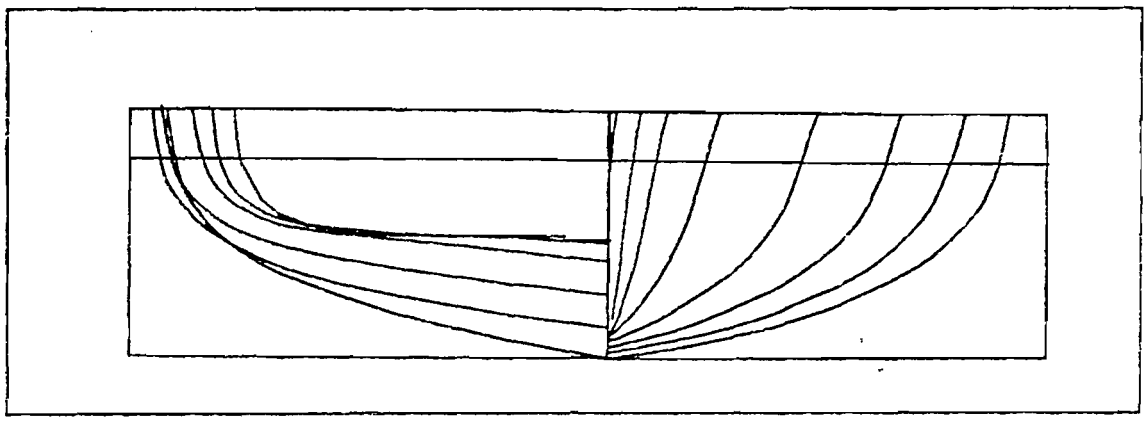

Fig.34: Athena hull form [97]

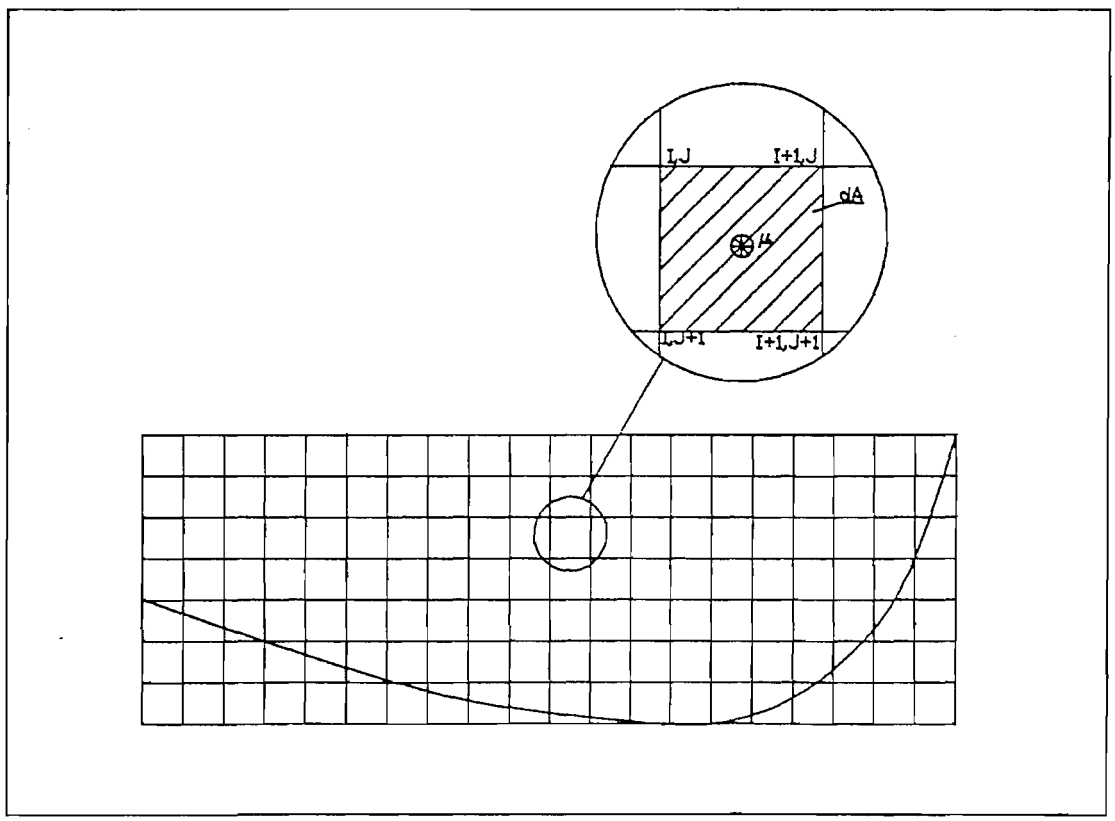

Fig.35: Source panels distributed at the centreplane

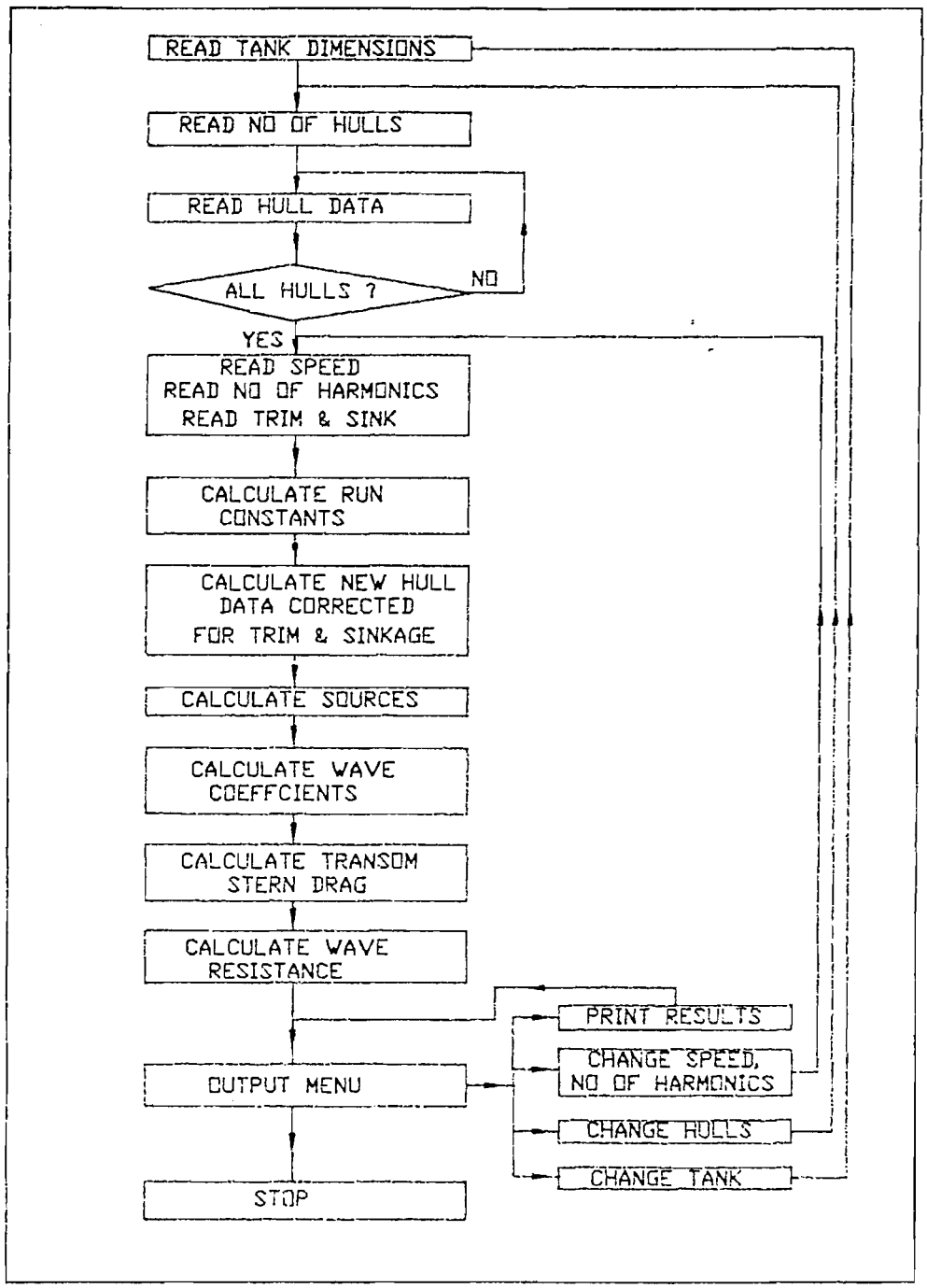

Fig.36: Flow diagram of theoretical wave resistance calculation program

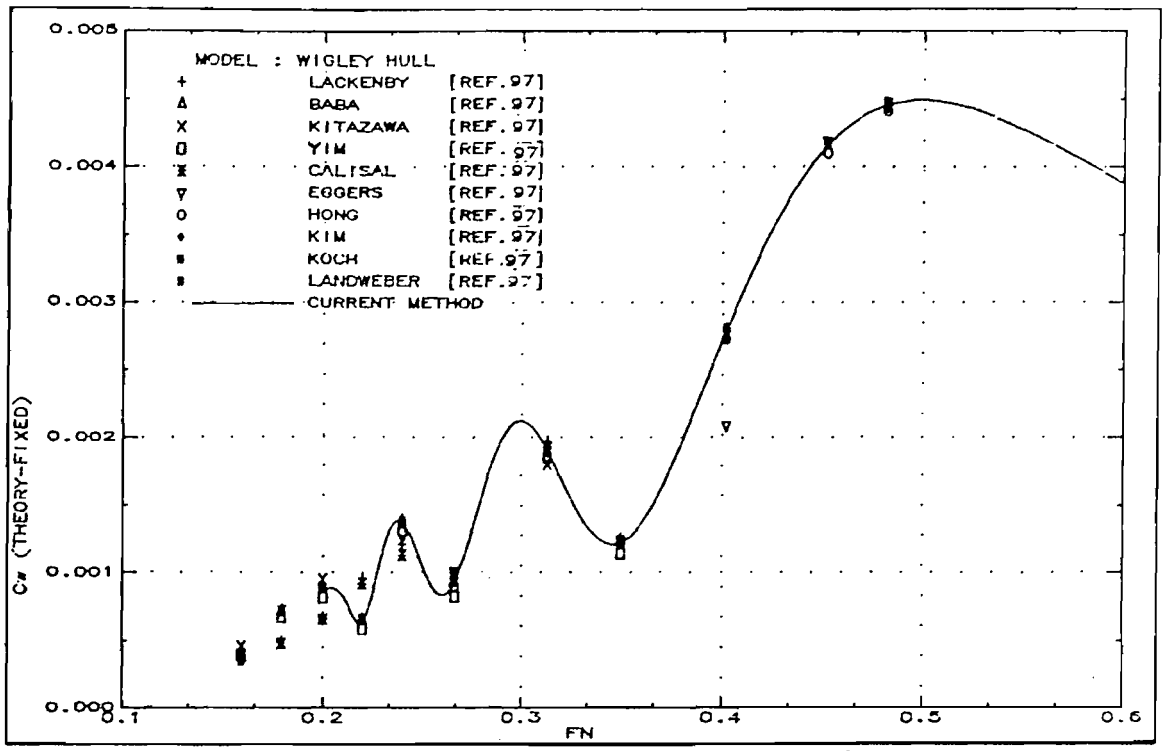

Fig.37: Comparison of theoretical wave resistance calculations by linearised thin ship theory (Wigley Hull-Fixed)

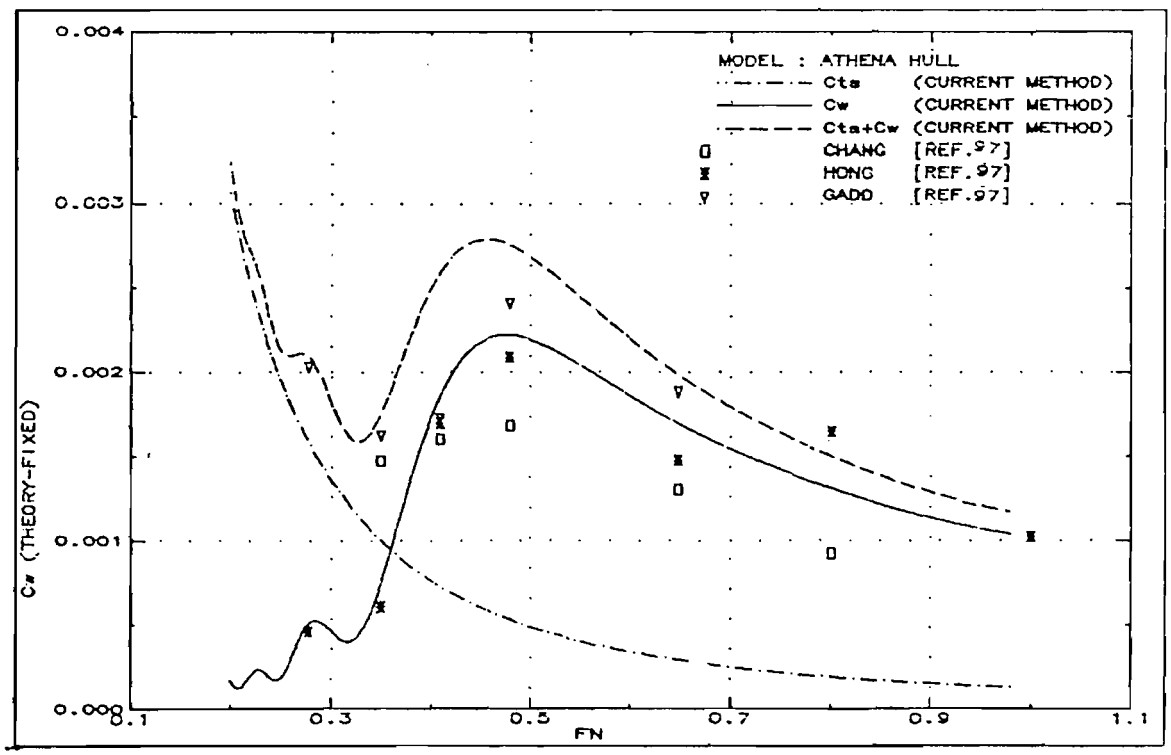

Fig.38: Comparison of theoretical wave resistance calculations by linearised thin ship theory (Athena Hull-Fixed)

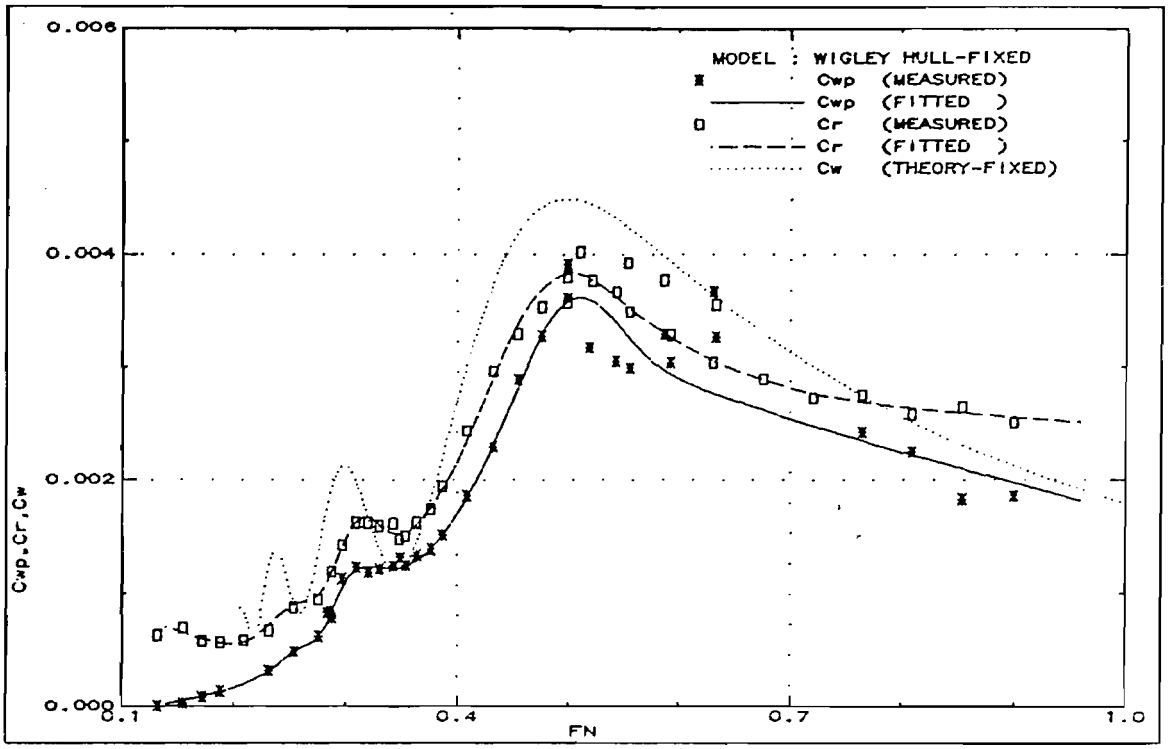

Fig.39: Comparison of theoretical wave resistance calculations with experimental measurements (Wigley Hull-Fixed)

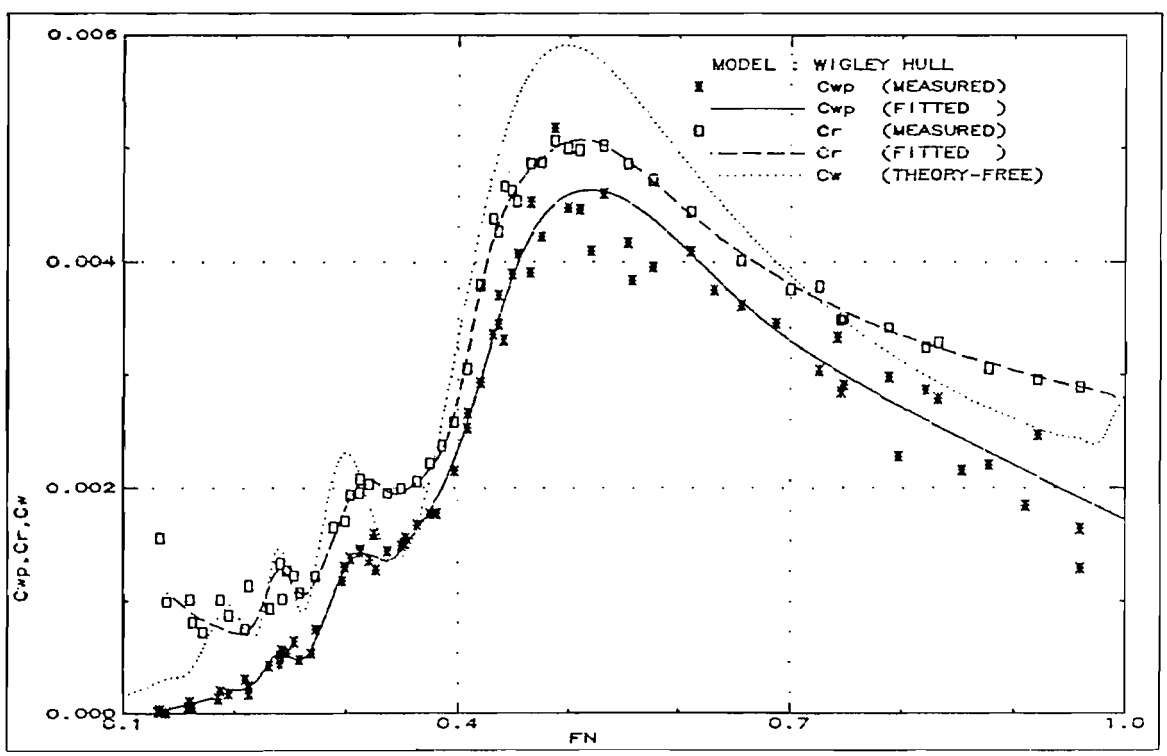

Fig.40: Comparison of theoretical wave resistance calculations with experimental measurements (Wigley Hull-Free)

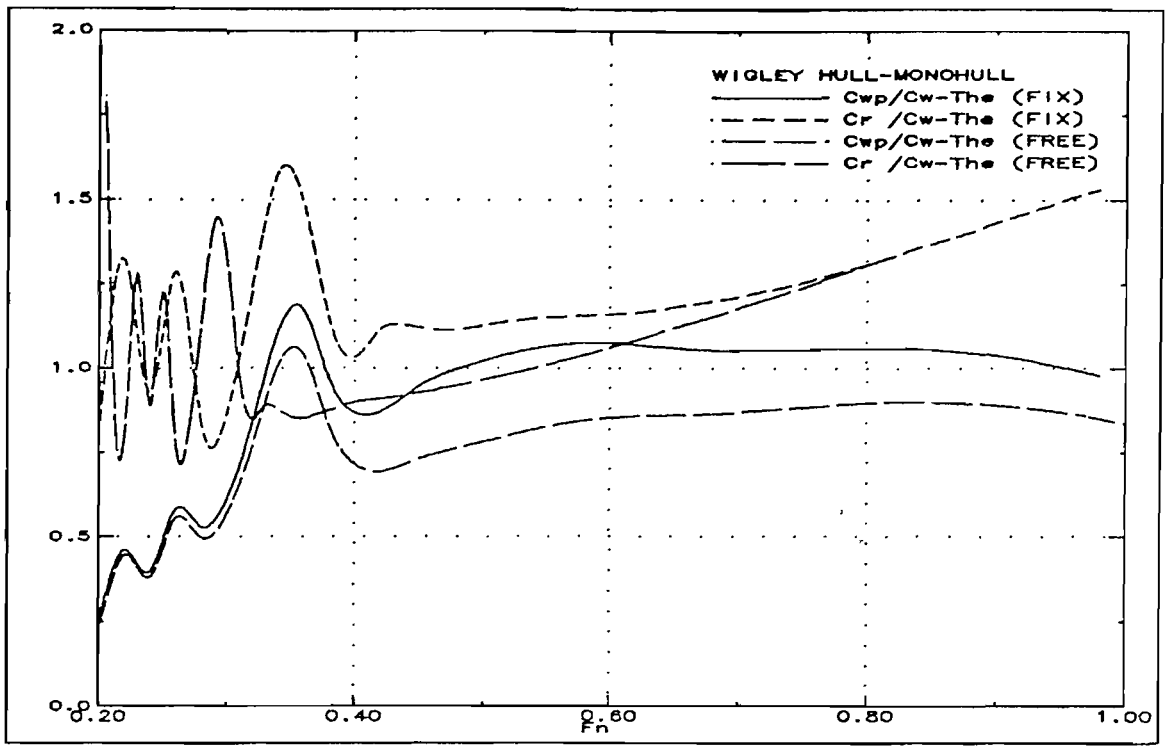

Fig.41: Correlation between fixed and free to trim and sink conditions (Wigley Hull)

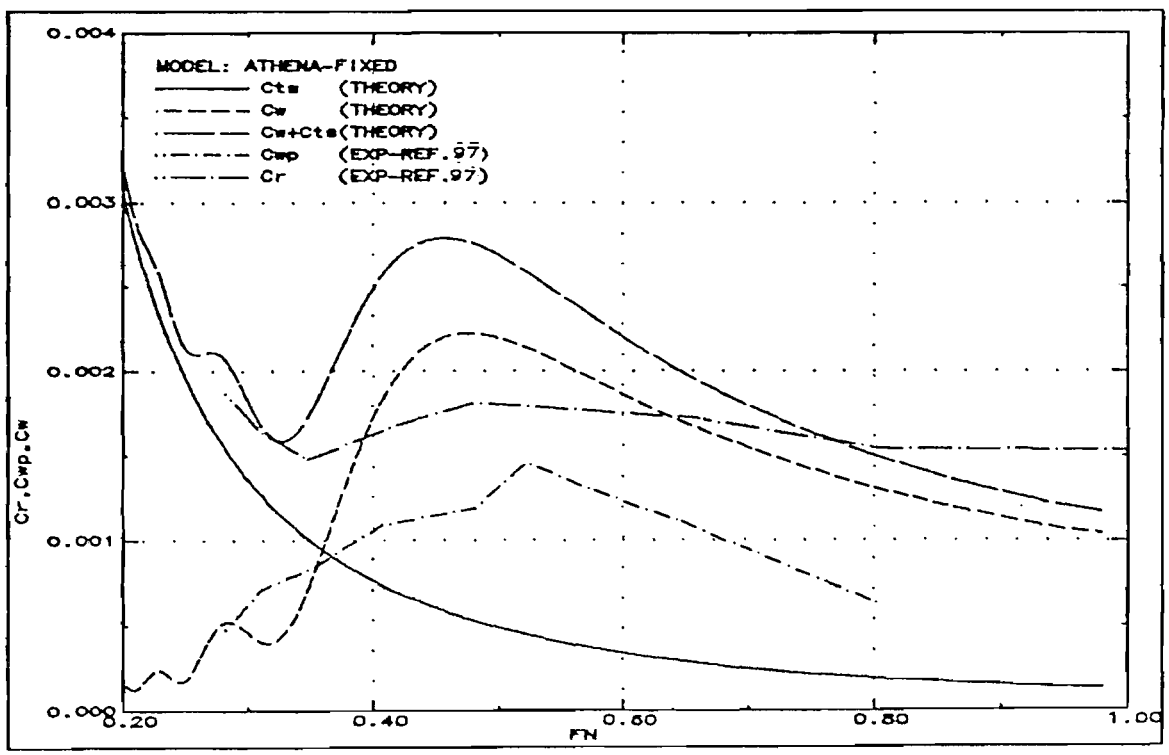

Fig.42: Comparison of wave resistance calculations with experiments (Athena Hull-Fixed)

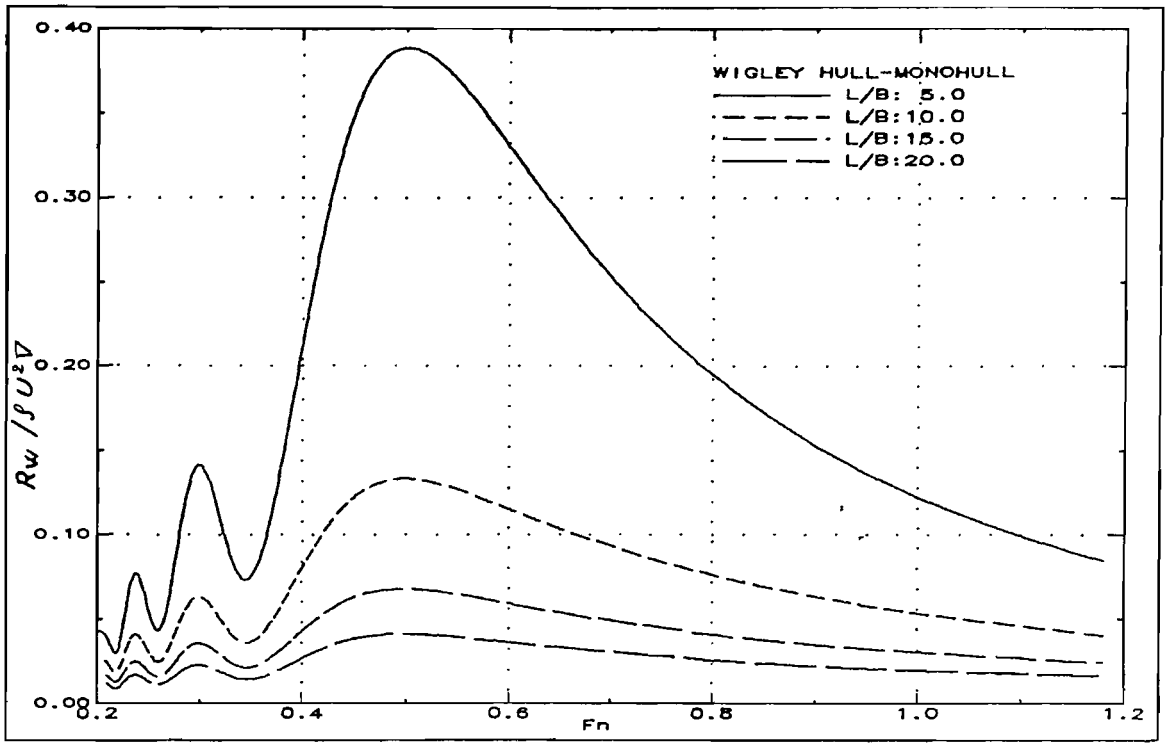

Fig.43: Theoretical wave resistance change with length to beam ratio (L/B) variation (Wigley Hull)

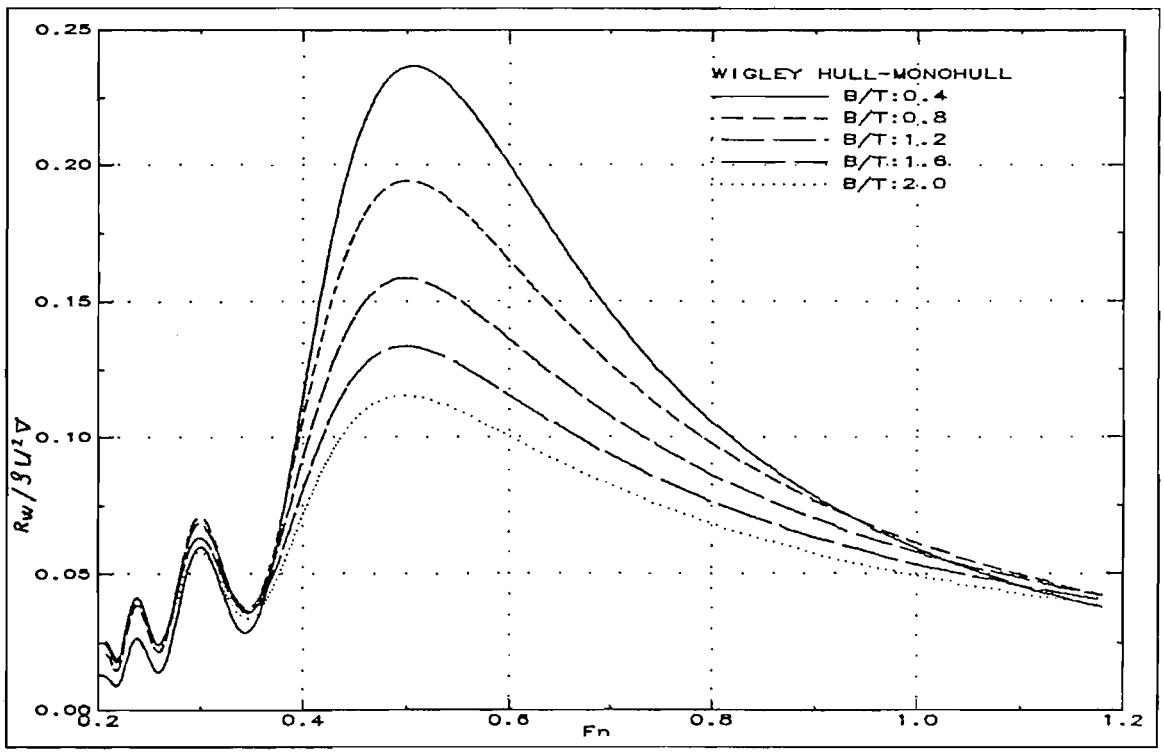

Fig.44: Theoretical wave resistance change with beam to draught ratio (B/T) variation (Wigley Hull)

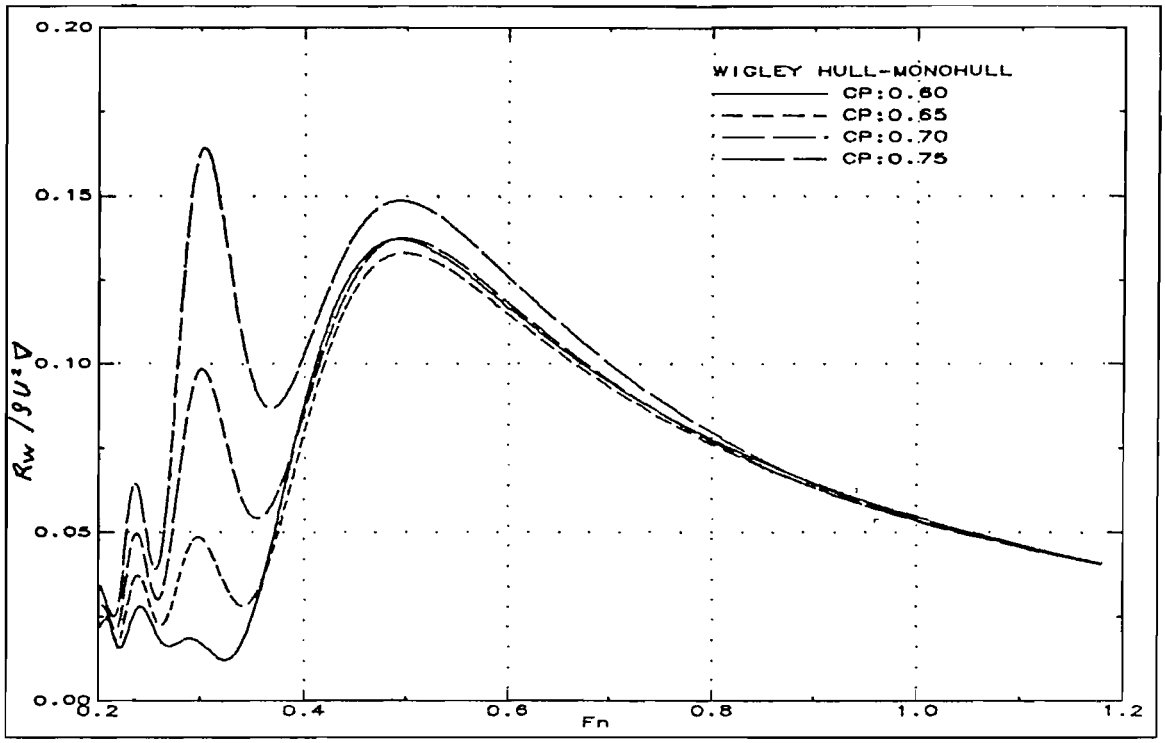

Fig.45: Theoretical wave resistance change with prismatic coefficient (C_P) variation (Wigley Hull)

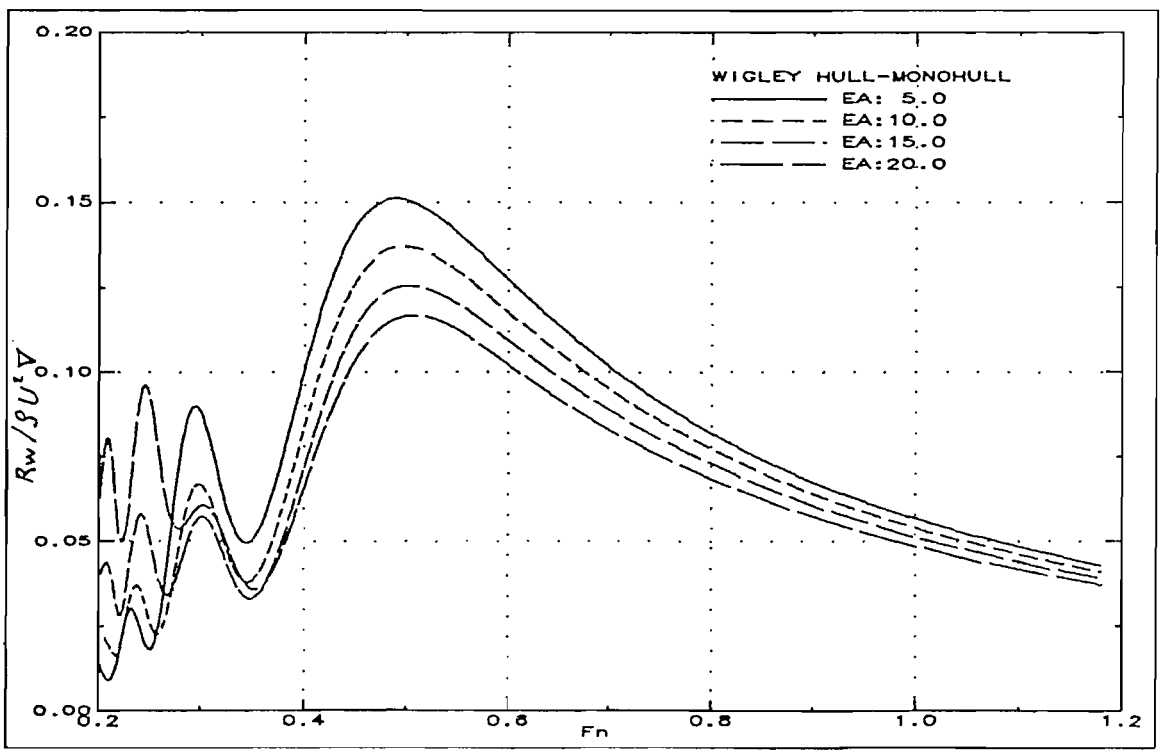

Fig.46: Theoretical wave resistance change with entrance angle (α_E) variation (Wigley Hull)

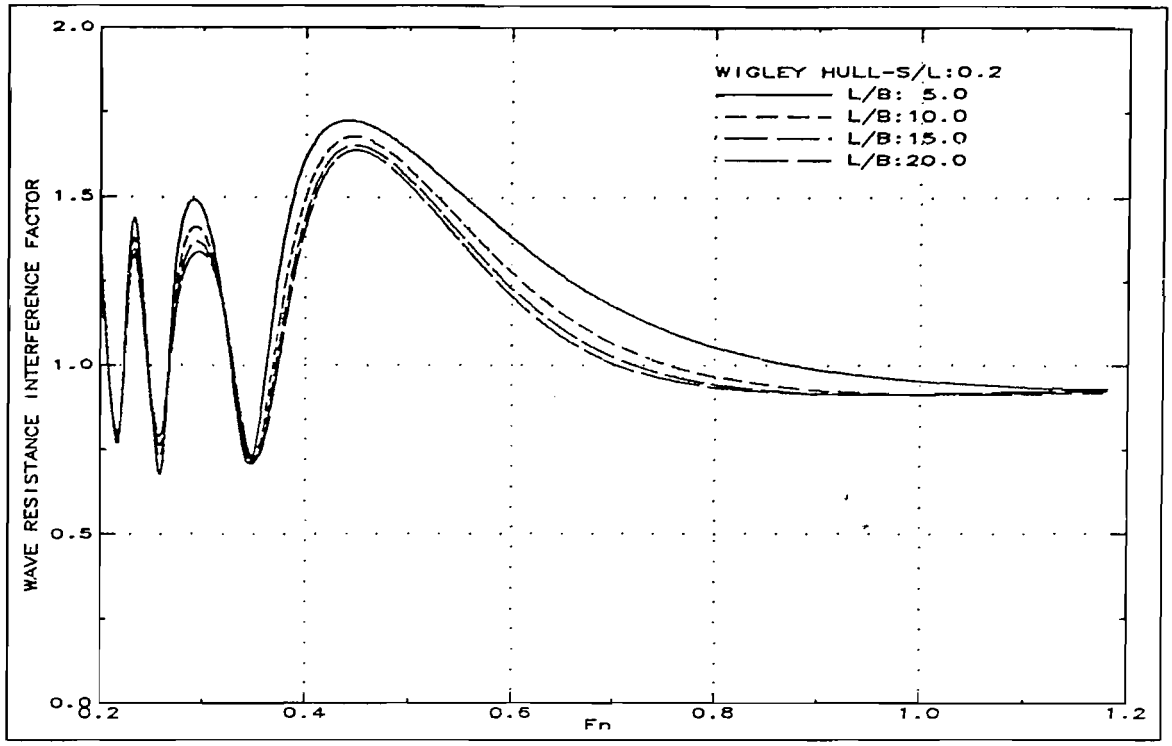

Fig.47: Theoretical wave resistance interference factor change with length to beam ratio change (Wigley Hull-S/L:Ø.2)

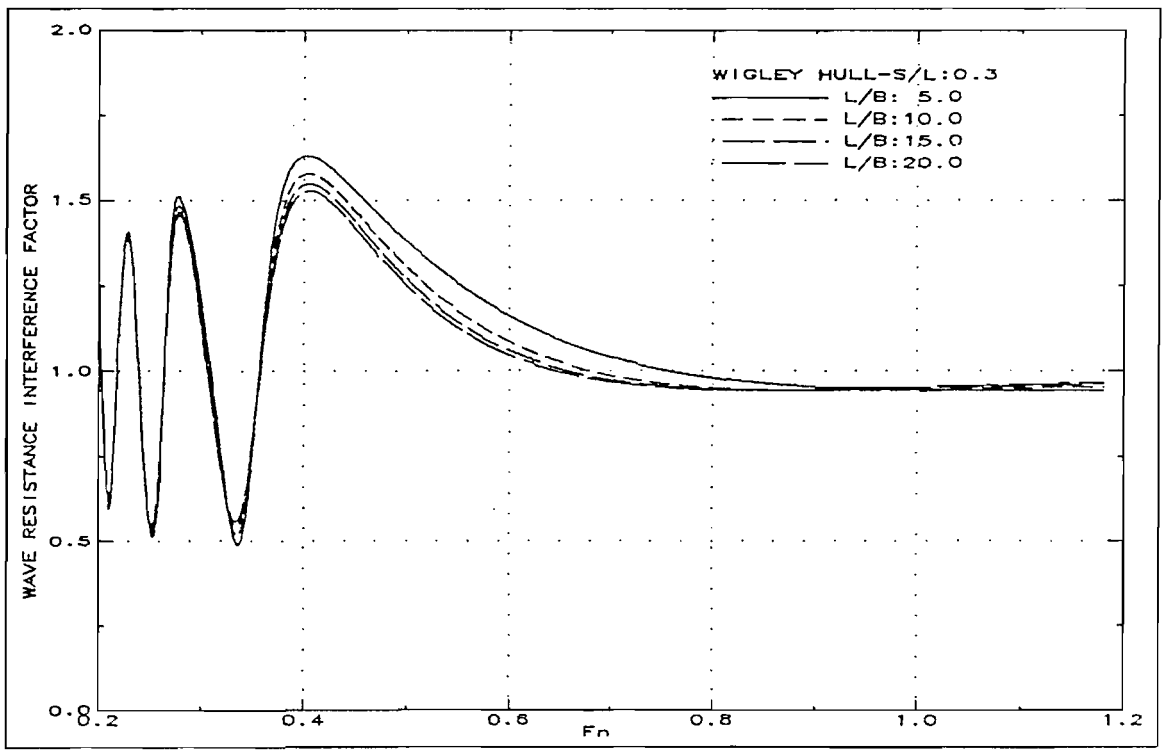

Fig.48: Theoretical wave resistance interference factor change with length to beam ratio change (Wigley Hull-S/L:Ø.3)

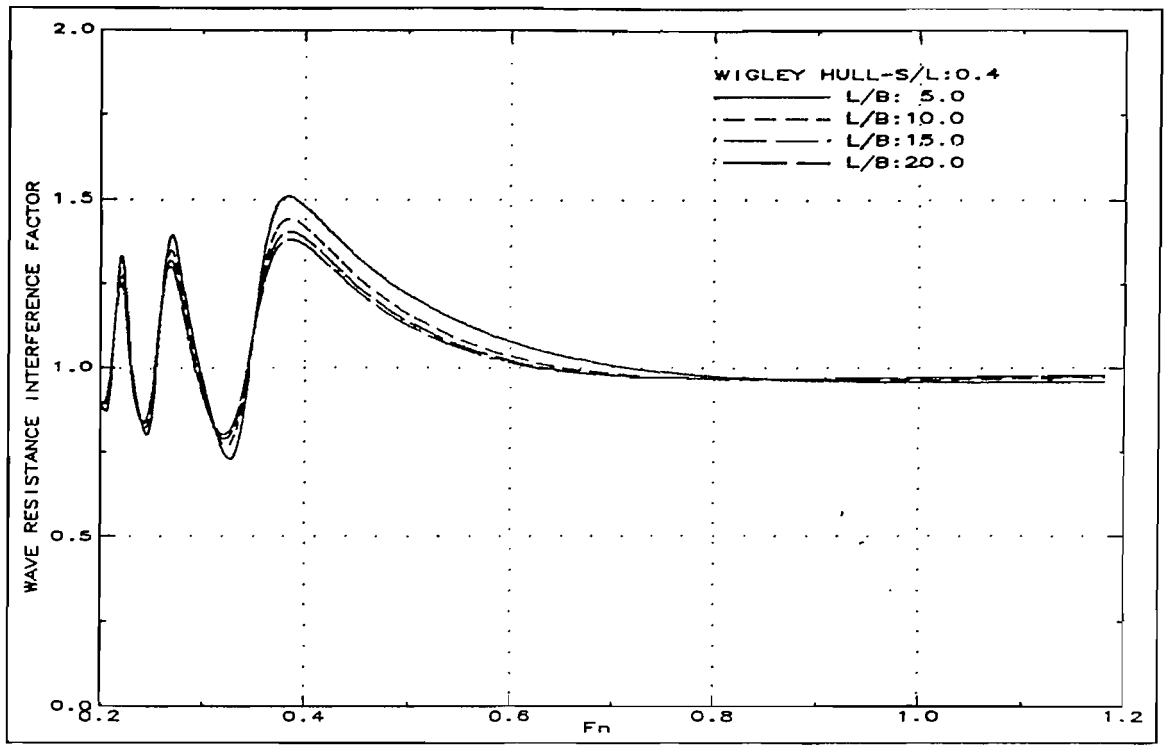

Fig.49: Theoretical wave resistance interference factor change with length to beam ratio change (Wigley Hull-S/L:0.4)

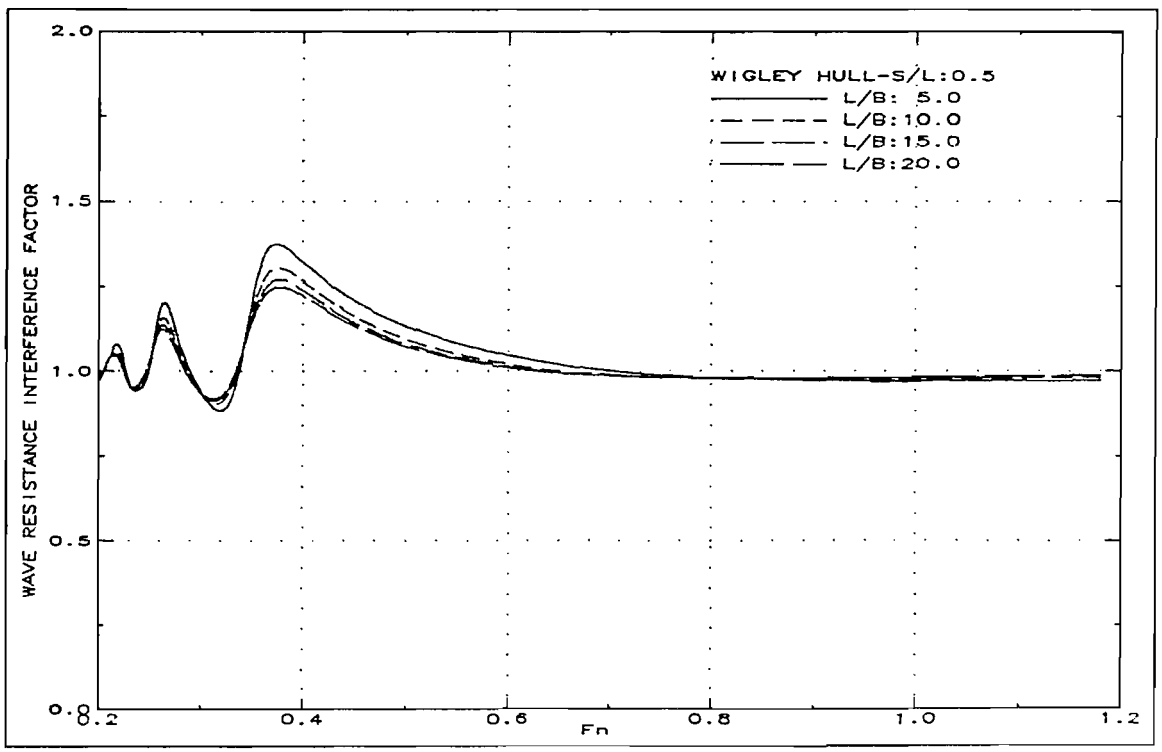

Fig.50: Theoretical wave resistance interference factor change with length to beam ratio change (Wigley Hull-S/L:0.5)

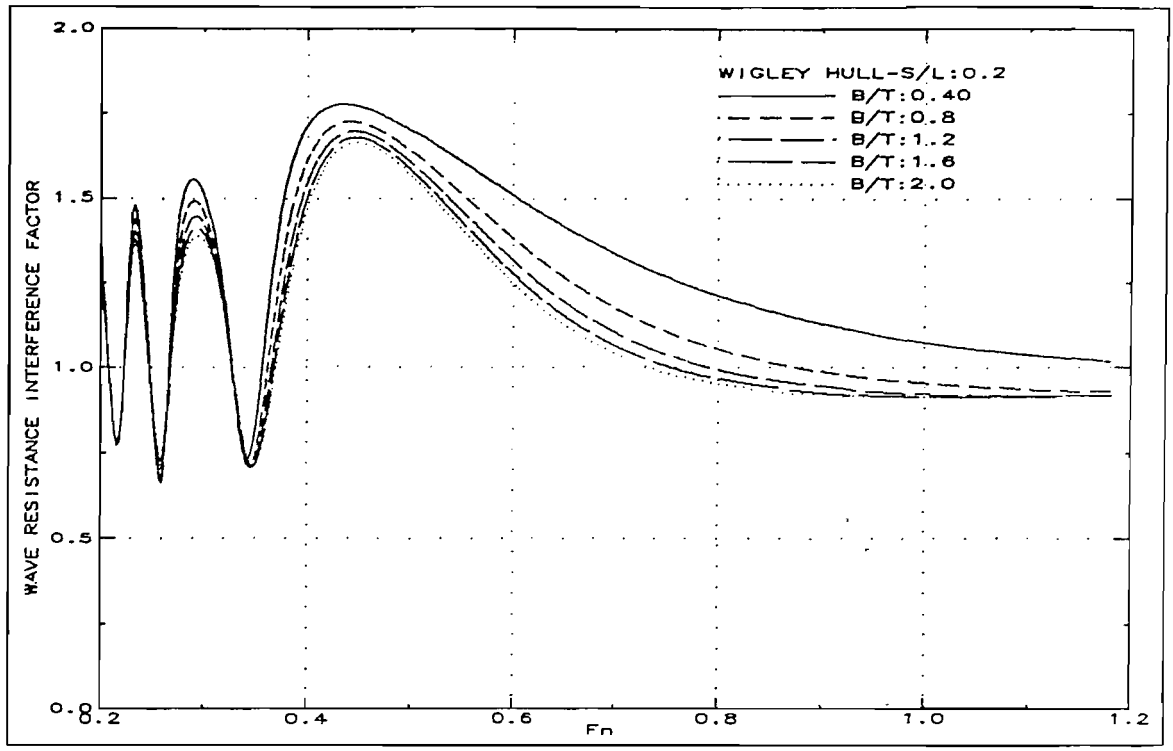

Fig.51: Theoretical wave resistance interference factor change with beam to draught ratio change (Wigley Hull-S/L:0.2)

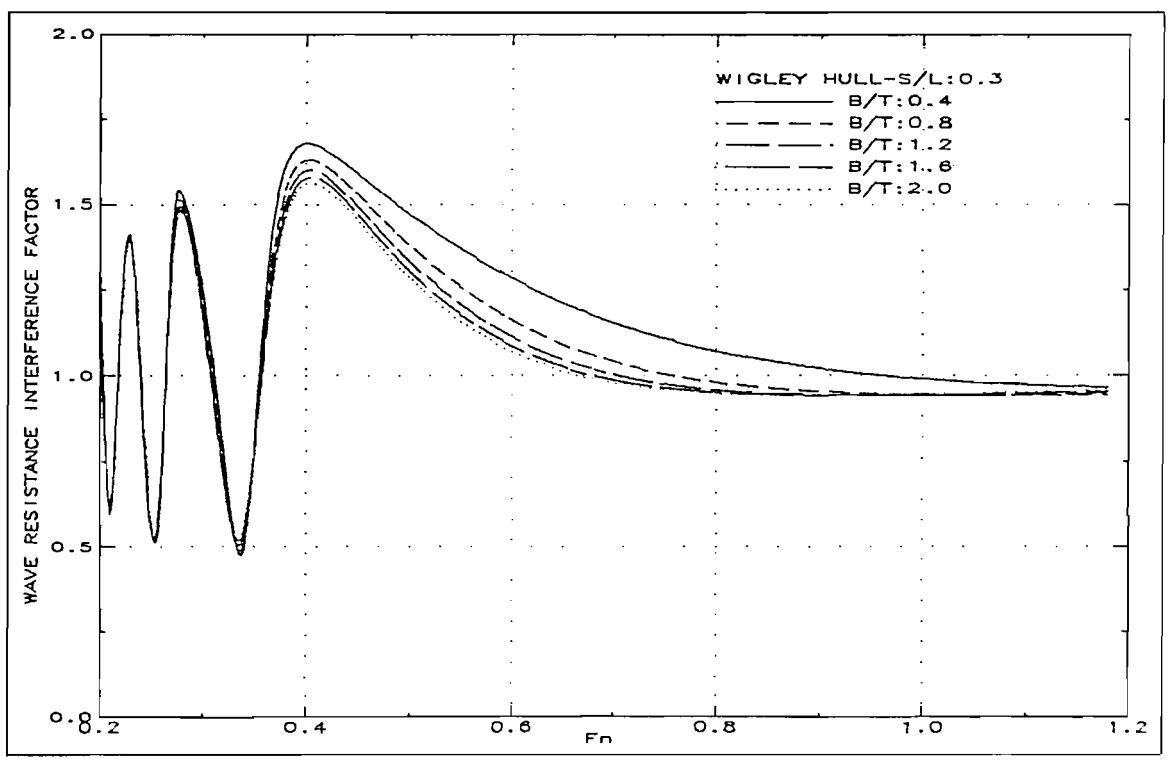

Fig.52: Theoretical wave resistance interference factor change with beam to draught ratio change (Wigley Hull-S/L:0.3)

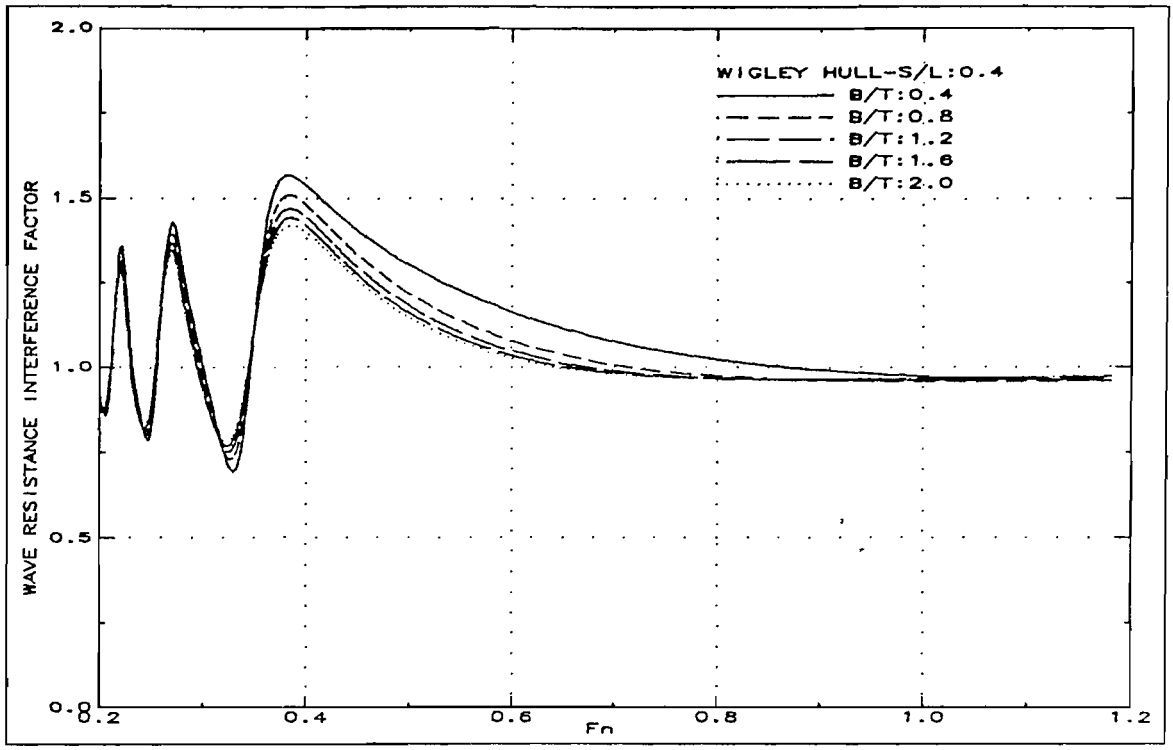

Fig.53: Theoretical wave resistance interference factor change with beam to draught ratio change (Wigley Hull-S/L:0.4)

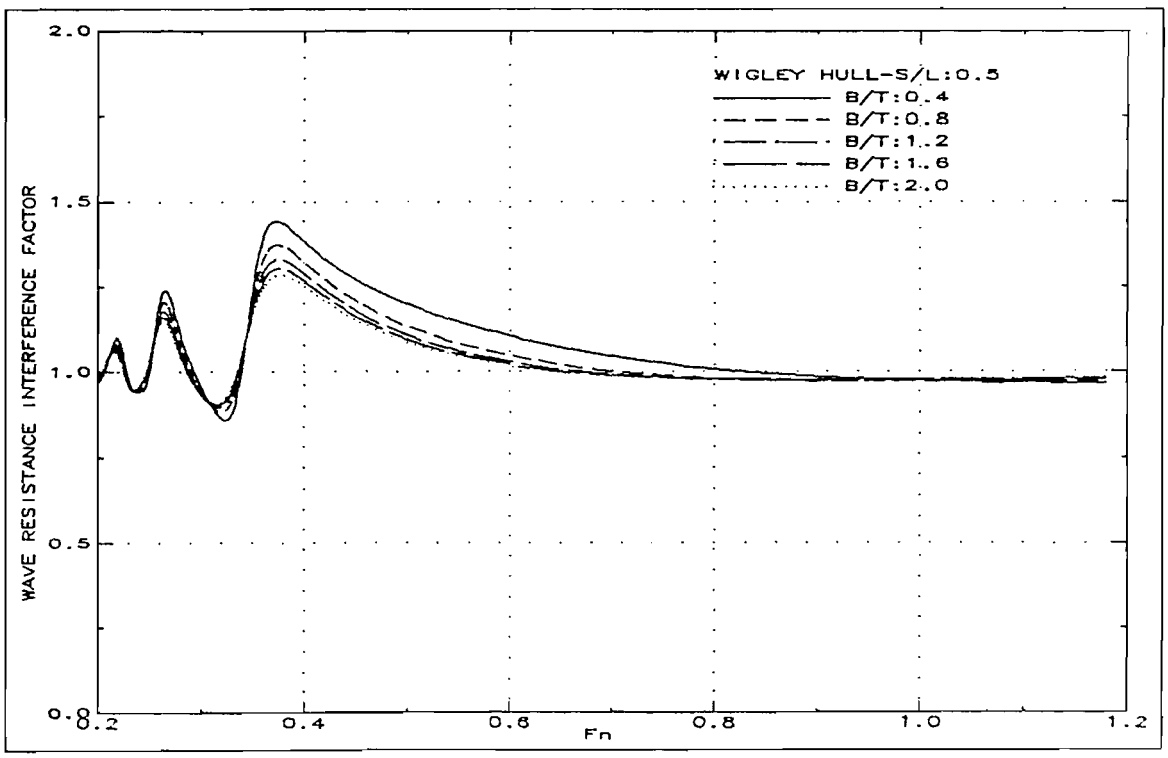

Fig.54: Theoretical wave resistance interference factor change with beam to draught ratio change (Wigley Hull-S/L:0.5)

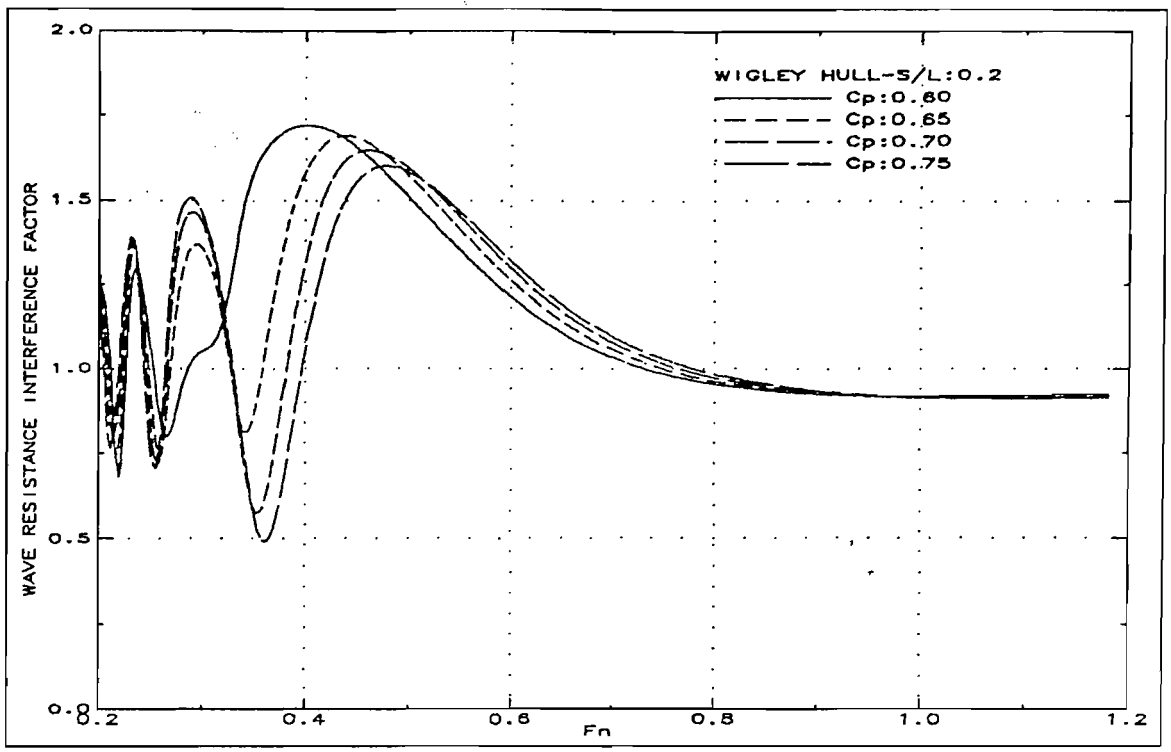

Fig.55: Theoretical wave resistance interference factor change with prismatic coefficient change (Wigley Hull-S/L:0.2)

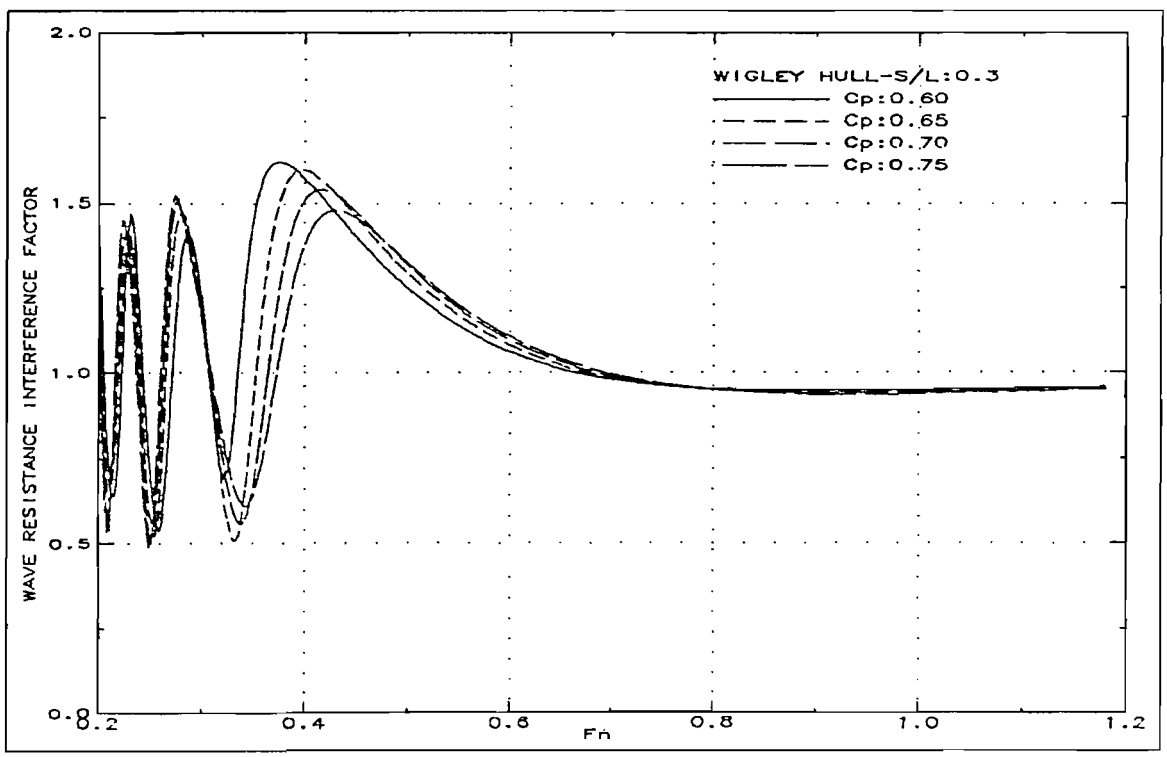

Fig.56: Theoretical wave resistance interference factor change with prismatic coefficient change (Wigley Hull-S/L:0.3)

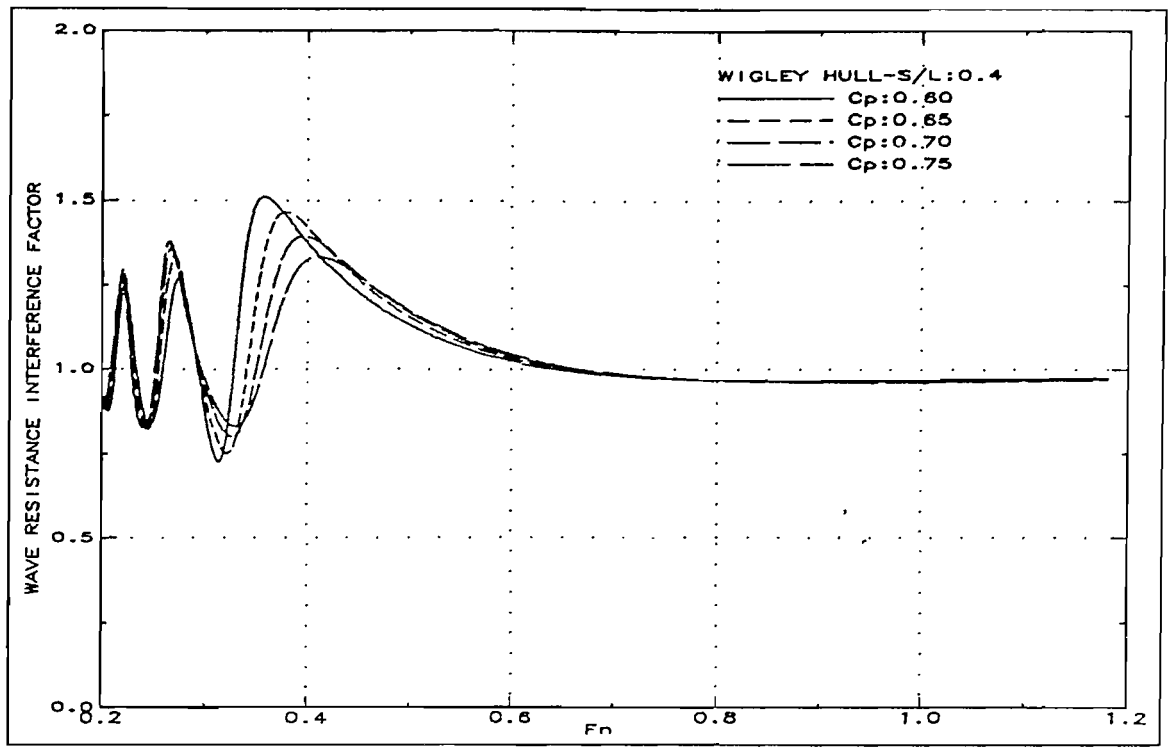

Fig.57: Theoretical wave resistance interference factor change with prismatic coefficient change (Wigley Hull-S/L:0.4)

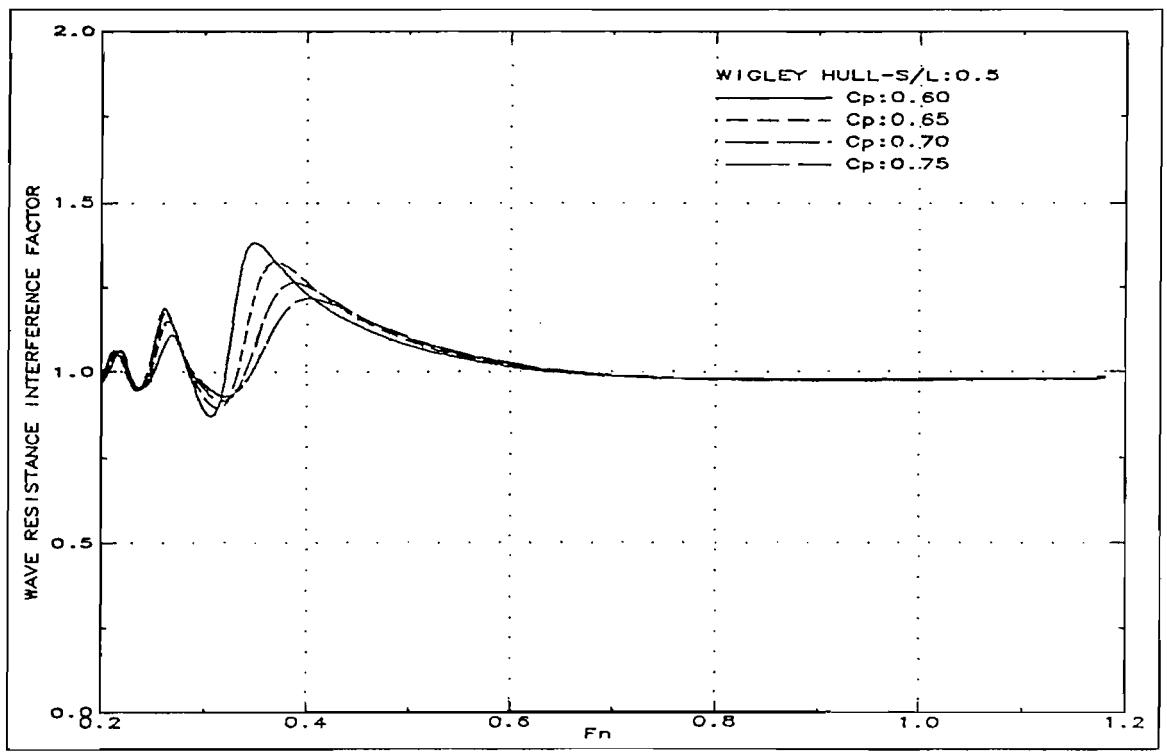

Fig.58: Theoretical wave resistance interference factor change with prismatic coefficient change (Wigley Hull-S/L:0.5)

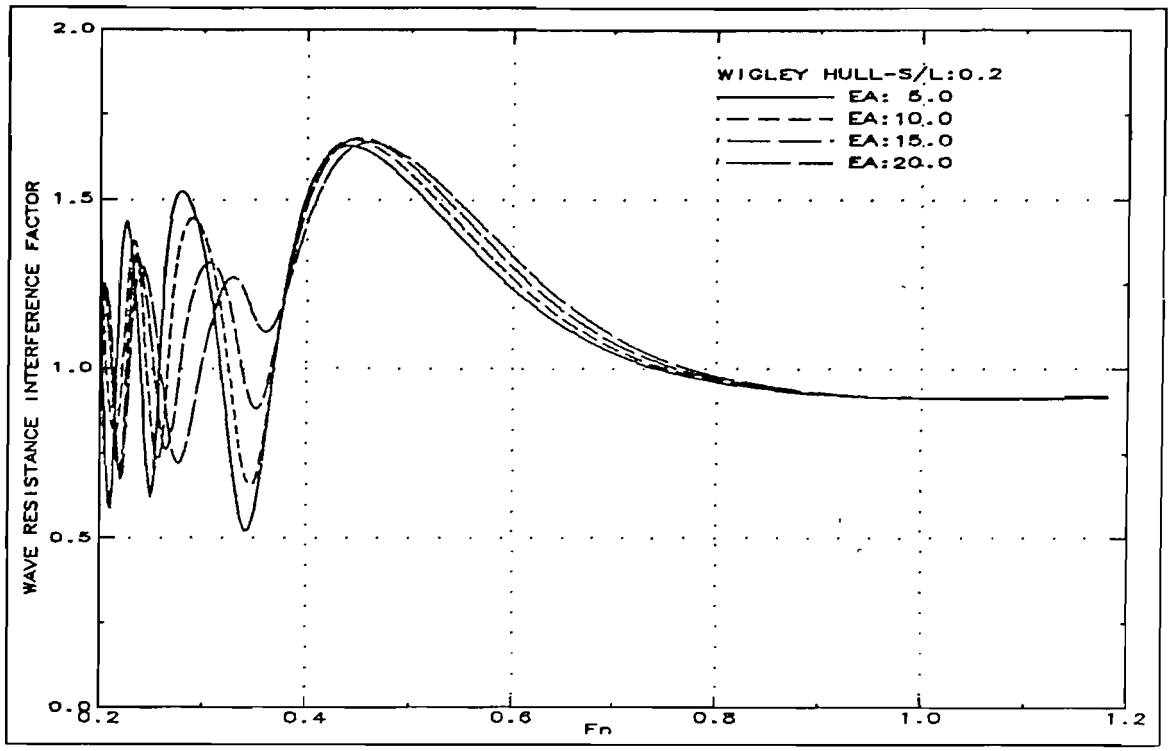

Fig.59: Theoretical wave resistance interference factor change with entrance angle change (Wigley Hull-S/L:Ø.2)

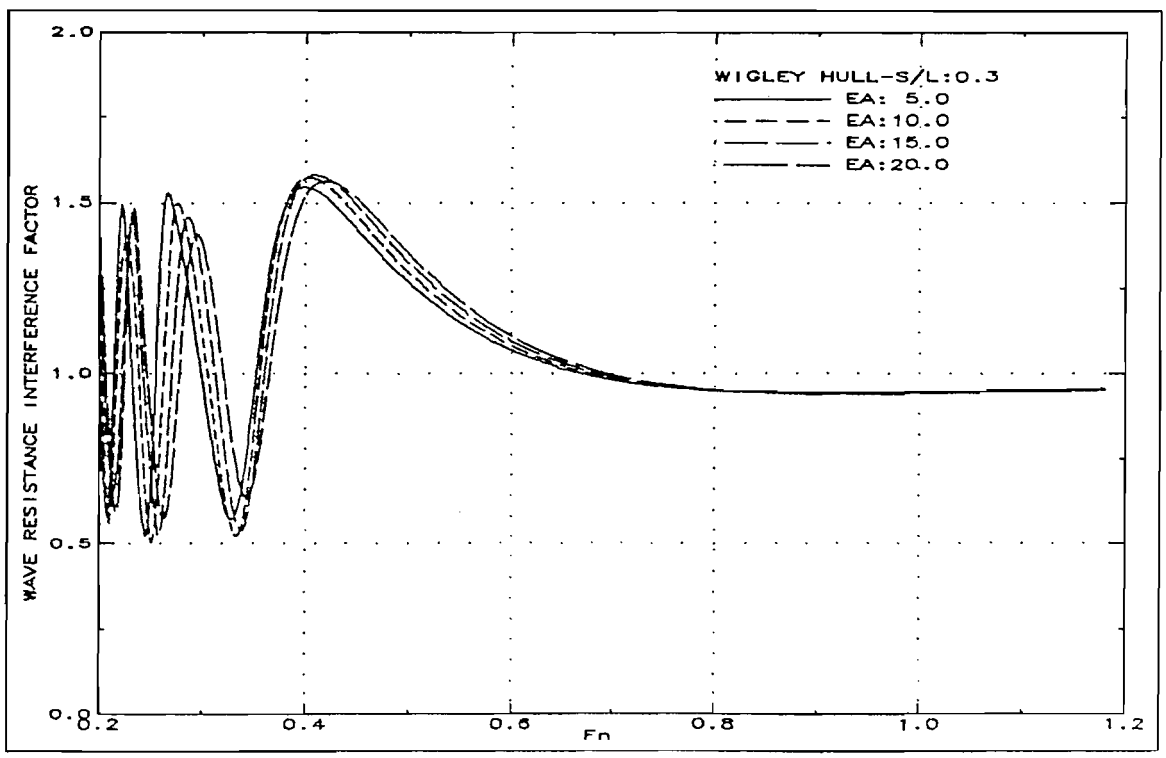

Fig.6Ø: Theoretical wave resistance interference factor change with entrance angle change (Wigley Hull-S/L:Ø.3)

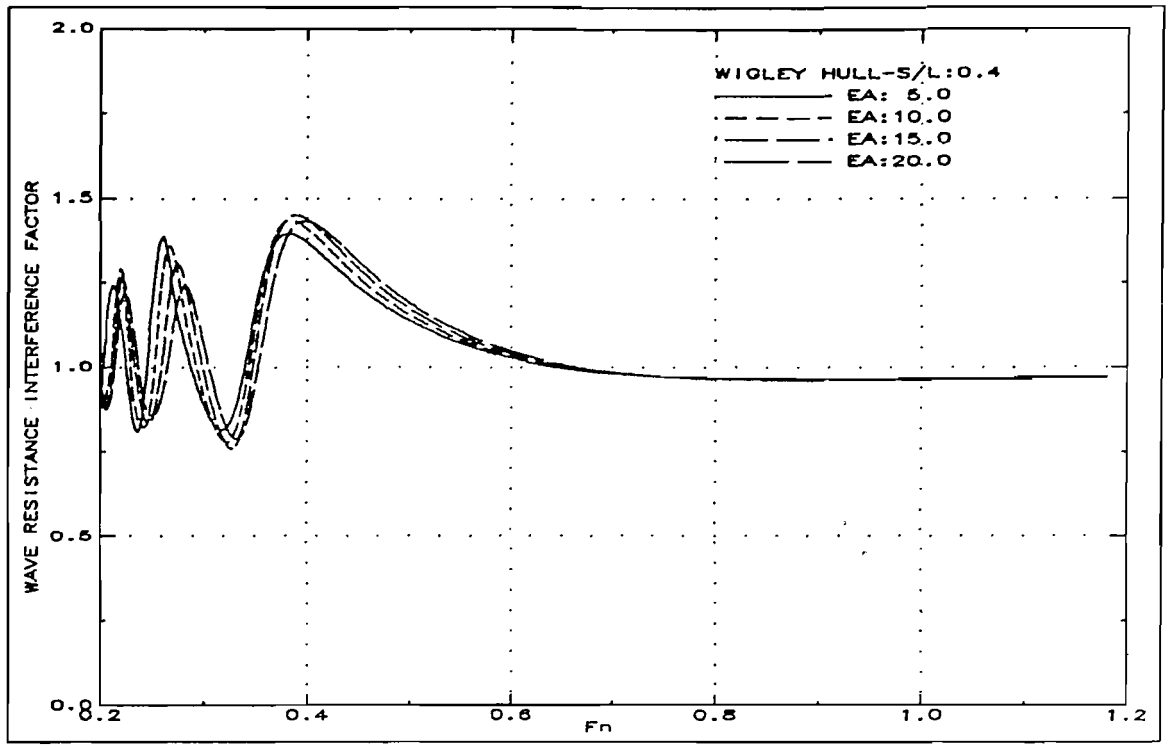

Fig.61: Theoretical wave resistance interference factor change with entrance angle change (Wigley Hull-S/L:0.4)

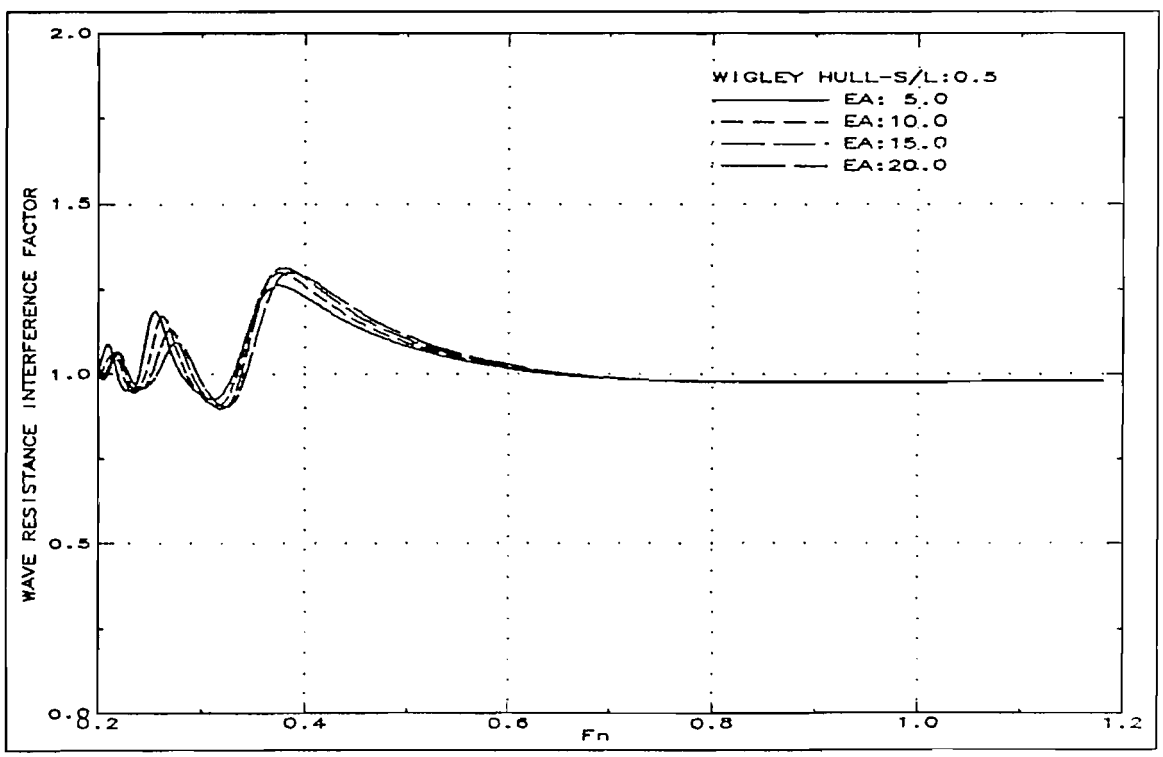

Fig.62: Theoretical wave resistance interference factor change with entrance angle change (Wigley Hull-S/L:0.5)

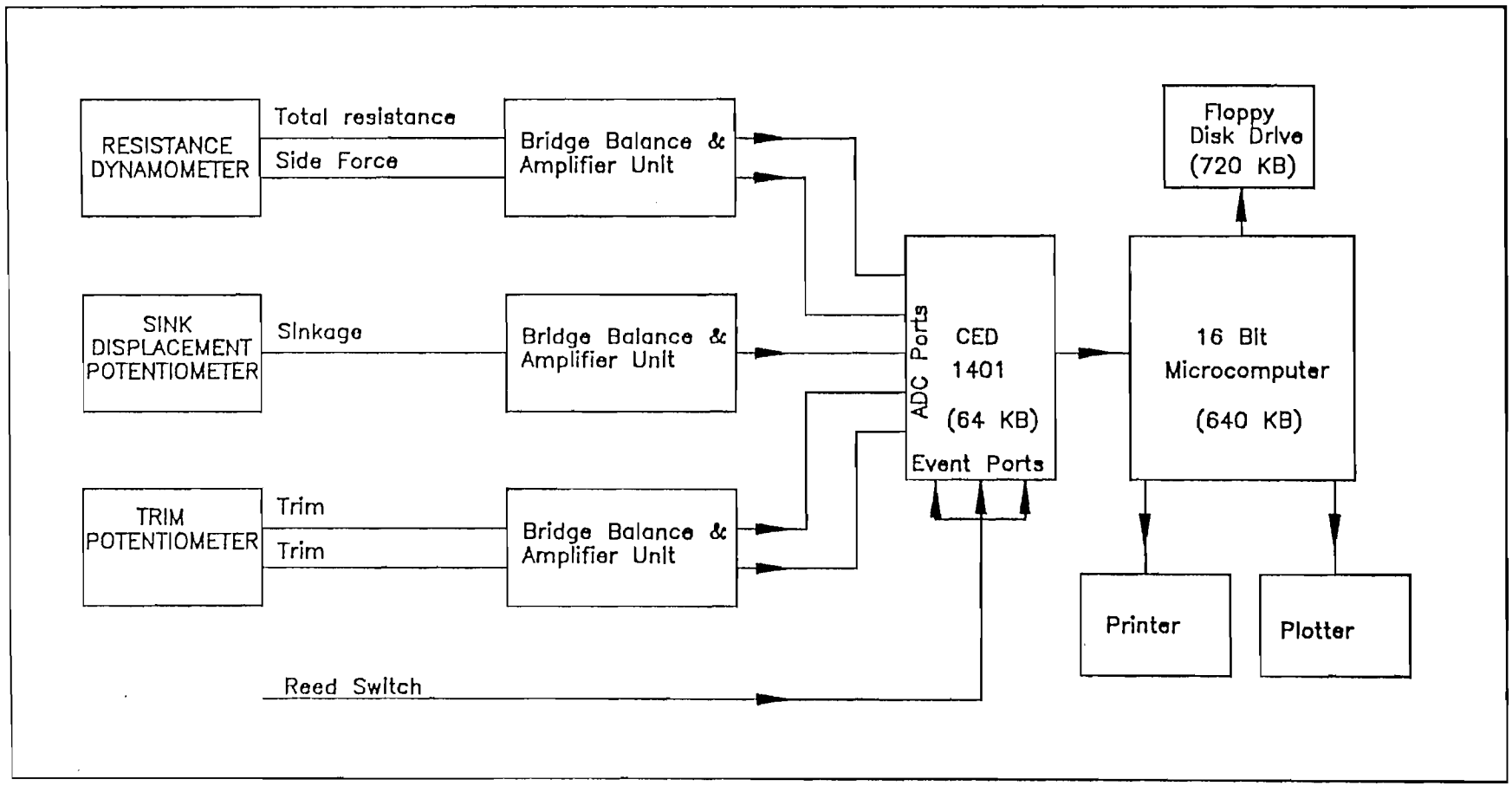

Fig.63: Setup for resistance/trim/sinkage tests

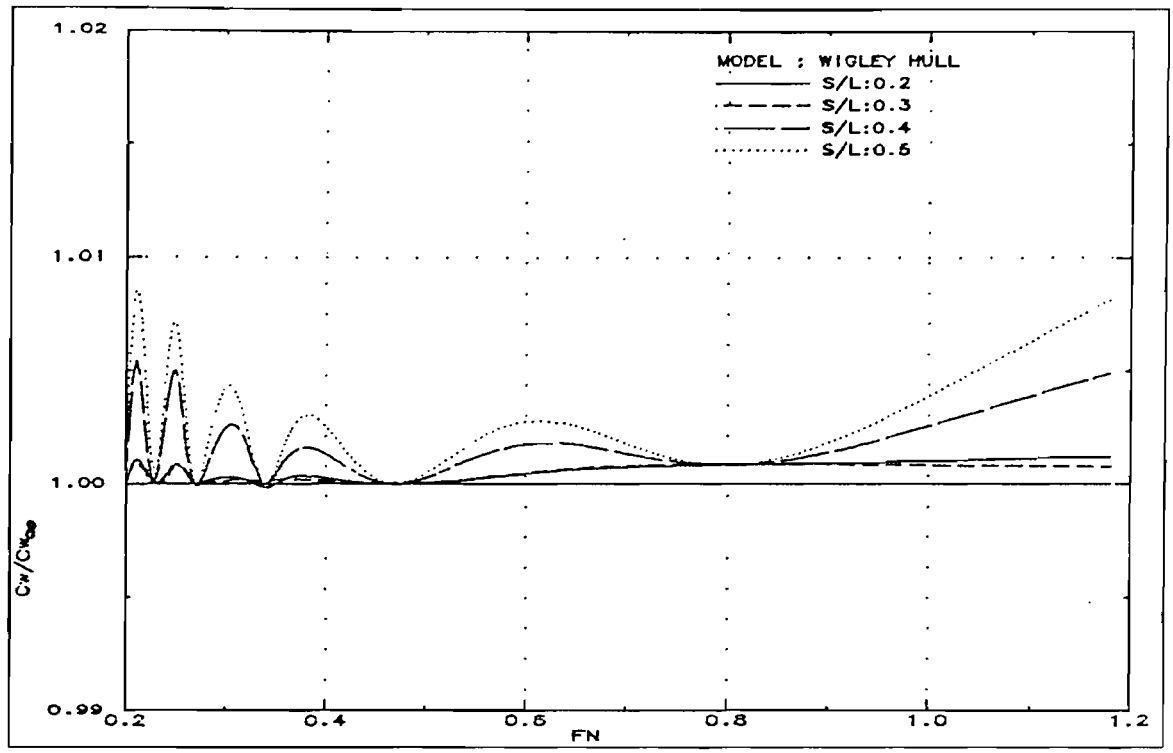

Fig.64: Tank width effect on catamaran wave resistance (Wigley Hull - H=10L)

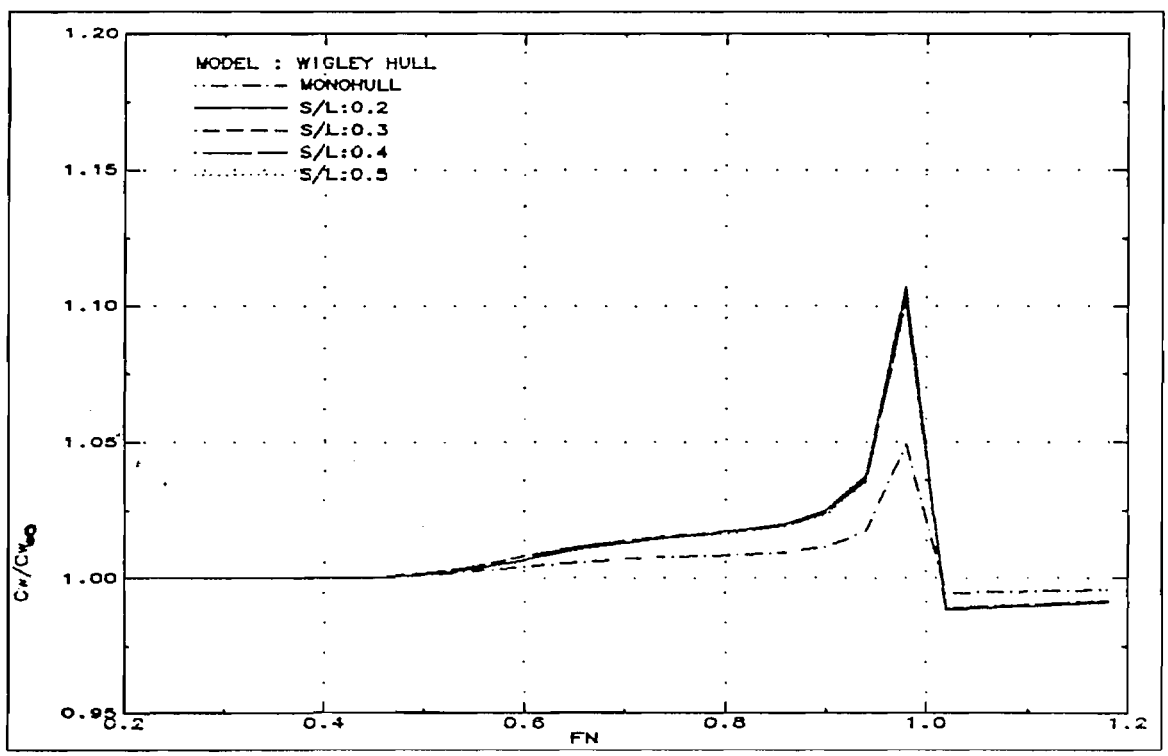

Fig.65: Tank depth effect on catamaran wave resistance (Wigley Hull - W=10L)

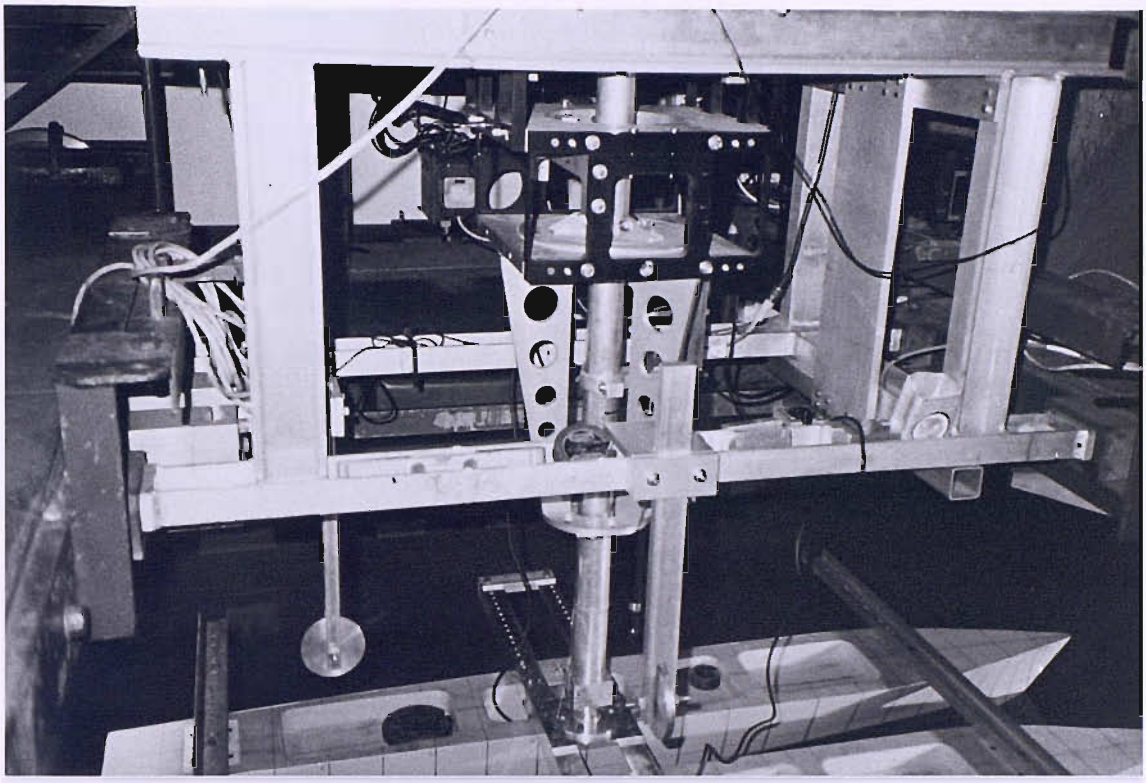

Fig. 66 : Resistance dynamometer

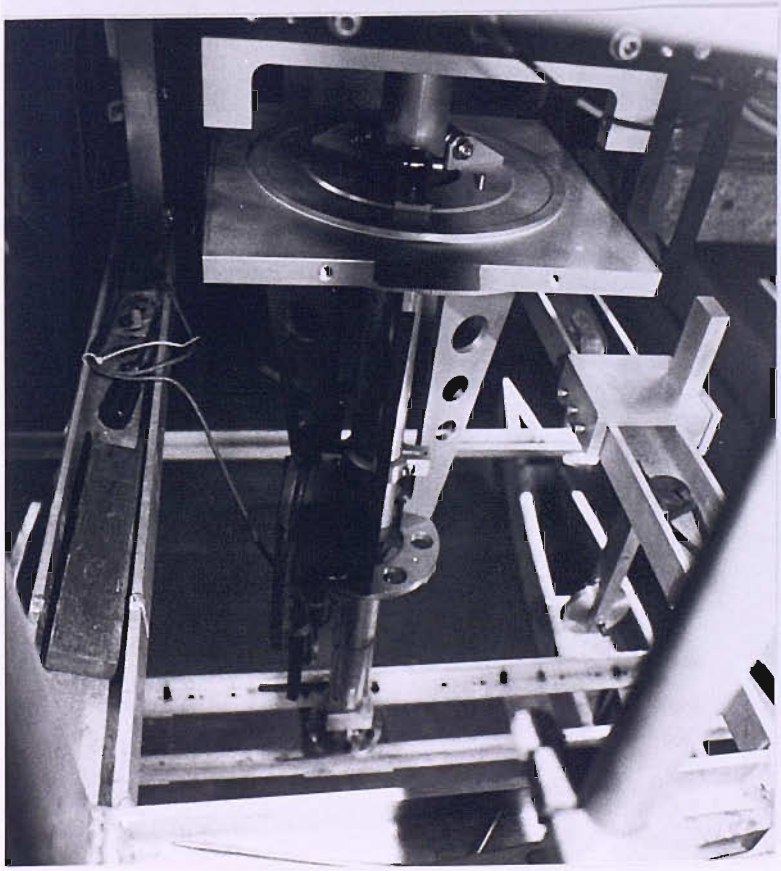

Fig. 67 : Tow post fixing arrangement

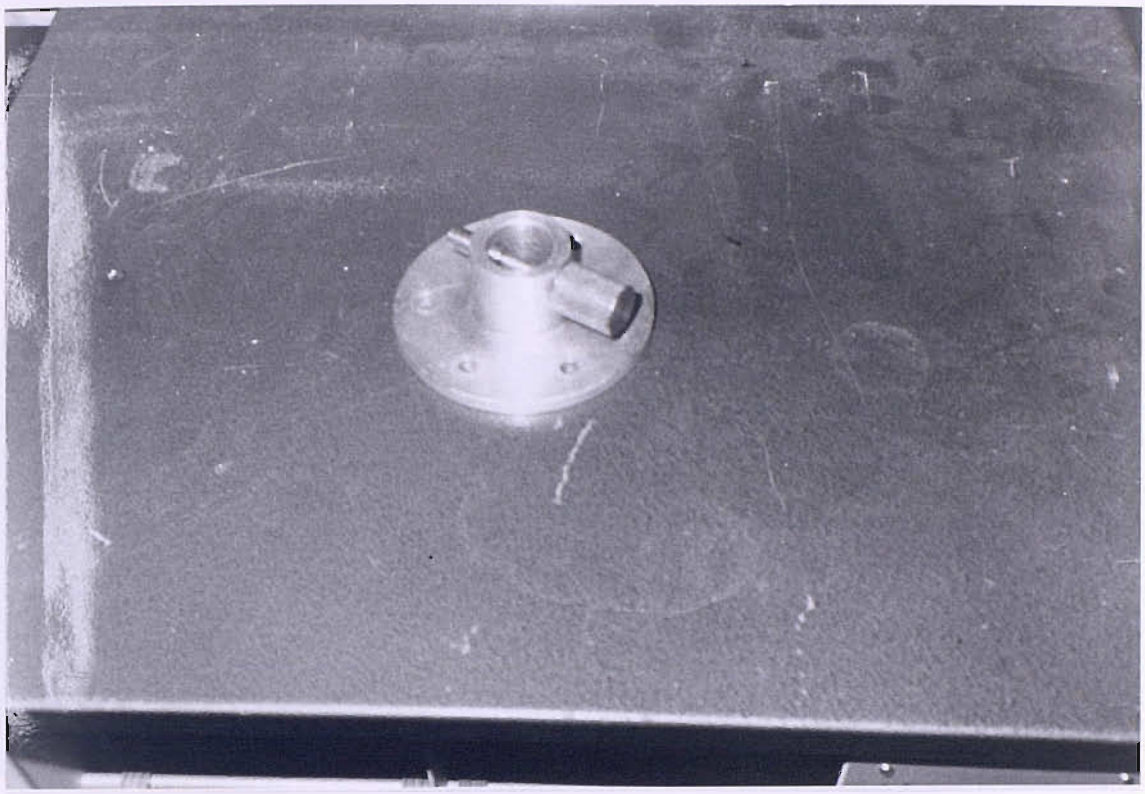

Fig. 68 : Monohull tow fitting (Fixed to trim and sink)

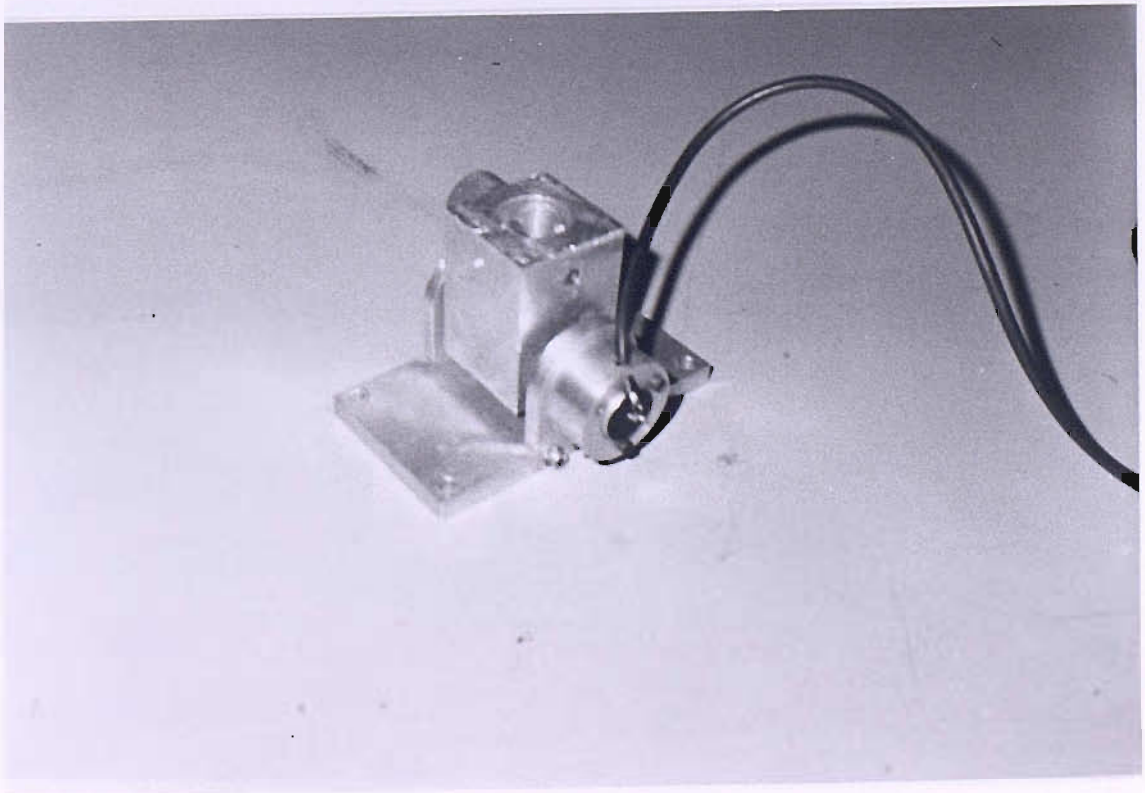

Fig. 69 : Monohull tow fitting (Free to trim and sink)

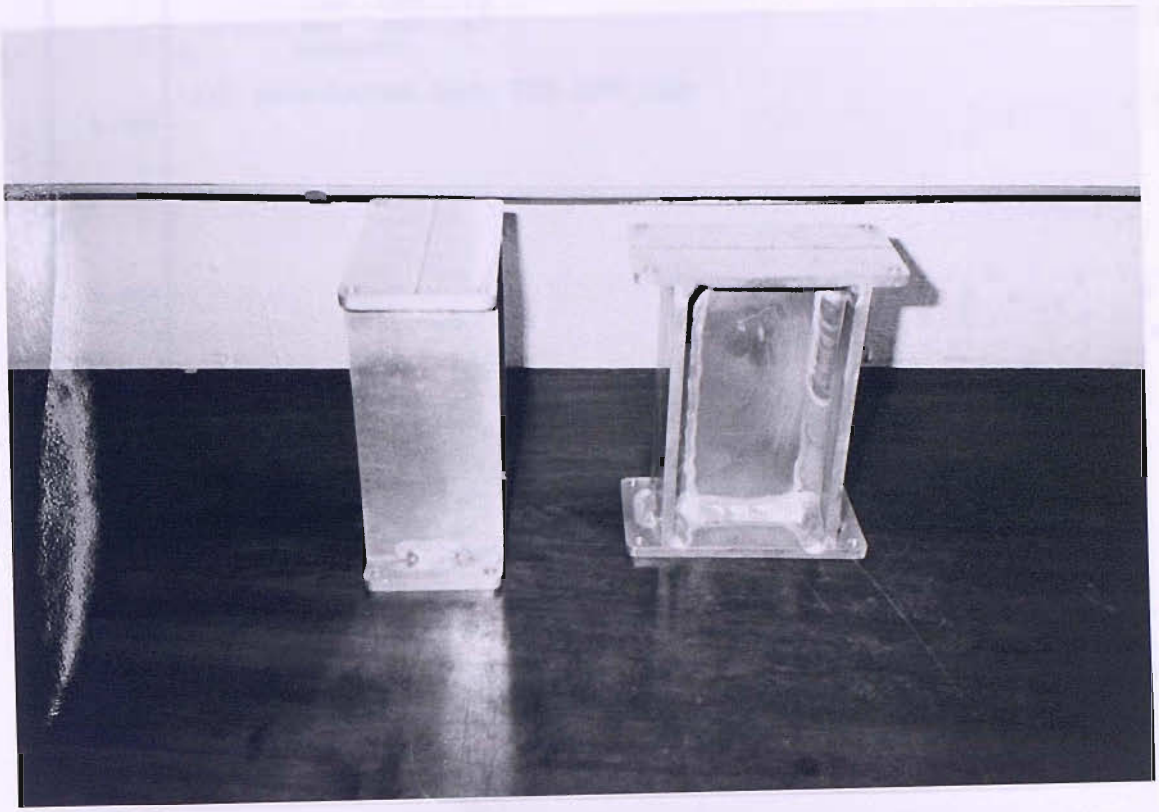

Fig. 7Ø : Catamaran tow fittings (Fixed to trim and sink)

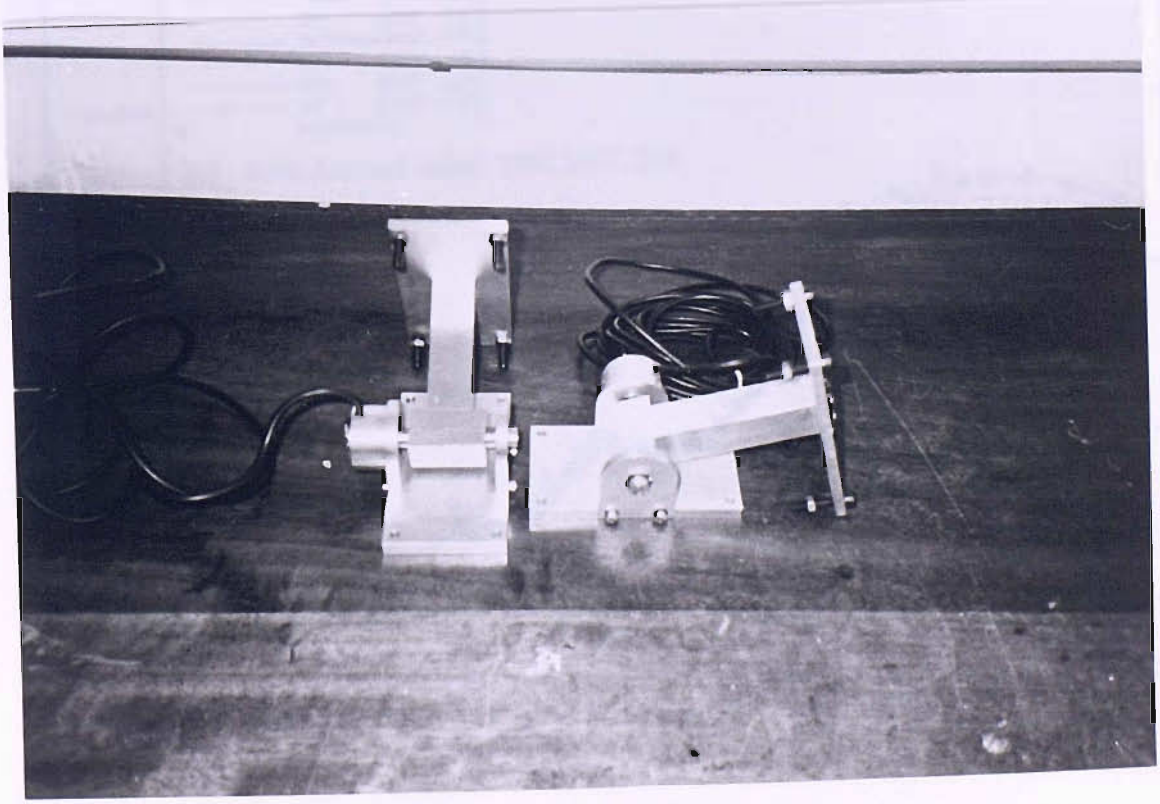

Fig. 71 : Catamaran tow fittings (Free to trim and sink)

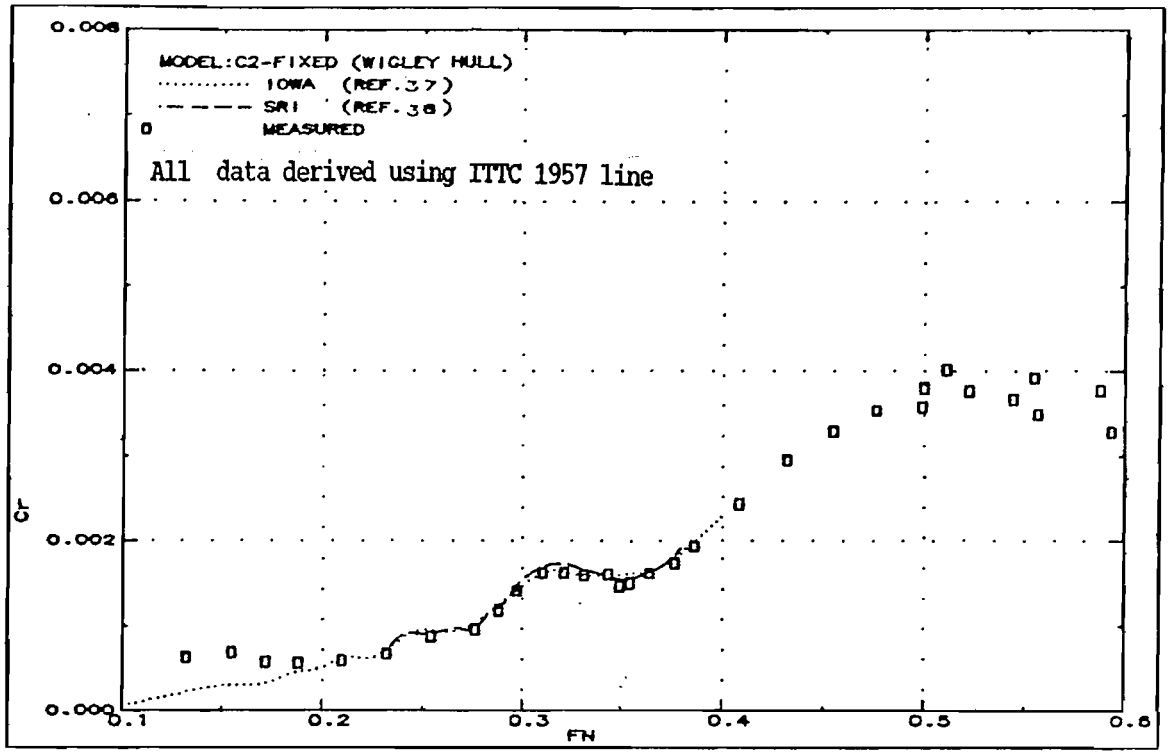

Fig.72: Comparison of measured residuary resistance with available experimental data (Wigley Hull-Fixed)

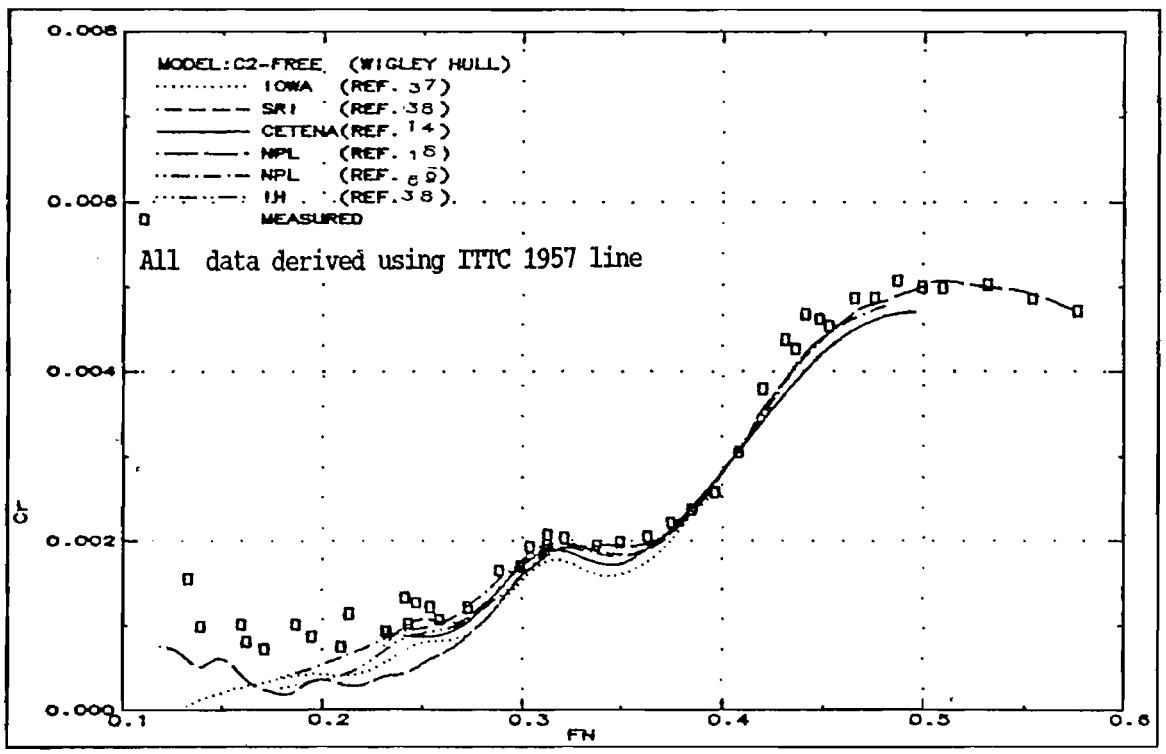

Fig.73: Comparison of measured residuary resistance with available experimental data (Wigley Hull-Free)

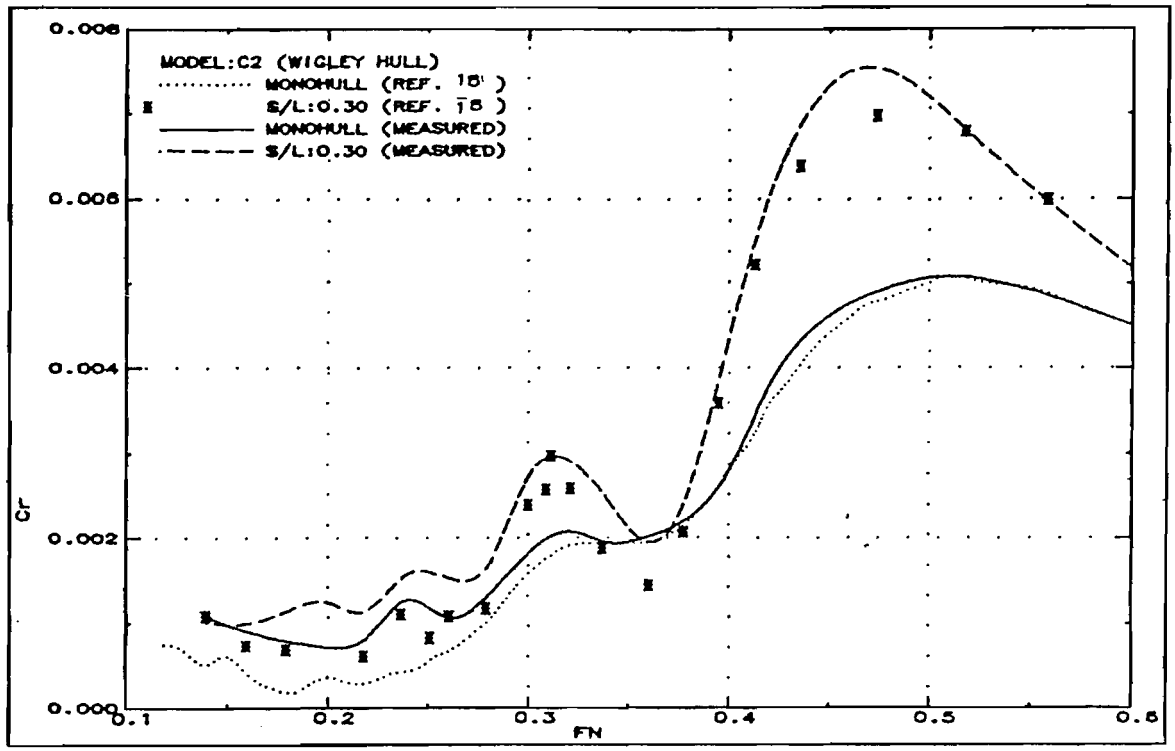

Fig.74: Comparison of measured residuary resistance with available experimental data (Wigley Hull Catamaran-S/L:Ø.3-Free)

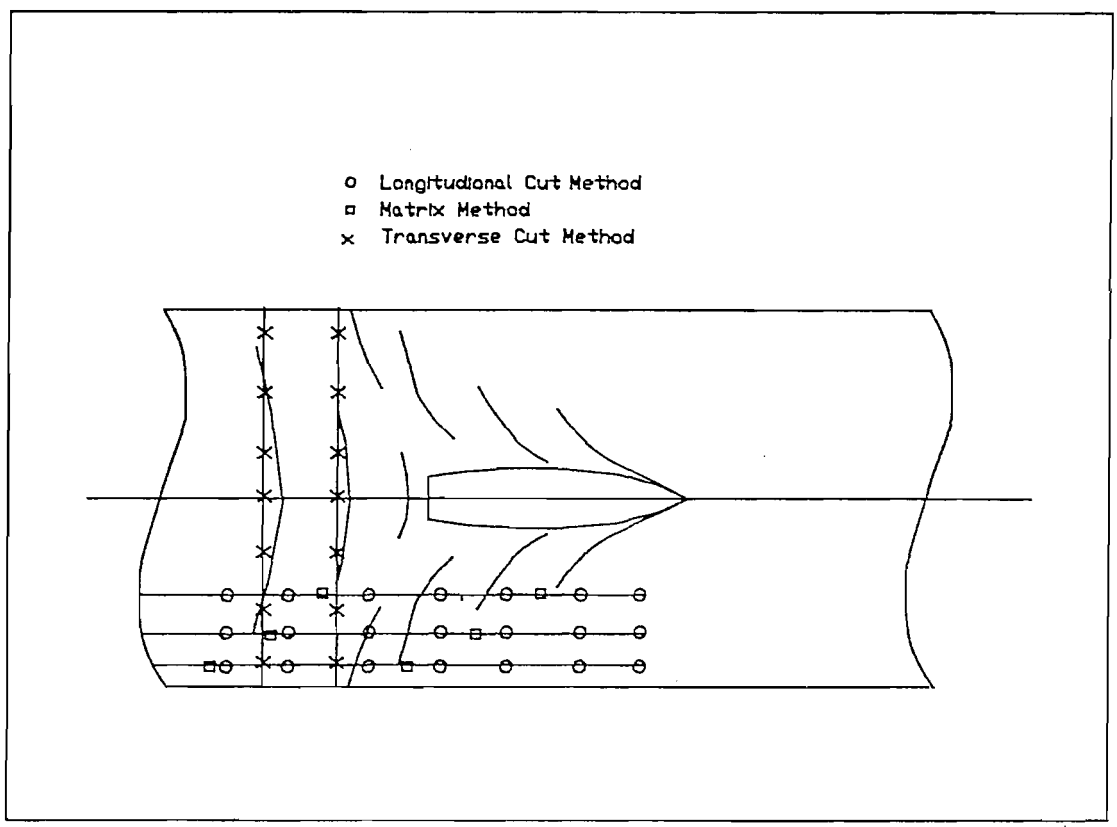

Fig.75: Wave pattern measurement points

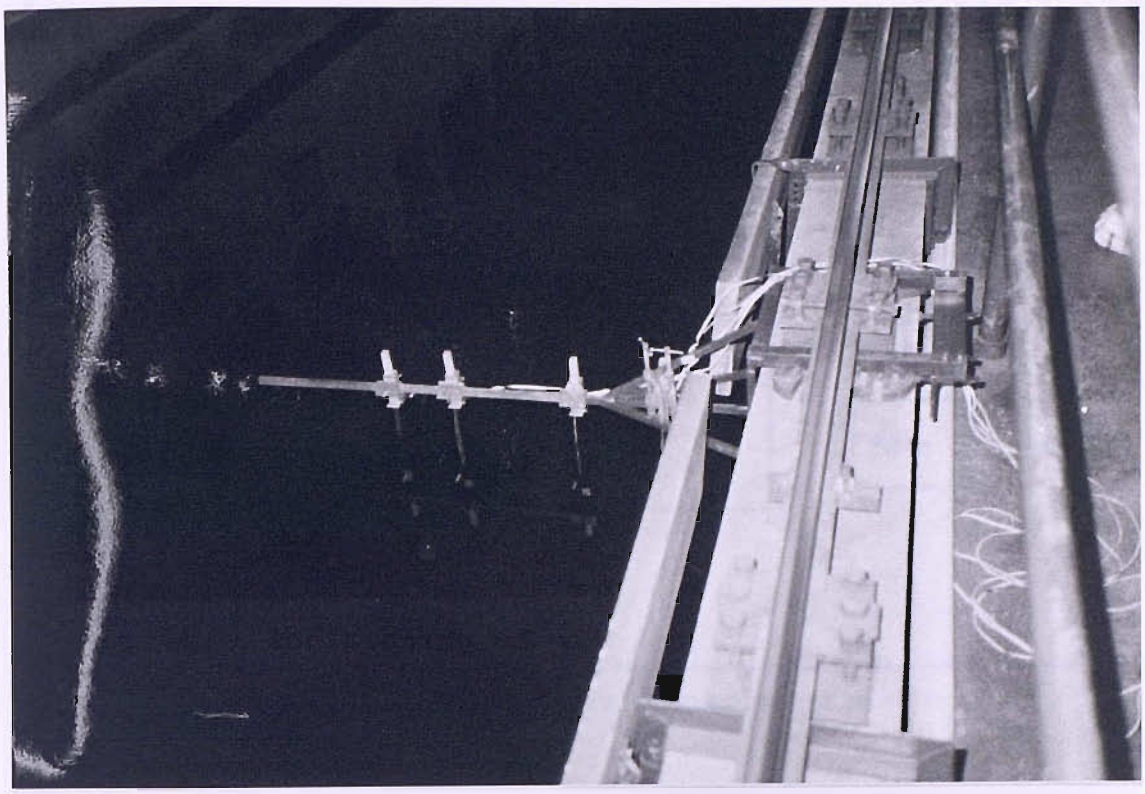

Fig. 76 : Positioning of wave probes

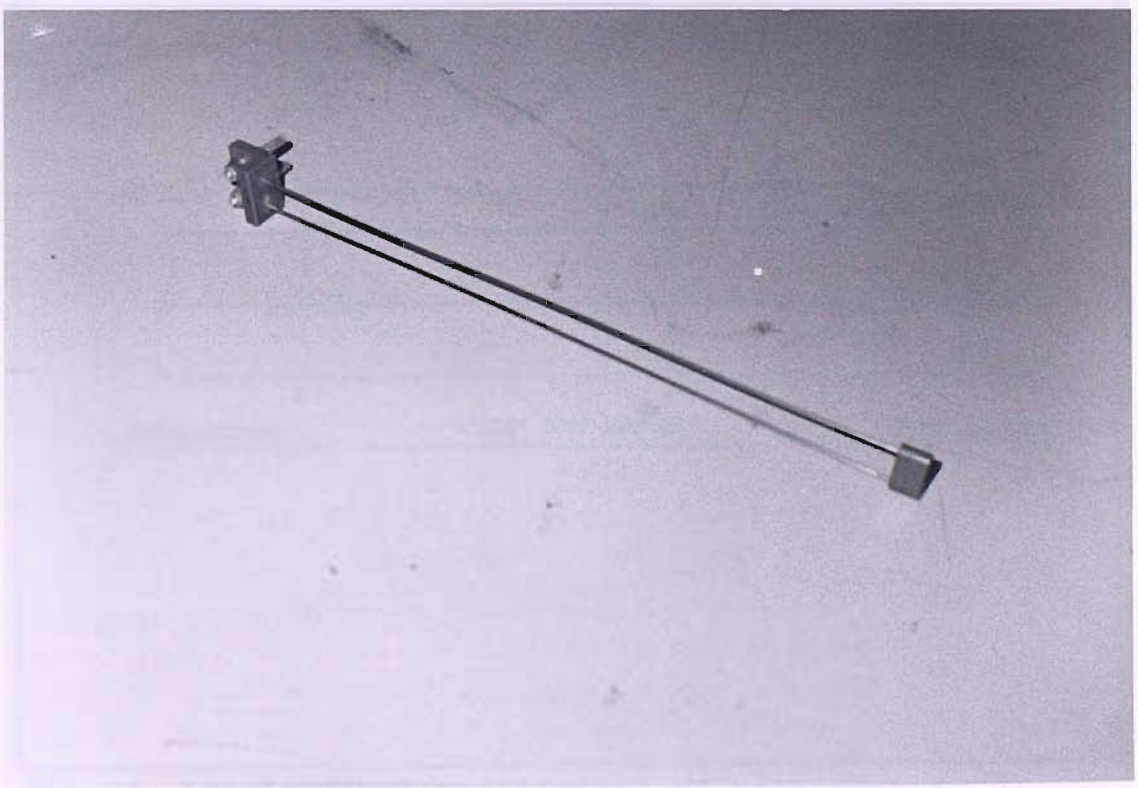

Fig. 77 : Resistance wave probe

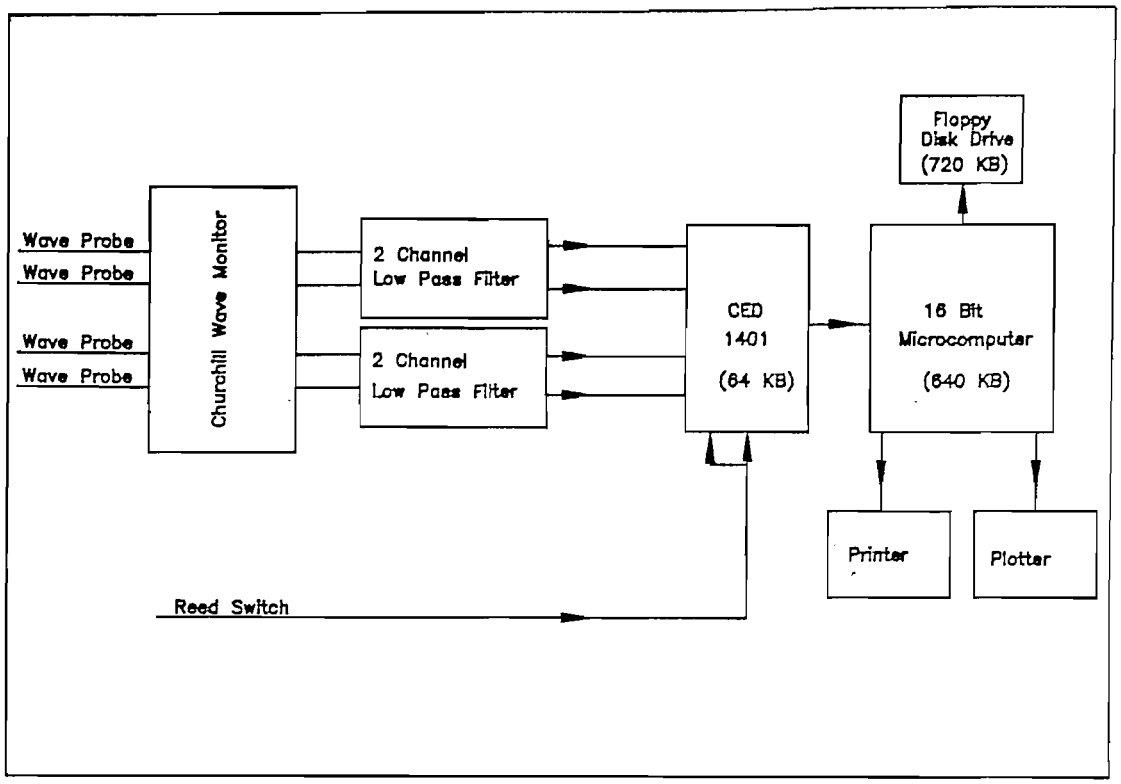

Fig.78: Setup for wave pattern experiments

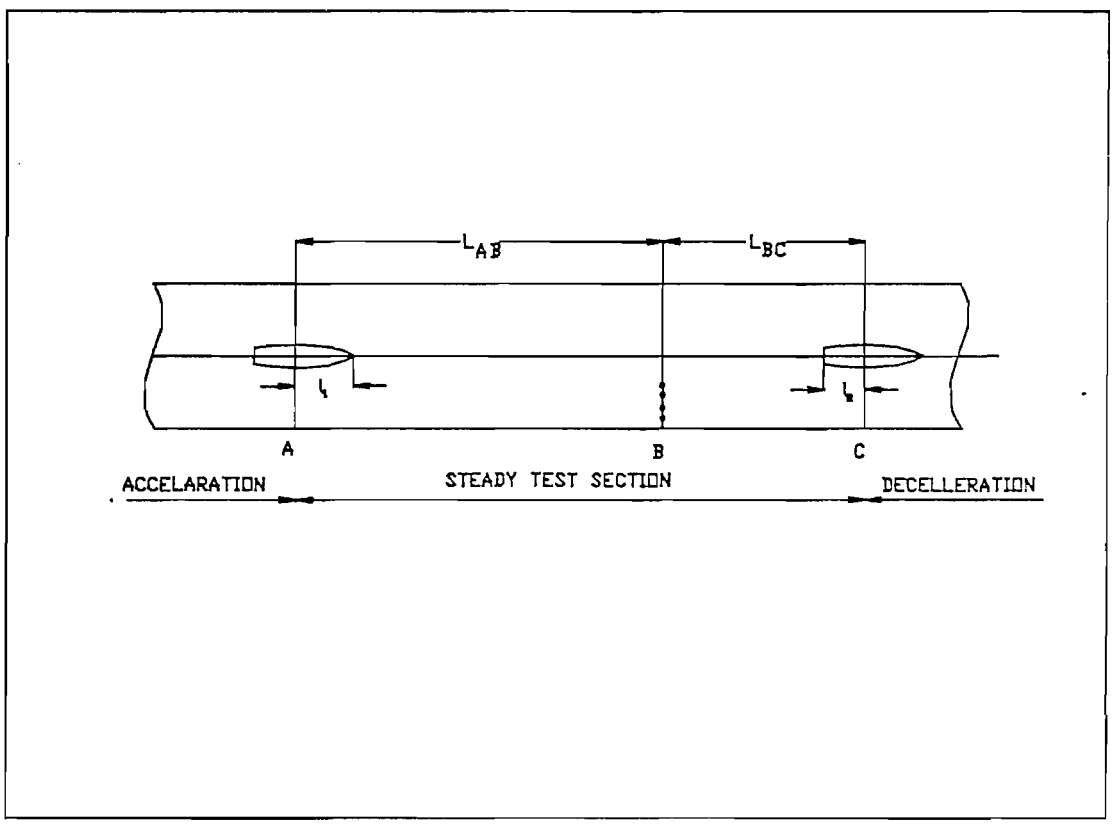

Fig.79: Longitudinal positioning of wave probes

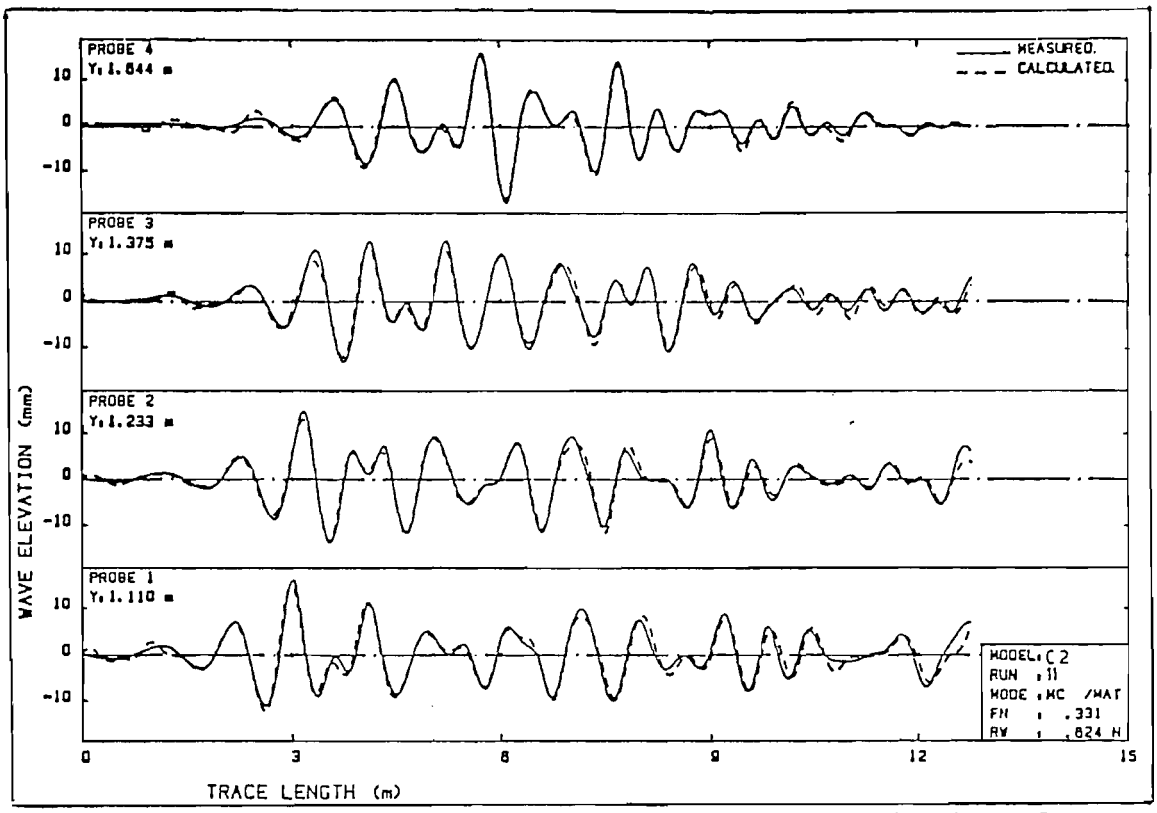

Fig.80: Typical comparison of measured and calculated wave patterns

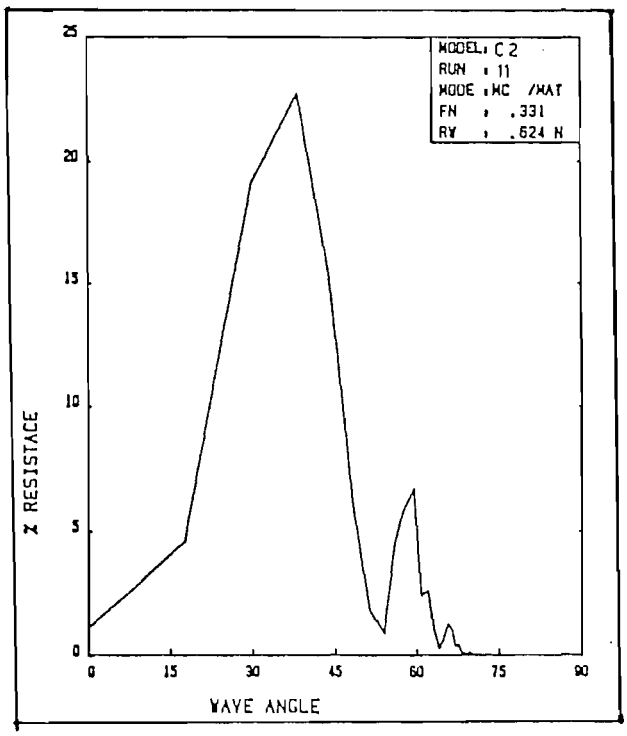

Fig.81: Typical wave pattern resistance distribution across the wave spectrum

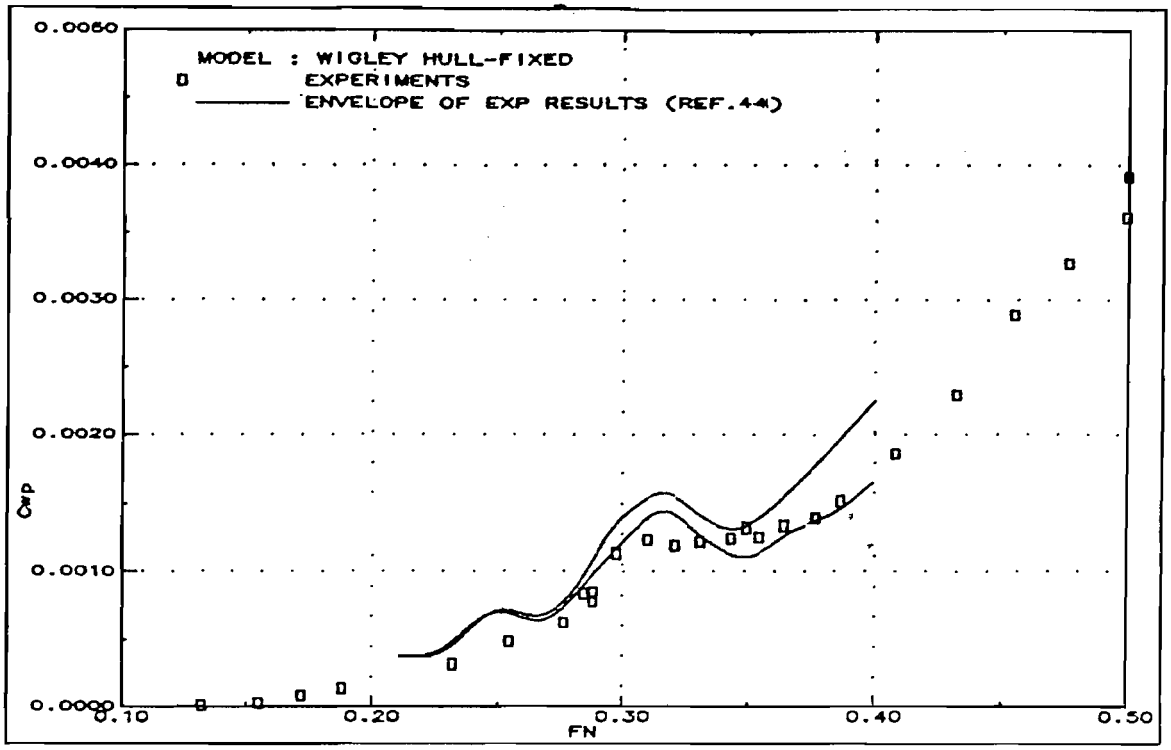

Fig.82: Comparison of measured wave pattern resistance with available experimental data (Wigley Hull-Fixed)

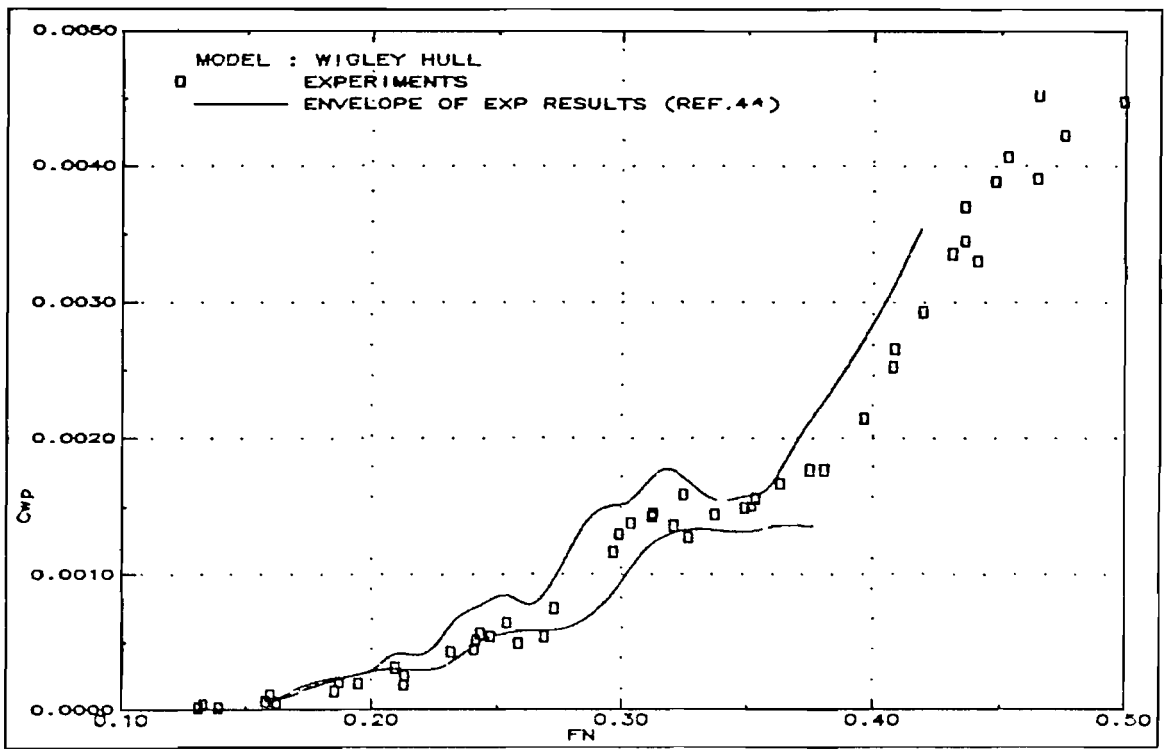

Fig.83: Comparison of measured wave pattern resistance with available experimental data (Wigley Hull-Free)

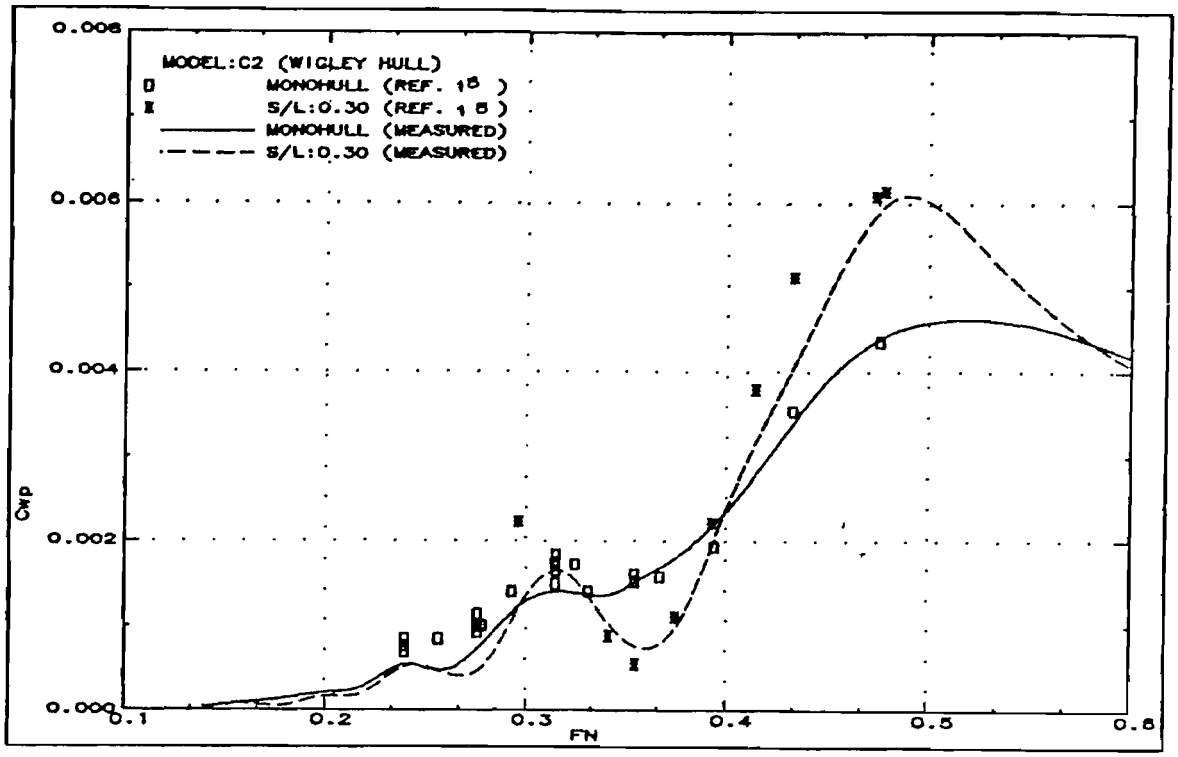

Fig.84: Comparison of measured wave pattern resistance with available experimental data (Wigley Hull Catamaran-S/L:Ø.3-Free)

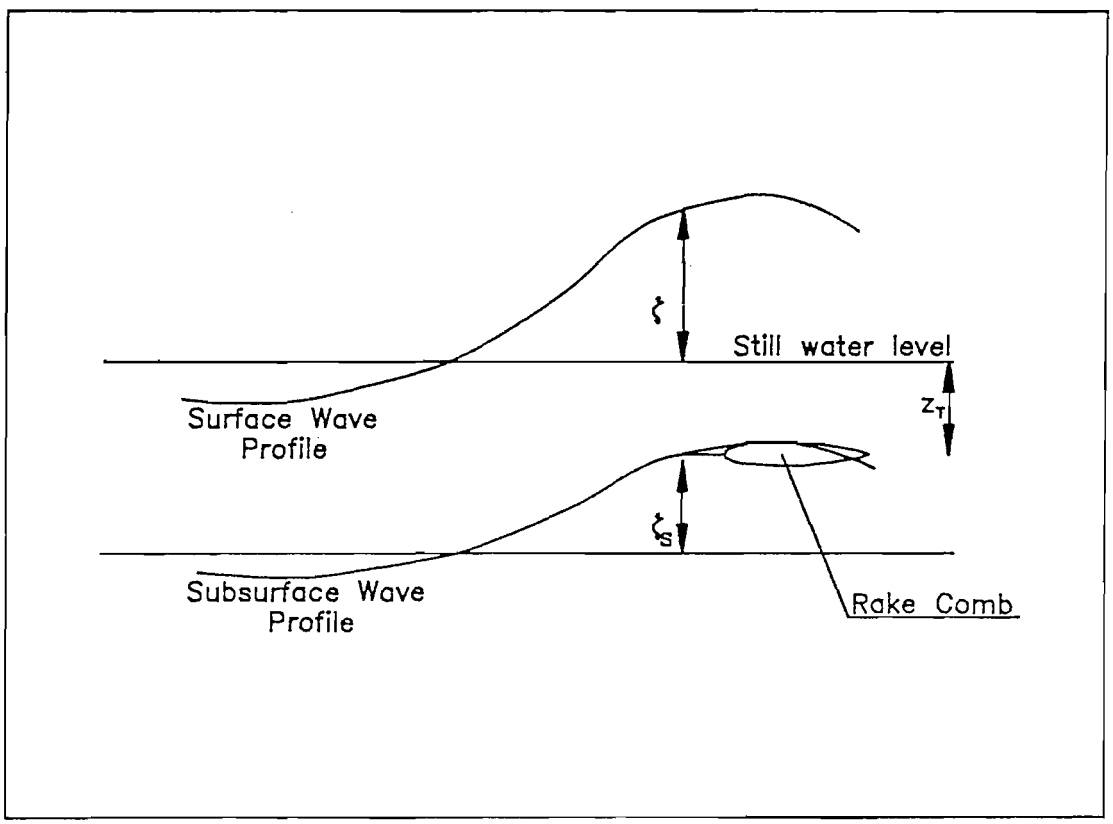

Fig.85: Determination of static pressure by wave height measurement

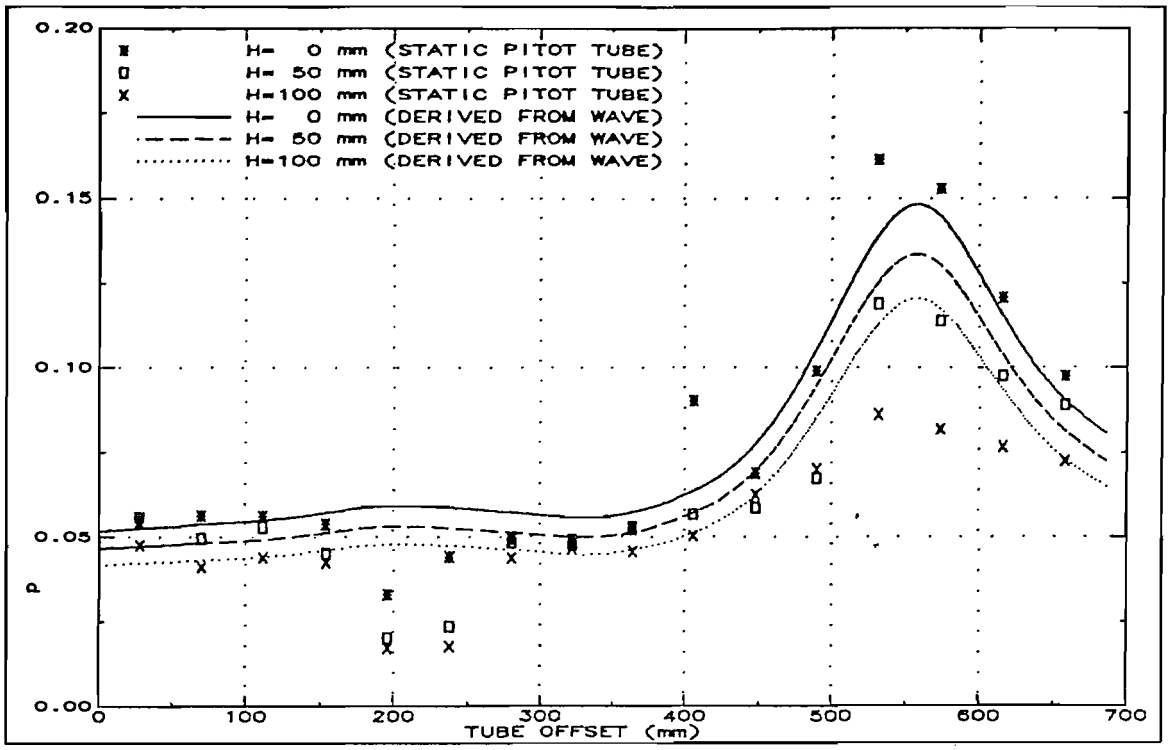

Fig.86: Comparison of static pressures derived from wave elevation with measured static pressures

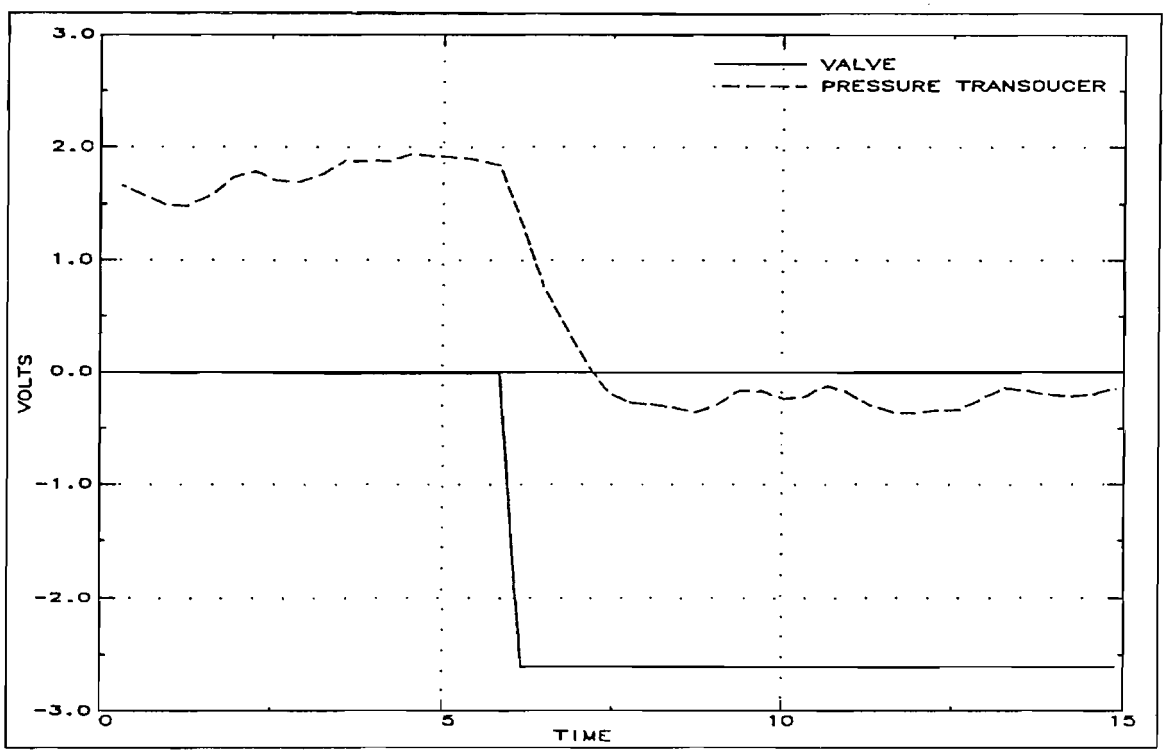

Fig.87: Transient signal due to valve actuation

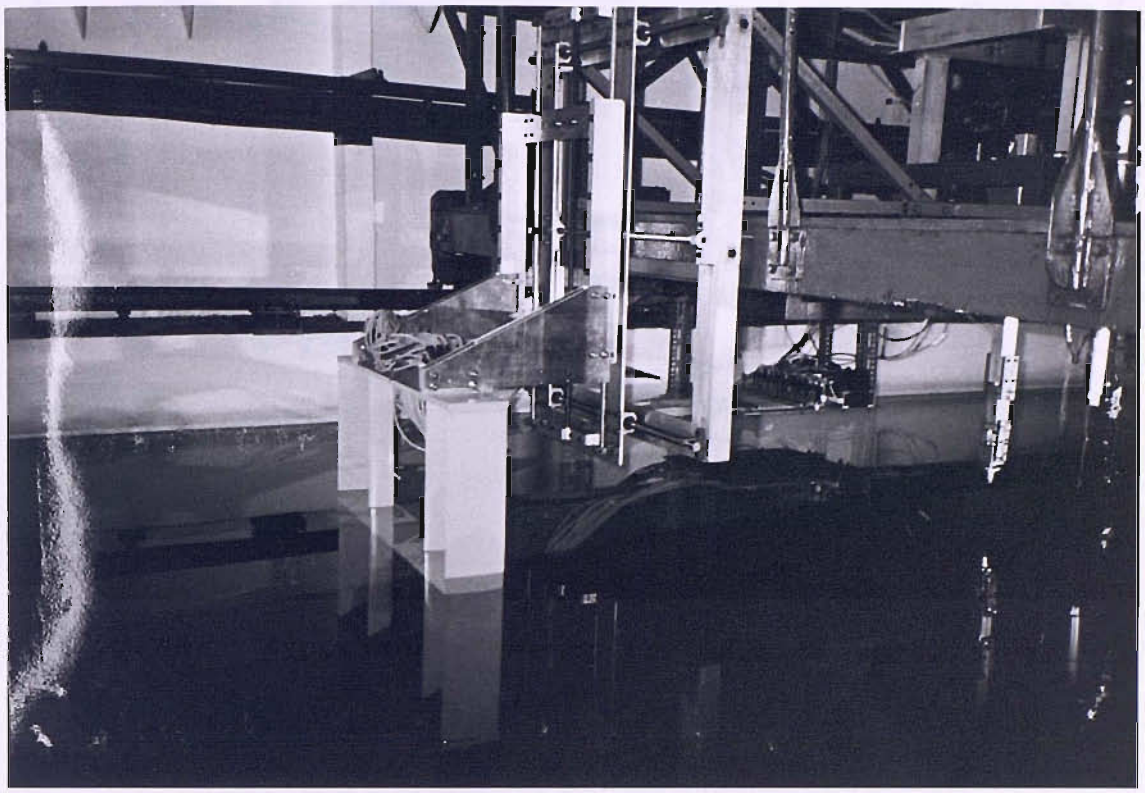

Fig. 88 : Experimental setup for wave traverse experiments

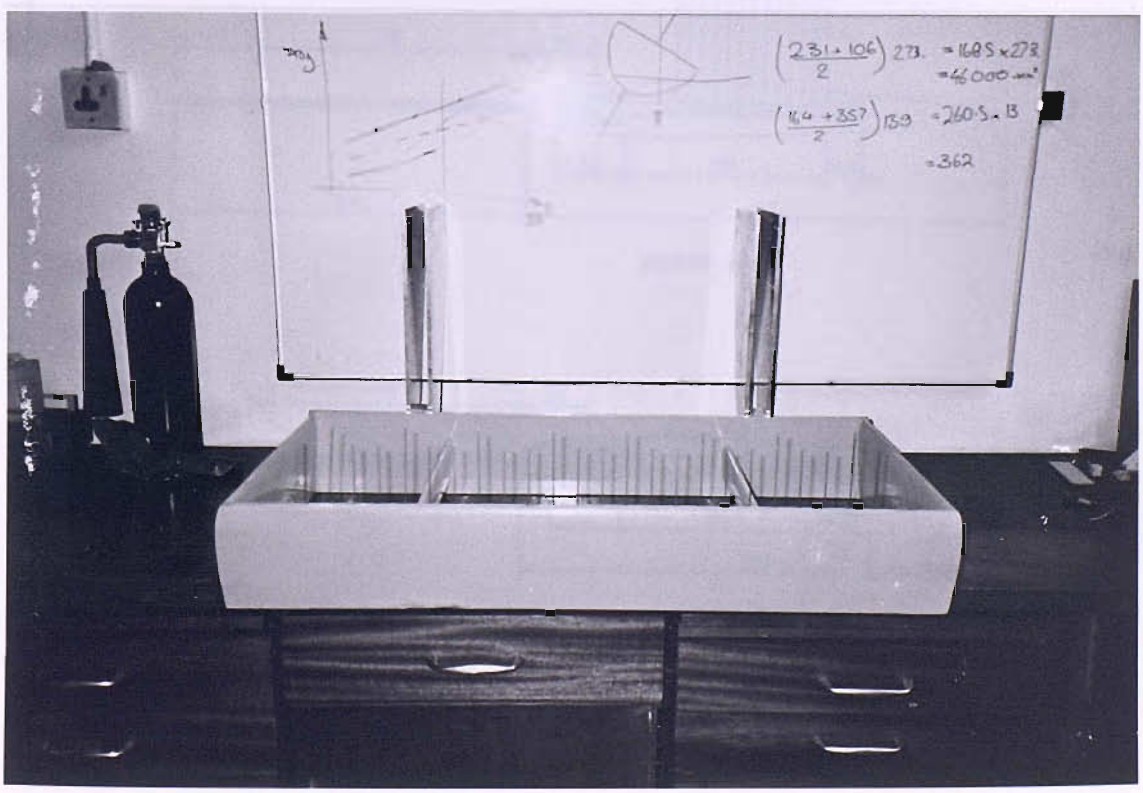

Fig. 89 : Wake rake

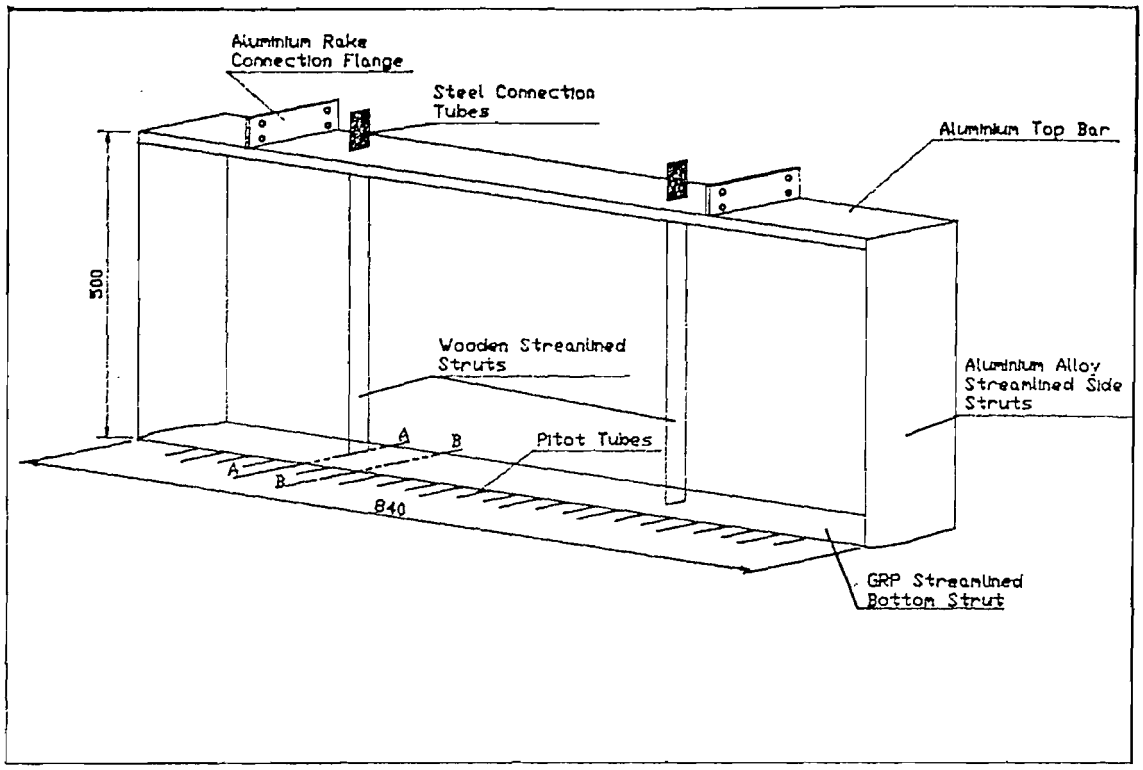

Fig.90: Wake traverse rake

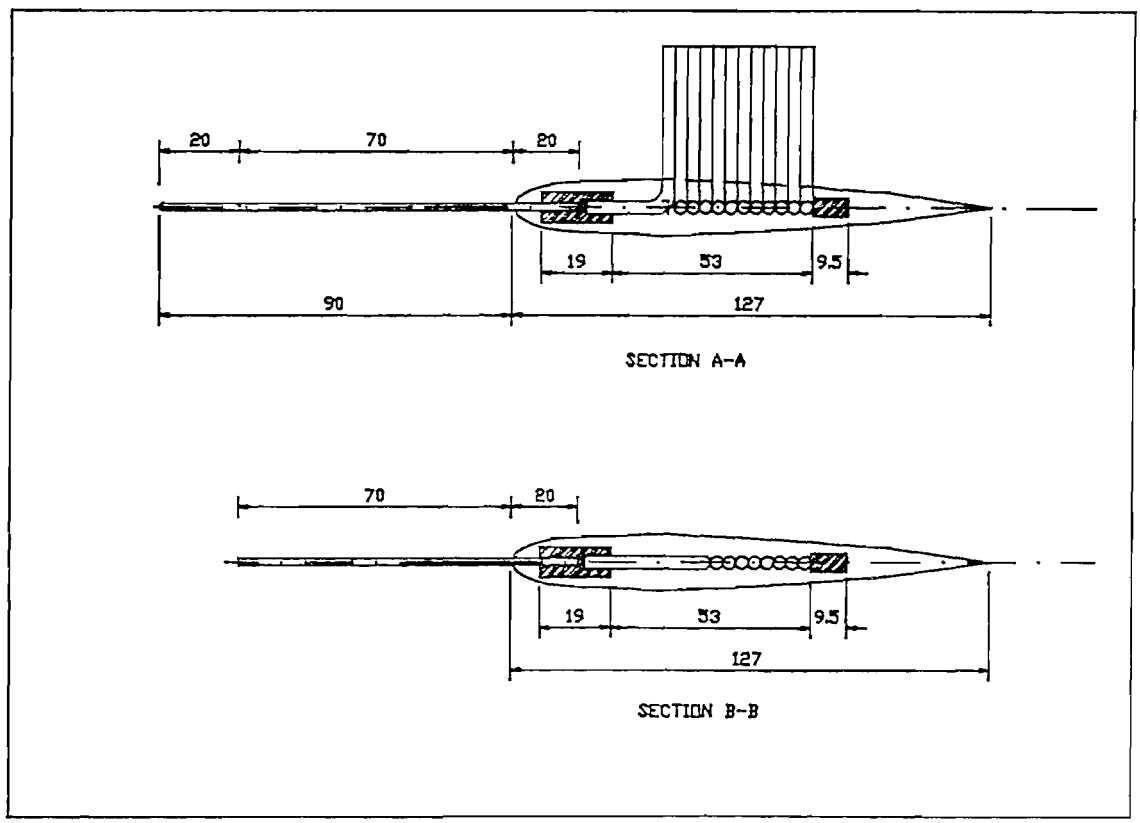

Fig.90: Wake traverse rake (Cross Sections)

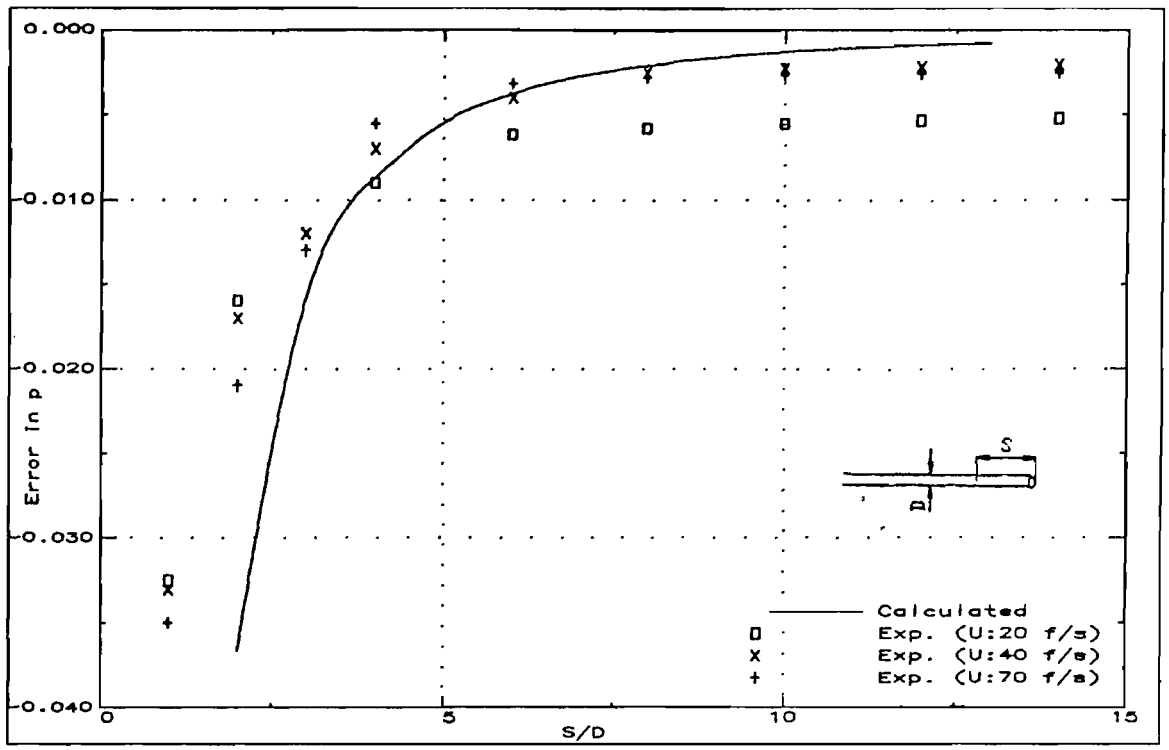

Fig.91: Error in static pressure due to tip to static orifice distance

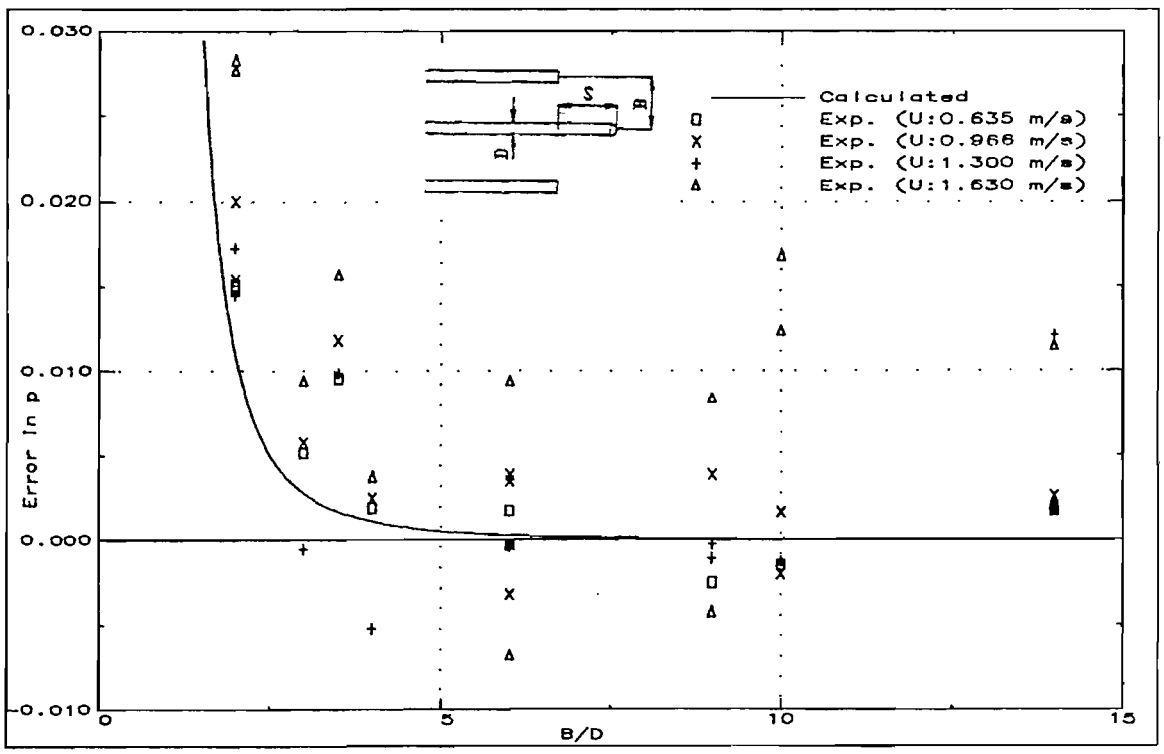

Fig.92: Error in static pressure due to tube interference

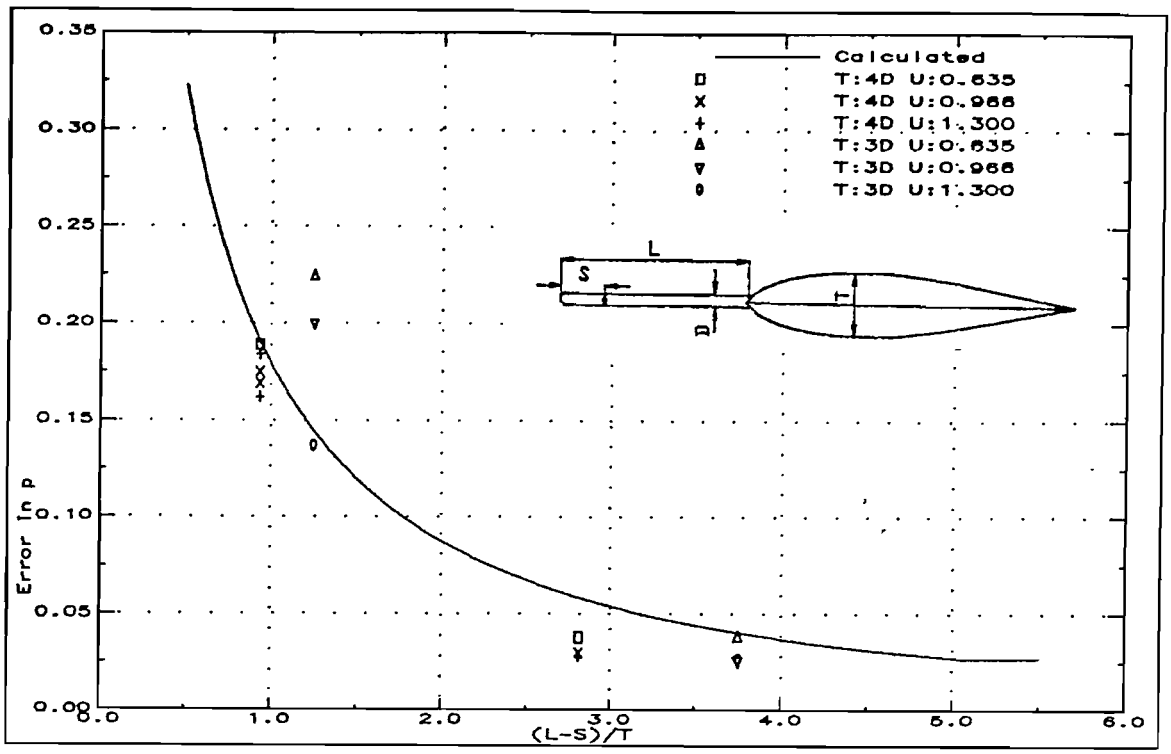

Fig.93: Error in static pressure due to support strut

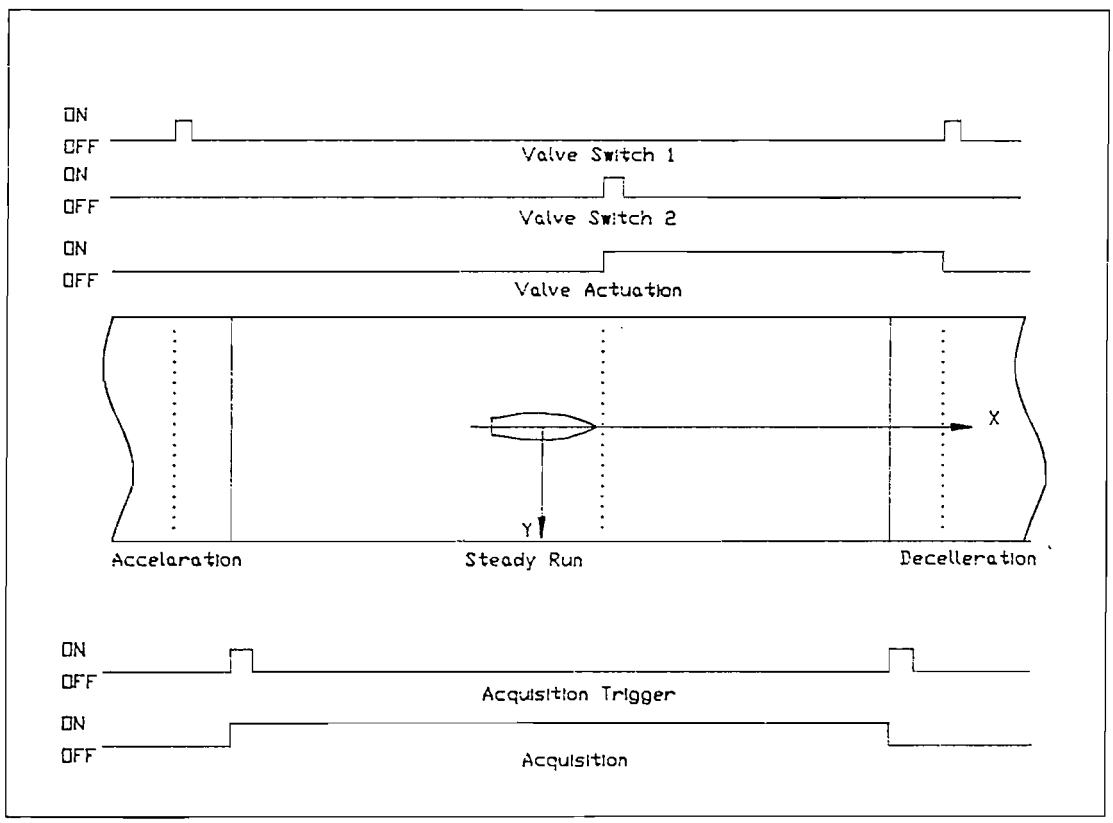

Fig.94: Wake traverse data acquisition, and valve actuation along the tank

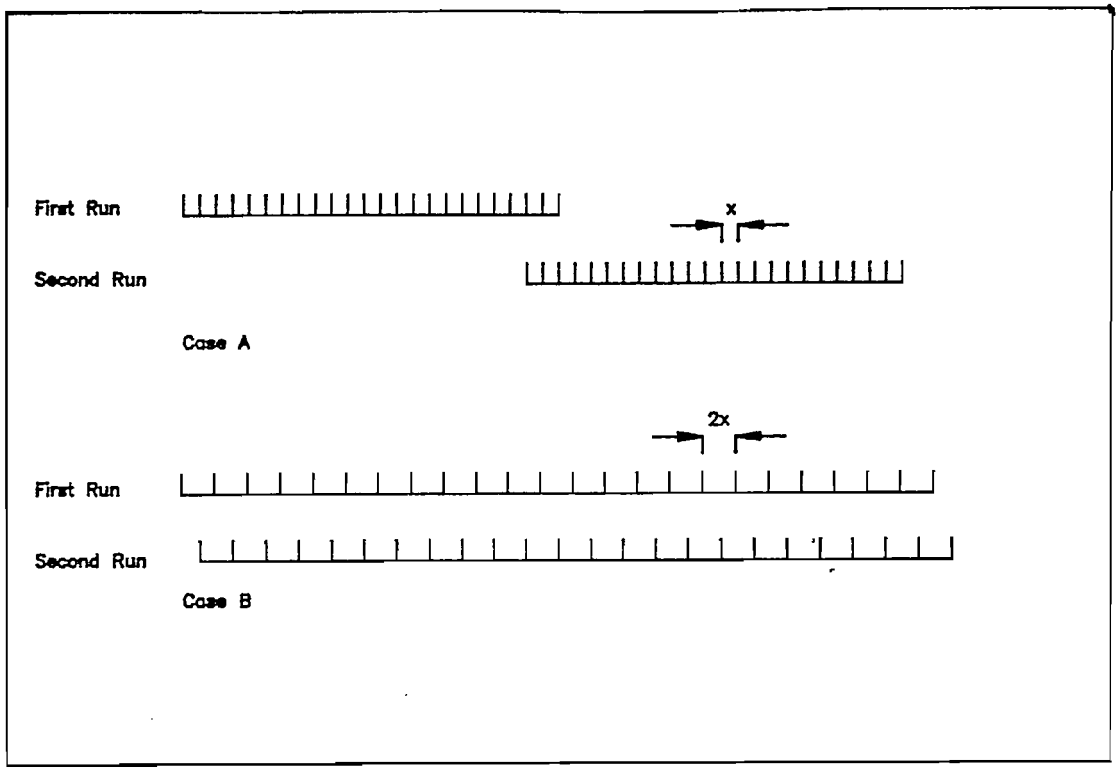

Fig.95: Possible tube distributions to cover a wide rake

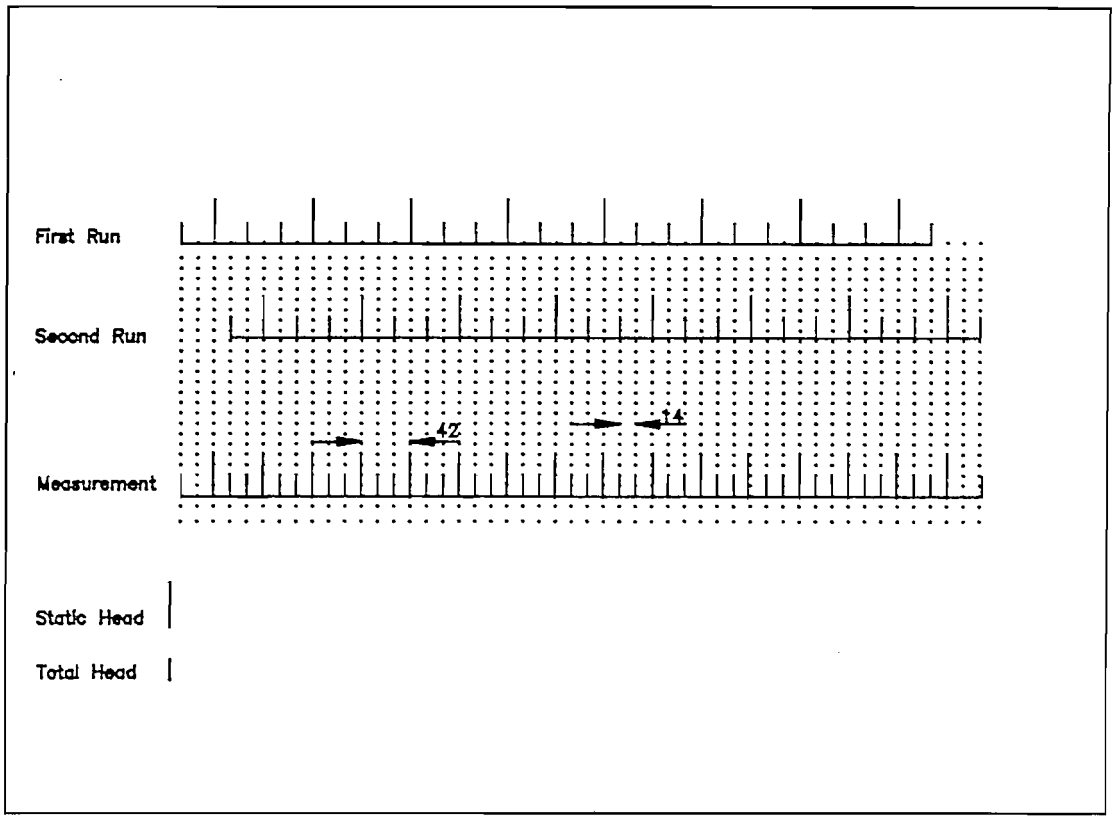

Fig.96: Distribution of static and total pitot tubes across the rake

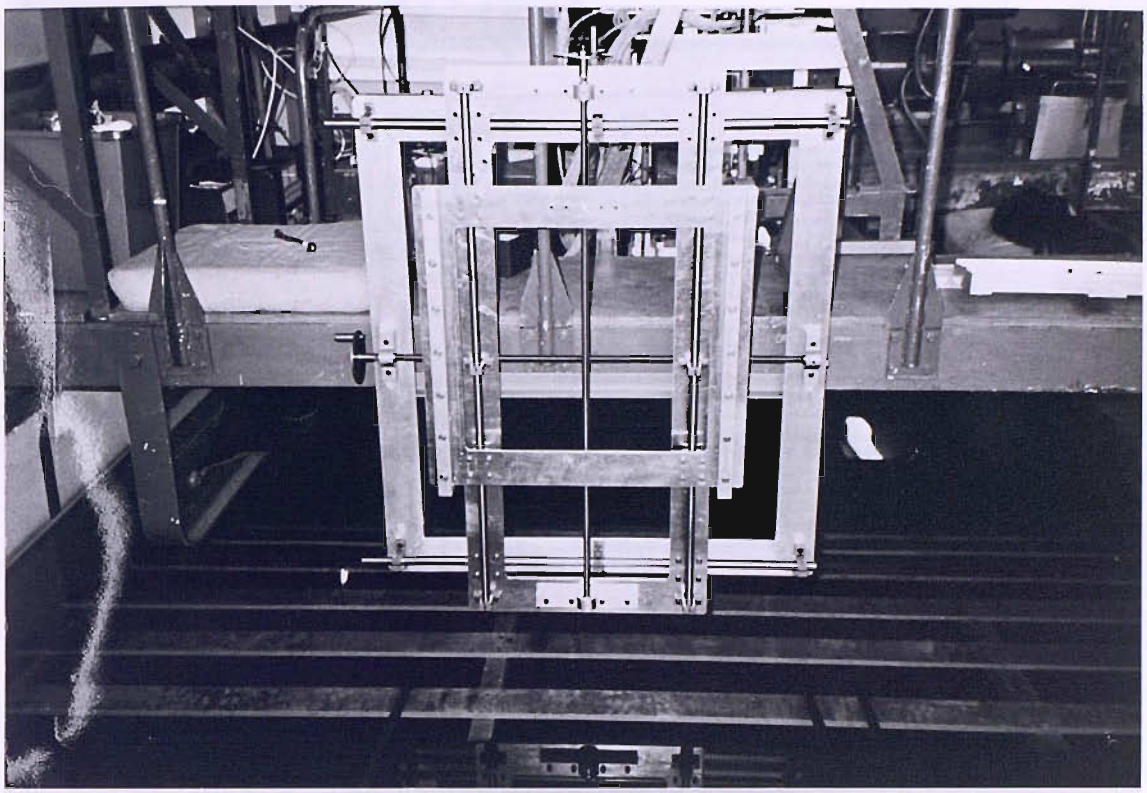

Fig. 97 : Horizontal and vertical movement table

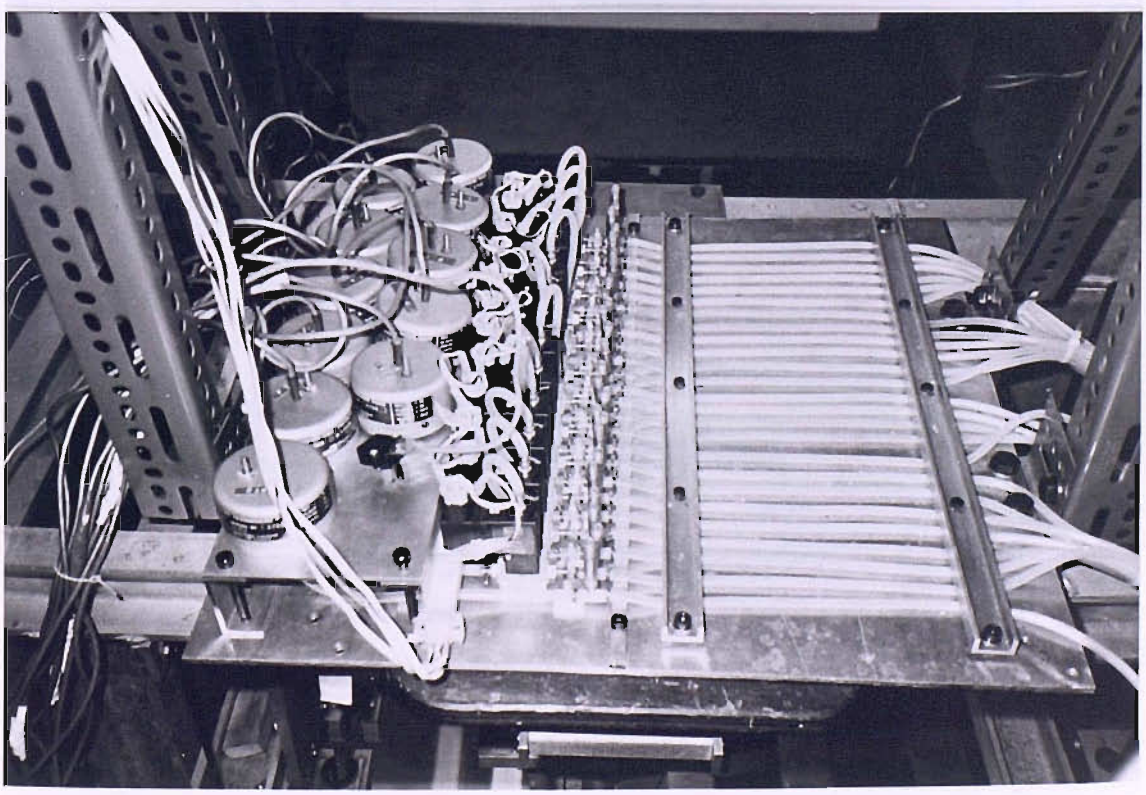

Fig. 98 : Horizontal plate

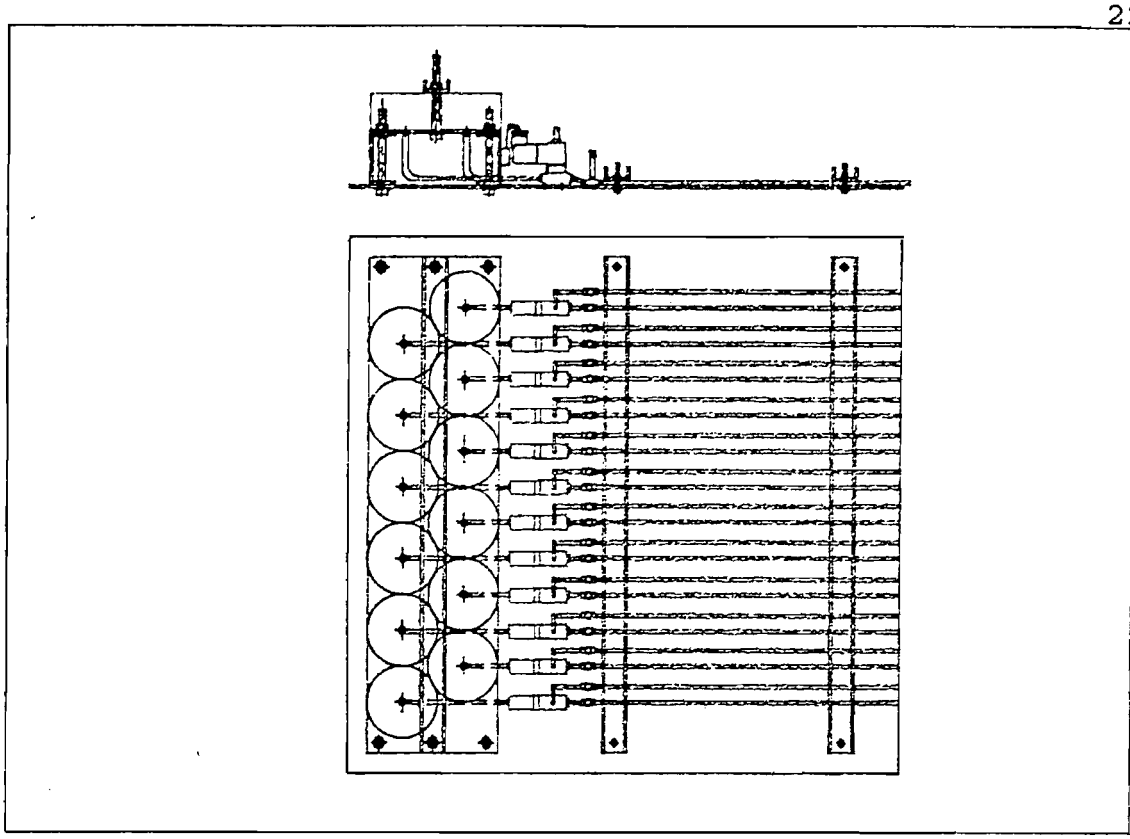

Fig.99: Horizontal plate layout

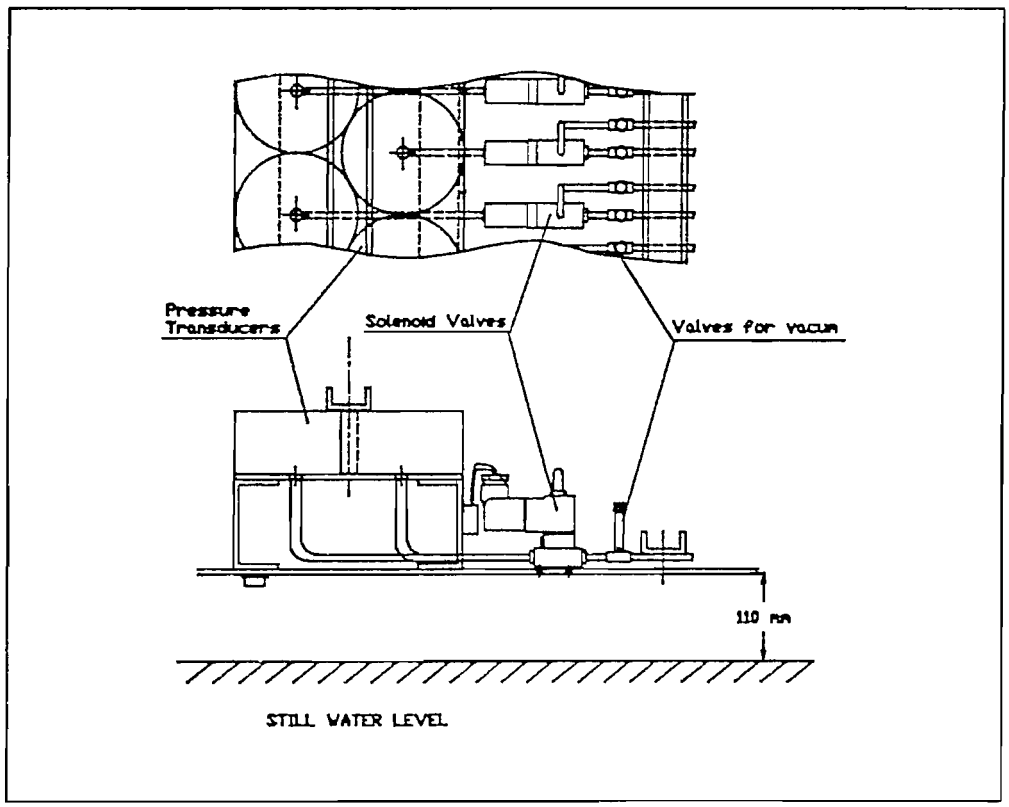

Fig.100: Valve-pressure transducer connection

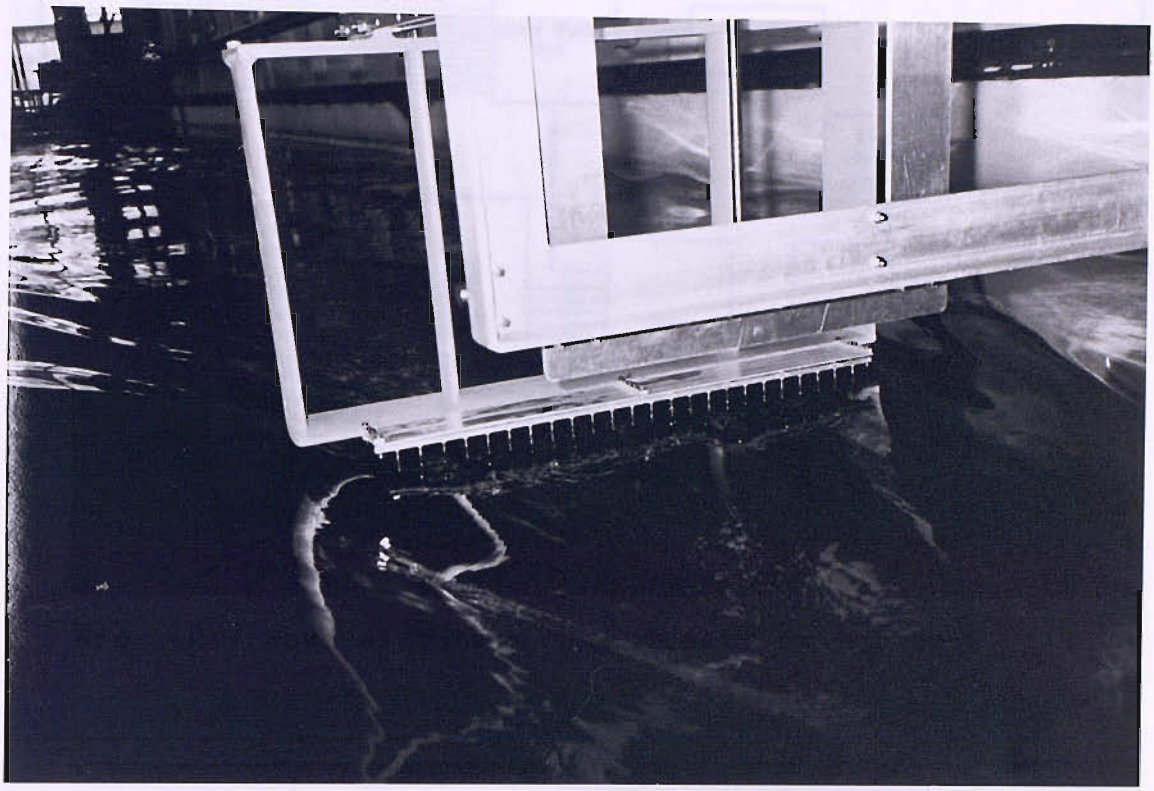

Fig. 101: Wave elevation measurement by pointers

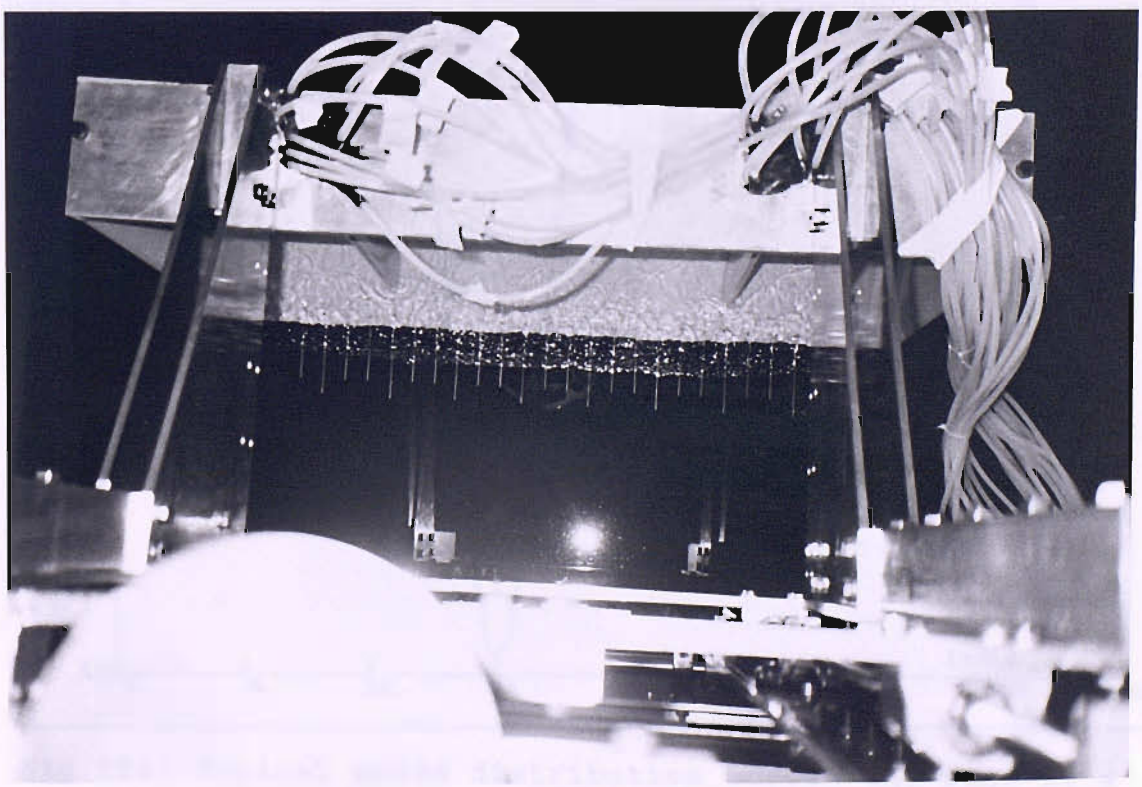

Fig. 102 : Disturbance due to support strut near to free surface

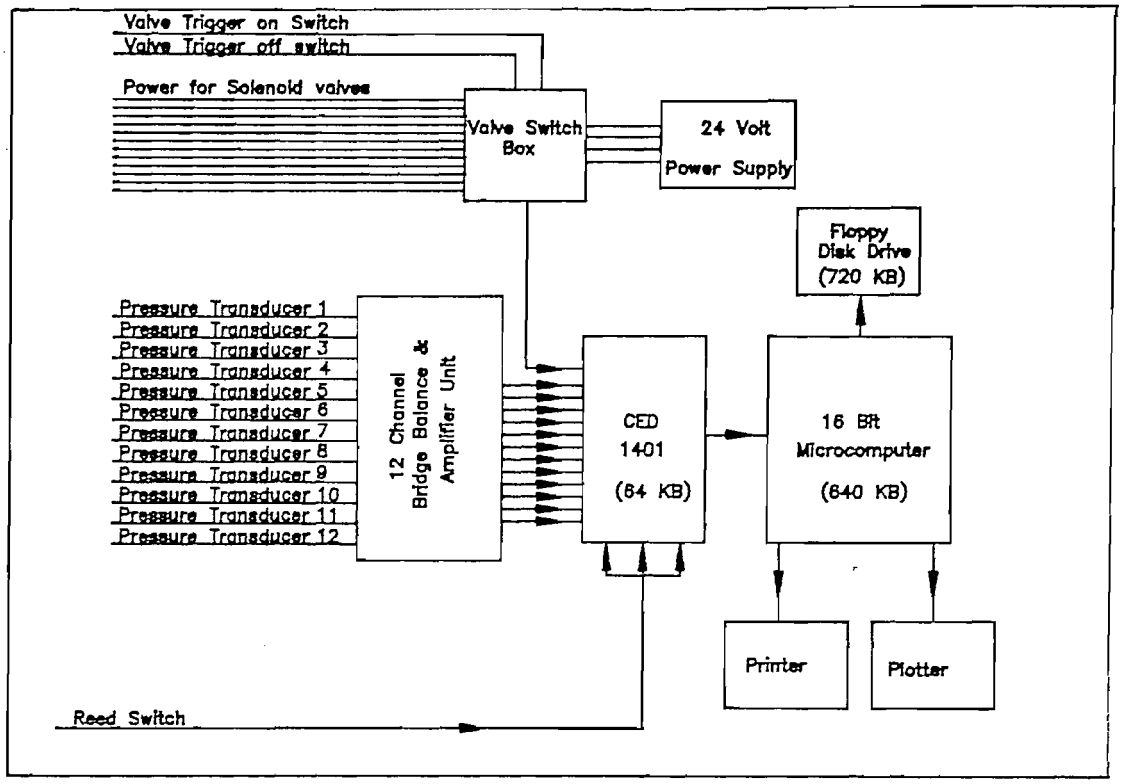

Fig.103: Setup for wake traverse experiments

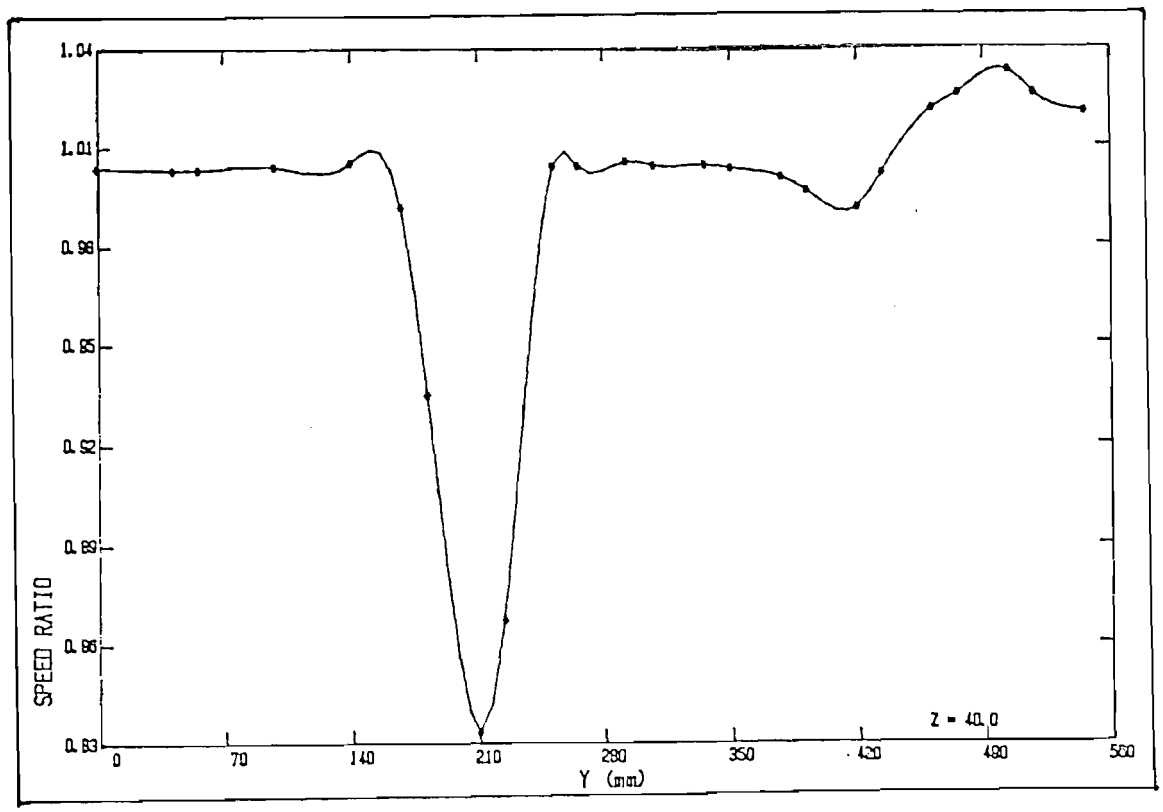

Fig.104: Typical speed distribution across the wake at a constant depth

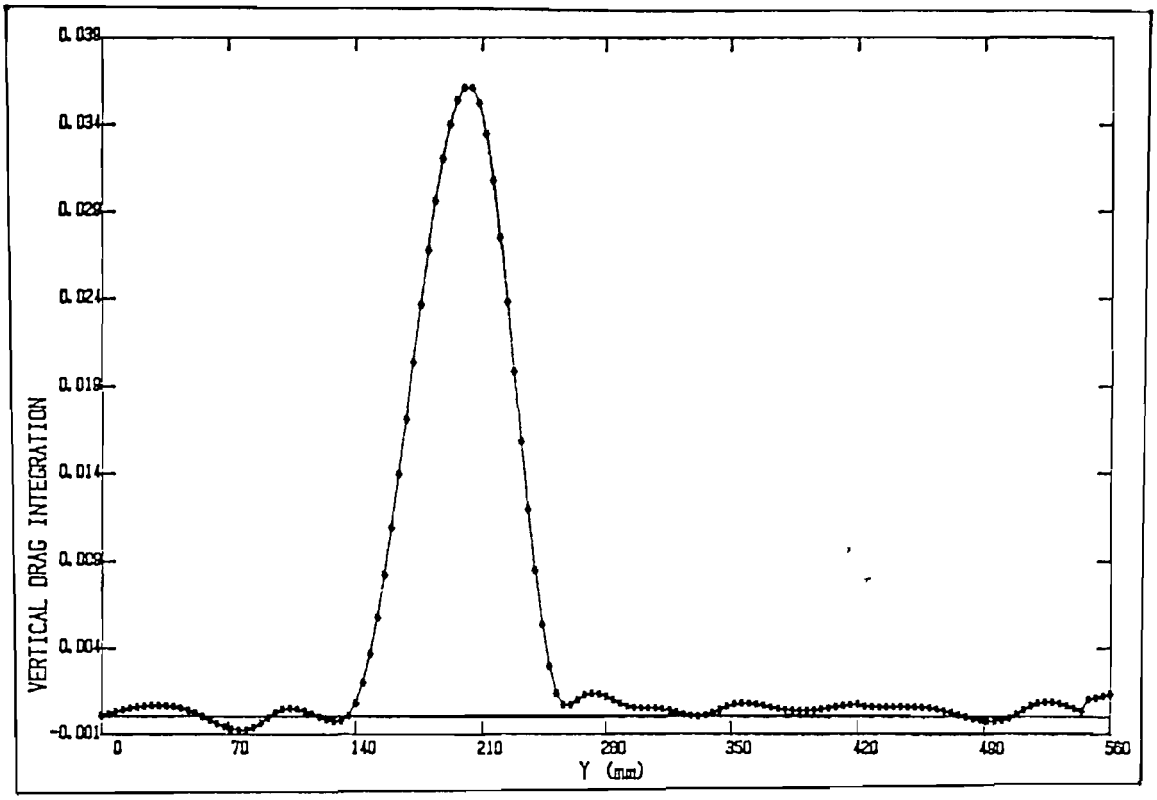

Fig.105: Typical drag distribution across the wake

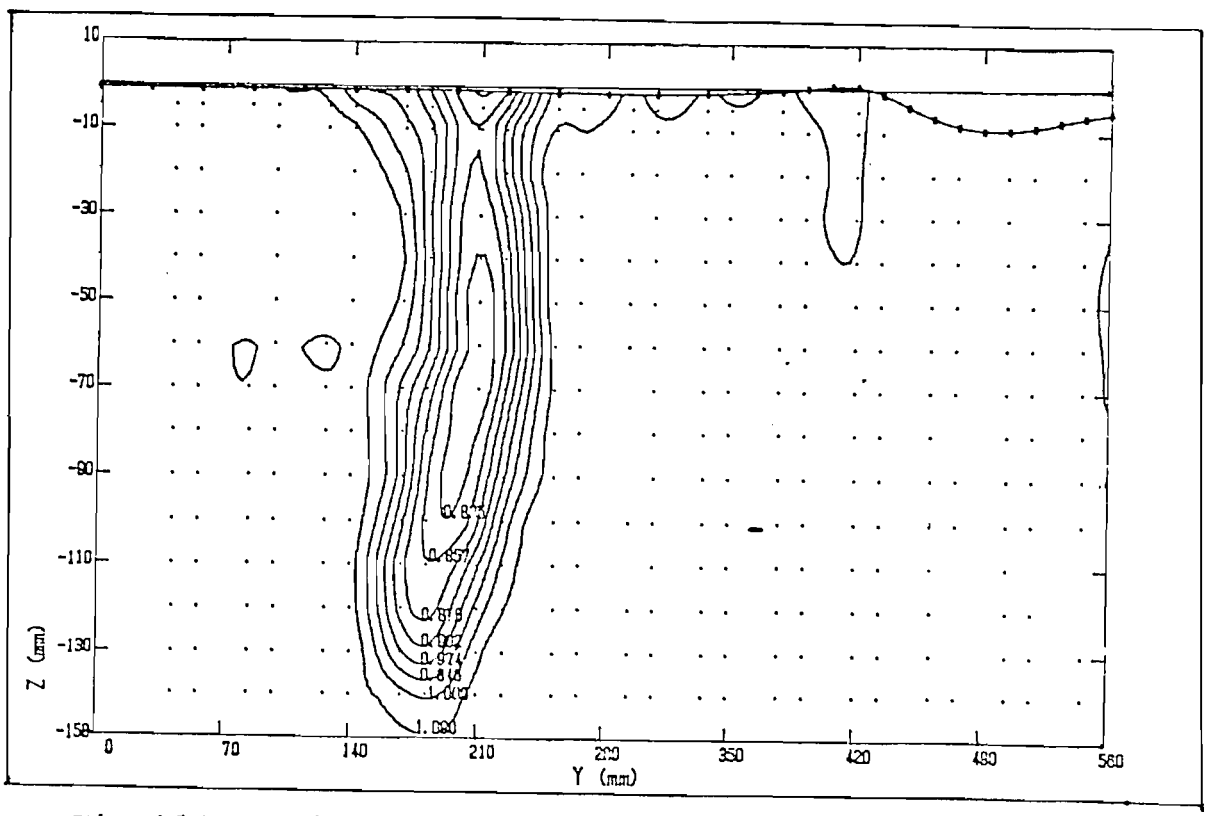

Fig.106: Typical wake contours

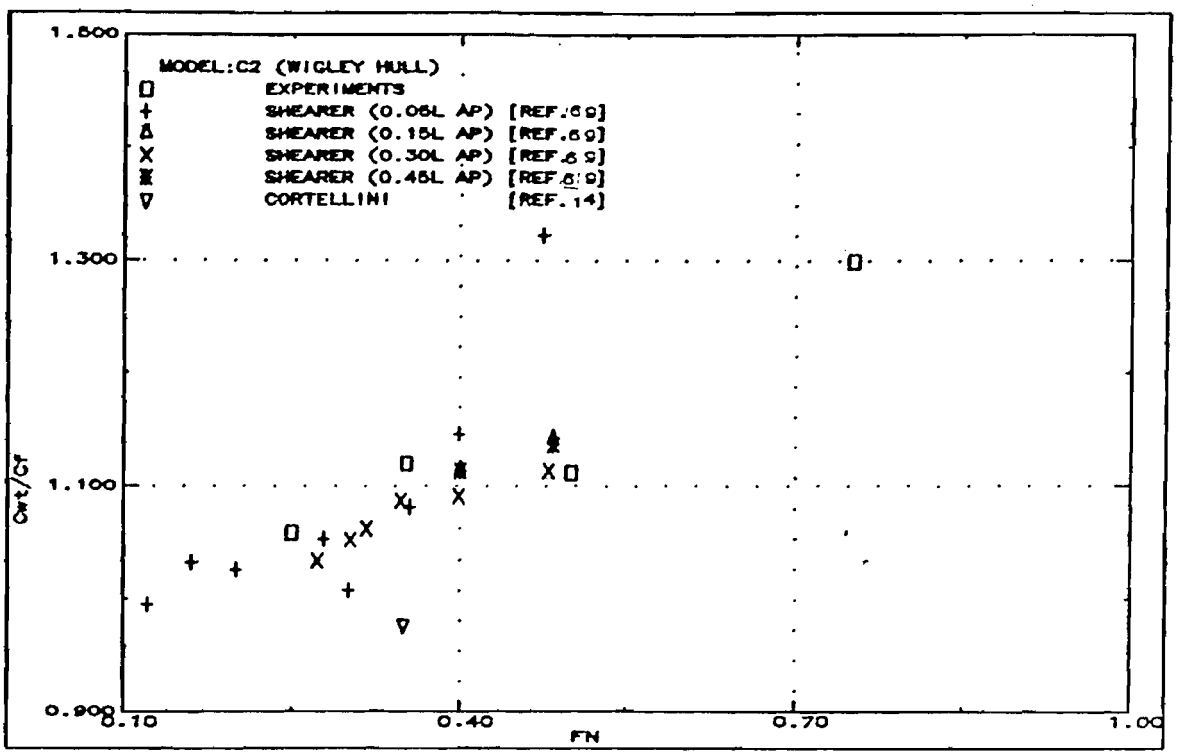

Fig.107: Comparison of wake traverse results with available experimental data (Wigley Hull-Free)

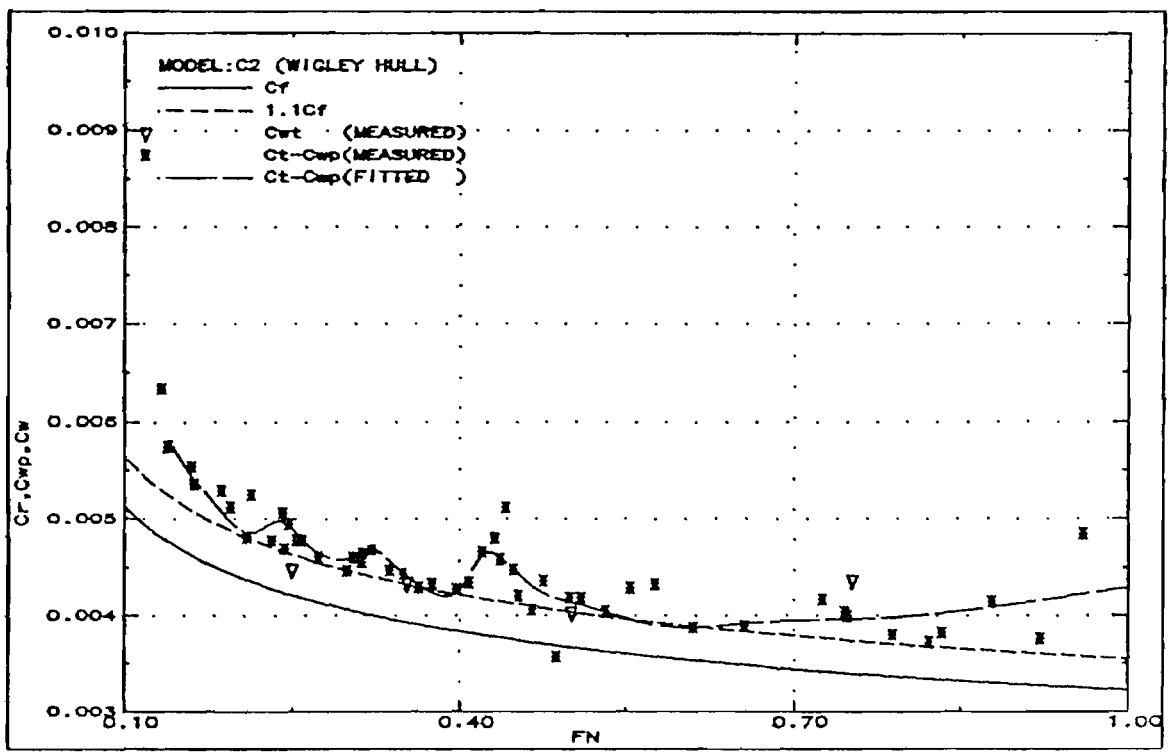

Fig.108: Comparison of wake traverse results with total resistance-wave pattern resistance (Wigley Hull-Free)

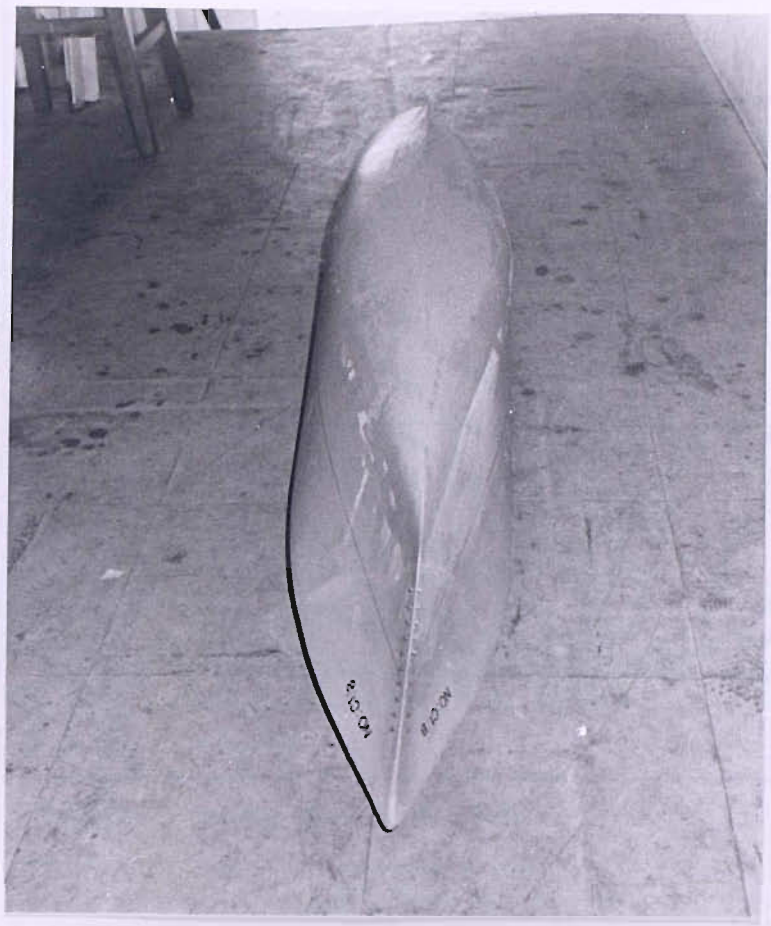

Fig. 109: Front view of model: C1

Fig. 110: Side view of model: C1

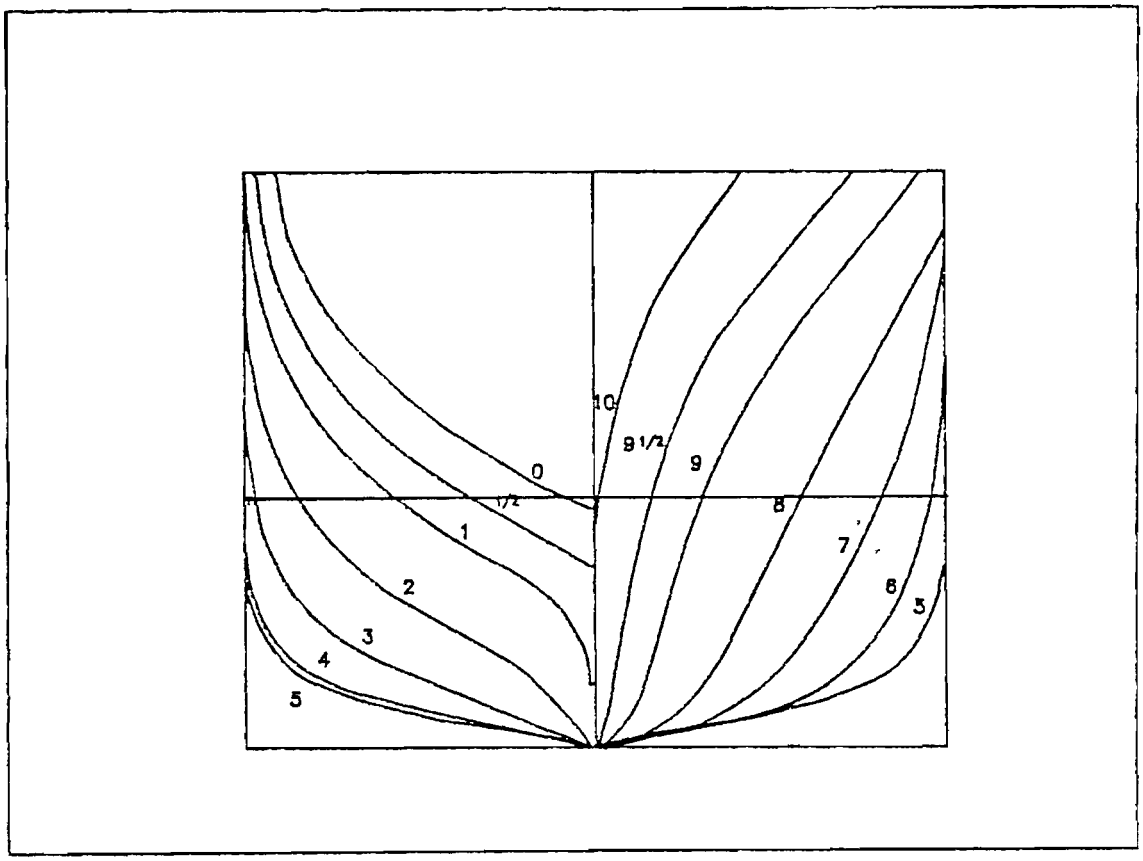

Fig.111: Body plan of model : C1

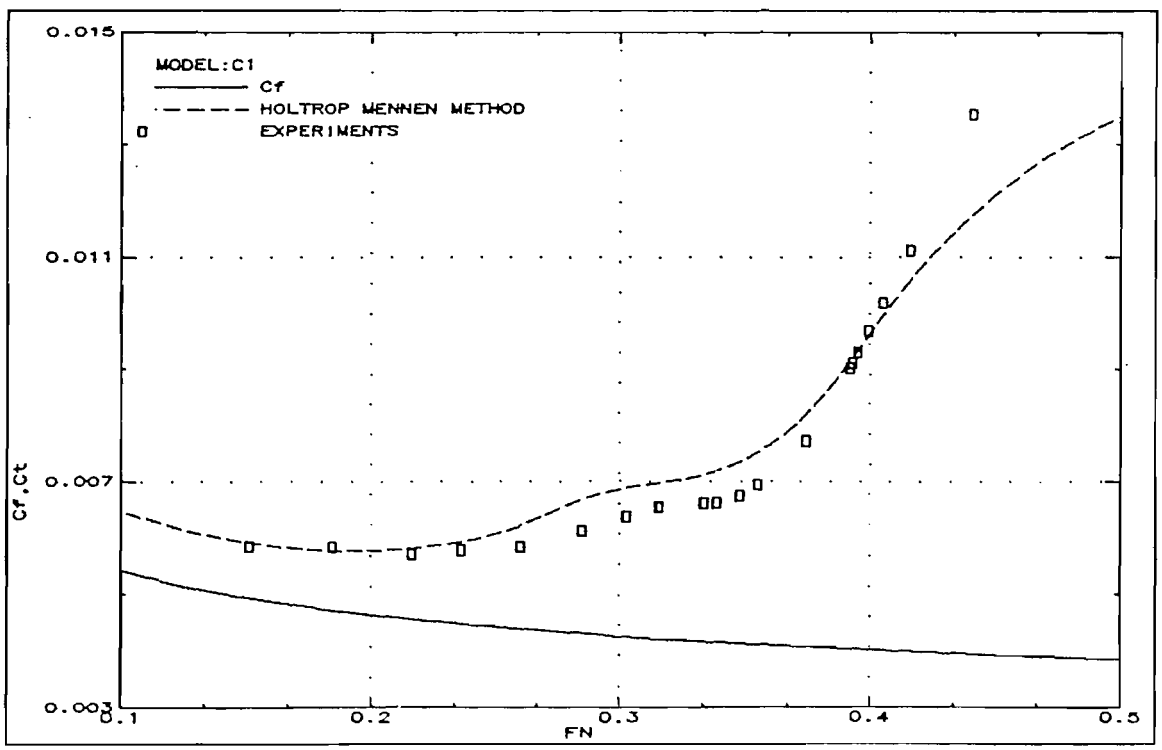

Fig.112: Comparison of measured residuary resistance with predictions (C1-Monohull)

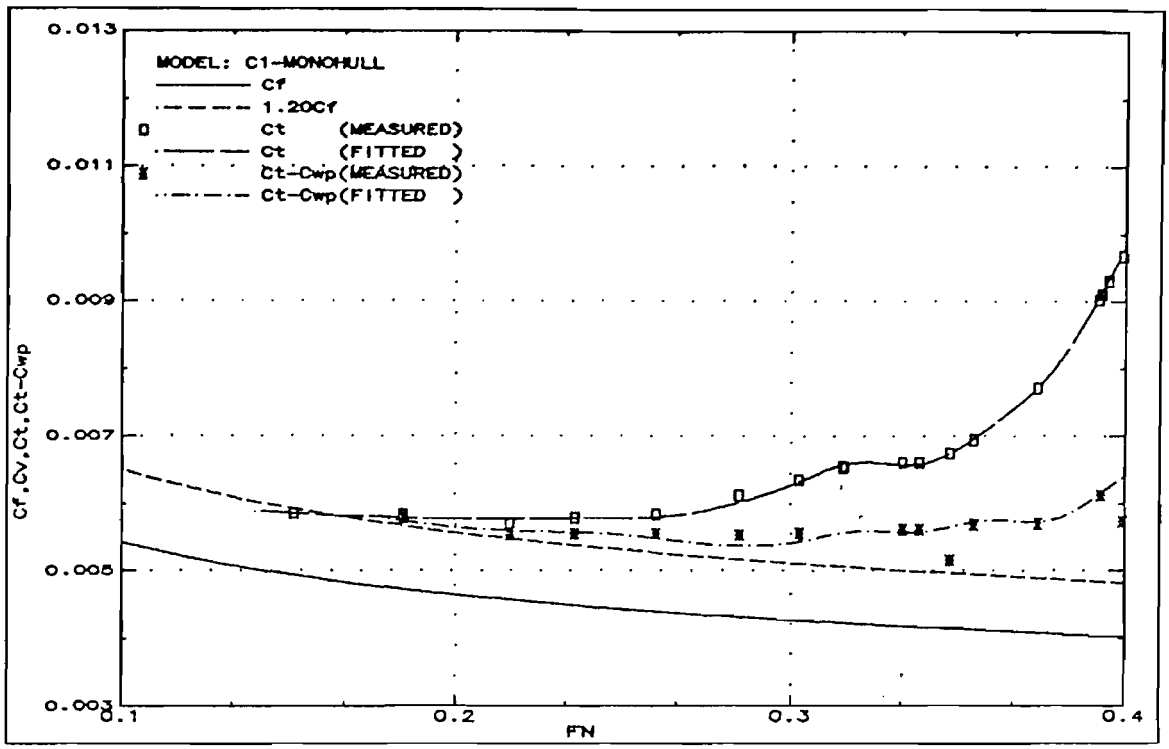

Fig.113: Resistance components (C1-Monohull)

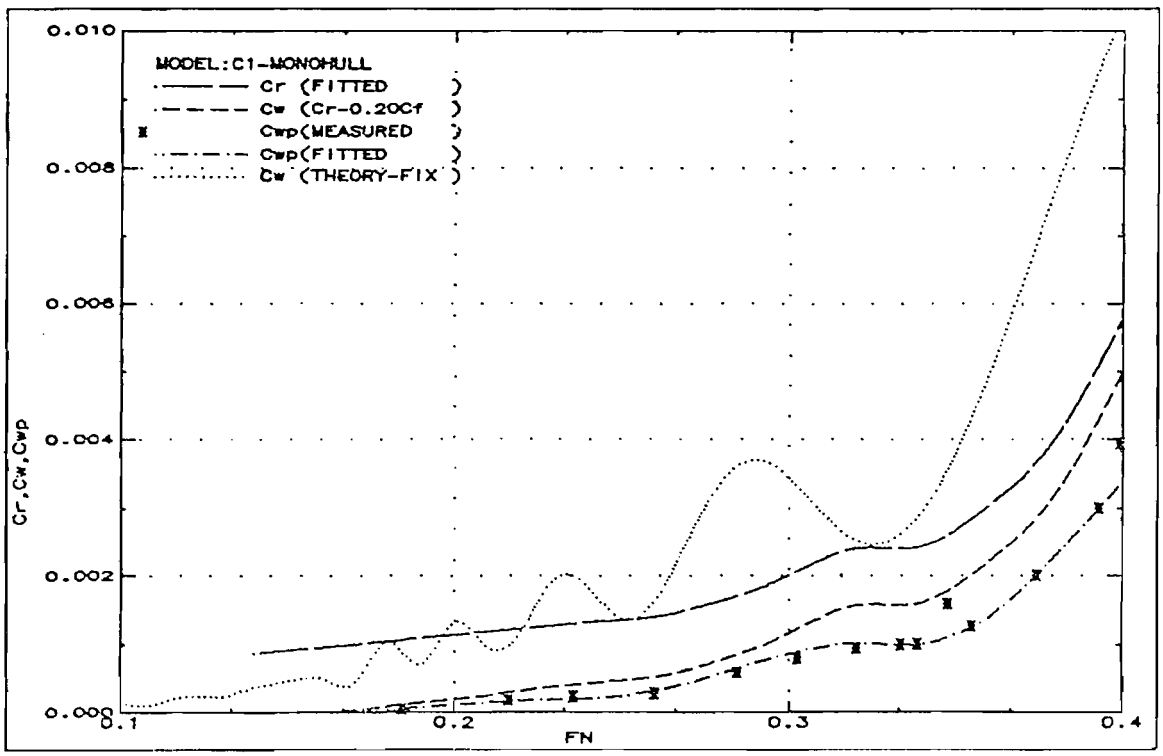

Fig.114: Wave resistance comparison (C1-Monohull)

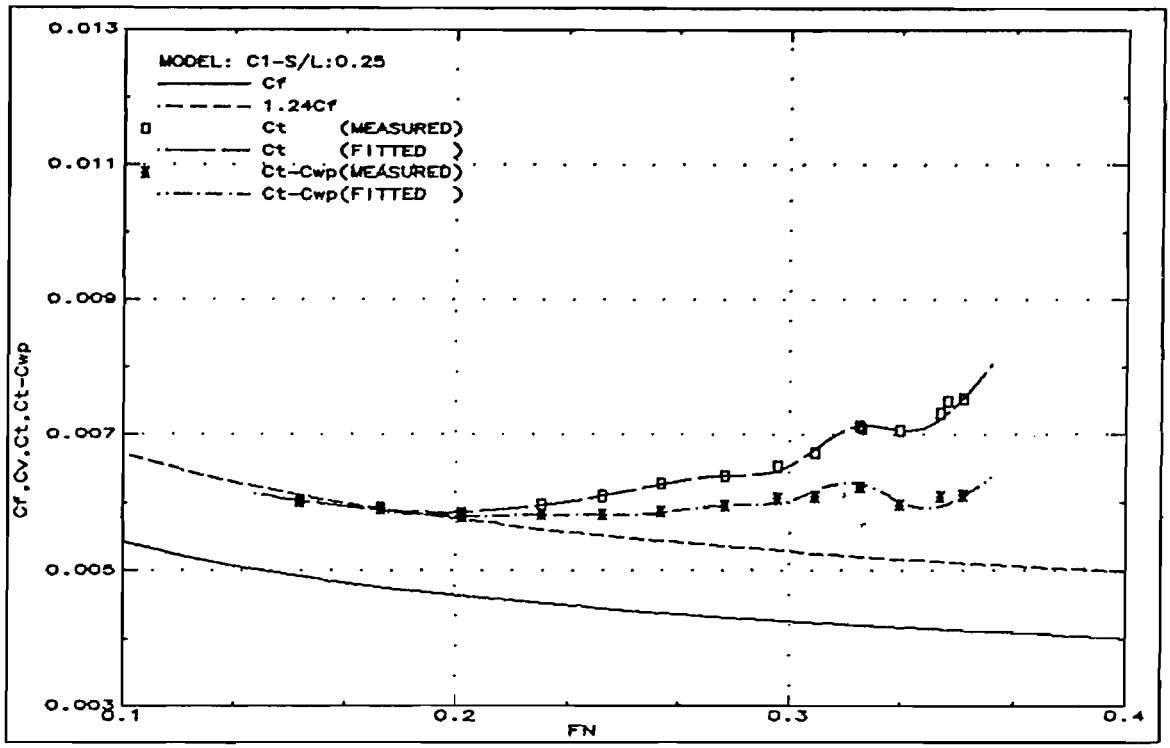

Fig.115: Resistance components (C1-S/L:0.25

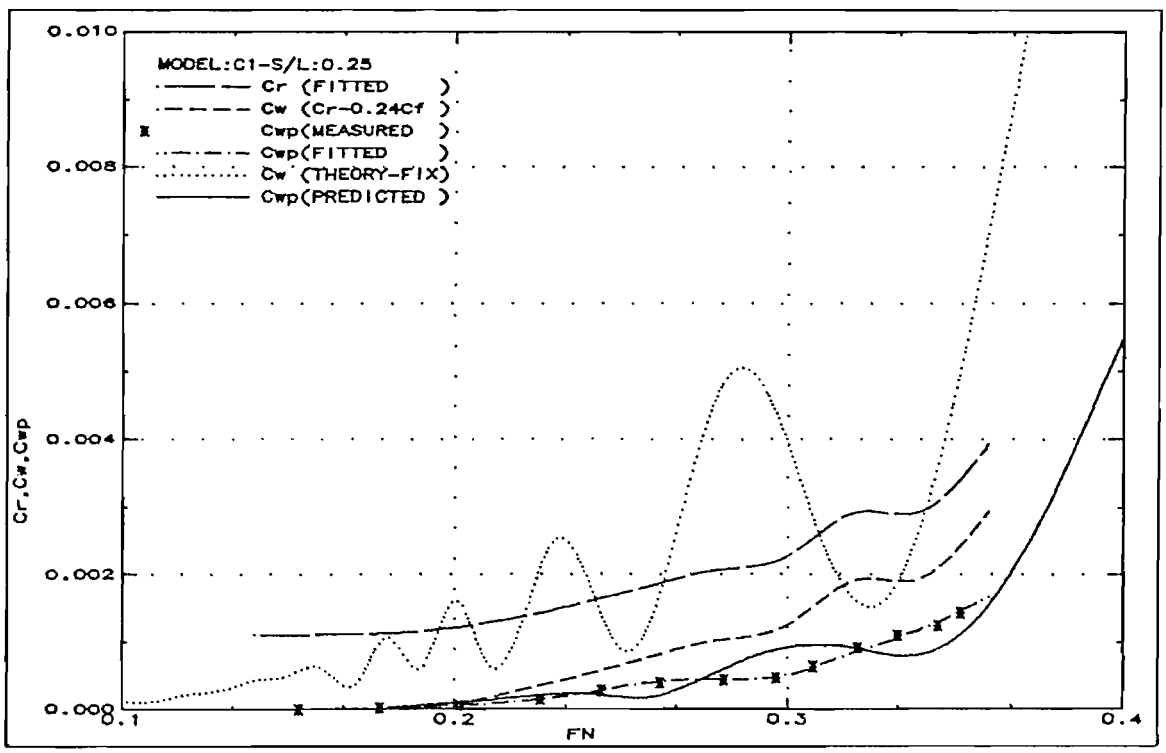

Fig.116: Wave resistance comparison (C1-S/L:0.25)

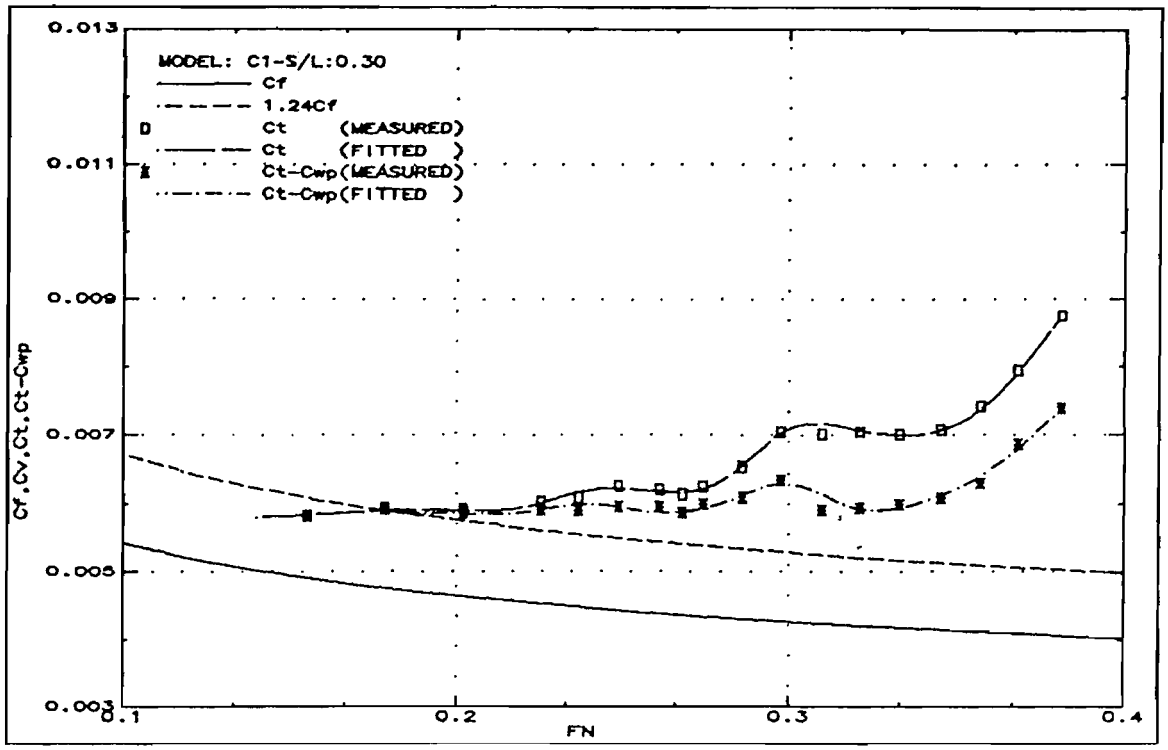

Fig.117: Resistance components (C1-S/L:Ø.3)

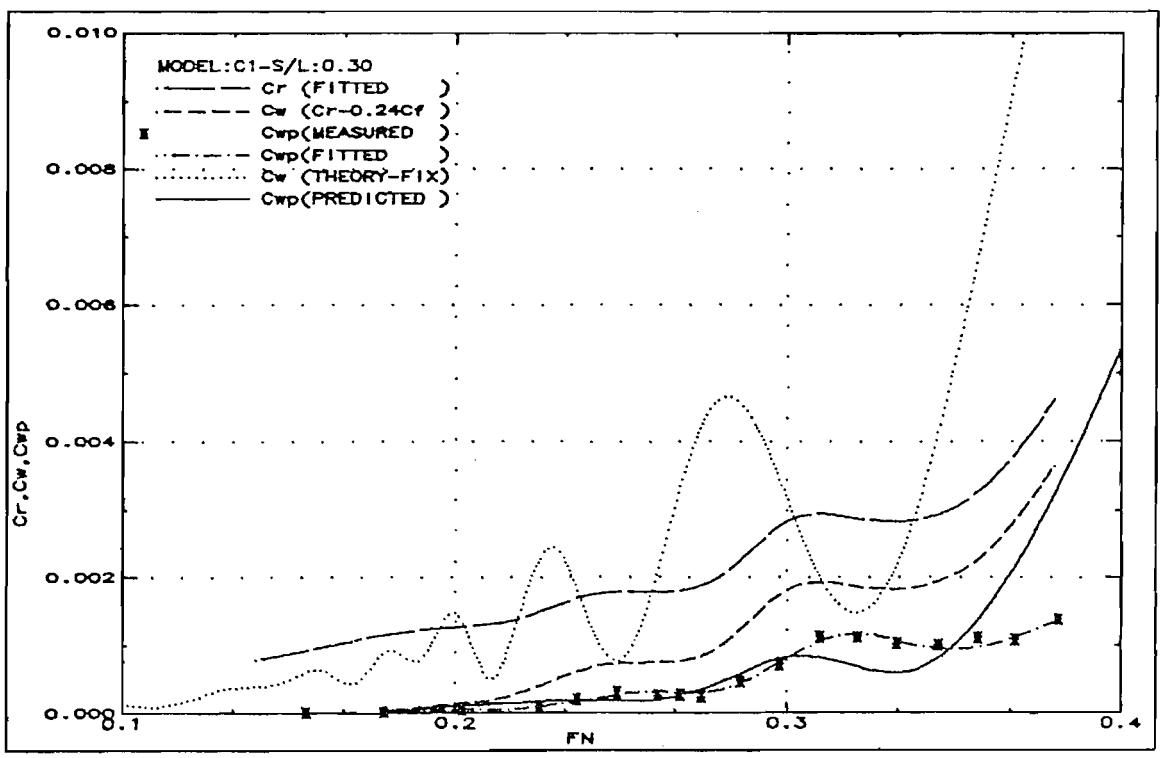

Fig.118: Wave resistance comparison (C1-S/L:Ø.3)

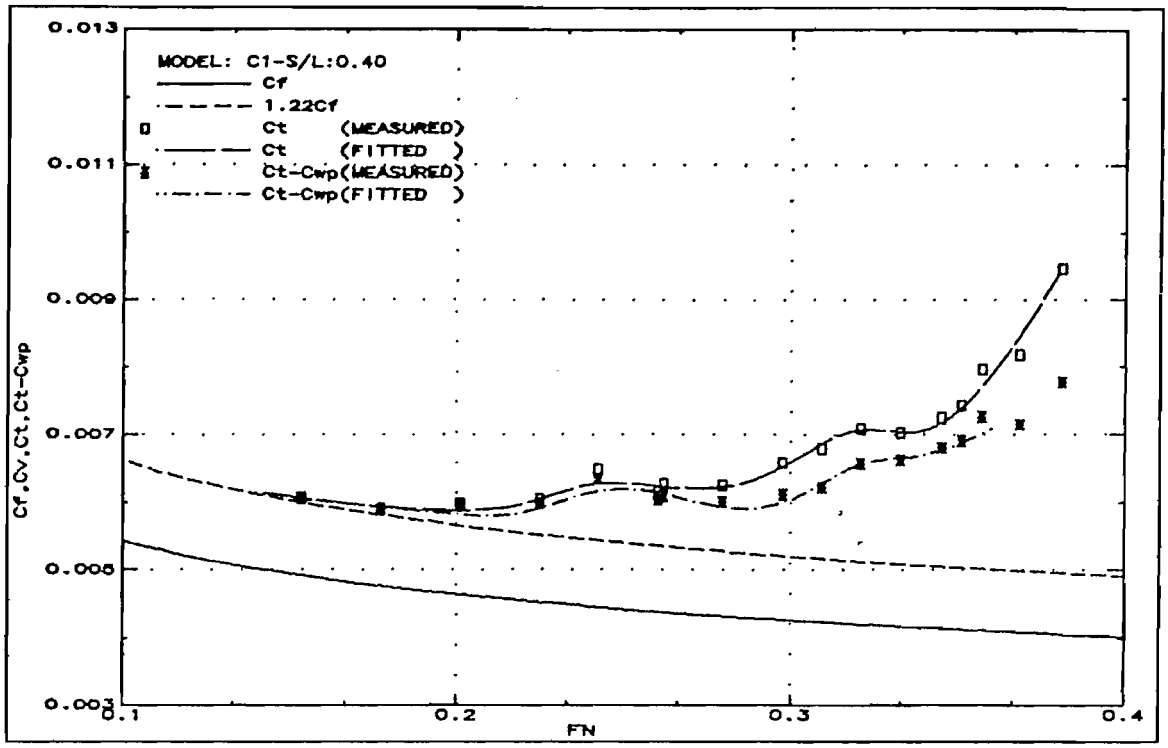

Fig.119: Resistance components (C1-S/L:Ø.4)

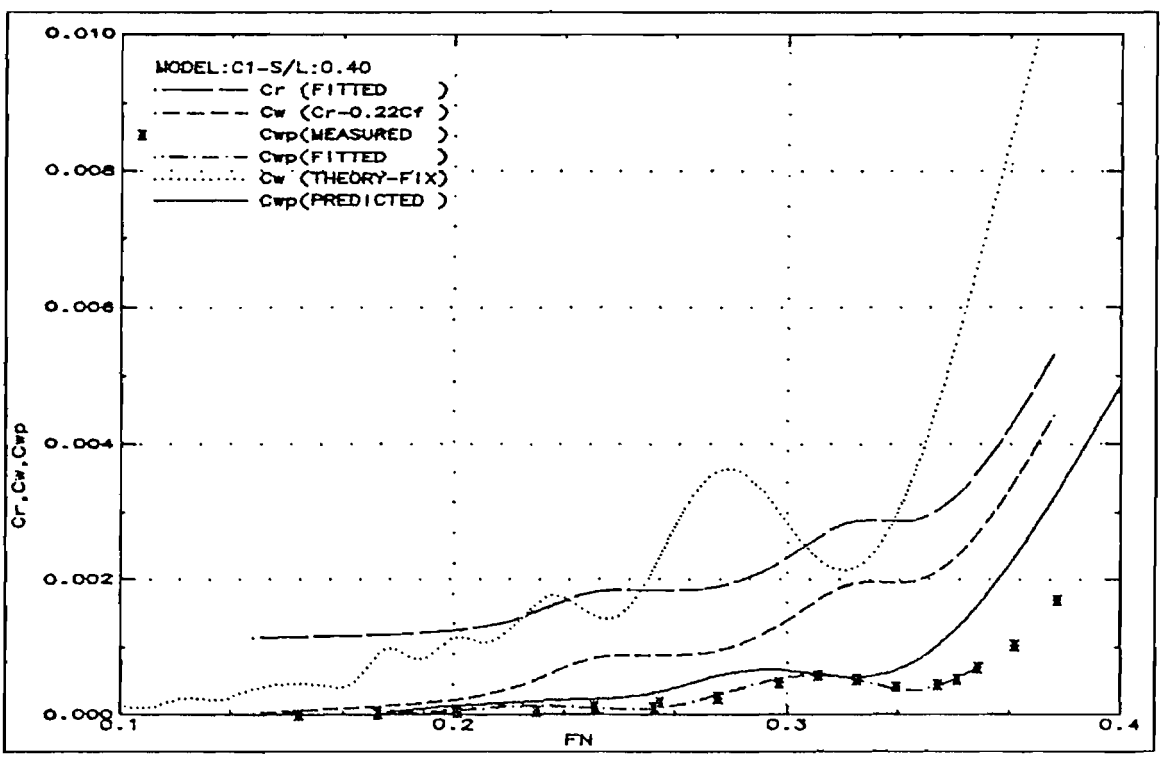

Fig.12Ø: Wave resistance comparison (C1-S/L:Ø.4)

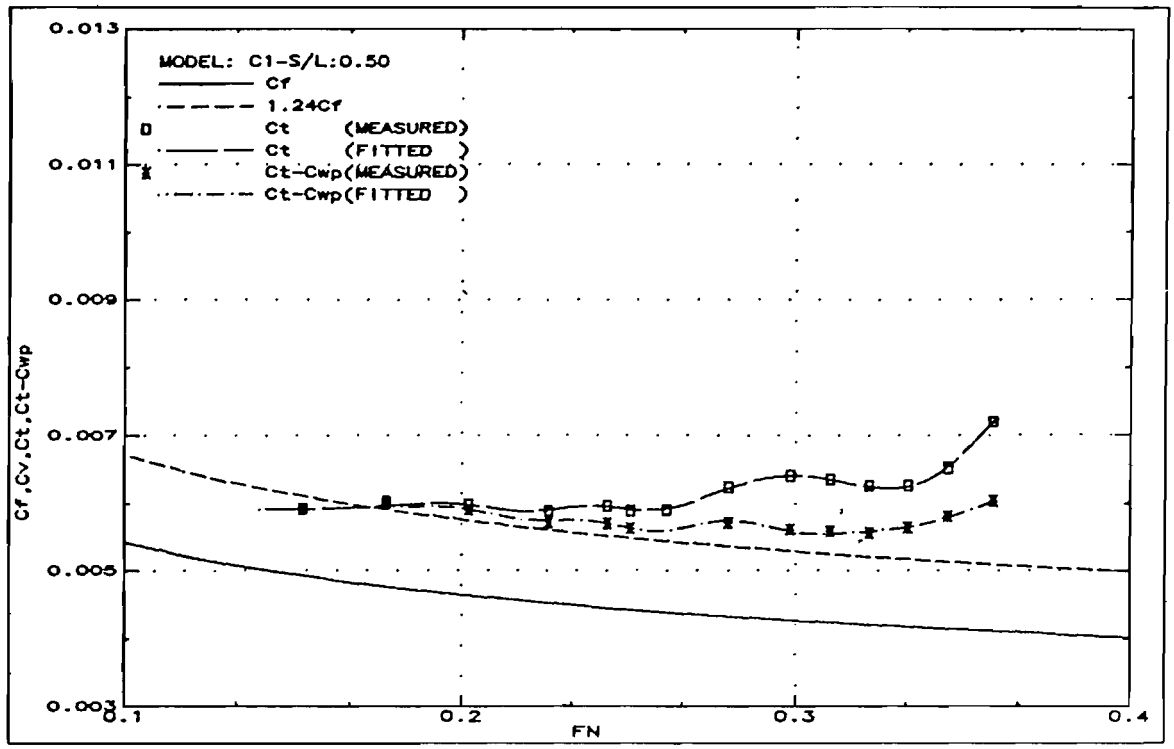

Fig.121 : Resistance components (C1-S/L:Ø.5)

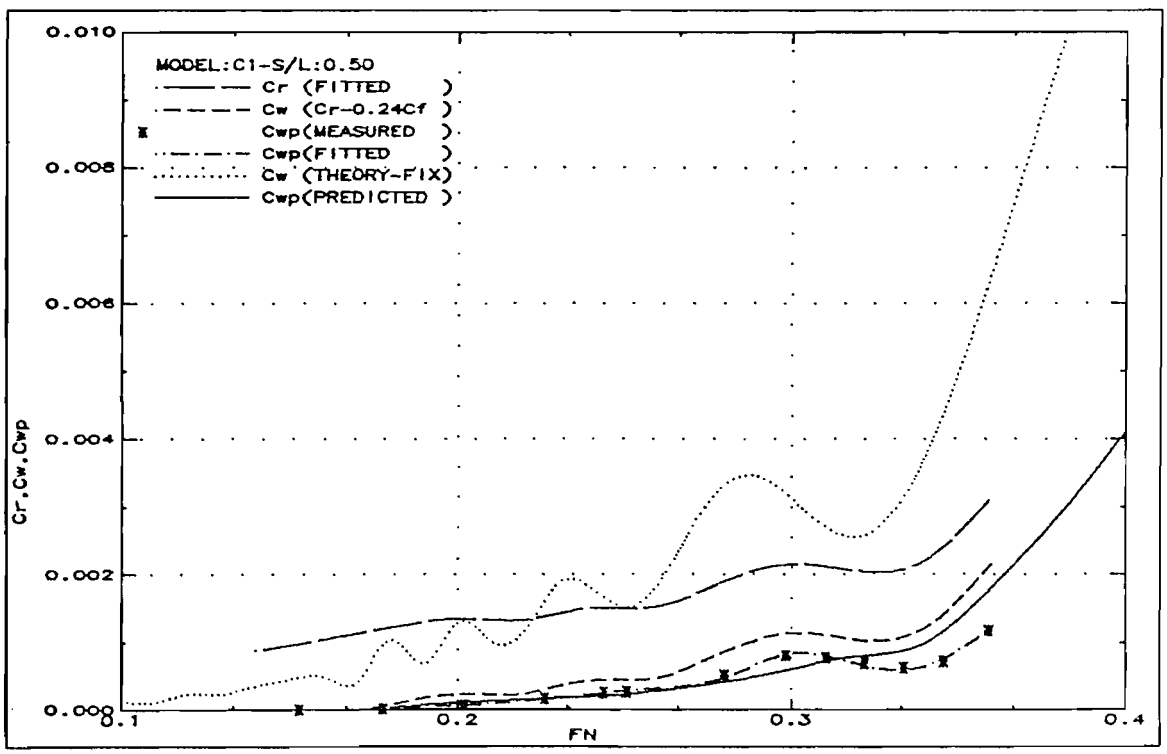

Fig.122: Wave resistance comparison (C1-S/L:Ø.5)

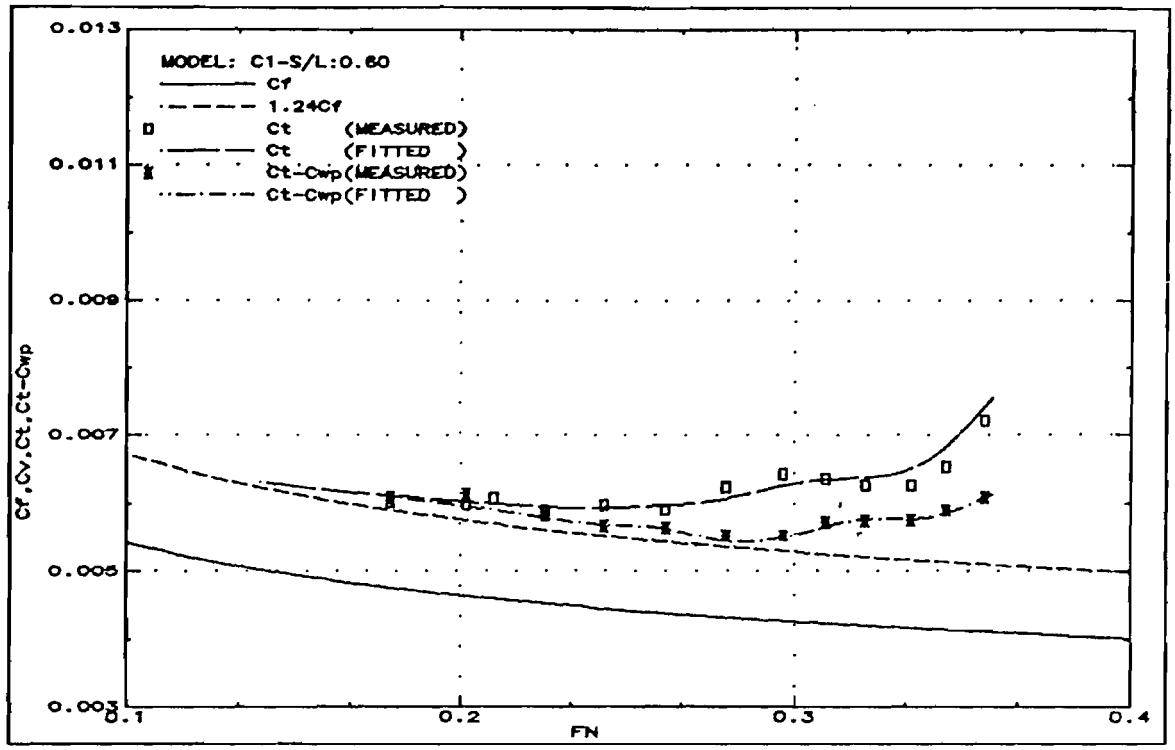

Fig.123: Resistance components (C1-S/L:Ø.6)

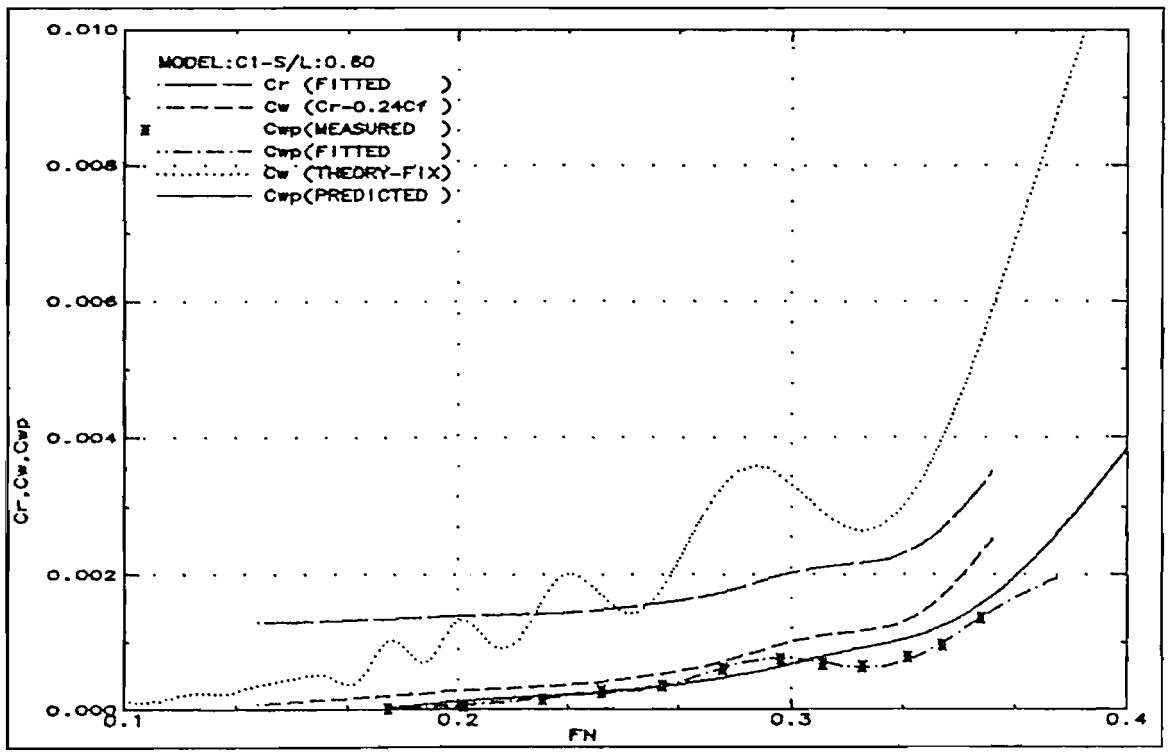

Fig.124: Wave resistance comparison (C1-S/L:Ø.6)

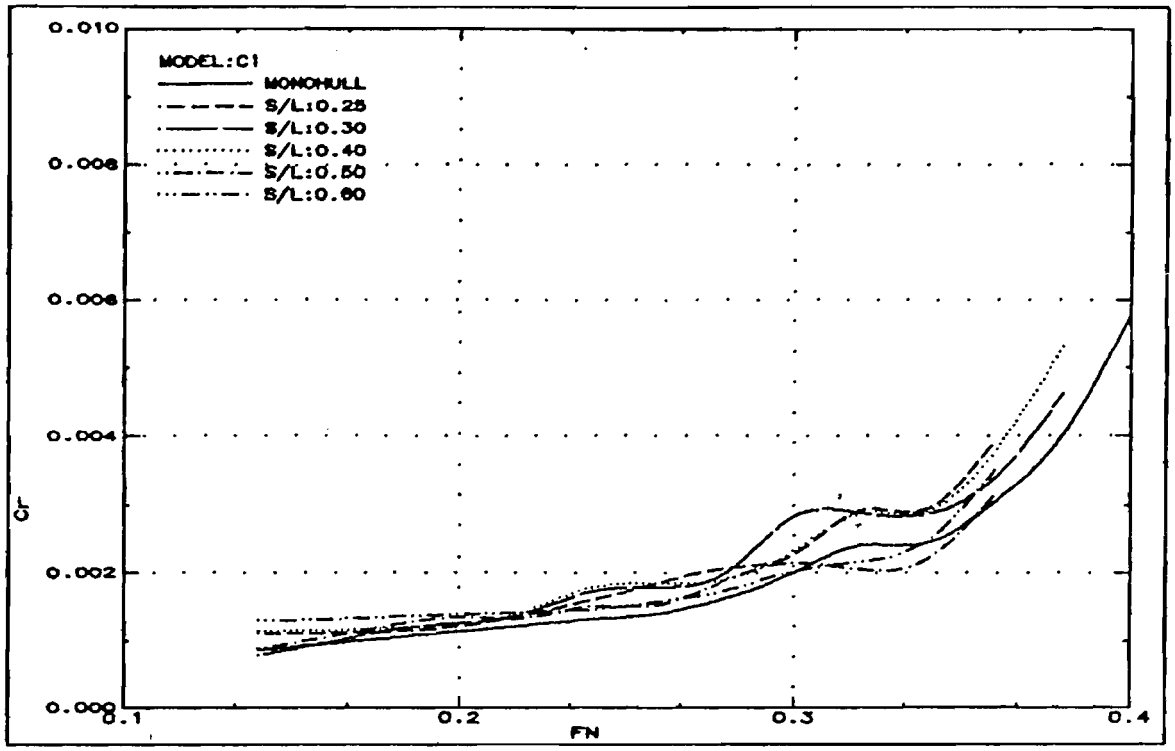

Fig.125: Residuary resistance (C1)

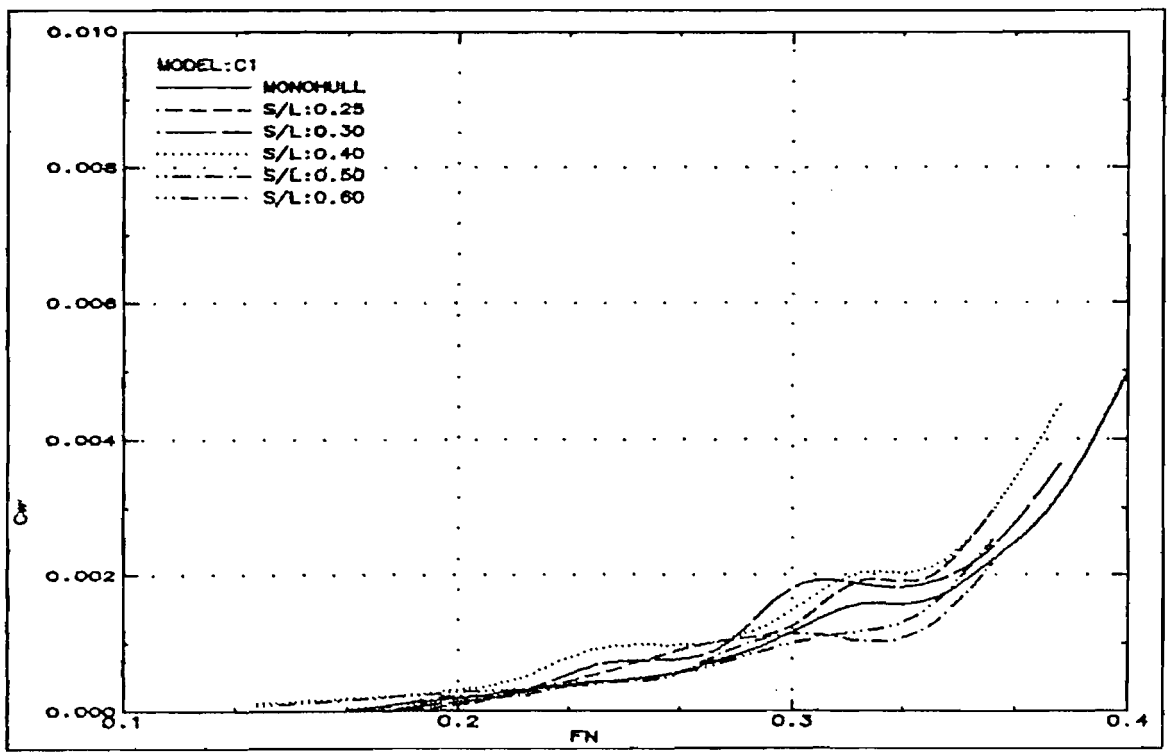

Fig.126: Wave resistance (C1)

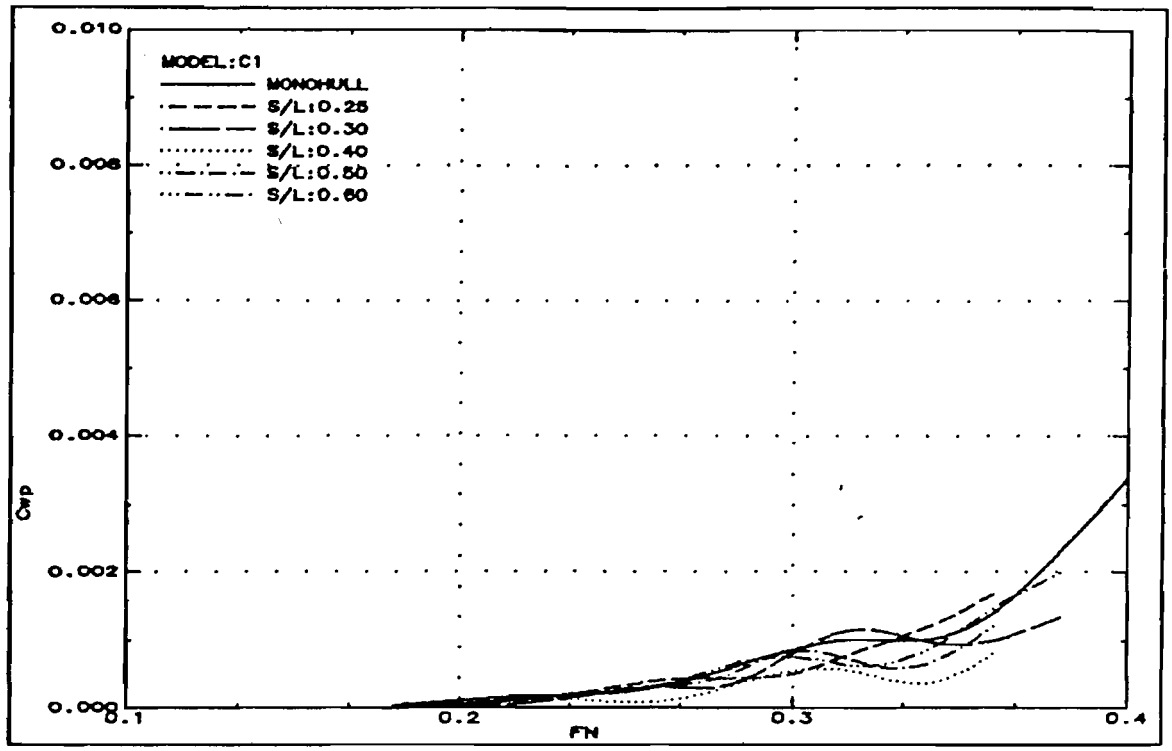

Fig.127: Wave pattern resistance (C1)

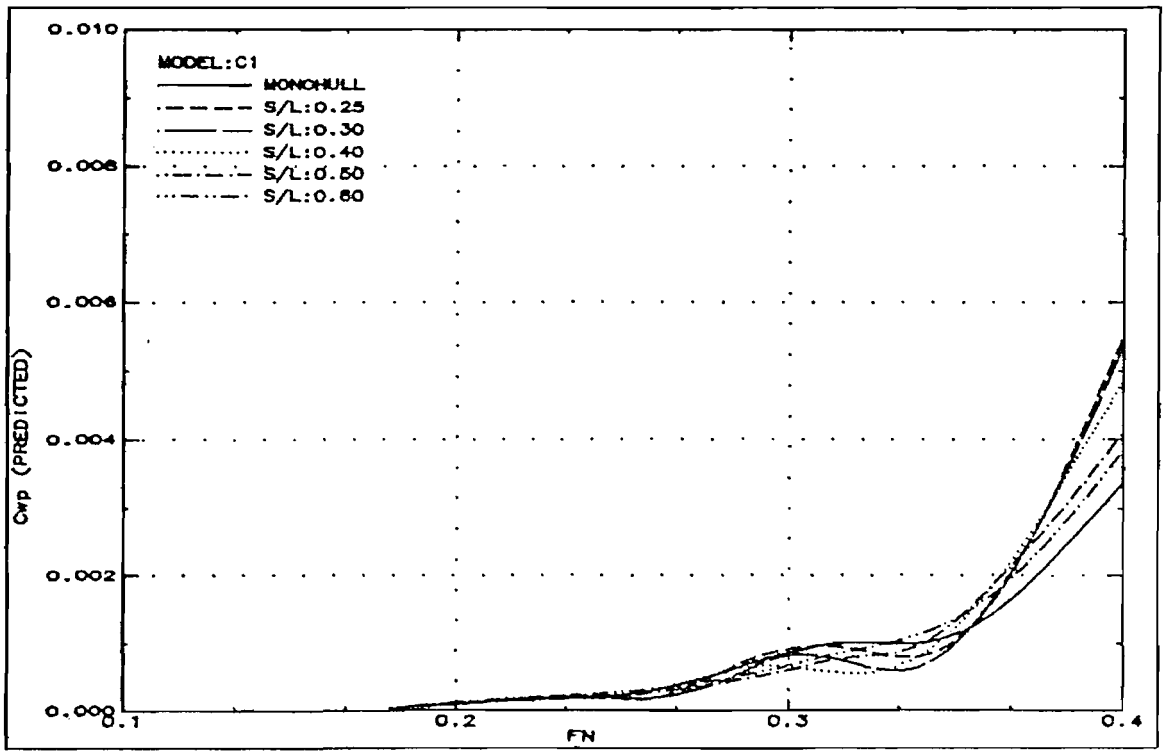

Fig.128: Wave pattern resistance predicted from monohull wave pattern analysis (C1)

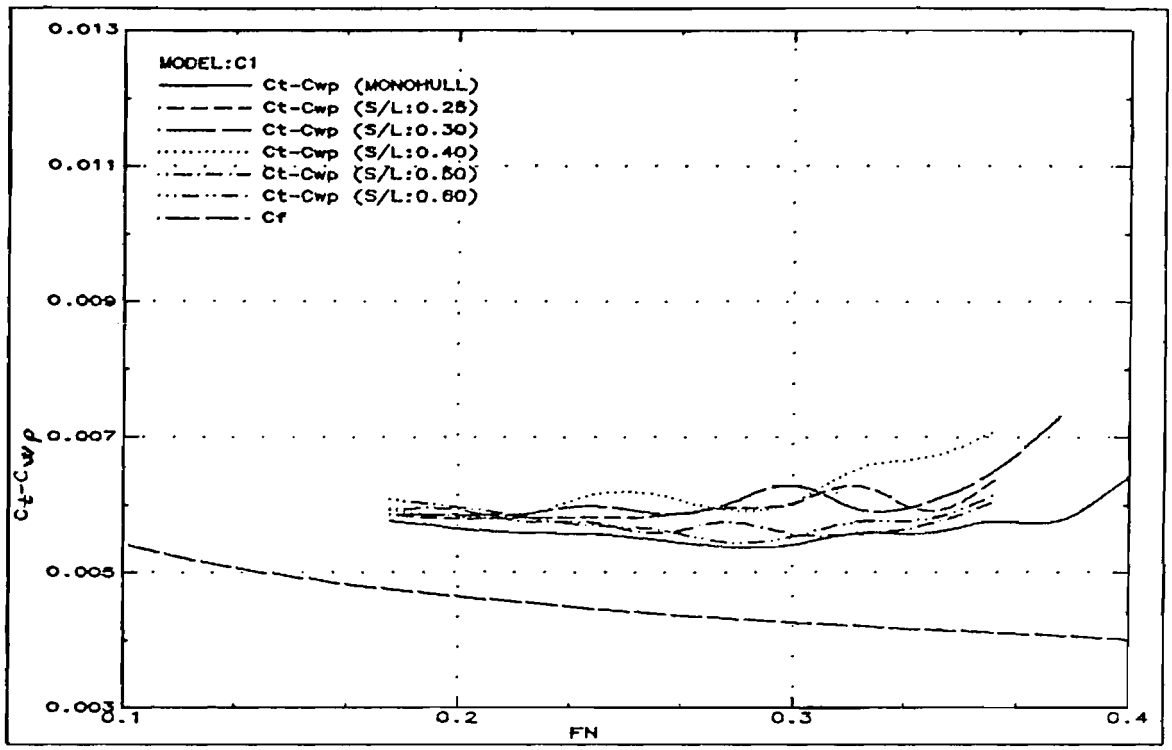

Fig.129: Total resistance minus wave pattern resistance (C1)

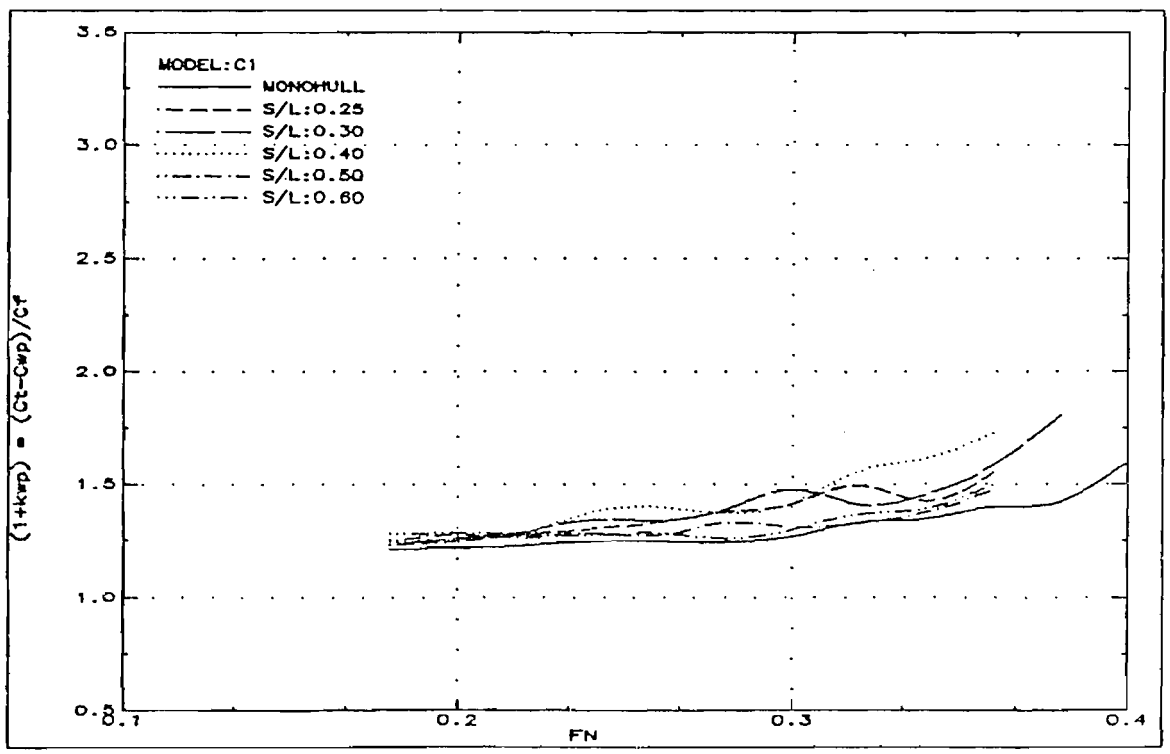

Fig.130: Form factor, i.e. $1+k_{WP}=(C_T-C_{WP})/C_F$ (C1)

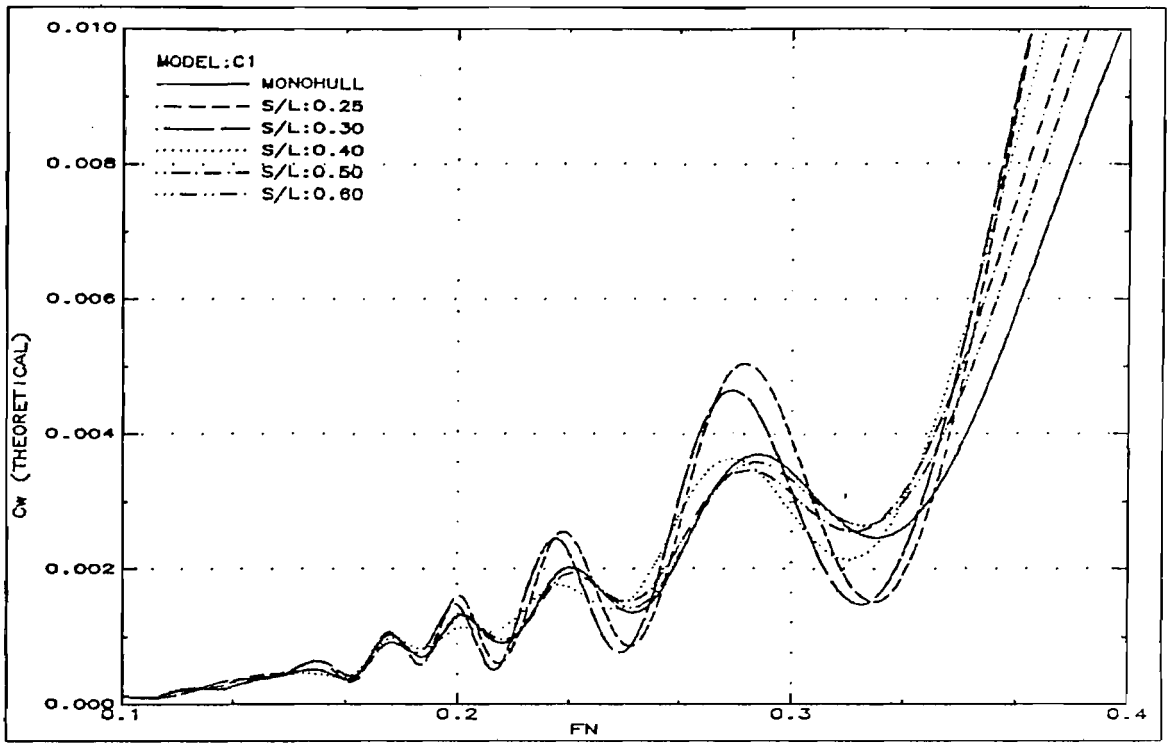

Fig.131: Theoretical wave resistance (C1)

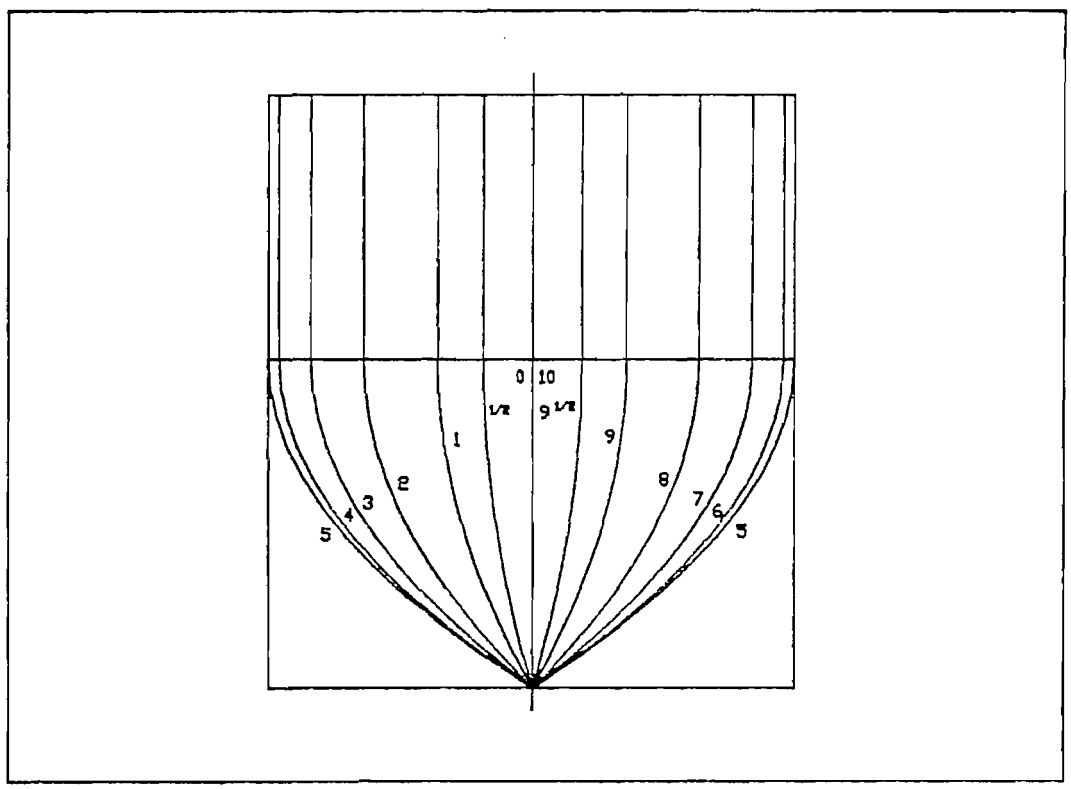

Fig.132: Body plan of model : C2 (Wigley Hull)

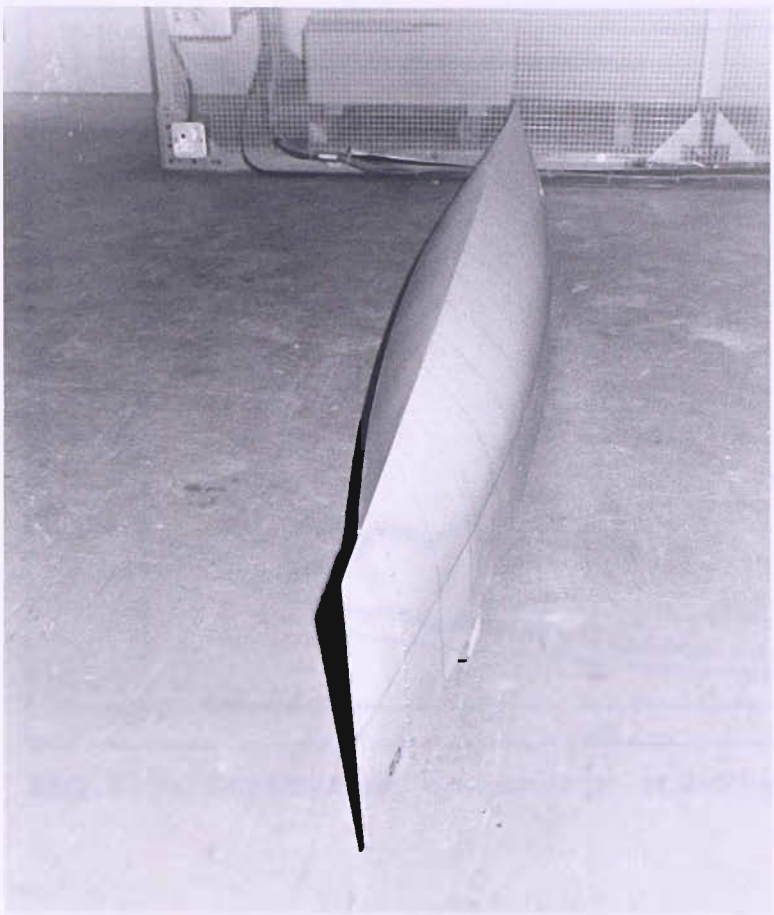

Fig. 133 : Front view of model: C2

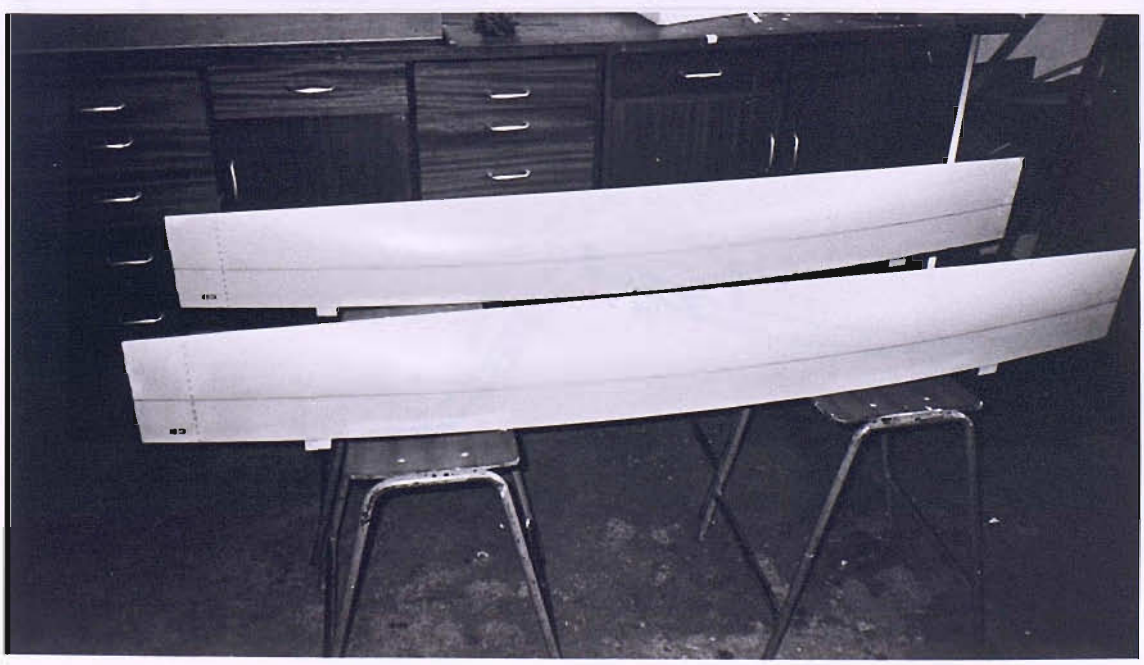

Fig. 134 : Side view of model: C2

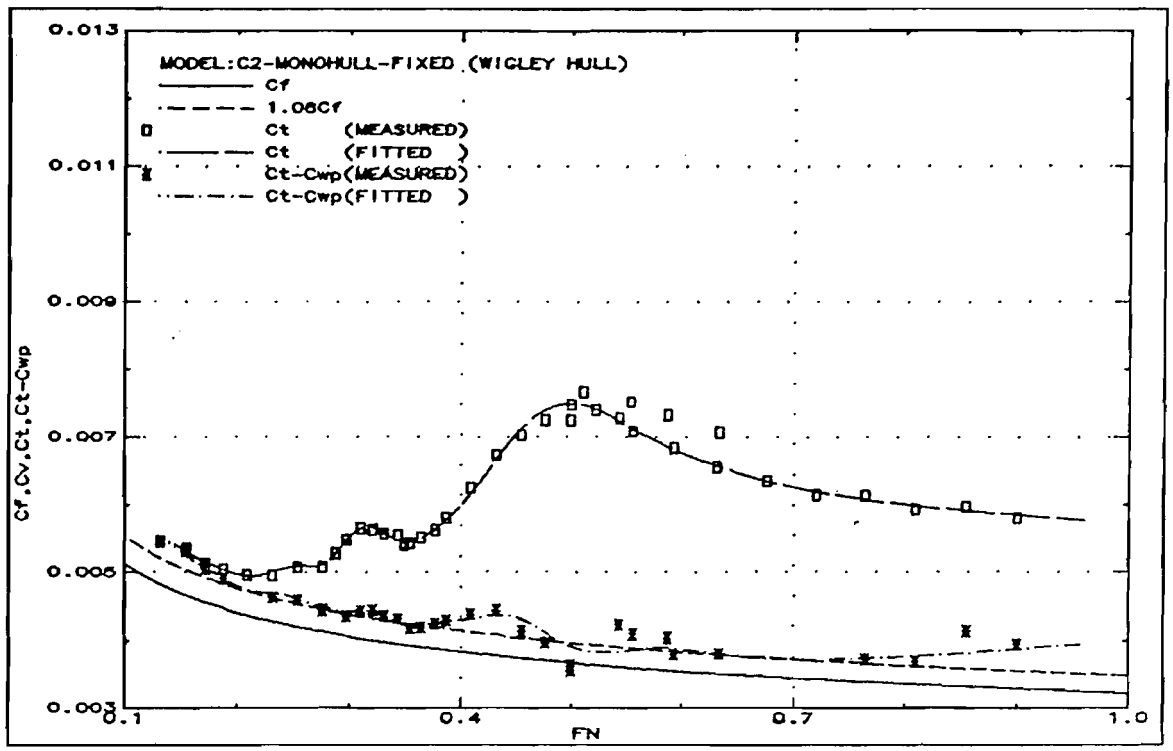

Fig.135: Resistance components (C2-Fixed-Monohull)

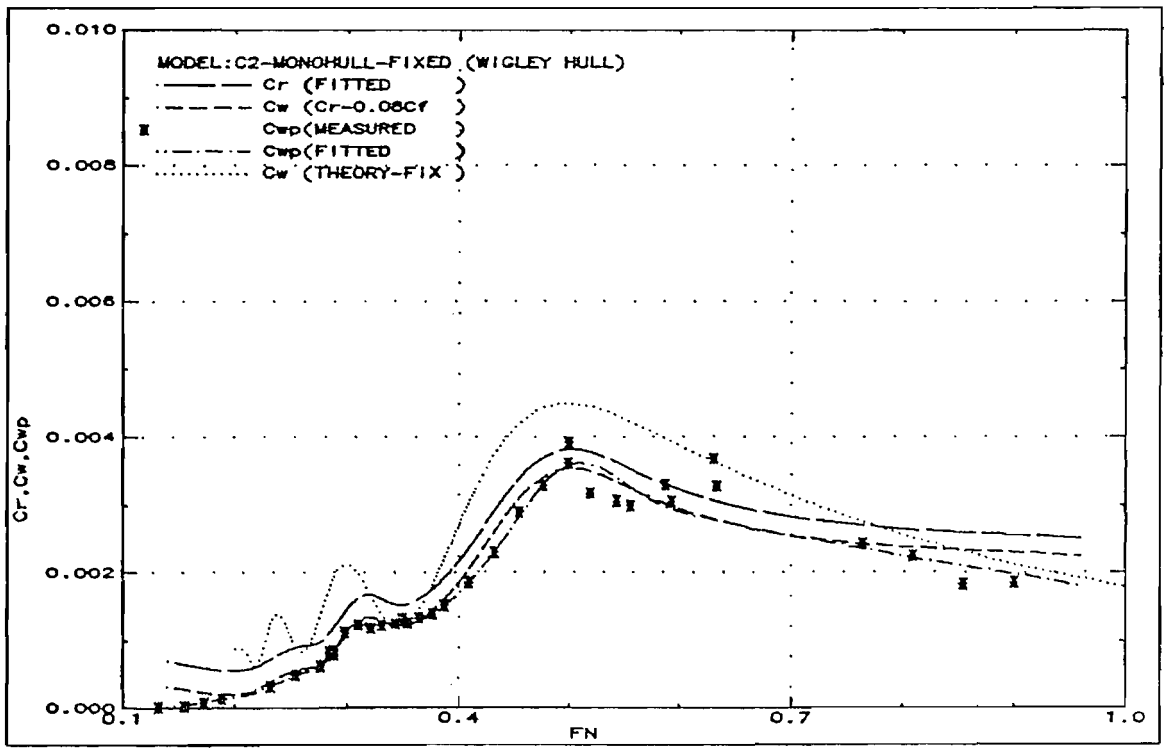

Fig.136: Wave resistance comparison (C2-Fixed-Monohull)

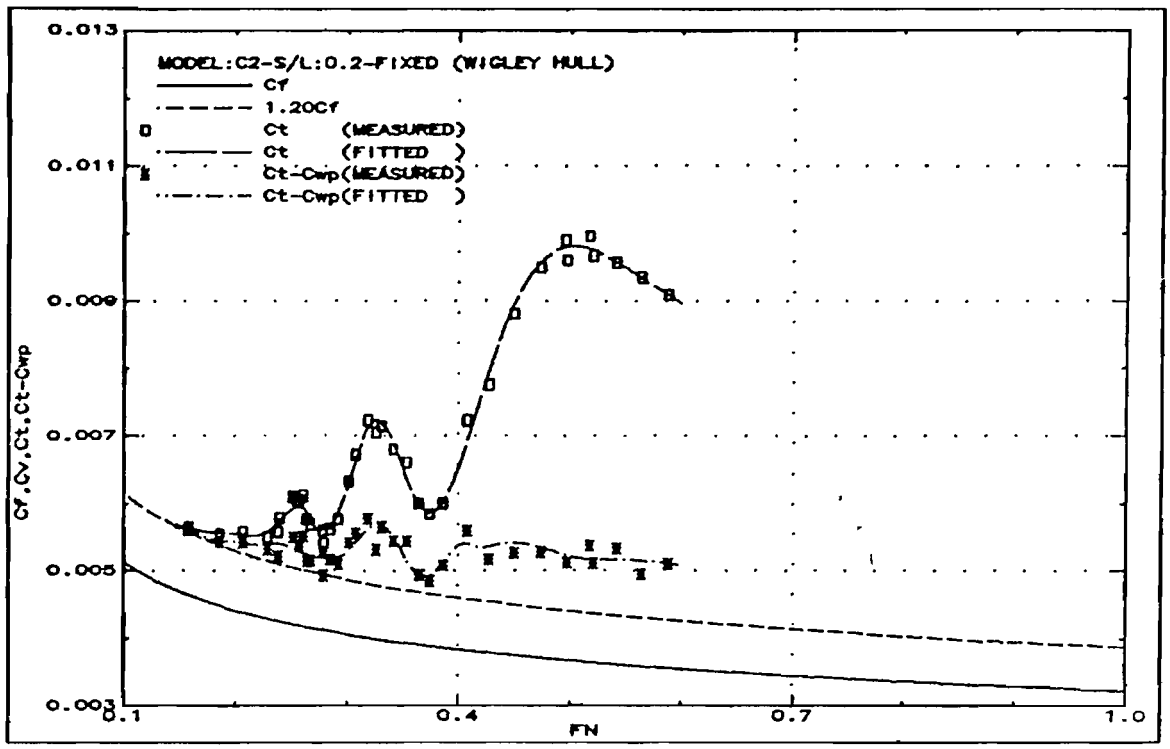

Fig.137: Resistance components (C2-Fixed-S/L:Ø.2)

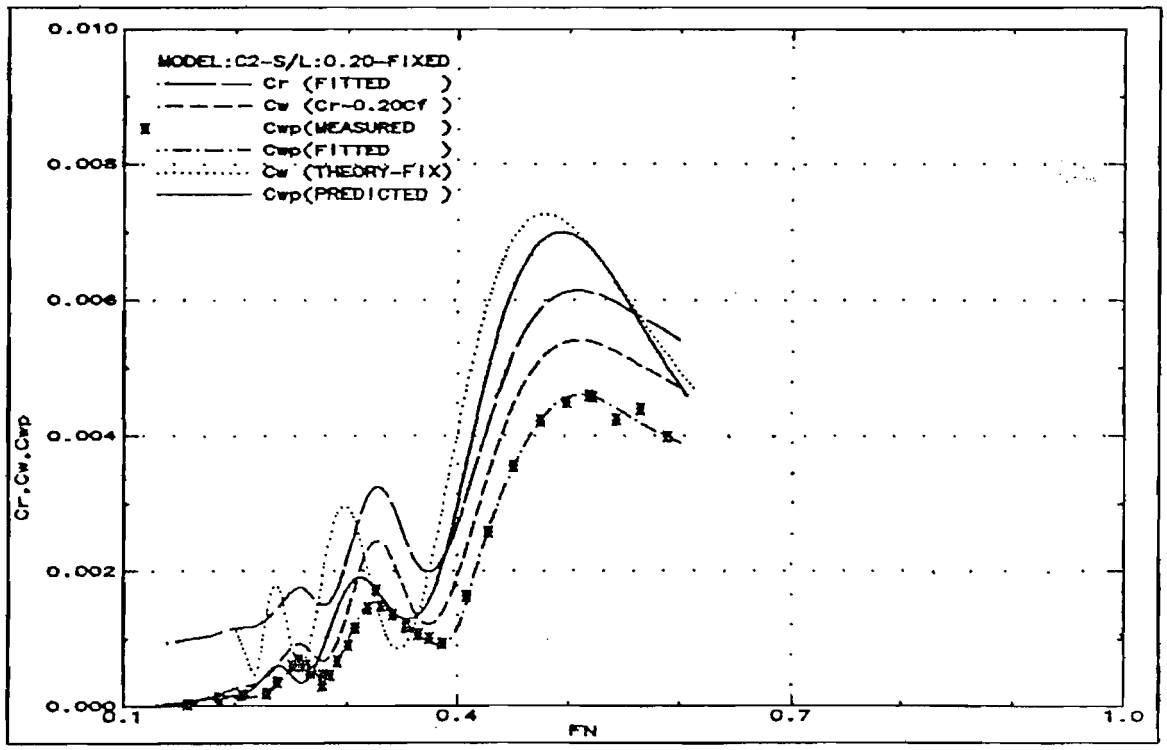

Fig.138: Wave resistance comparison (C2-Fixed-S/L:Ø.2)

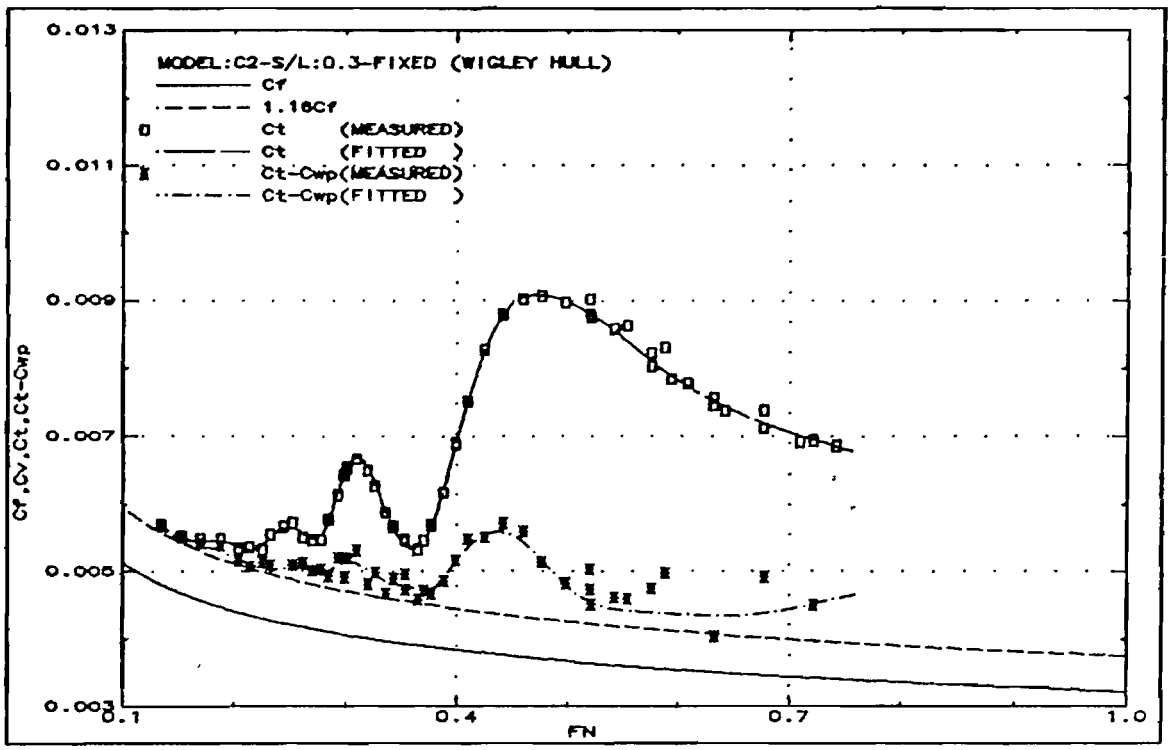

Fig.139: Resistance components (C2-Fixed-S/L:Ø.3)

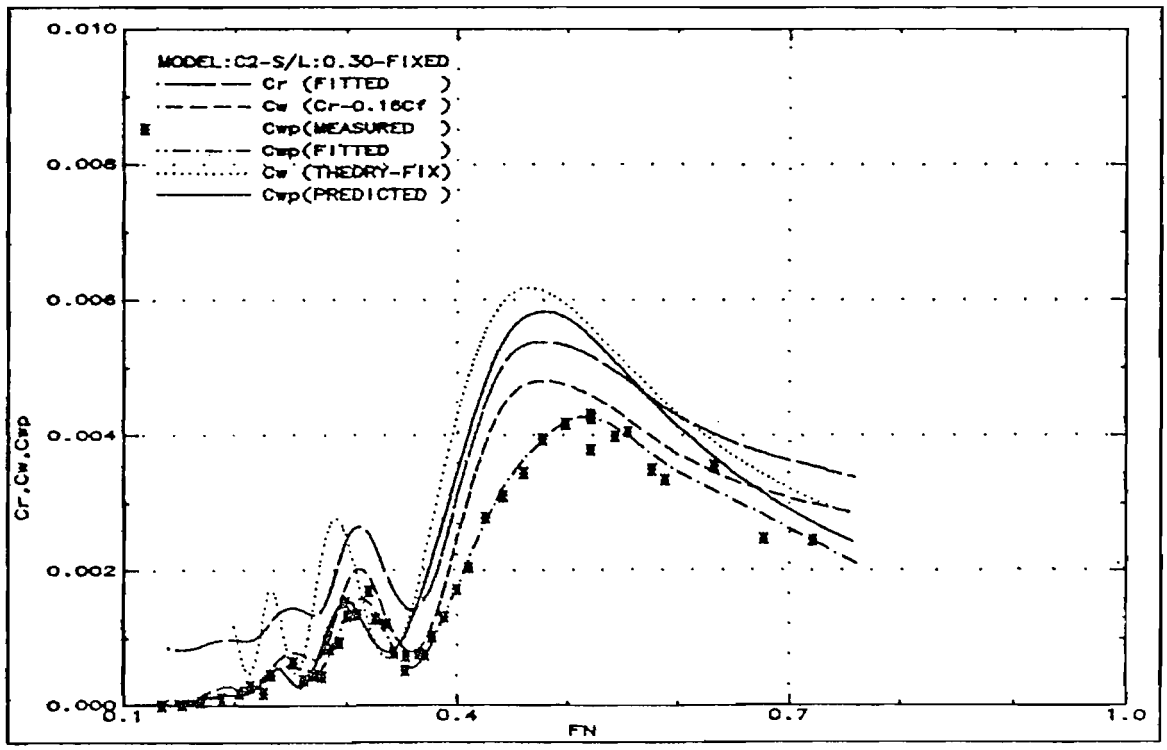

Fig.140: Wave resistance comparison (C2-Fixed-S/L:Ø.3)

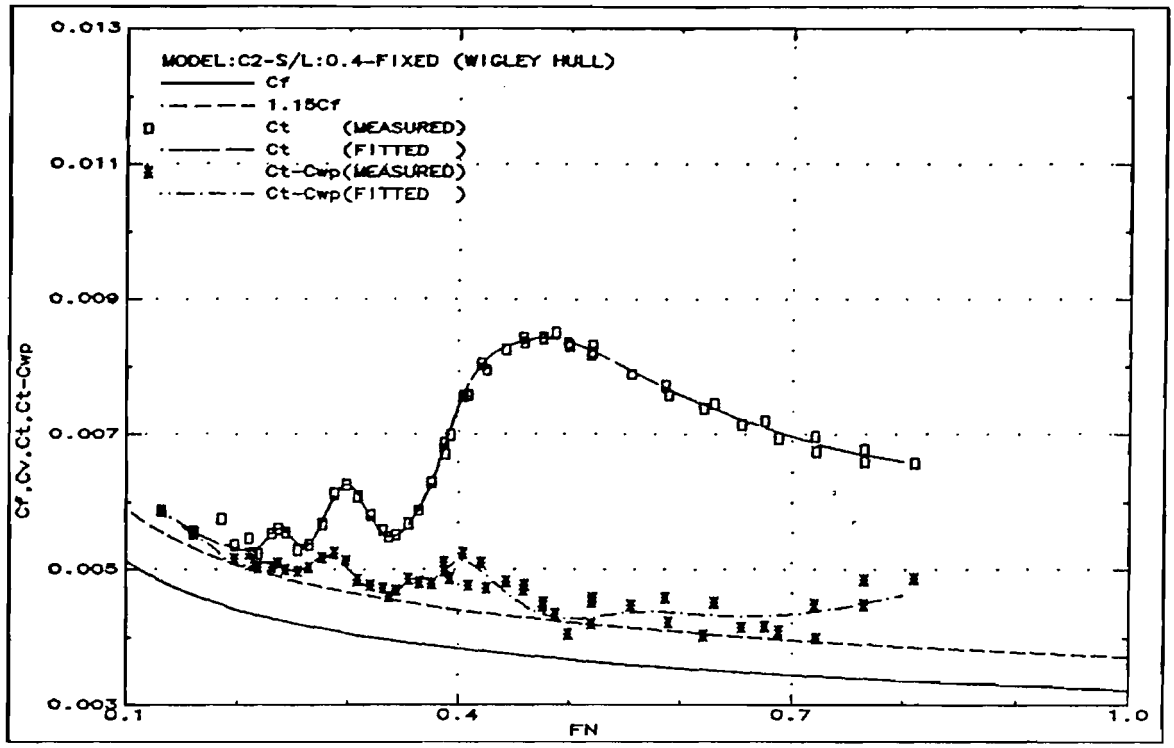

Fig.141: Resistance components (C2-Fixed-S/L:Ø.4)

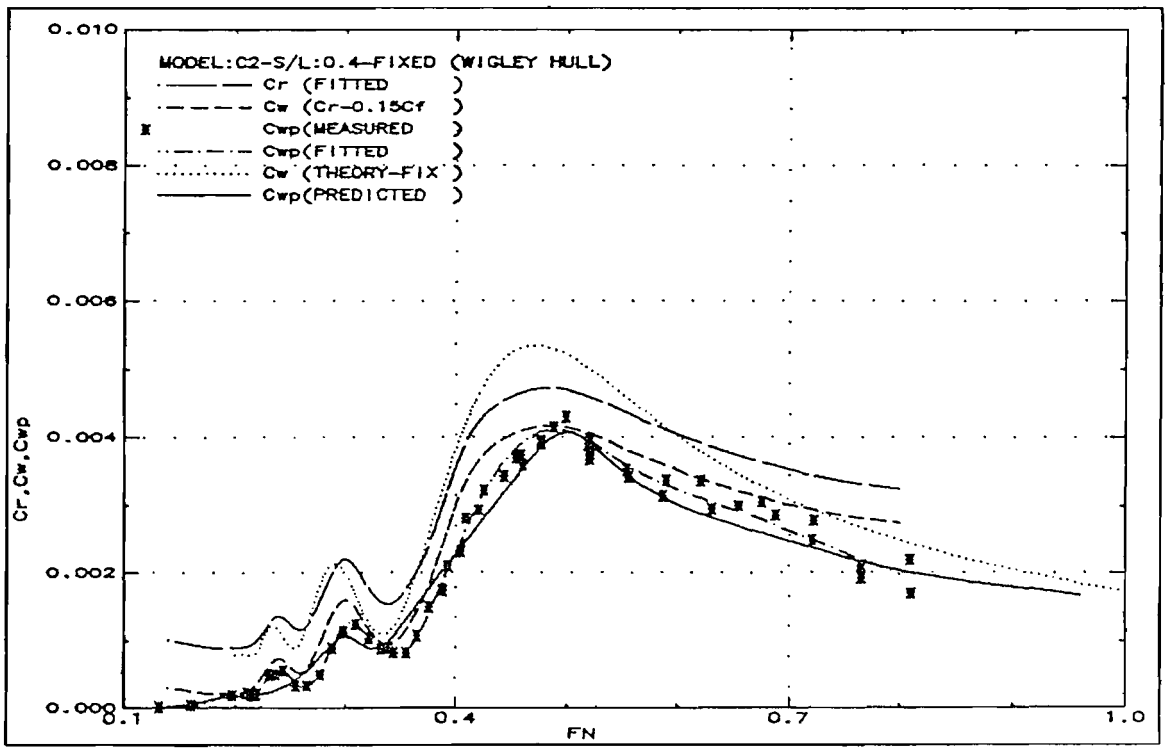

Fig.142: Wave resistance comparison (C2-Fixed-S/L:Ø.4)

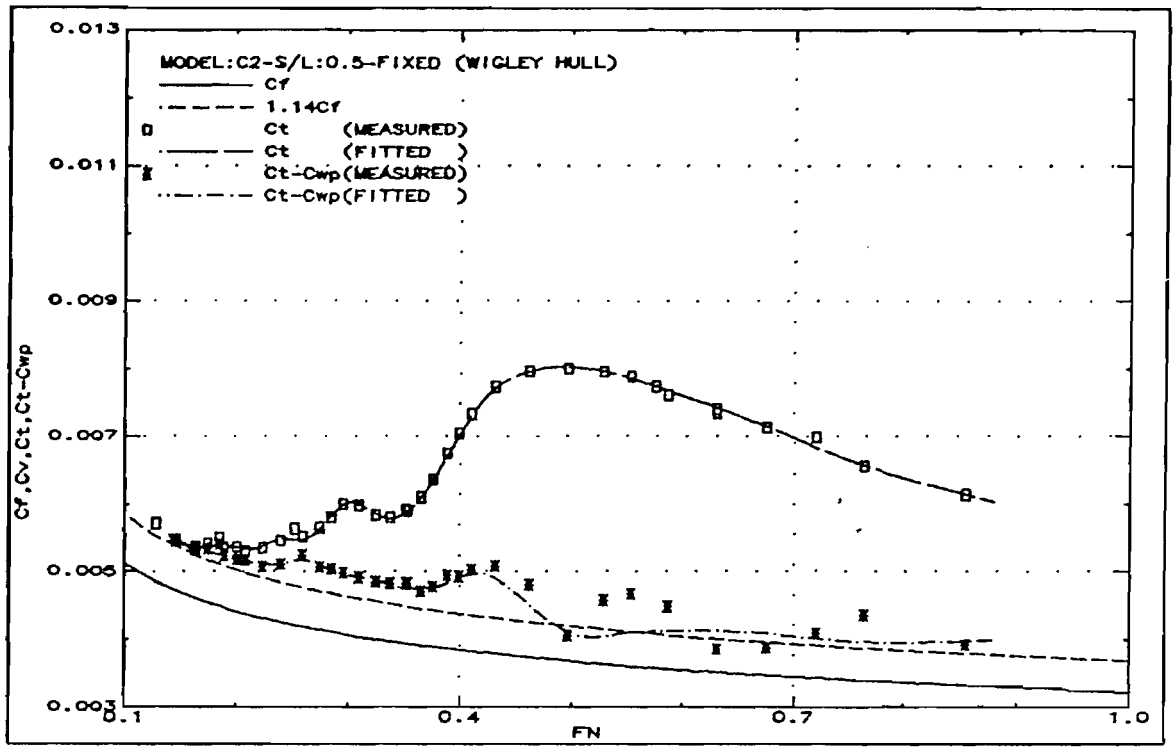

Fig.143: Resistance components (C2-Fixed-S/L:Ø.5)

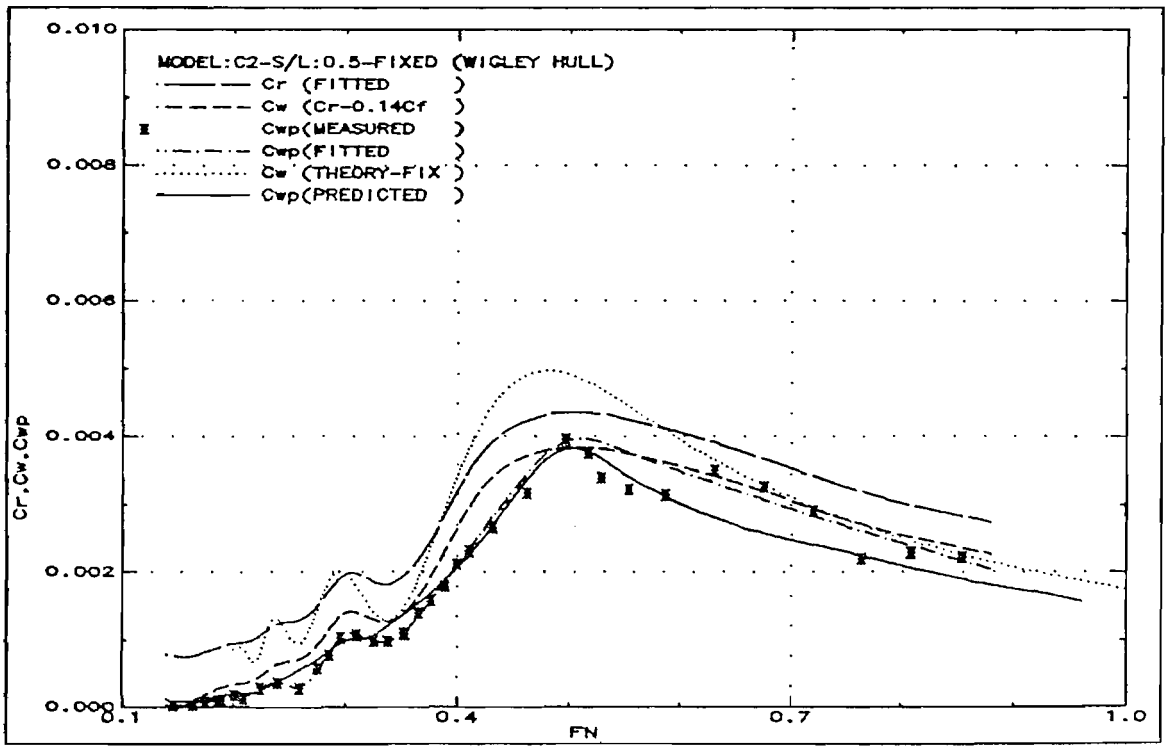

Fig.144: Wave resistance comparison (C2-Fixed-S/L:Ø.5)

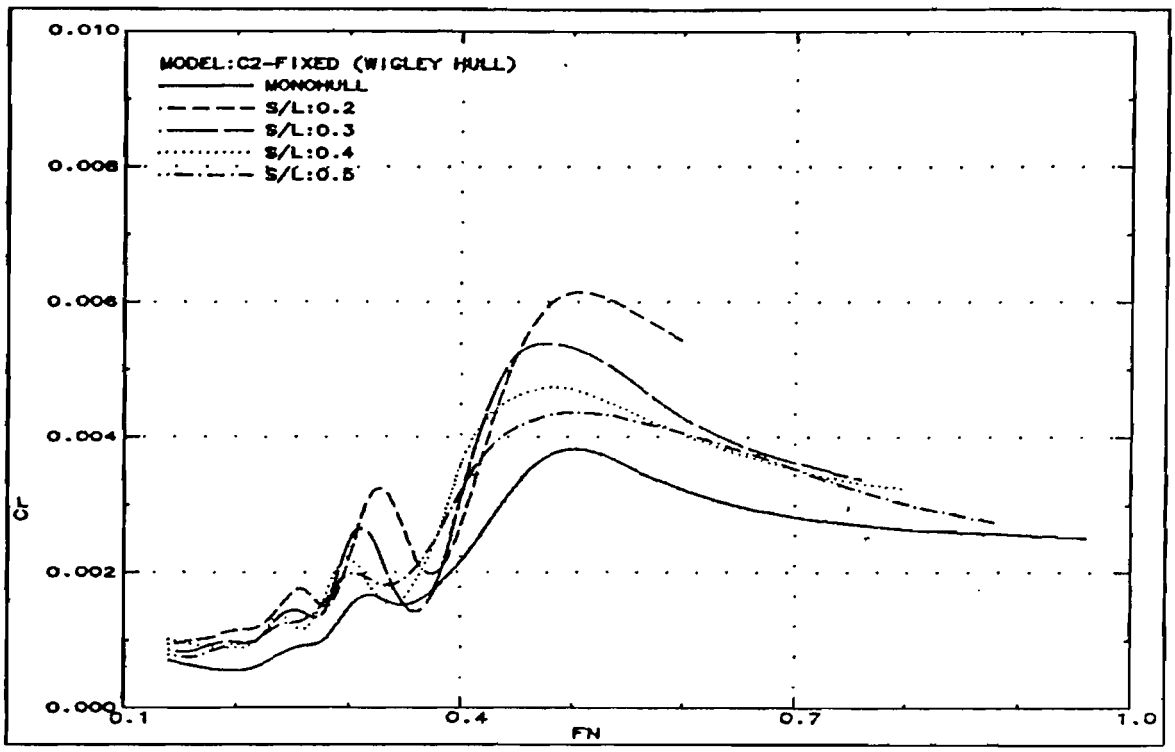

Fig.145: Residuary resistance (C2-Fixed)

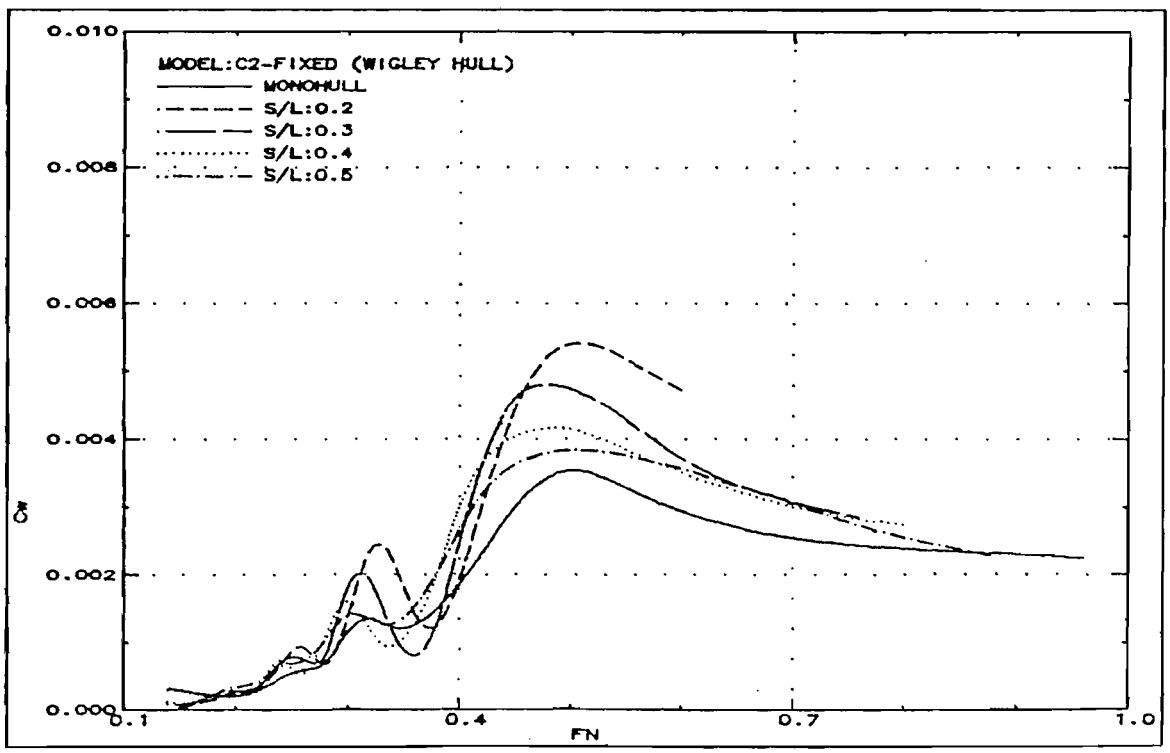

Fig.146: Wave resistance (C2-Fixed)

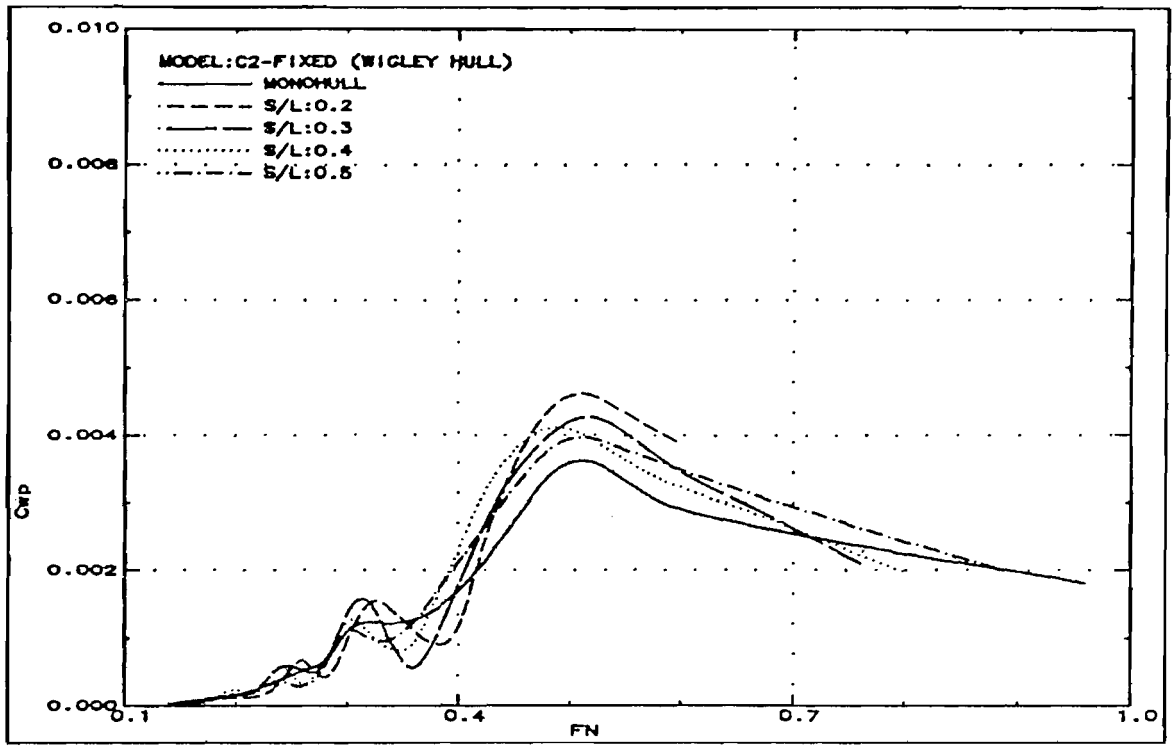

Fig.147: Wave pattern resistance (C2-Fixed)

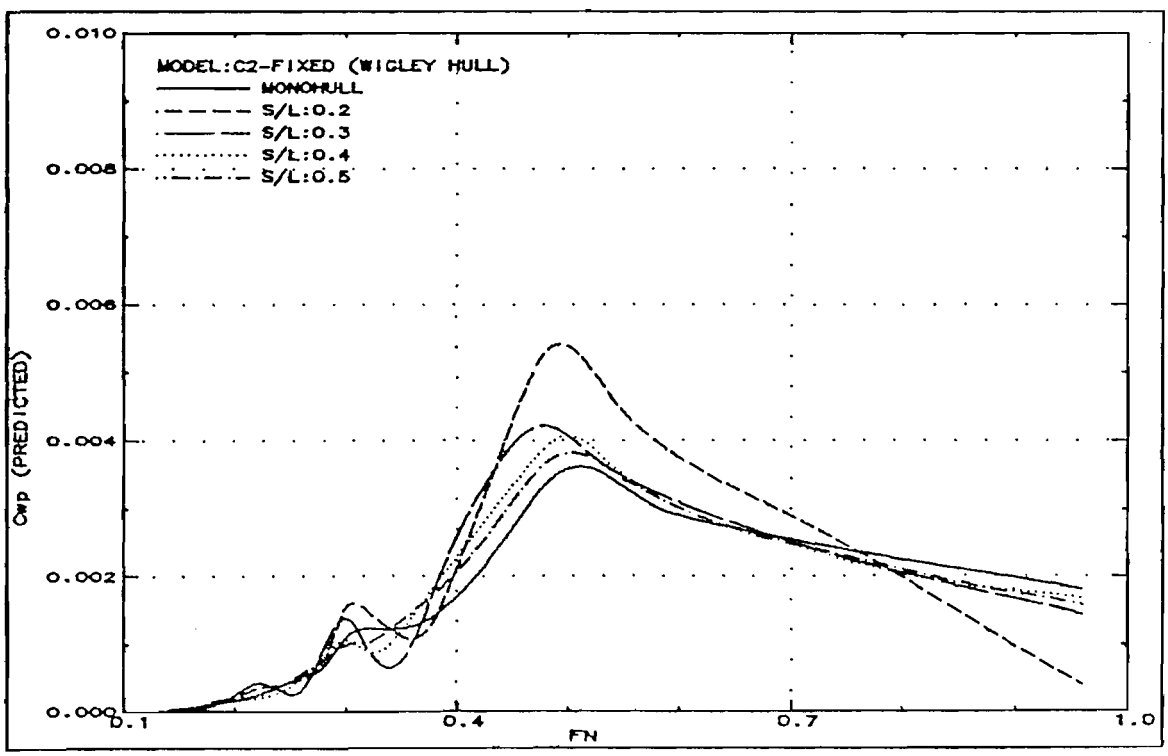

Fig.148:Wave pattern resistance predicted from monohull wave pattern analysis (C2-Fixed)

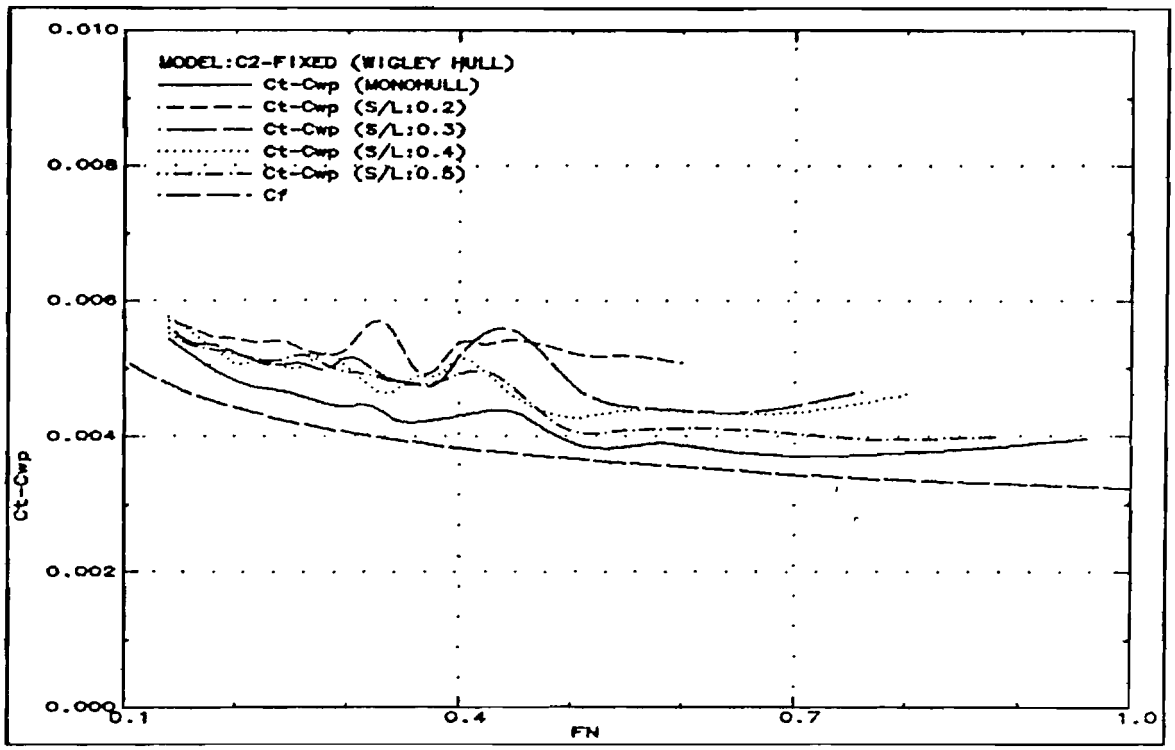

Fig.149: Total resistance minus wave pattern resistance (C2-Fixed)

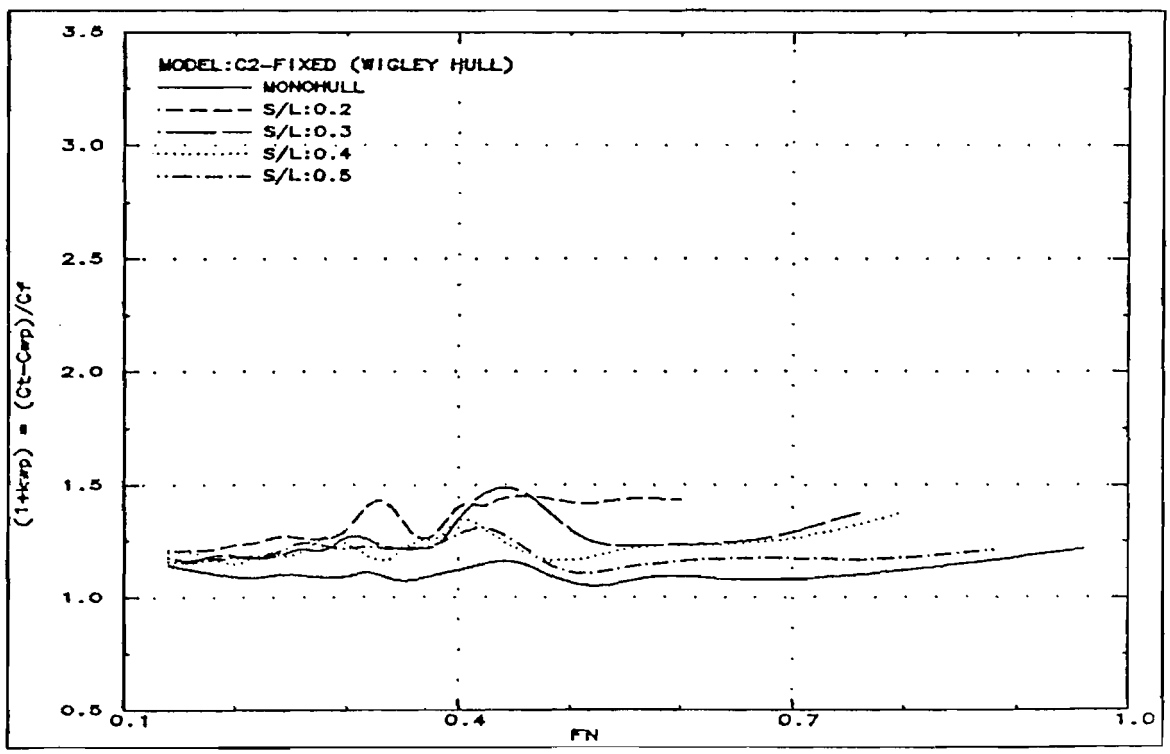

Fig.150: Form factor, i.e. $1+k_{WP}=(C_T-C_{WP})/C_F$ (C2-Fixed)

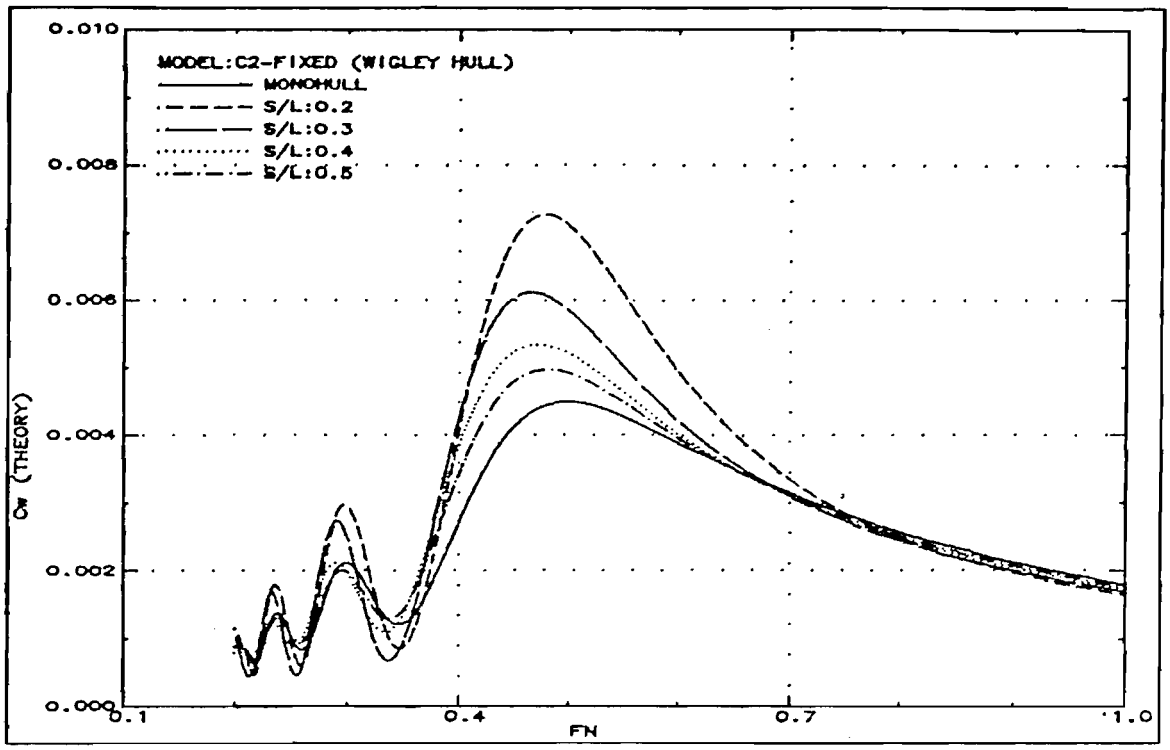

Fig.151: Theoretical wave resistance (C2-Fixed)

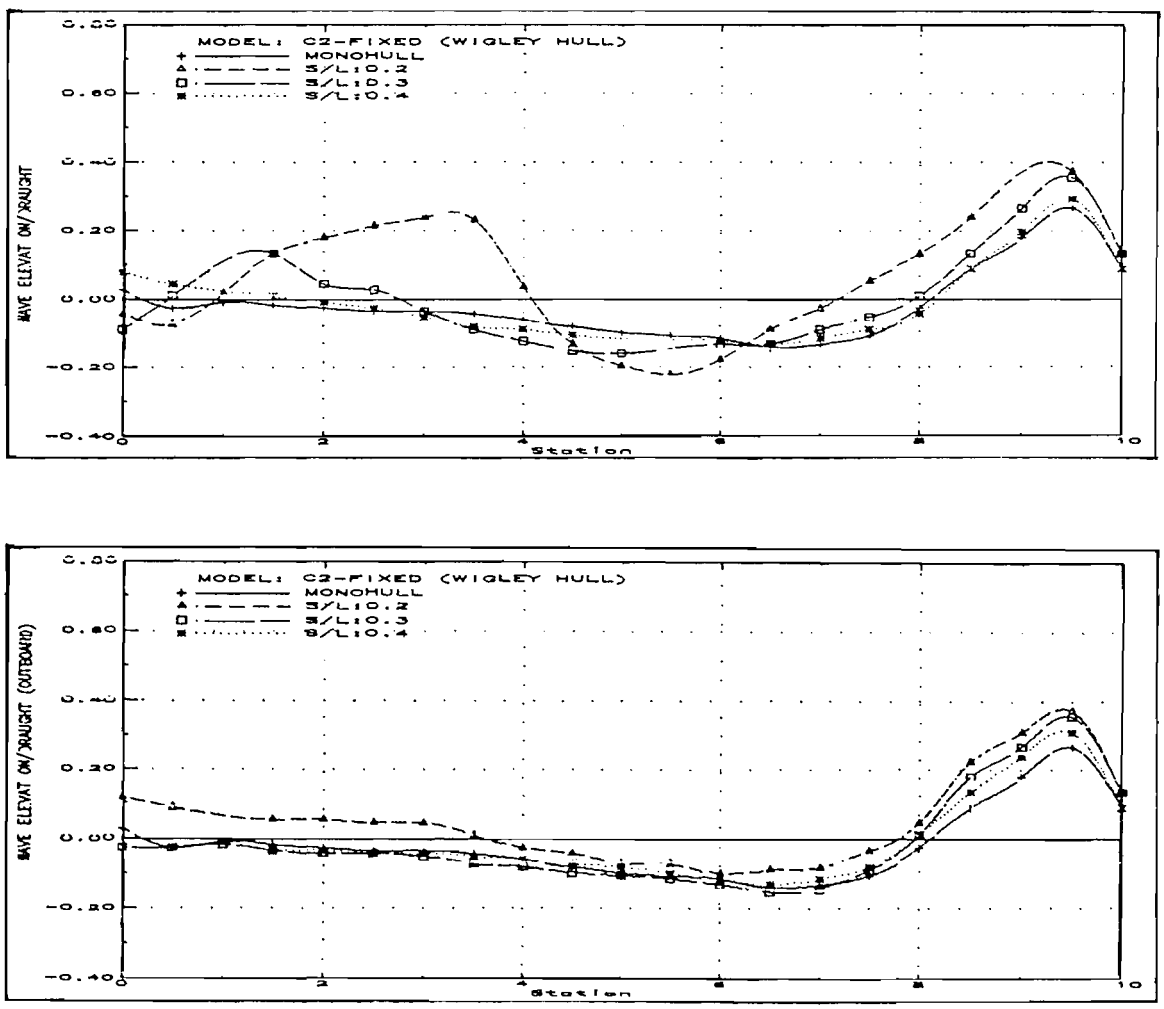

Fig.152: Wave elevation along the hull surface at Fn:0.35 (C2-Fixed)

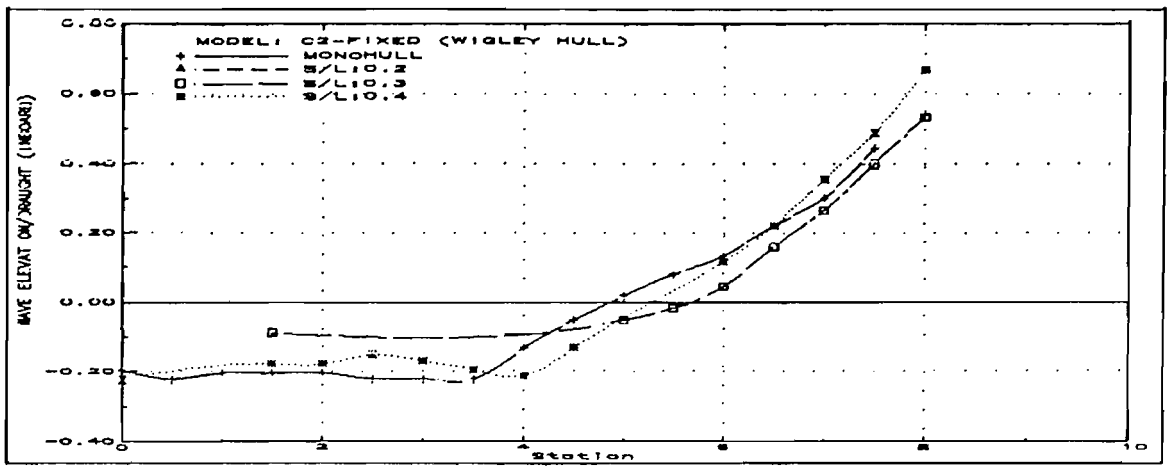

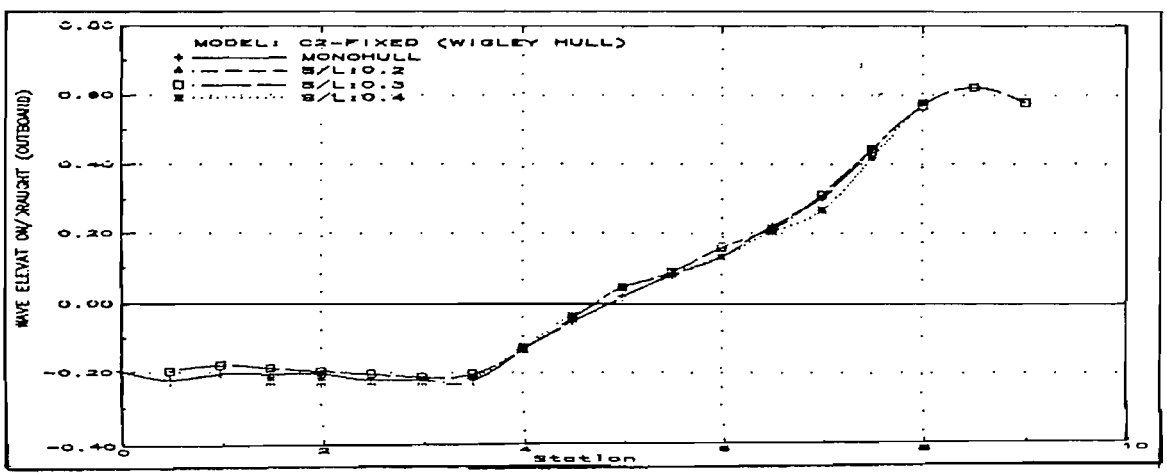

Fig.153: Wave elevation along the hull surface at Fn:0.50 (C2-Fixed)

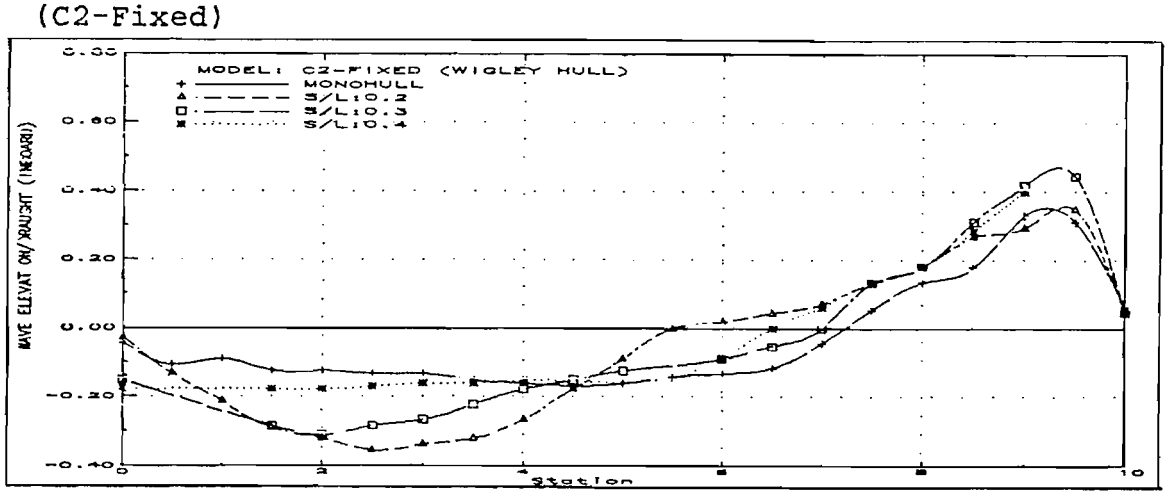

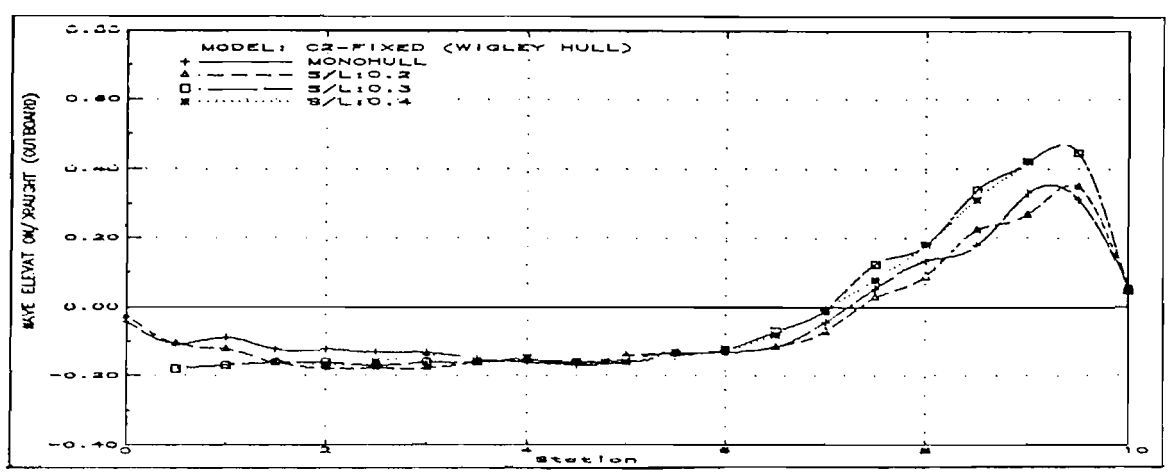

Fig.154: Wave elevation along the hull surface at Fn:0.75 (C2-Fixed)

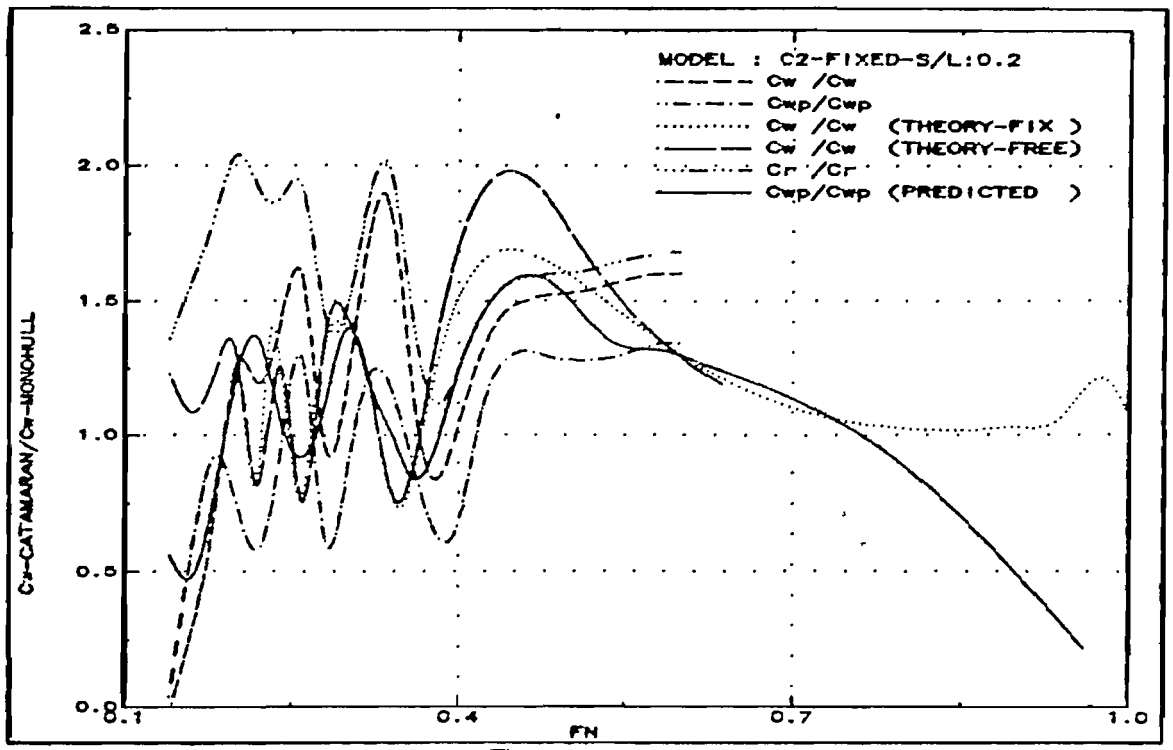

Fig.155: Wave resistance interference ratio (C2-Fixed-S/L:Ø.2)

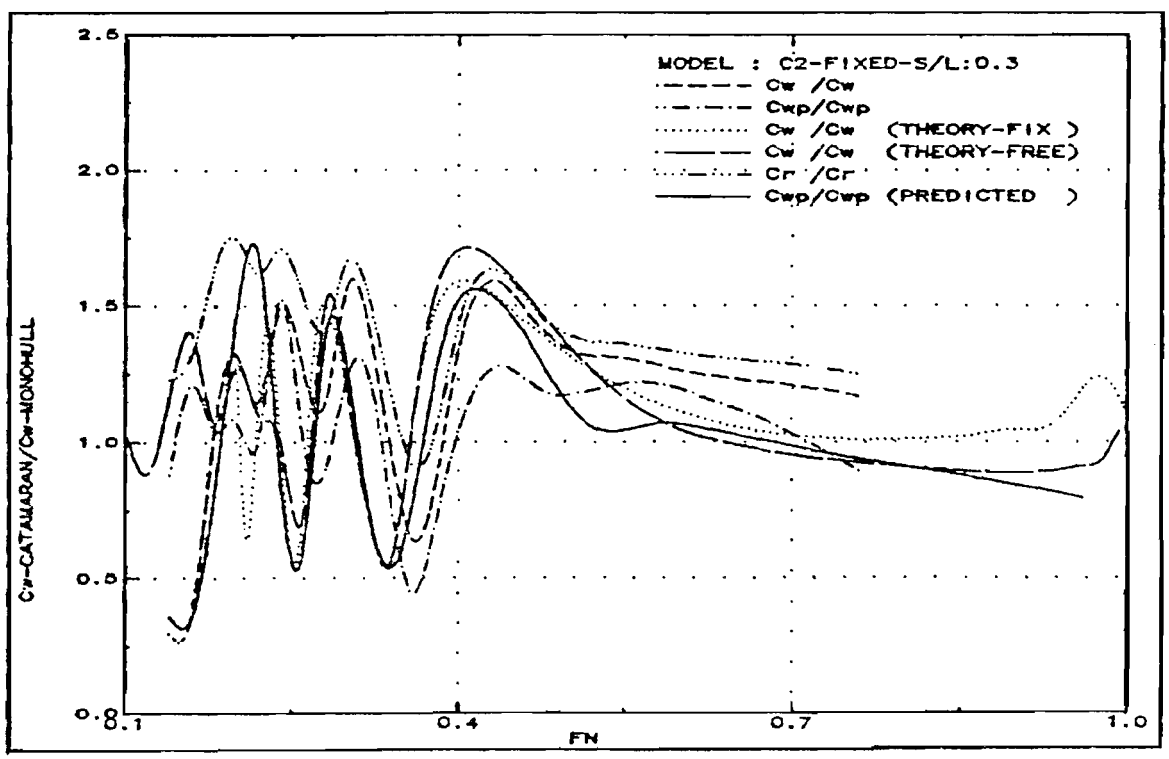

Fig.156: Wave resistance interference ratio (C2-Fixed-S/L:Ø.3)

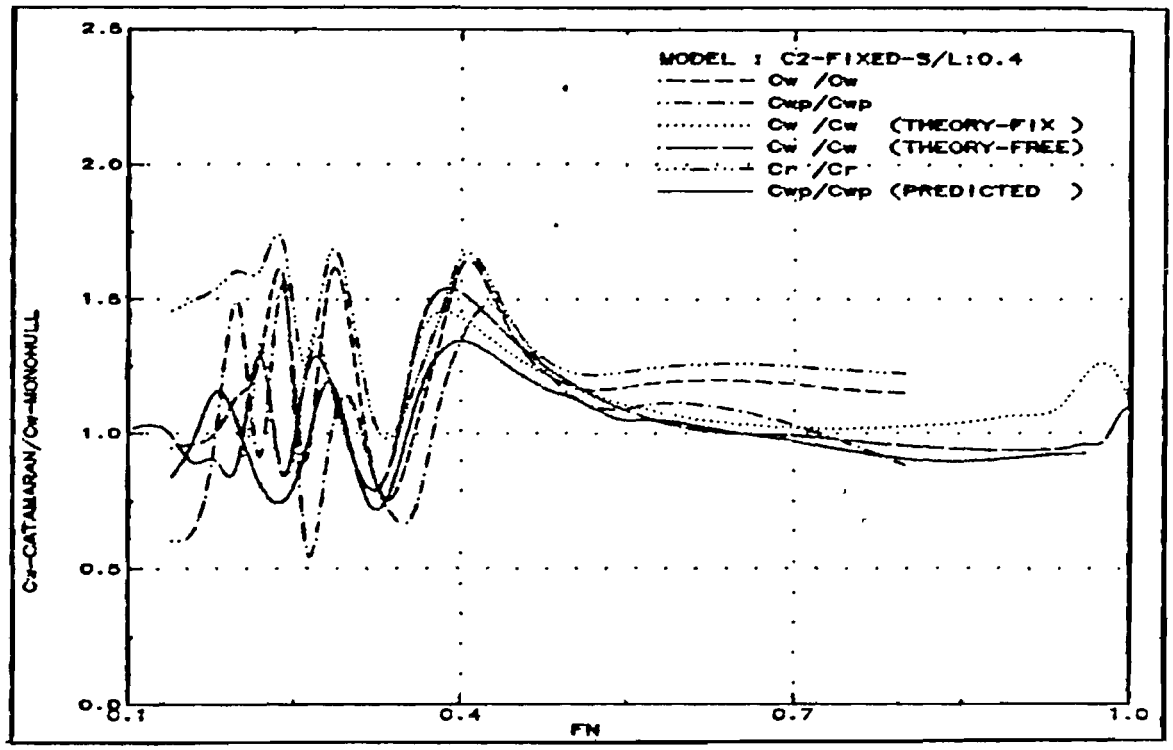

Fig.157: Wave resistance interference ratio (C2-Fixed-S/L:0.4)

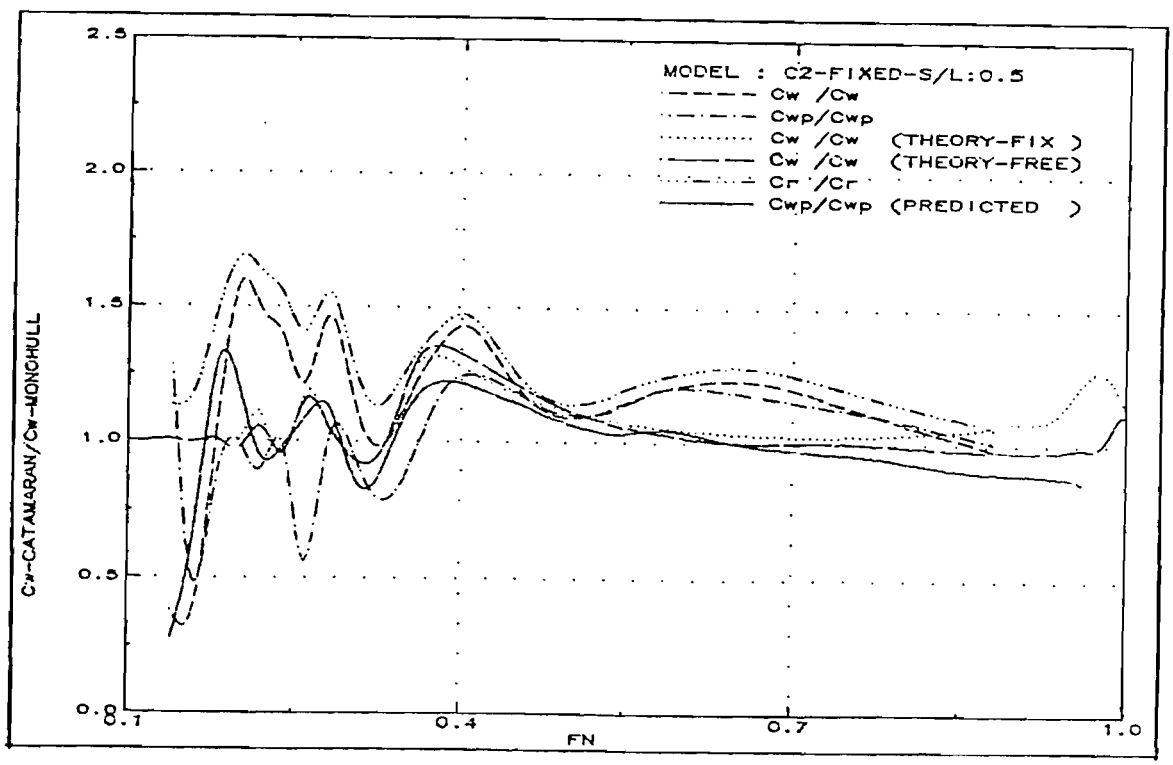

Fig.158: Wave resistance interference ratio (C2-Fixed-S/L:0.5)

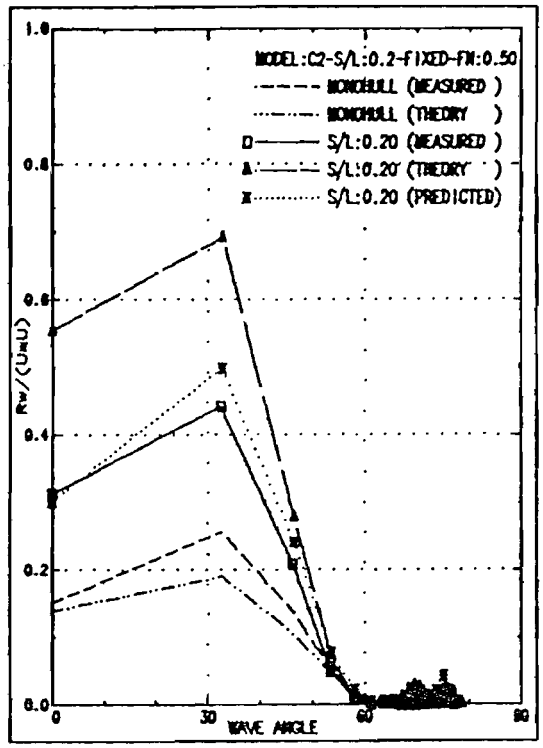

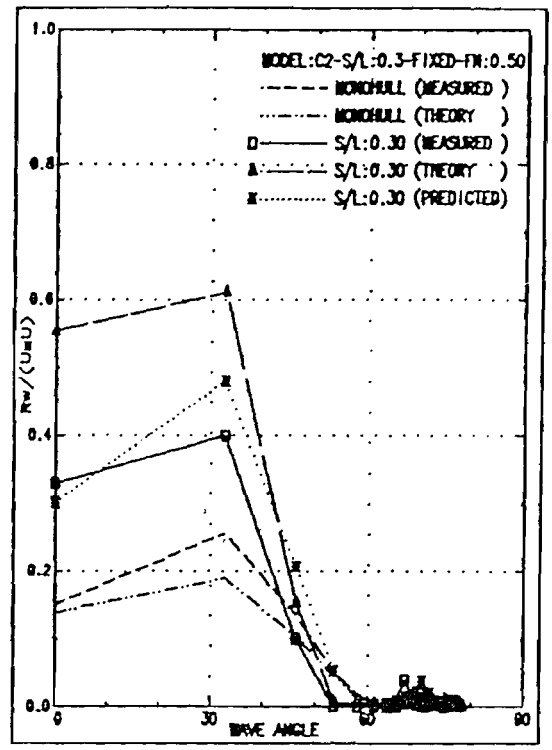

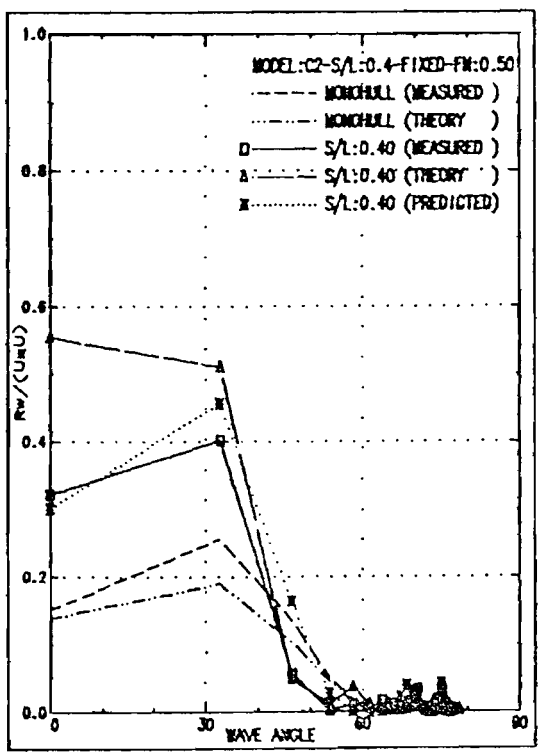

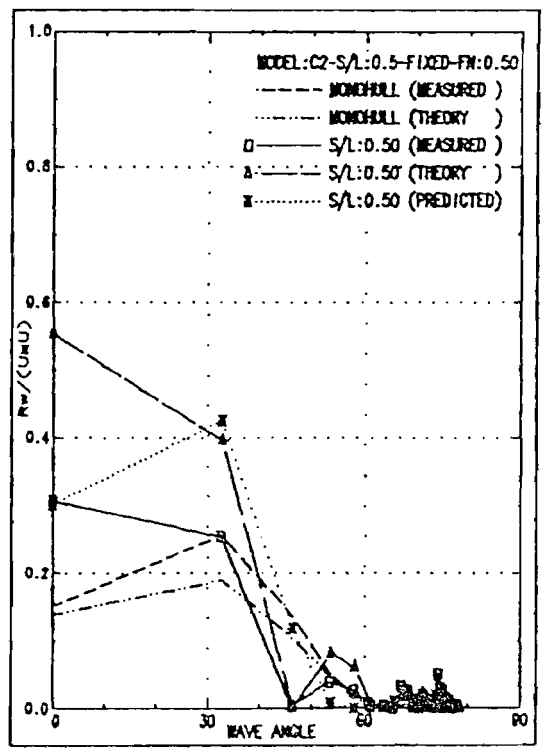

Fig.159: Wave resistance distribution across the wave spectrum at Fn:0.50 (C2-Fixed)

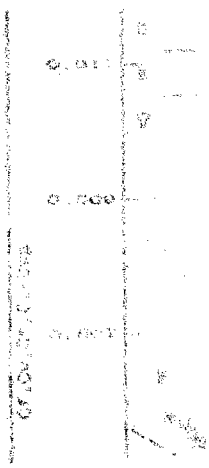

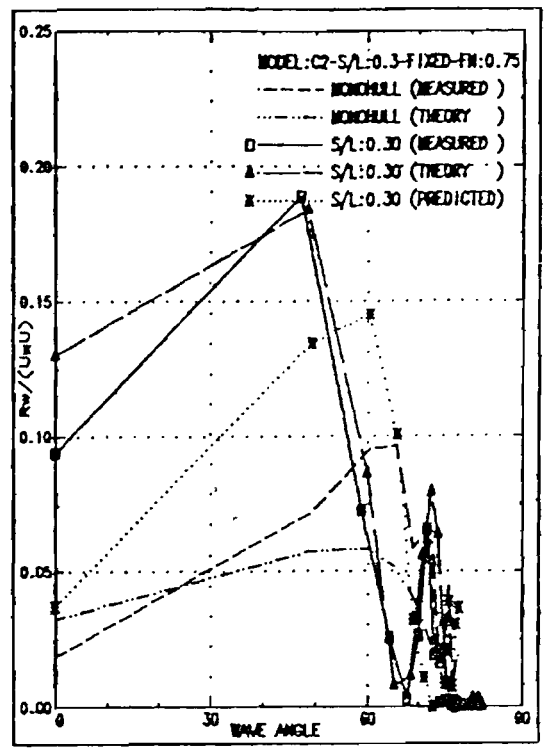

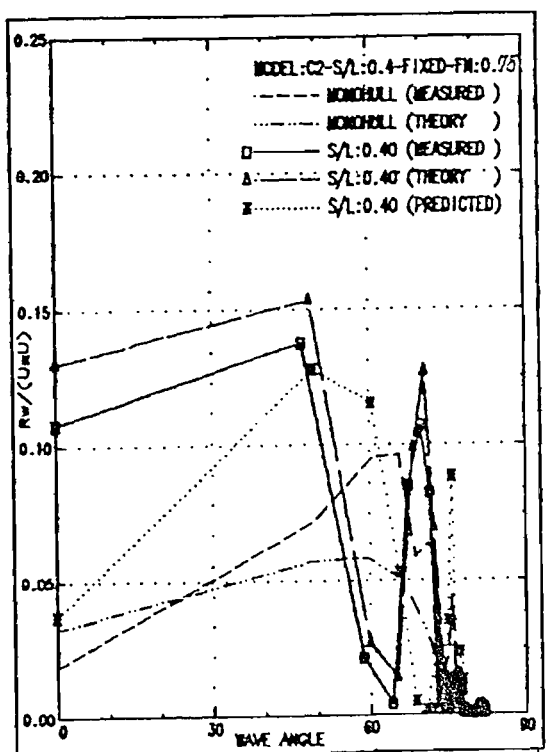

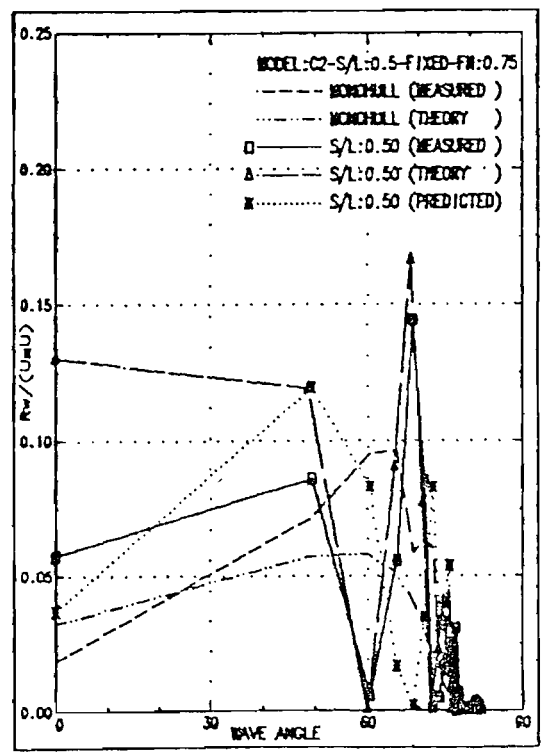

Fig.160: Wave resistance distribution across the wave spectrum at Fn:0.75 (C2-Fixed)

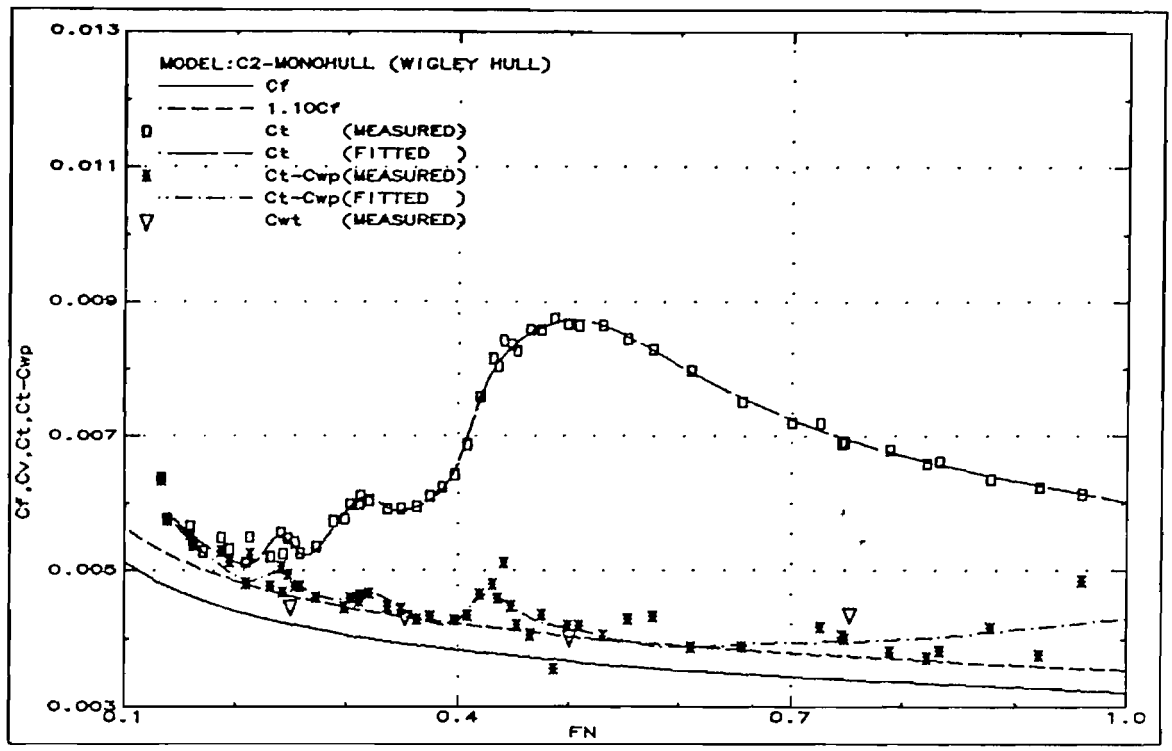

Fig.161: Resistance components (C2-Monohull)

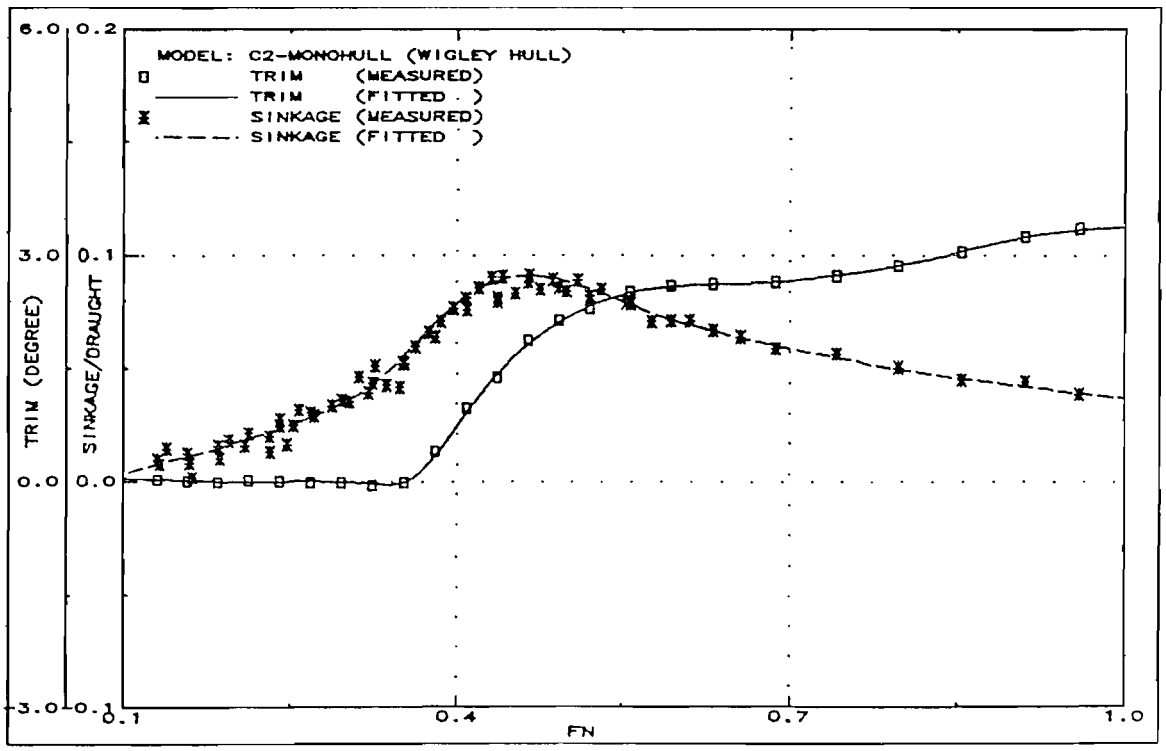

Fig.162: Running trim and sinkage (C2-Monohull)

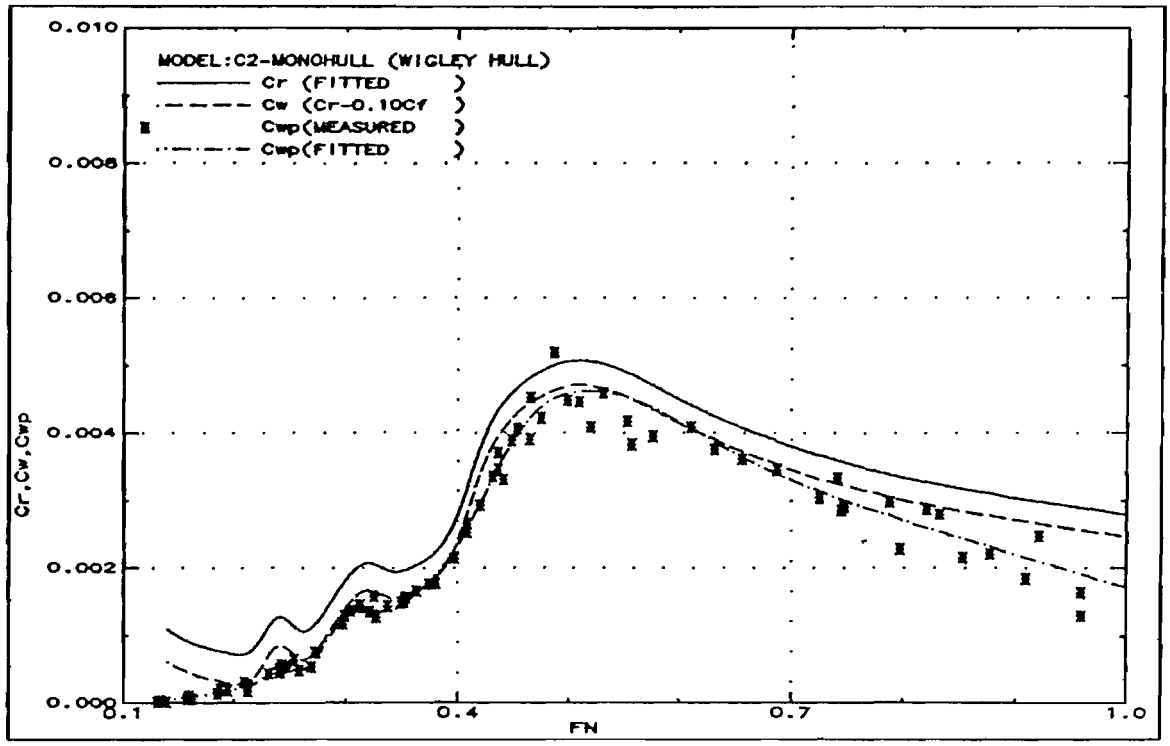

Fig.163: Measured wave resistance (C2-Monohull)

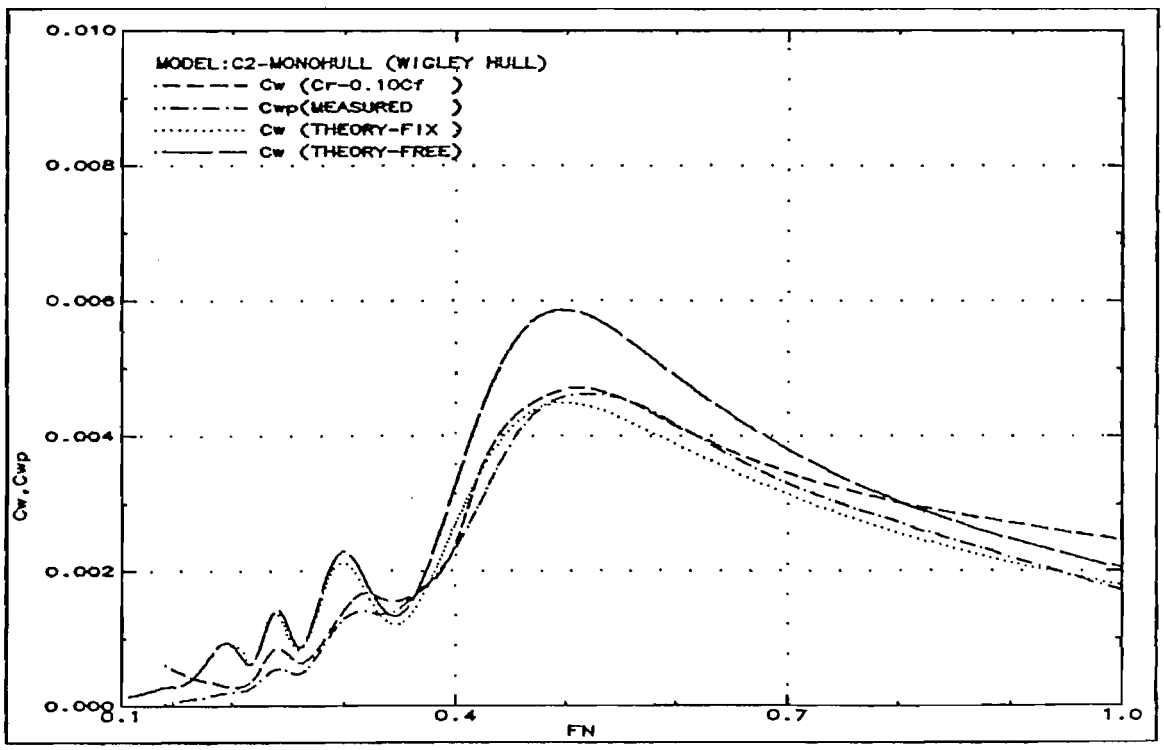

Fig.164: Wave resistance comparison (C2-Monohull)

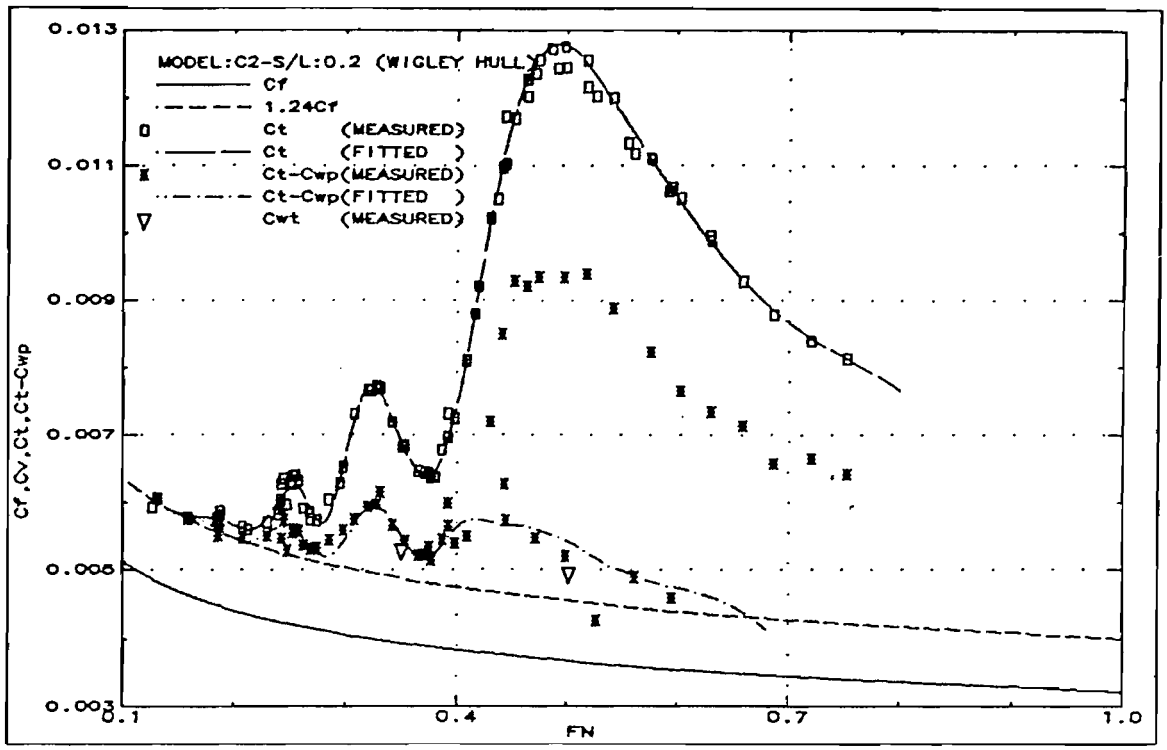

Fig.165: Resistance components (C2-S/L:0.2)

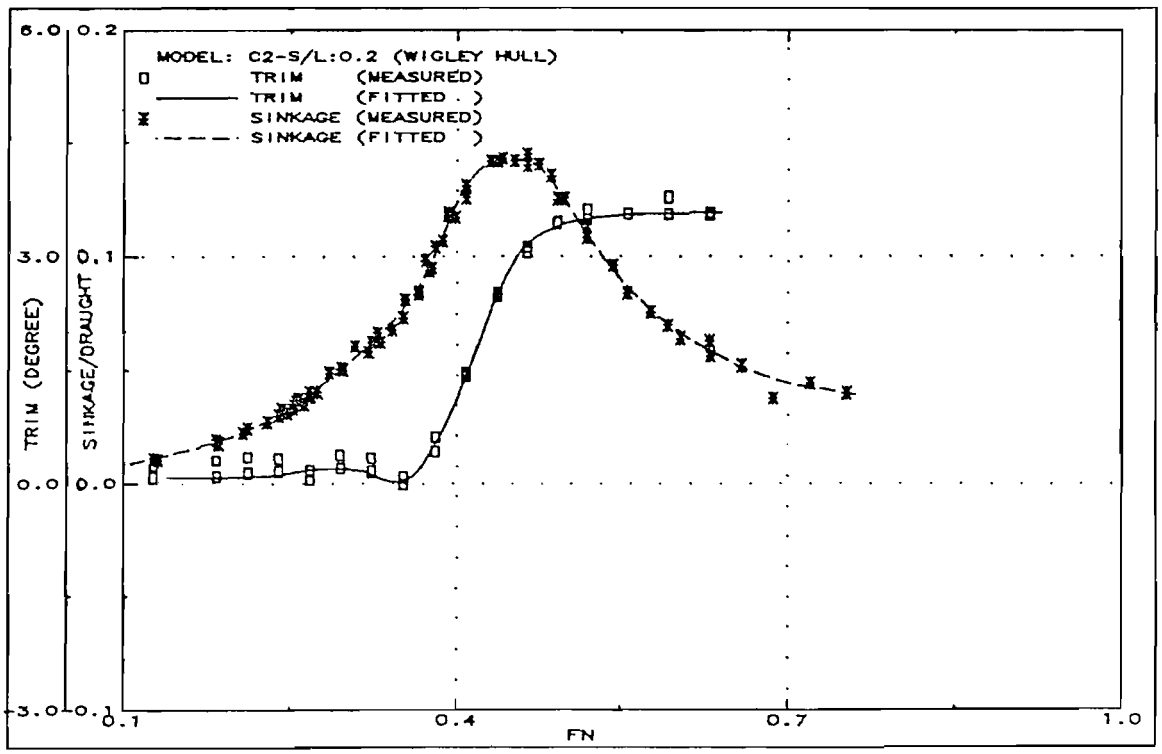

Fig.166: Running trim and sinkage (C2-S/L:0.2)

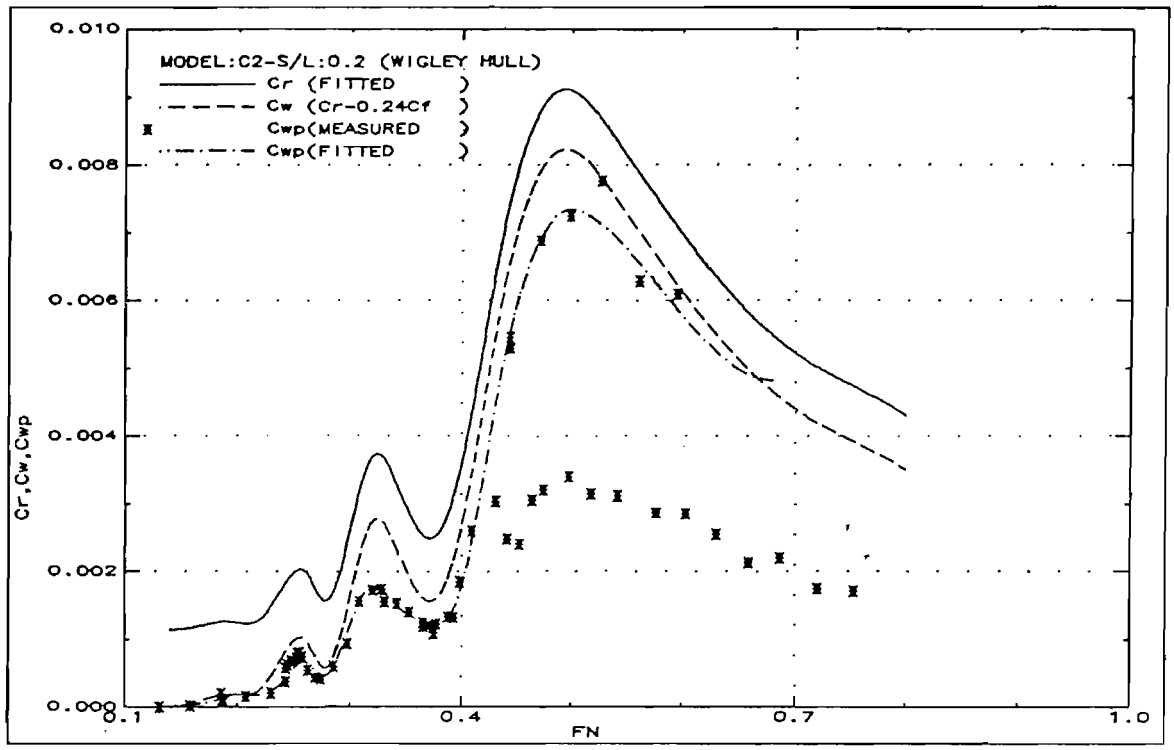

Fig.167: Measured wave resistance (C2-S/L:Ø.2)

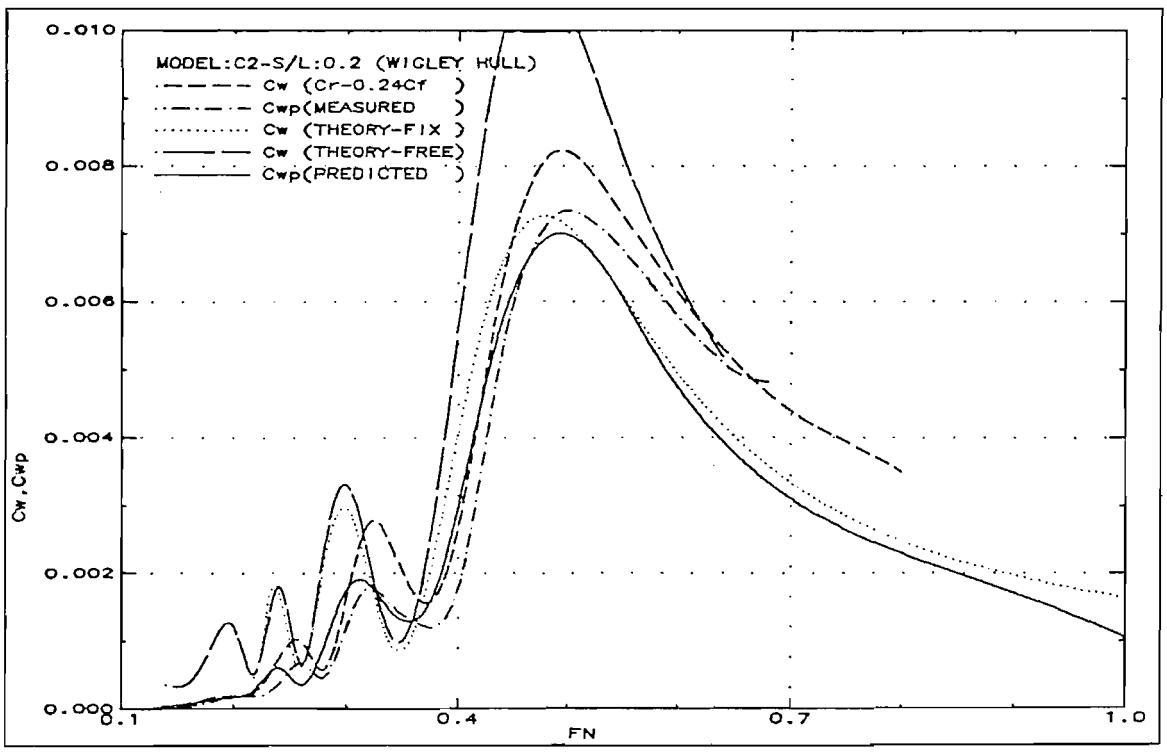

Fig.168: Wave resistance comparison (C2-S/L:Ø.2)

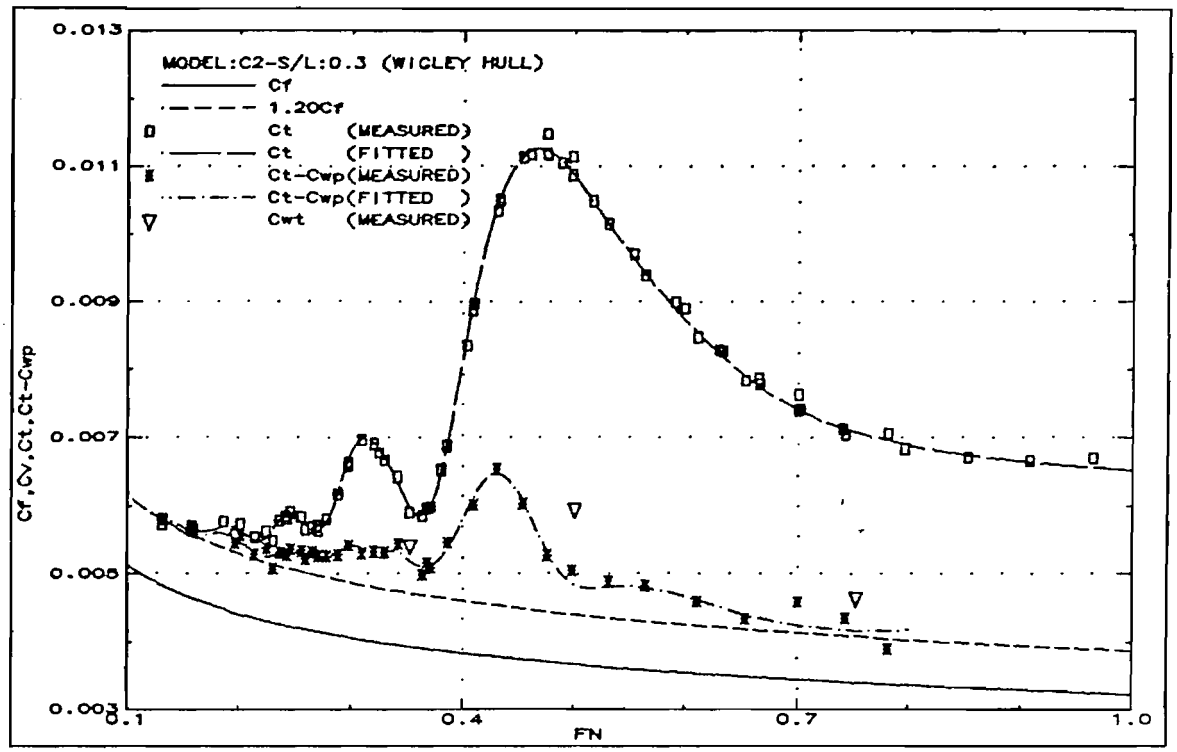

Fig.169: Resistance components (C2-S/L:0.3)

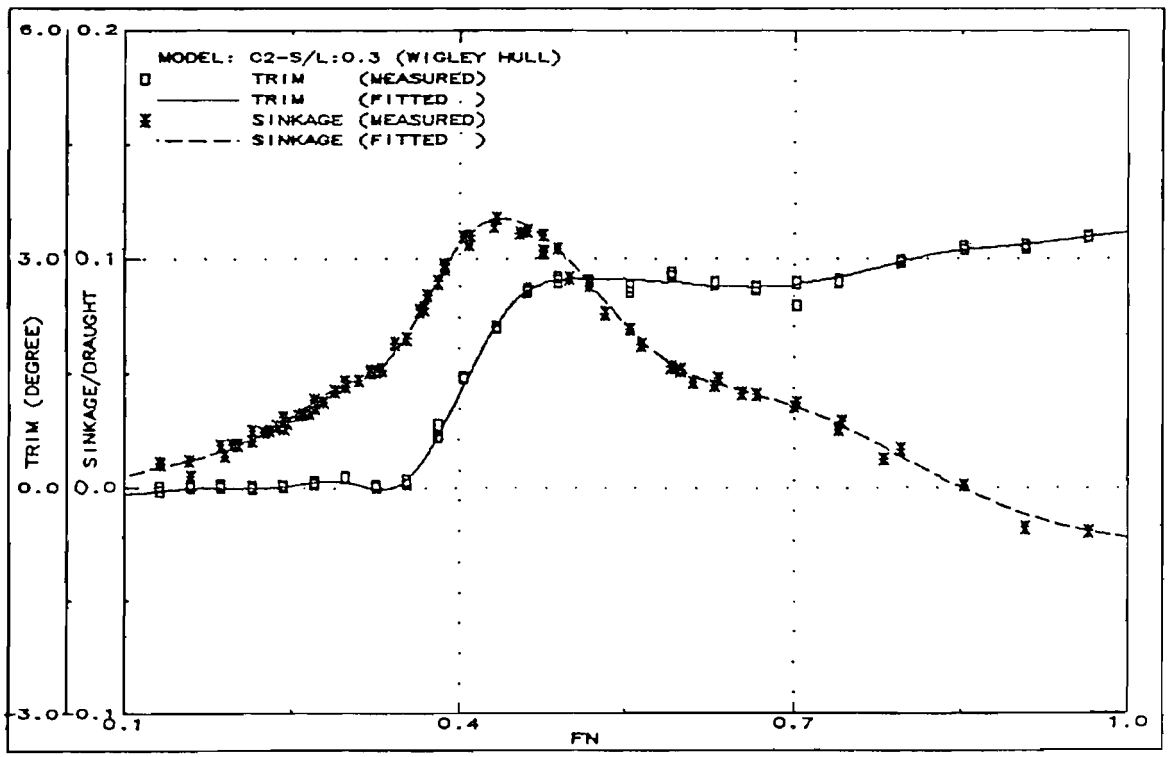

Fig.170: Running trim and sinkage (C2-S/L:0.3)

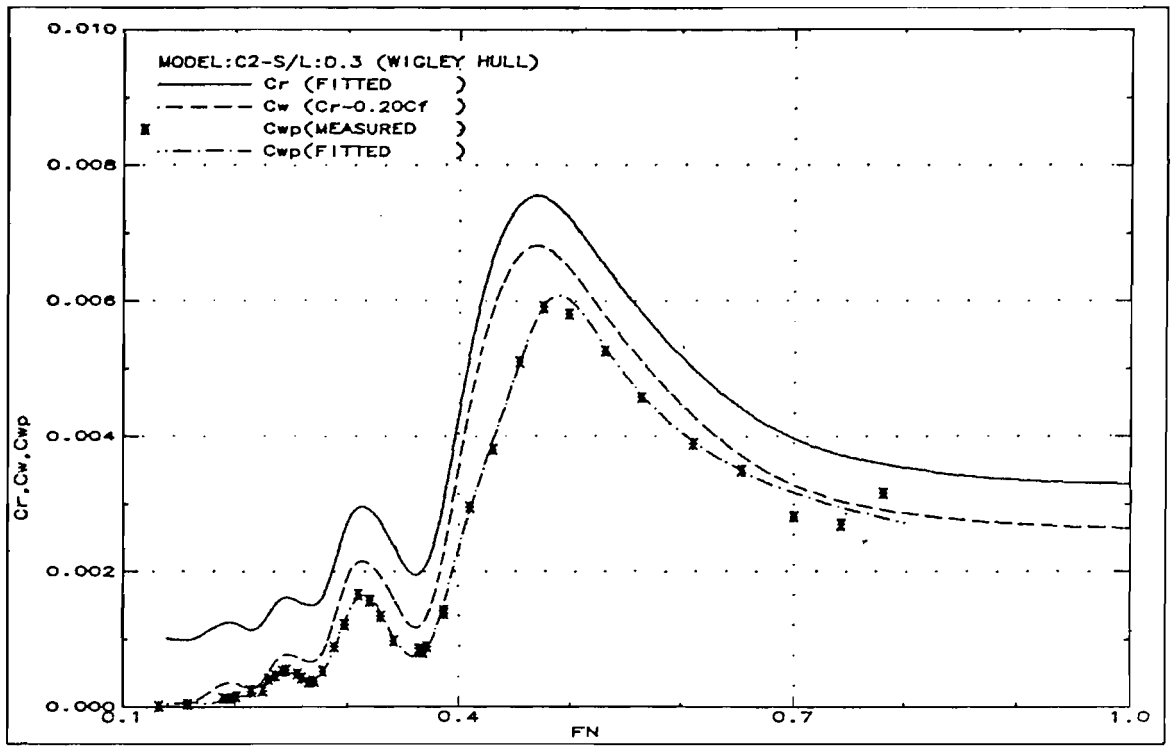

Fig.171: Measured wave resistance (C2-S/L:Ø.3)

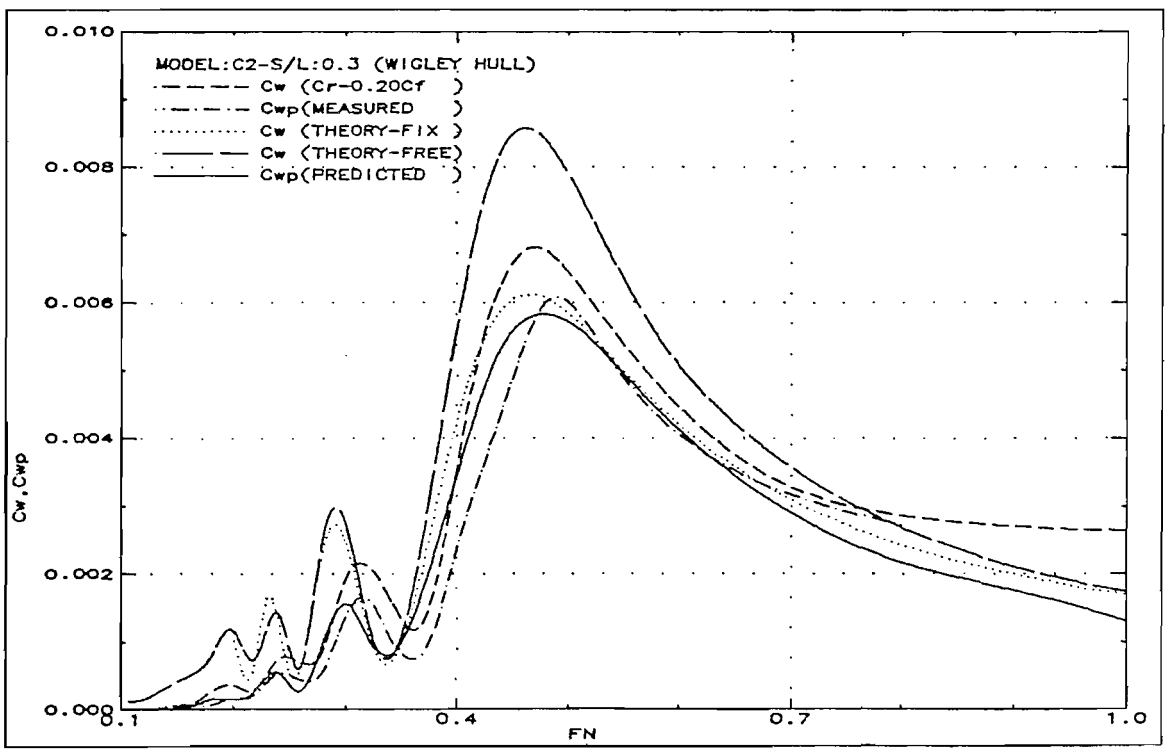

Fig.172: Wave resistance comparison (C2-S/L:Ø.3)

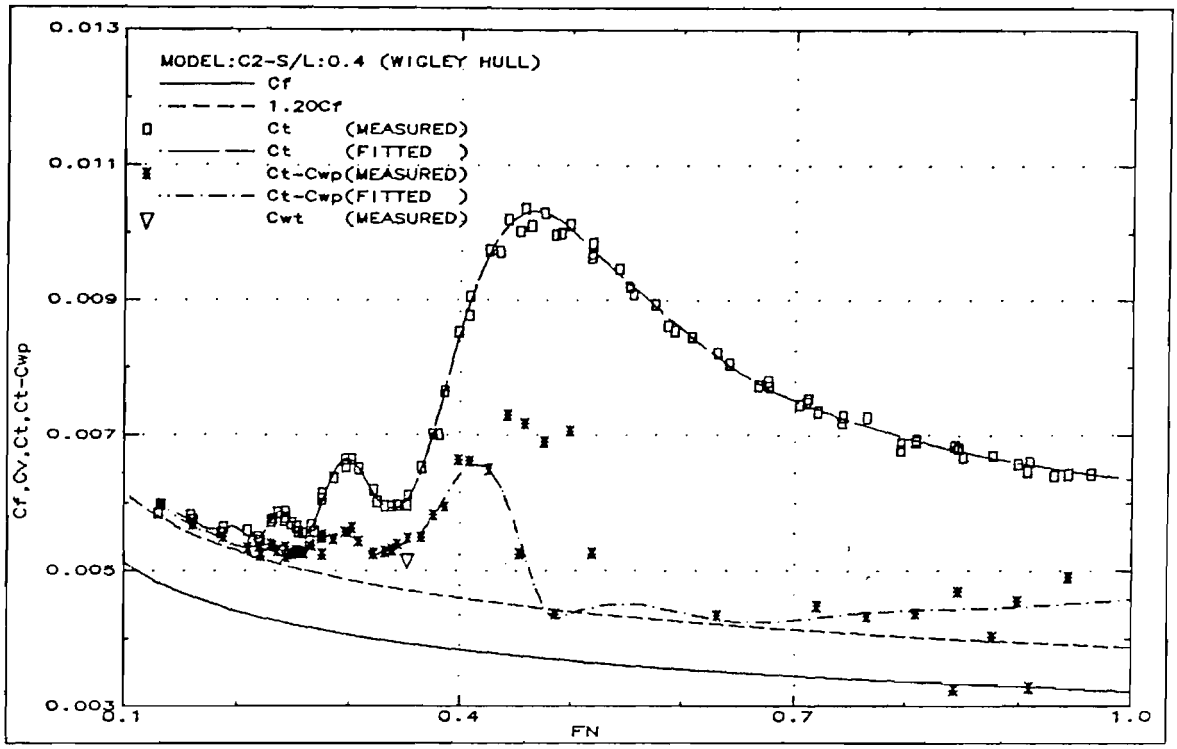

Fig.173: Resistance components (C2-S/L:0.4)

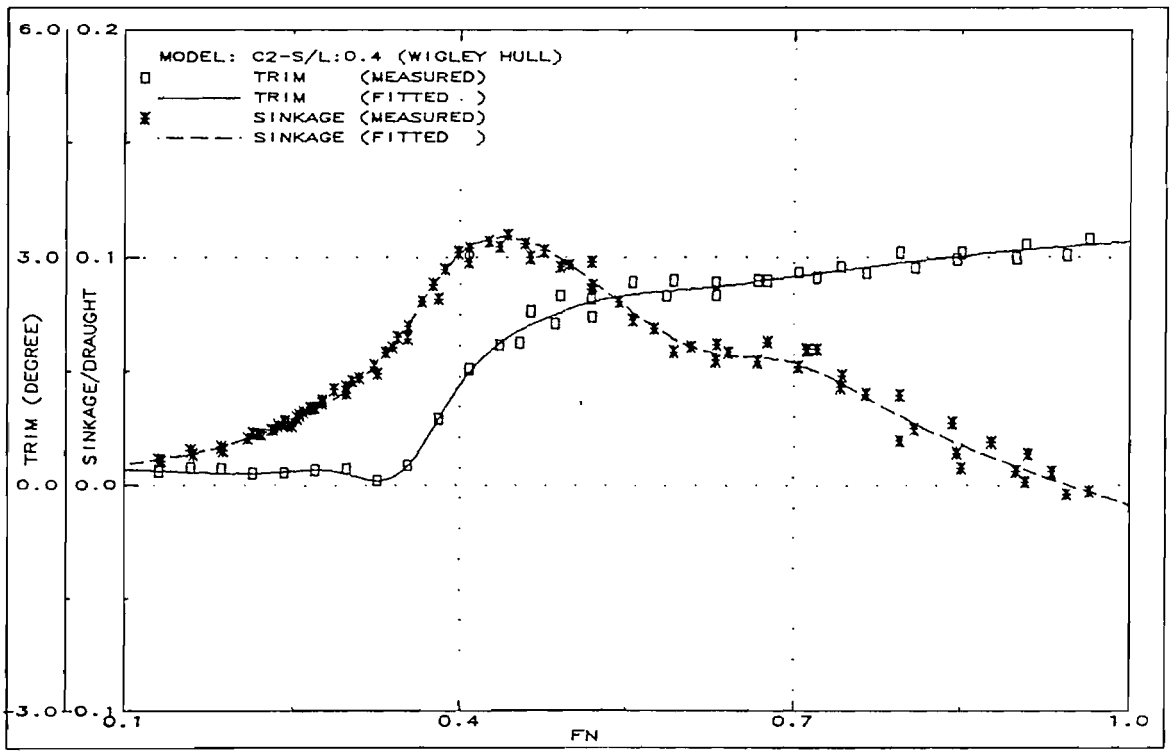

Fig.174: Running trim and sinkage (C2-S/L:0.4)

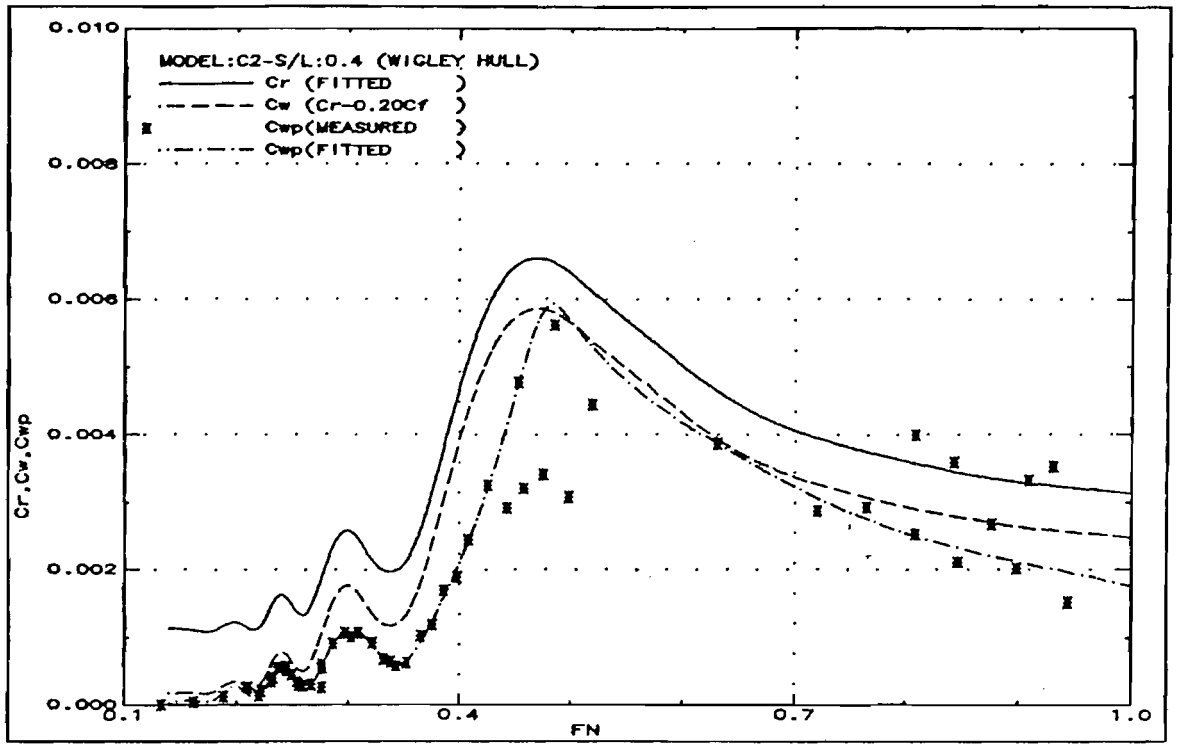

Fig.175: Measured wave resistance (C2-S/L:0.4)

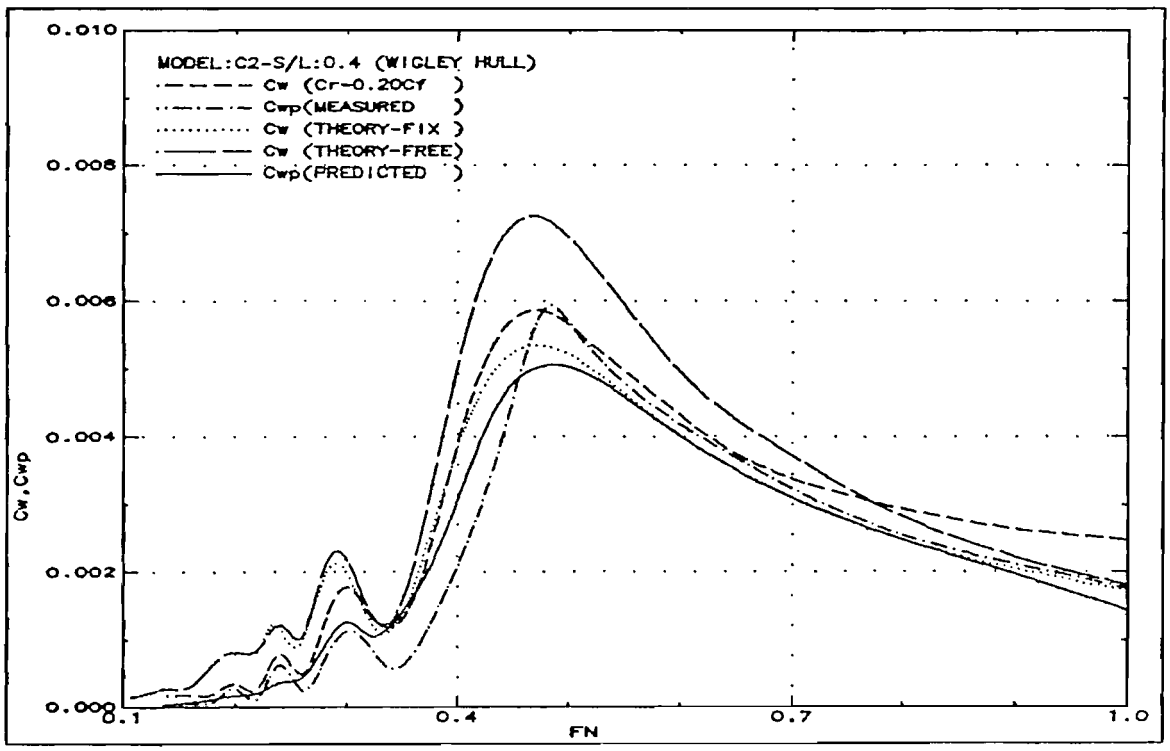

Fig.176: Wave resistance comparison (C2-S/L:0.4)

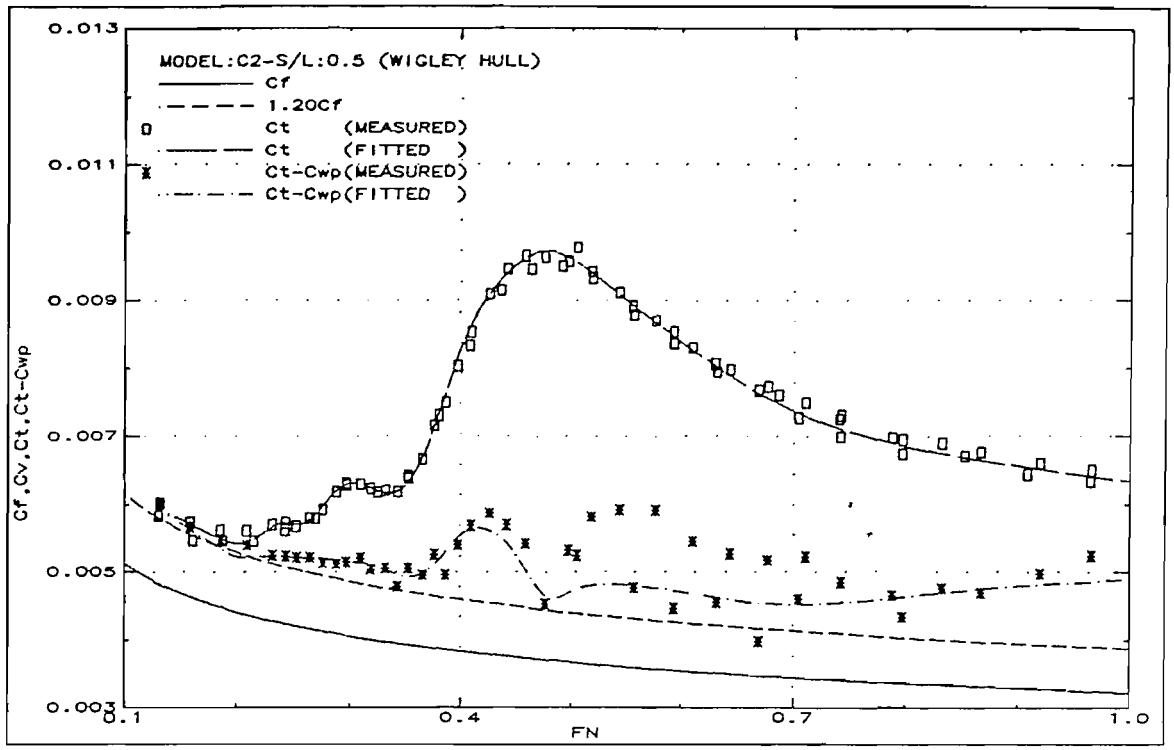

Fig.177: Resistance components (C2-S/L:0.5)

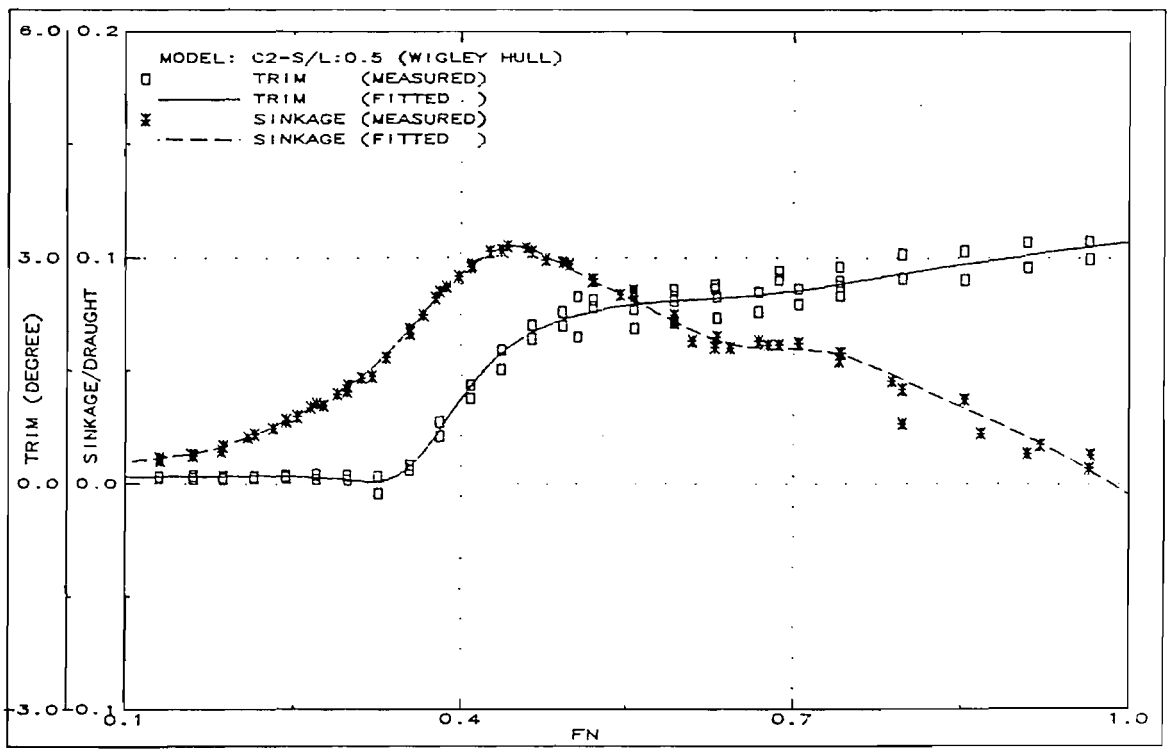

Fig.178: Running trim and sinkage (C2-S/L:0.5)

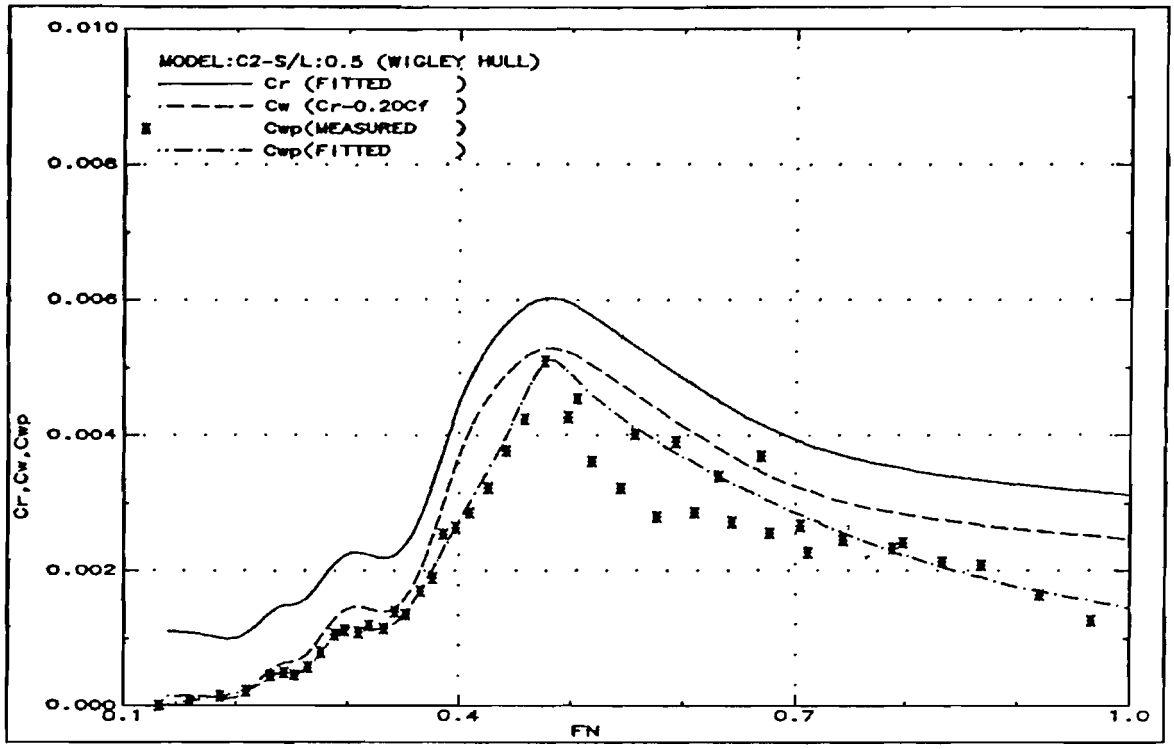

Fig.179: Measured wave resistance (C2-S/L:0.5)

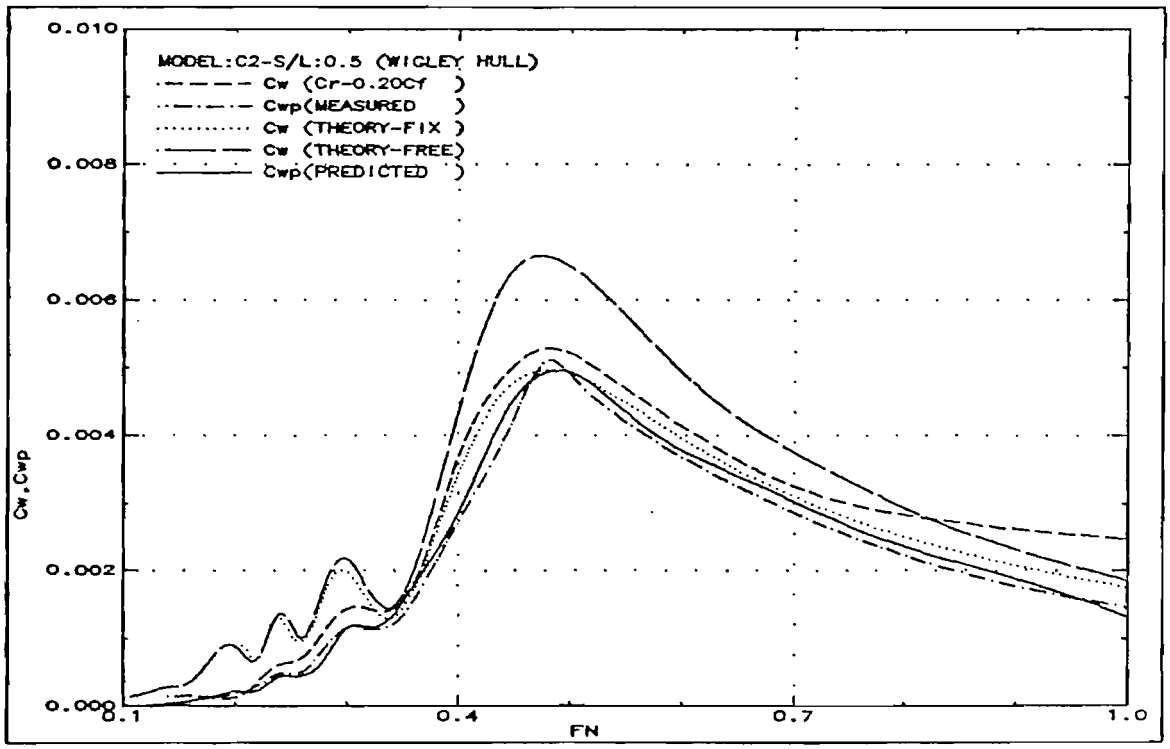

Fig.180: Wave resistance comparison (C2-S/L:0.5)

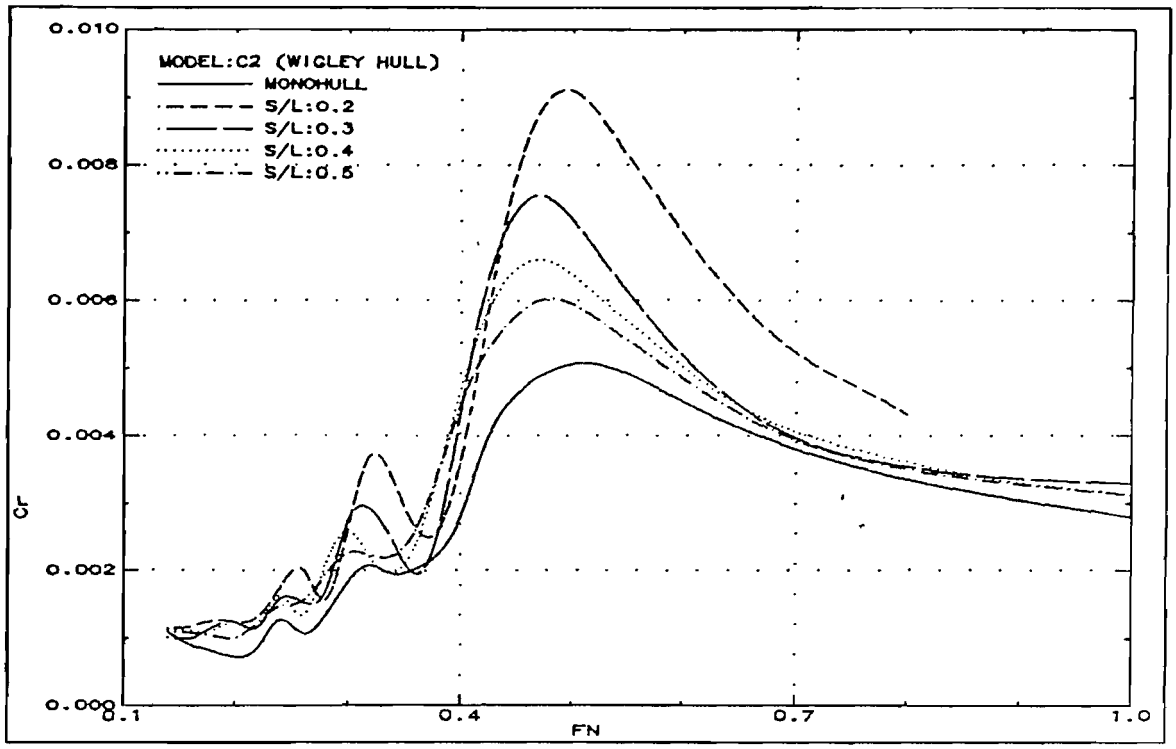

Fig.181: Residuary resistance (C2)

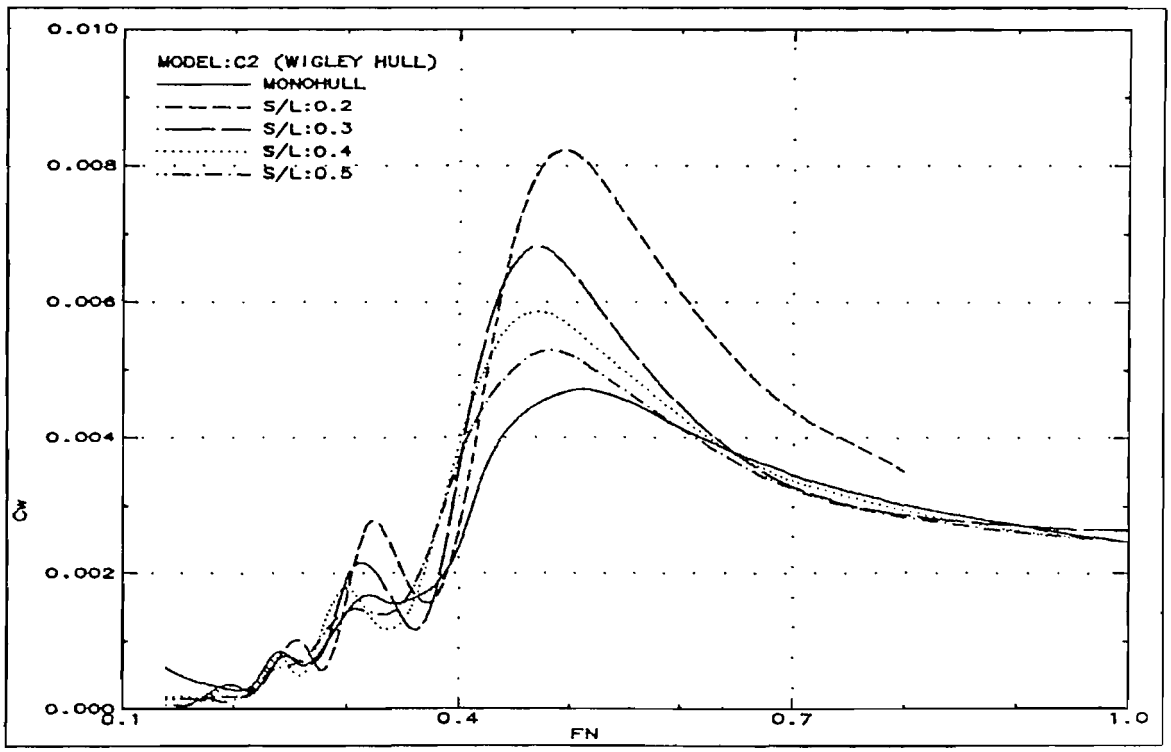

Fig.182: Wave resistance (C2)

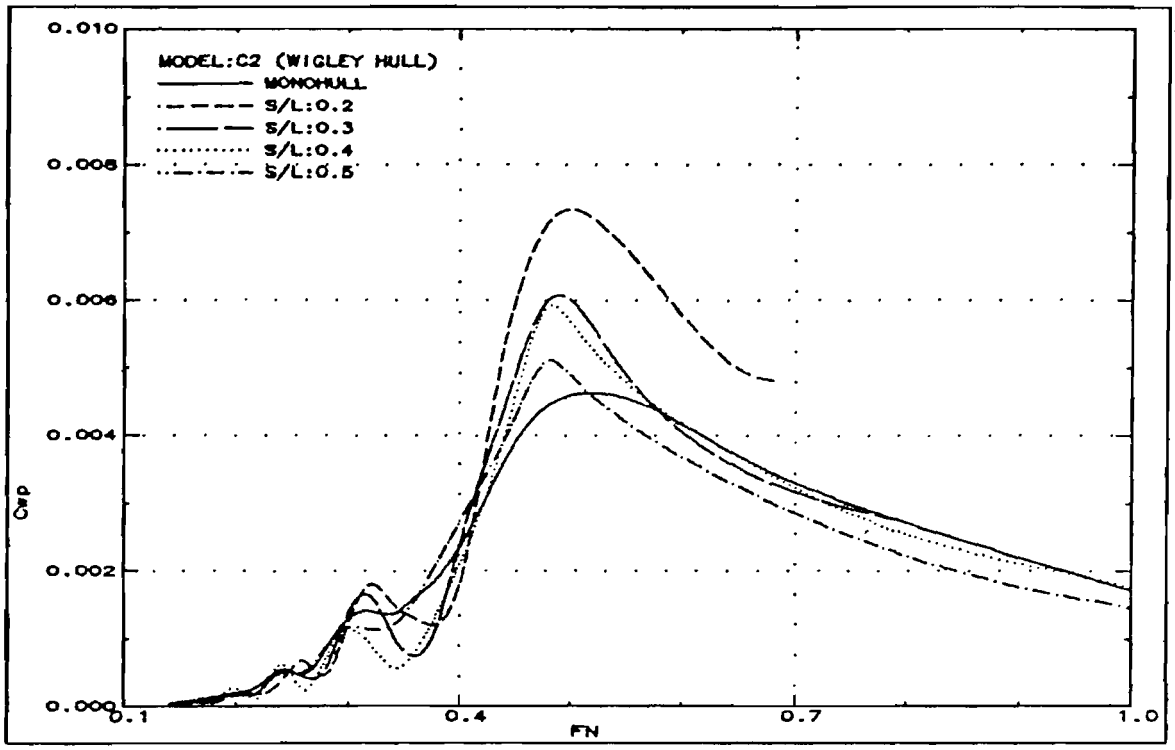

Fig.183: Wave pattern resistance (C2)

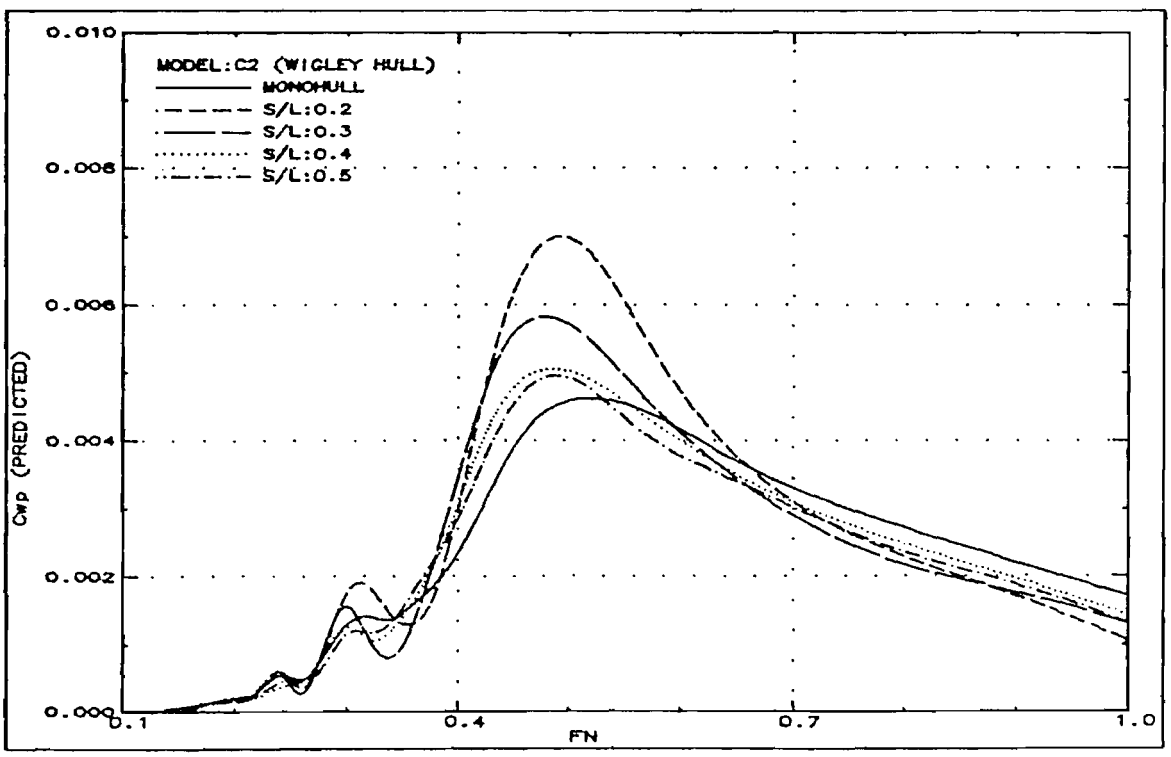

Fig.184: Wave pattern resistance predicted from monohull wave pattern analysis (C2)

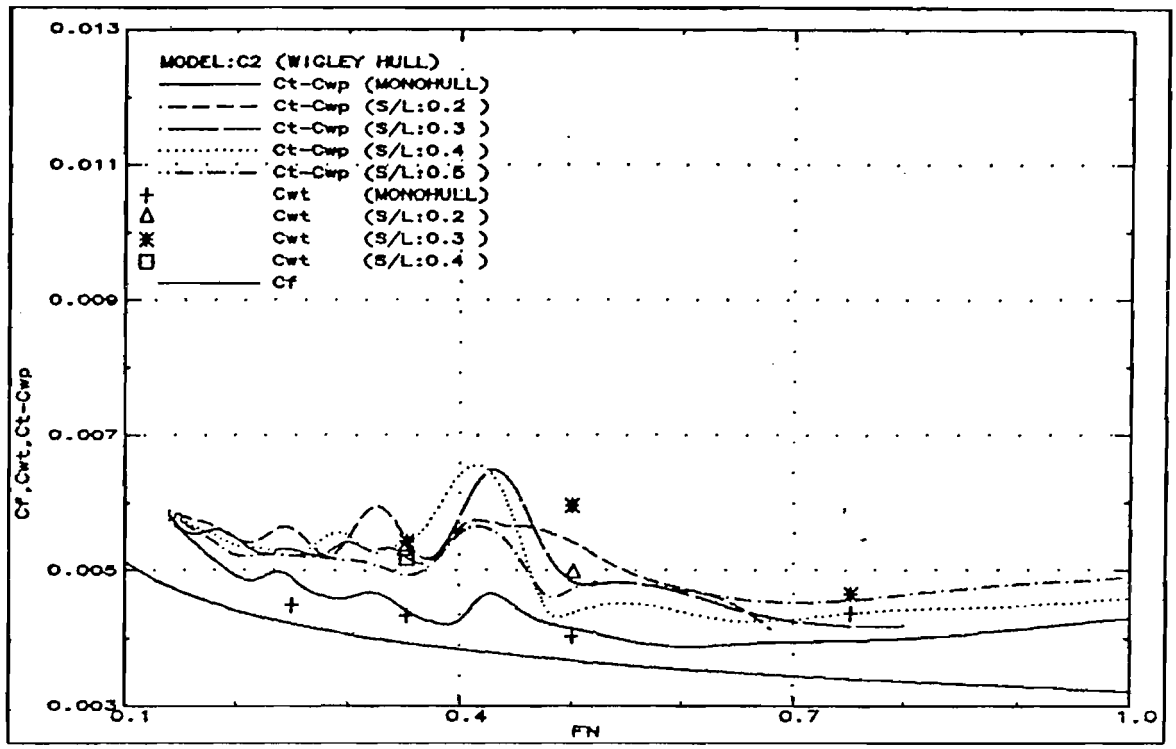

Fig.185: Total resistance minus wave pattern resistance (C2)

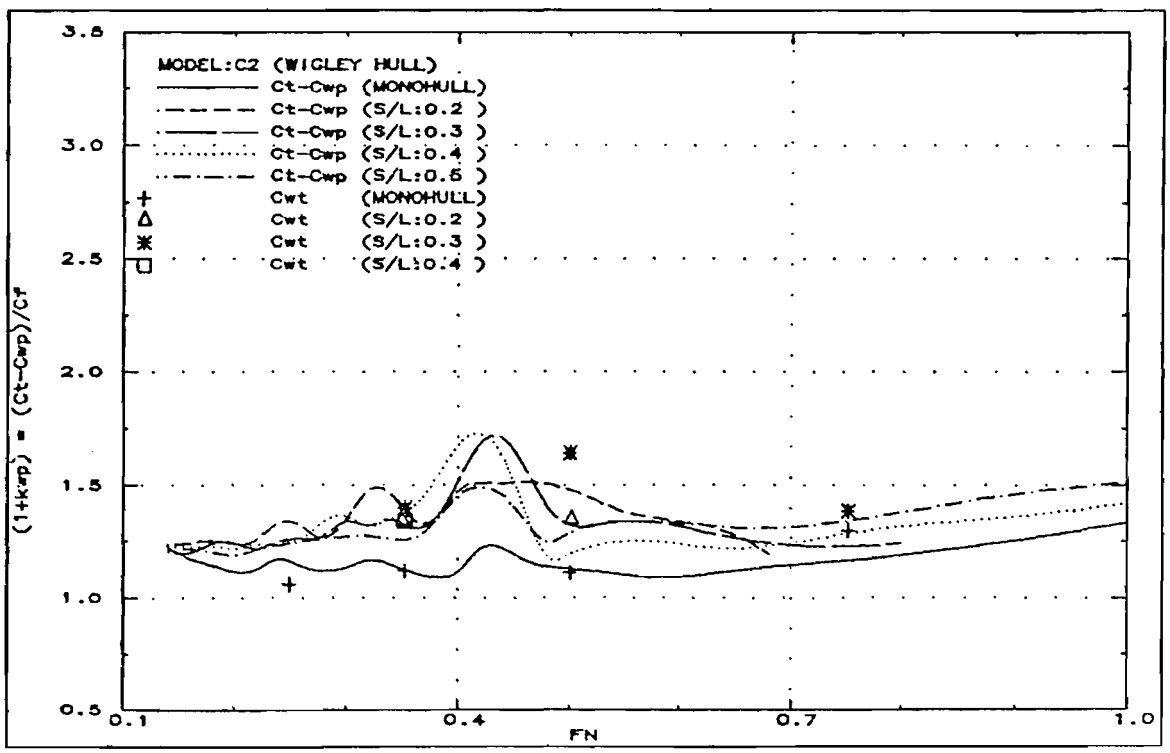

Fig.186: Form factor, i.e. $1+k_{WP}=(C_T-C_{WP})/C_F$ (C2)

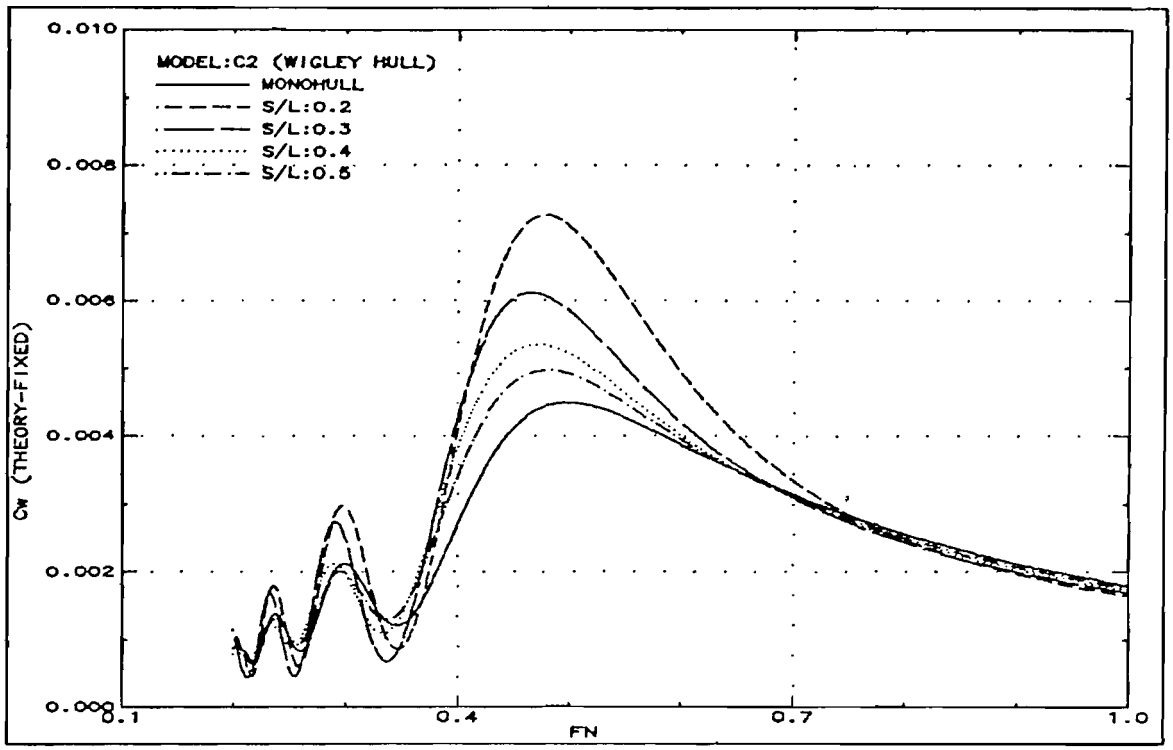

Fig.187: Theoretical wave resistance in fixed condition (C2)

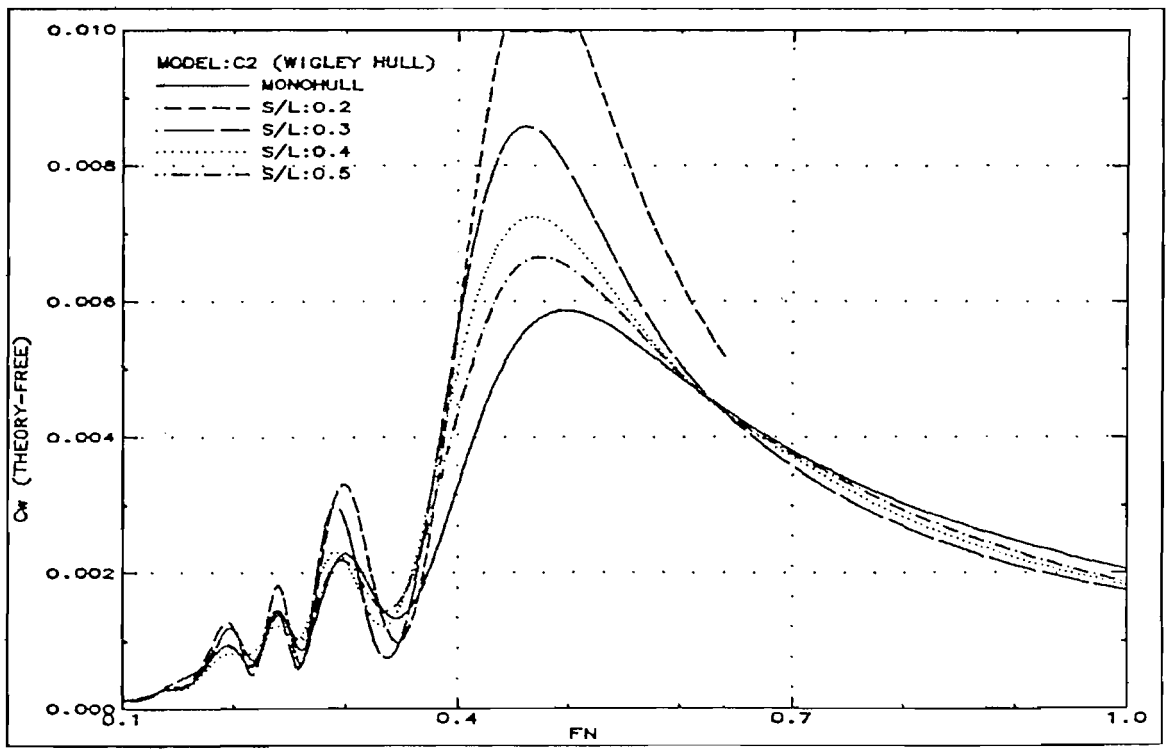

Fig.188: Theoretical wave resistance in free condition (C2)

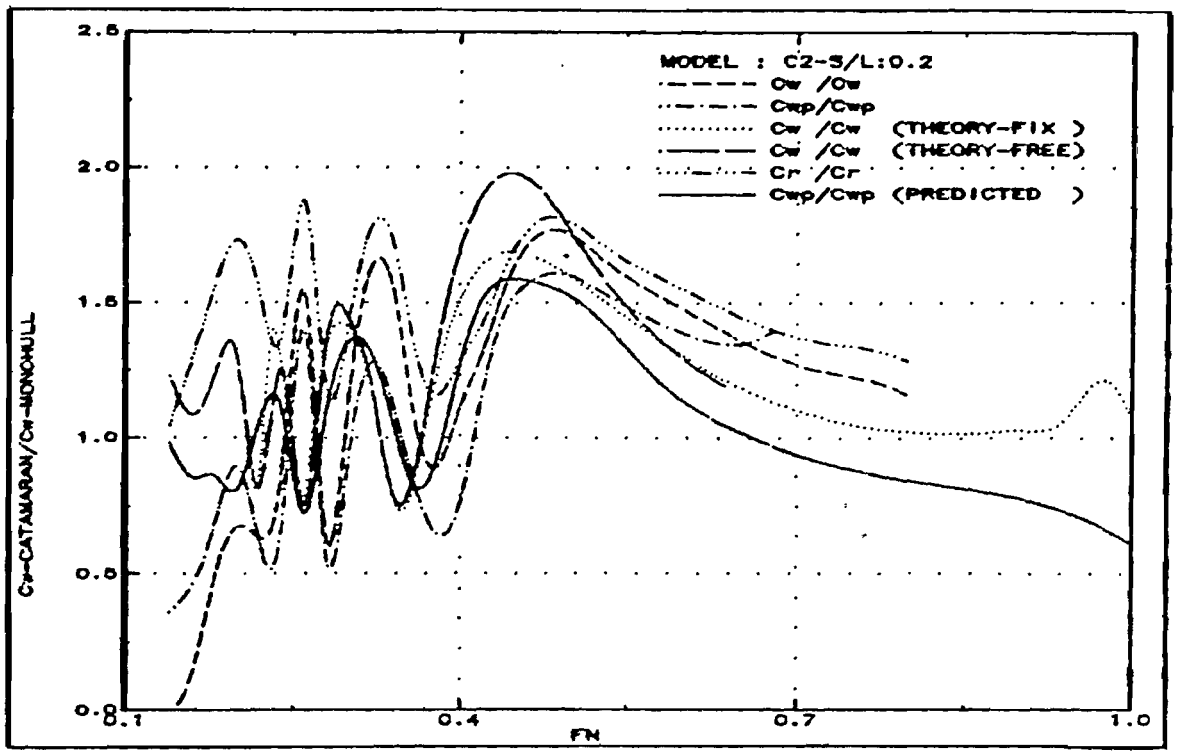

Fig.189: Wave resistance interference ratio (C2-S/L:0.2)

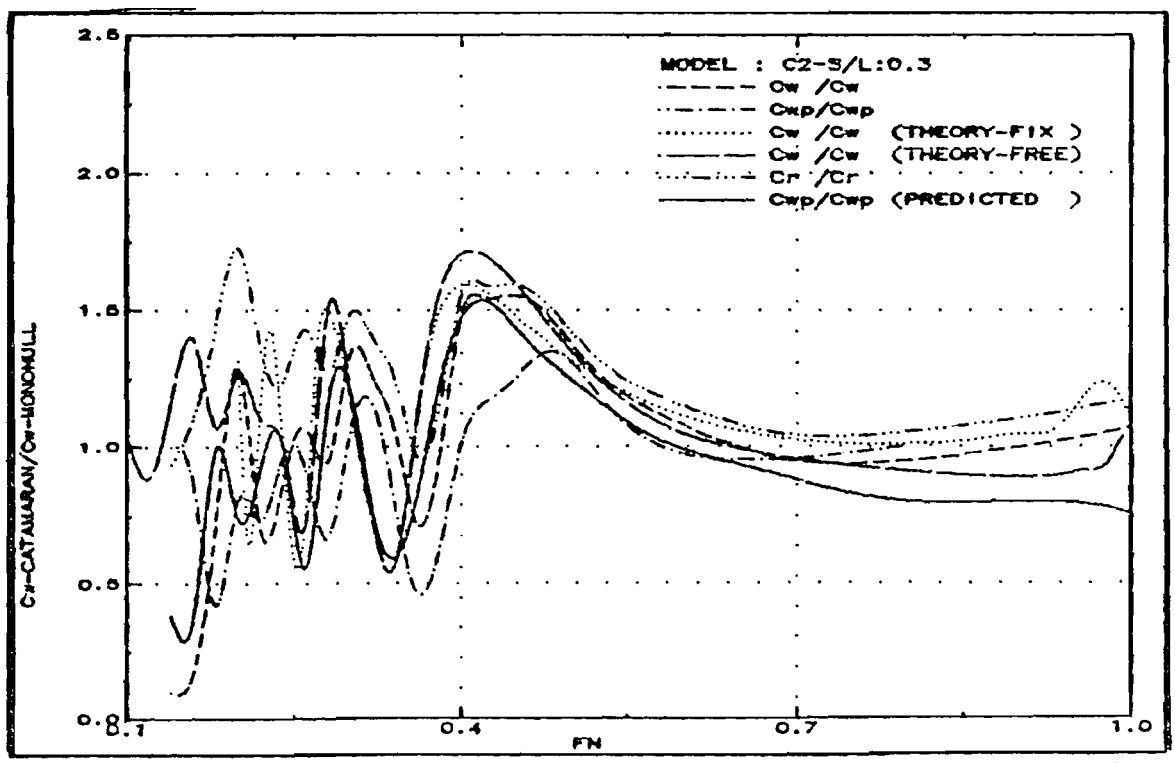

Fig.190: Wave resistance interference ratio (C2-S/L:0.3)

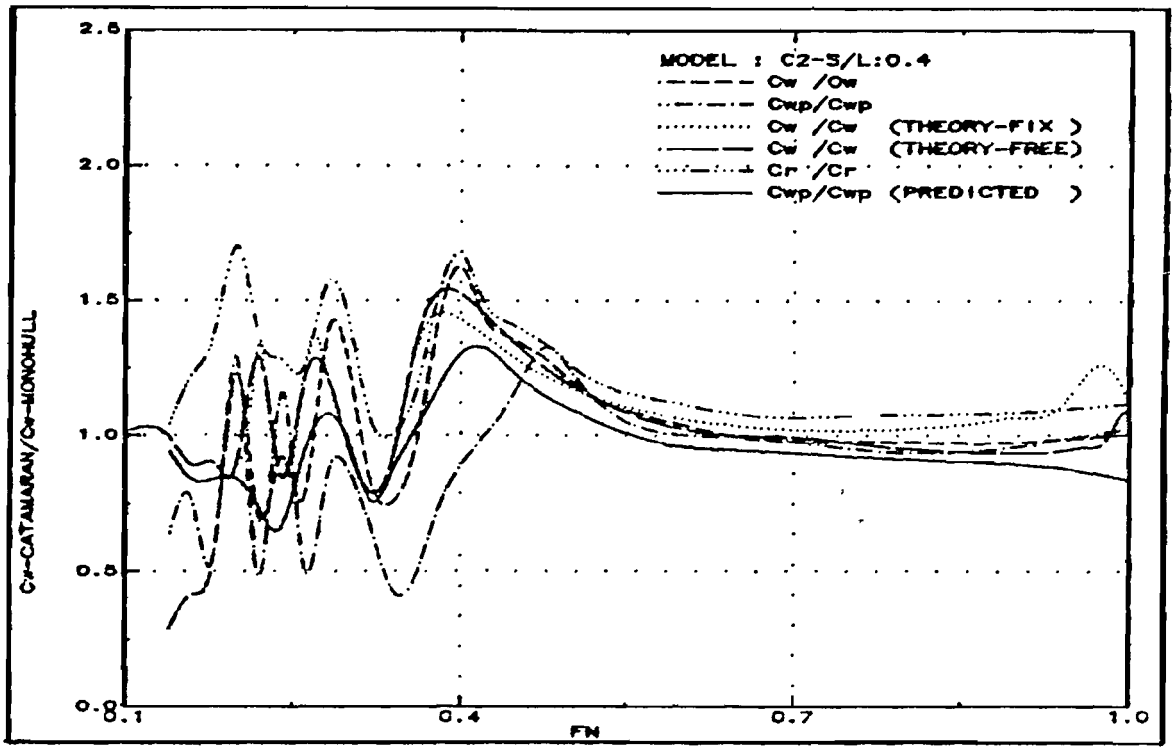

Fig.191: Wave resistance interference ratio (C2-S/L:Ø.4)

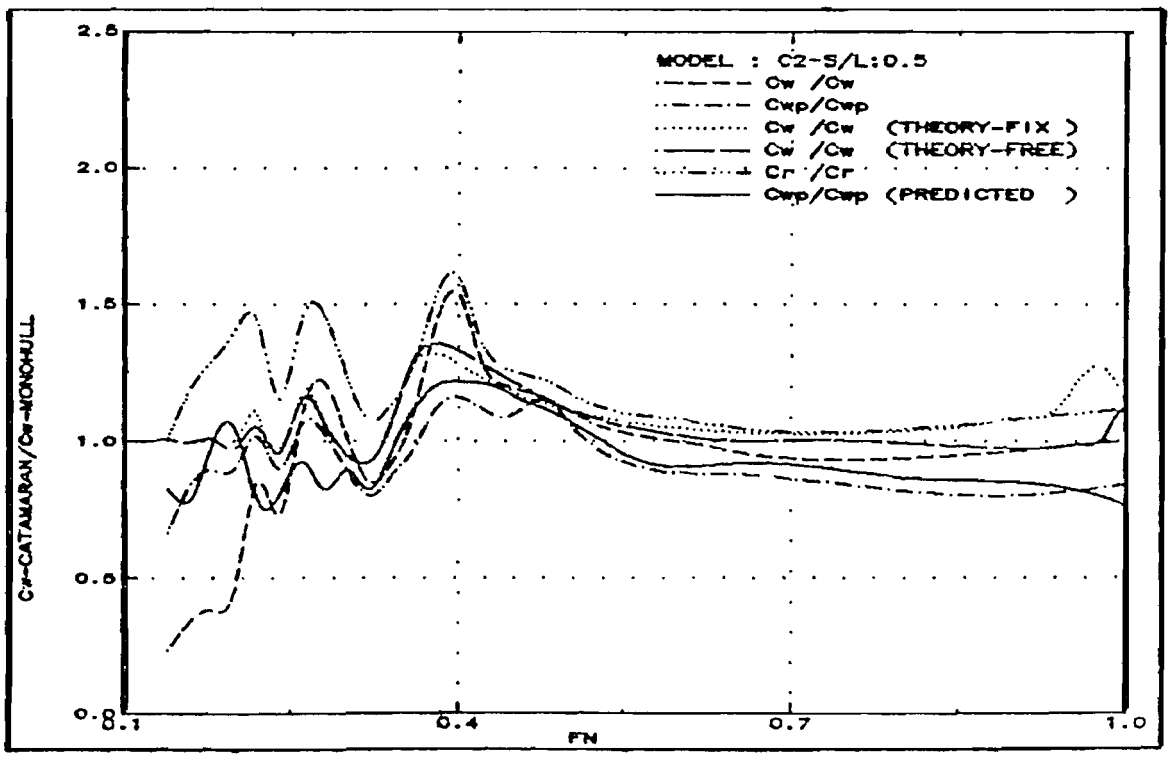

Fig.192: Wave resistance interference ratio (C2-S/L:Ø.5)

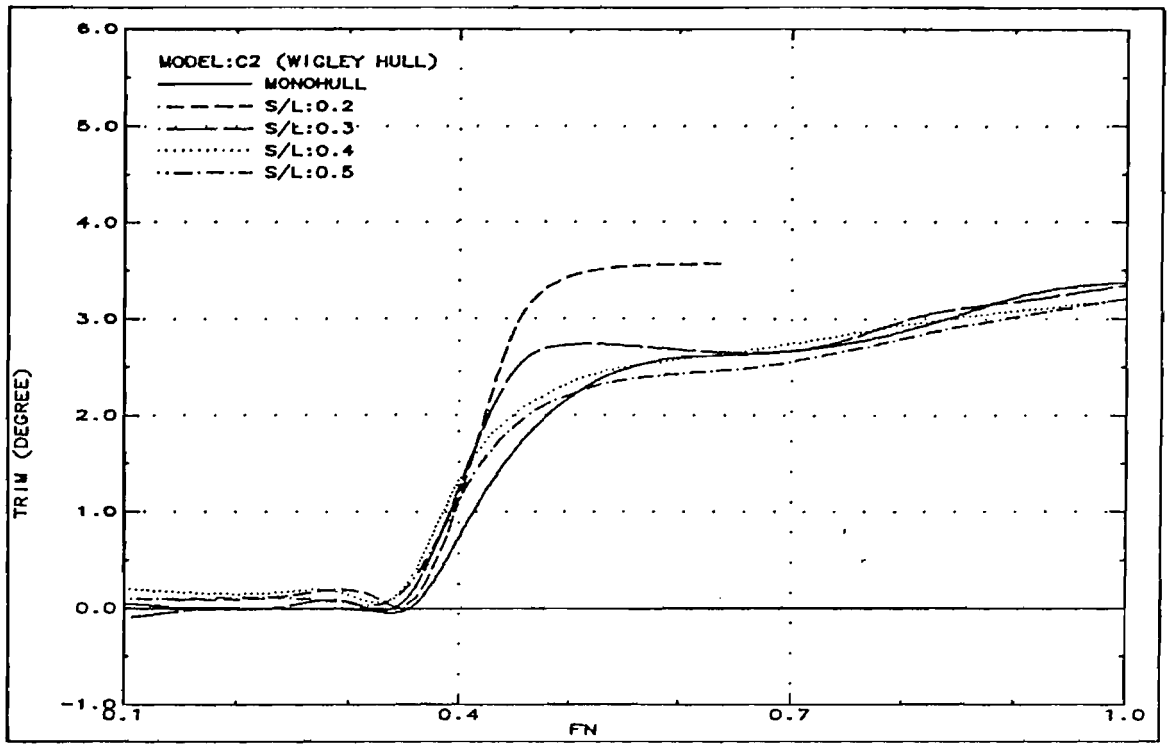

Fig.193: Running trim (C2)

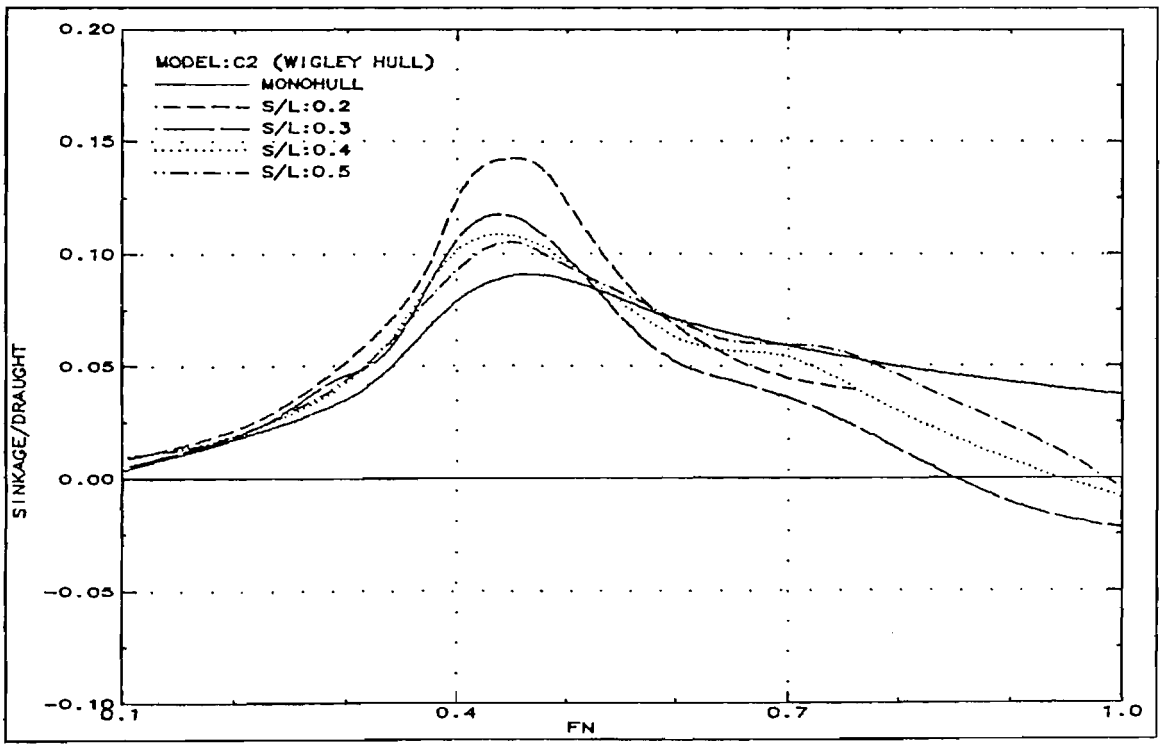

Fig.194: Sinkage (C2)

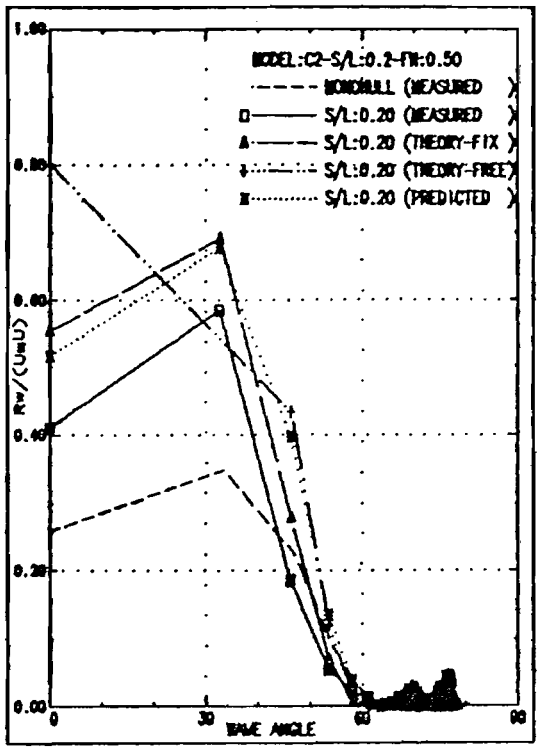

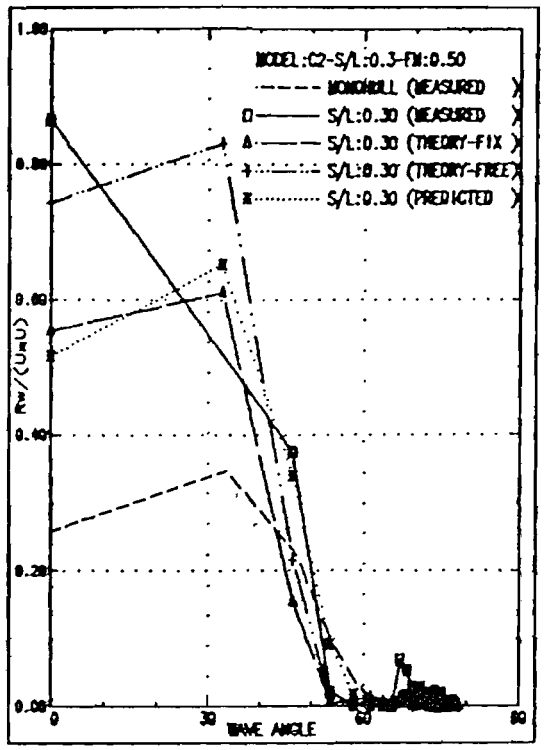

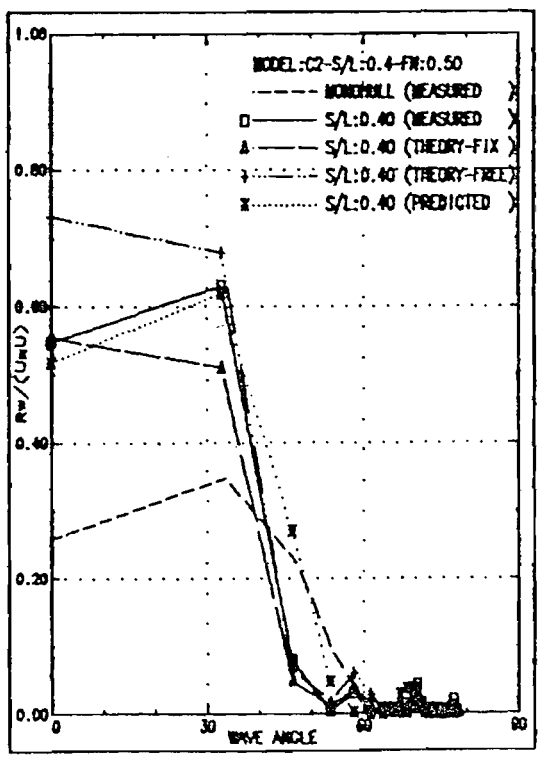

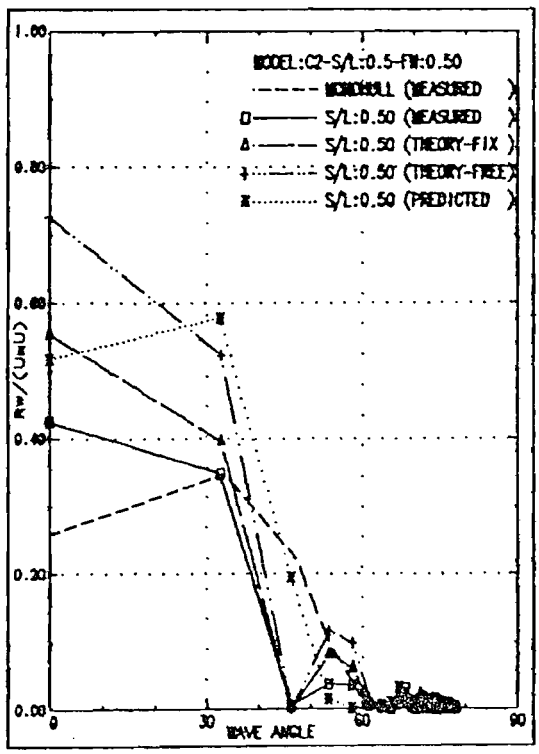

Fig.195: Wave resistance distribution across the wave spectrum at Fn:0.50 (C2)

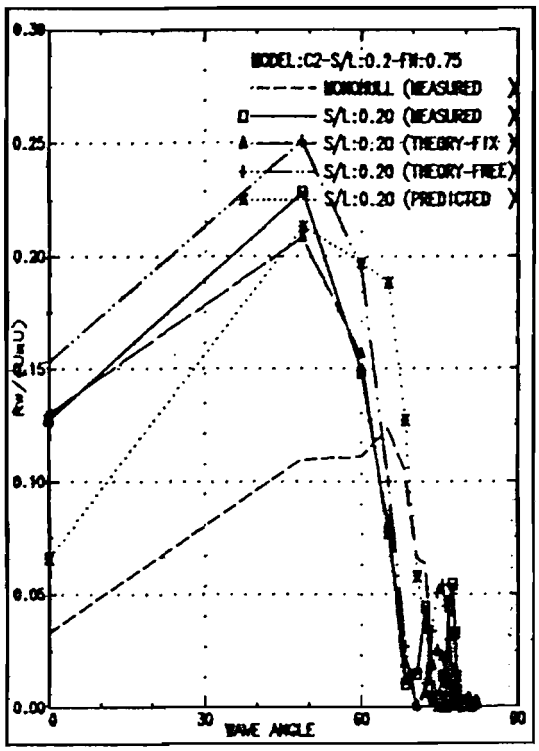

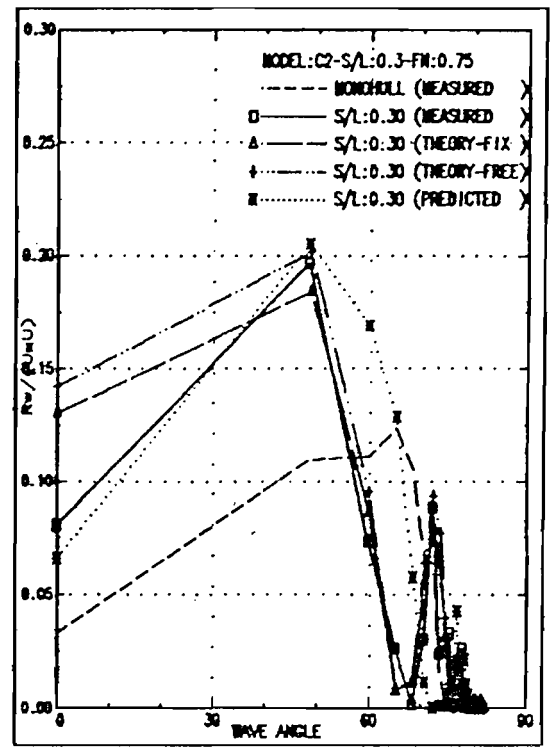

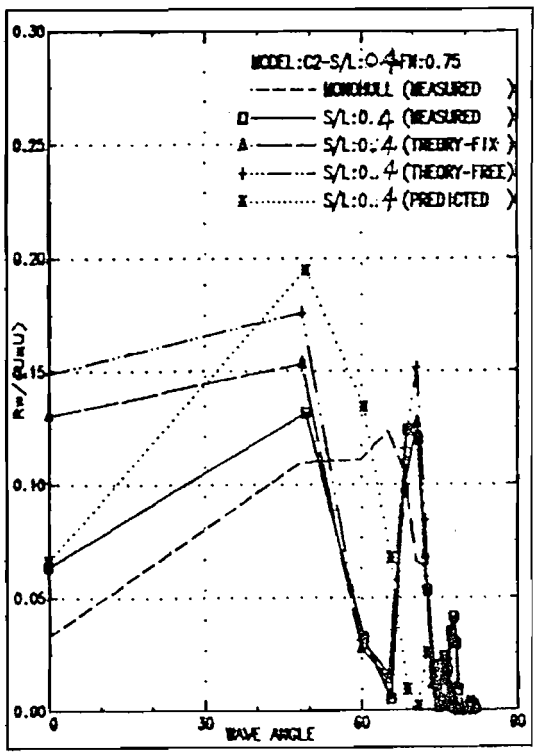

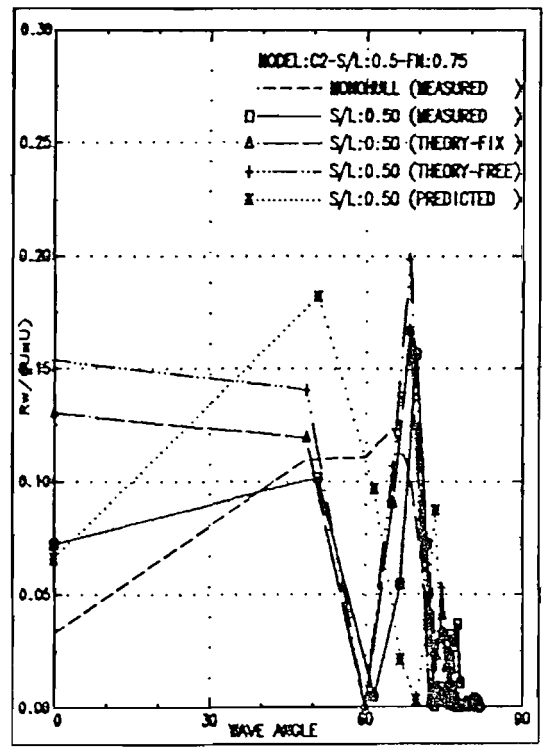

Fig.196: Wave resistance distribution across the wave spectrum at Fn:0.75 (C2-Fixed)

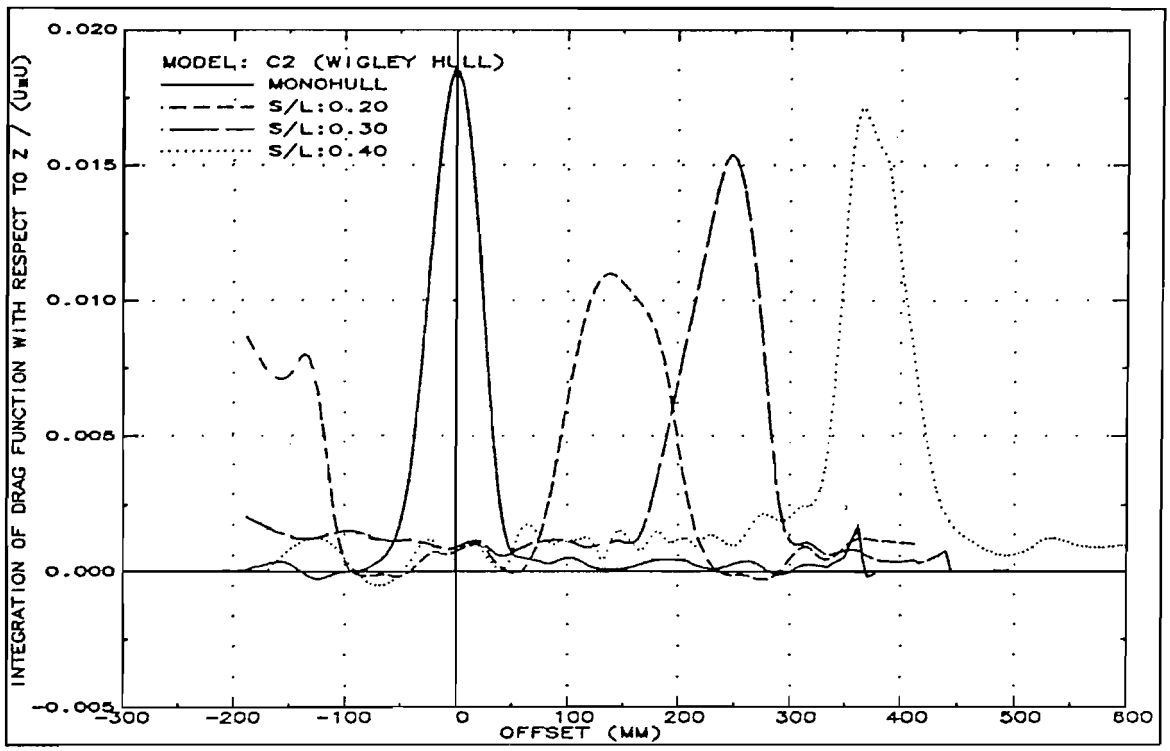

Fig.197: Integration of drag function with respect to z (C2-Fn:Ø.35)

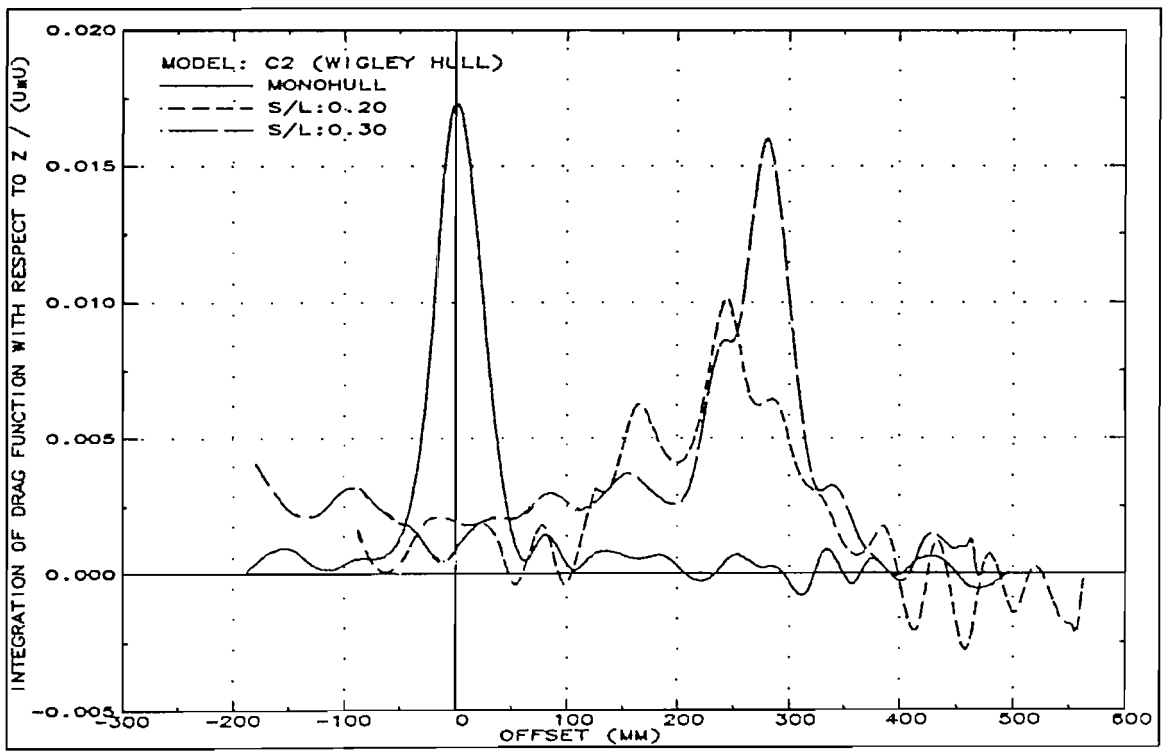

Fig.198: Integration of drag function with respect to z (C2-Fn:Ø.5Ø)

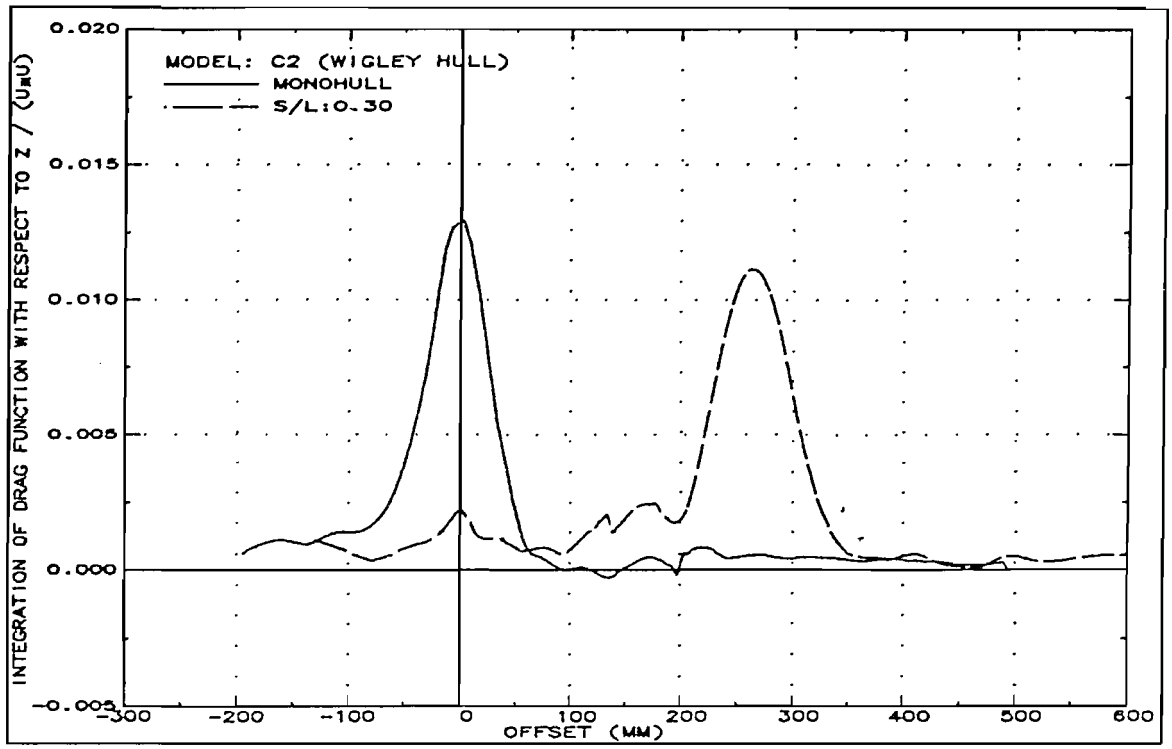

Fig.199: Integration of drag function with respect to z (C2-Fn:0.75)

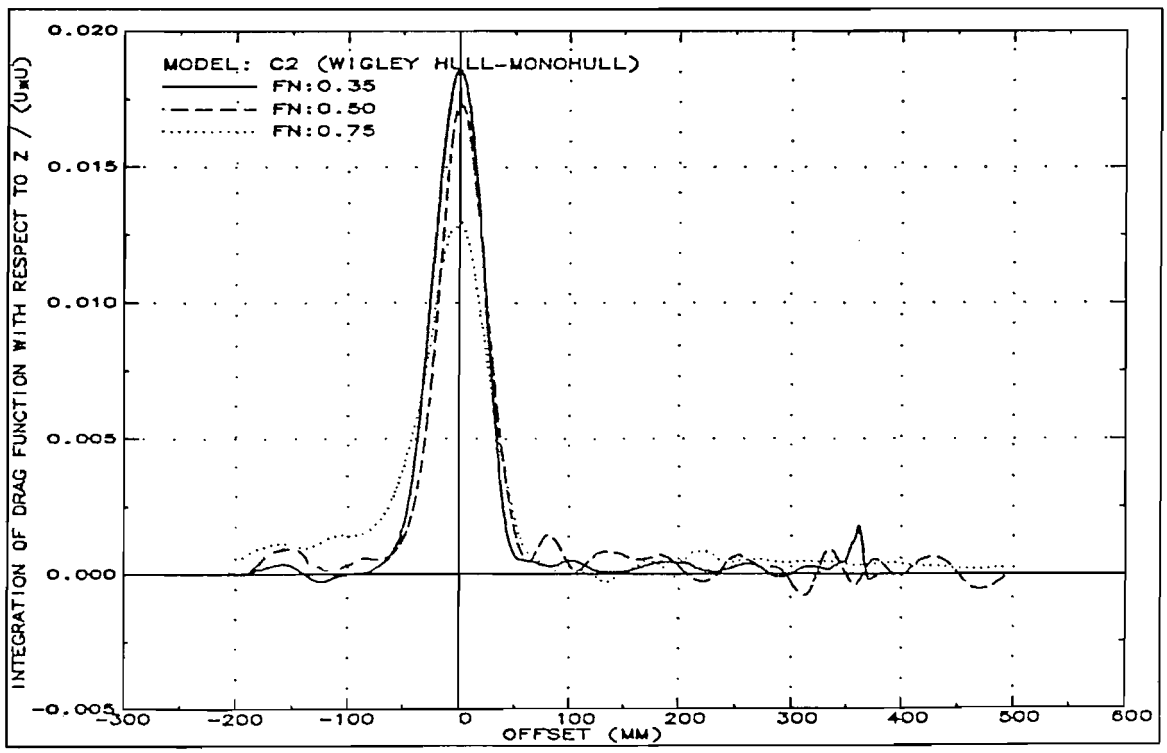

Fig.200: Integration of drag function with respect to z (C2-Monohull)

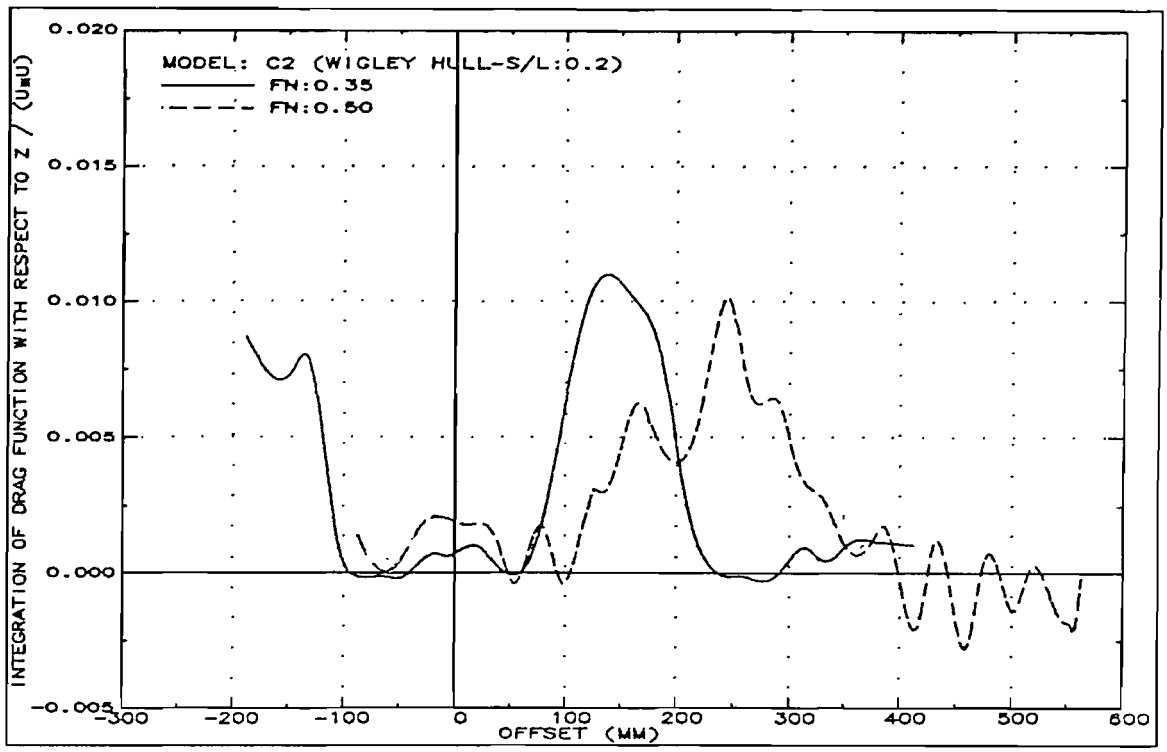

Fig.201: Integration of drag function with respect to z (C2-S/L:0.2)

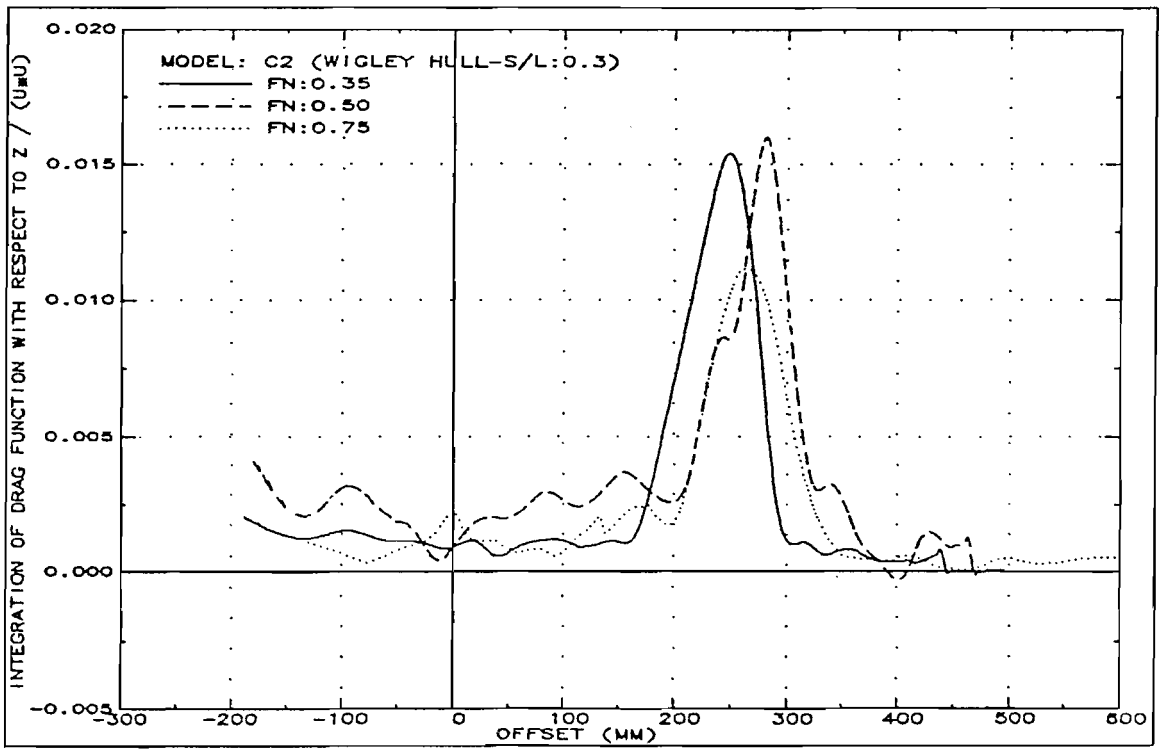

Fig.202: Integration of drag function with respect to z (C2-S/L:0.3)

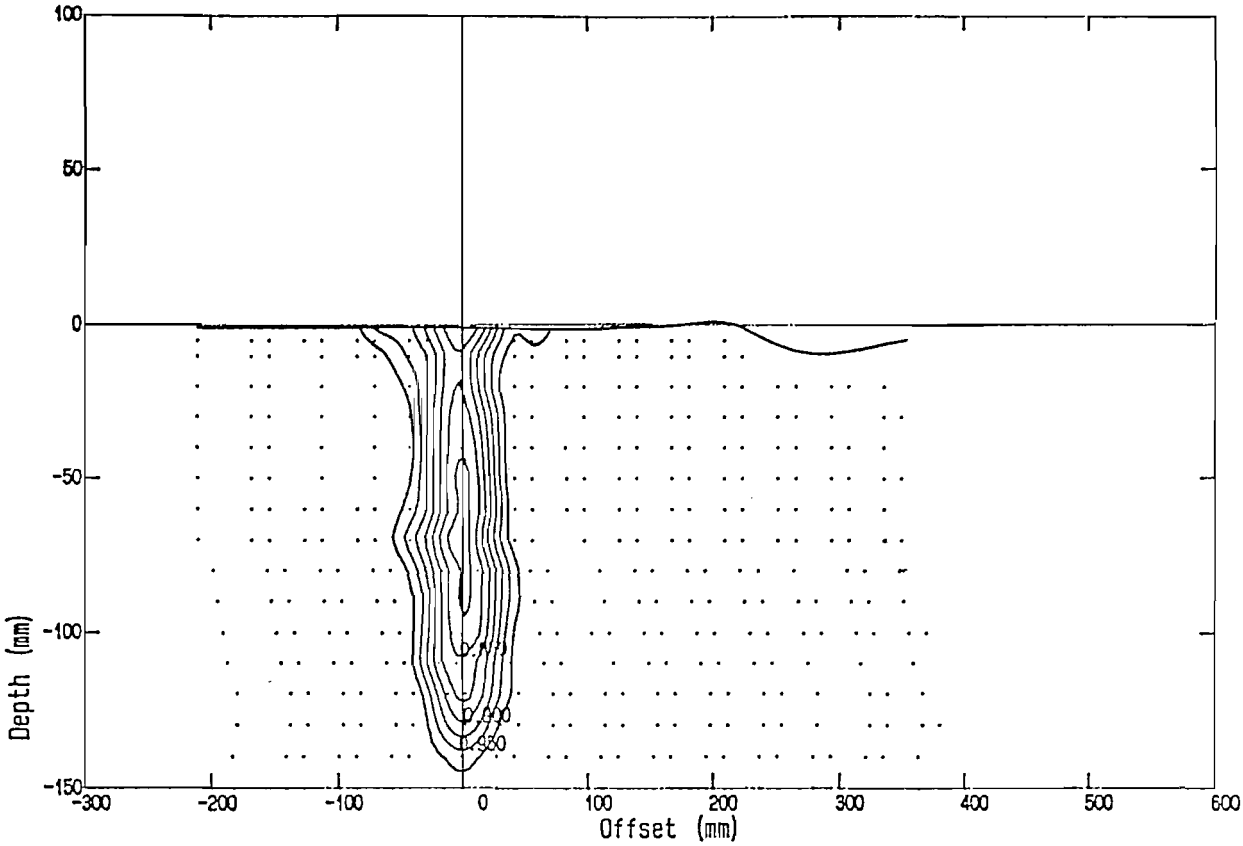

Fig.203: Wake contours at Fn:0.35 (C2-Monohull)

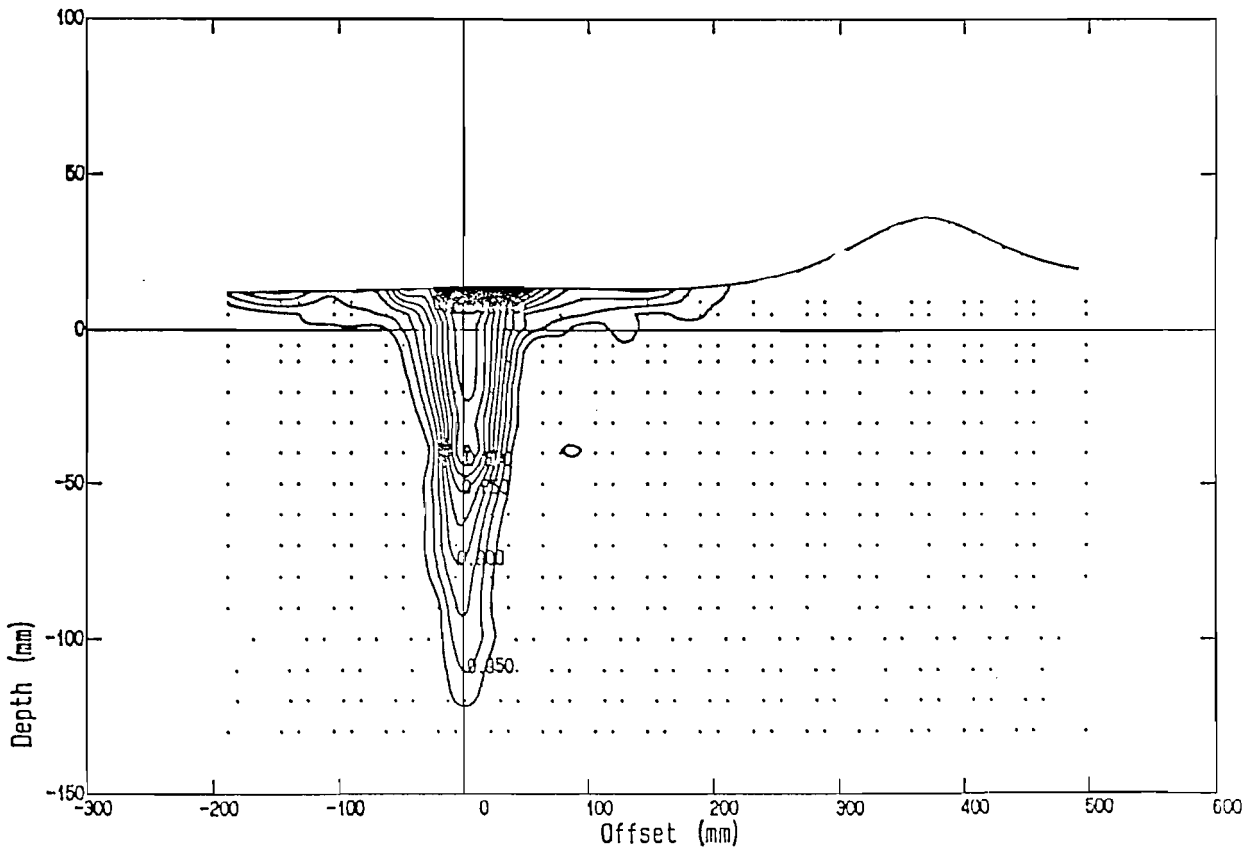

Fig.204: Wake contours at Fn:0.50 (C2-Monohull)

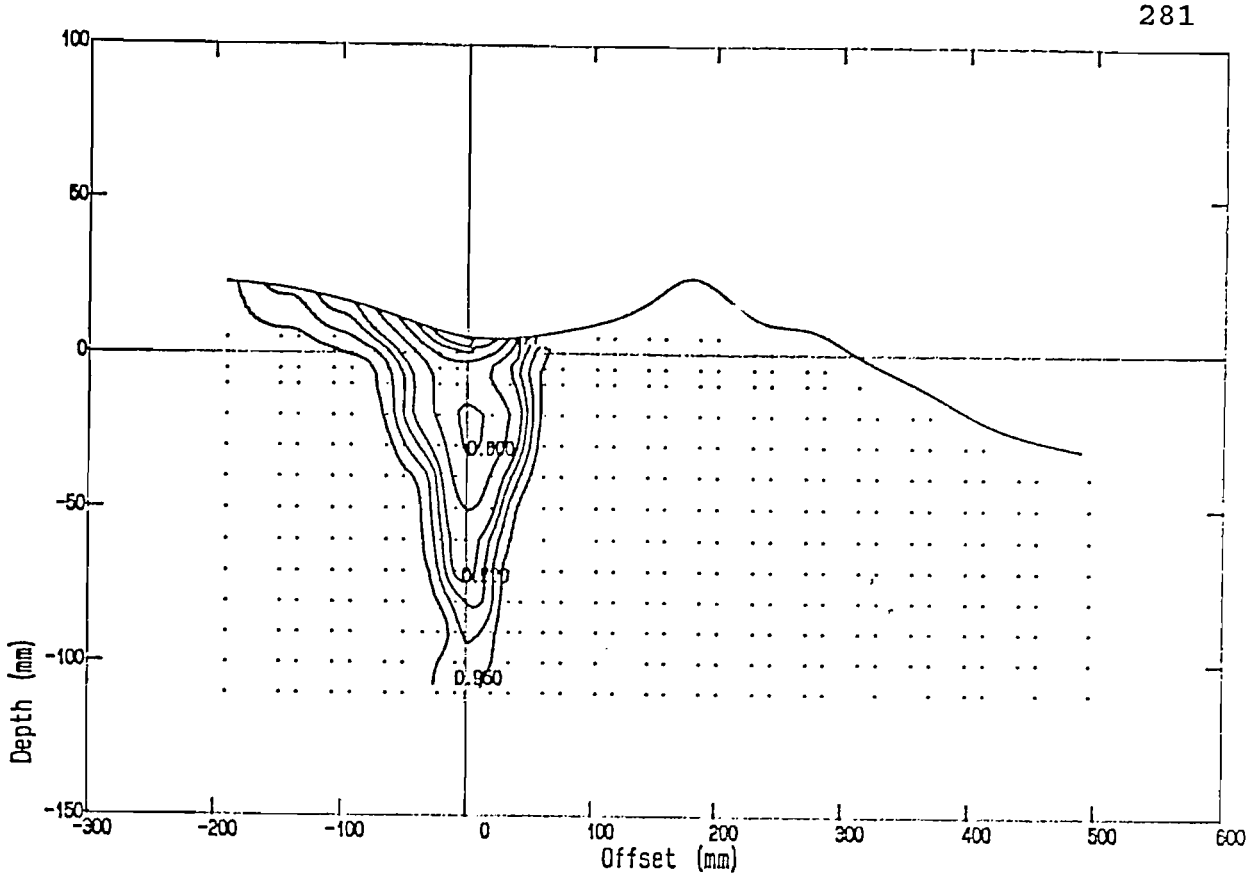

Fig.205: Wake contours at Fn:0.75 (C2-Monohull)

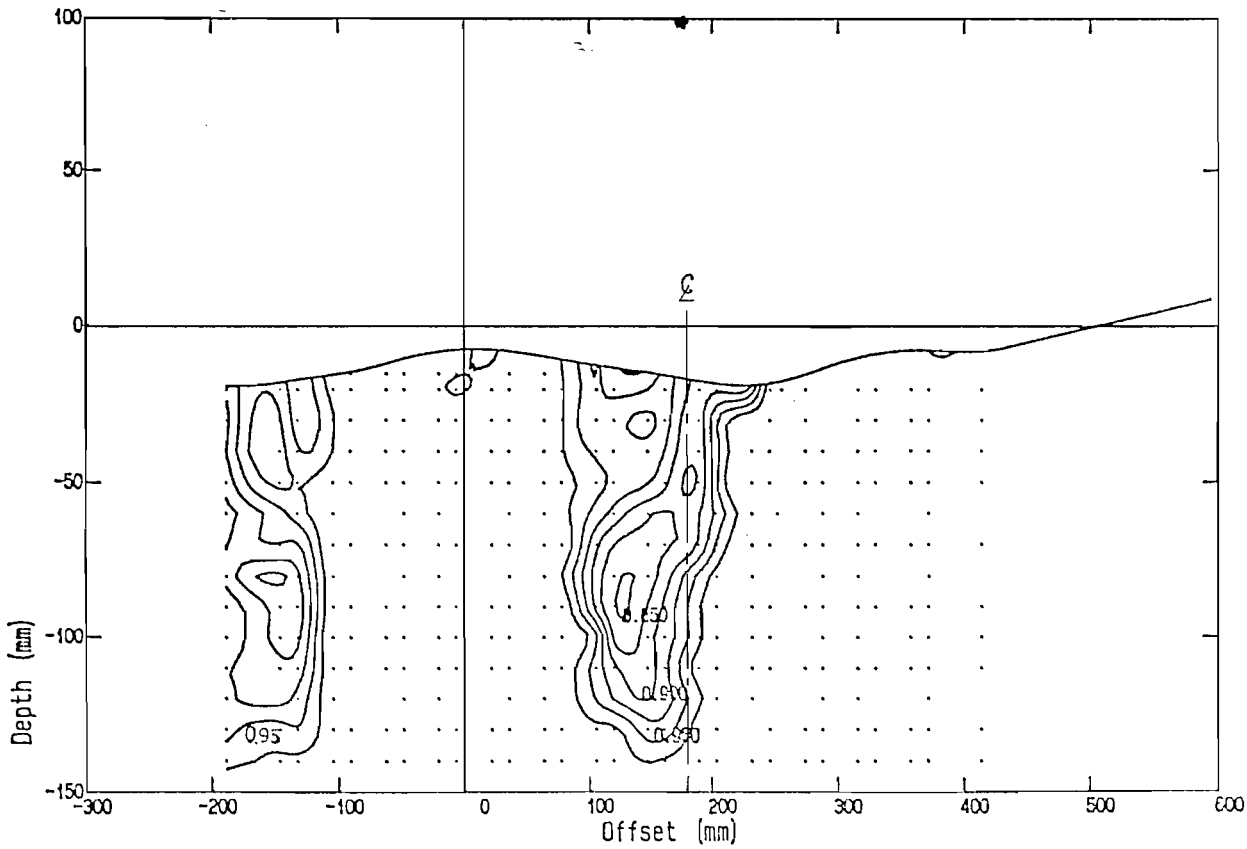

Fig.206: Wake contours at Fn:0.35 (C2-S/L:0.2)

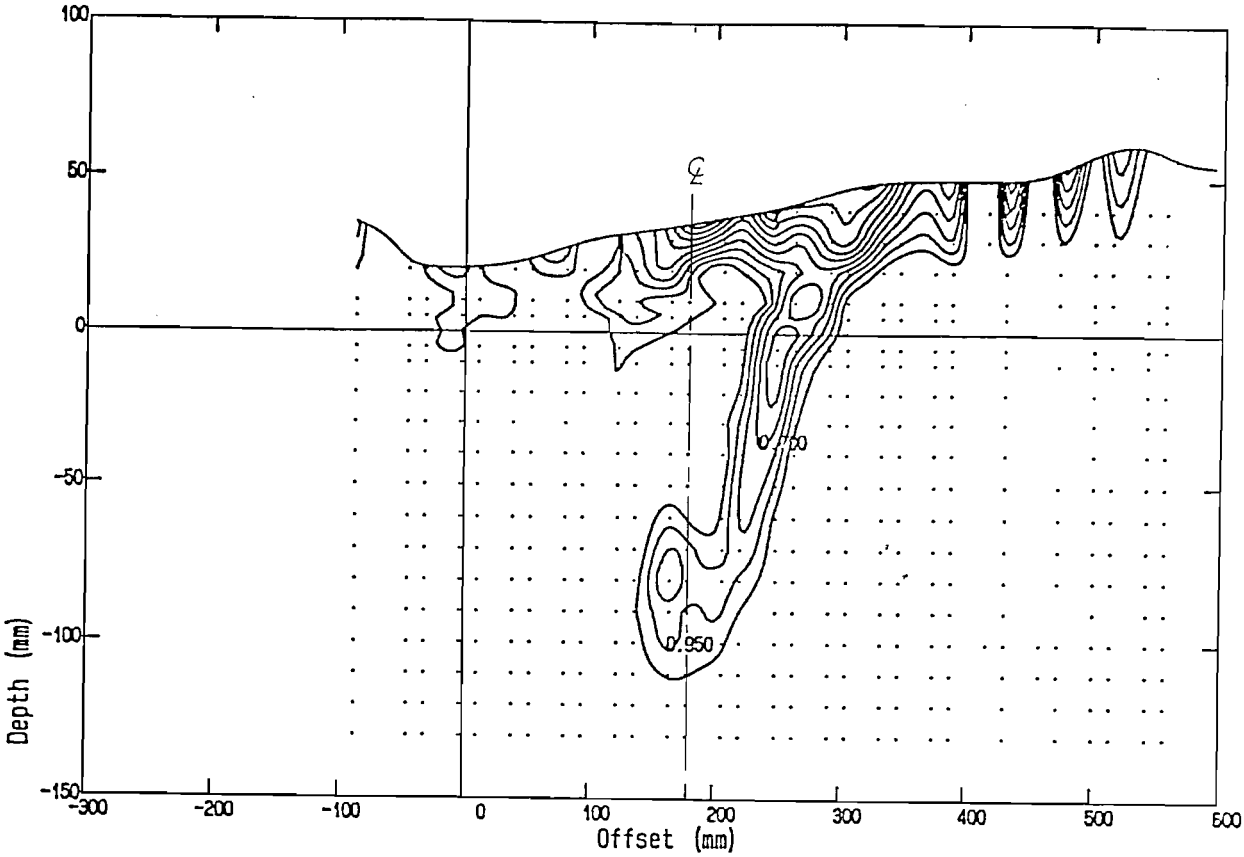

Fig.207: Wake contours at Fn:0.50 (C2-S/L:0.2)

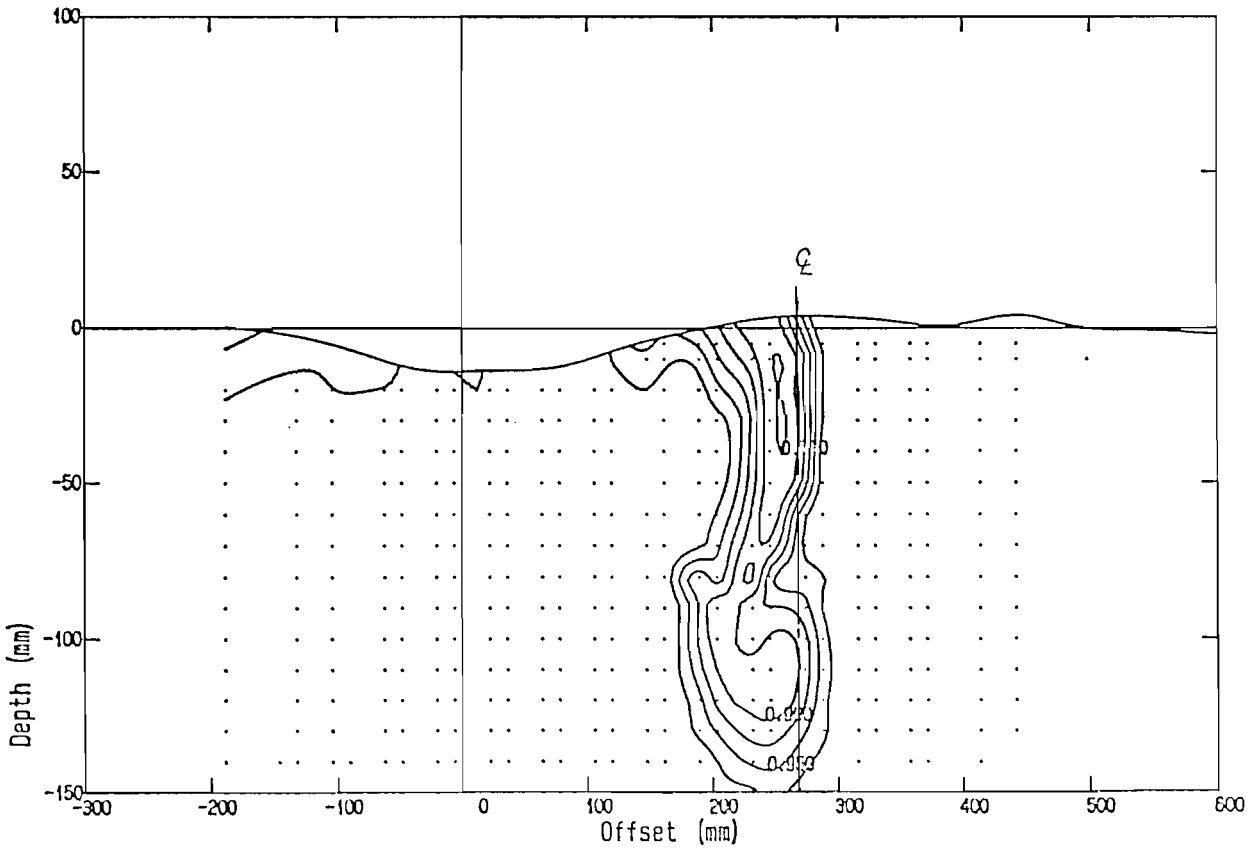

Fig.208: Wake contours at Fn:0.35 (C2-S/L:0.3)

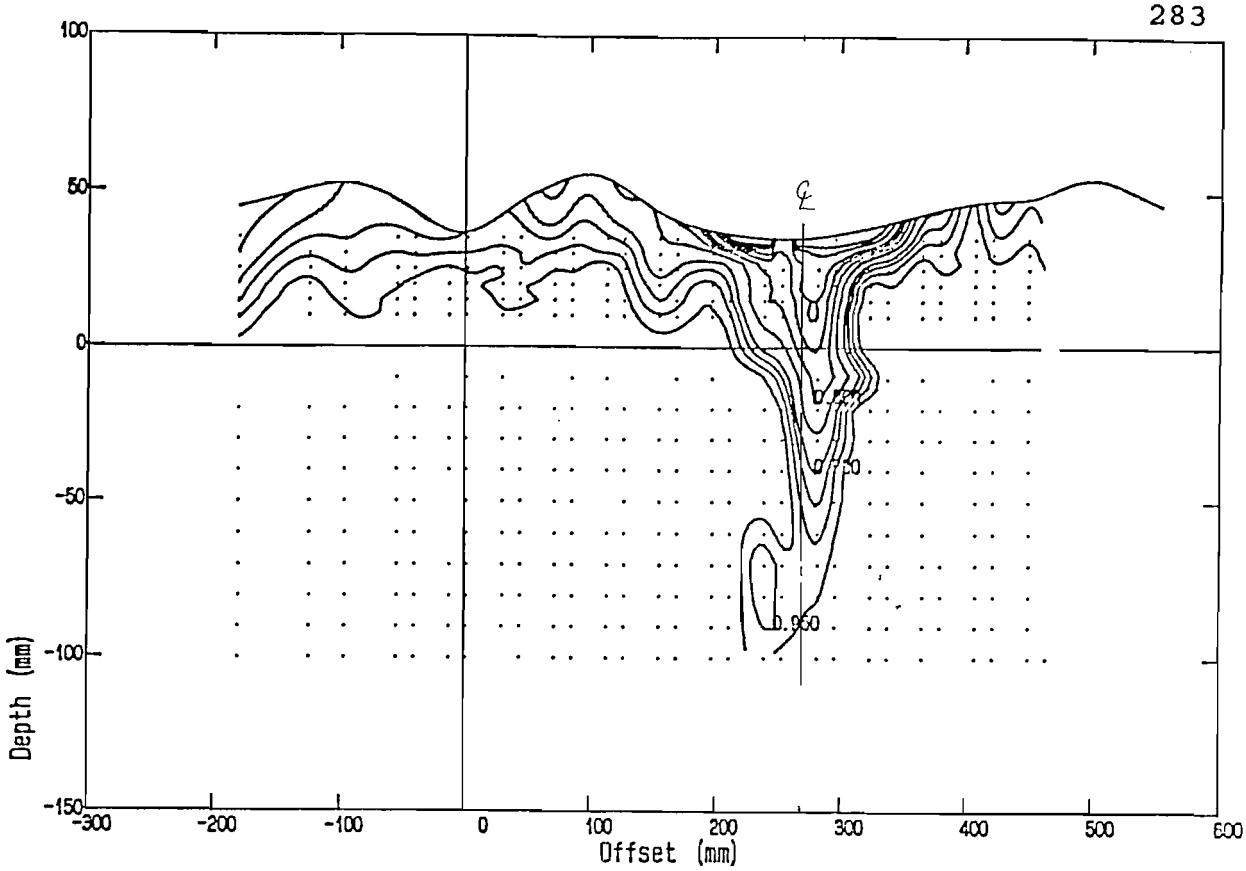

Fig.209: Wake contours at Fn:0.50 (C2-S/L:0.3)

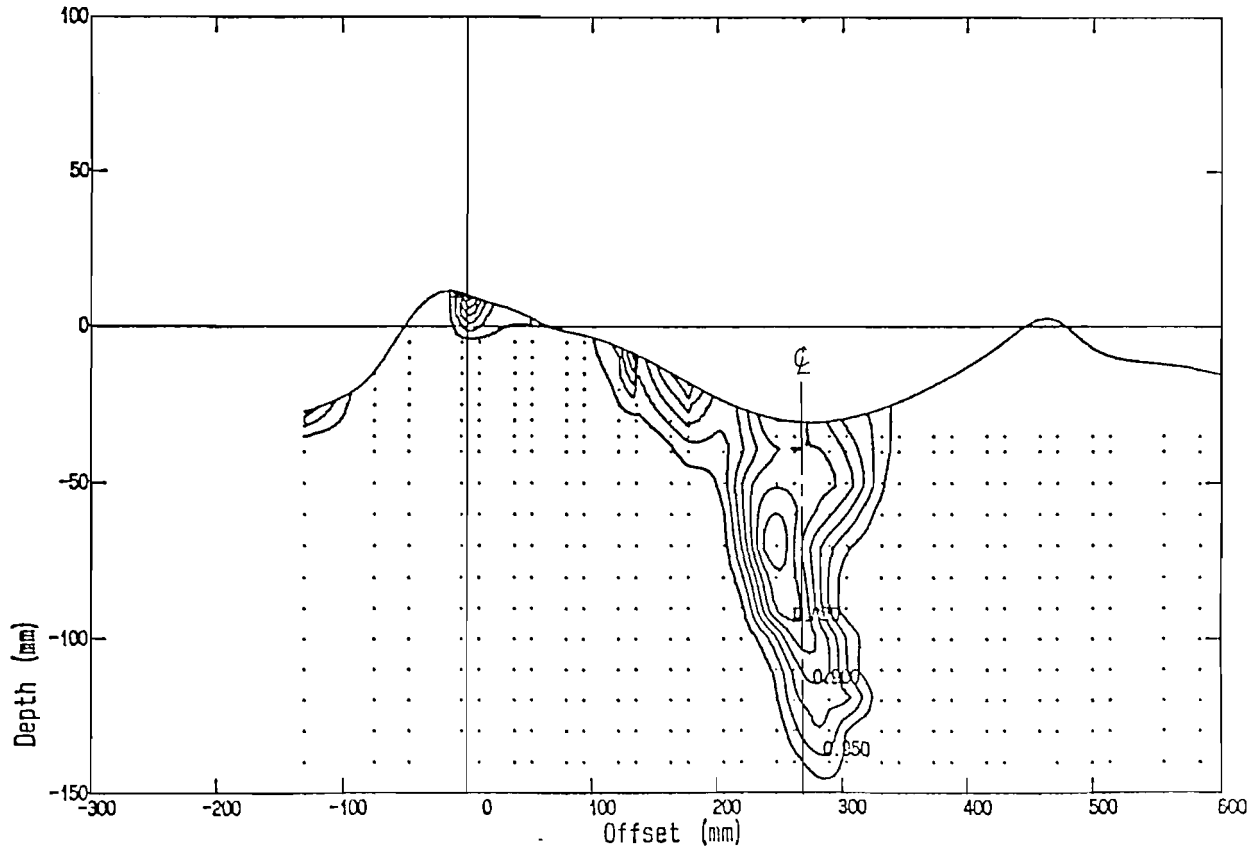

Fig.210: Wake contours at Fn:0.75 (C2-S/L:0.3)

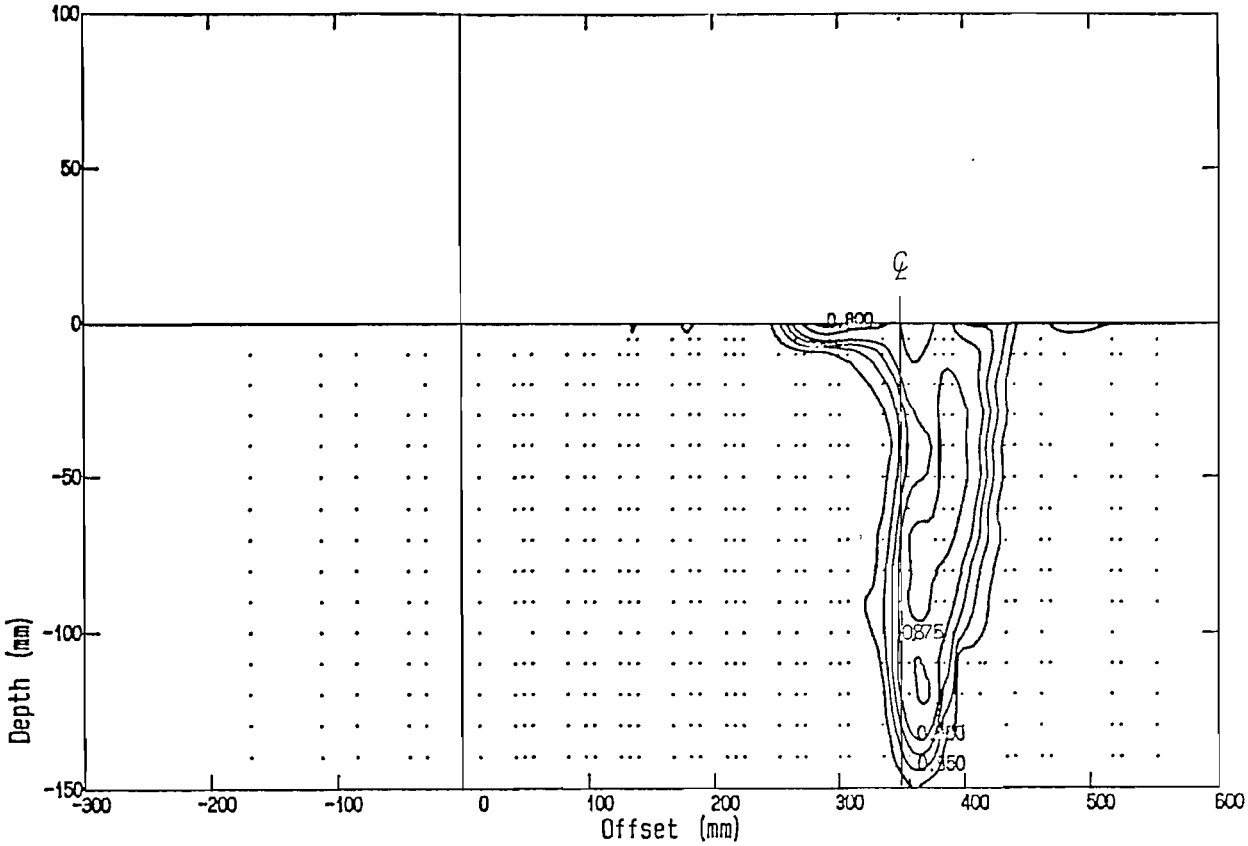

Fig.211: Wake contours at Fn:0.35 (C2-S/L:0.4)

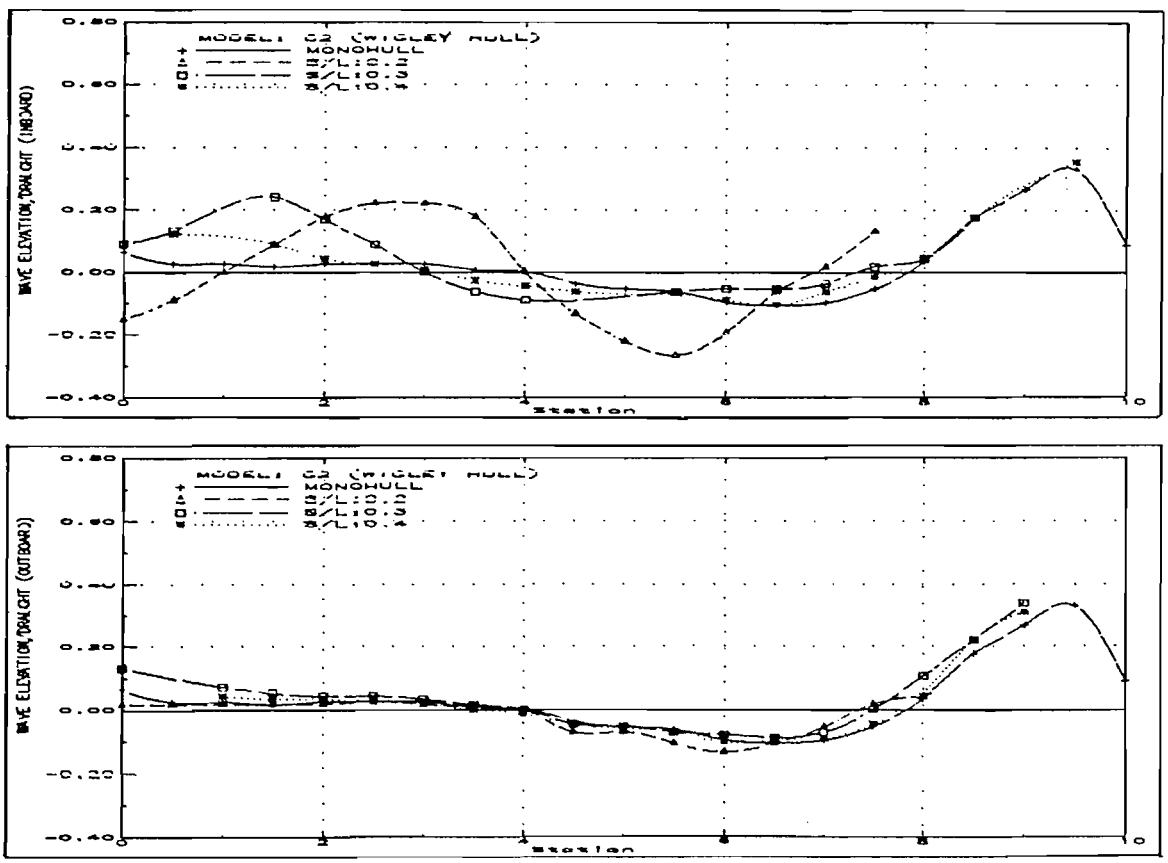

Fig.212: Wave elevation along the hull surface at Fn:0.35 (C2)

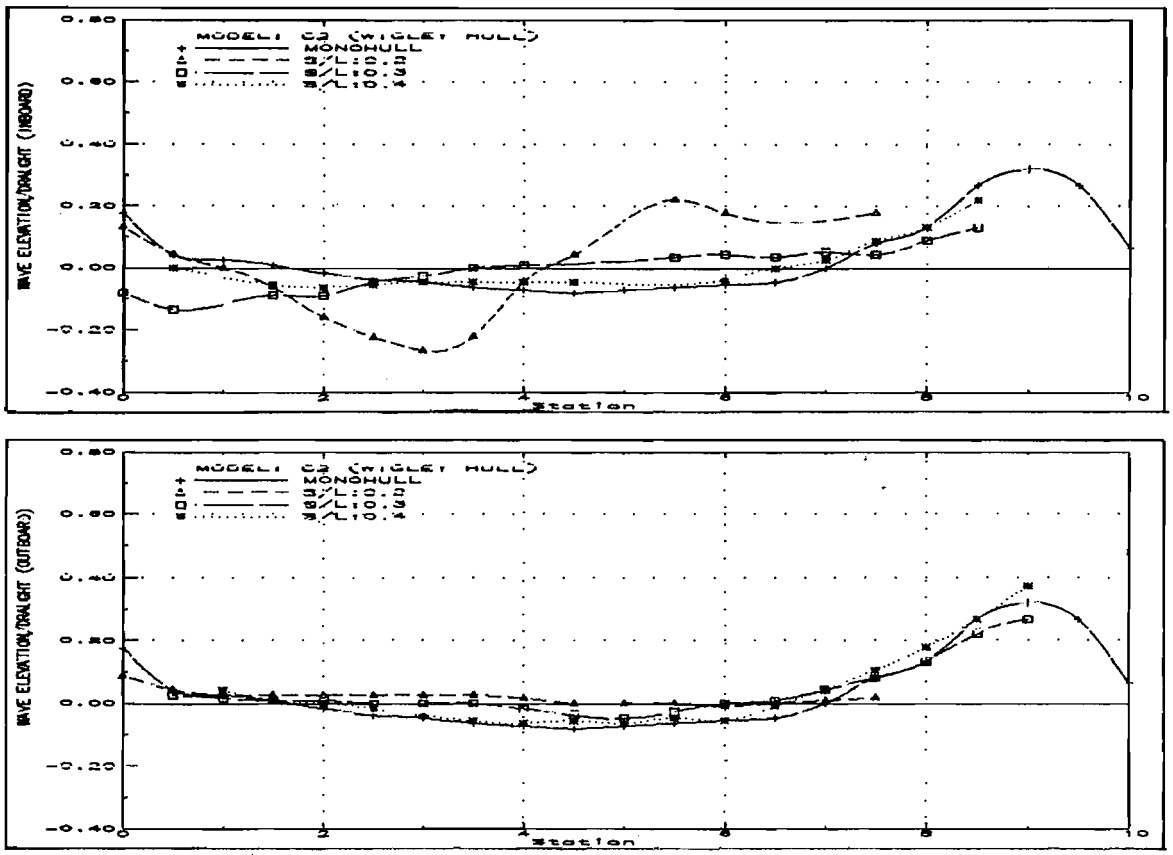

Fig.213: Wave elevation along the hull surface at Fn:0.50 (C2)

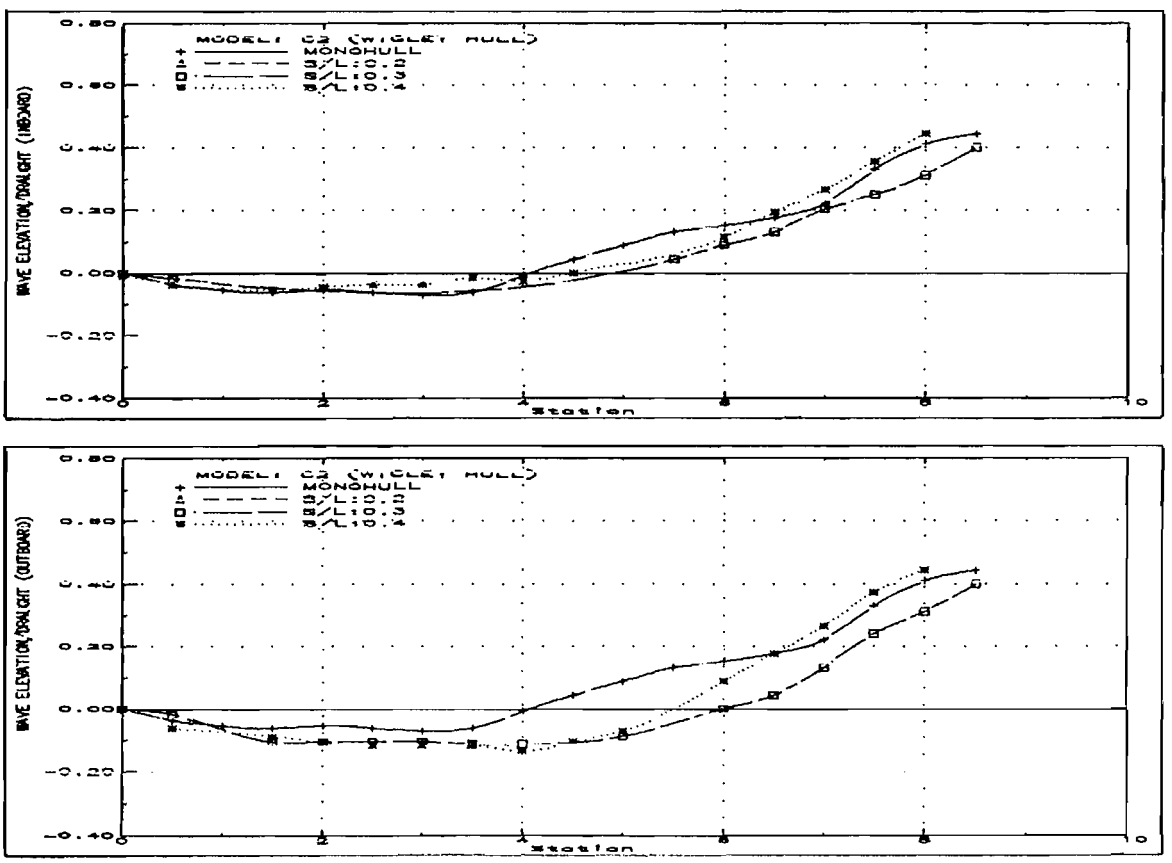

Fig.214: Wave elevation along the hull surface at Fn:0.75 (C2)

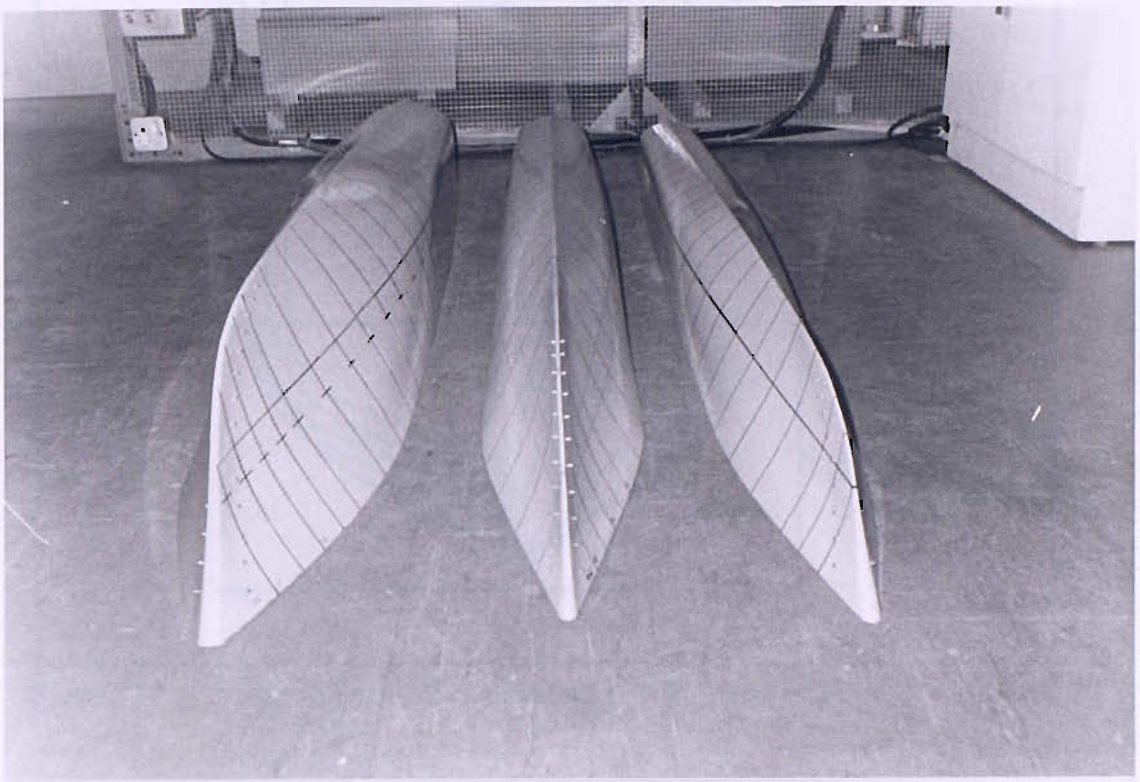

Fig. 215 : Front view of models : C3, C4 and C5
(Left to right)

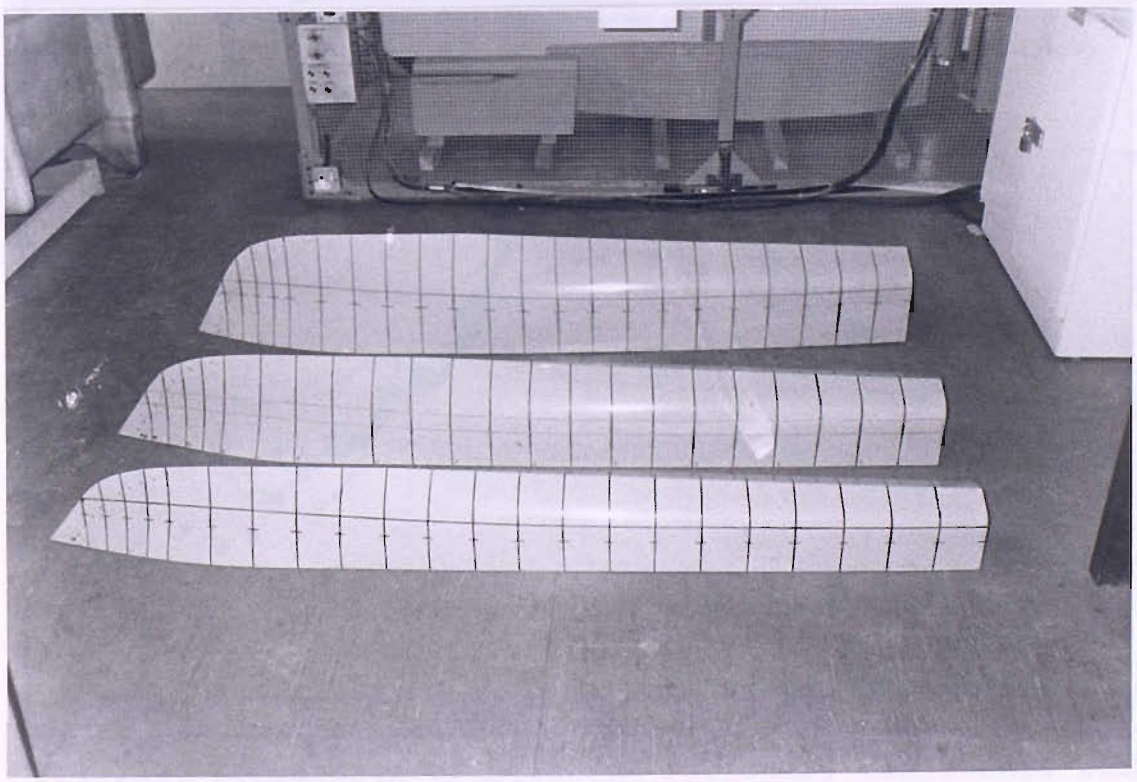

Fig. 216 : Side view of models : C3, C4 and C5
(Furthest to nearest)

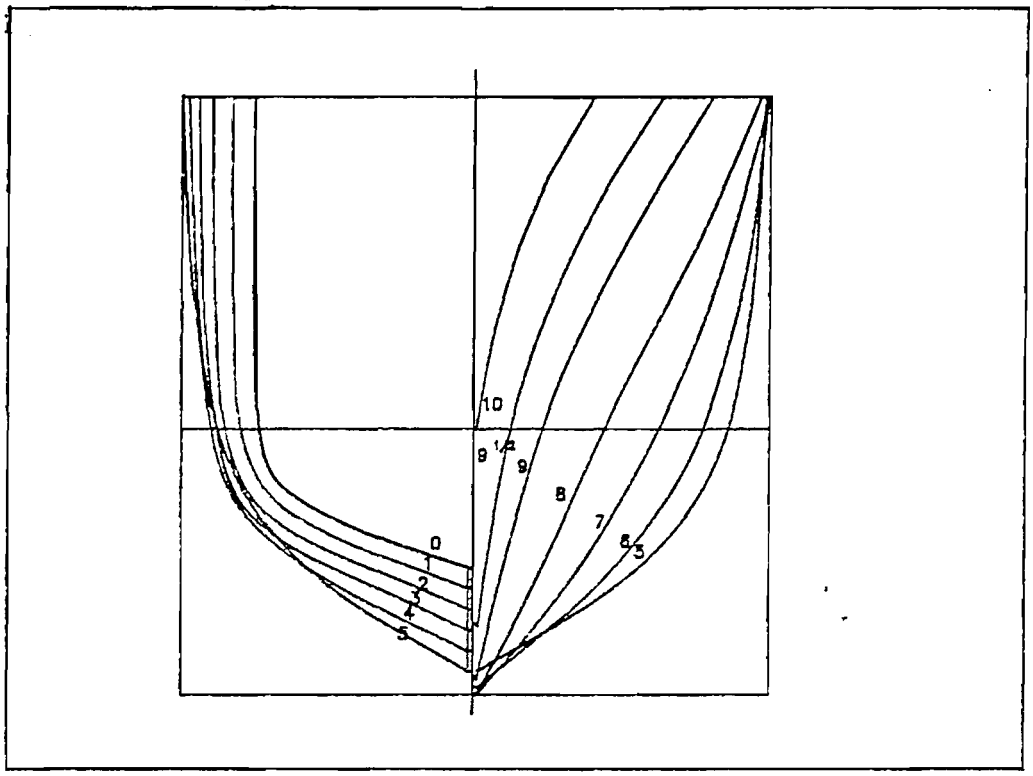

Fig.217: Body plan of models : C3, C4, C5

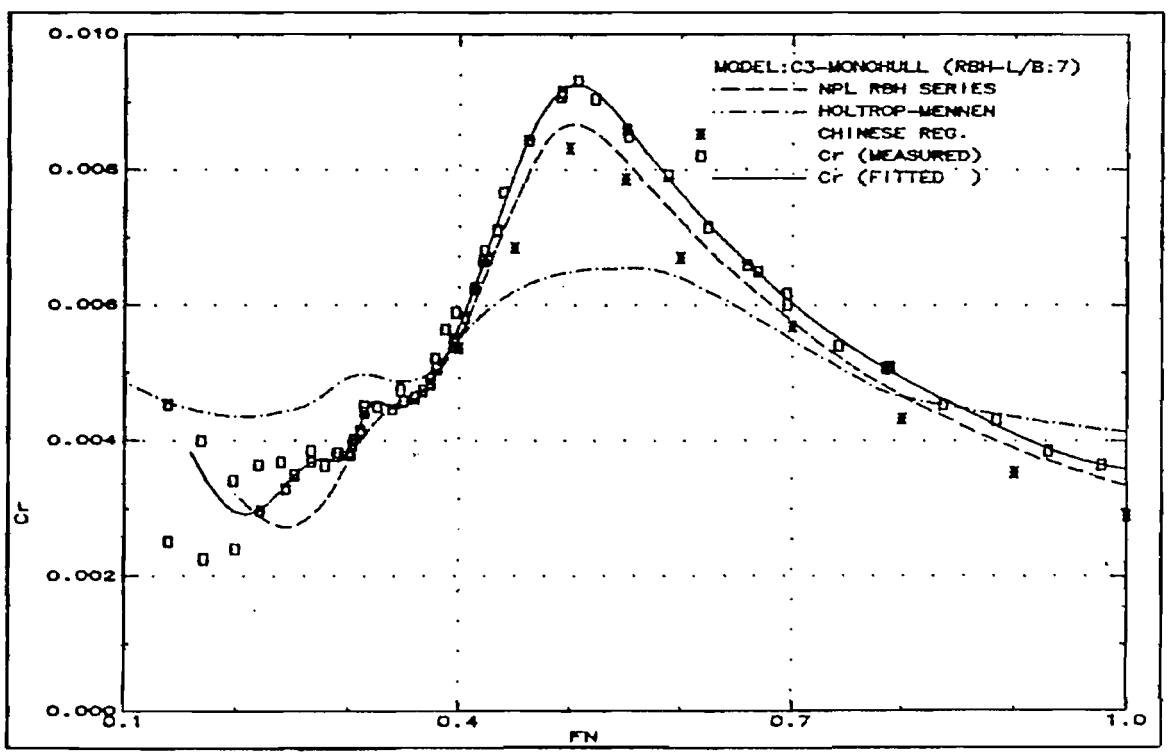

Fig.218: Comparison of measured residuary resistance with predictions (C3-Monohull)

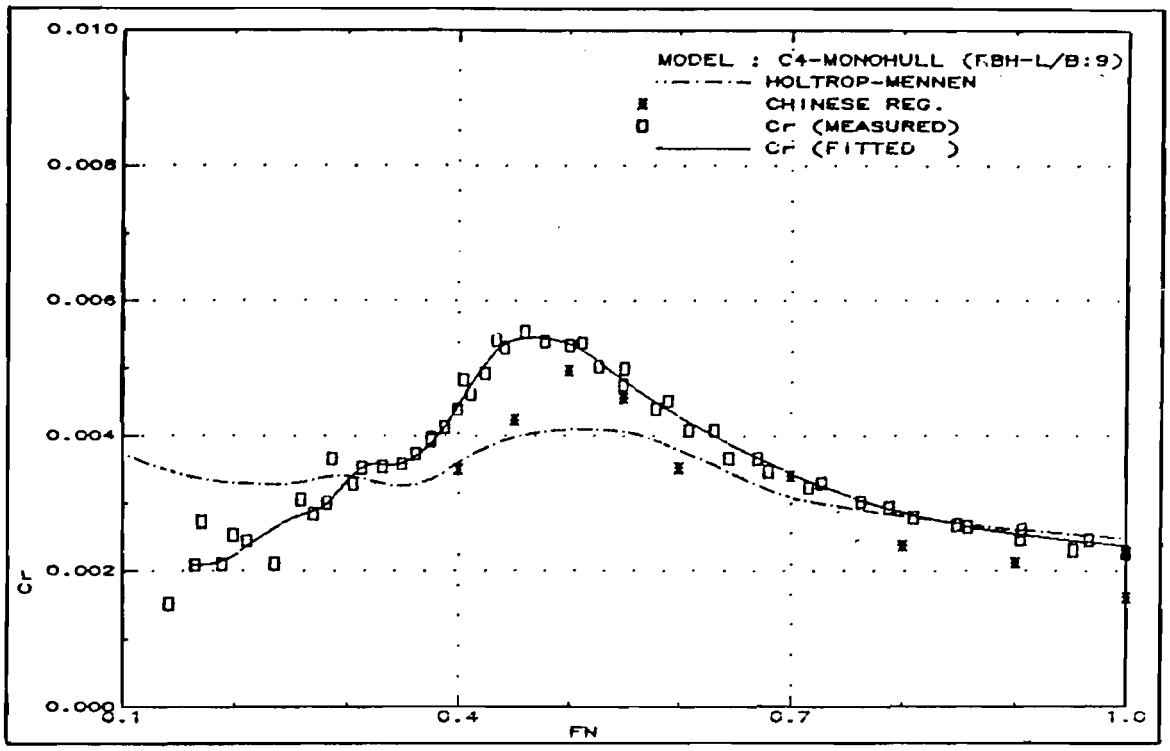

Fig.219: Comparison of measured residuary resistance with predictions (C4-Monohull)

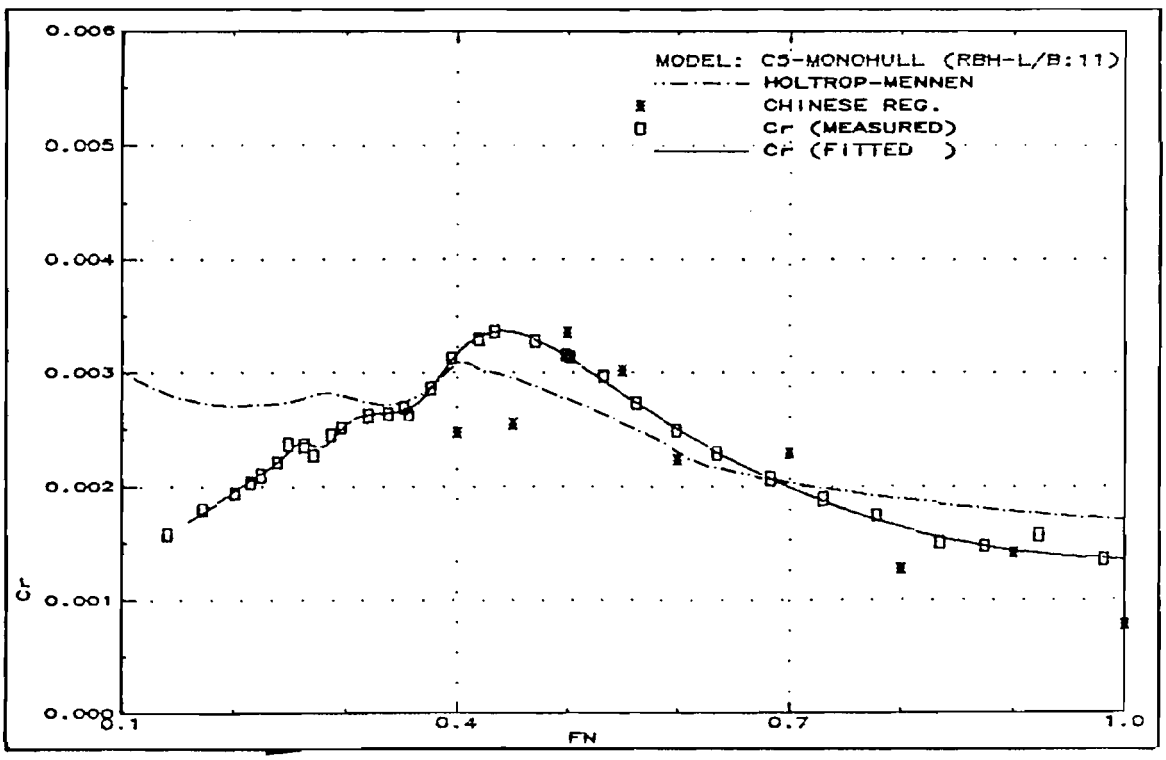

Fig.220: Comparison of measured residuary resistance with predictions (C5-Monohull)

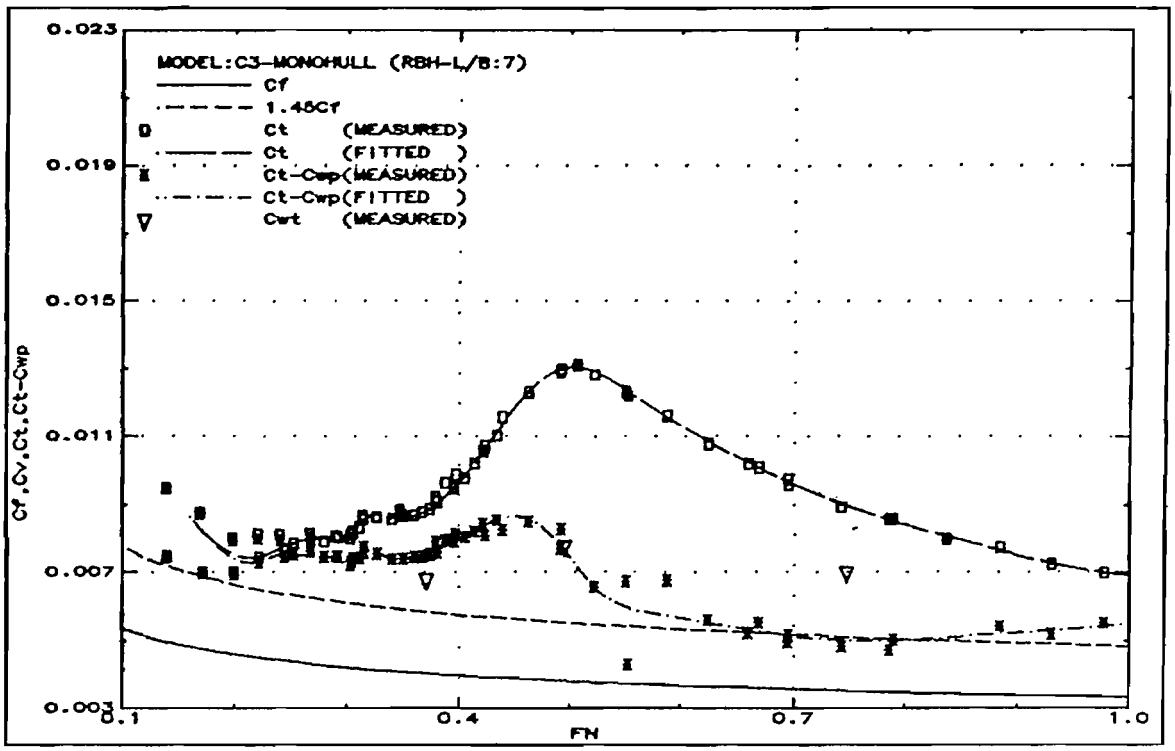

Fig.221: Resistance components (C3-Monohull)

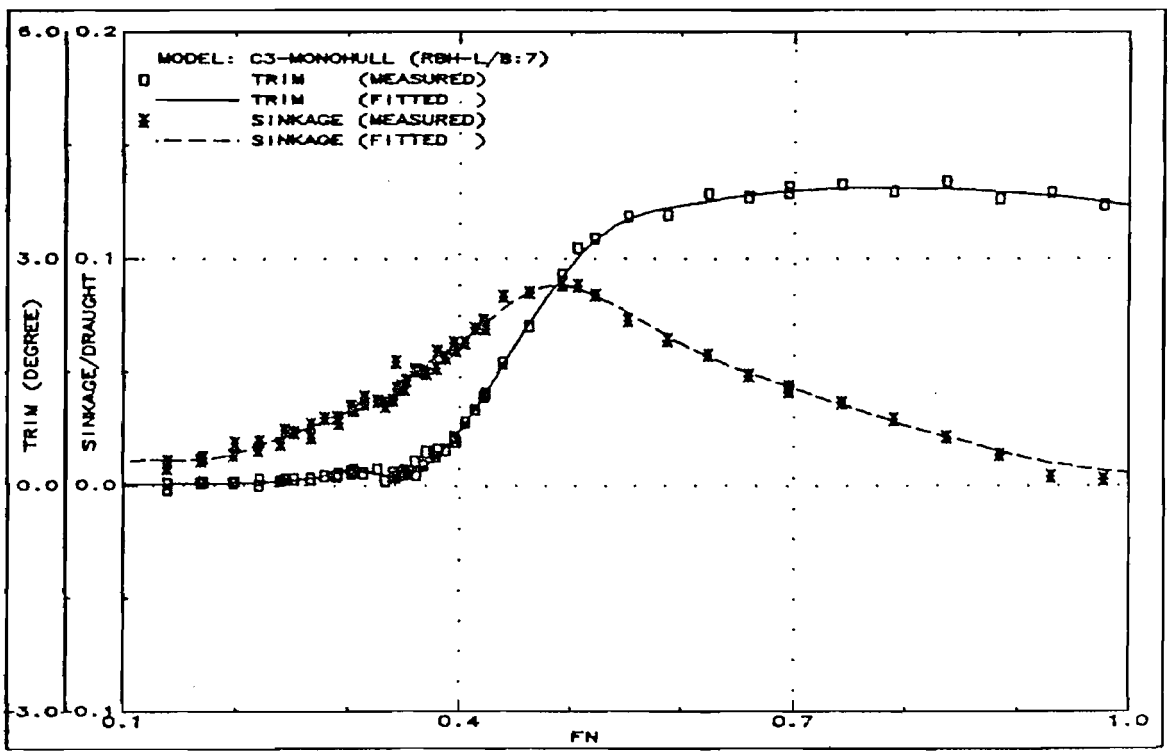

Fig.222: Running trim and sinkage (C3-Monohull)

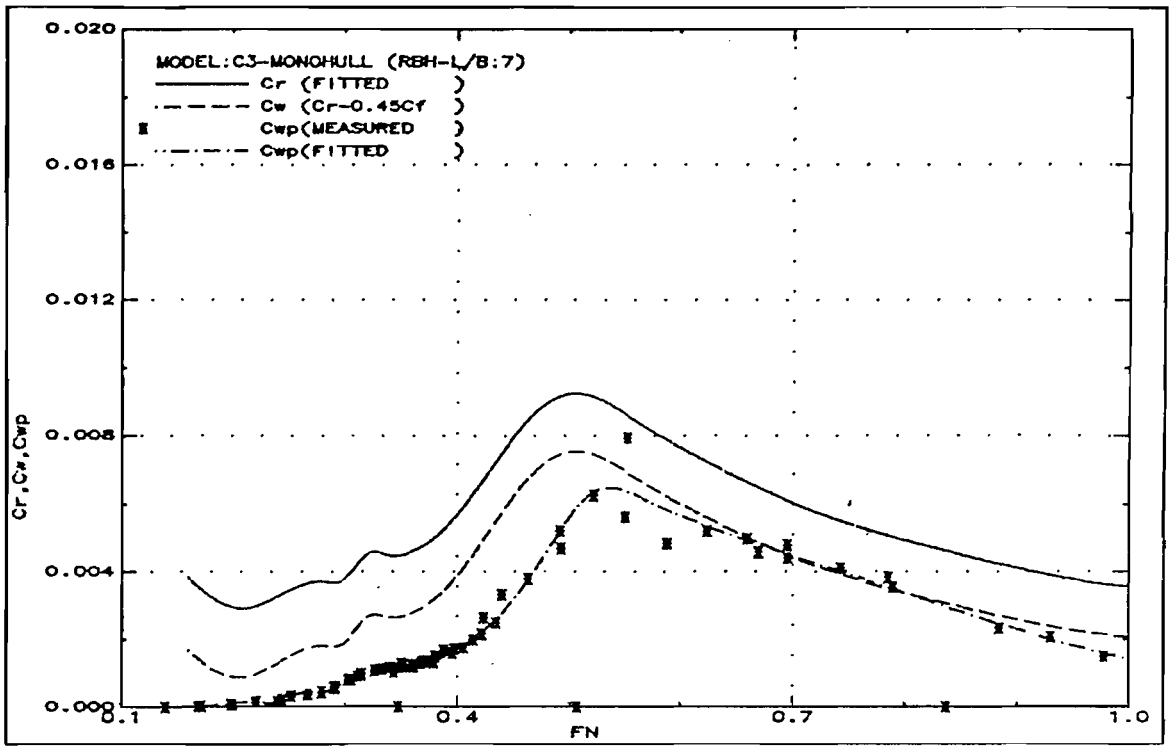

Fig.223: Measured wave resistance (C3-Monohull)

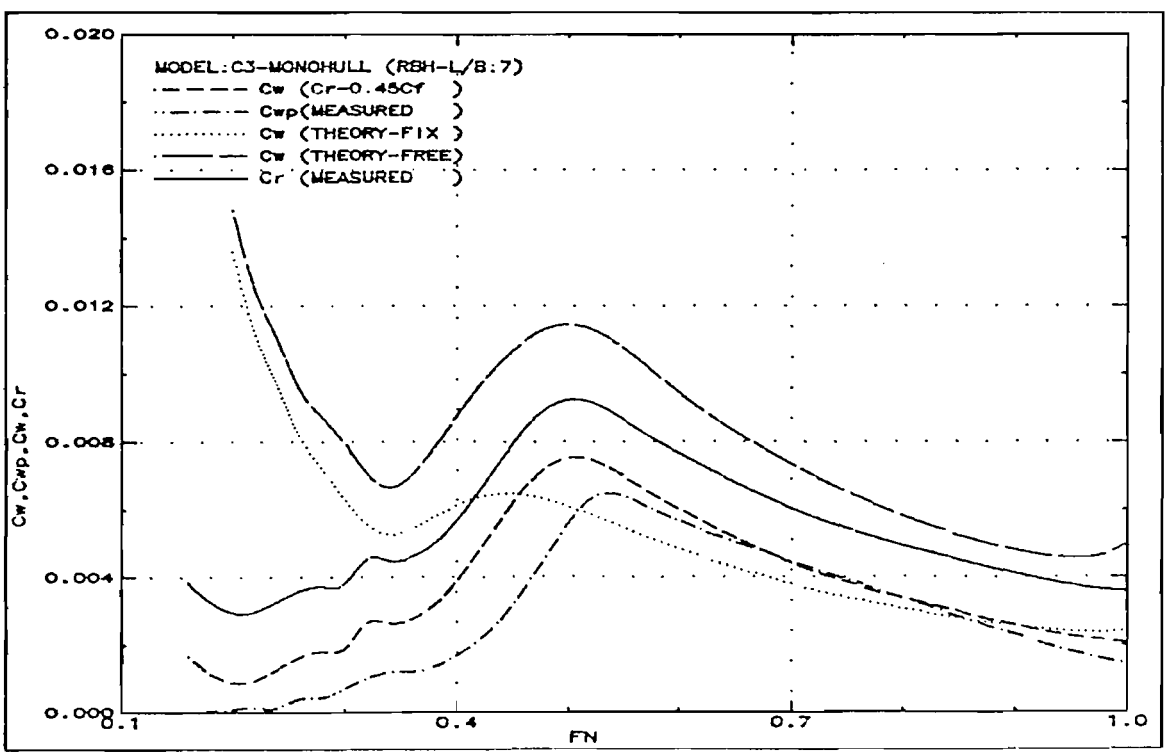

Fig.224: Wave resistance comparison (C3-Monohull)

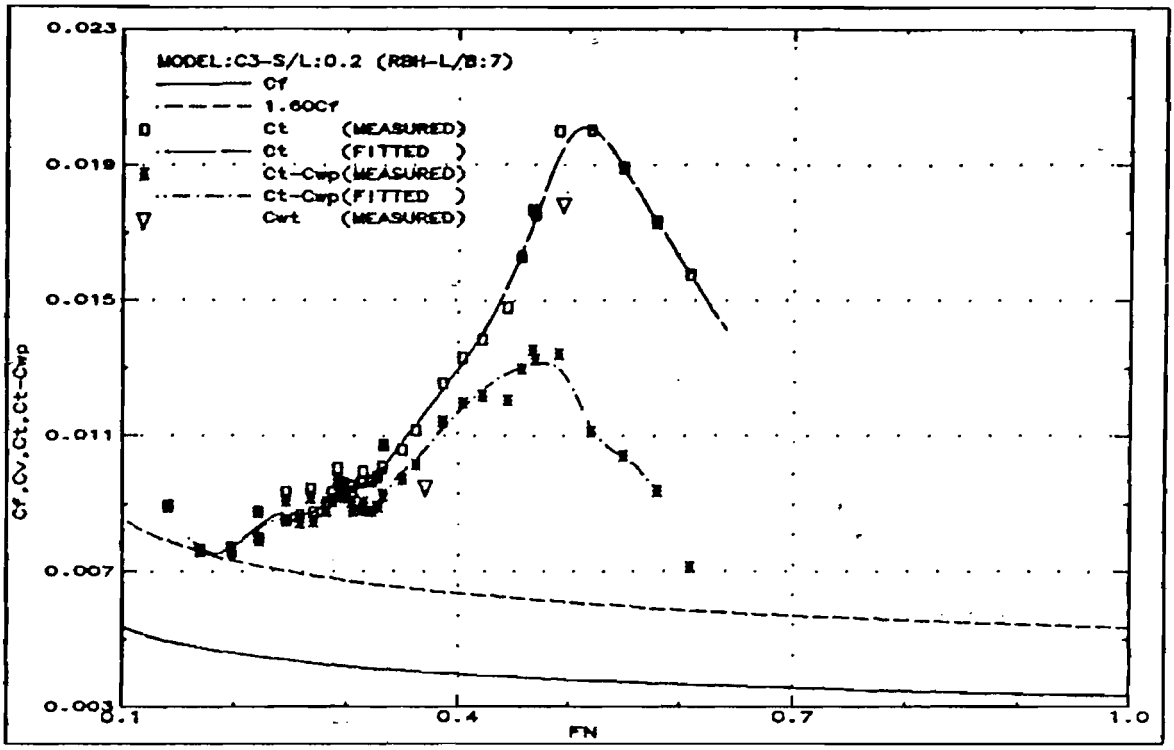

Fig.225: Resistance components (C3-S/L:Ø.2)

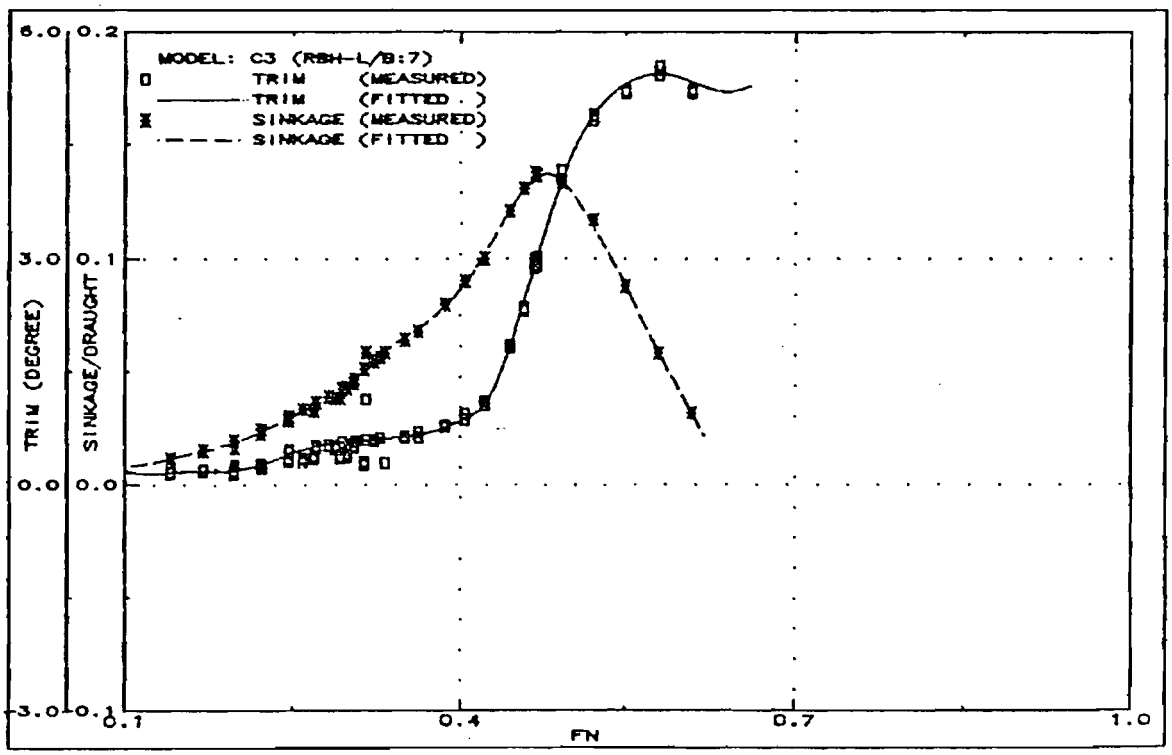

Fig.226: Running trim and sinkage (C3-S/L:Ø.2)

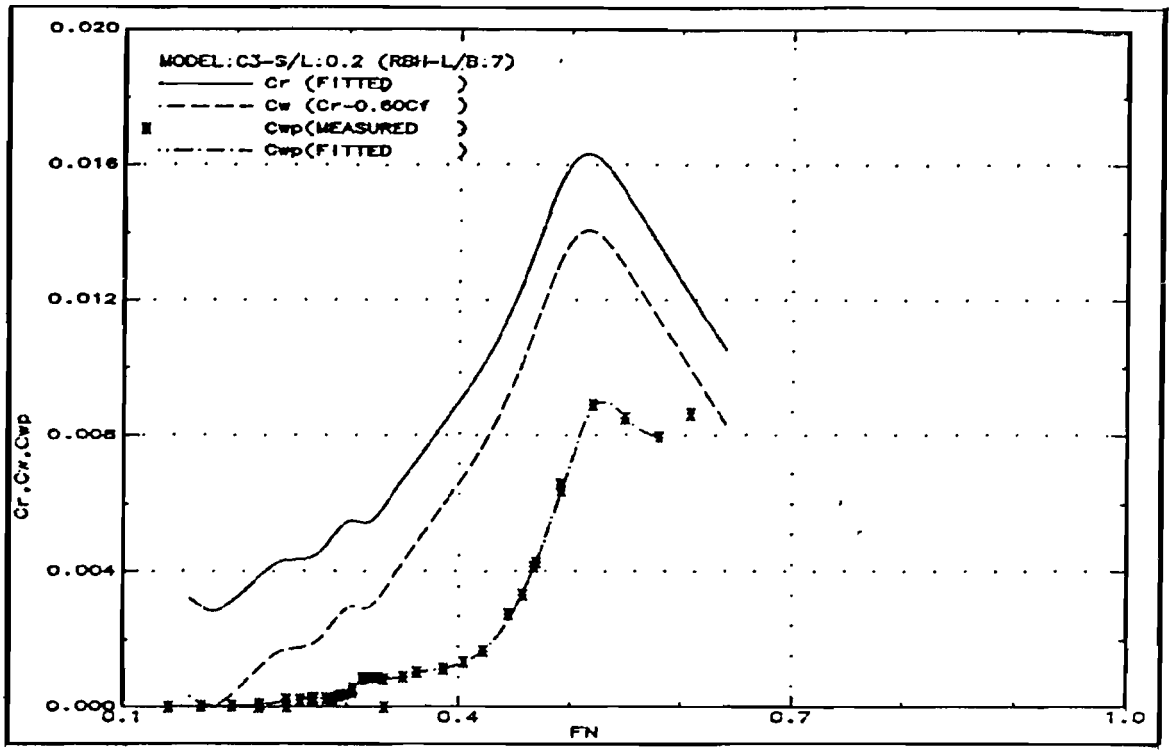

Fig.227: Measured wave resistance (C3-S/L:Ø.2)

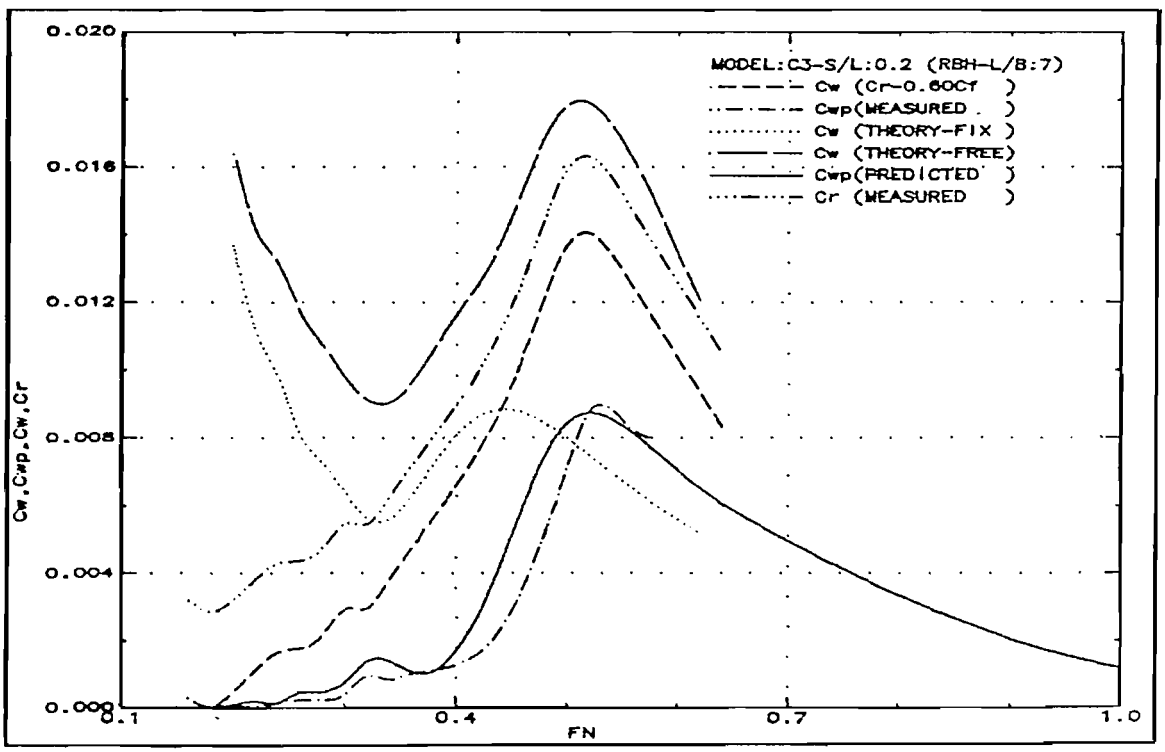

Fig.228: Wave resistance comparison (C3-S/L:Ø.2)

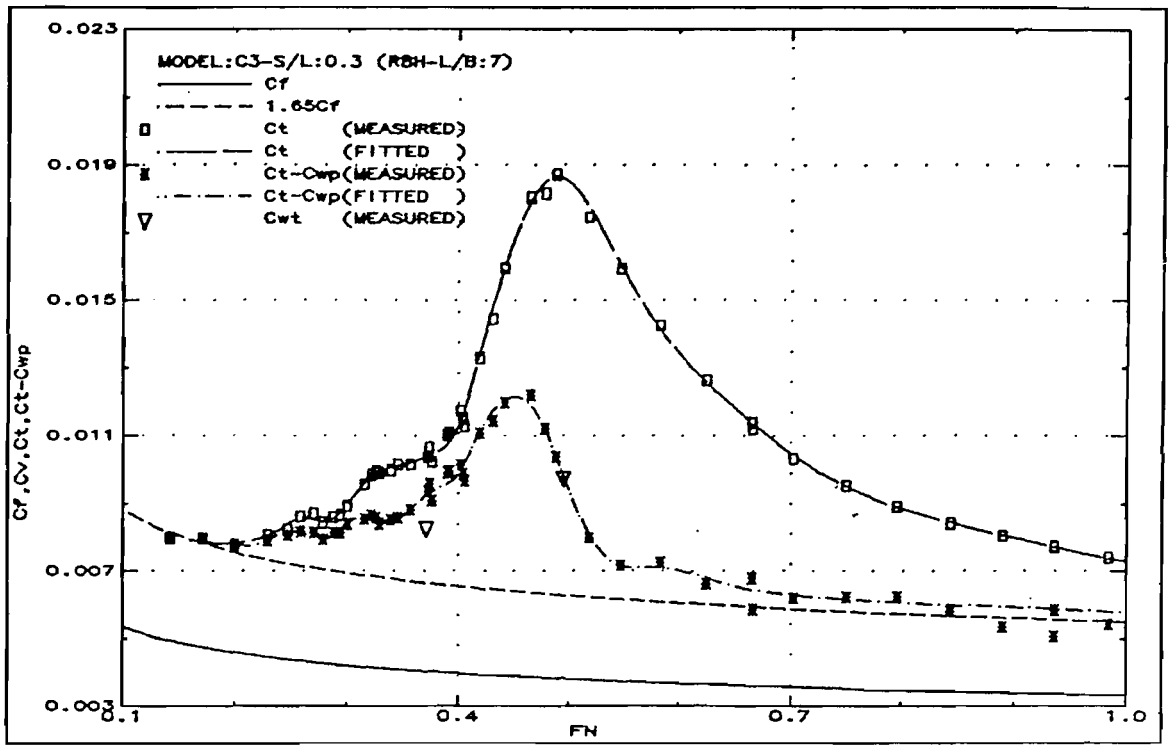

Fig.229: Resistance components (C3-S/L:Ø.3)

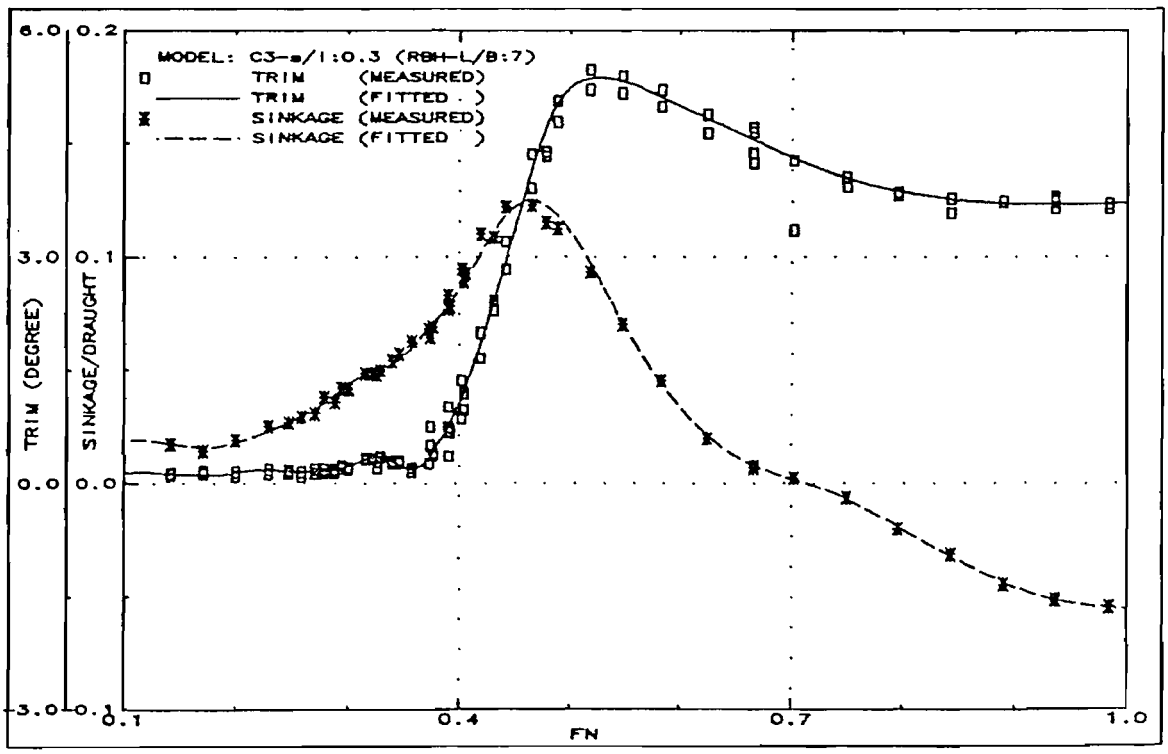

Fig.230: Running trim and sinkage (C3-S/L:Ø.3)

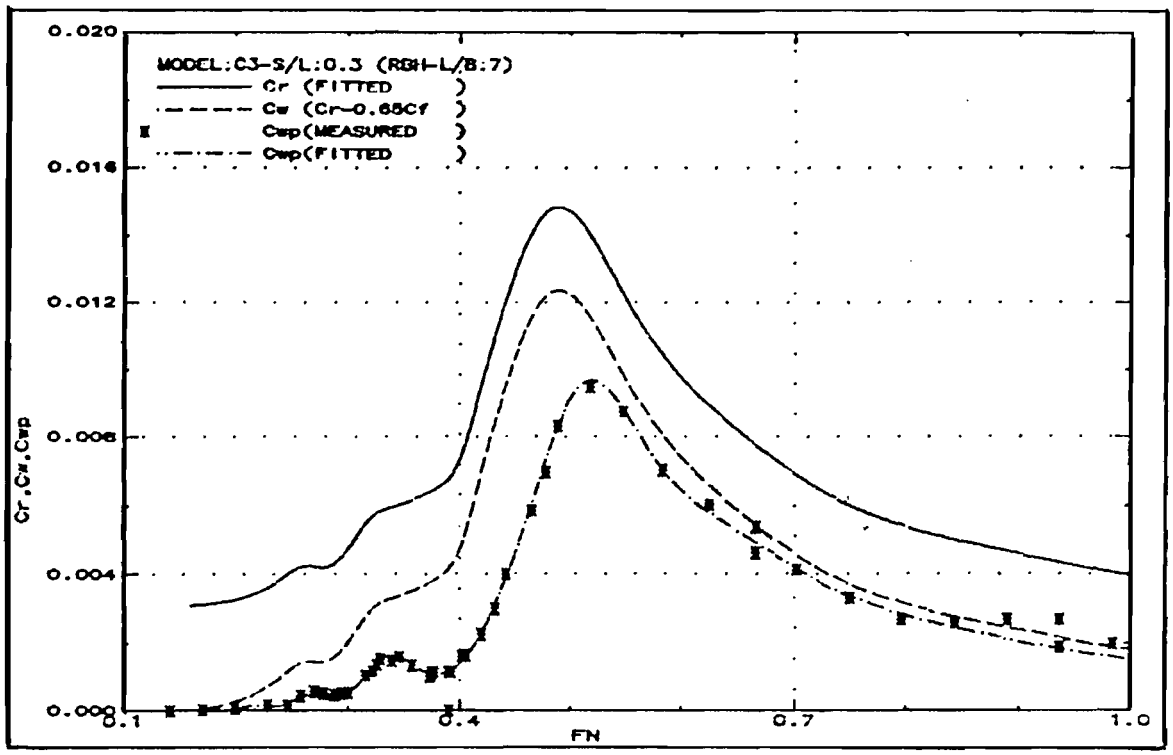

Fig.231: Measured wave resistance (C3-S/L:Ø.3)

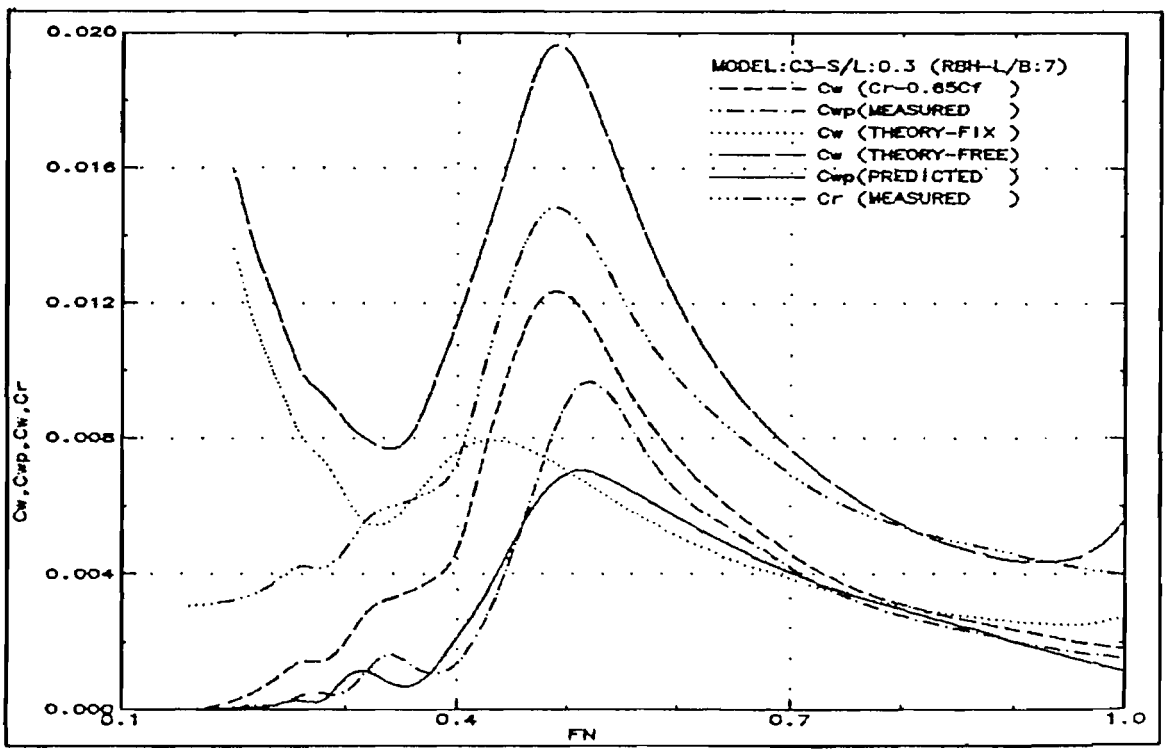

Fig.232: Wave resistance comparison (C3-S/L:Ø.3)

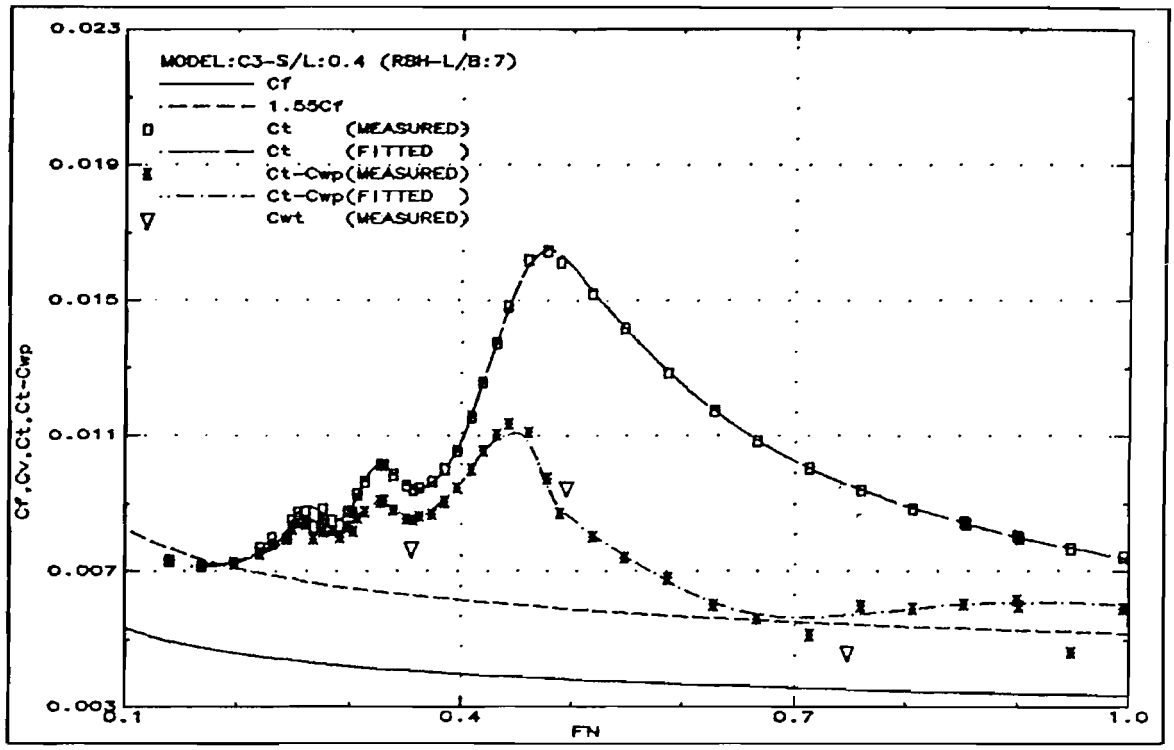

Fig.233: Resistance components (C3-S/L:Ø.4)

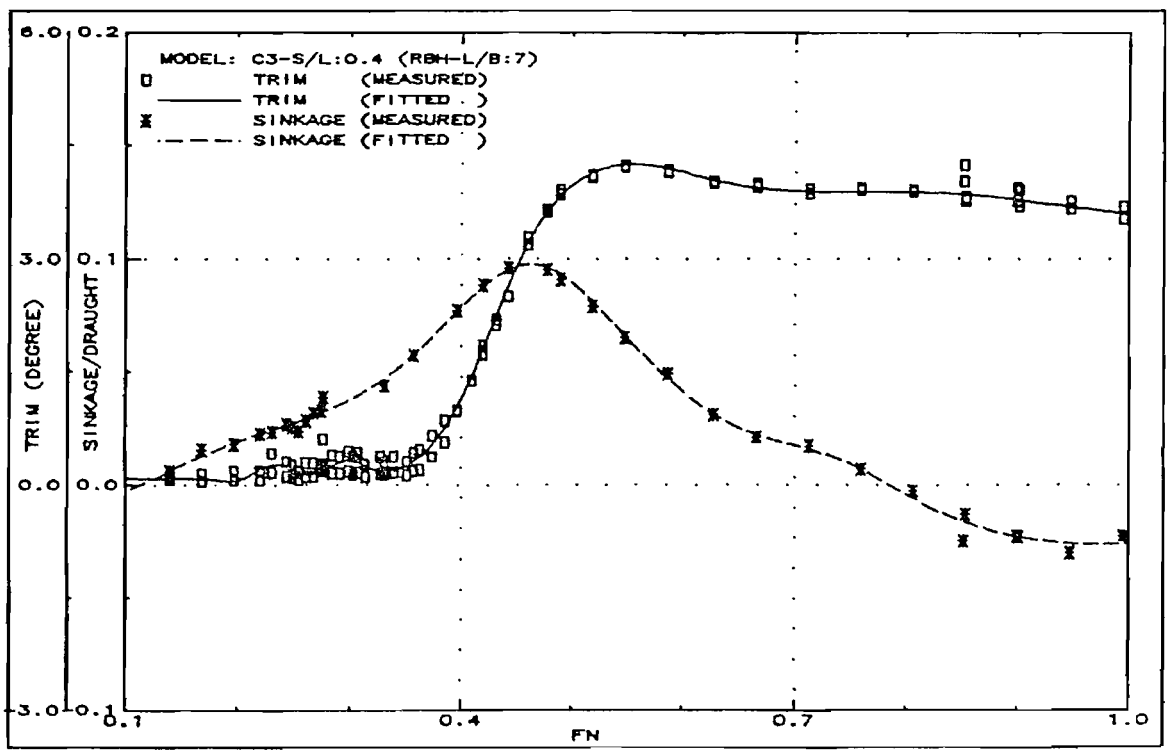

Fig.234: Running trim and sinkage (C3-S/L:Ø.4)

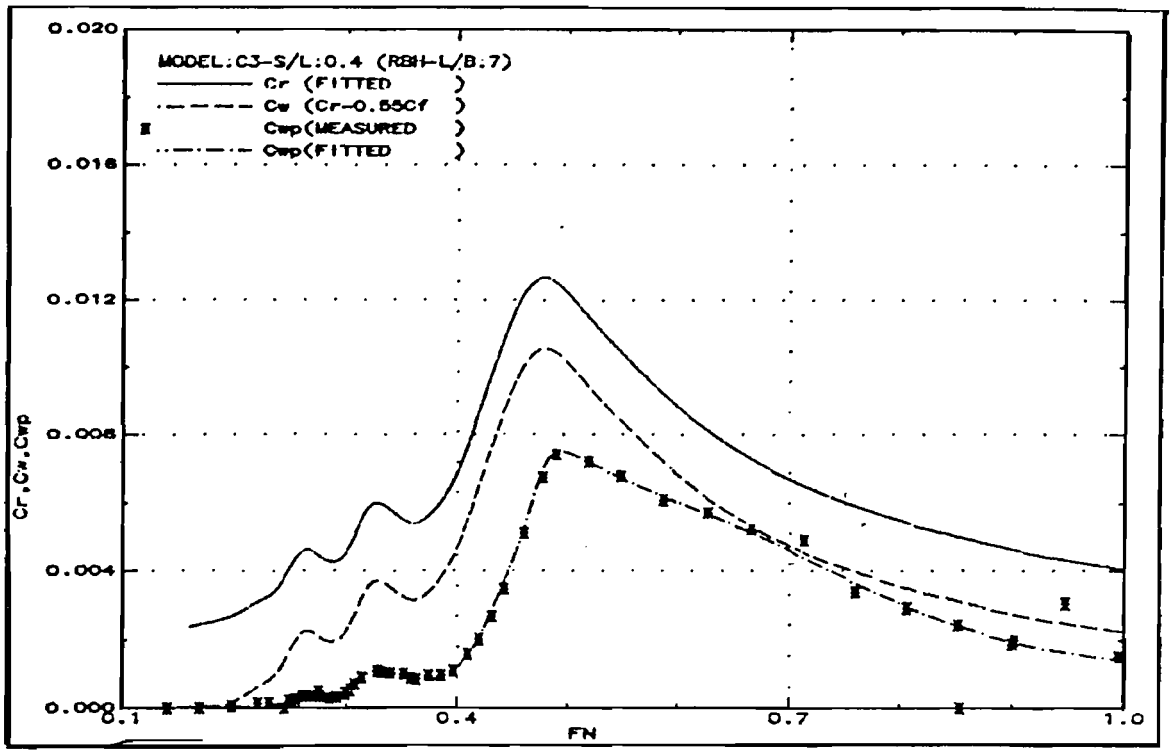

Fig.235: Measured wave resistance (C3-S/L:0.4)

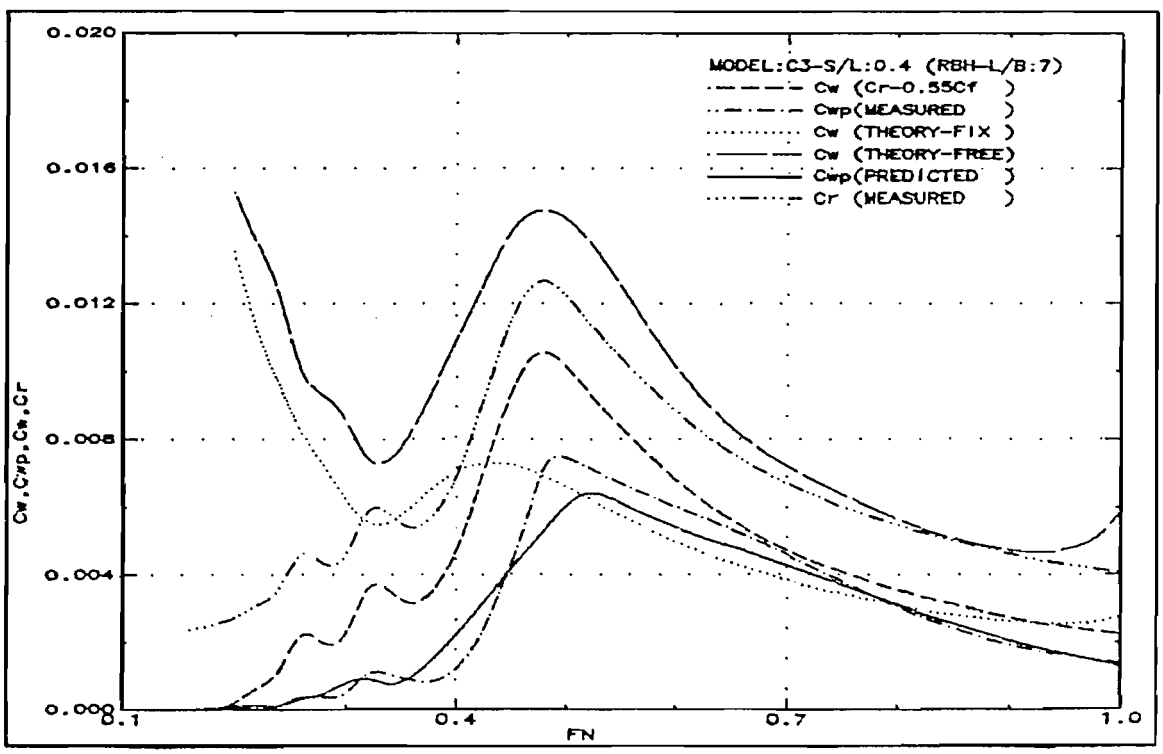

Fig.236: Wave resistance comparison (C3-S/L:0.4)

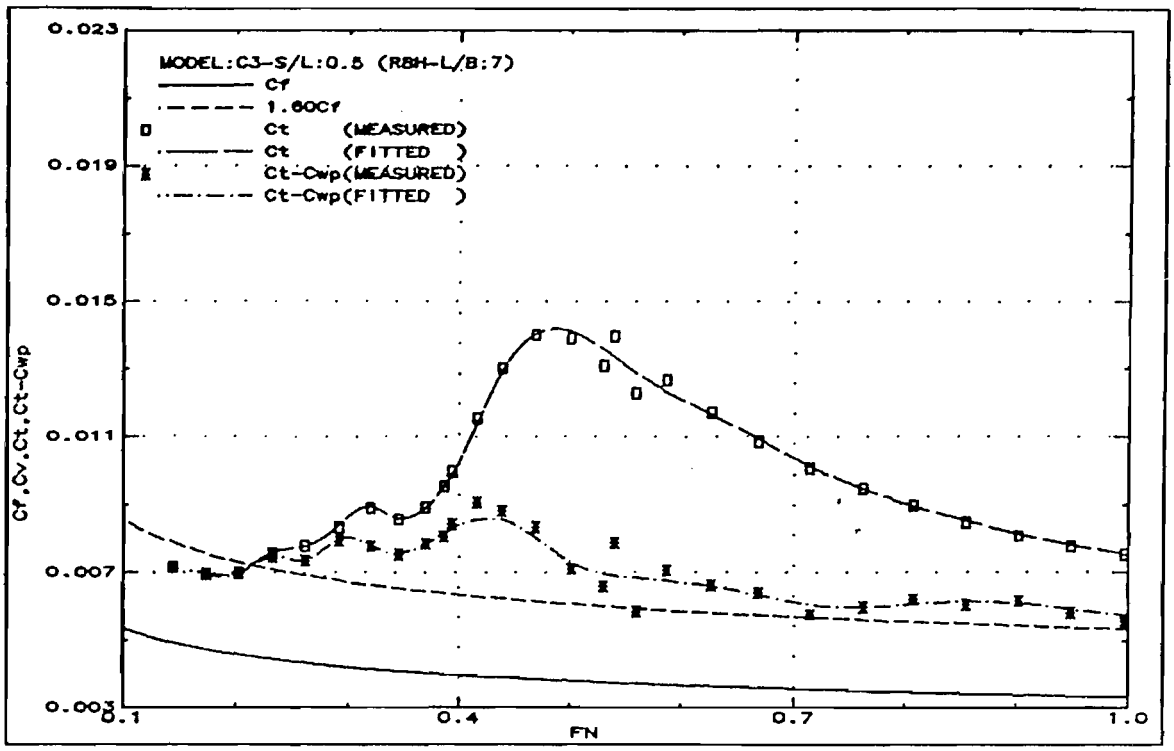

Fig.237: Resistance components (C3-S/L:Ø.5)

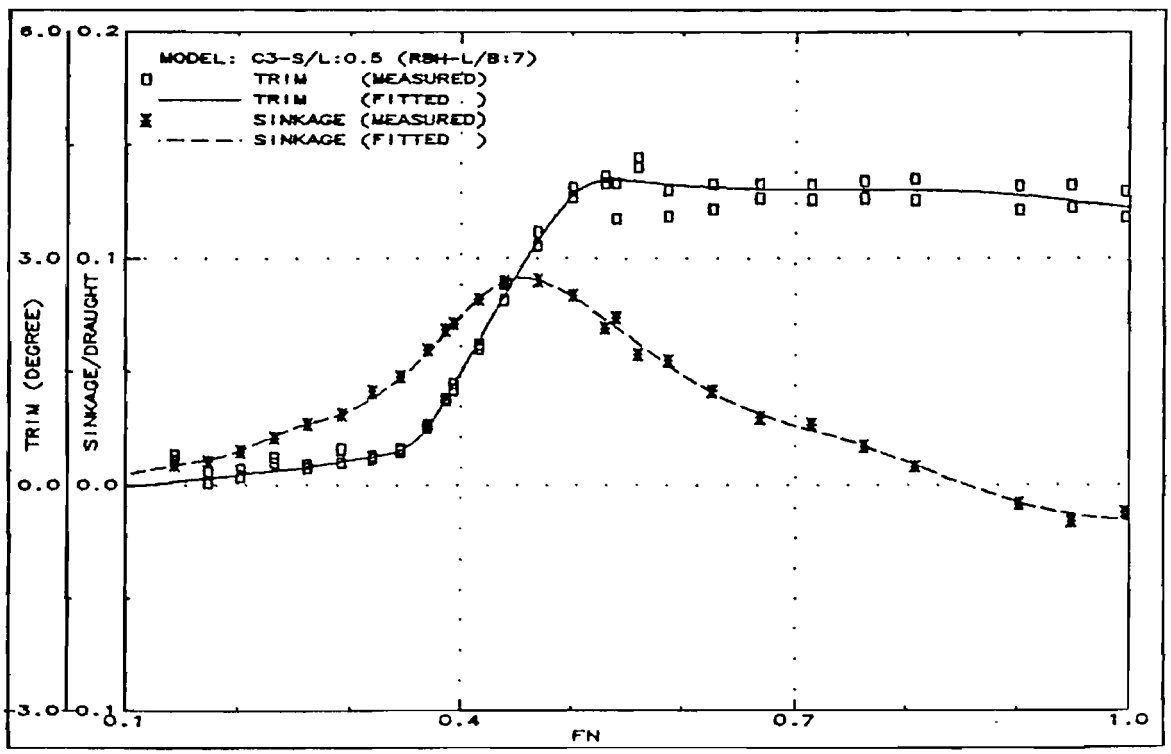

Fig.238: Running trim and sinkage (C3-S/L:Ø.5)

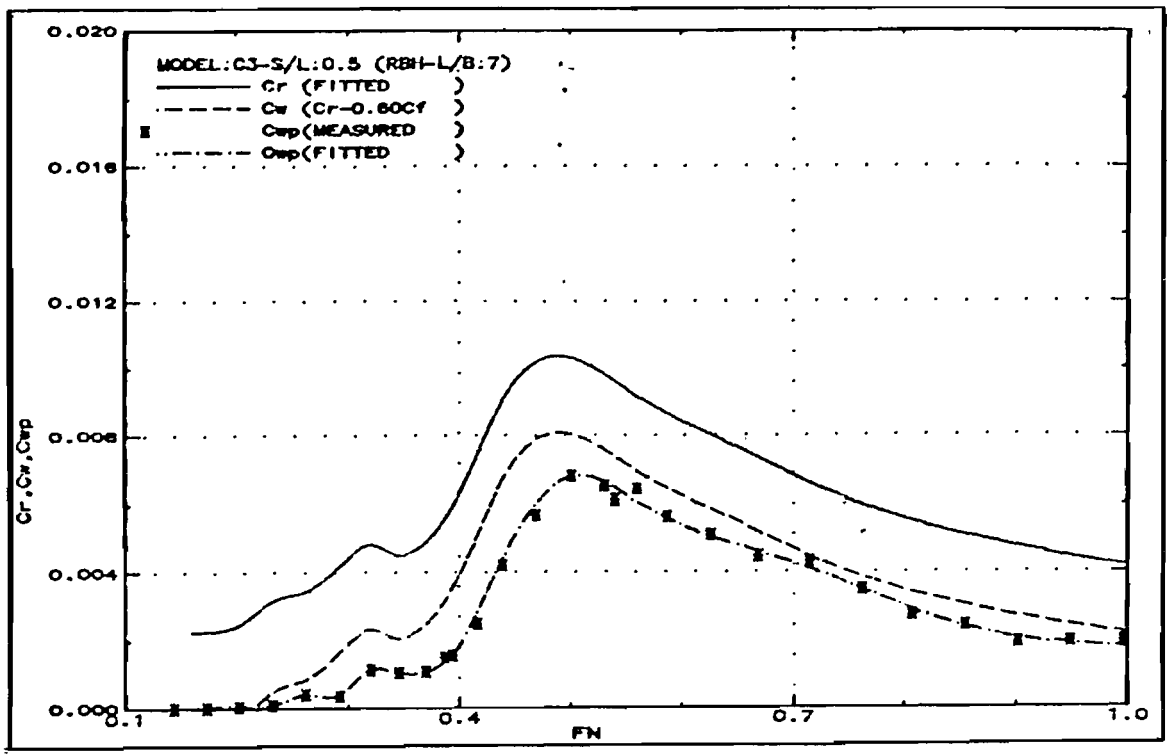

Fig.239: Measured wave resistance (C3-S/L:0.5)

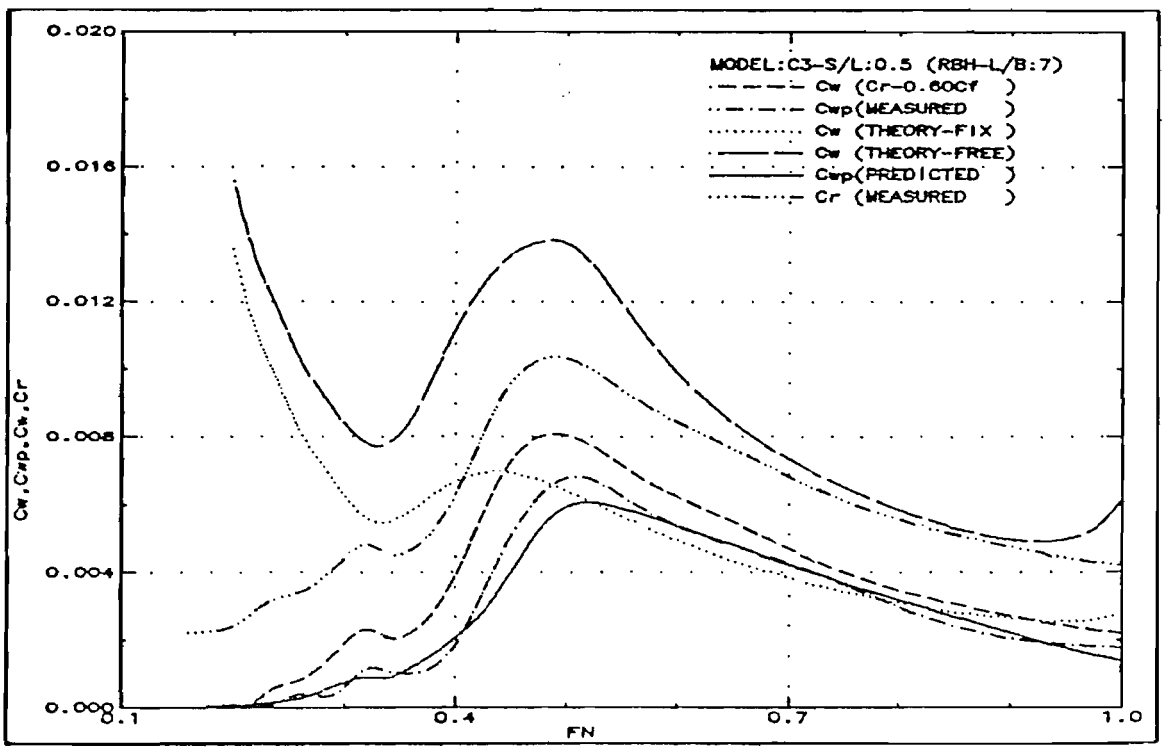

Fig.240: Wave resistance comparison (C3-S/L:0.5)

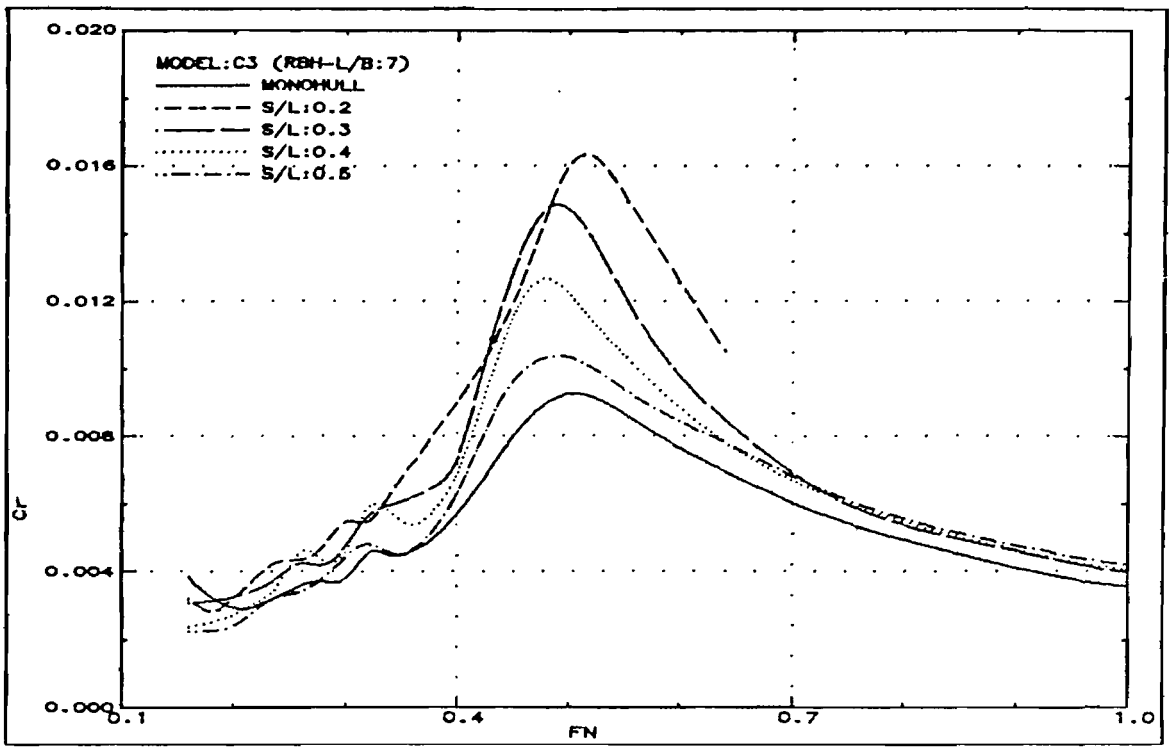

Fig.241: Residuary resistance (C3)

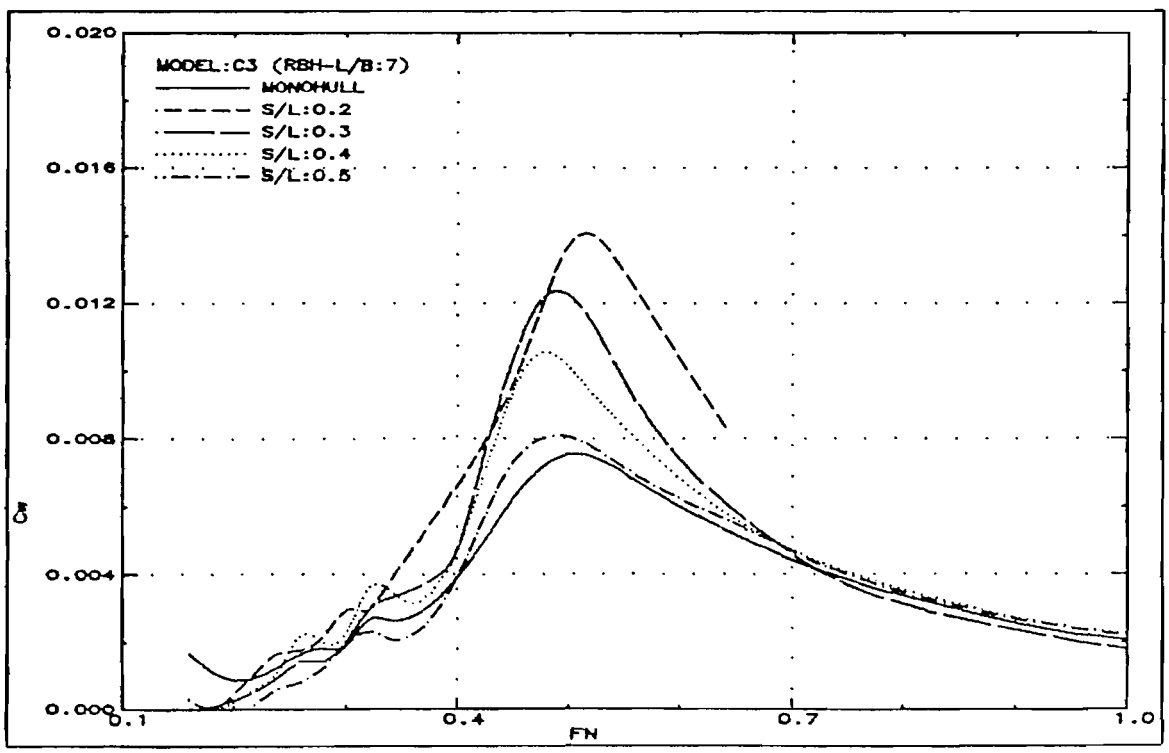

Fig.242: Wave resistance (C3)

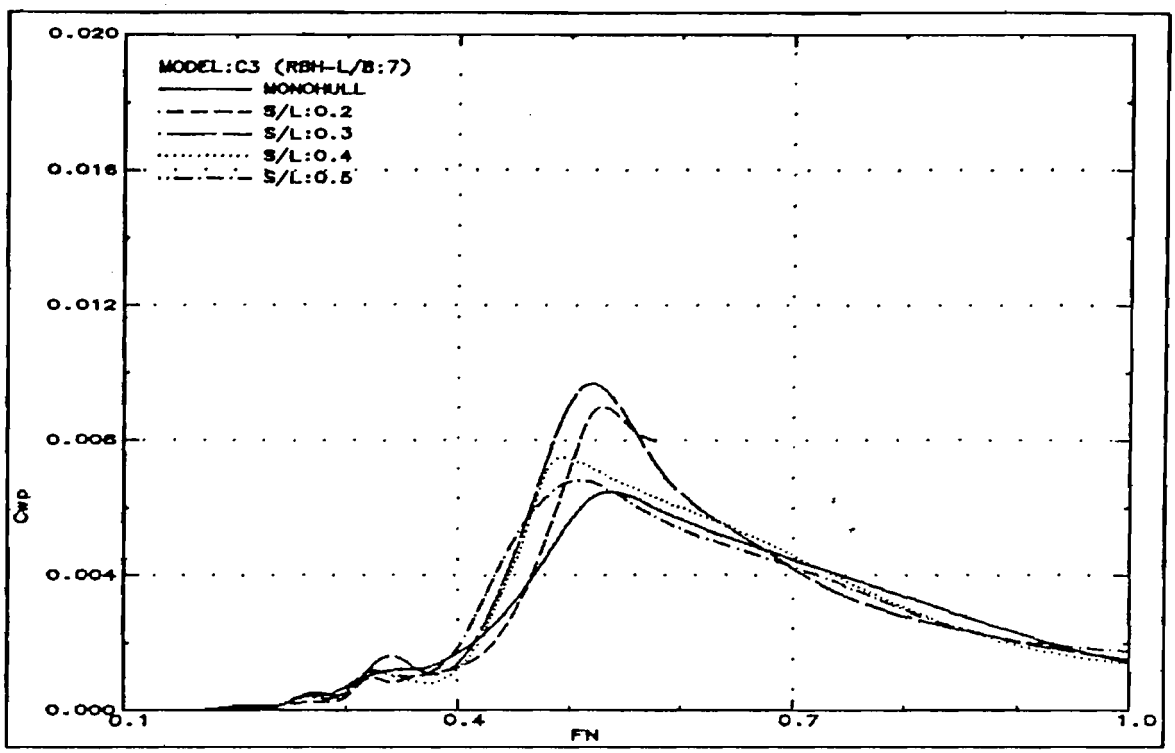

Fig.243: Wave pattern resistance (C3)

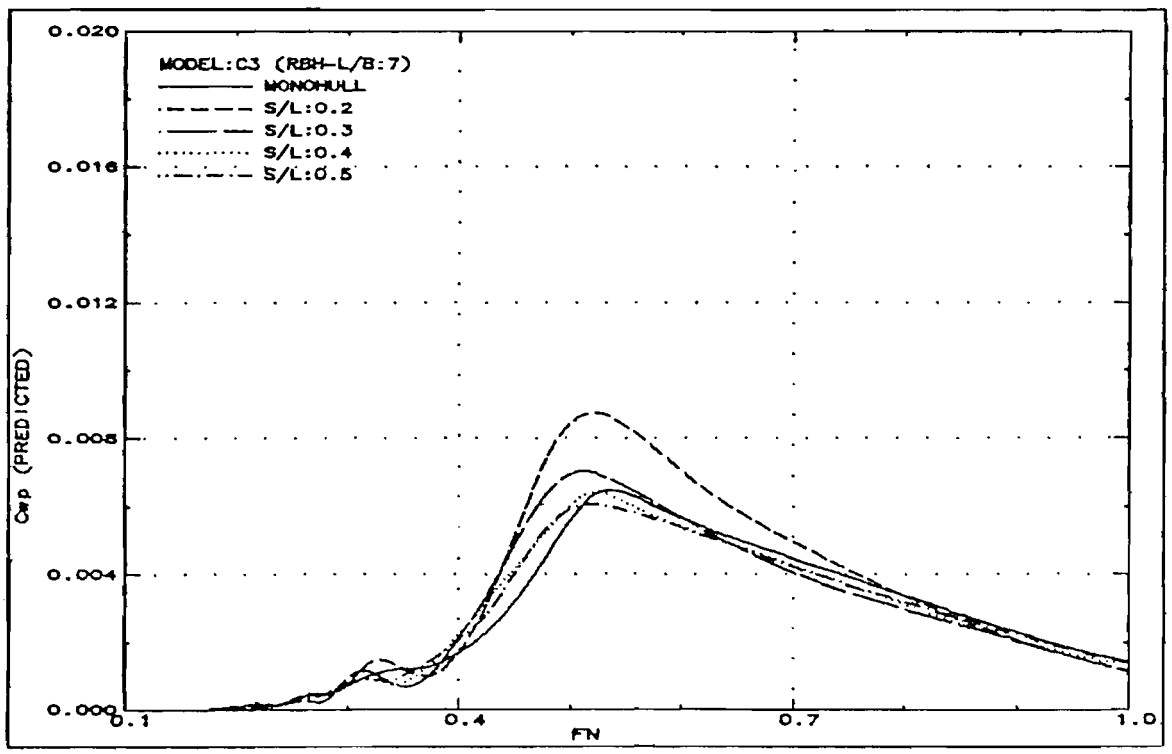

Fig.244: Wave pattern resistance predicted from monohull wave pattern analysis (C3)

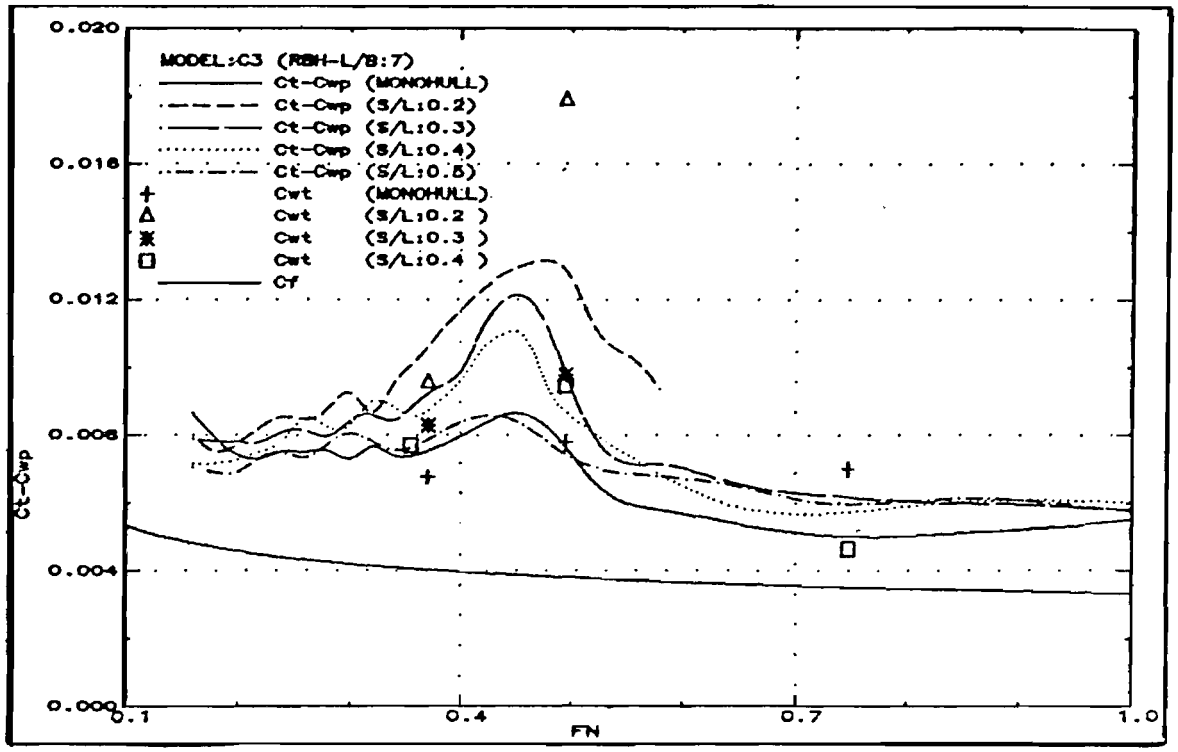

Fig.245: Total resistance minus wave pattern resistance (C3)

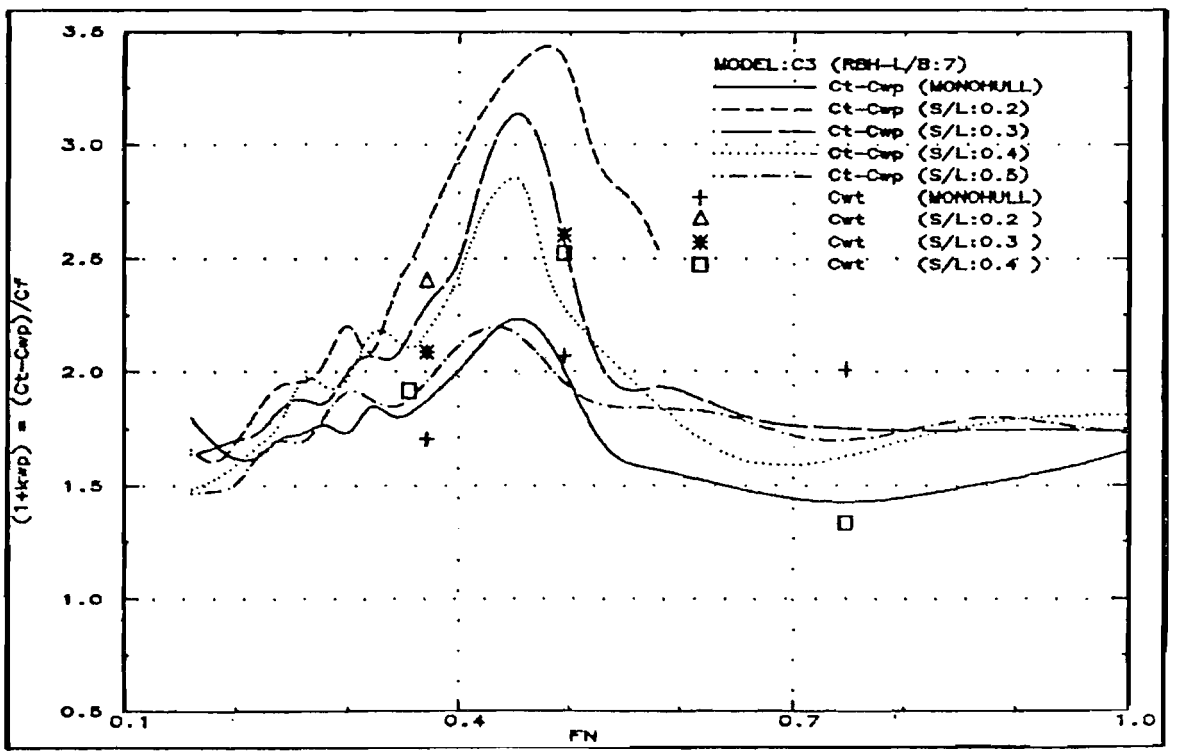

Fig.246: Form factor, i.e. $1+k_{WP}=(C_T-C_{WP})/C_F$ (C3)

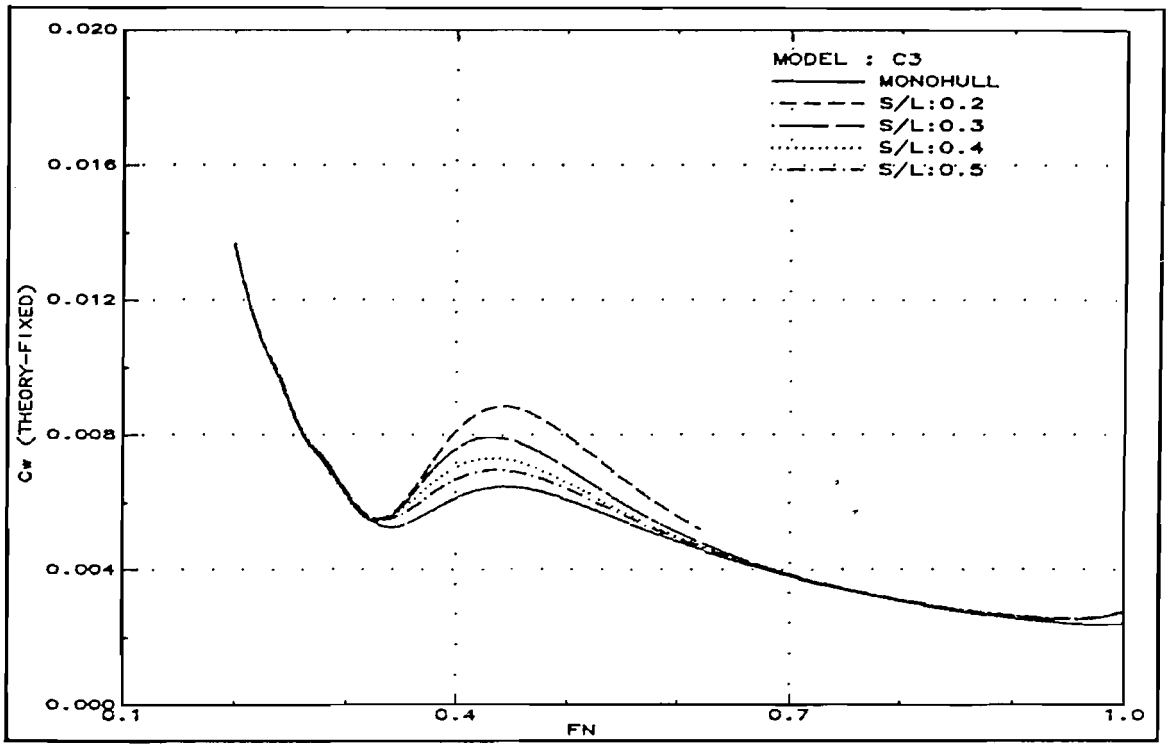

Fig.247: Theoretical wave resistance in fixed condition (C3)

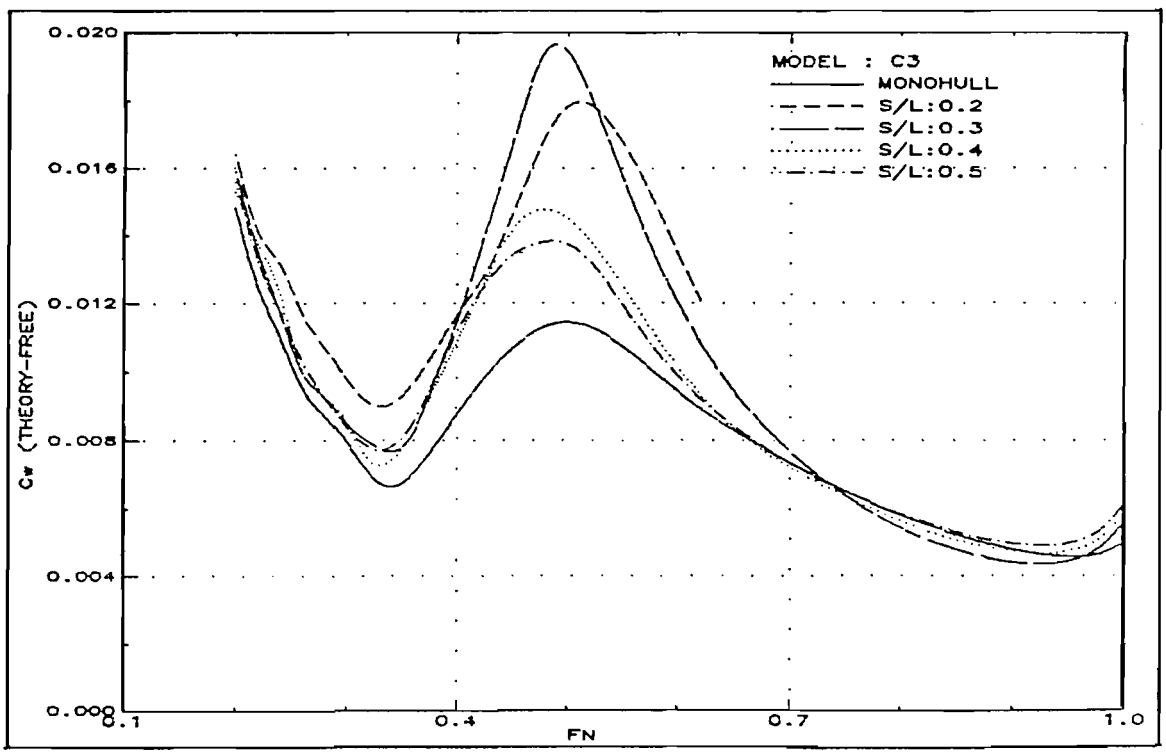

Fig.248: Theoretical wave resistance in free condition (C3)

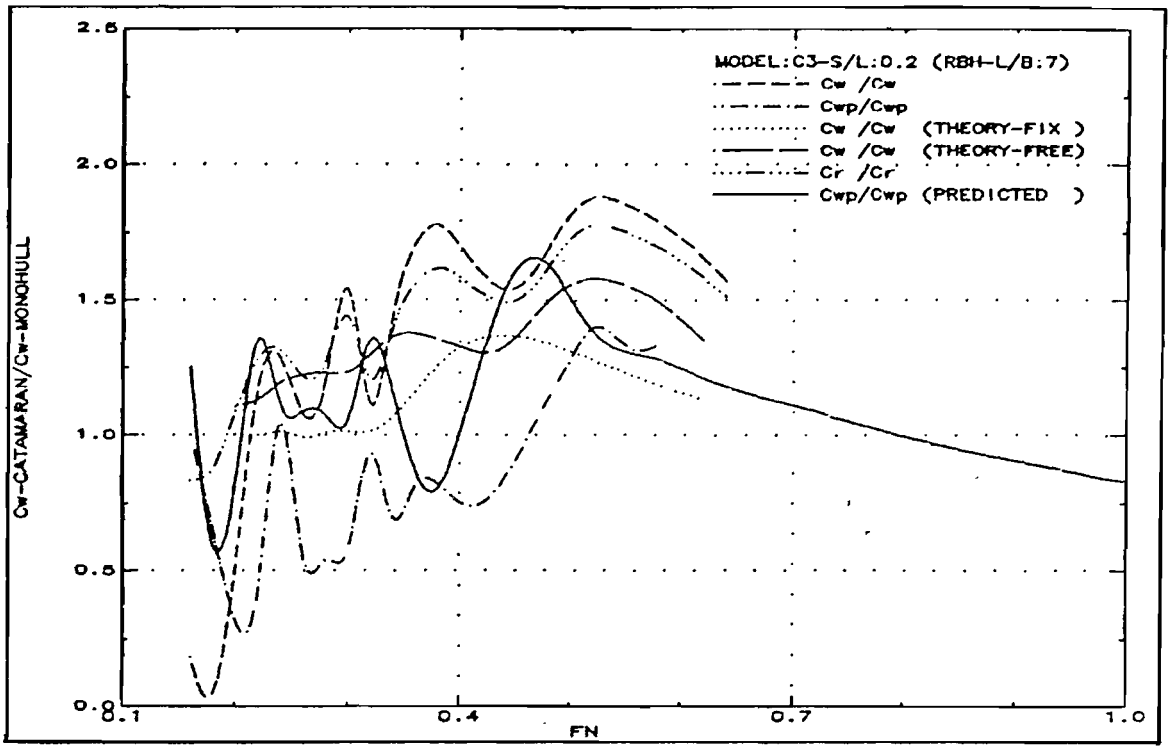

Fig.249: Wave resistance interference ratio (C3-S/L:0.2)

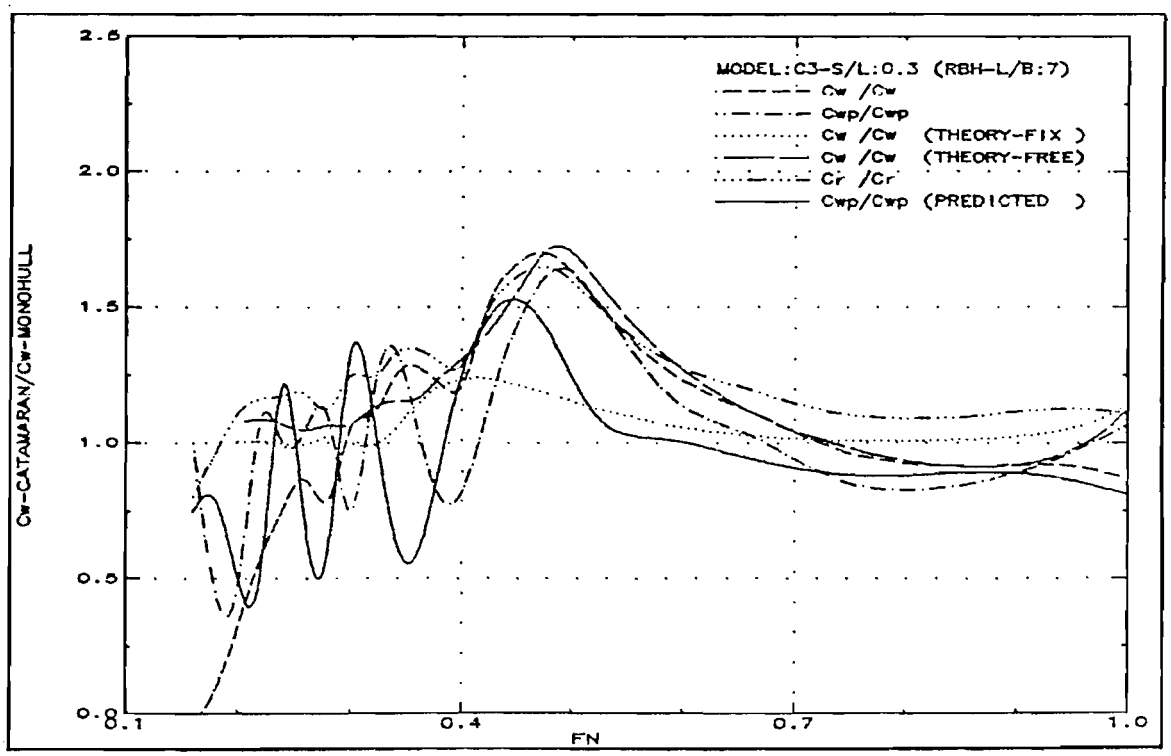

Fig.250: Wave resistance interference ratio (C3-S/L:0.3)

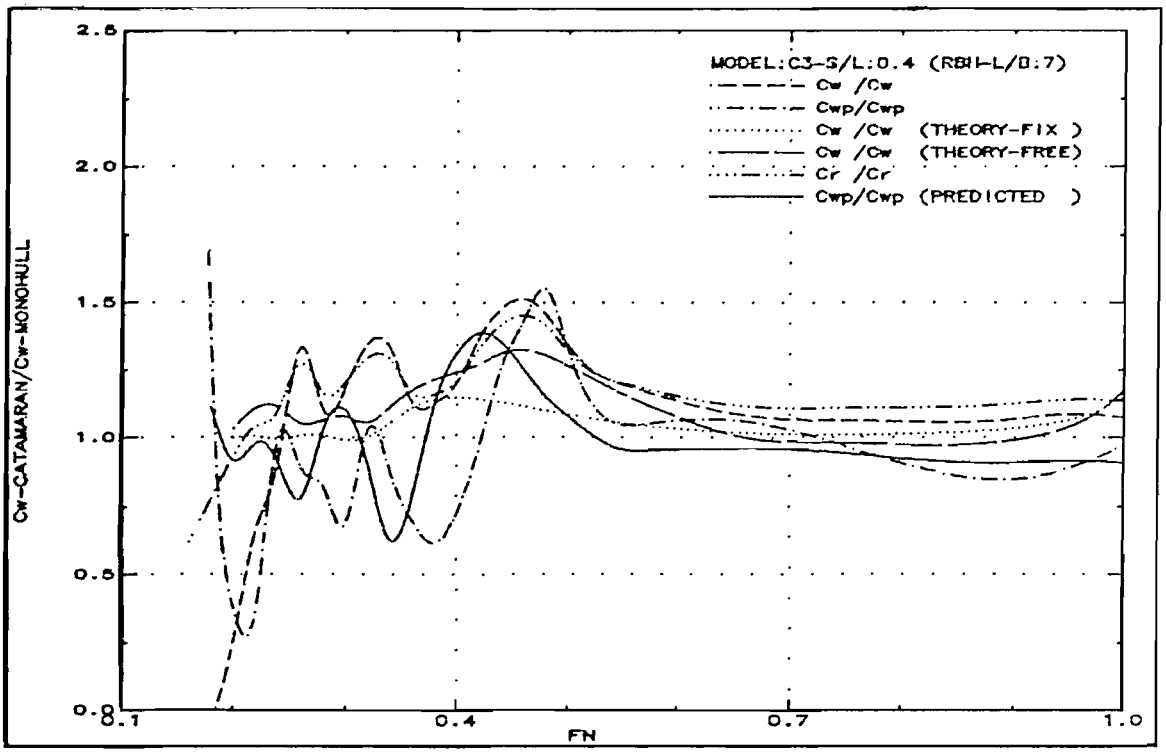

Fig.251: Wave resistance interference ratio (C3-S/L:0.4)

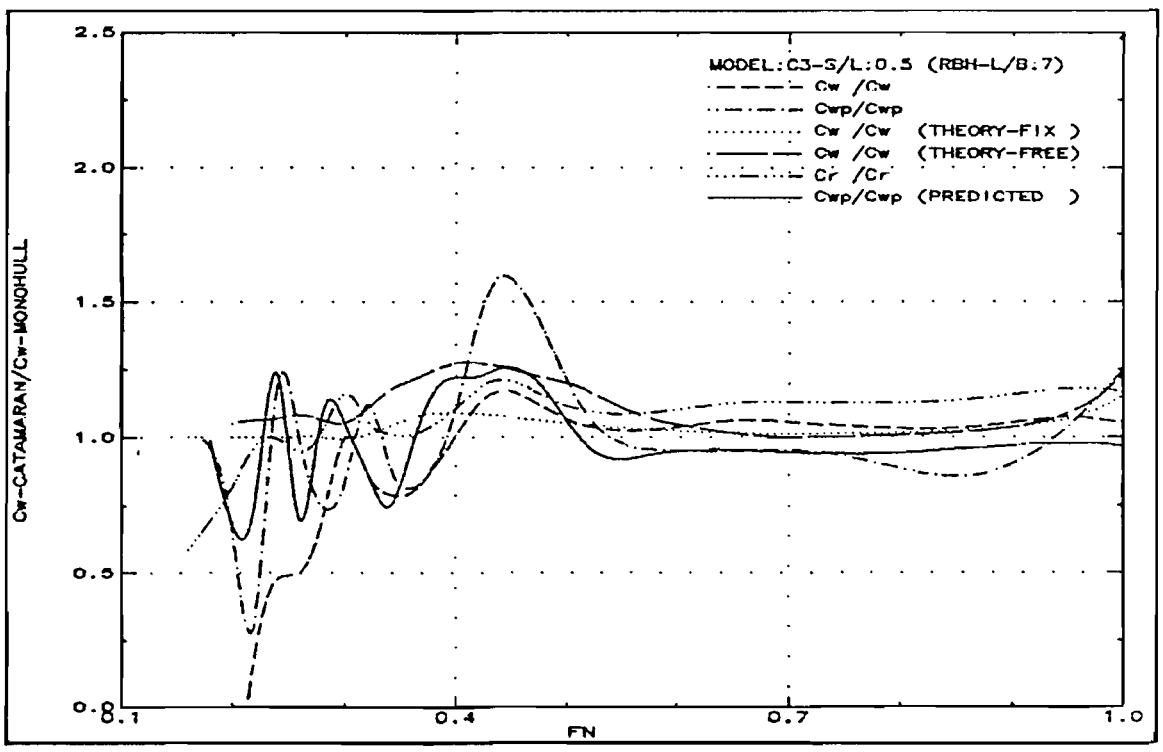

Fig.252: Wave resistance interference ratio (C3-S/L:0.5)

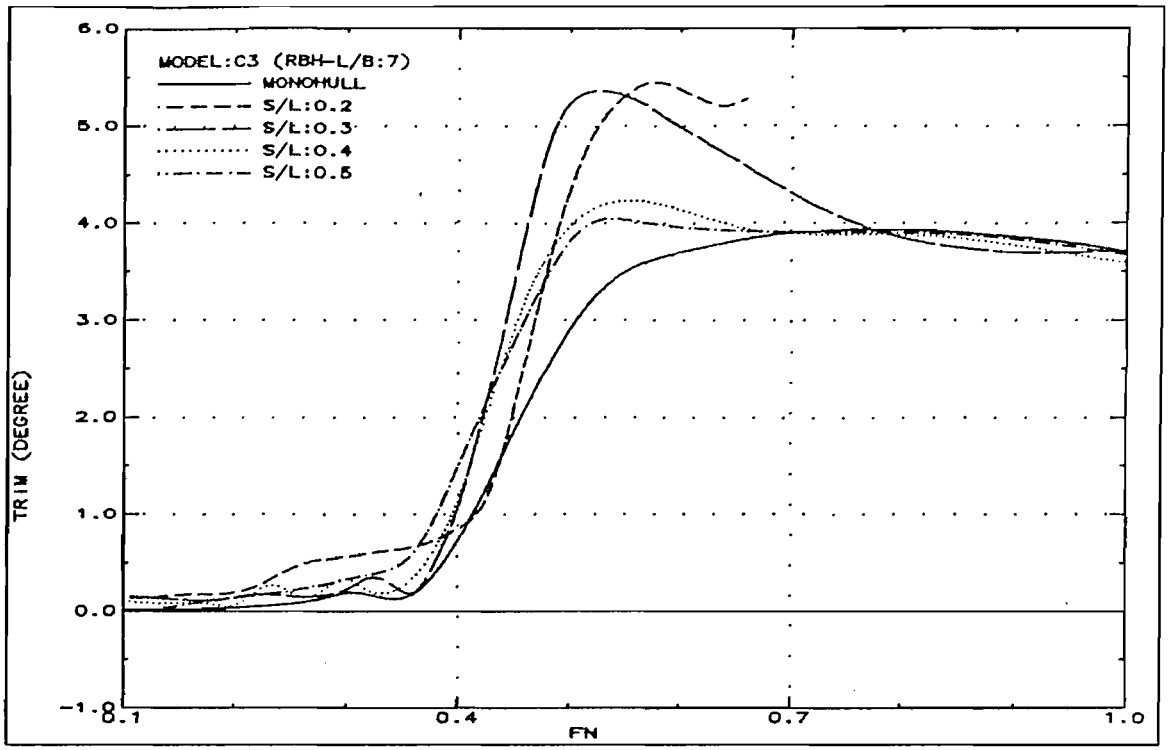

Fig.253: Running trim (C3)

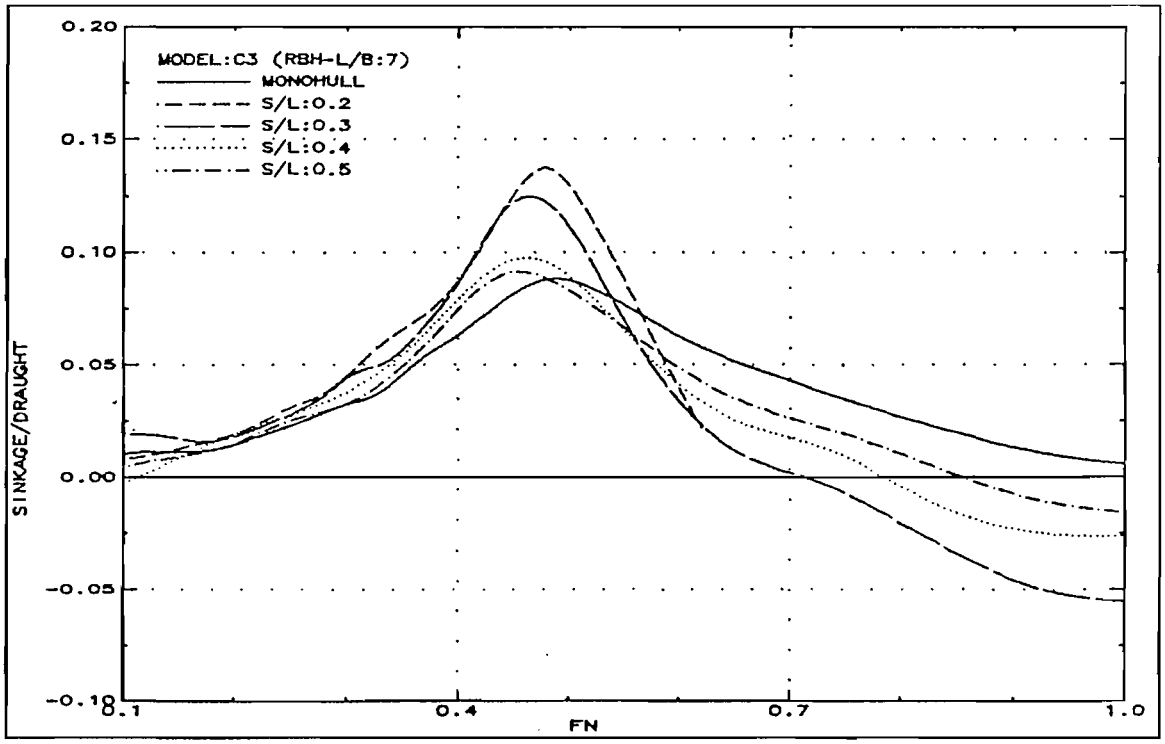

Fig.254: Sinkage (C3)

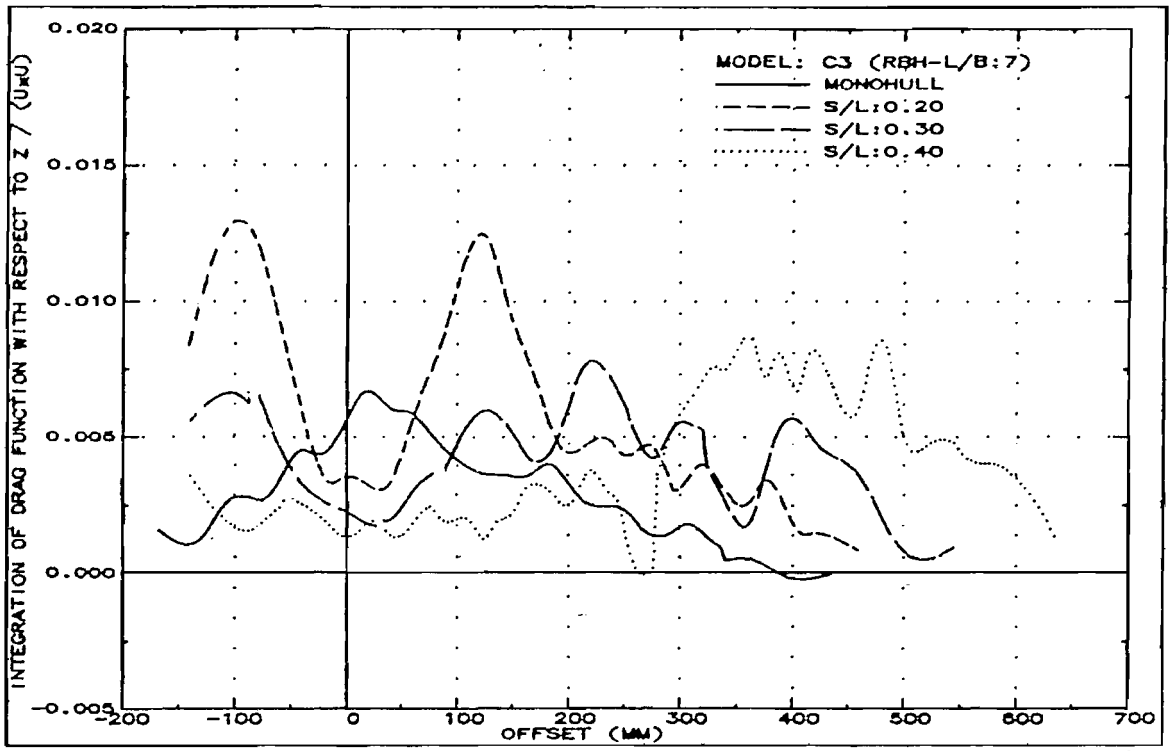

Fig.255: Integration of drag function with respect to z (C3-Fn:0.35)

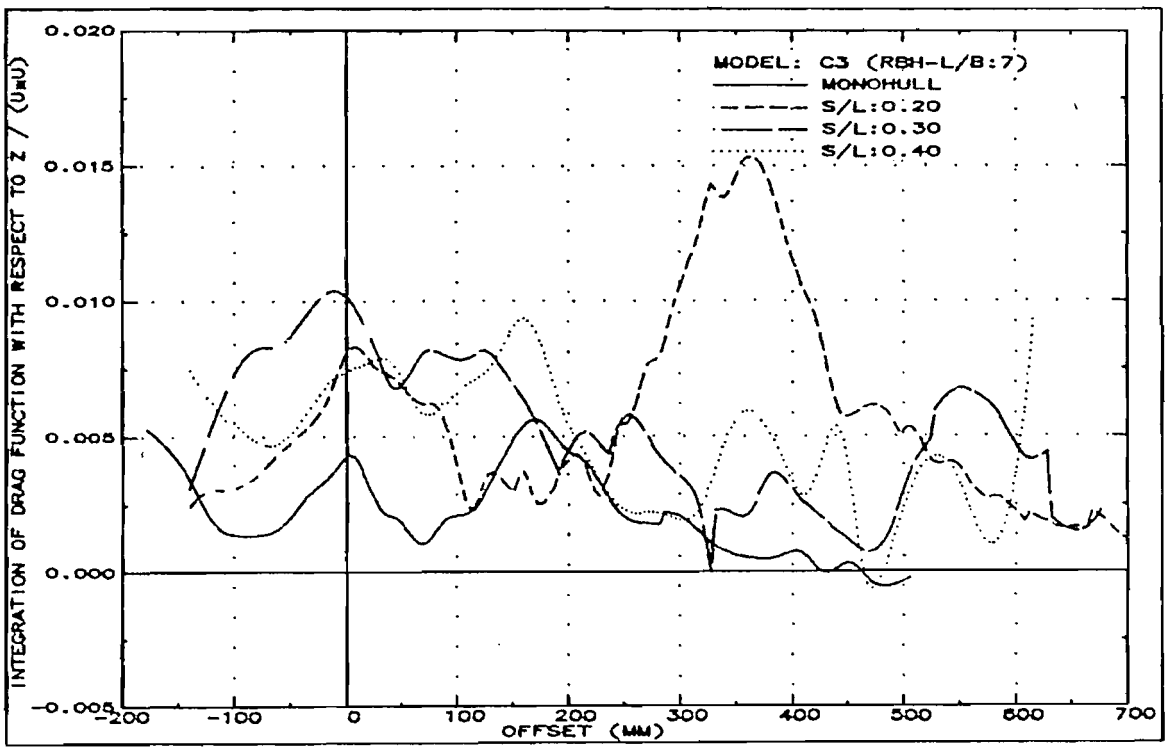

Fig.256: Integration of drag function with respect to z (C3-Fn:0.50)

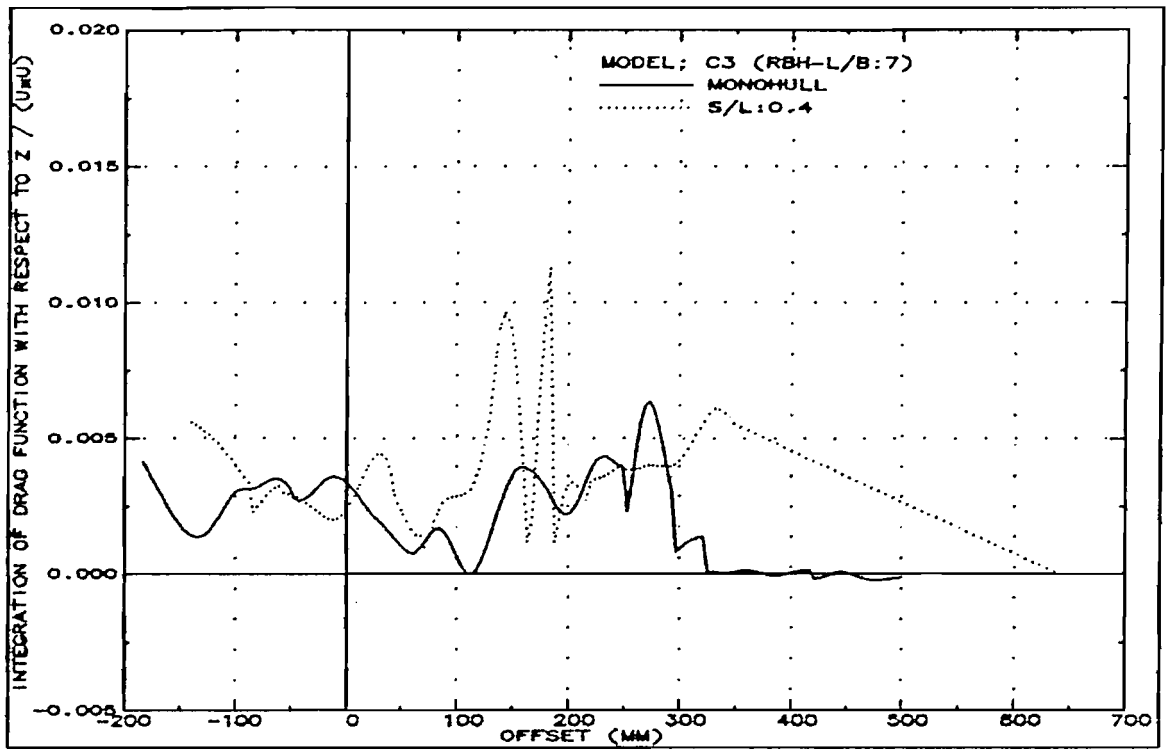

Fig.257: Integration of drag function with respect to z (C3-Fn:0.75)

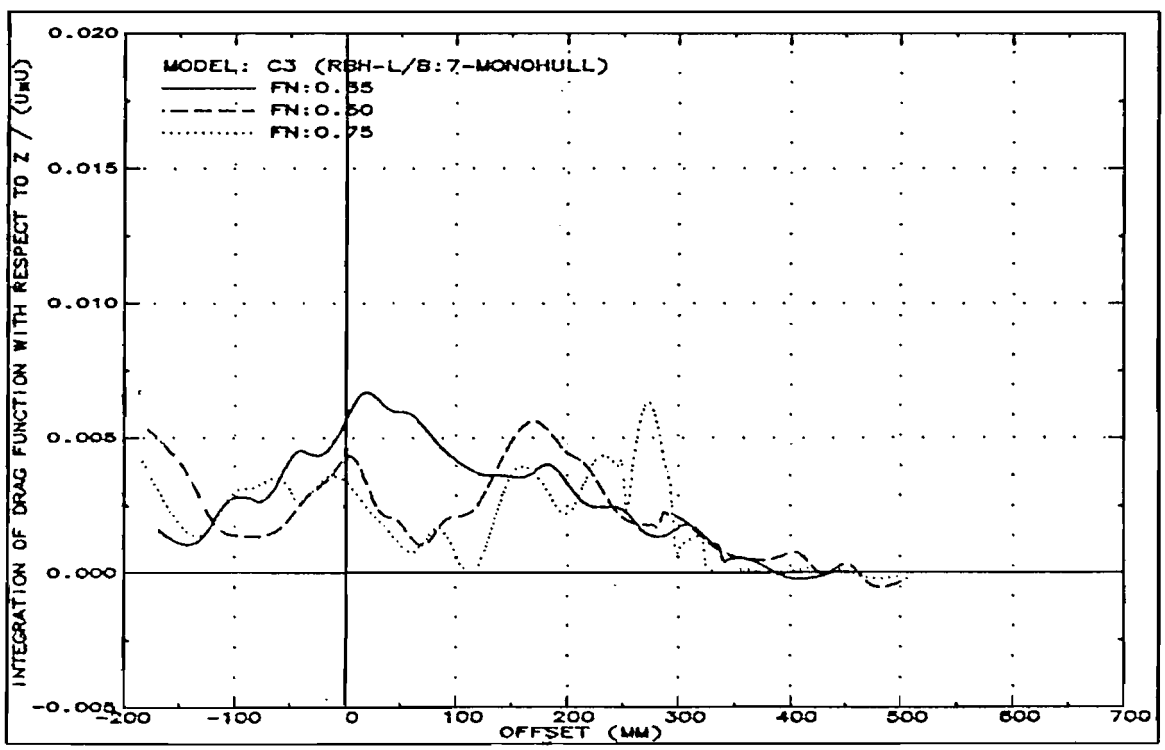

Fig.258: Integration of drag function with respect to z (C3-Monohull)

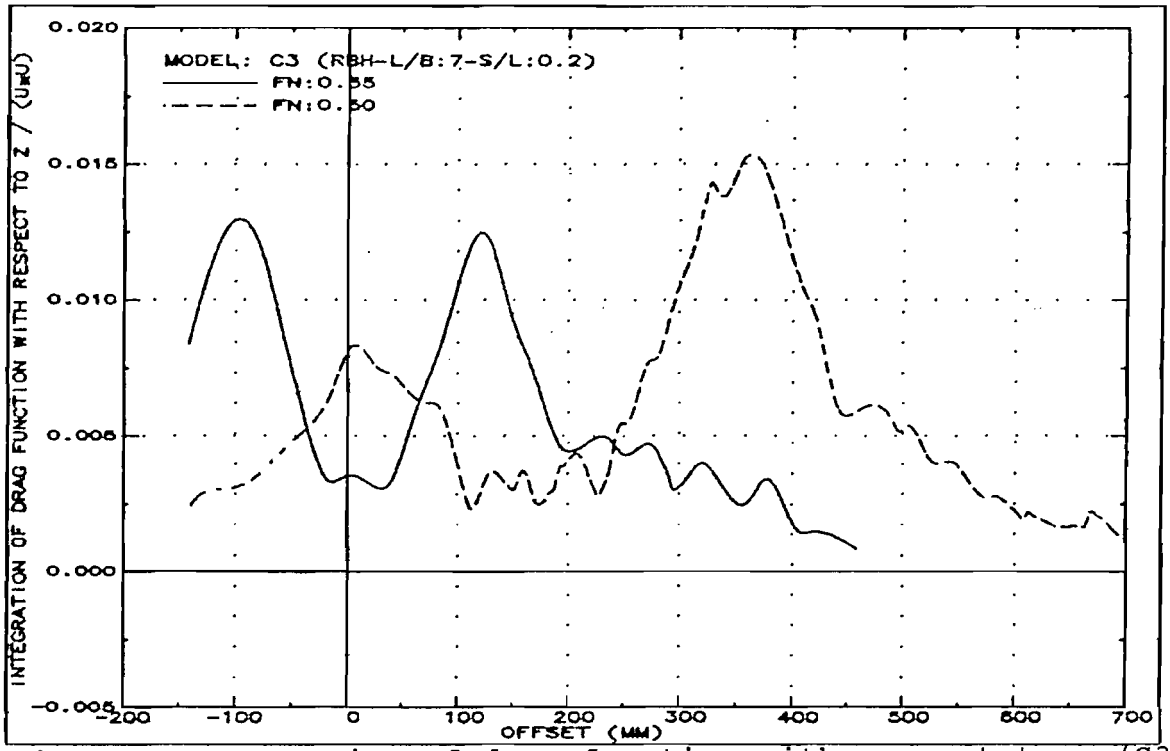

Fig.259: Integration of drag function with respect to z (C3-S/L:0.2)

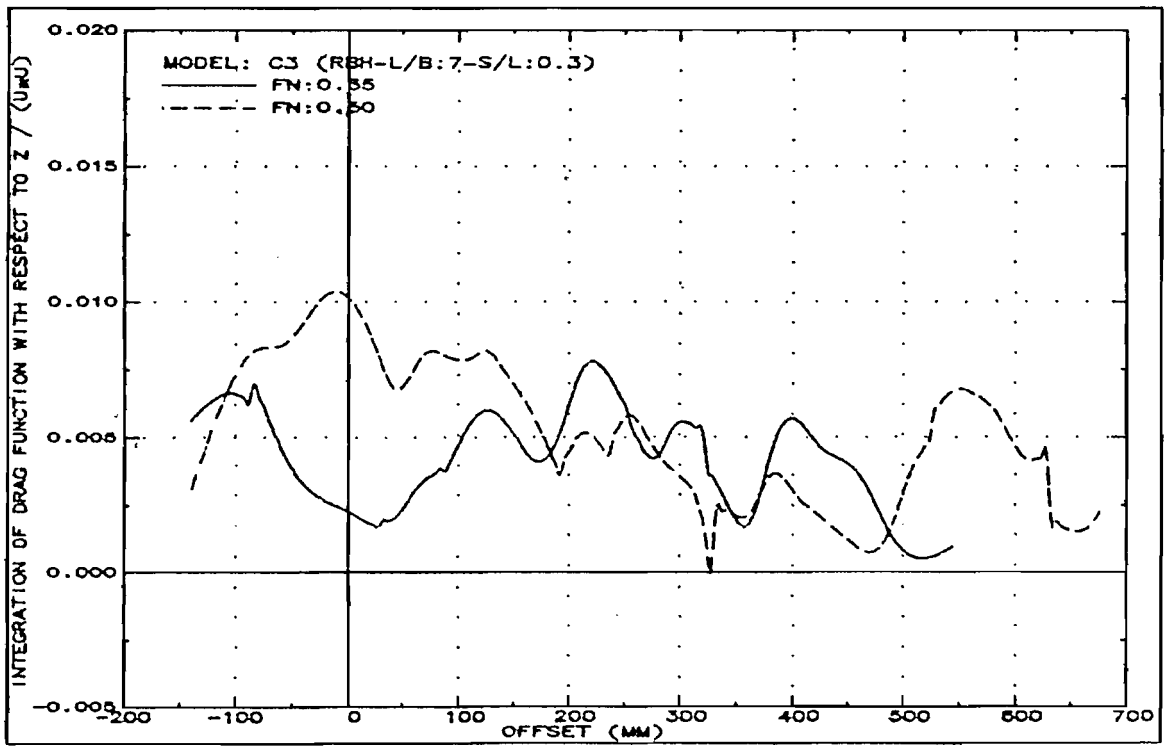

Fig.260: Integration of drag function with respect to z (C3-S/L:0.3)

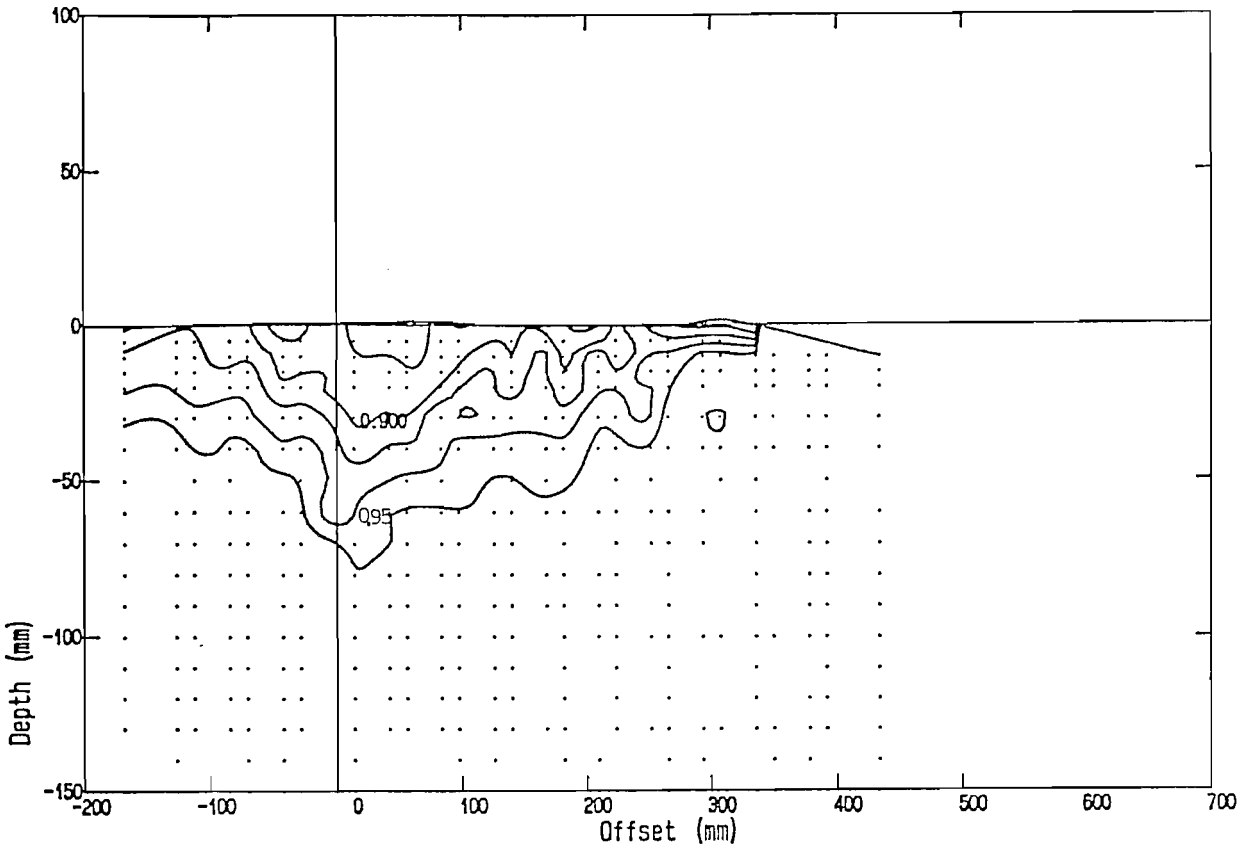

Fig.261: Wake contours at Fn:0.35 (C3-Monohull)

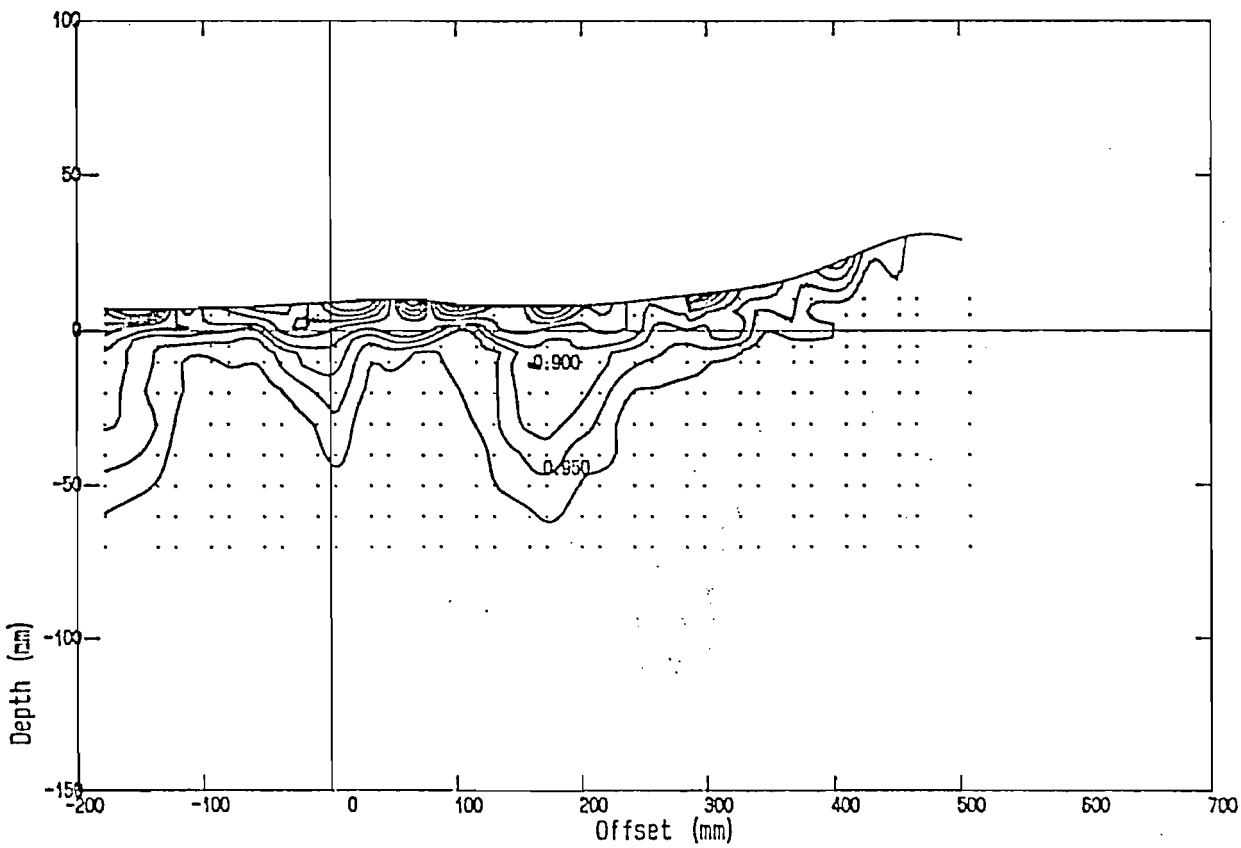

Fig.262: Wake contours at Fn:0.50 (C3-Monohull)

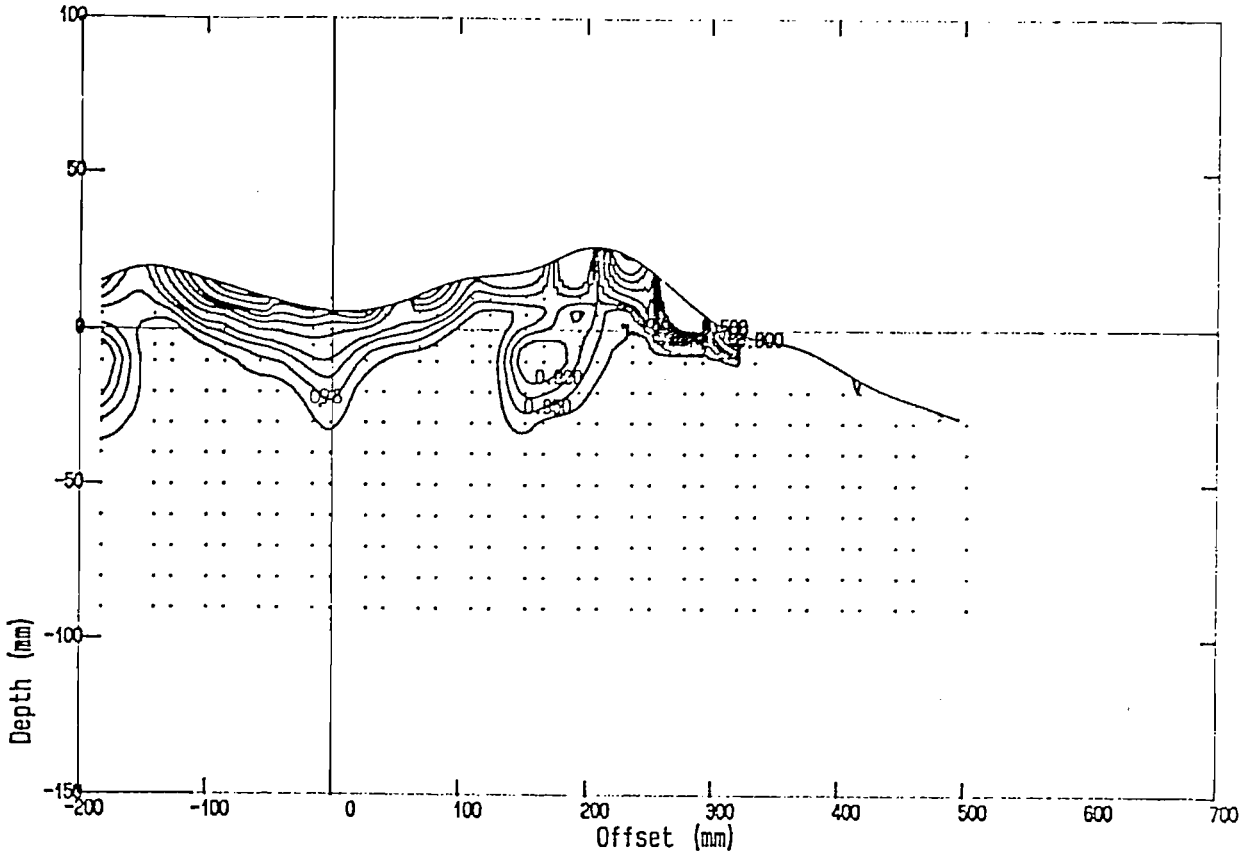

Fig.263: Wake contours at Fn:Ø.75 (C3-Monohull)

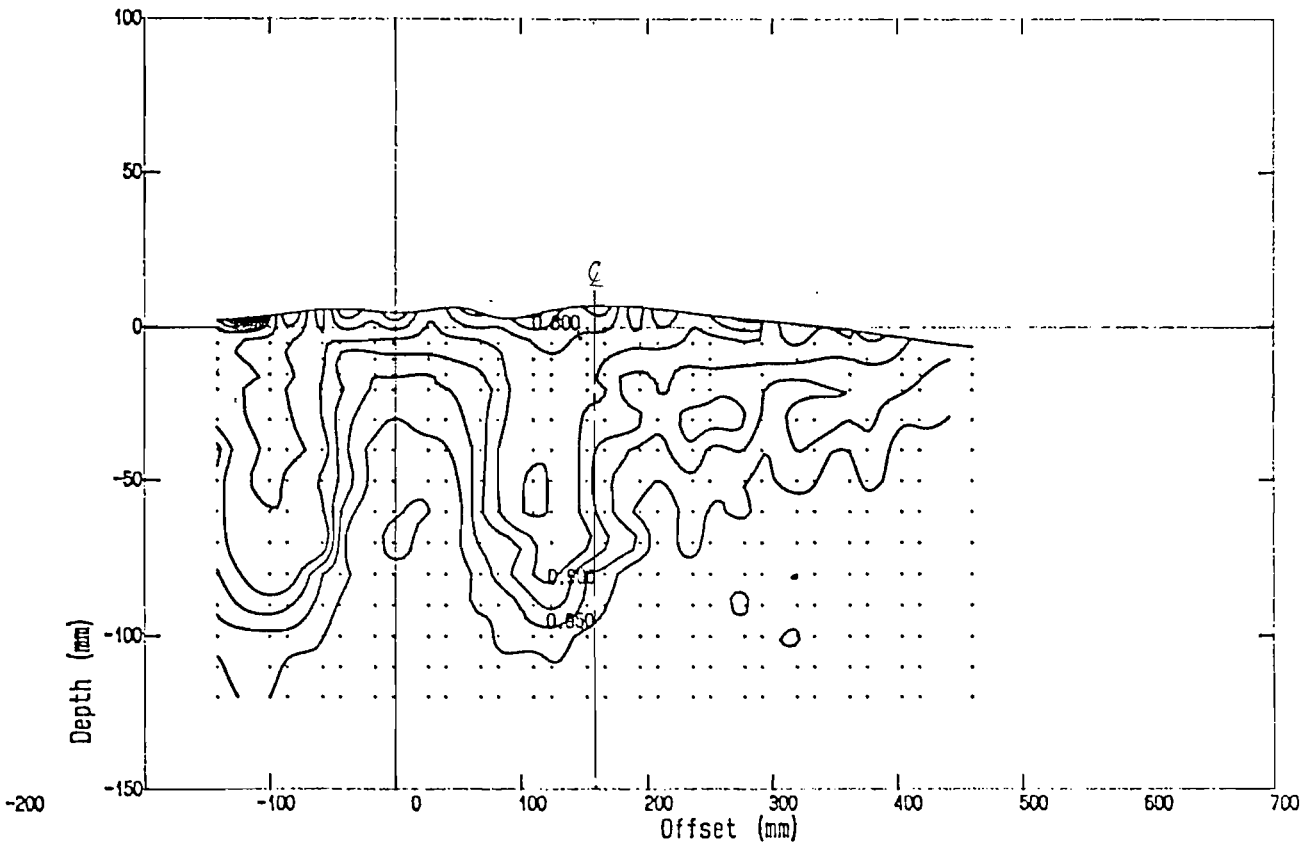

Fig.264: Wake contours at Fn:Ø.35 (C3-S/L:Ø.2)

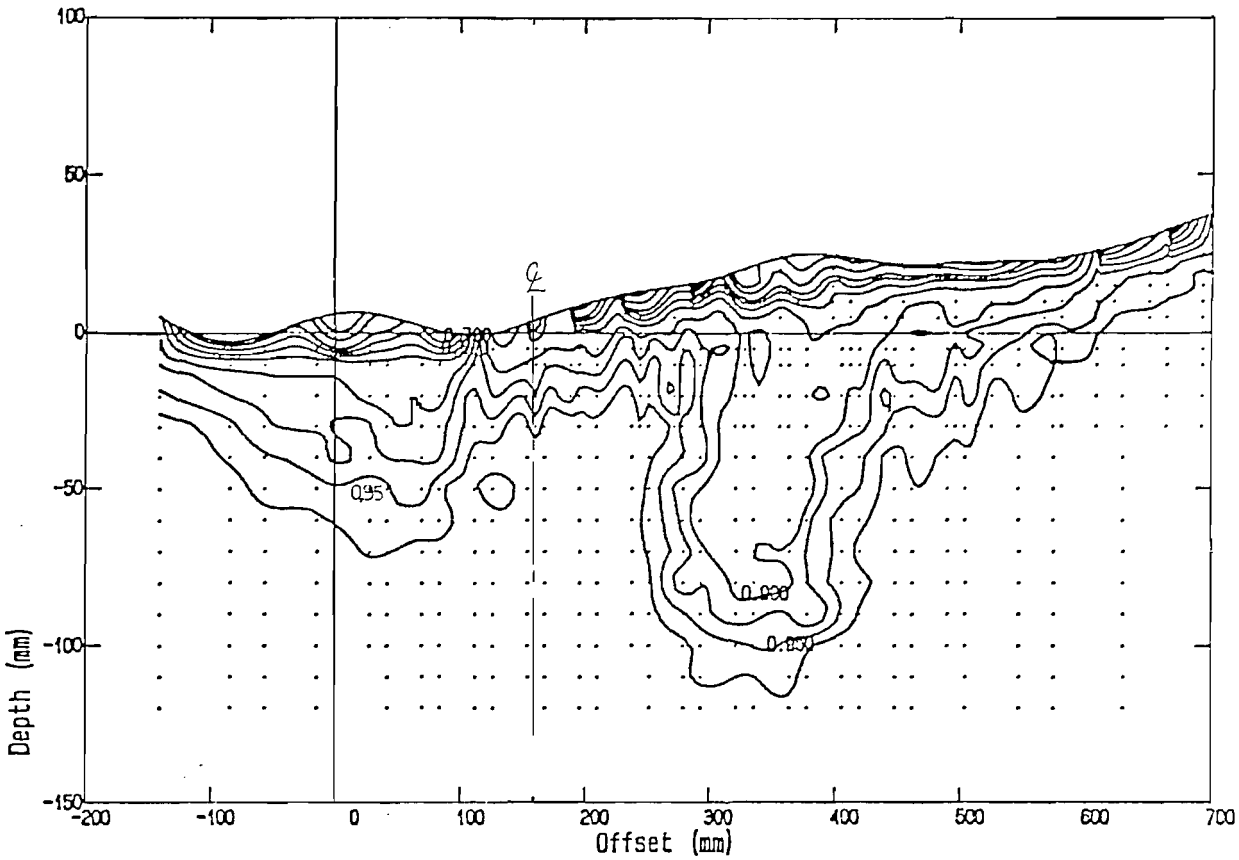

Fig.265: Wake contours at Fn:0.50 (C3-S/L:0.2)

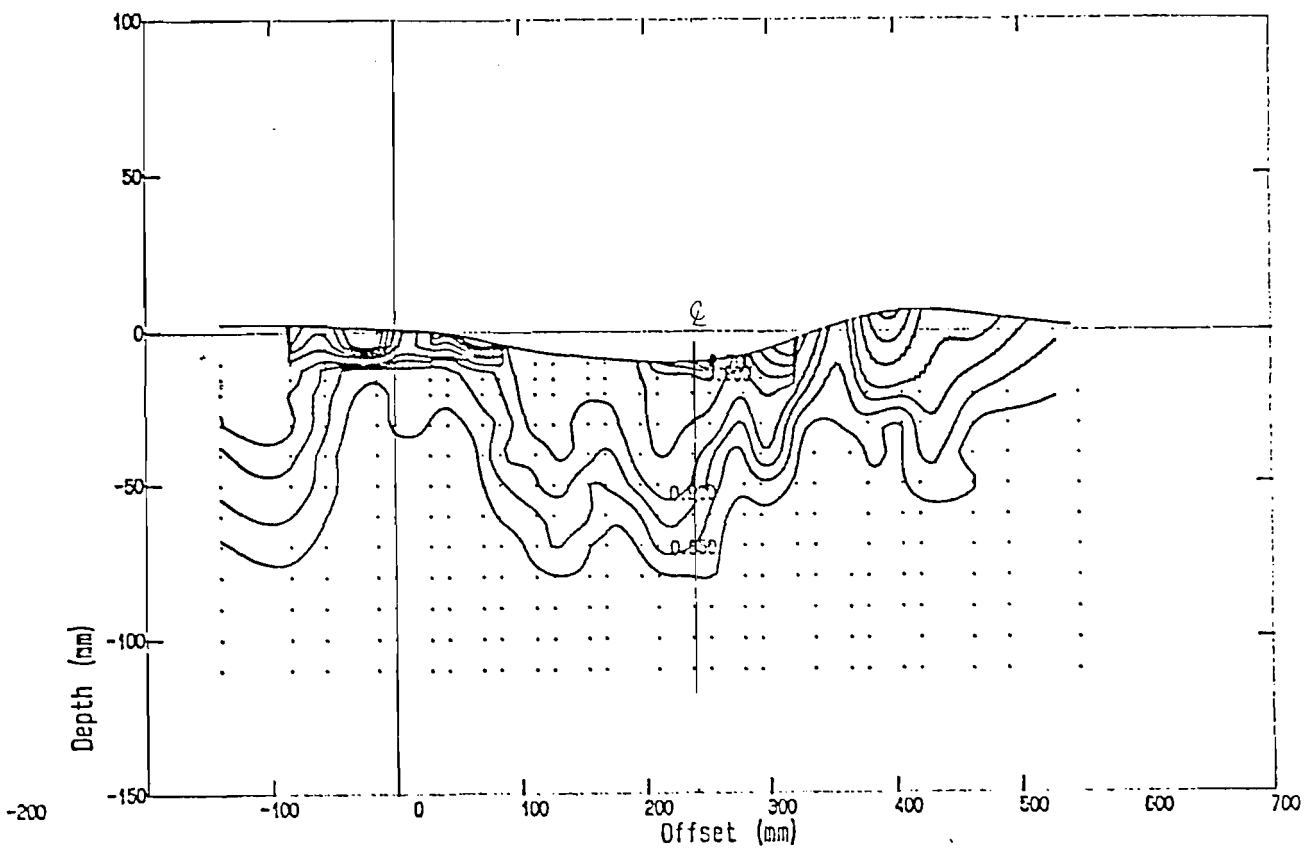

Fig.266: Wake contours at Fn:0.35 (C3-S/L:0.3)

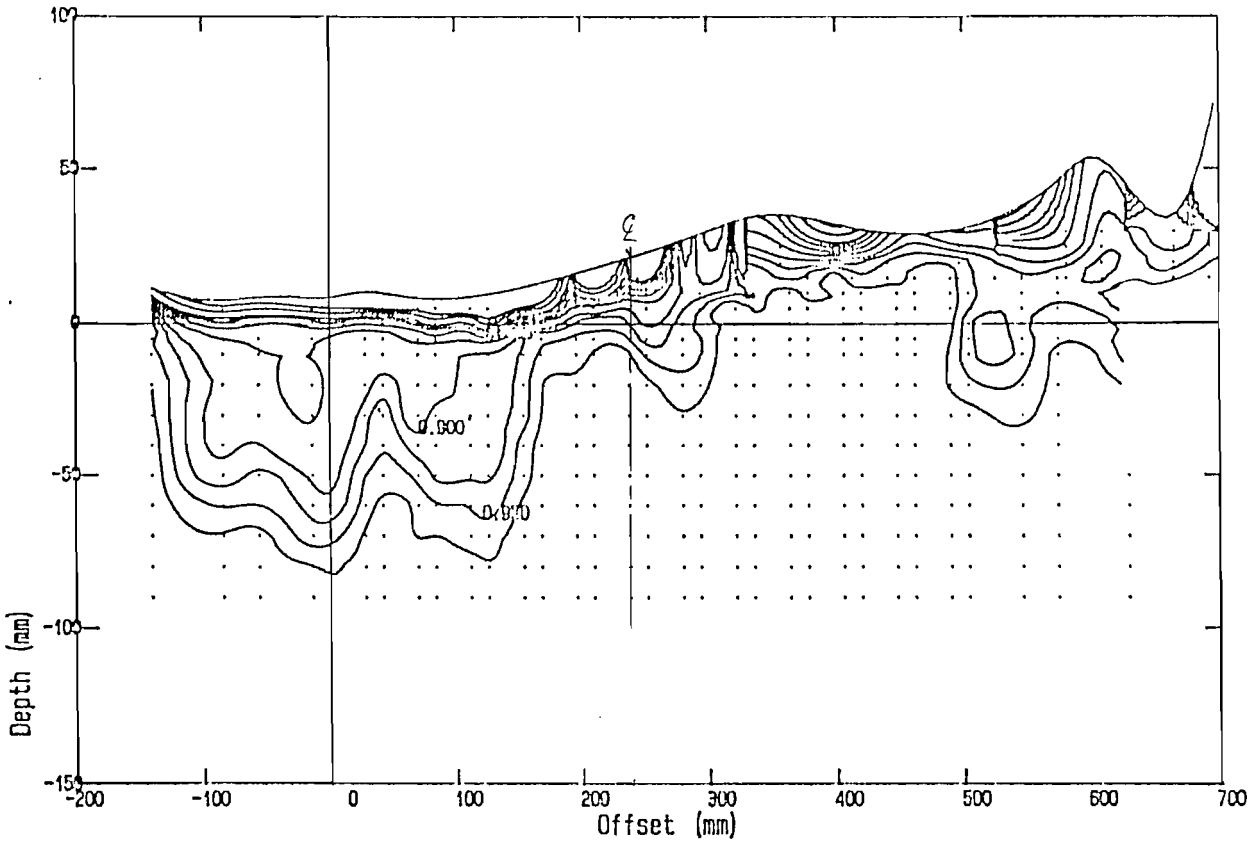

Fig.267: Wake contours at Fn:0.50 (C3-S/L:0.3)

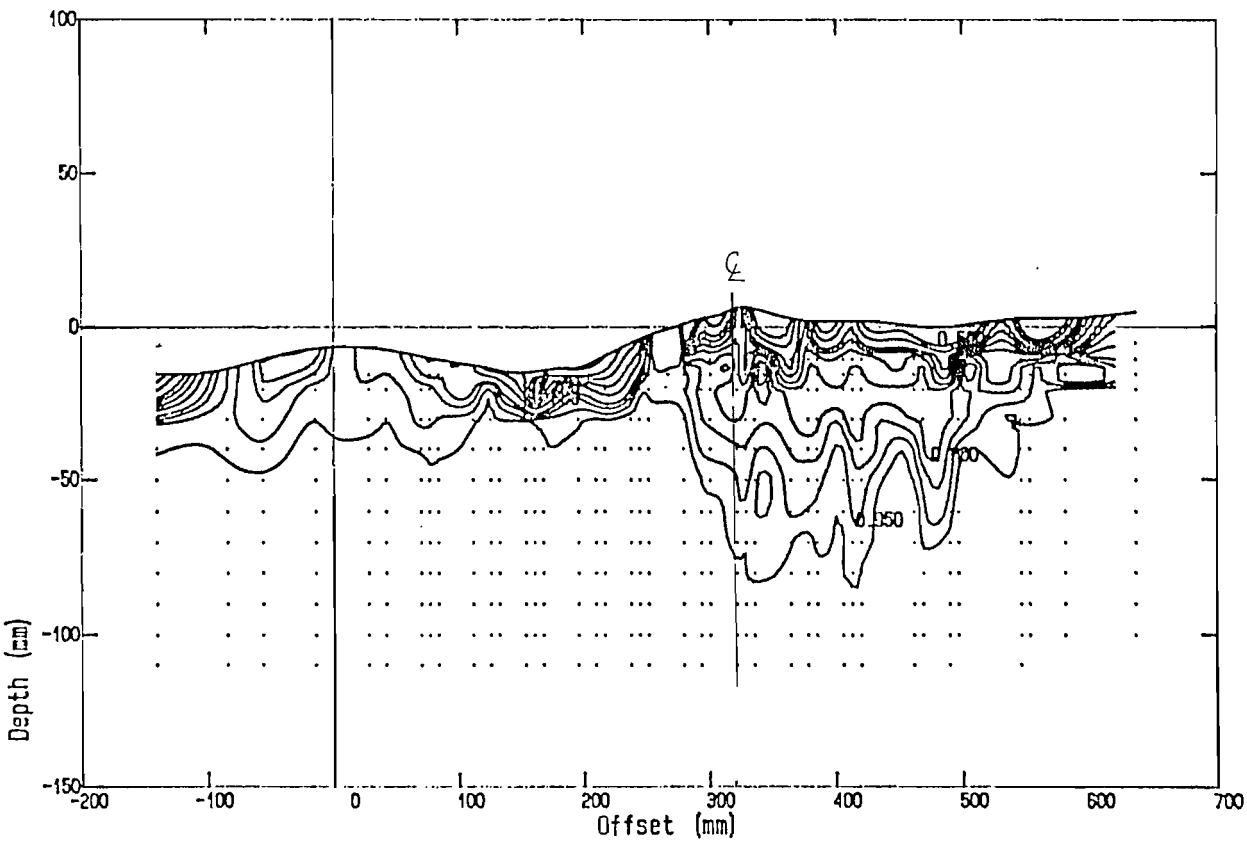

Fig.268: Wake contours at Fn:0.35 (C3-S/L:0.4)

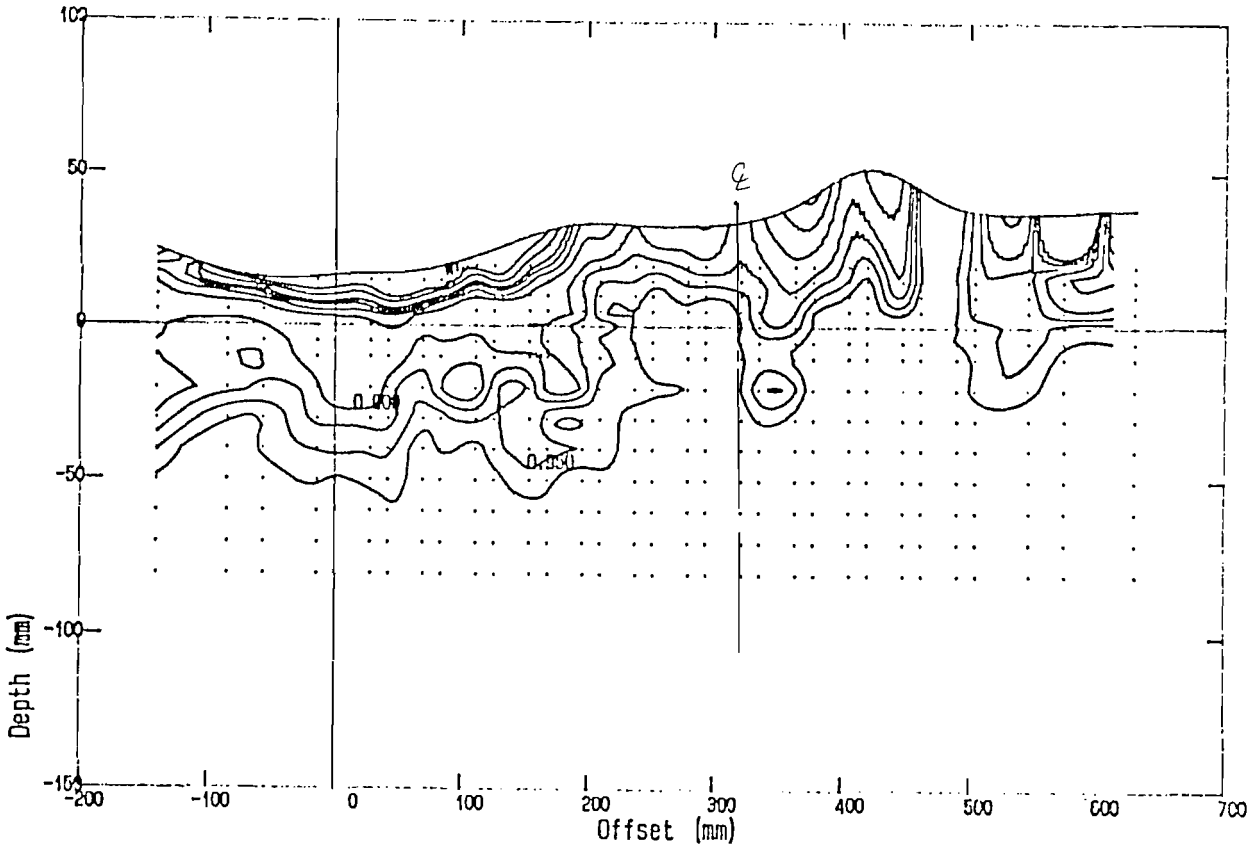

Fig.269: Wake contours at Fn:0.50 (C3-S/L:0.4)

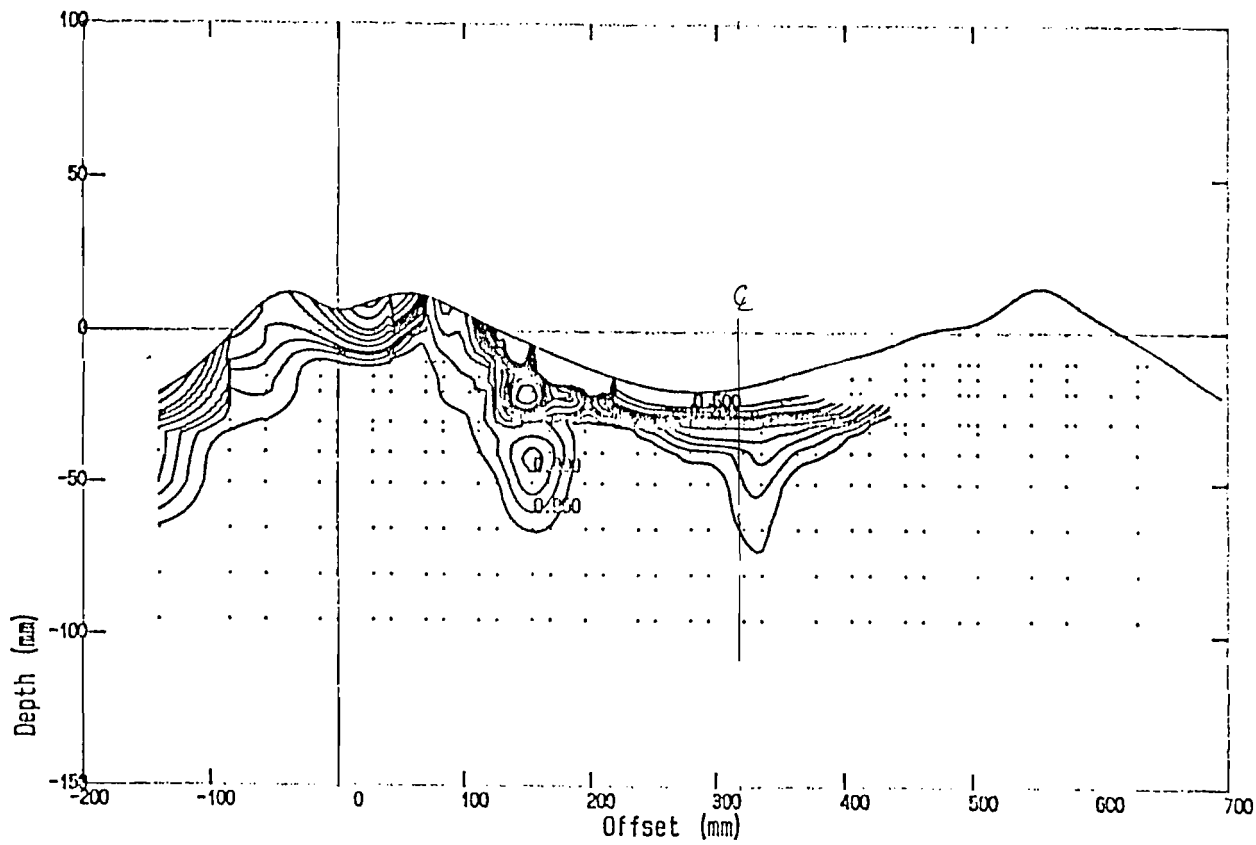

Fig.270: Wake contours at Fn:0.75 (C3-S/L:0.4)

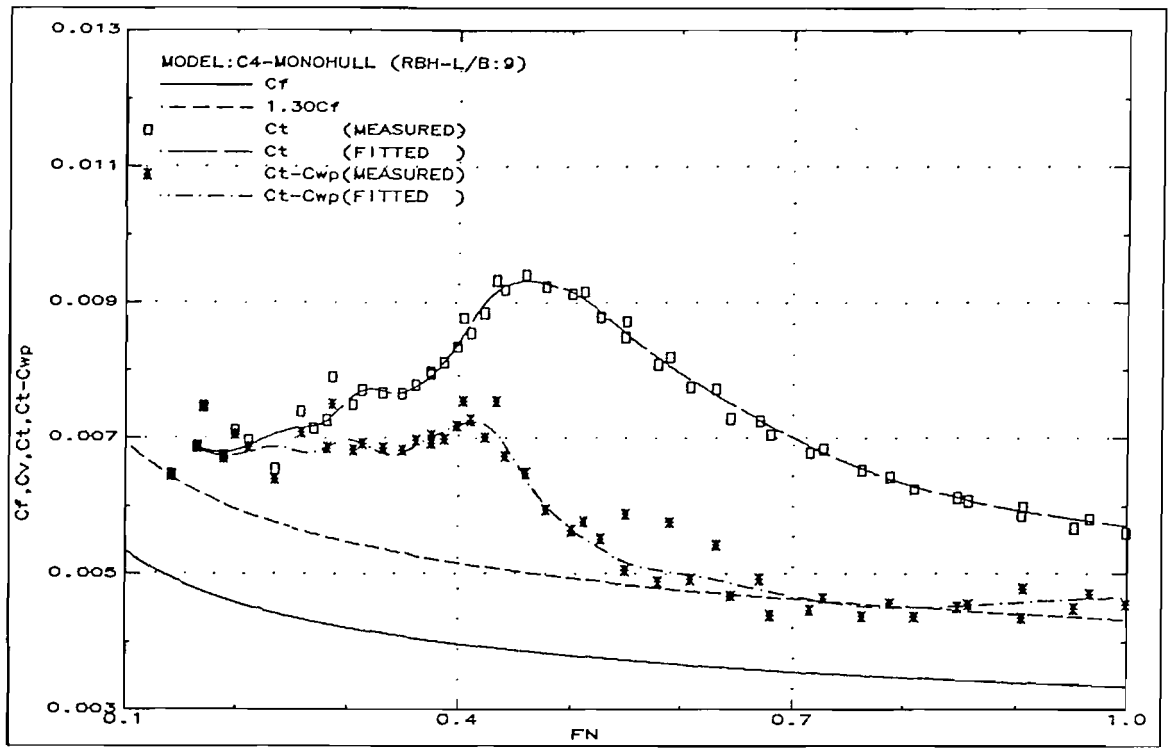

Fig.271: Resistance components (C4-Monohull)

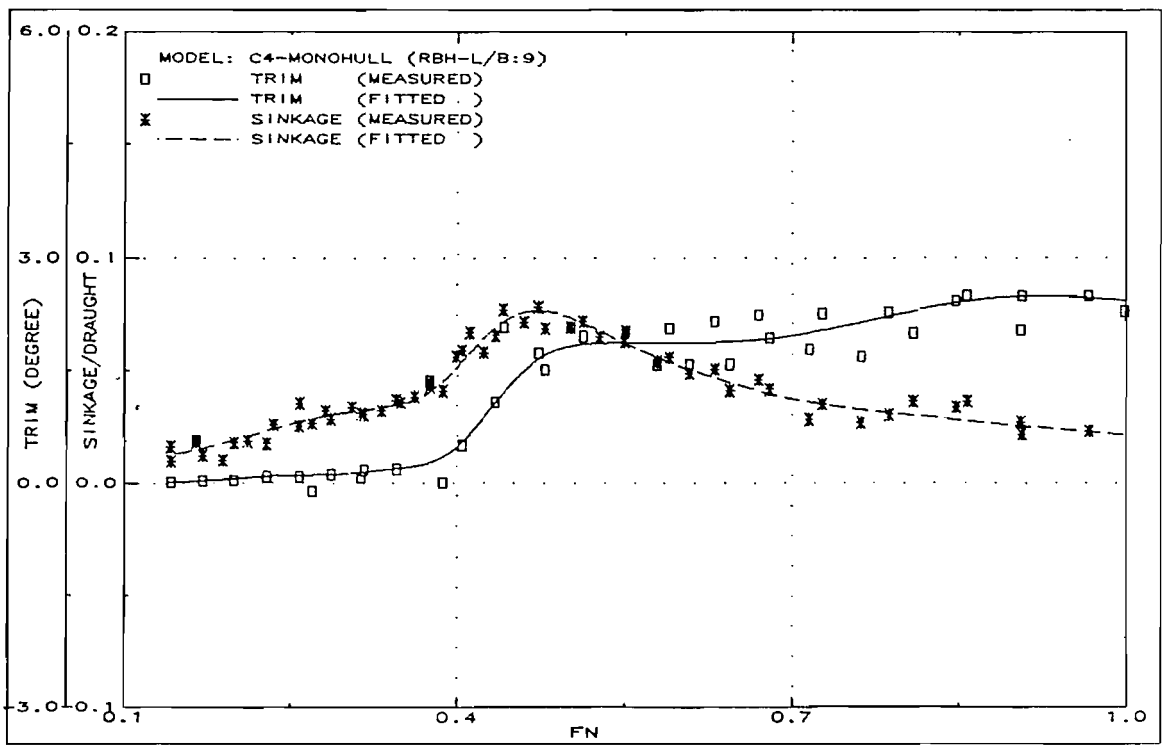

Fig.272: Running trim and sinkage (C4-Monohull)

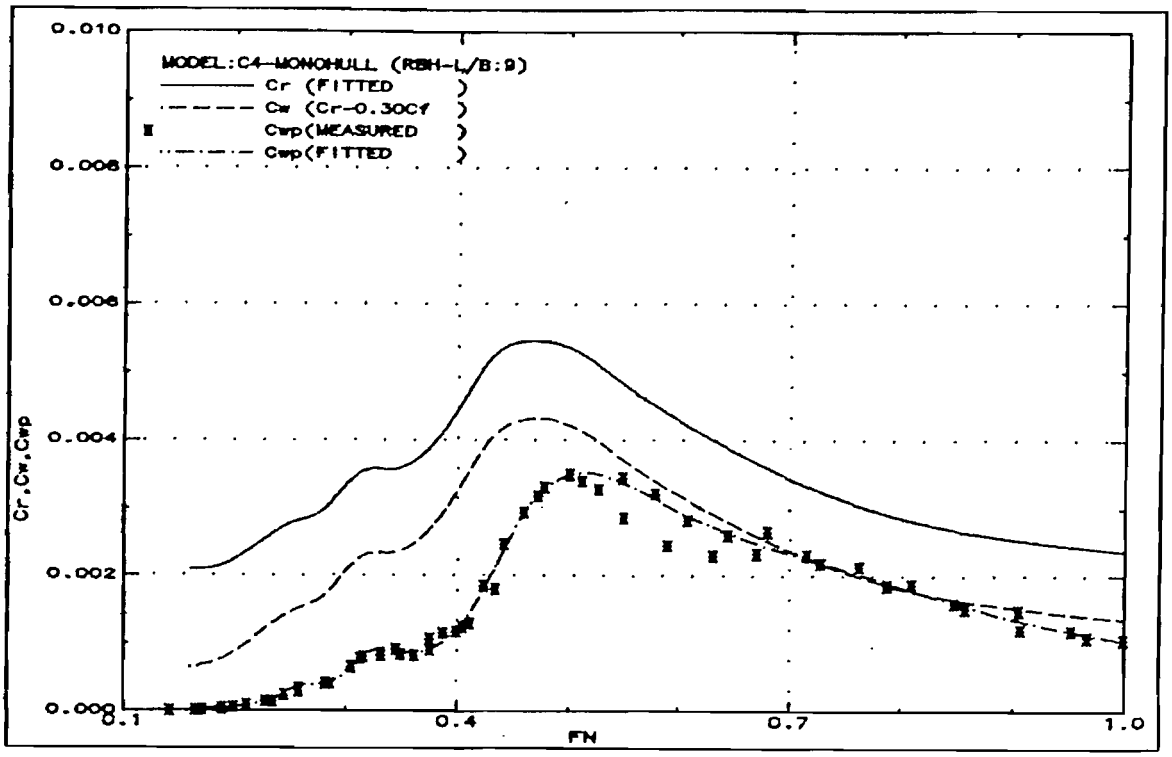

Fig.273: Measured wave resistance (C4-Monohull)

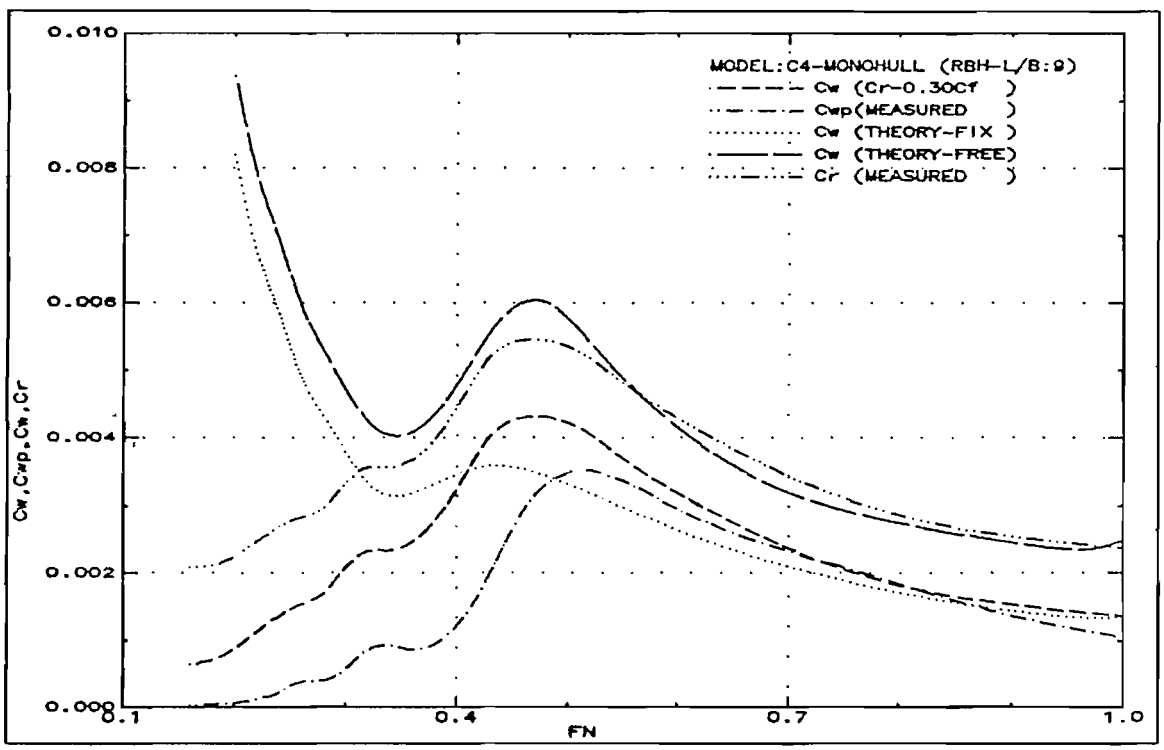

Fig.274: Wave resistance comparison (C4-Monohull)

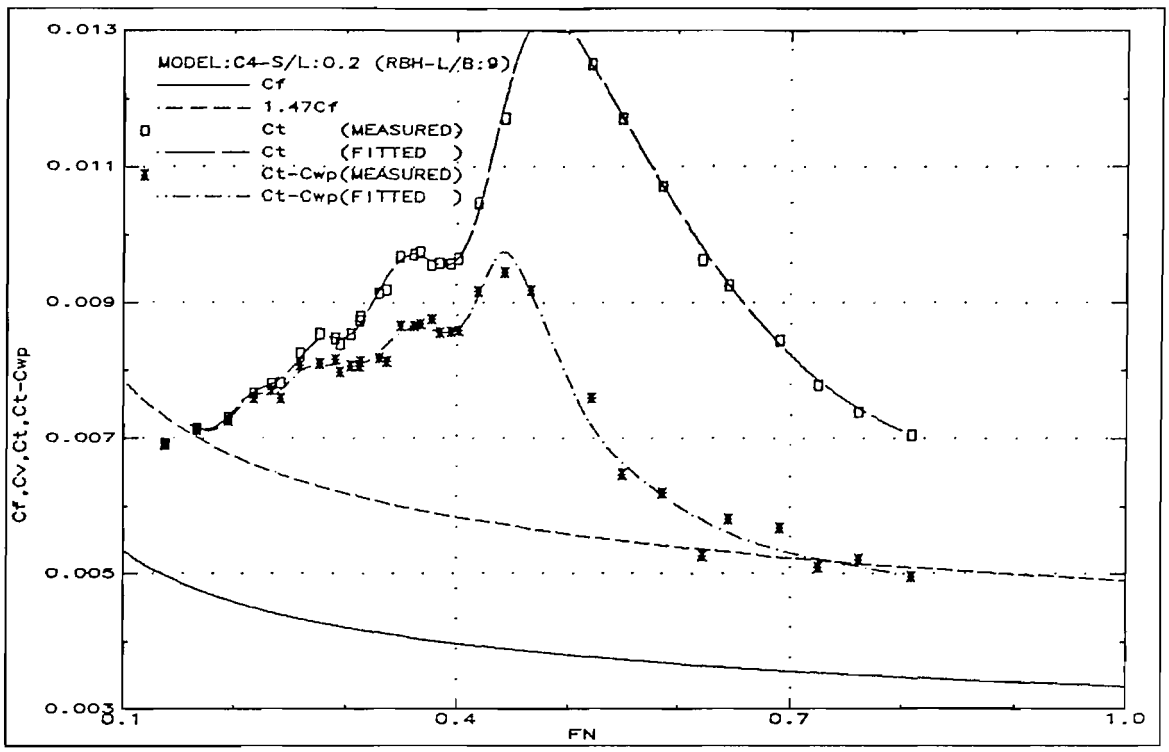

Fig.275: Resistance components (C4-S/L:Ø.2)

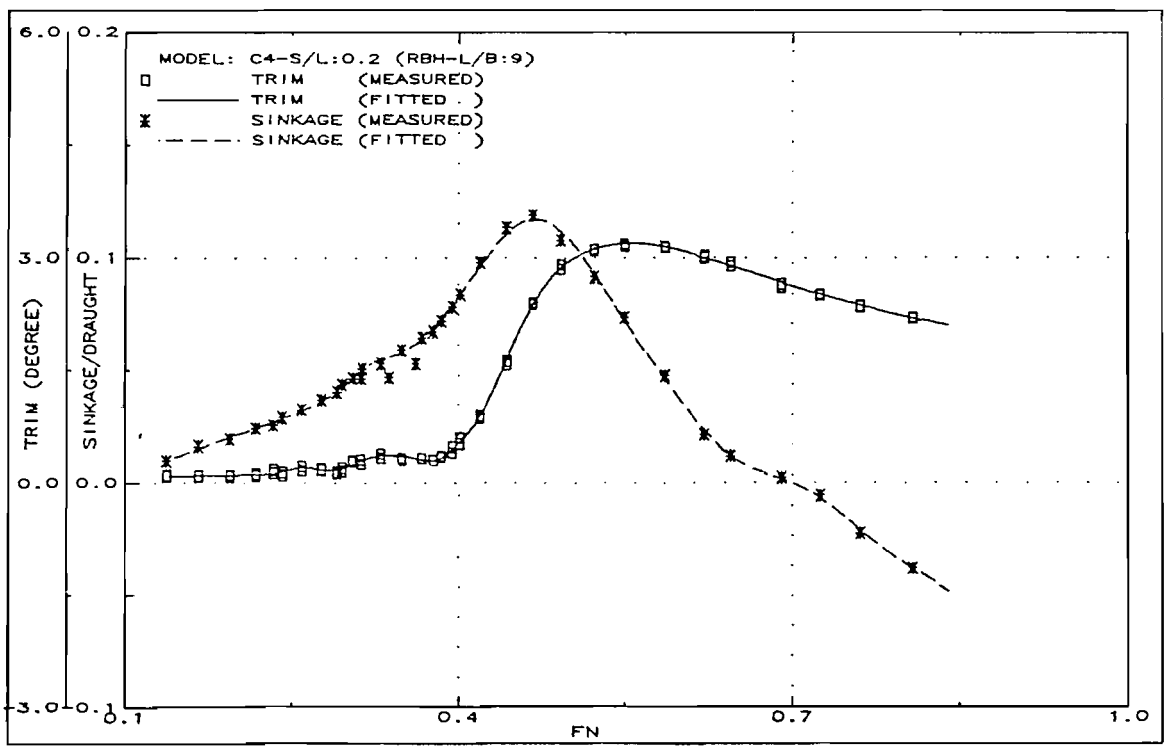

Fig.276: Running trim and sinkage (C4-S/L:Ø.2)

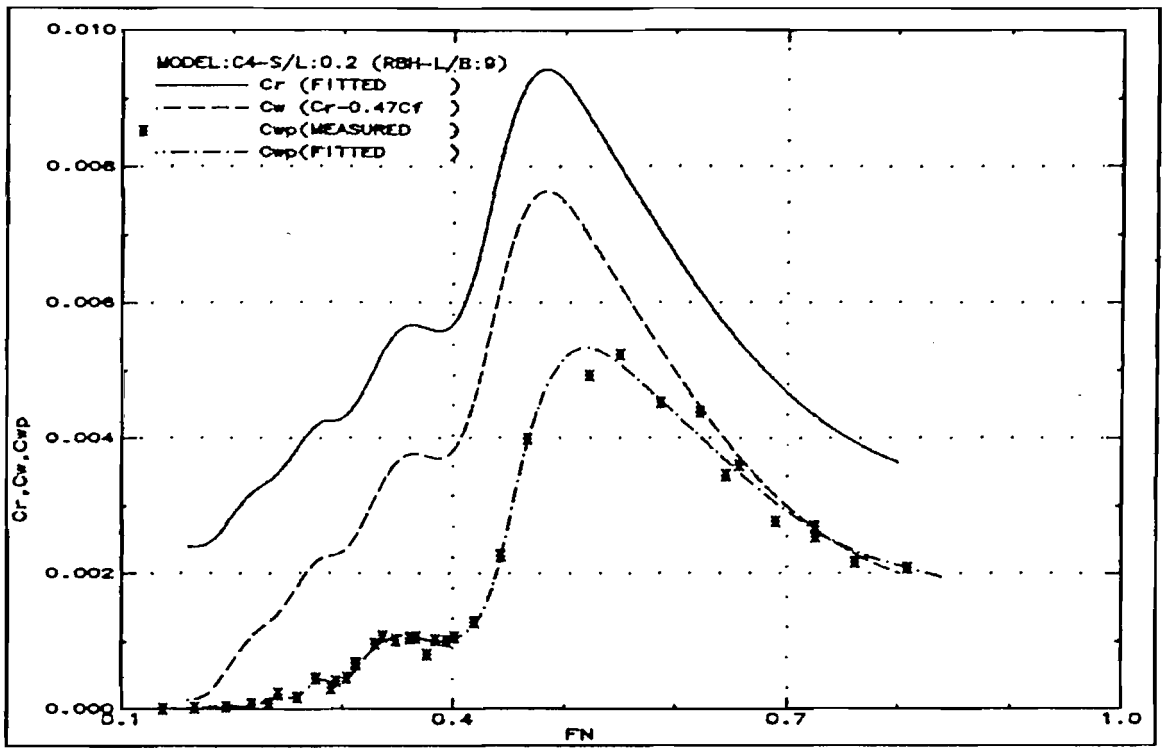

Fig.277: Measured wave resistance (C4-S/L:Ø.2)

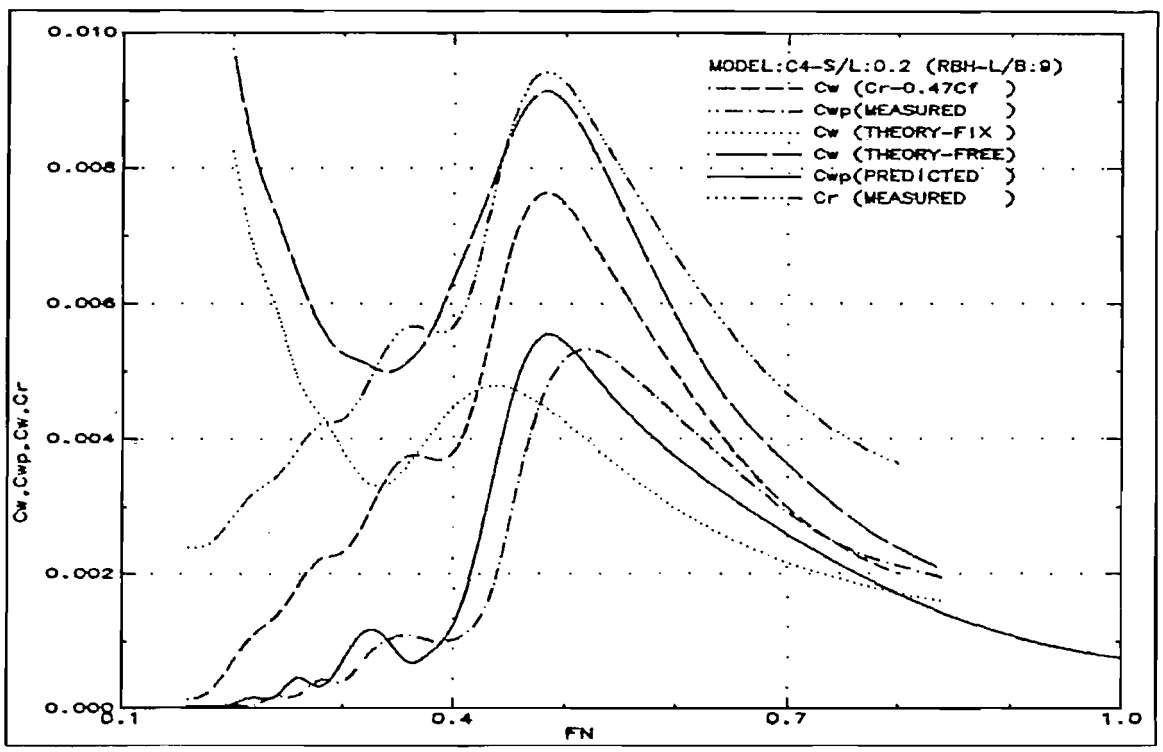

Fig.278: Wave resistance comparison (C4-S/L:Ø.2)

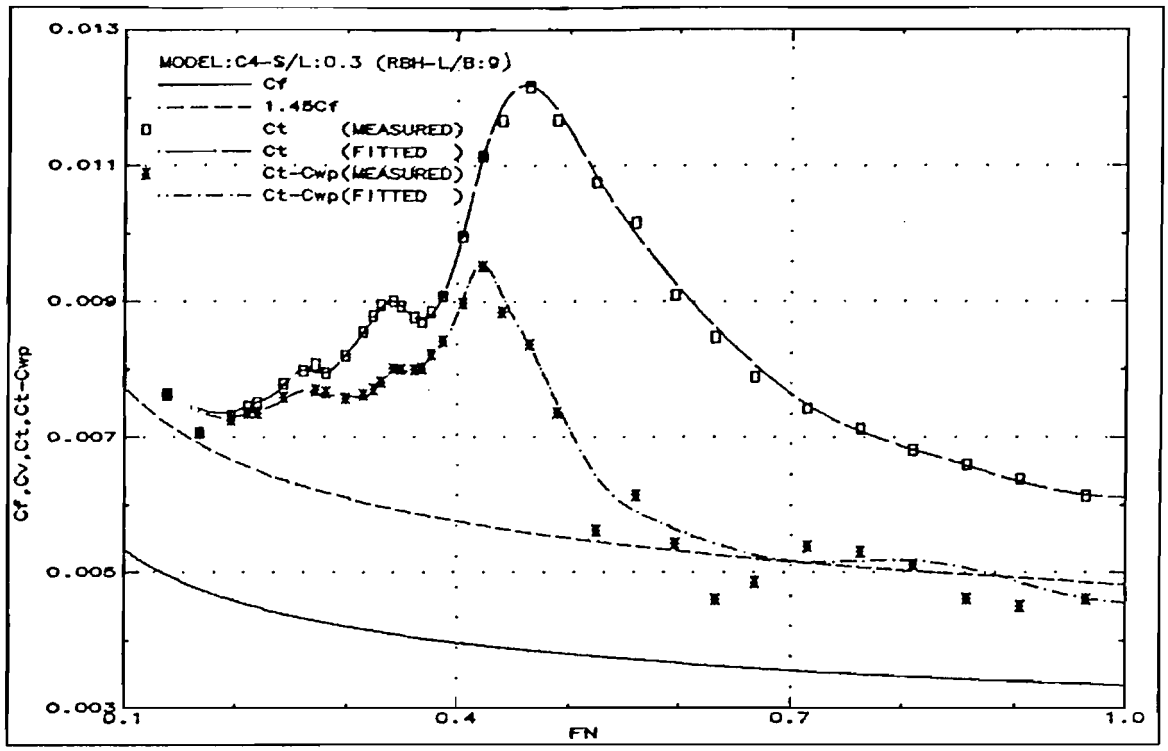

Fig.279: Resistance components (C4-S/L:Ø.3)

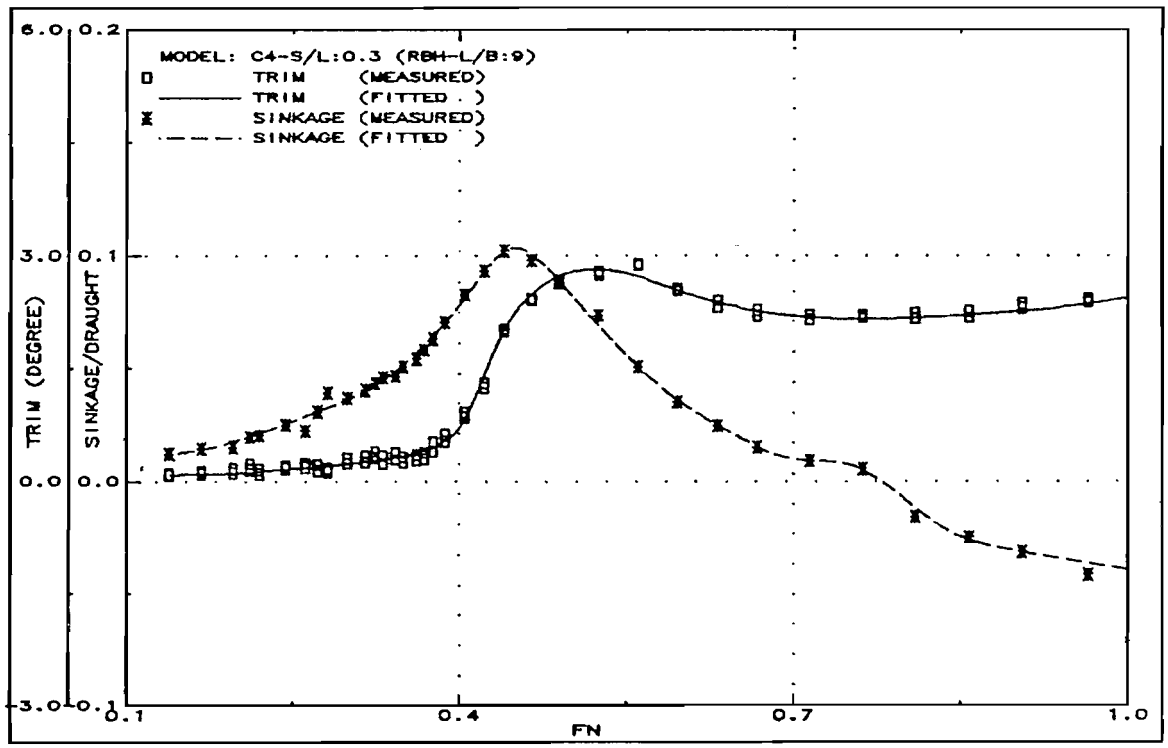

Fig.28Ø: Running trim and sinkage (C4-S/L:Ø.3)

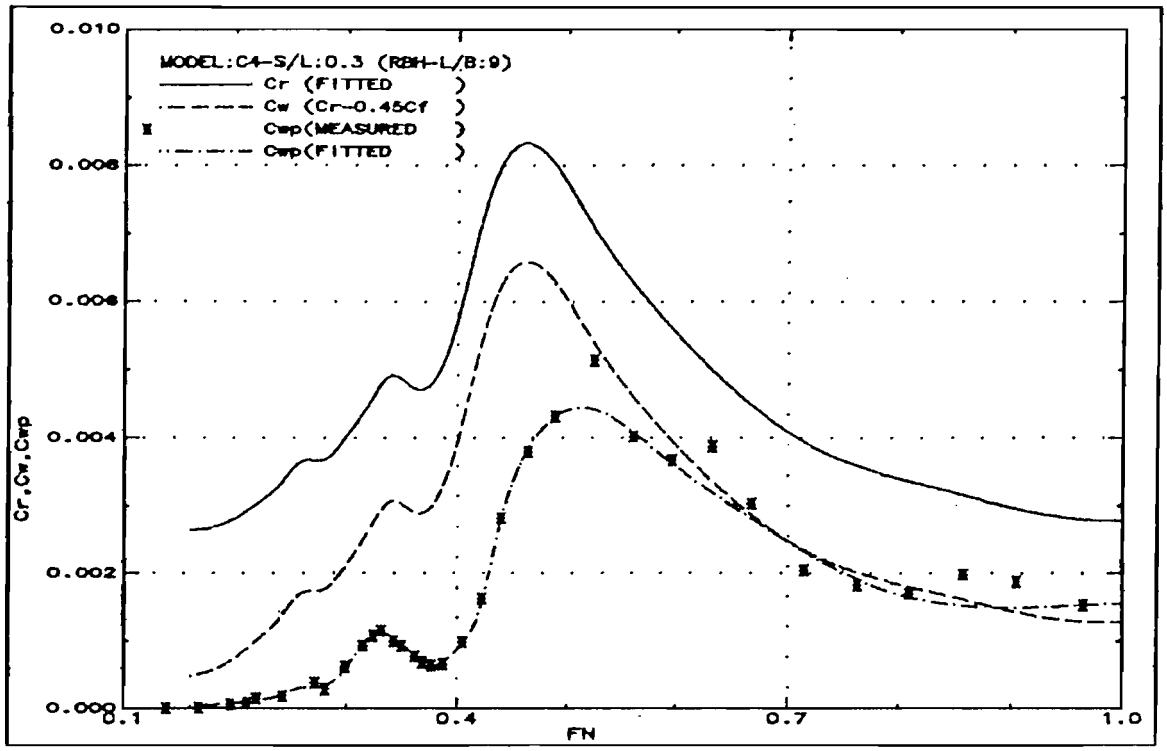

Fig.281: Measured wave resistance (C4-S/L:0.3)

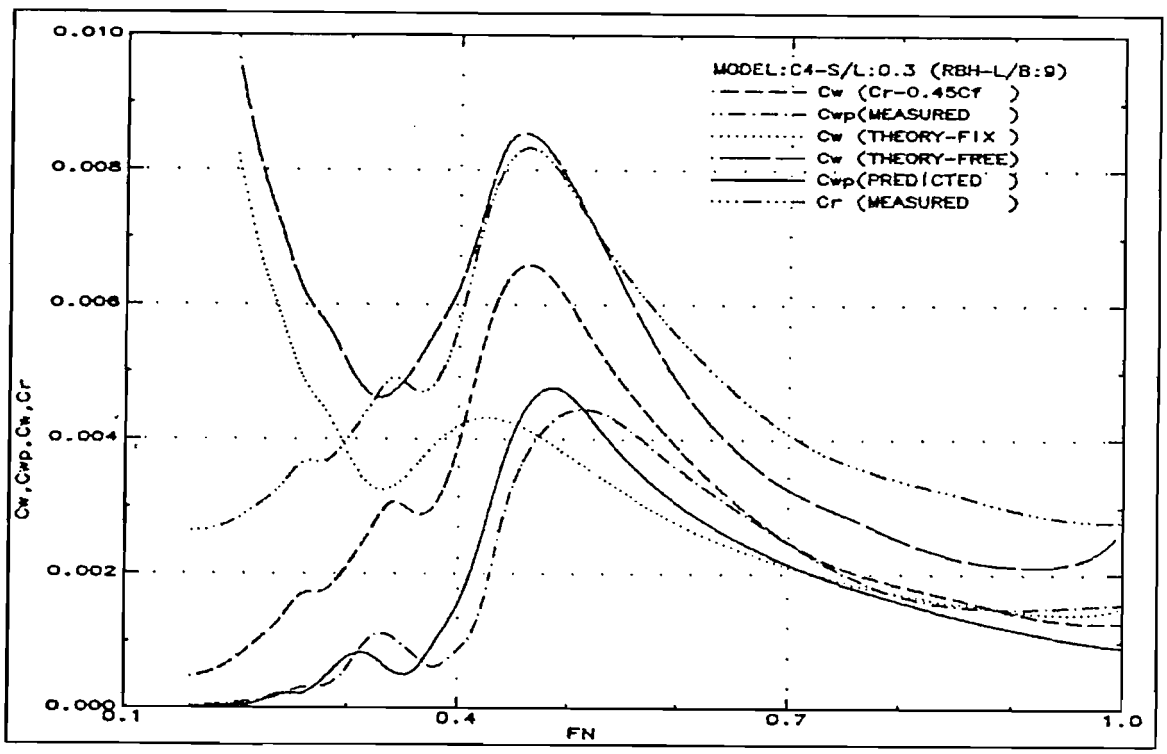

Fig.282: Wave resistance comparison (C4-S/L:0.3)

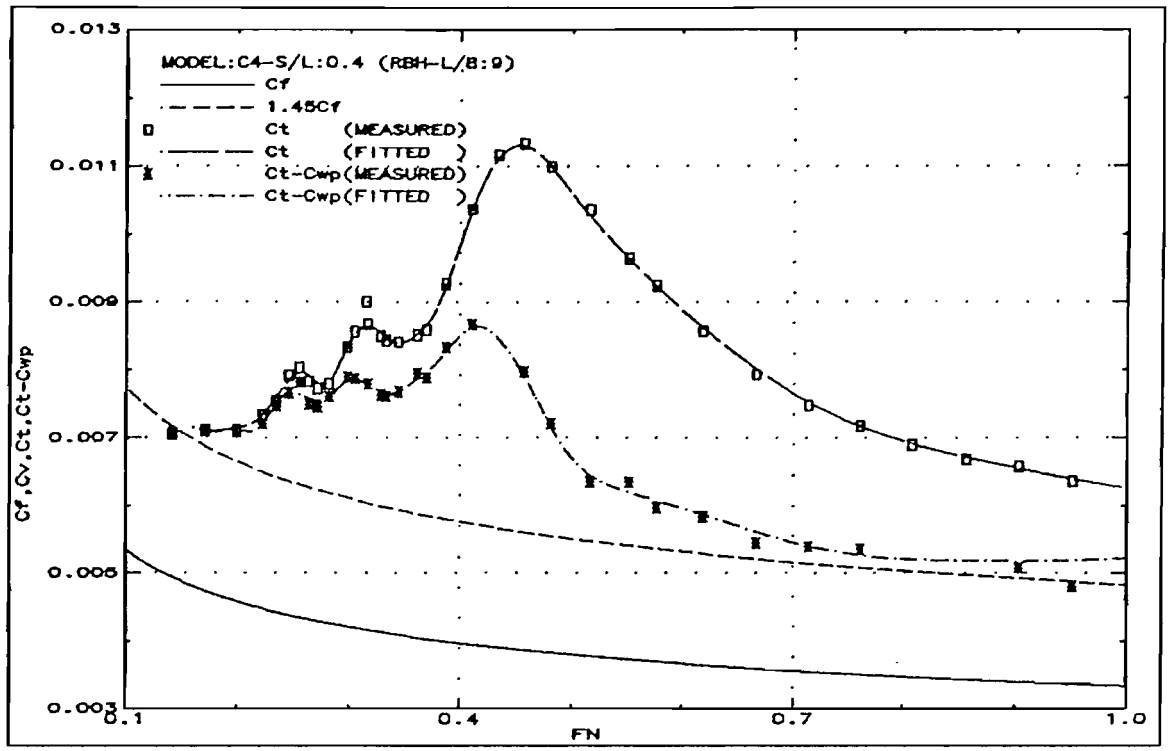

Fig.283: Resistance components (C4-S/L:0.4)

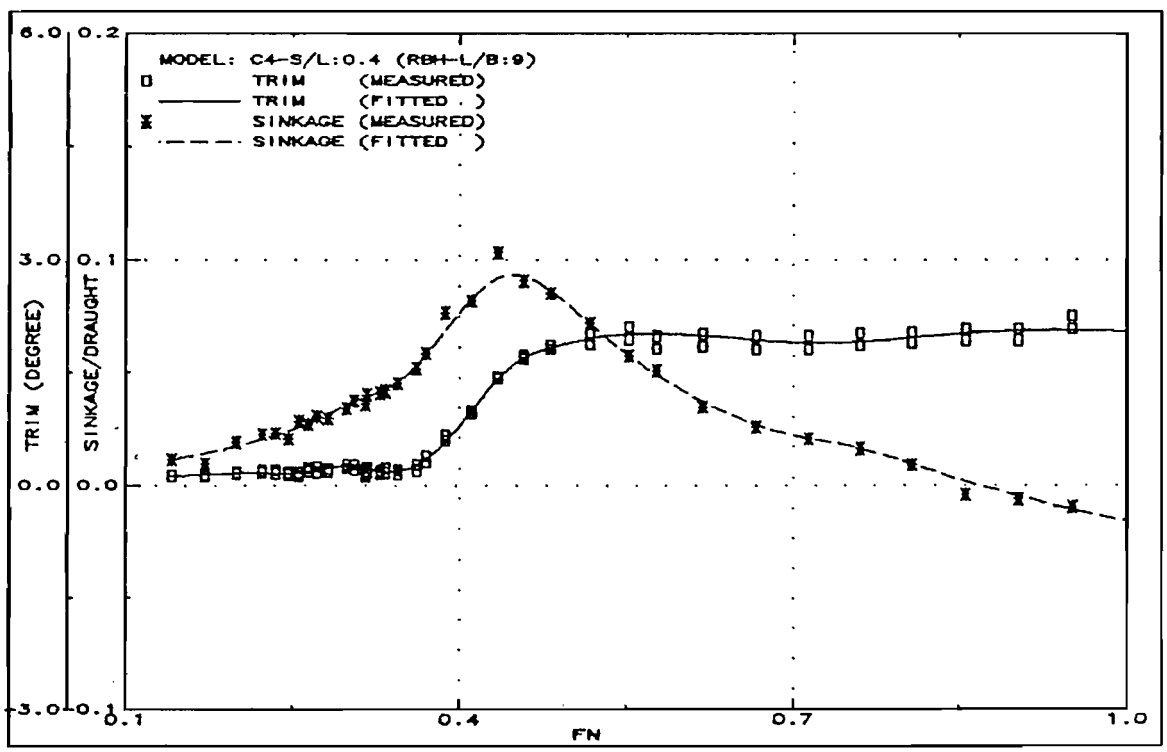

Fig.284: Running trim and sinkage (C4-S/L:0.4)

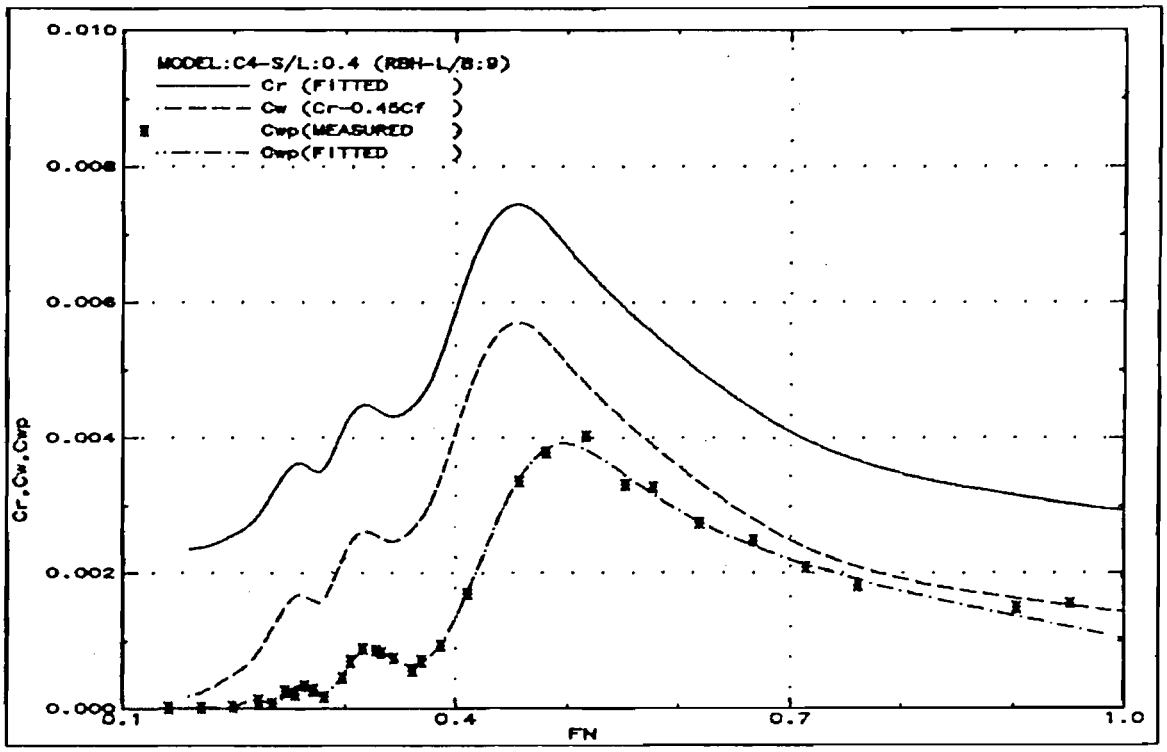

Fig.285: Measured wave resistance (C4-S/L:0.4)

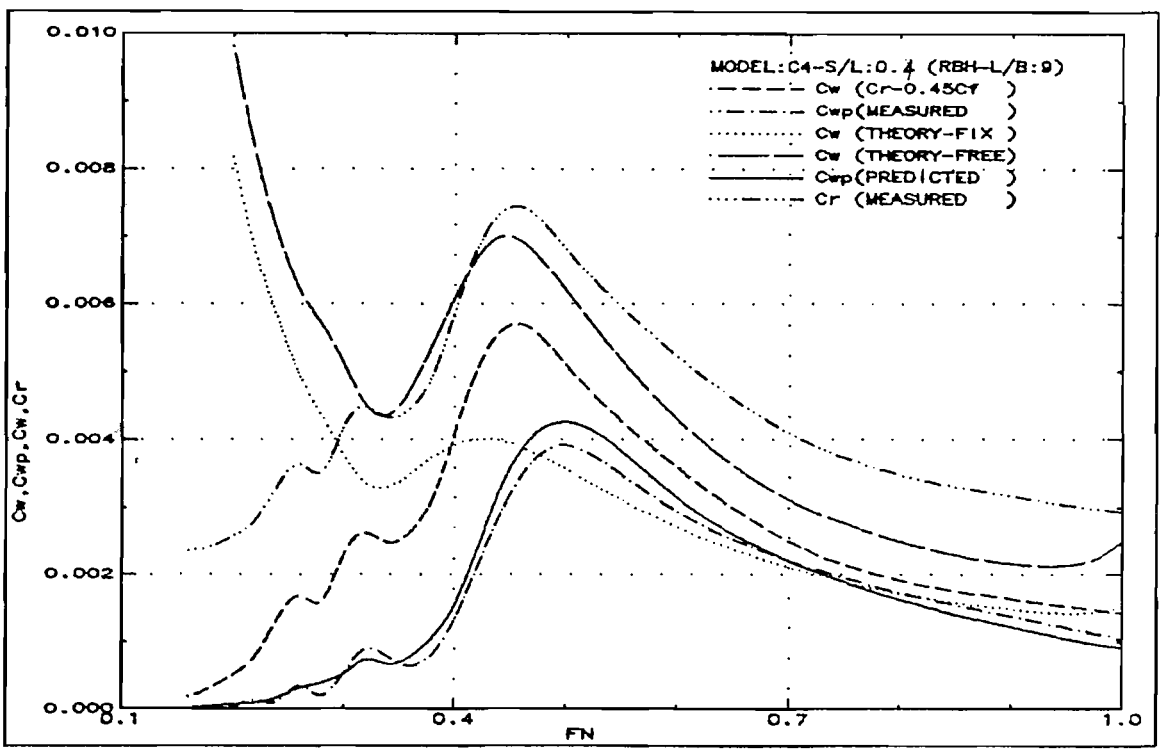

Fig.286: Wave resistance comparison (C4-S/L:0.4)

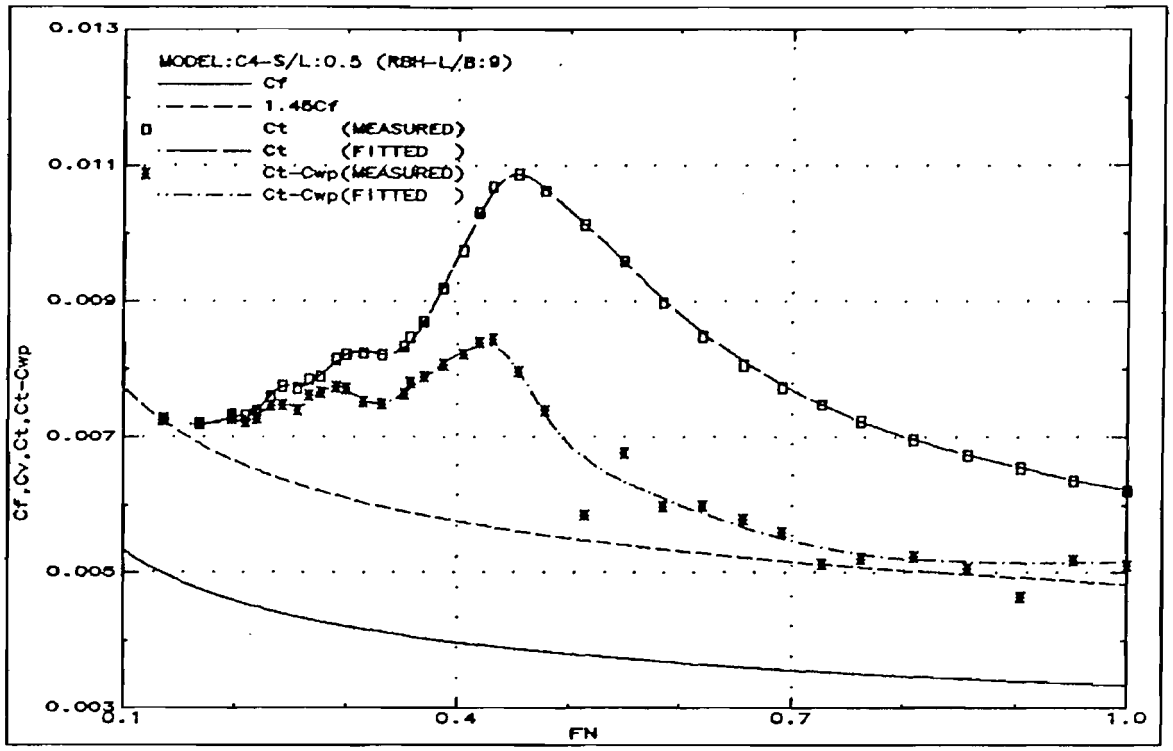

Fig.287: Resistance components (C4-S/L:Ø.5)

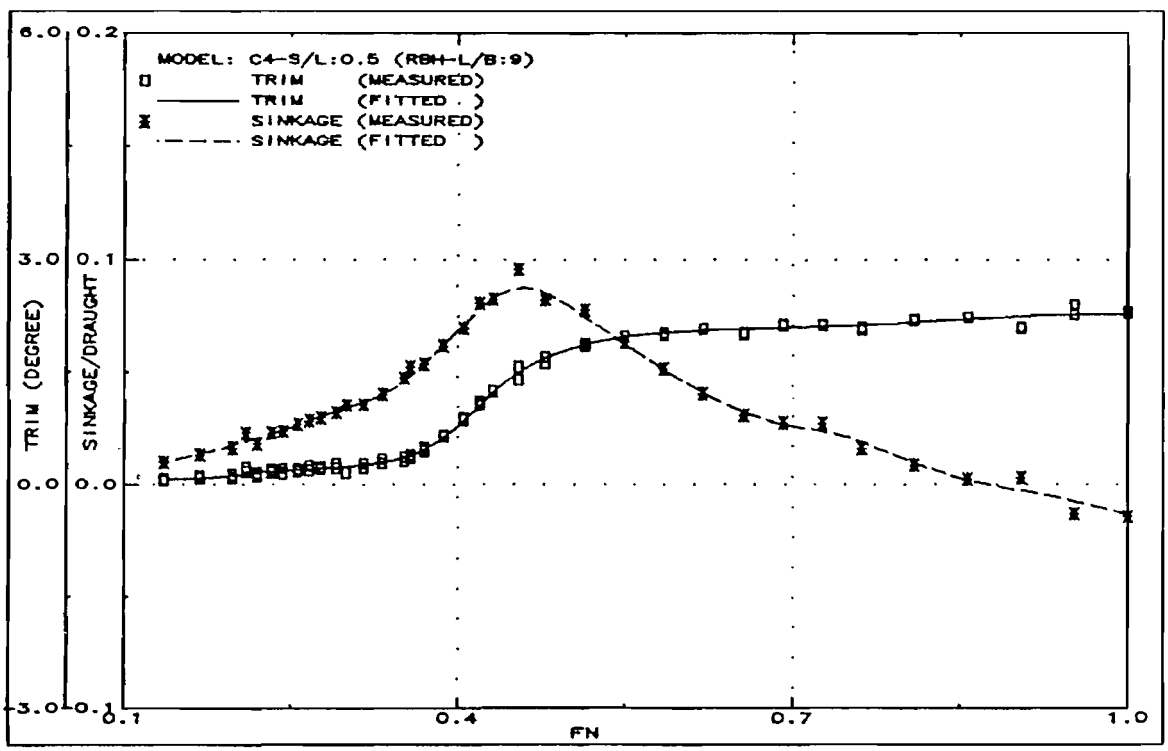

Fig.288: Running trim and sinkage (C4-S/L:Ø.5)

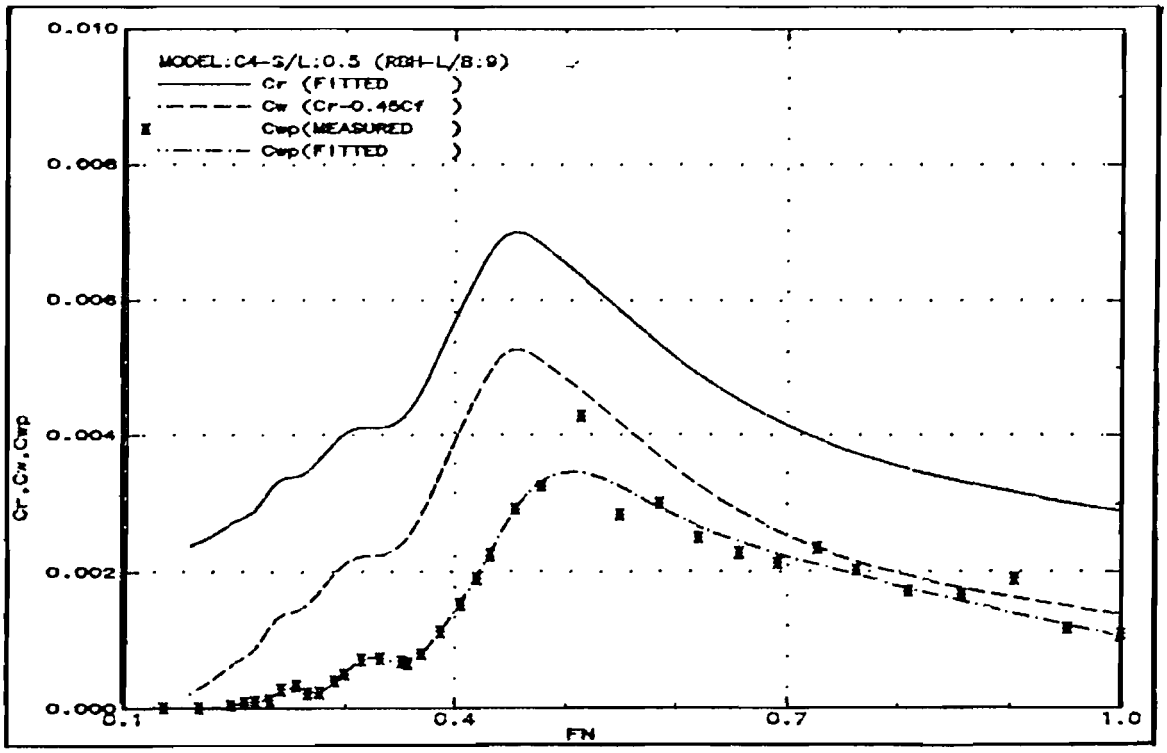

Fig.289: Measured wave resistance (C4-S/L:0.5)

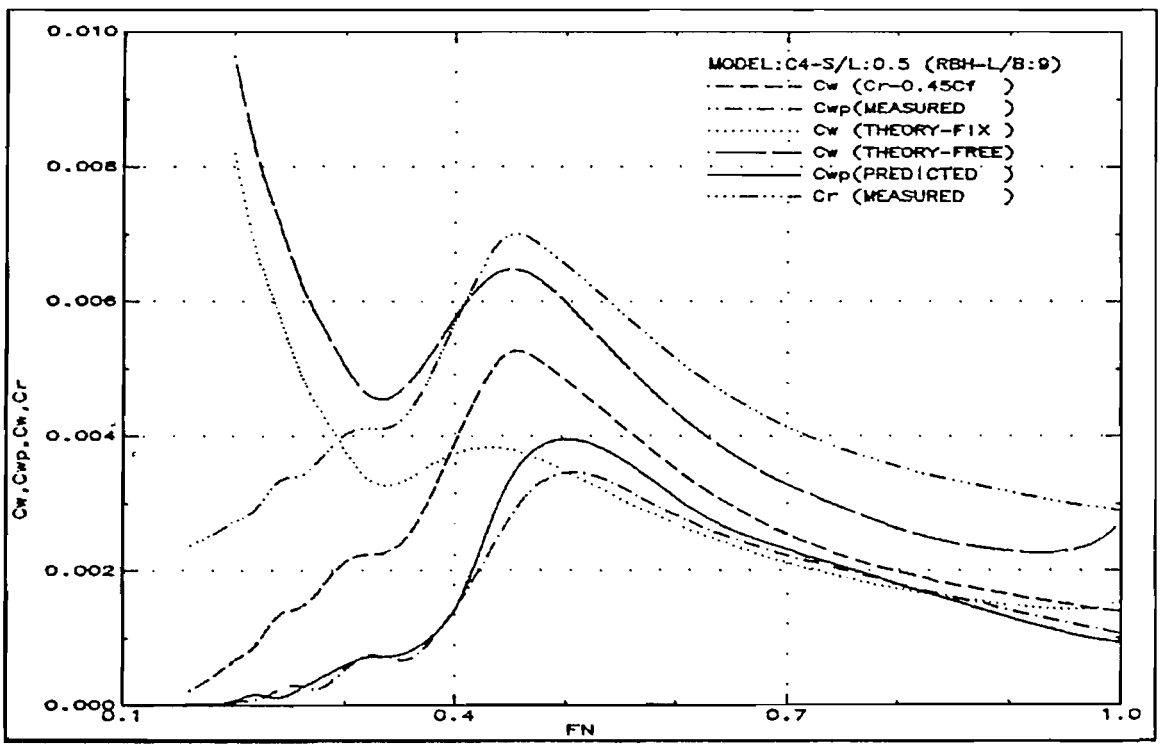

Fig.290: Wave resistance comparison (C4-S/L:0.5)

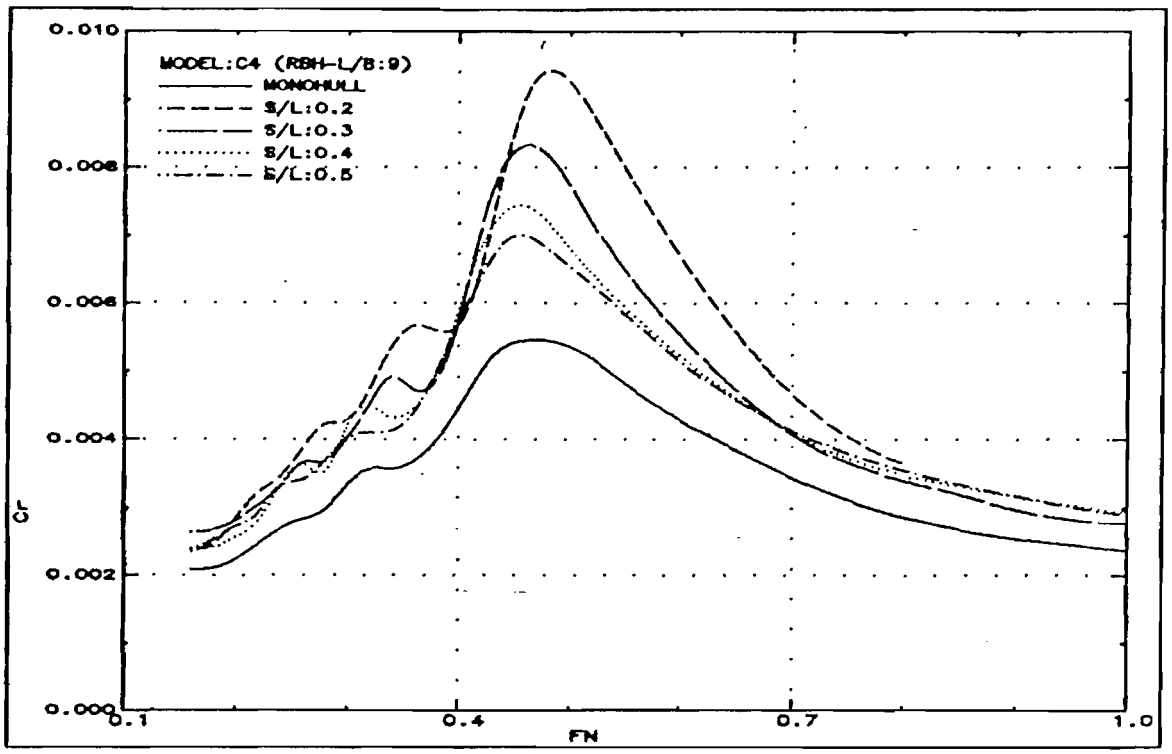

Fig.291: Residuary resistance (C4)

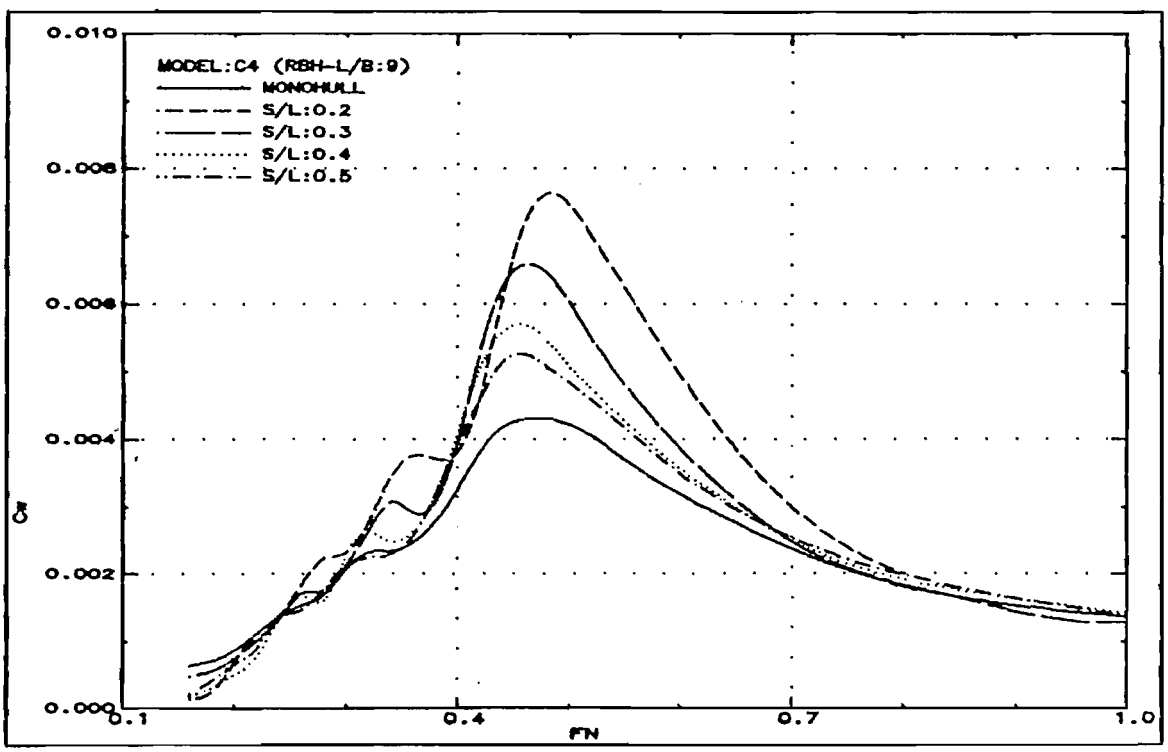

Fig.292: Wave resistance (C4)

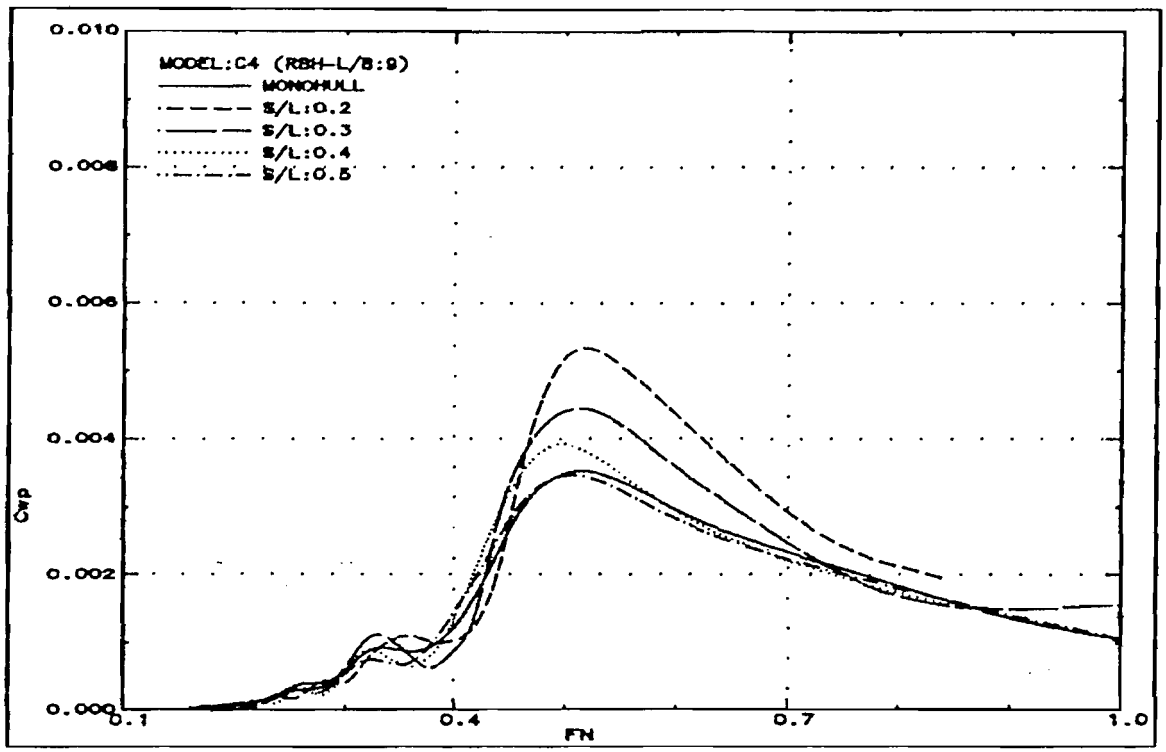

Fig.293: Wave pattern resistance (C4)

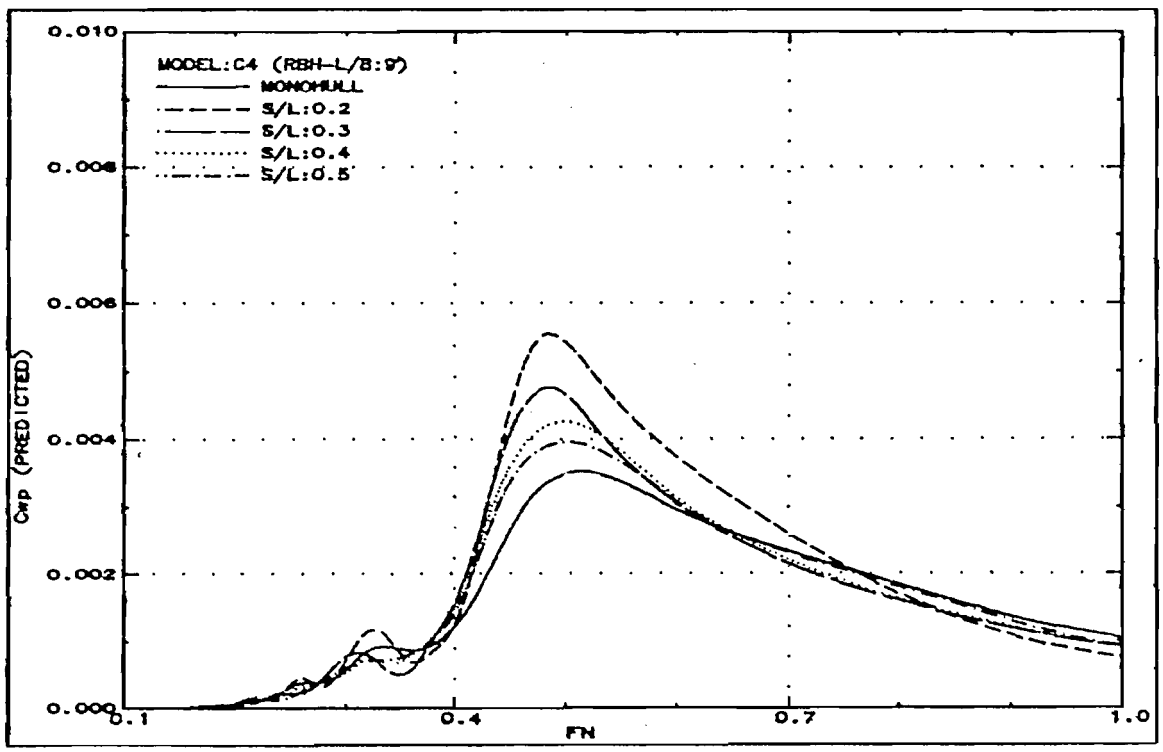

Fig.294: Wave pattern resistance predicted from monohull wave pattern analysis (C4)

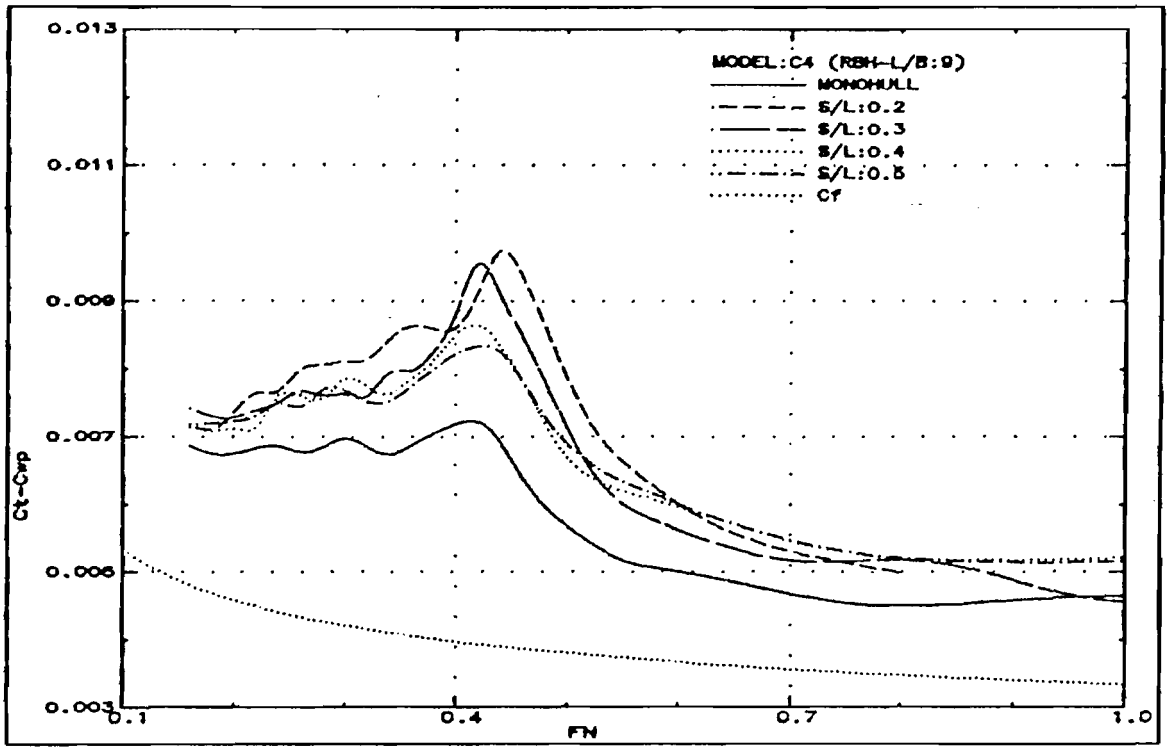

Fig.295: Total resistance minus wave pattern resistance (C4)

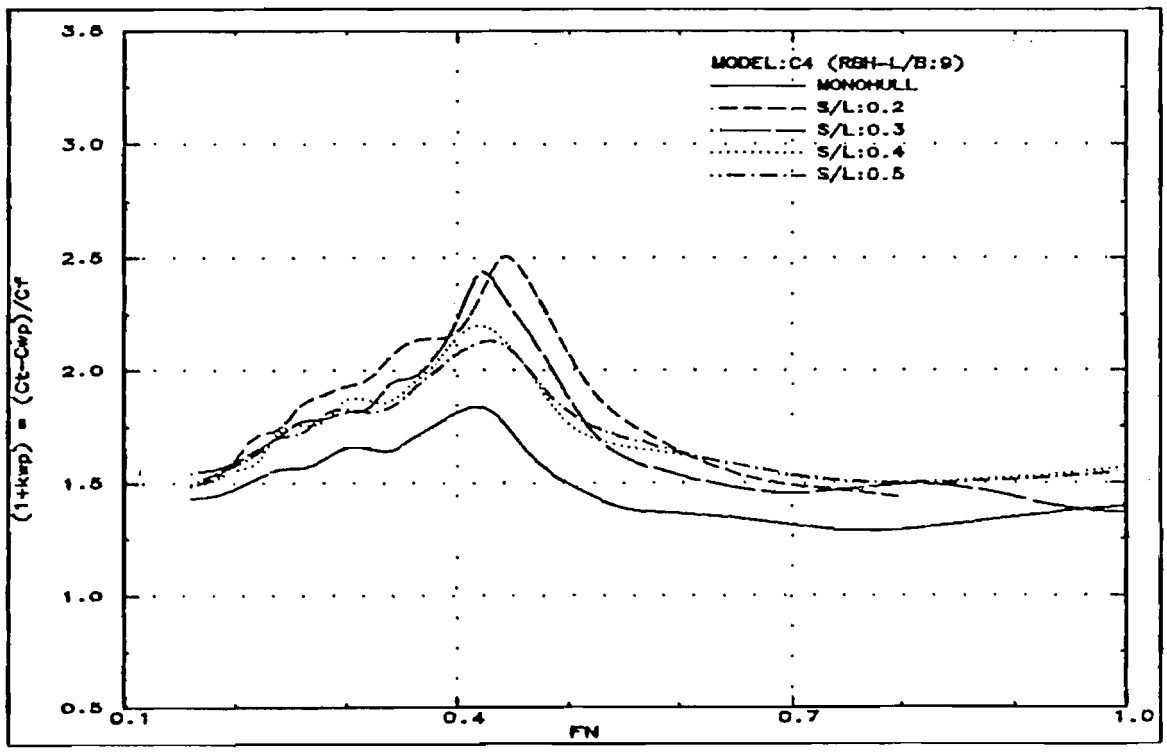

Fig.296: Form factor, i.e. $1+k_{WP}=(C_T-C_{WP})/C_F$ (C4)

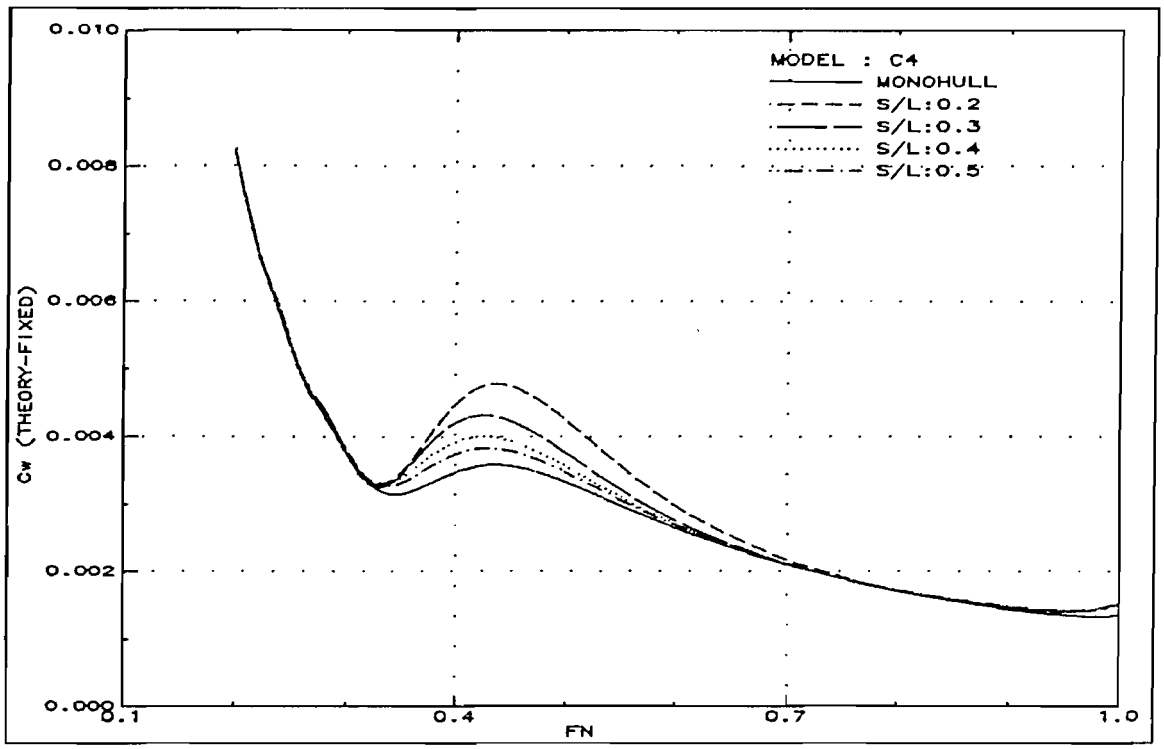

Fig.297: Theoretical wave resistance in fixed condition (C4)

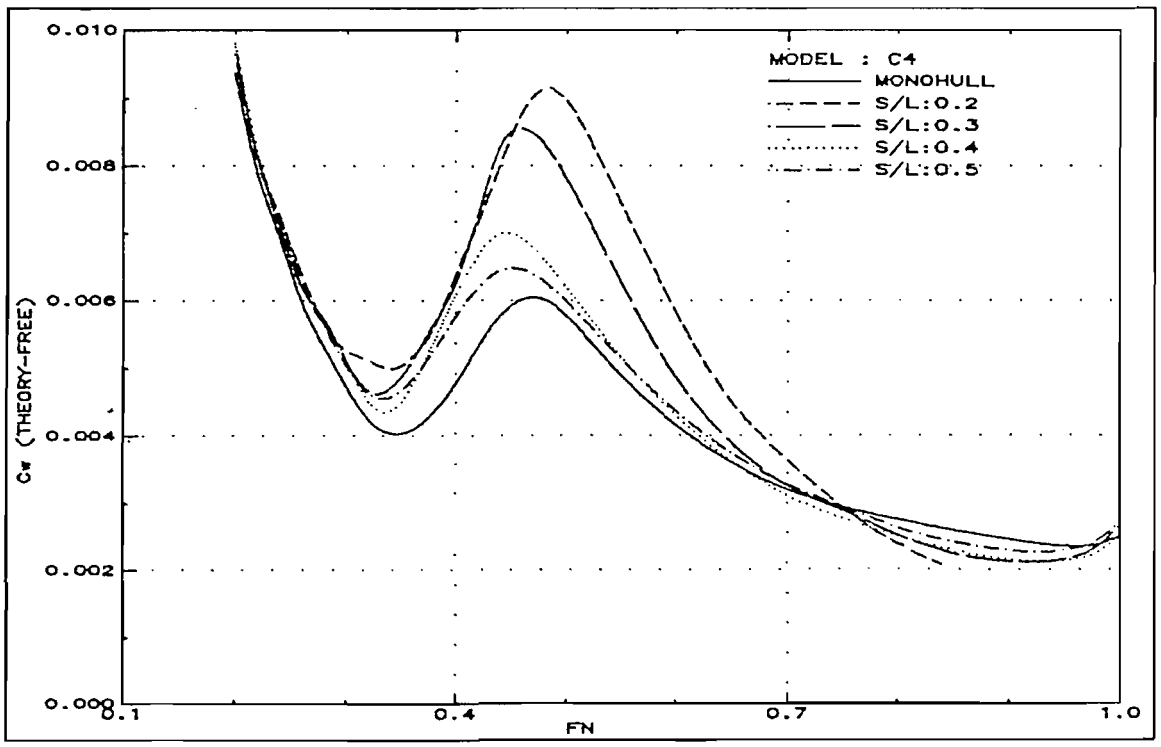

Fig.298: Theoretical wave resistance in free condition (C4)

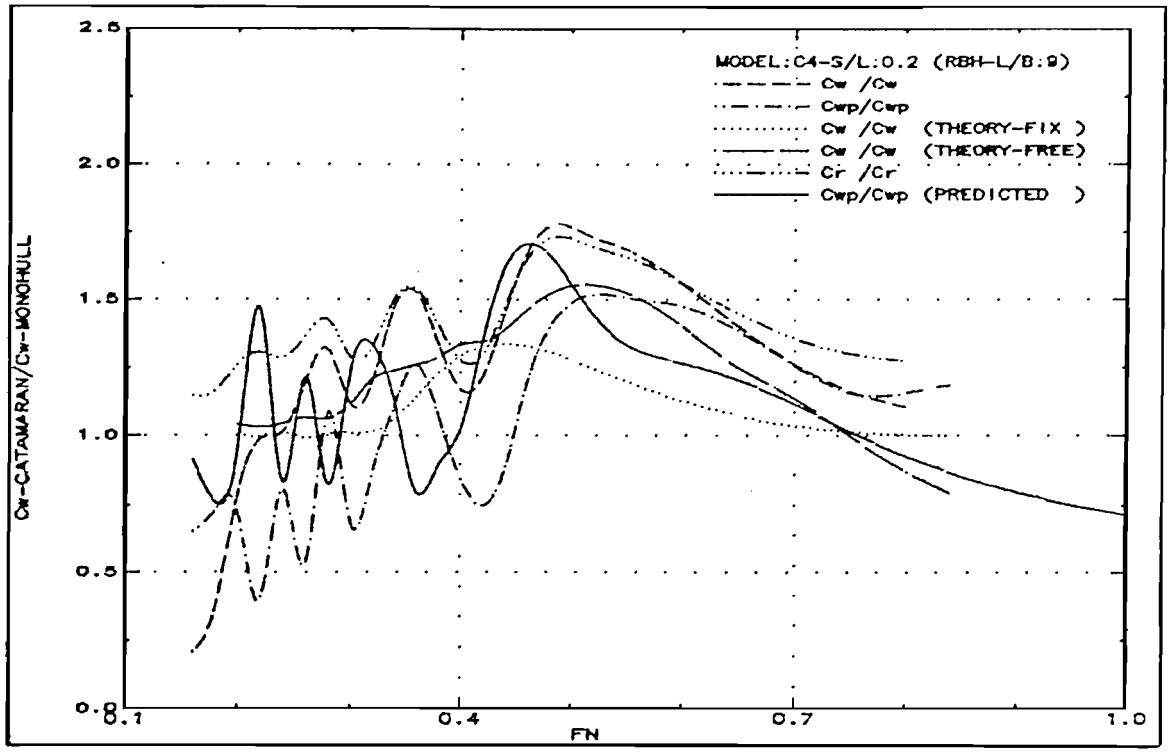

Fig.299: Wave resistance interference ratio (C4-S/L:Ø.2)

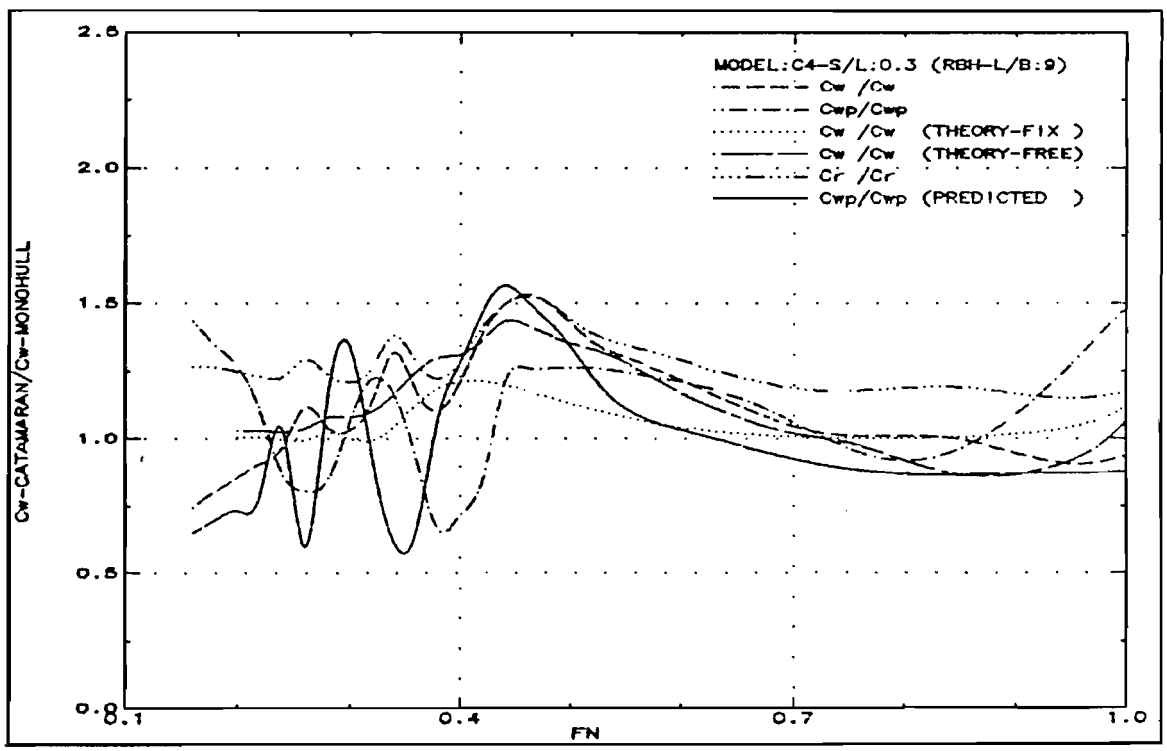

Fig.300: Wave resistance interference ratio (C4-S/L:Ø.3)

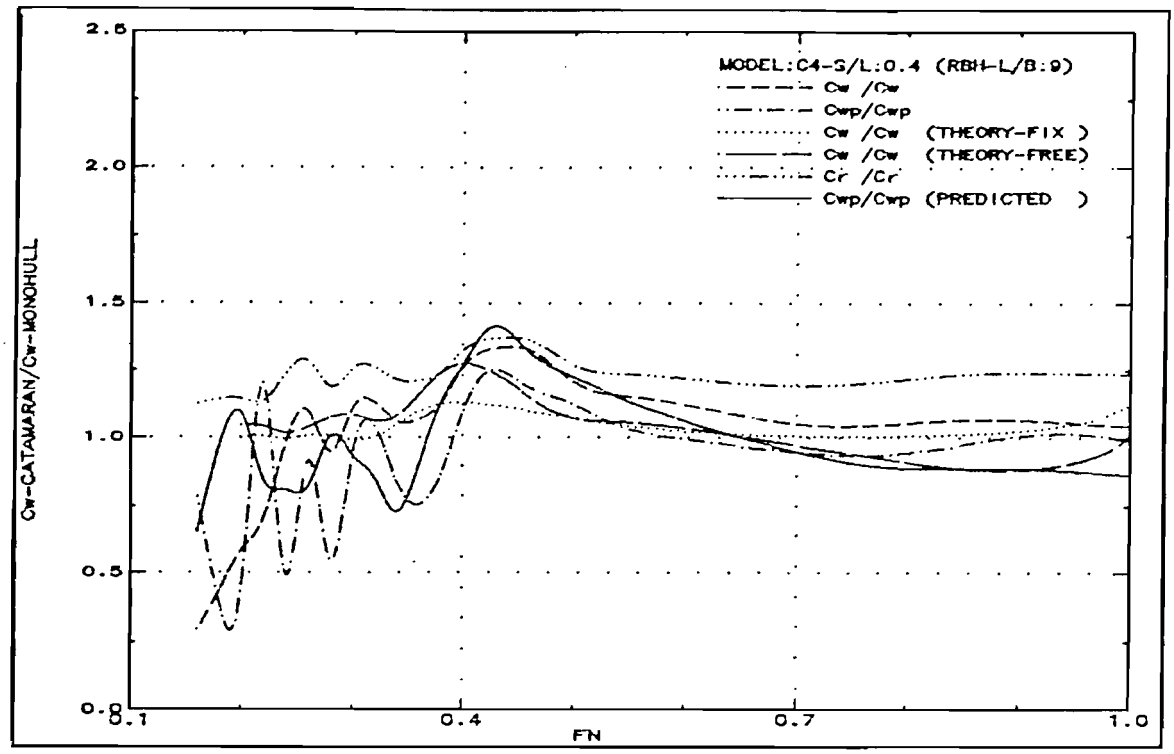

Fig.301: Wave resistance interference ratio (C4-S/L:0.4)

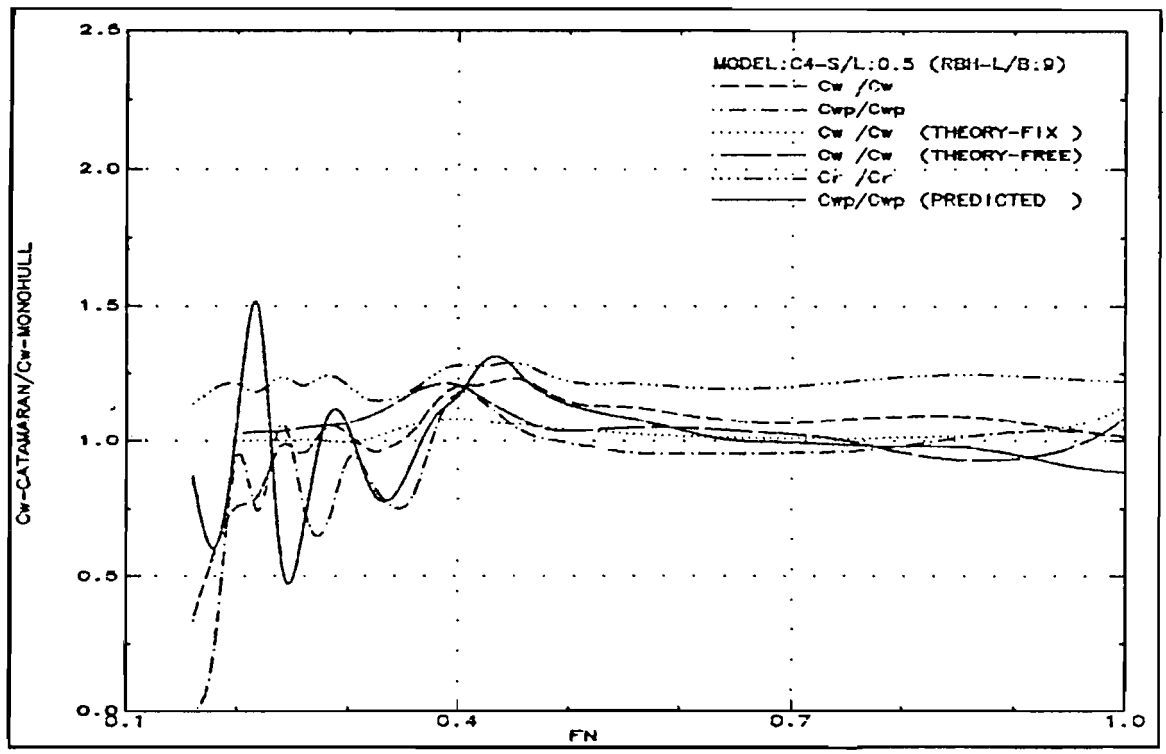

Fig.302: Wave resistance interference ratio (C4-S/L:0.5)

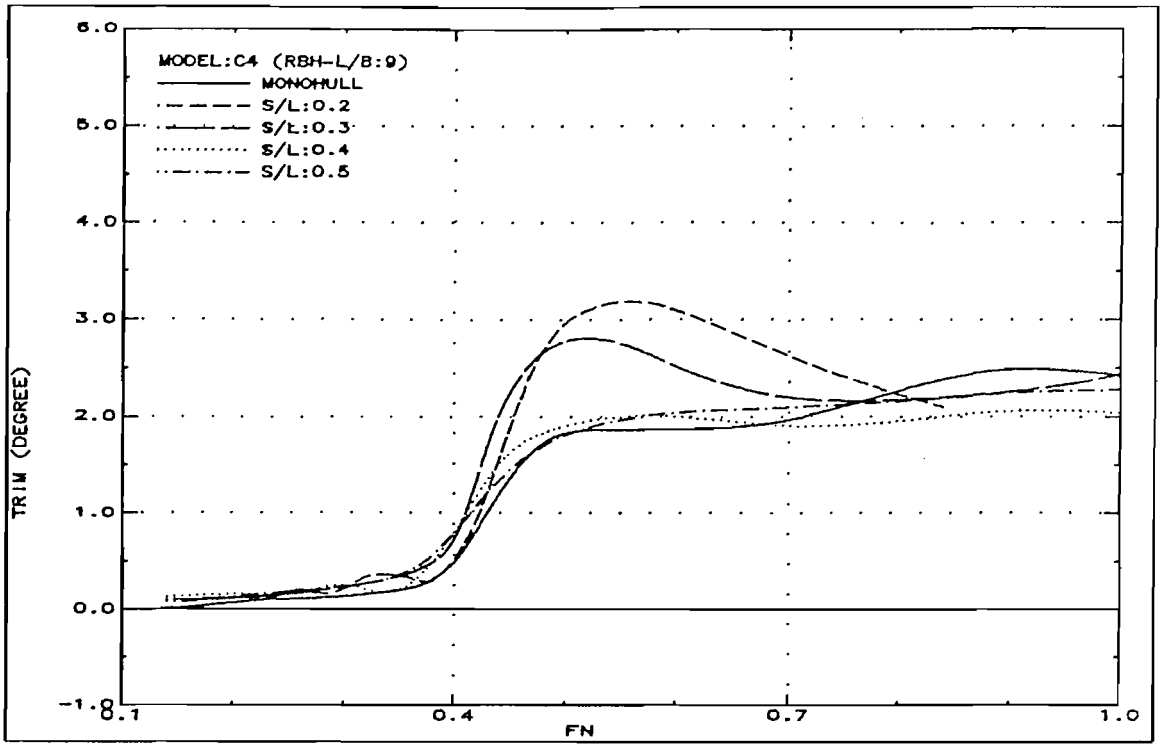

Fig.303: Running trim (C4)

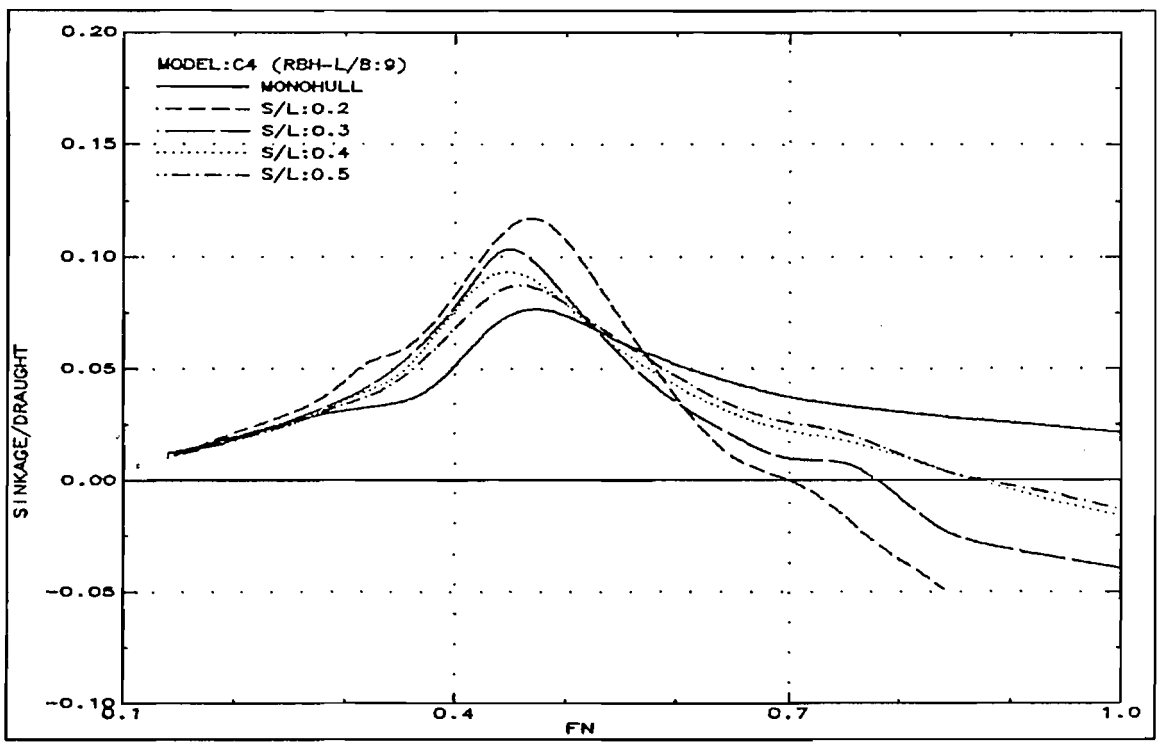

Fig.304: Sinkage (C4)

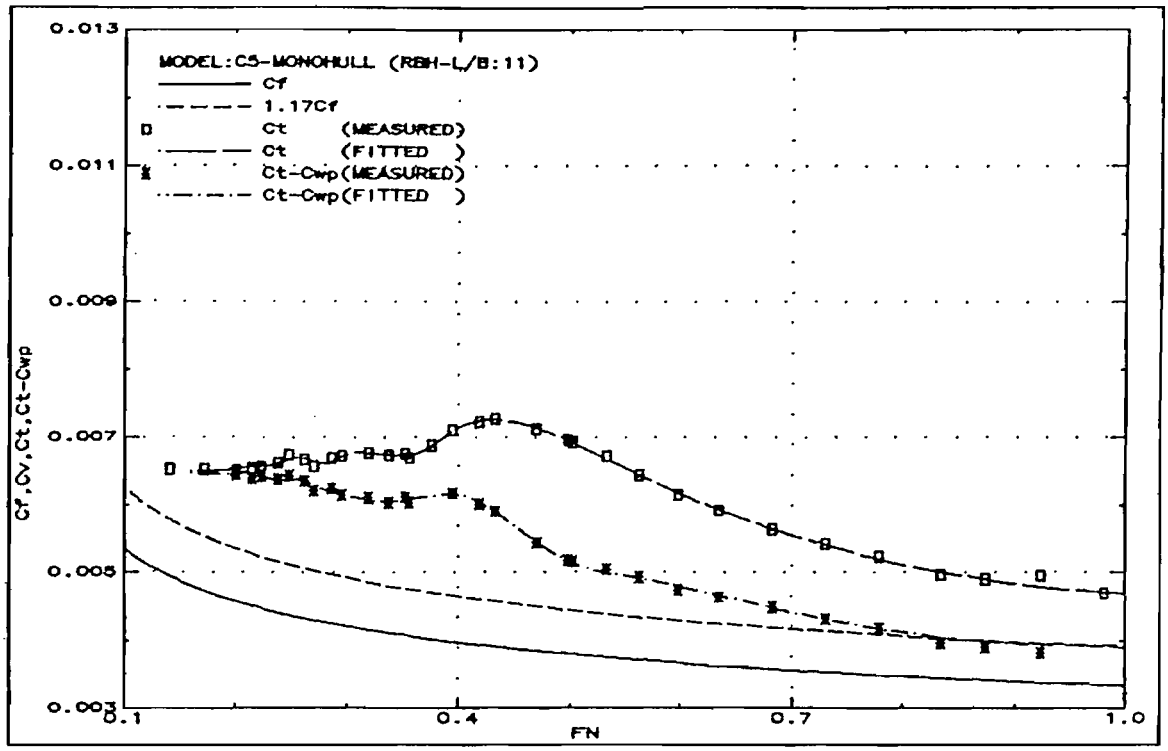

Fig.305: Resistance components (C5-Monohull)

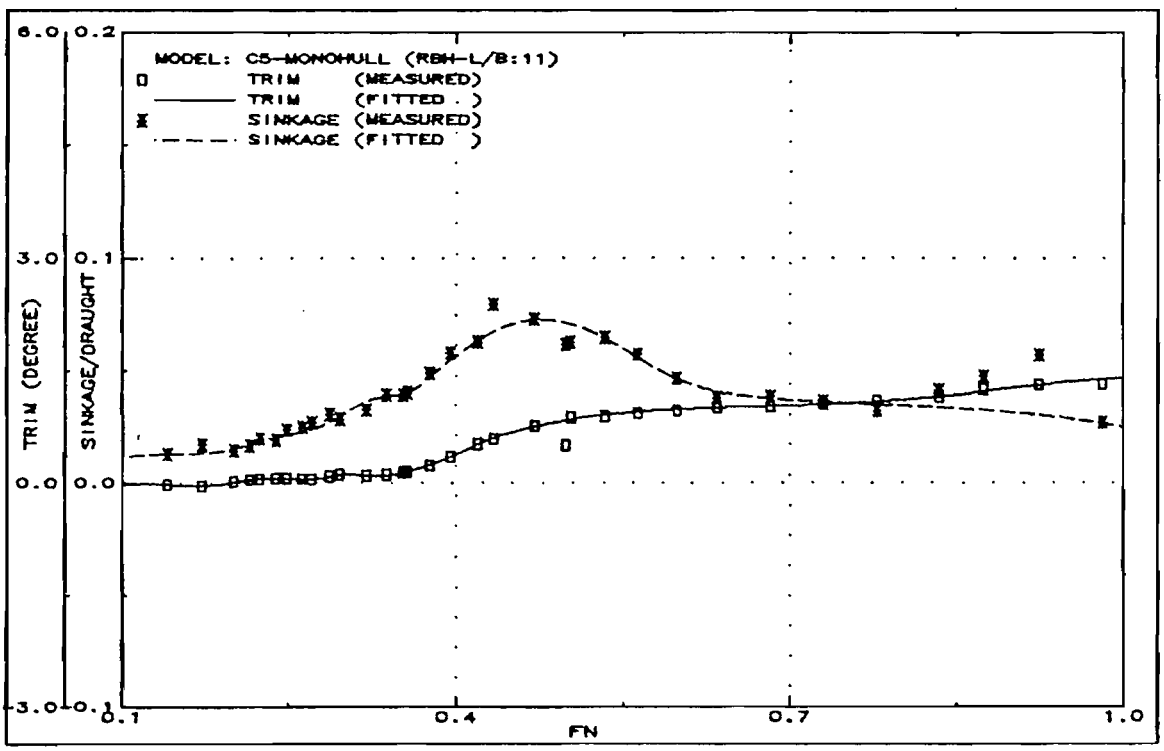

Fig.306: Running trim and sinkage (C5-Monohull)

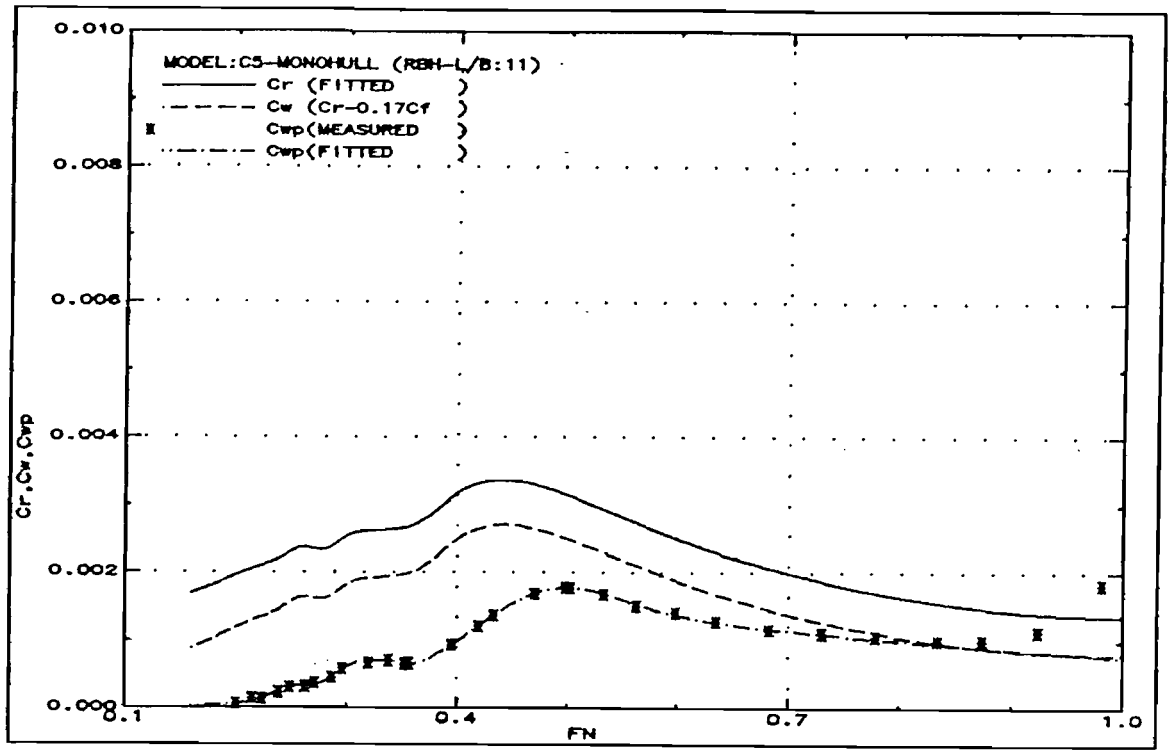

Fig.307: Measured wave resistance (C5-Monohull)

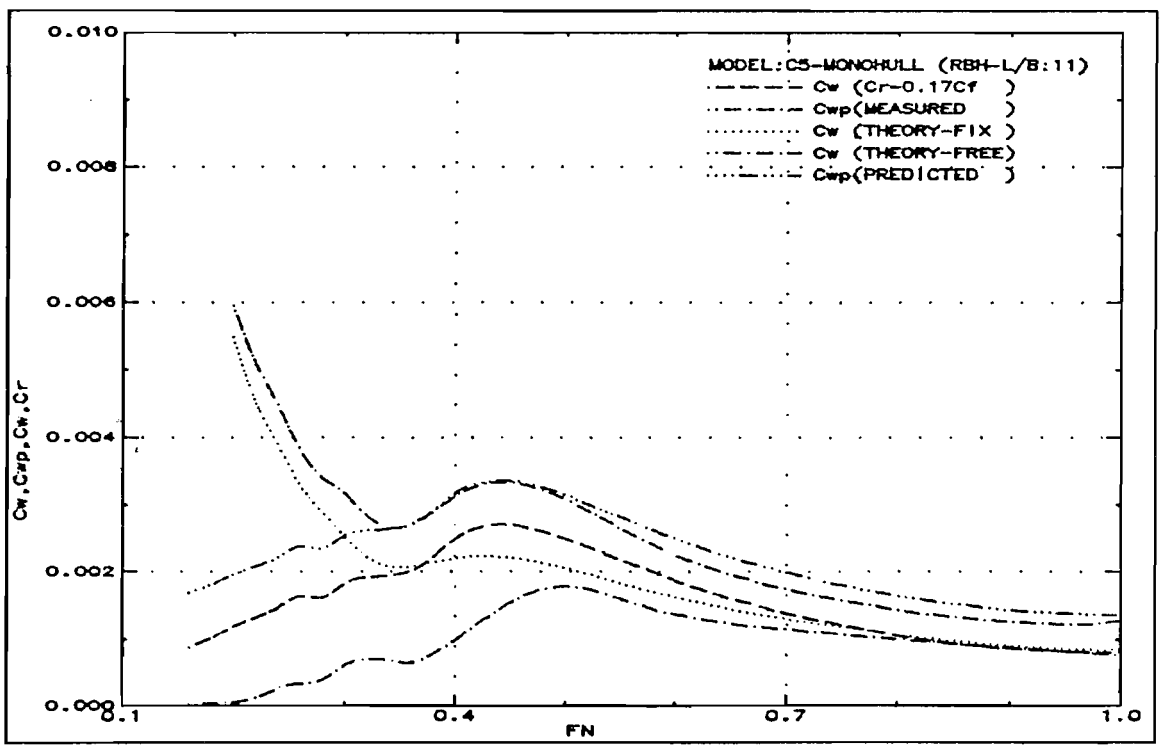

Fig.308: Wave resistance comparison (C5-Monohull)

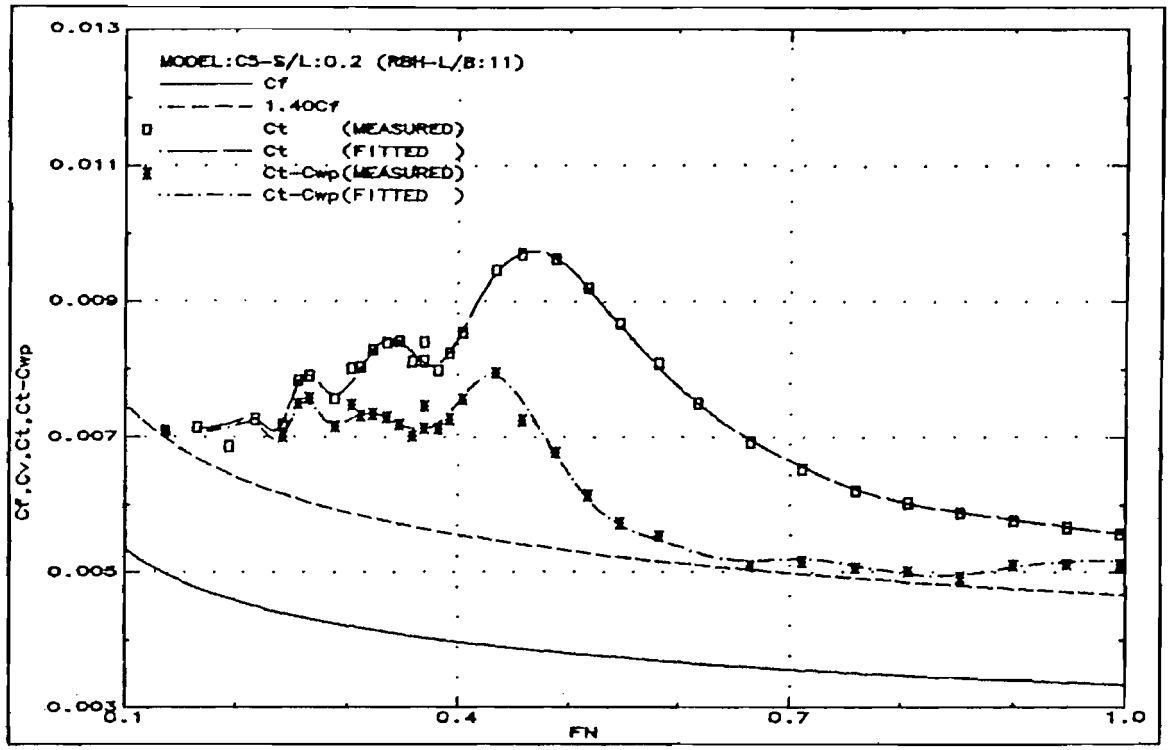

Fig.309: Resistance components (C5-S/L:0.2)

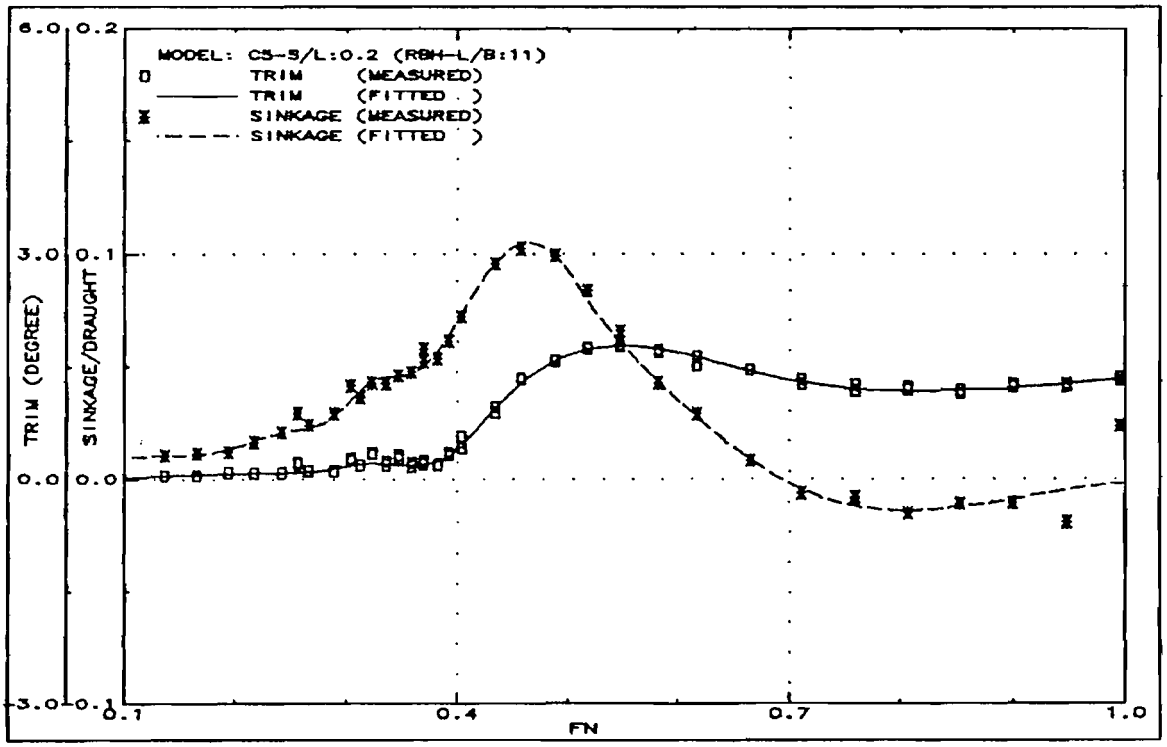

Fig.310: Running trim and sinkage (C5-S/L:0.2)

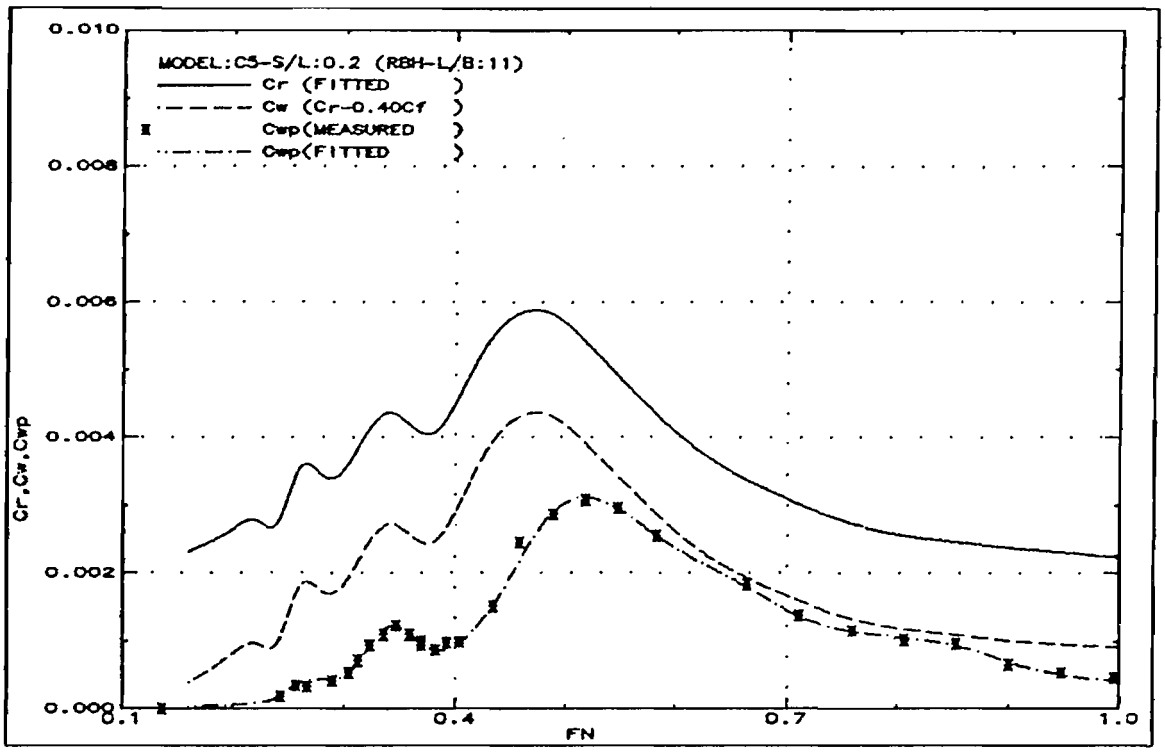

Fig.311: Measured wave resistance (C5-S/L:Ø.2)

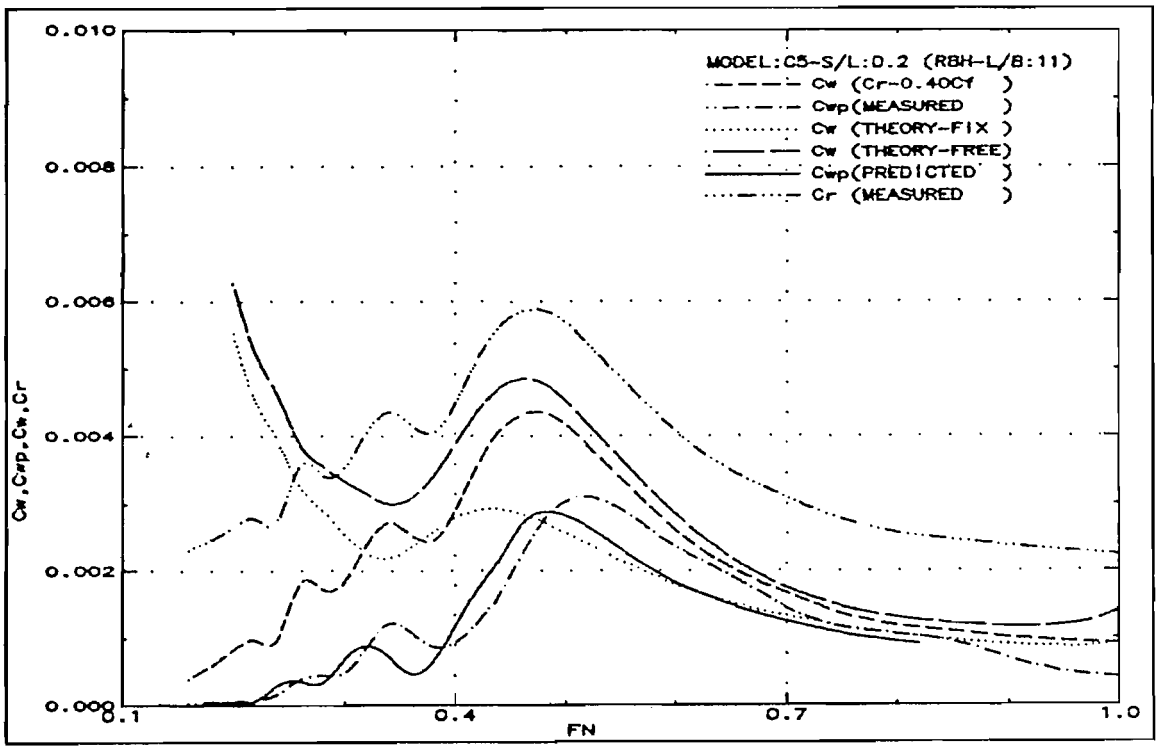

Fig.312: Wave resistance comparison (C5-S/L:Ø.2)

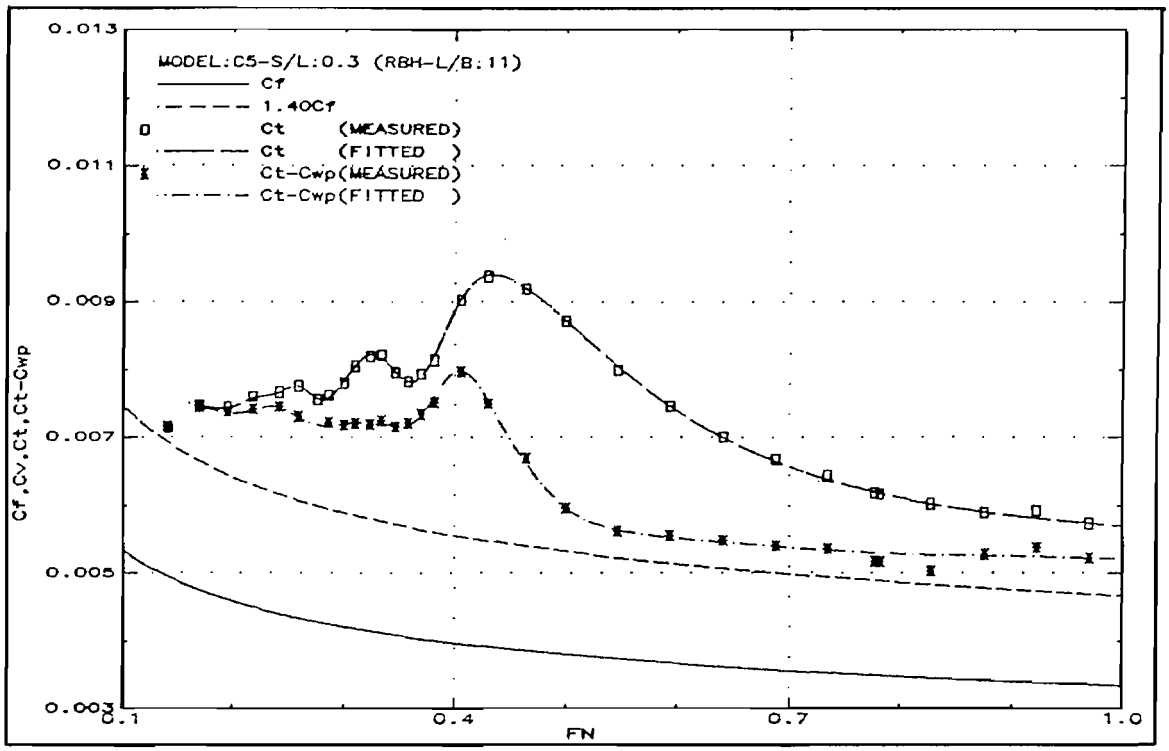

Fig.313: Resistance components (C5-S/L:Ø.3)

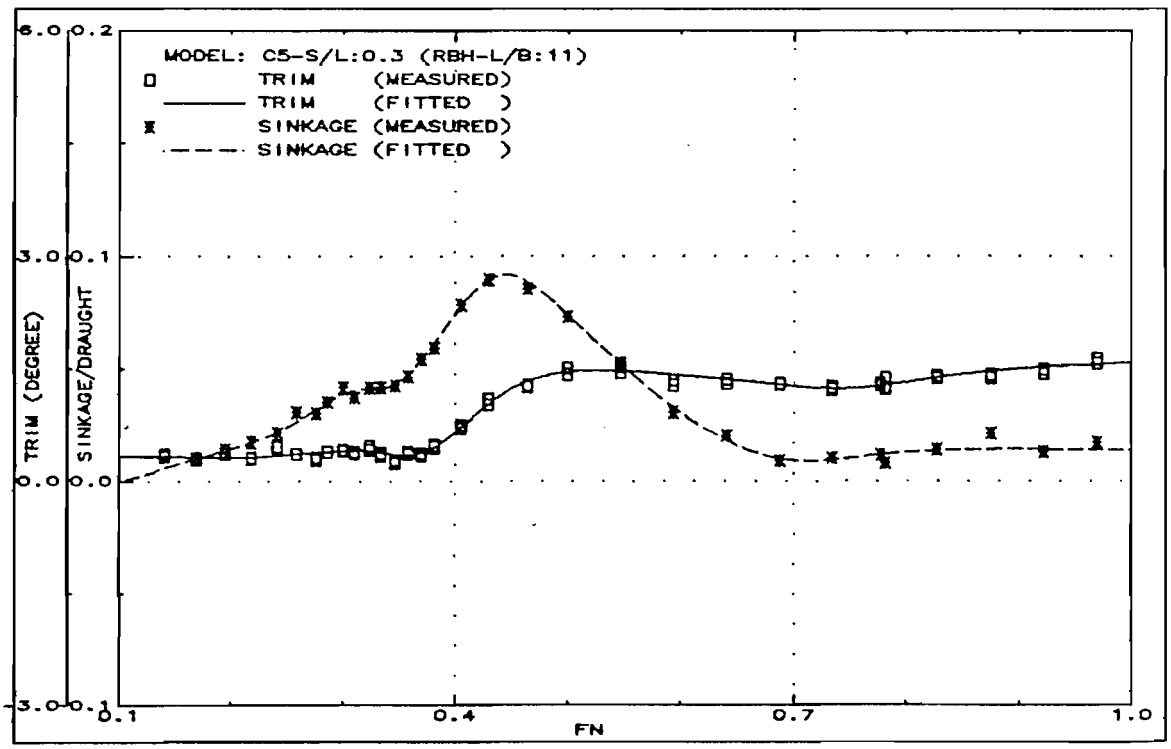

Fig.314: Running trim and sinkage (C5-S/L:Ø.3)

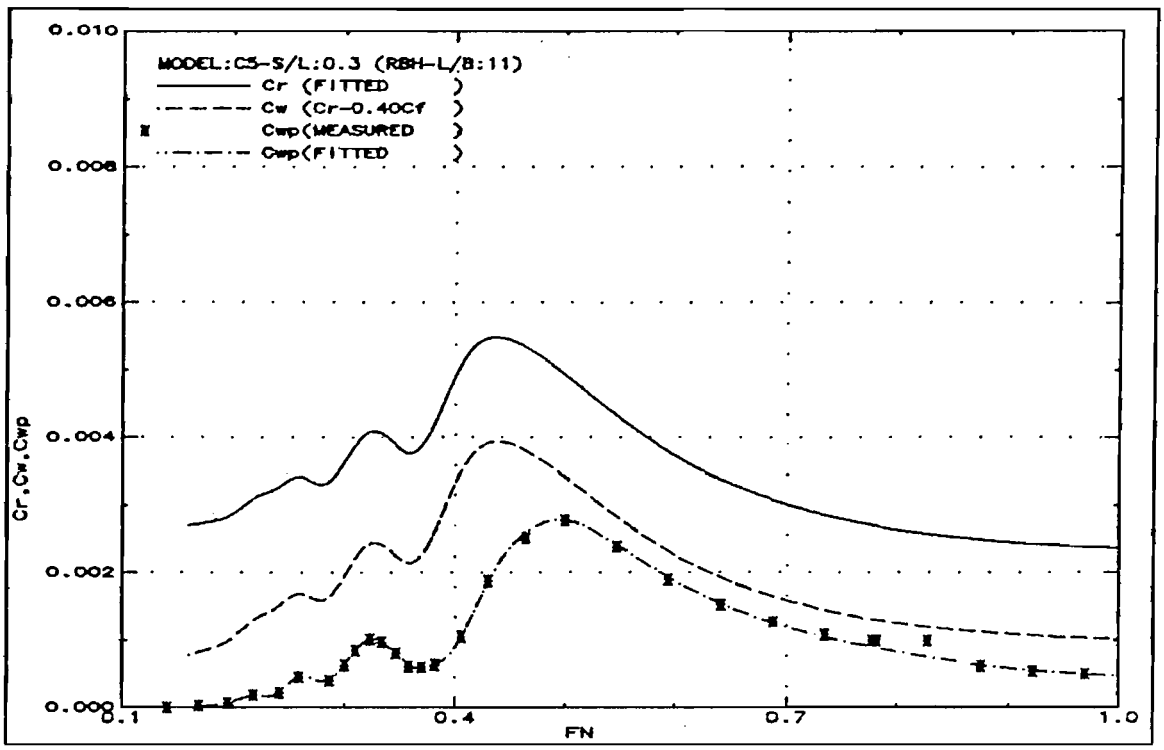

Fig.315: Measured wave resistance (C5-S/L:Ø.3)

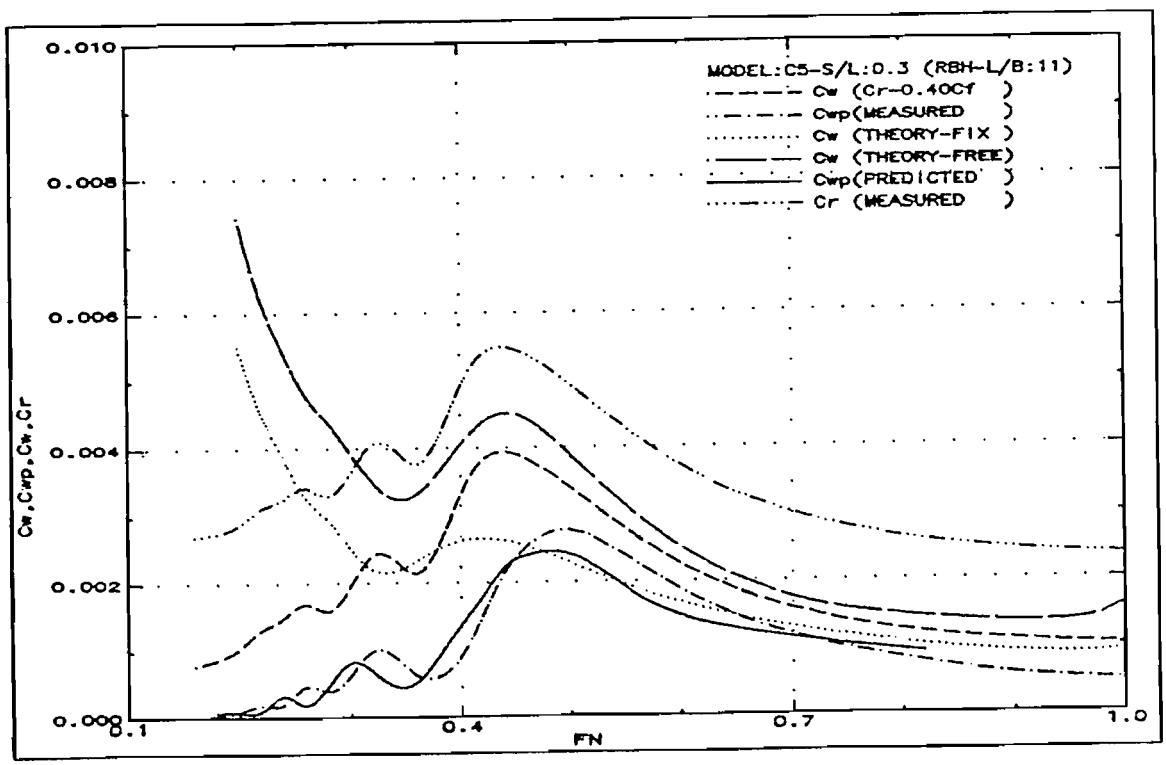

Fig.316: Wave resistance comparison (C5-S/L:Ø.3)

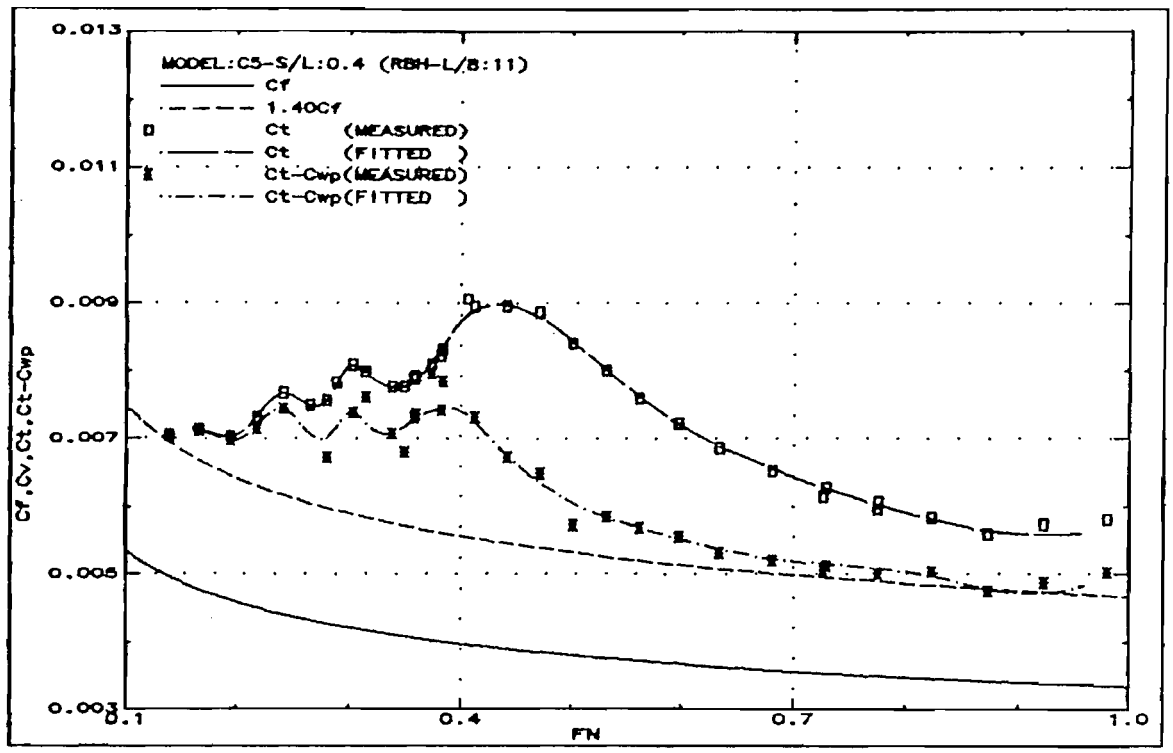

Fig.317: Resistance components (C5-S/L:Ø.4)

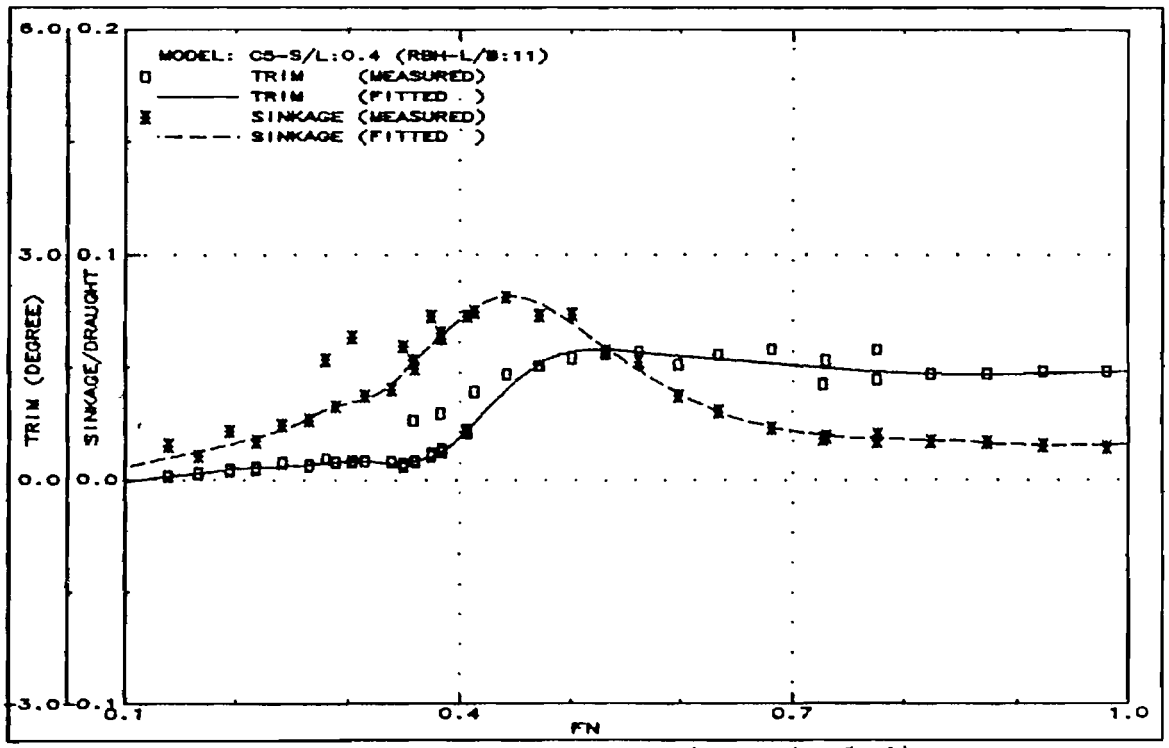

Fig.318: Running trim and sinkage (C5-S/L:Ø.4)

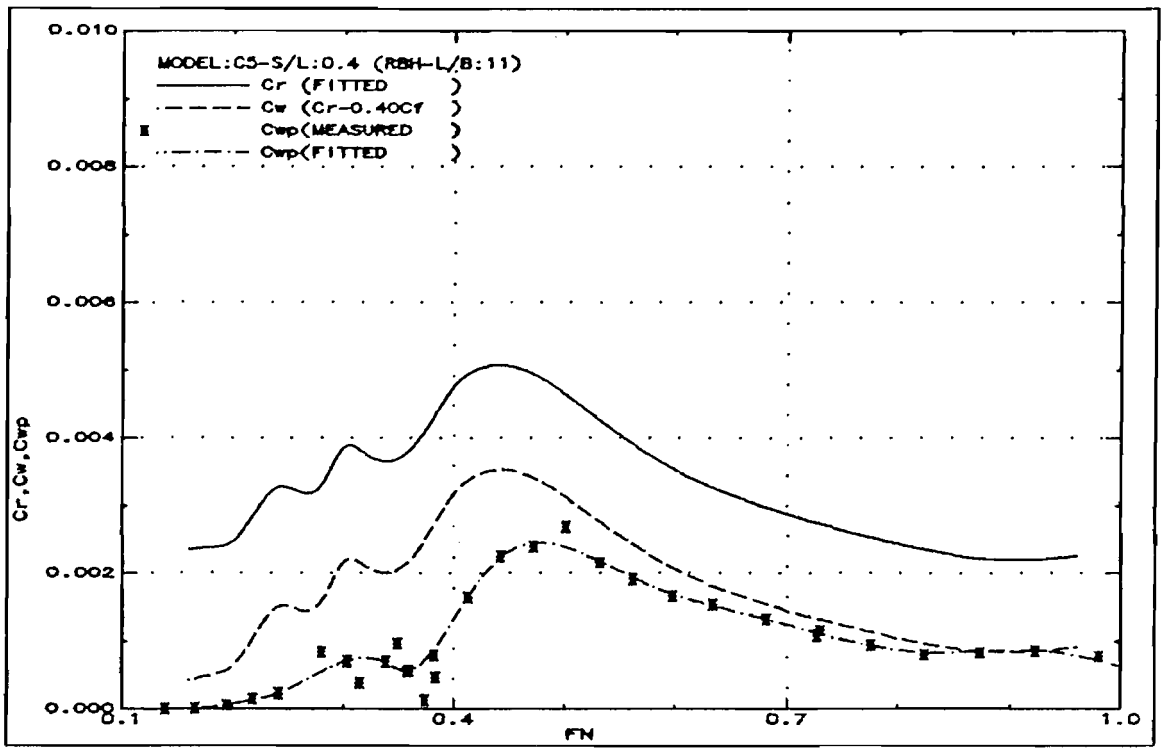

Fig.319: Measured wave resistance (C5-S/L:0.4)

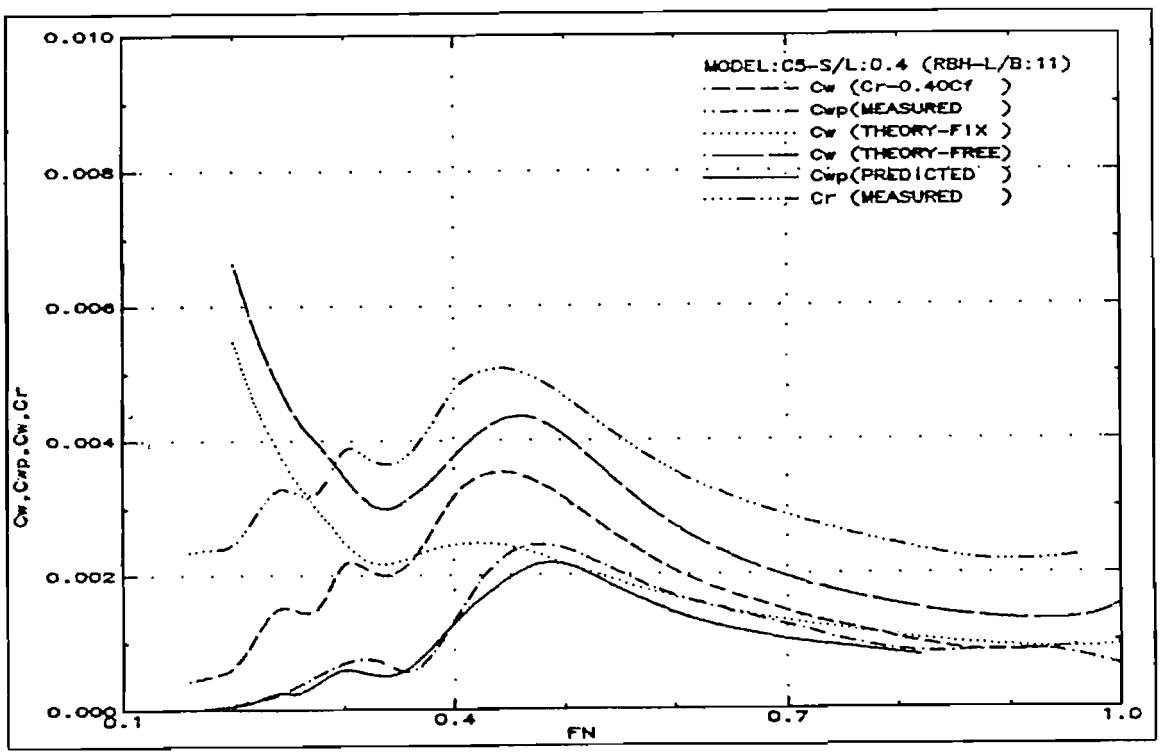

Fig.320: Wave resistance comparison (C5-S/L:0.4)

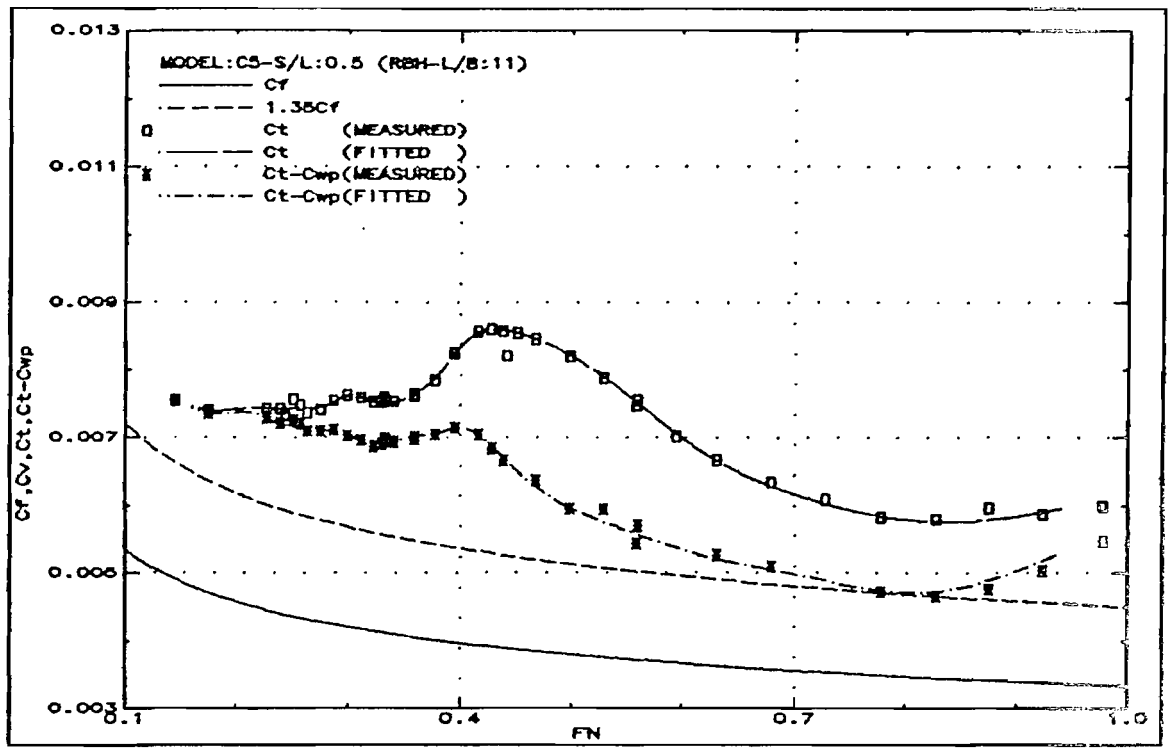

Fig.321: Resistance components (C5-S/L:Ø.5)

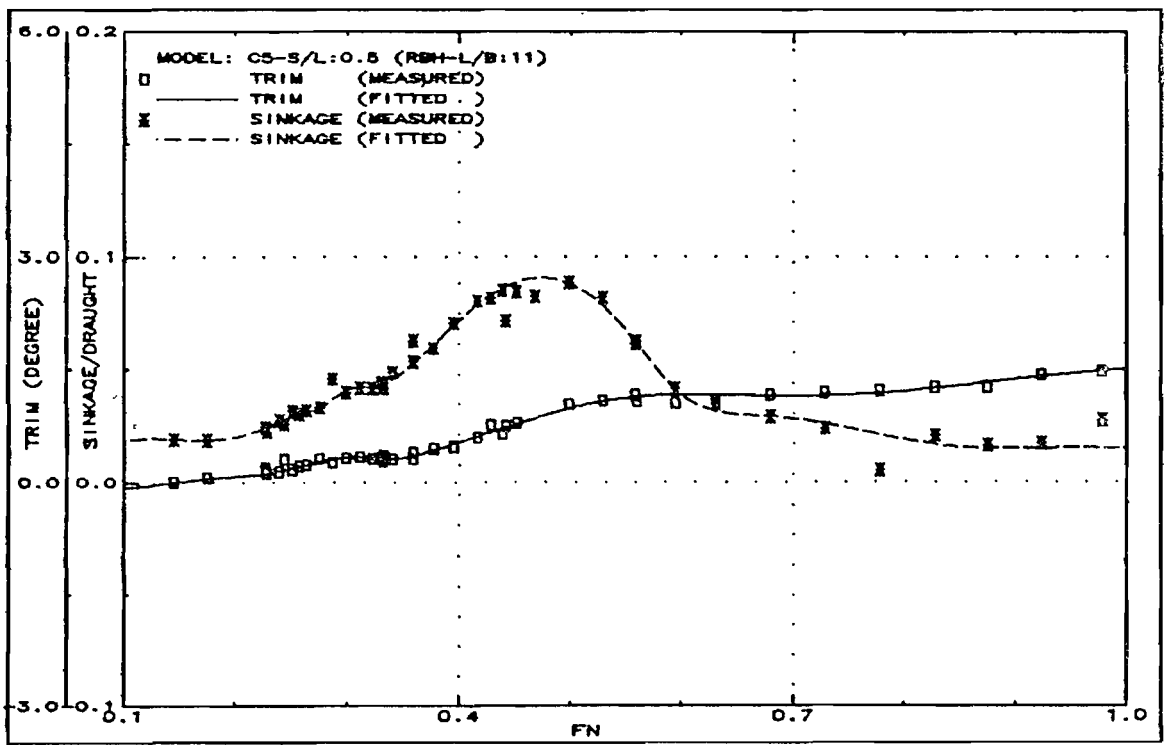

Fig.322: Running trim and sinkage (C5-S/L:Ø.5)

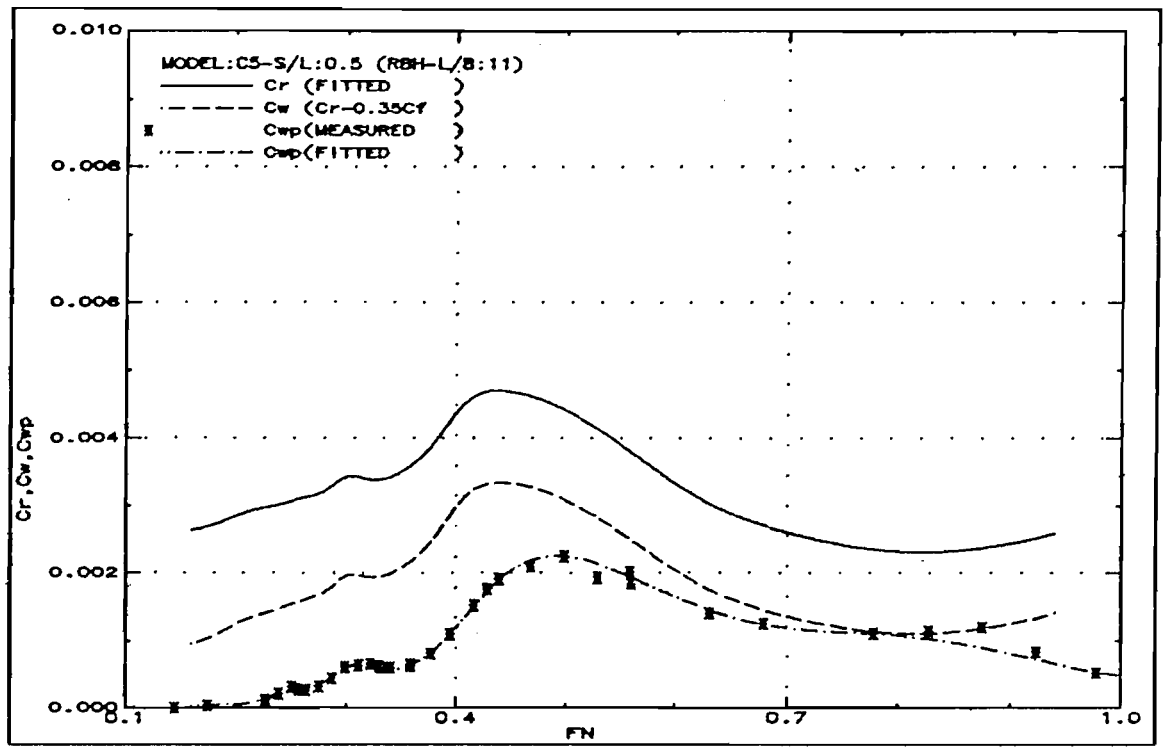

Fig.323: Measured wave resistance (C5-S/L:Ø.5)

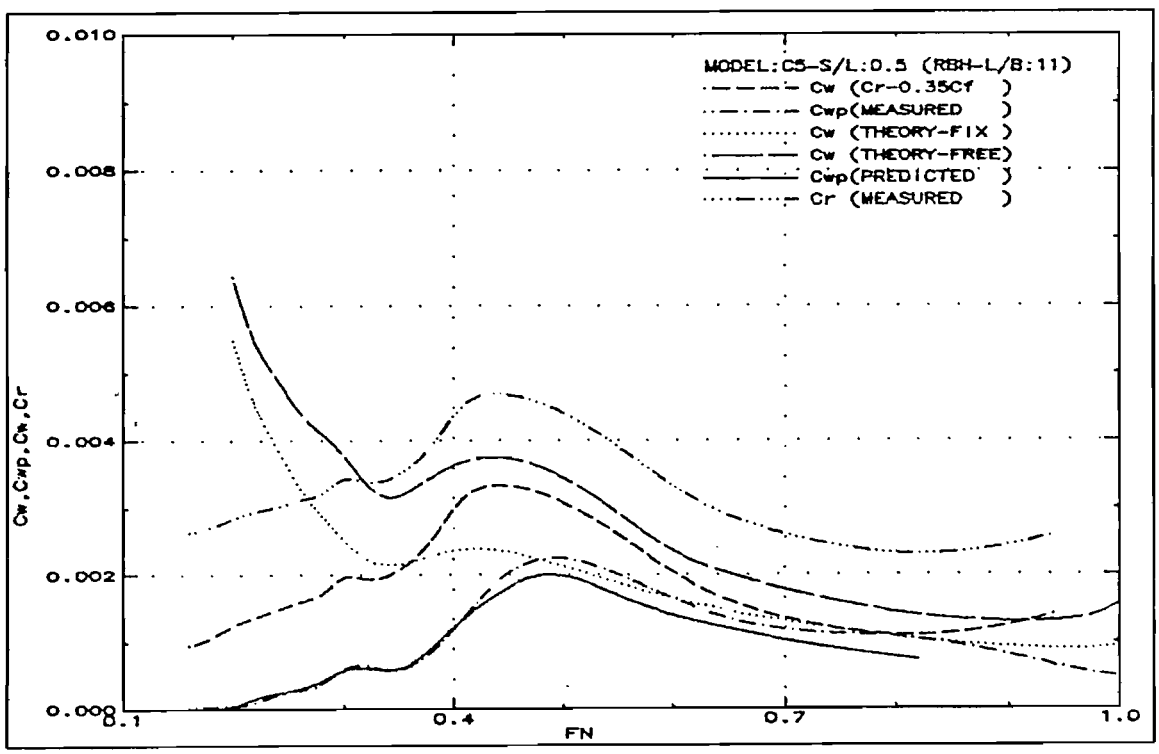

Fig.324: Wave resistance comparison (C5-S/L:Ø.5)

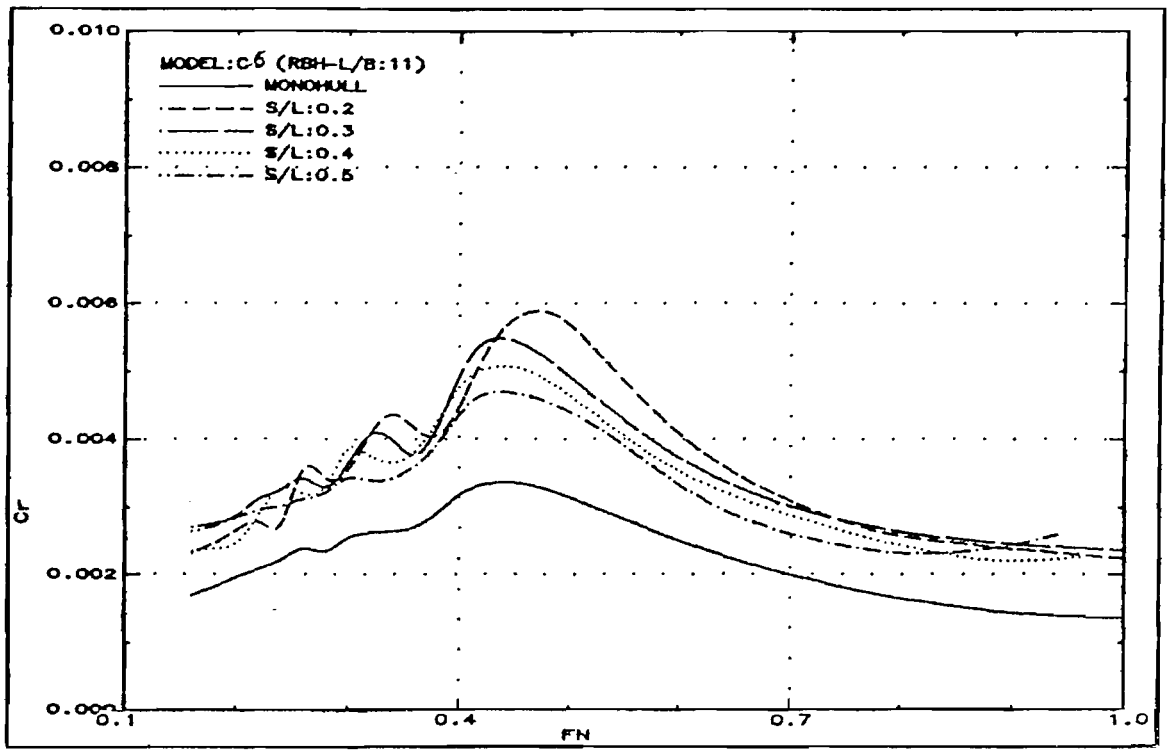

Fig.325: Residuary resistance (C5)

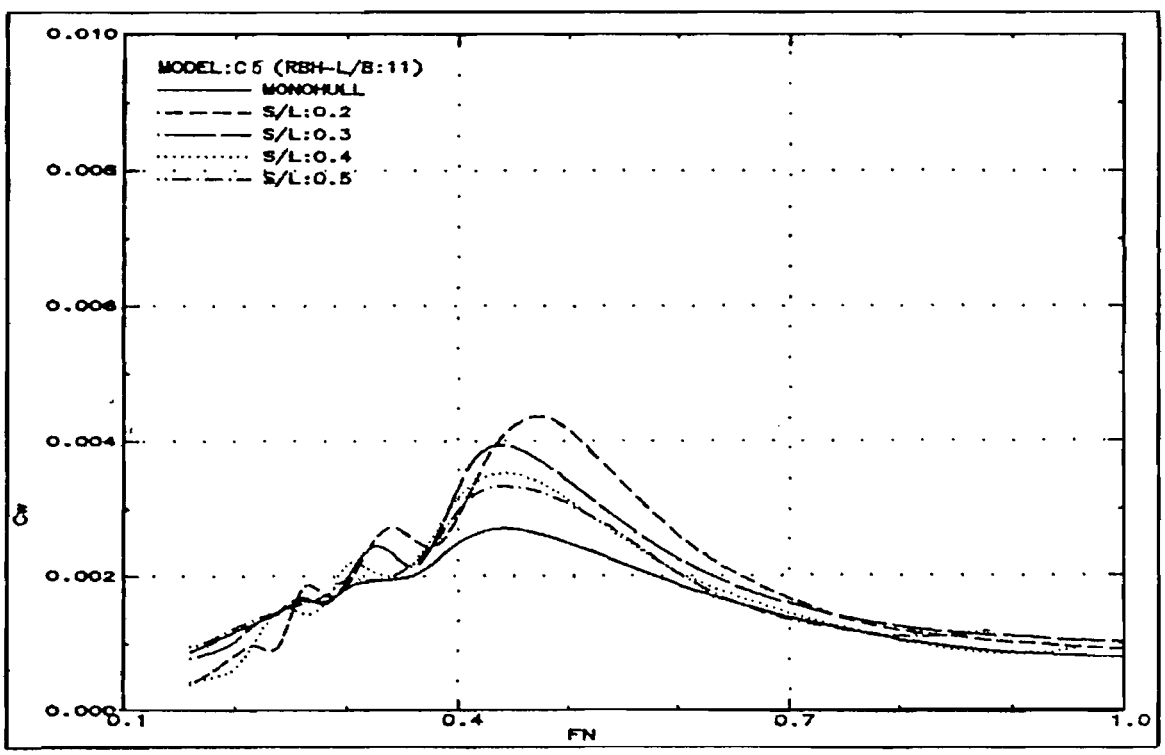

Fig.326: Wave resistance (C5)

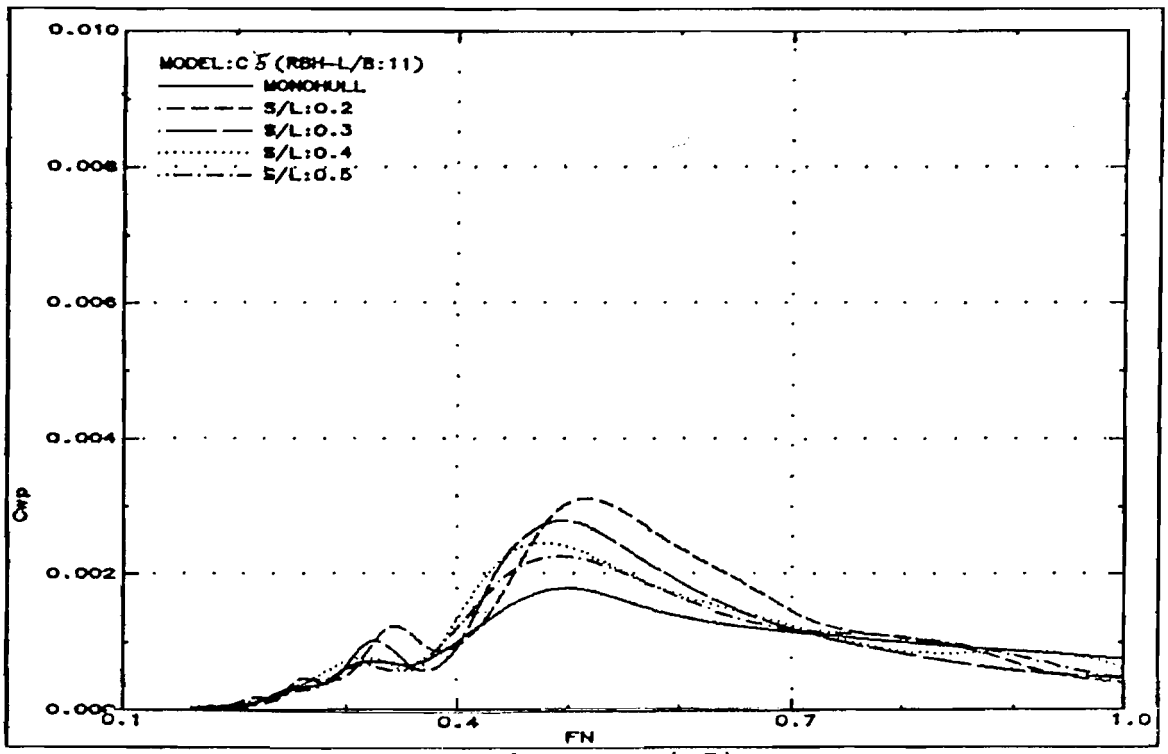

Fig.327: Wave pattern resistance (C5)

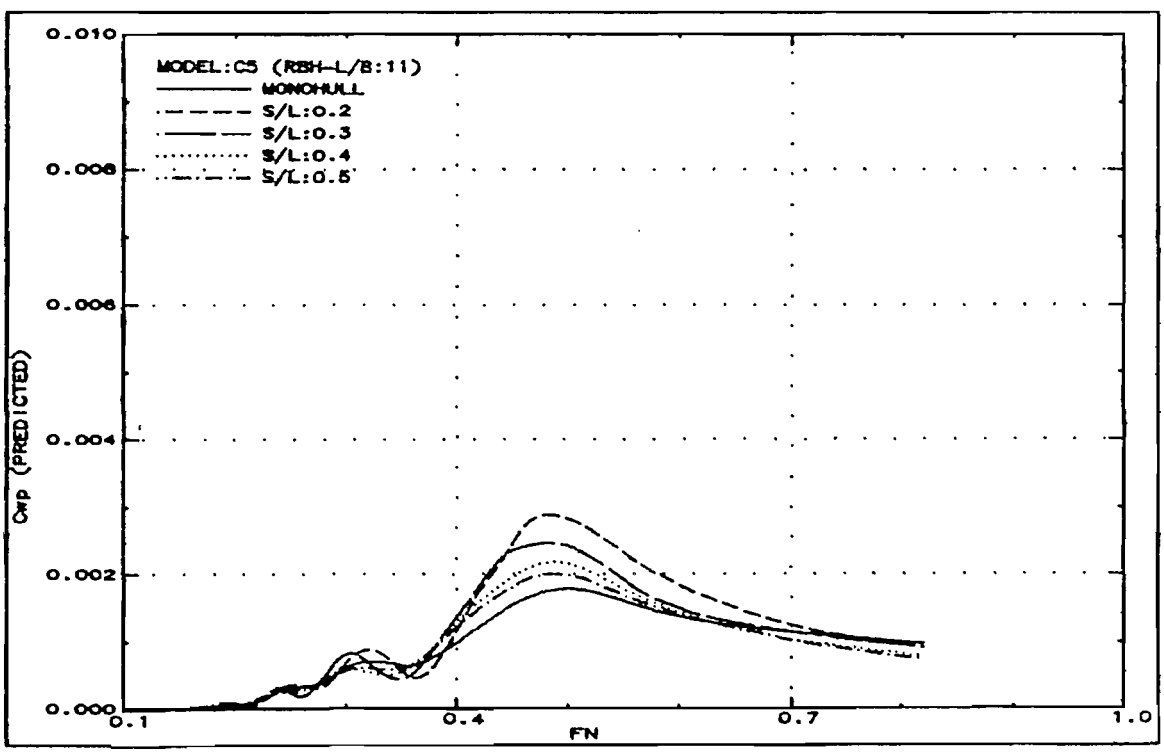

Fig.328: Wave pattern resistance predicted from monohull wave pattern analysis (C5)

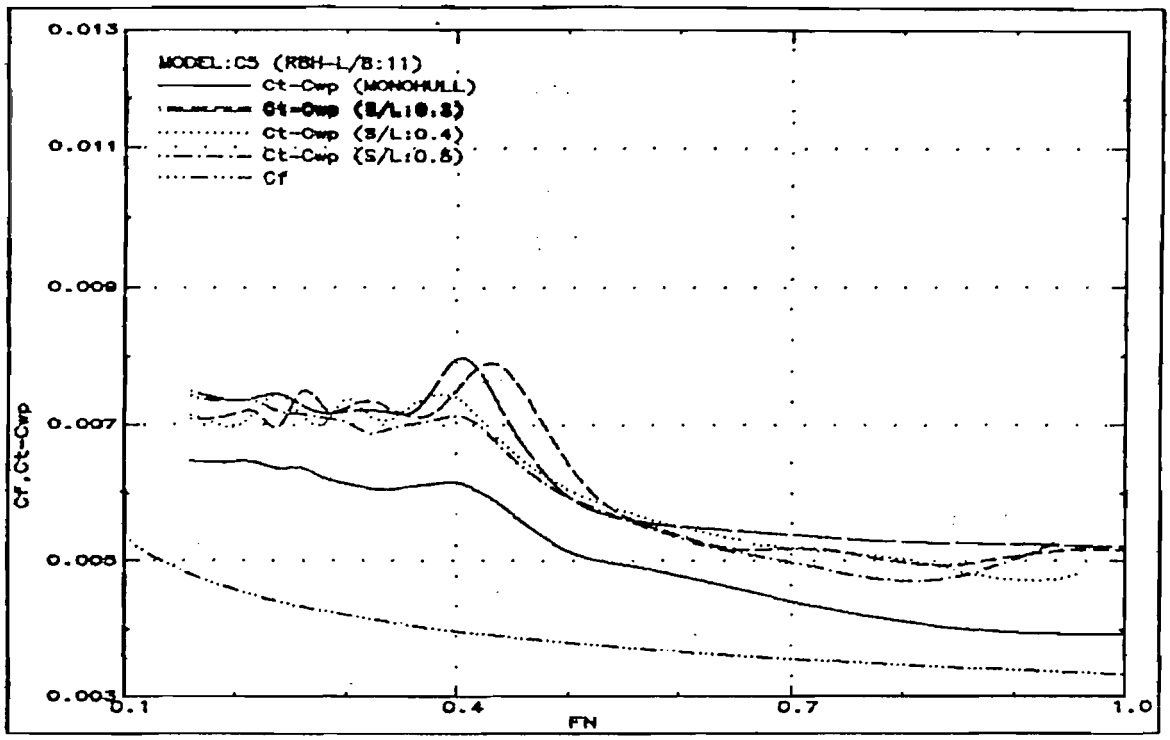

Fig.329: Total resistance minus wave pattern resistance (C5)

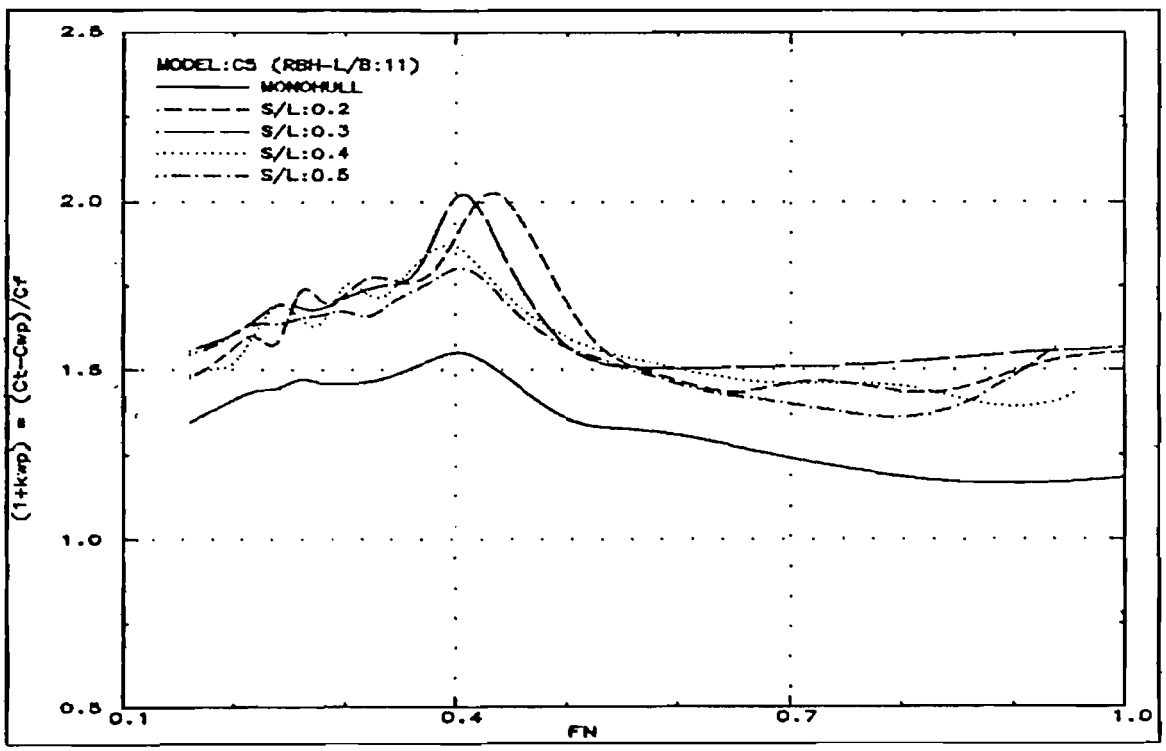

Fig.330: Form factor, i.e. $1+k_{WP}=(C_T-C_{WP})/C_F$ (C5)

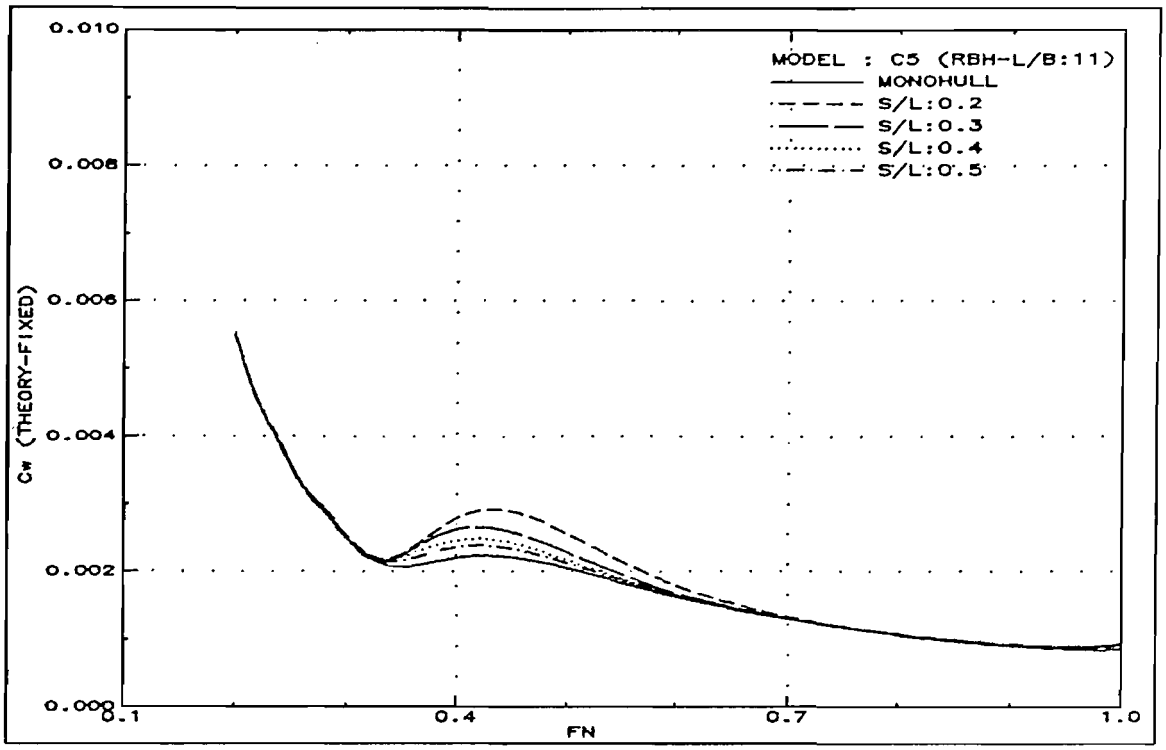

Fig.331: Theoretical wave resistance in fixed condition (C5)

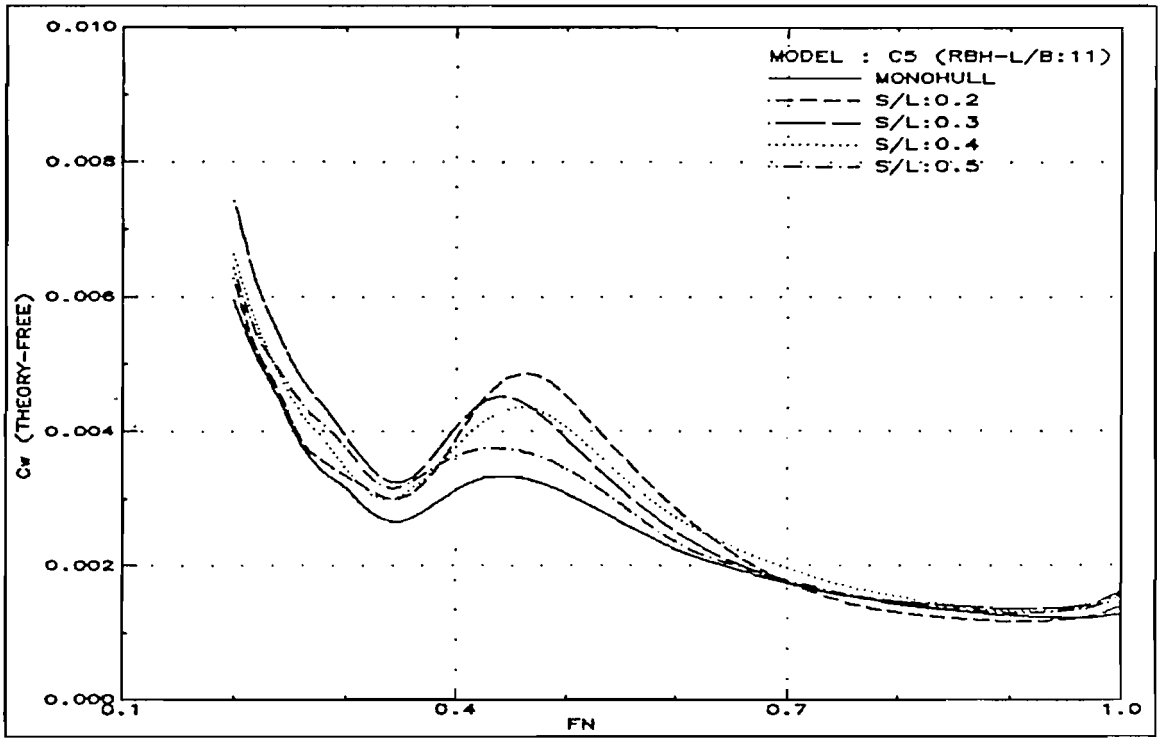

Fig.332: Theoretical wave resistance in free condition (C5)

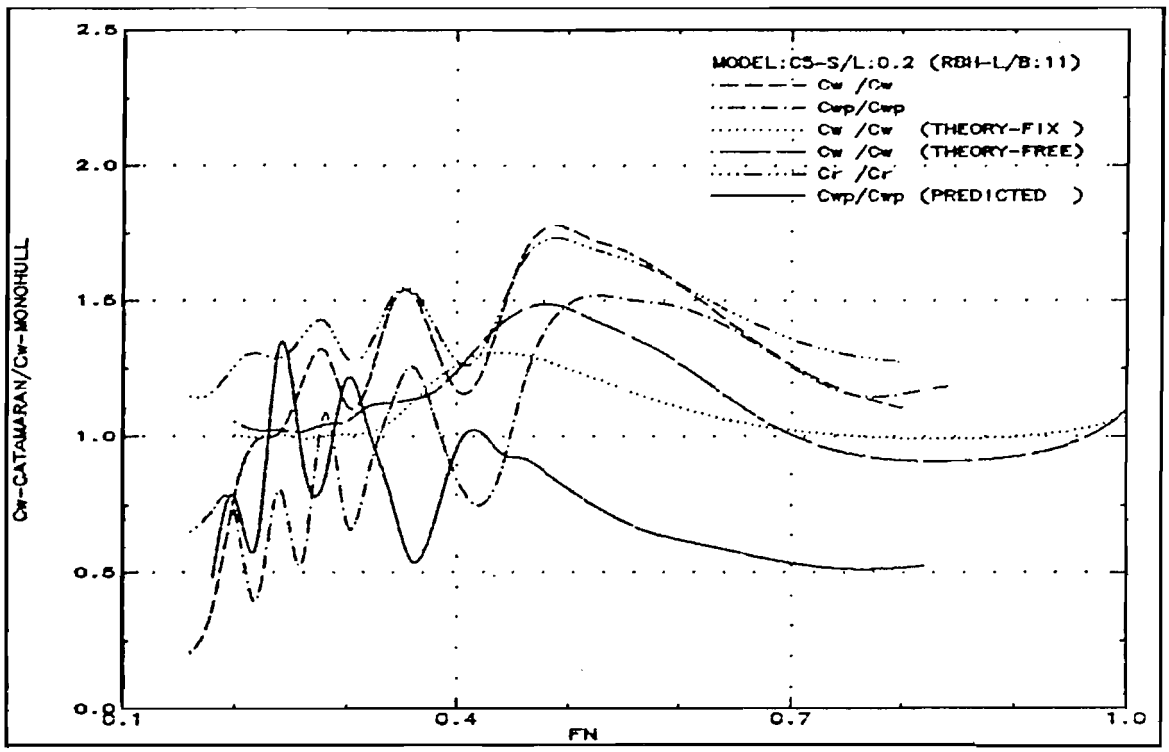

Fig.333: Wave resistance interference ratio (C5-S/L:Ø.2)

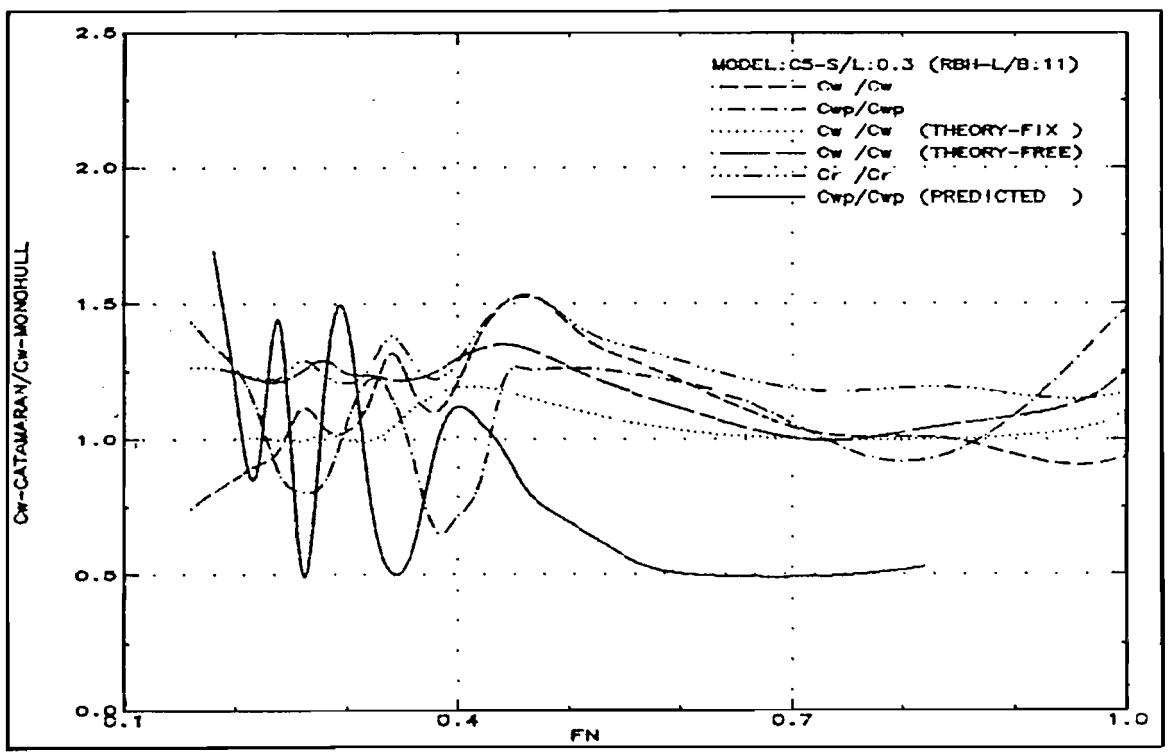

Fig.334: Wave resistance interference ratio (C5-S/L:Ø.3)

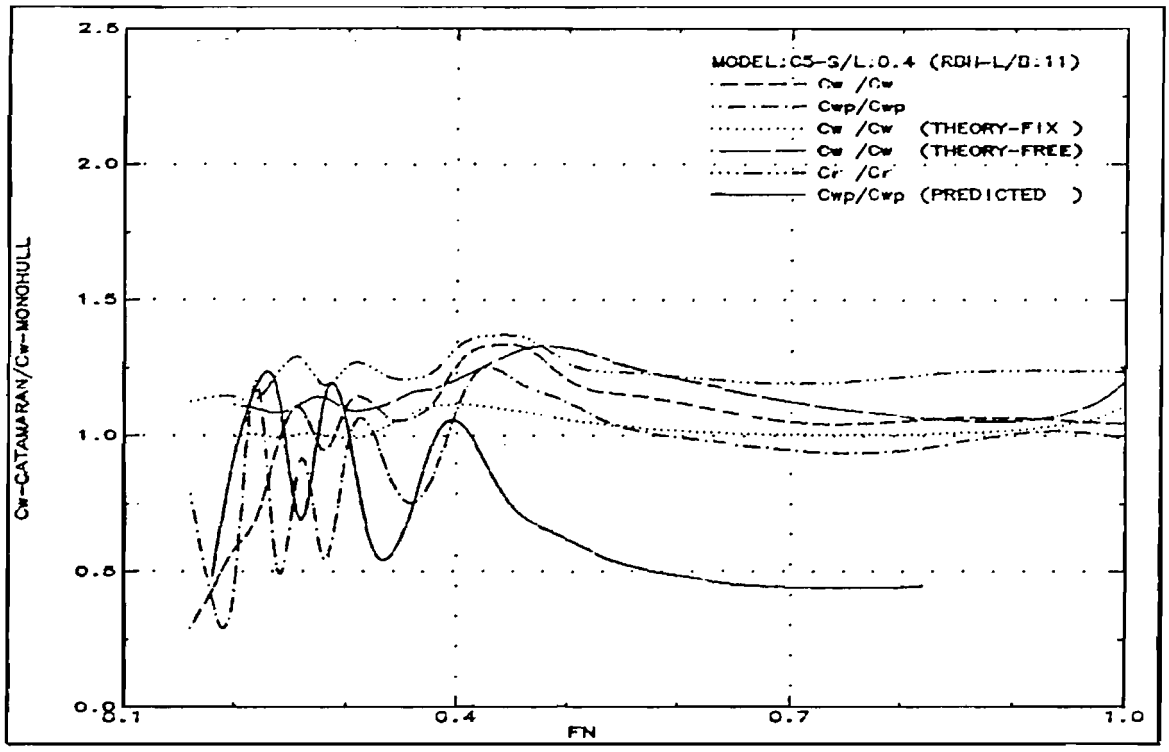

Fig.335: Wave resistance interference ratio (C5-S/L:Ø.4)

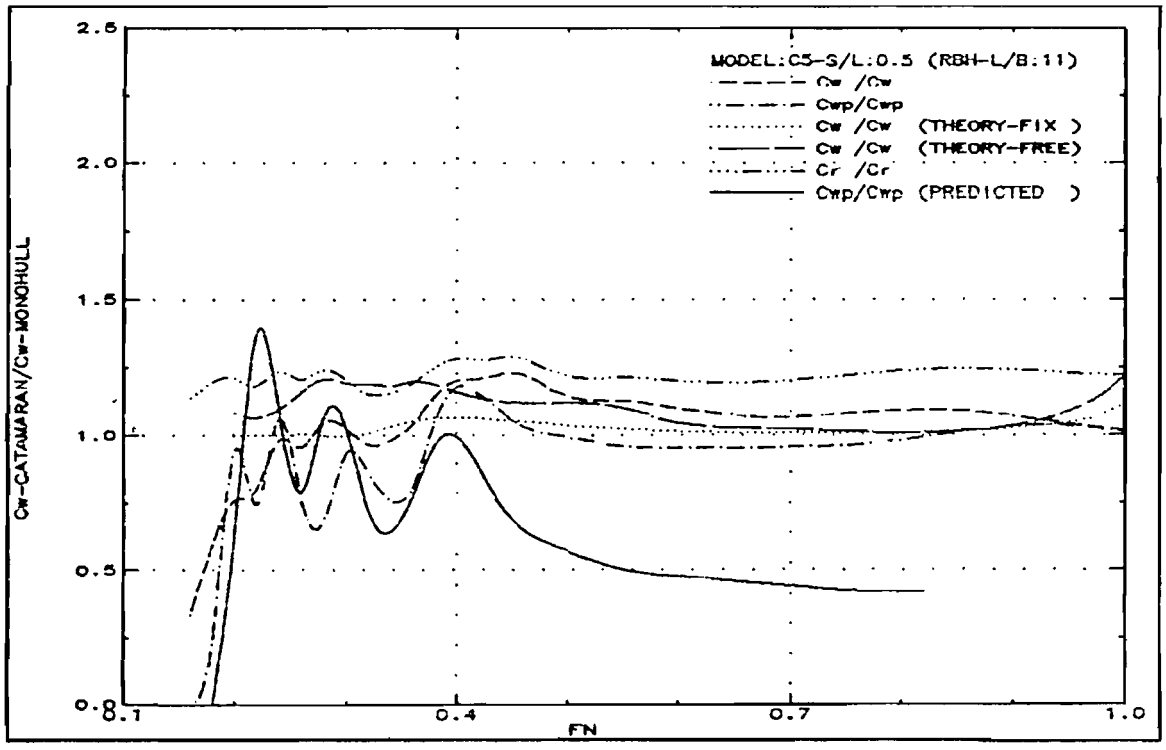

Fig.336: Wave resistance interference ratio (C5-S/L:Ø.5)

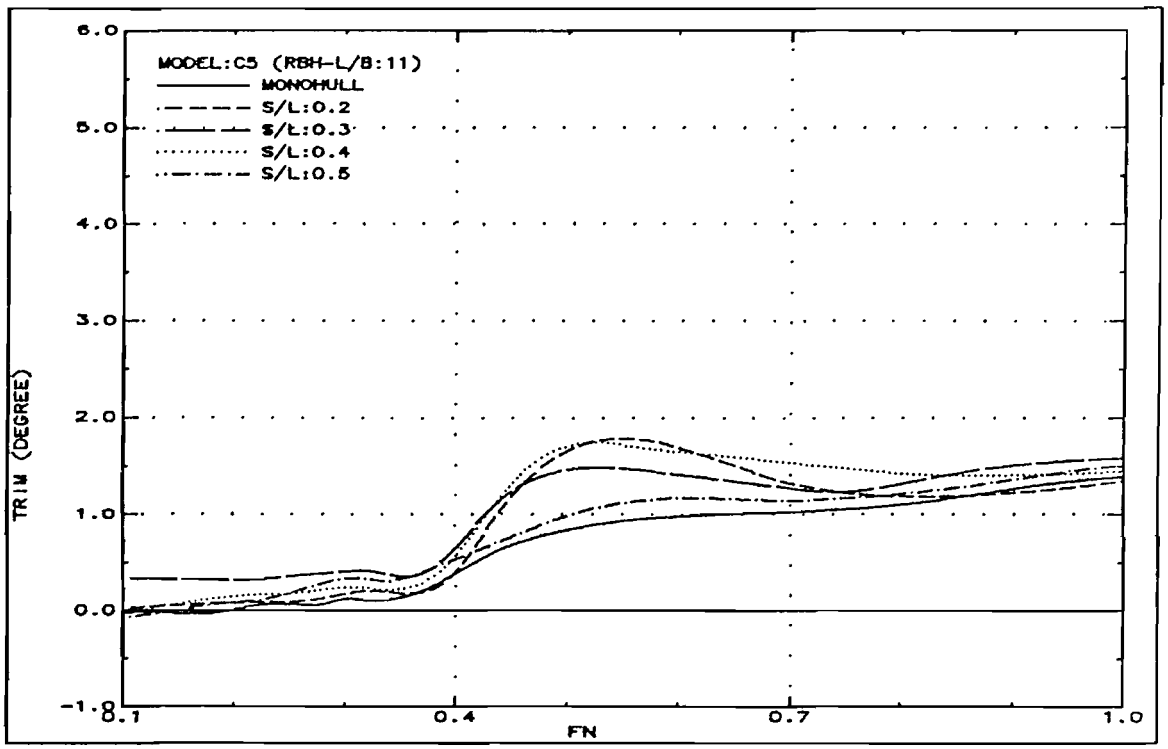

Fig.337: Running trim (C5)

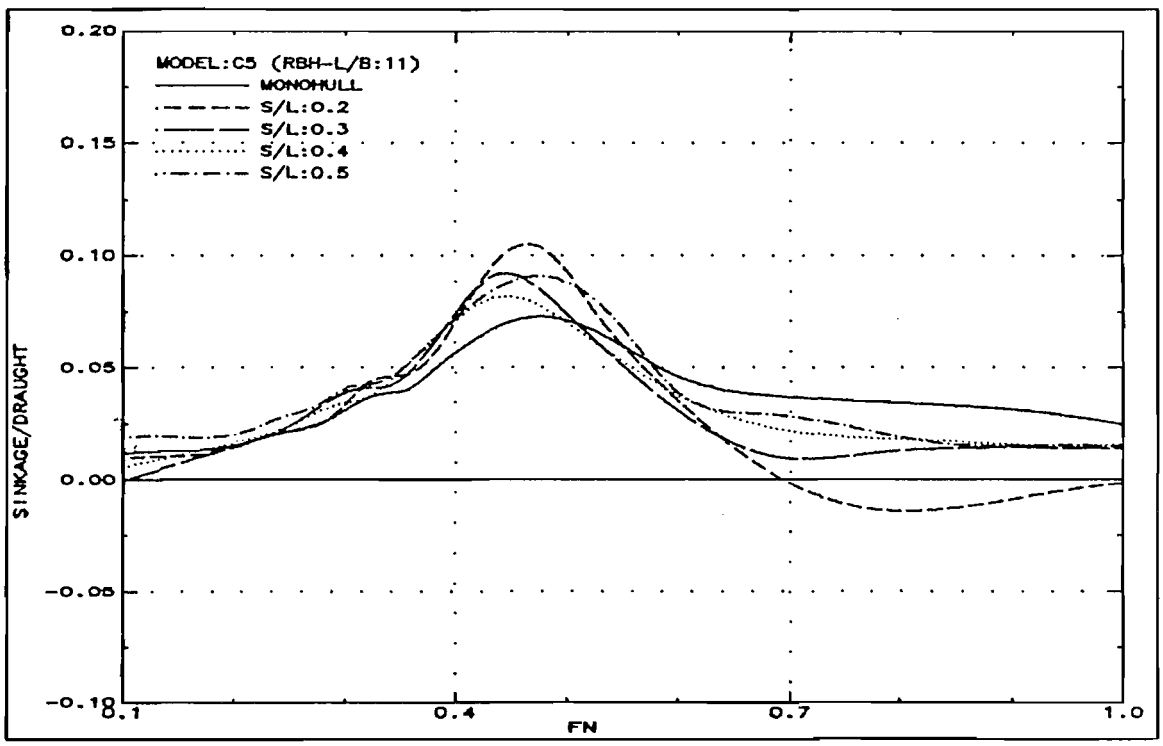

Fig.338: Sinkage (C5)

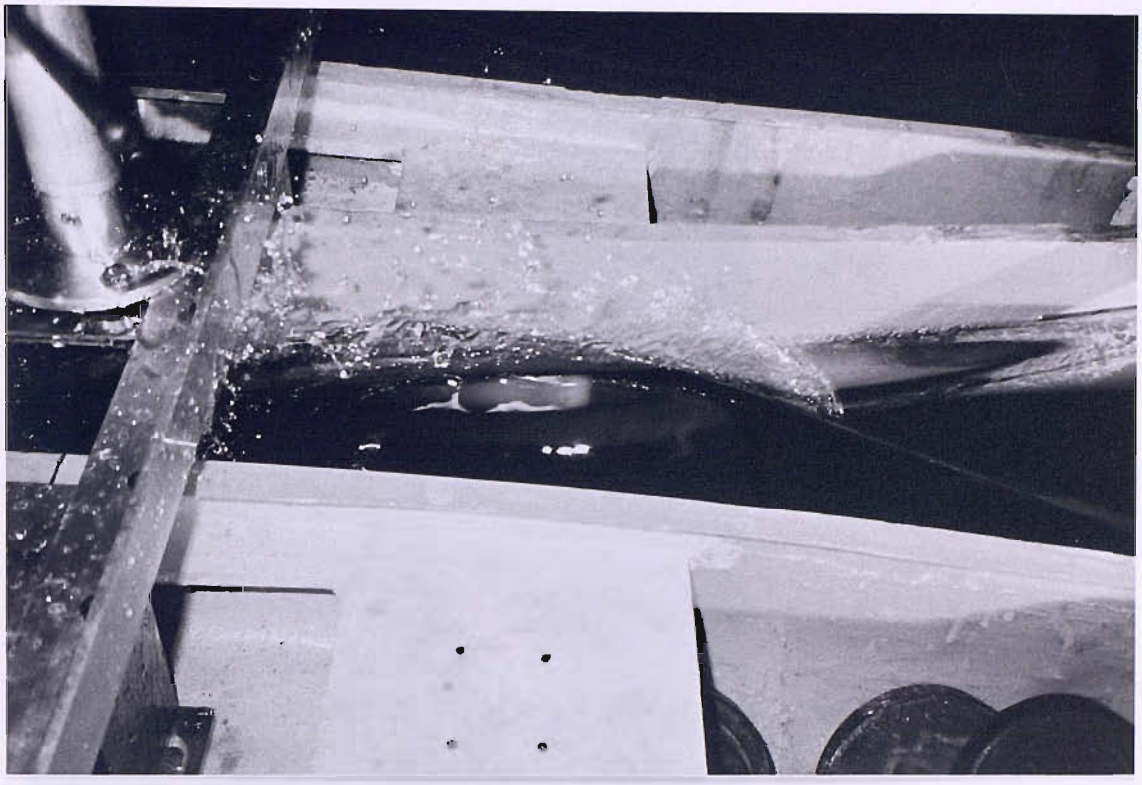

Fig. 339: Wave breaking between the demihulls
(Model: C2-S/L:Ø.2 Fn: Ø.59)

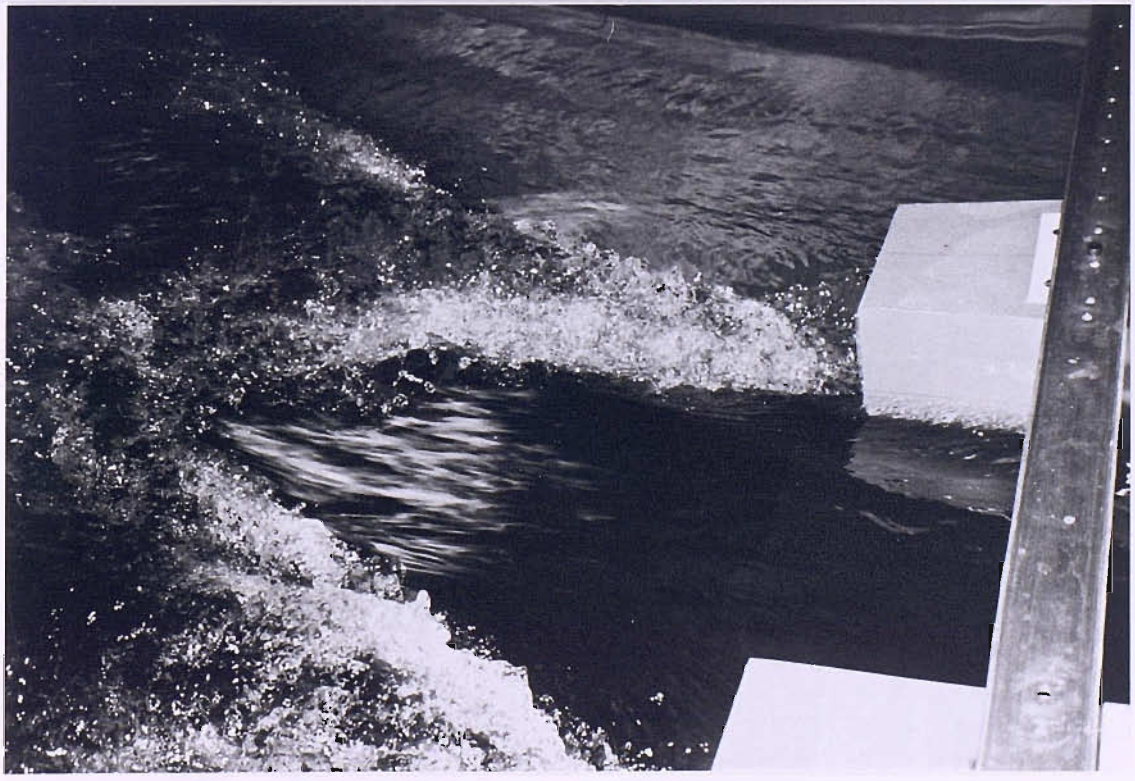

Fig. 340: Wave breaking due to transom stern
(Model: C4-S/L:Ø.3 Fn:Ø.45)

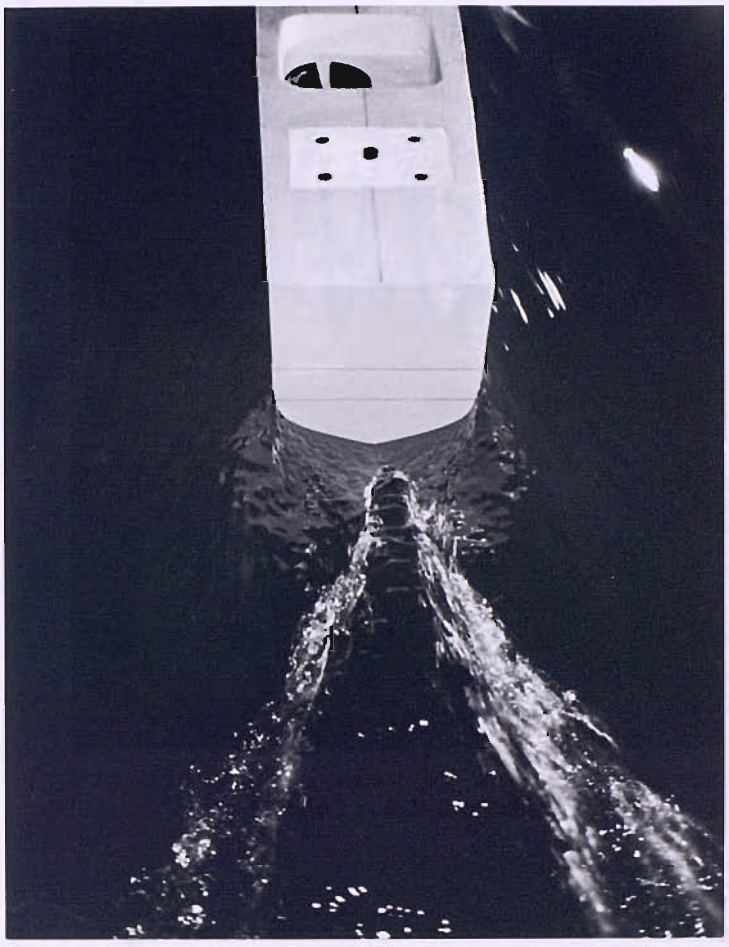

Fig.341 : Plan view of flow around transom stern
(Model: C4-Monohull Fn: 0.35)

Fig.342 : Side view of flow around transom stern
(Model: C4-S/L:0.5 Fn: 0.55)

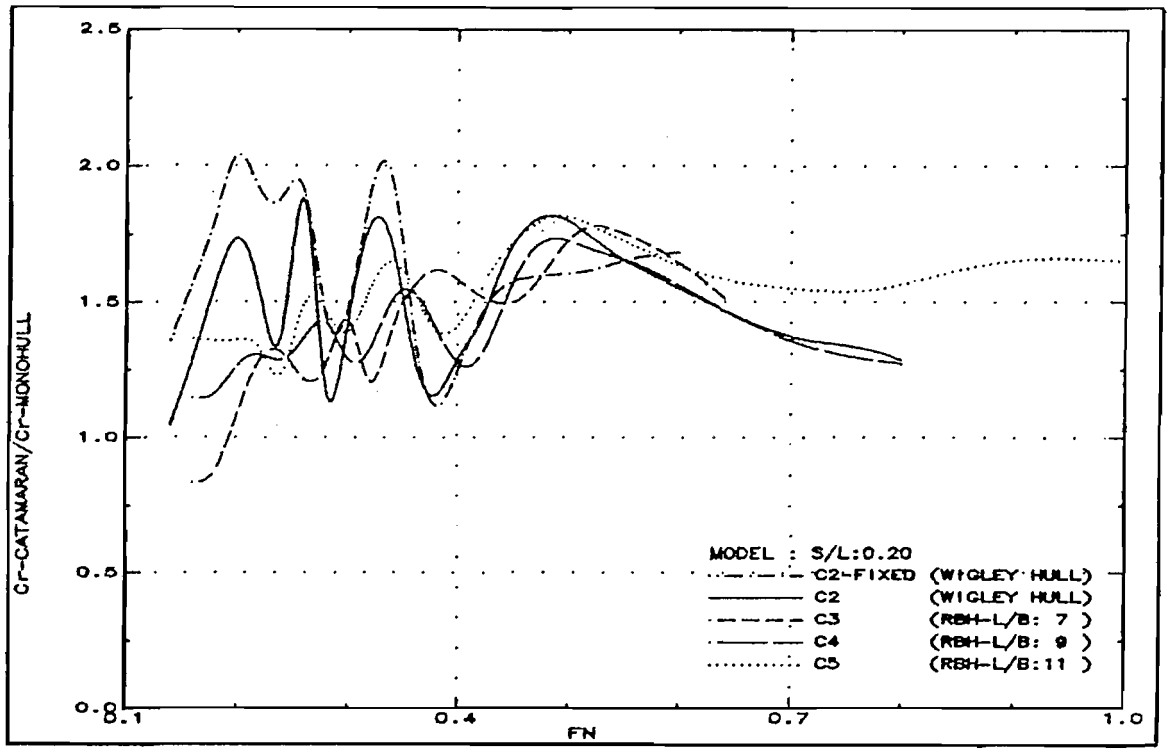

Fig.343: Residuary resistance interference ratio, Ω, comparison (S/L:0.2)

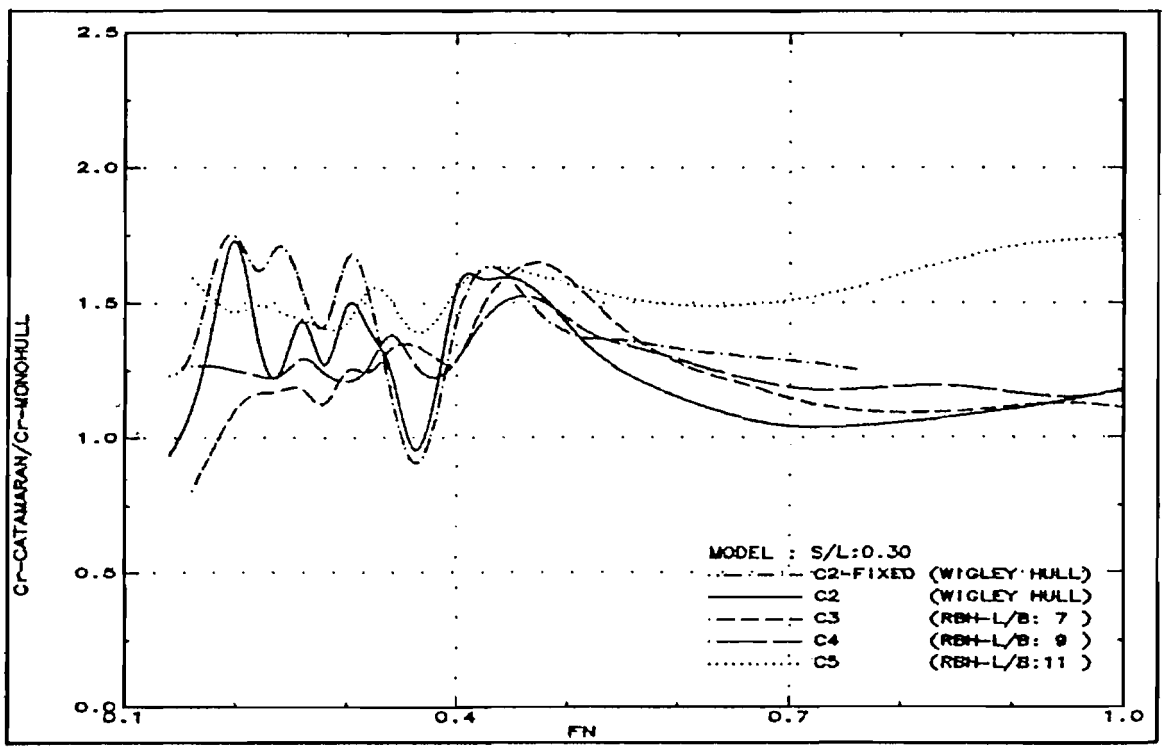

Fig.344: Residuary resistance interference ratio, Ω, comparison (S/L:0.3)

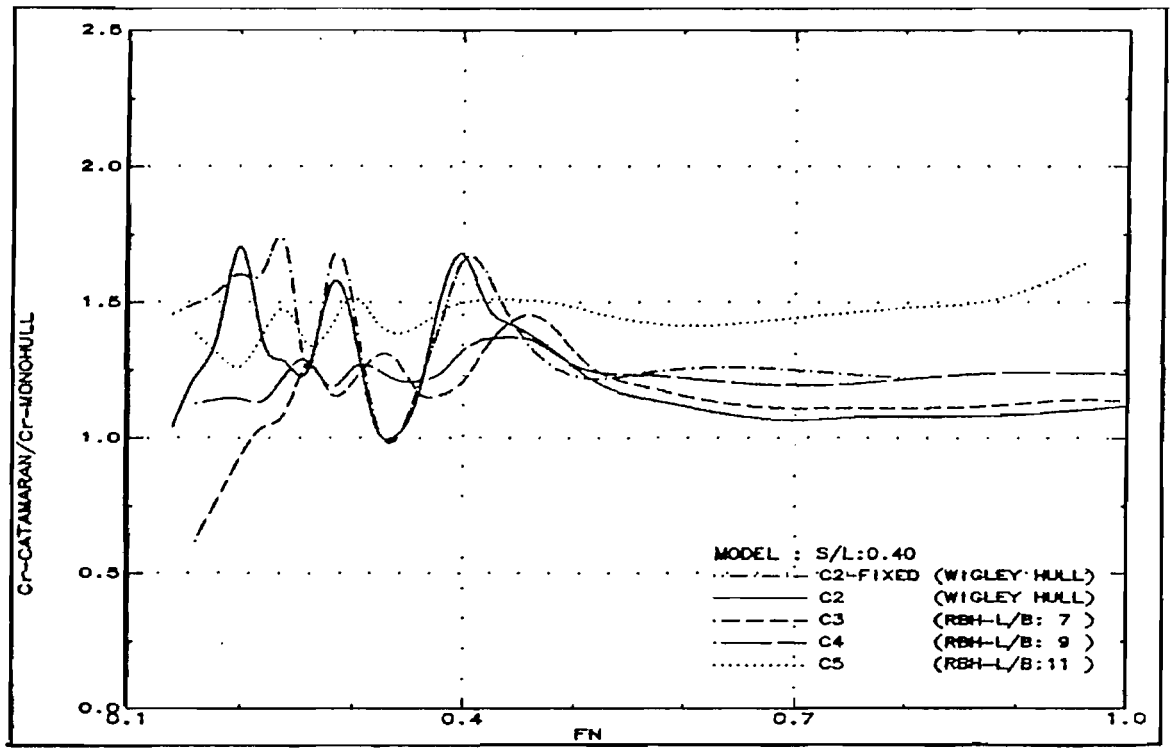

Fig.345: Residuary resistance interference ratio, Ω, comparison (S/L:Ø.4)

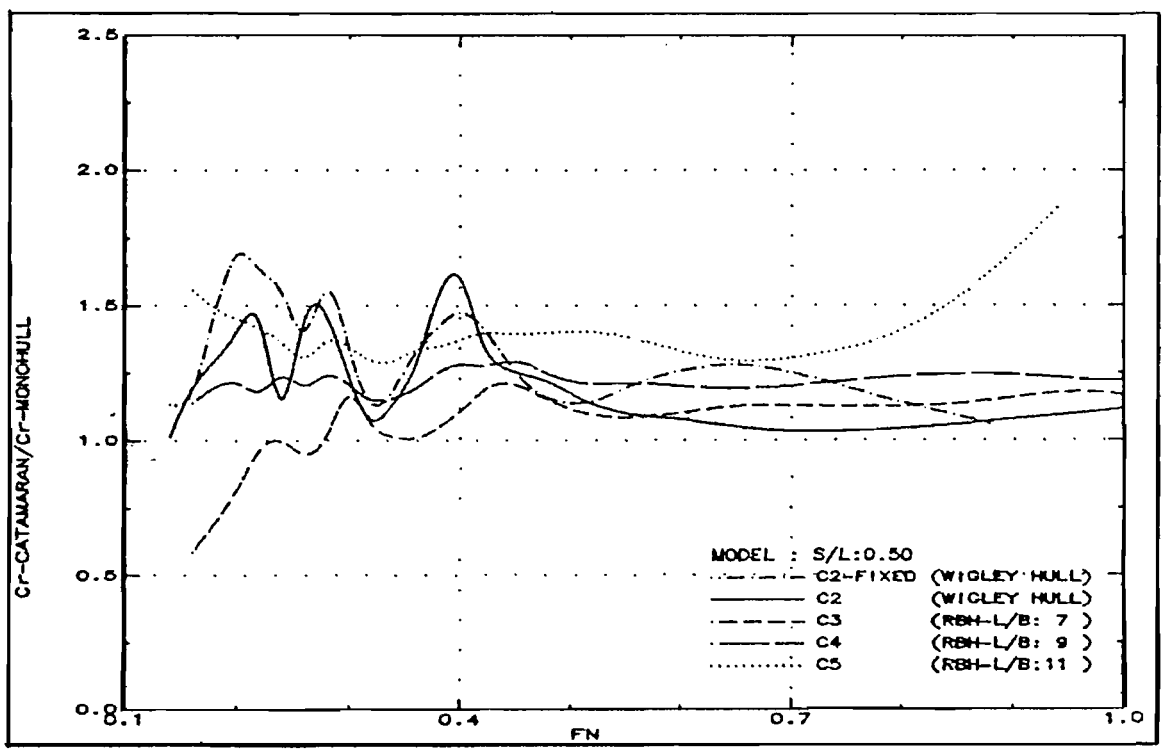

Fig.346: Residuary resistance interference ratio, Ω, comparison (S/L:Ø.5)

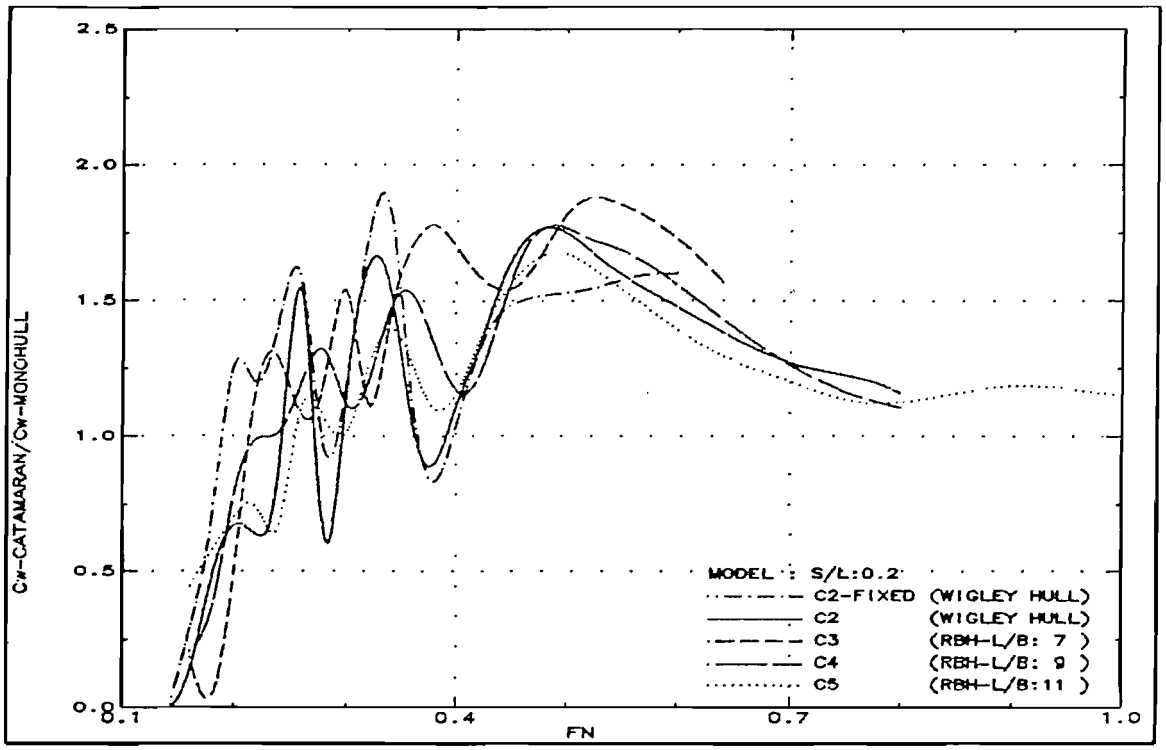

Fig.347: Wave resistance interference ratio, τ, comparison (S/L:Ø.2)

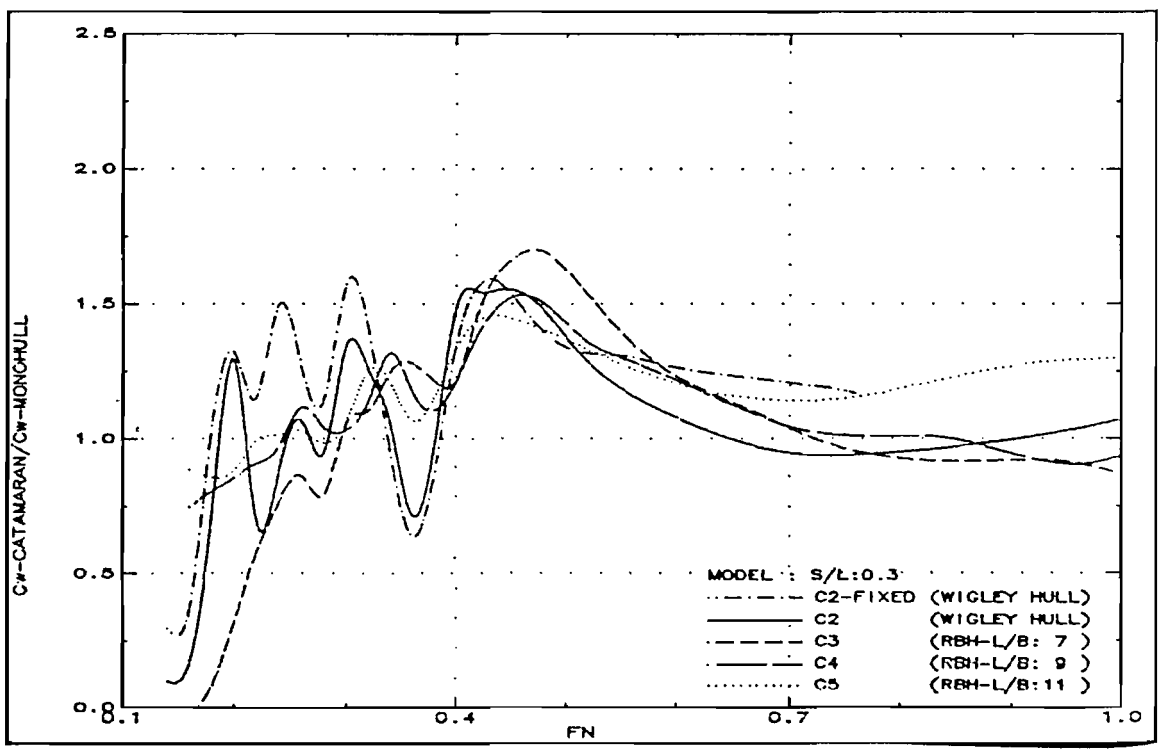

Fig.348: Wave resistance interference ratio, τ, comparison (S/L:Ø.3)

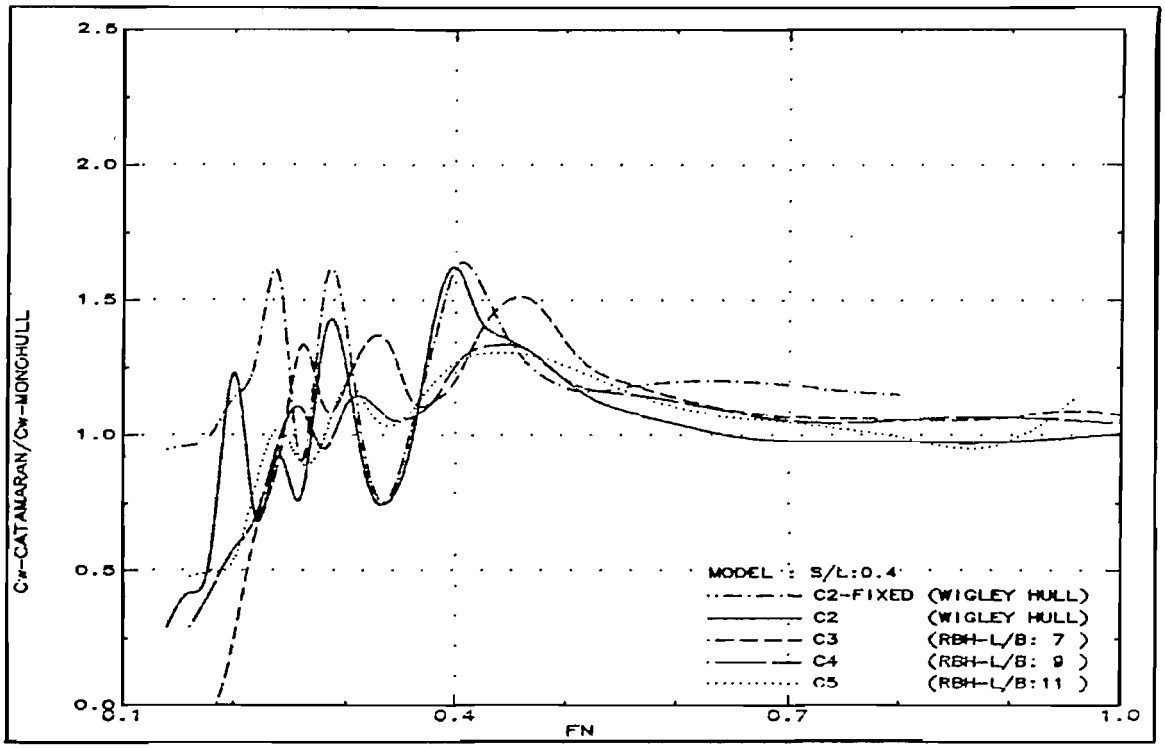

Fig.349: Wave resistance interference ratio, τ, comparison (S/L:Ø.4)

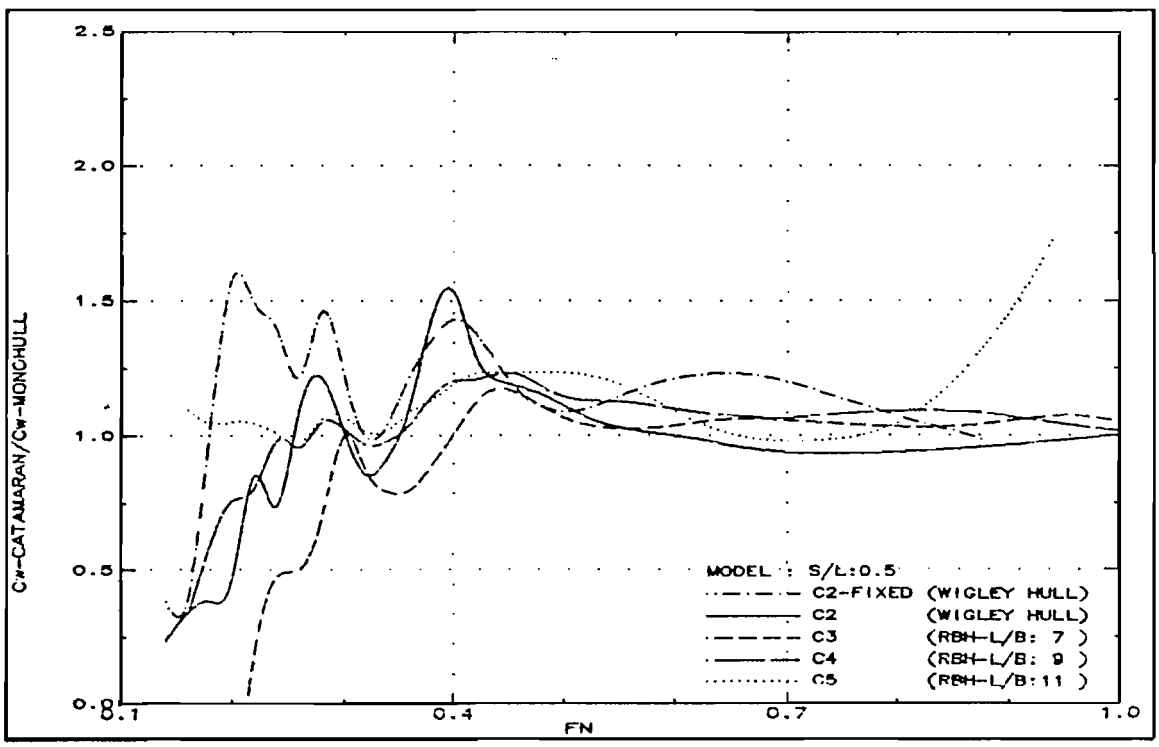

Fig.35Ø: Wave resistance interference ratio, τ, comparison (S/L:Ø.5)

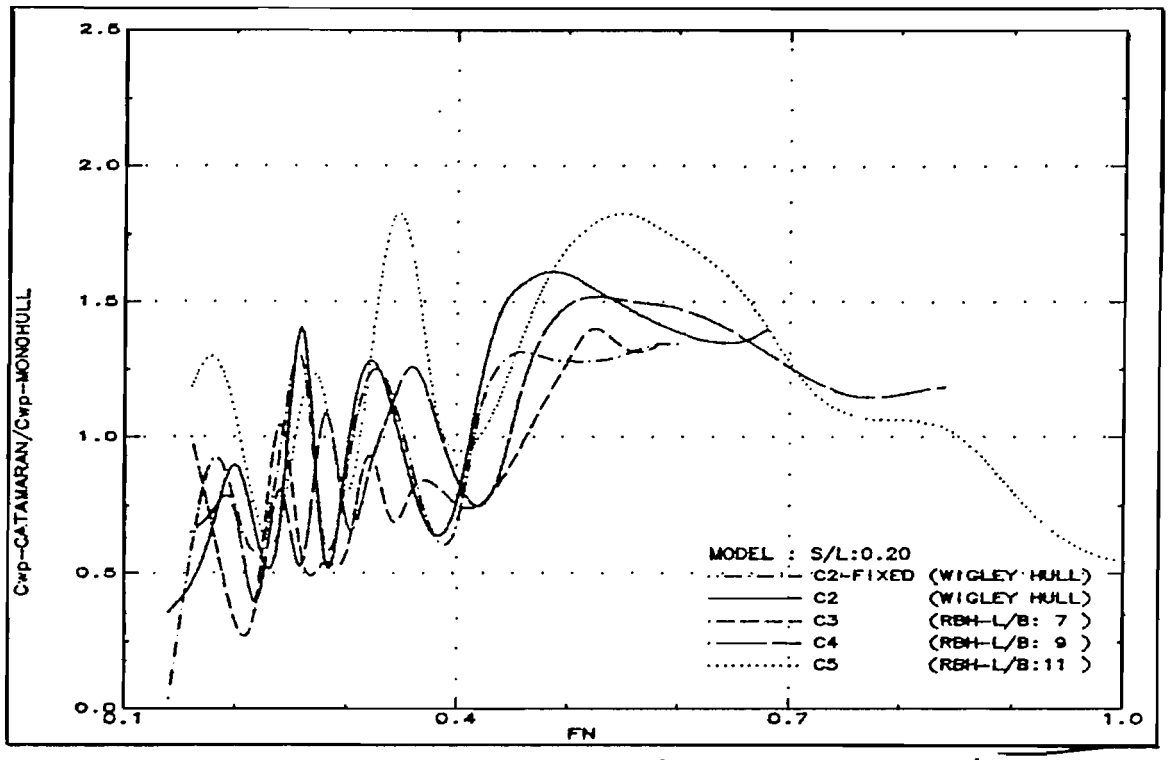

Fig.351: Wave pattern resistance interference ratio, μ, comparison (S/L:Ø.2)

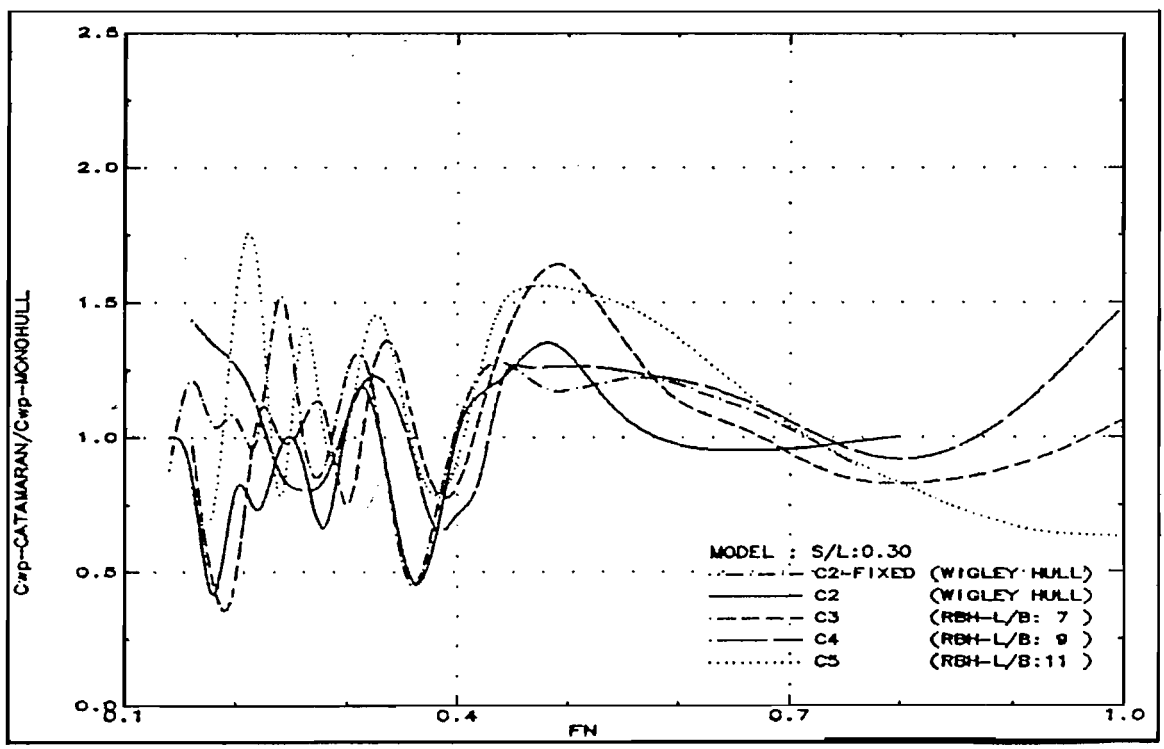

Fig.352: Wave pattern resistance interference ratio, μ, comparison (S/L:Ø.3)

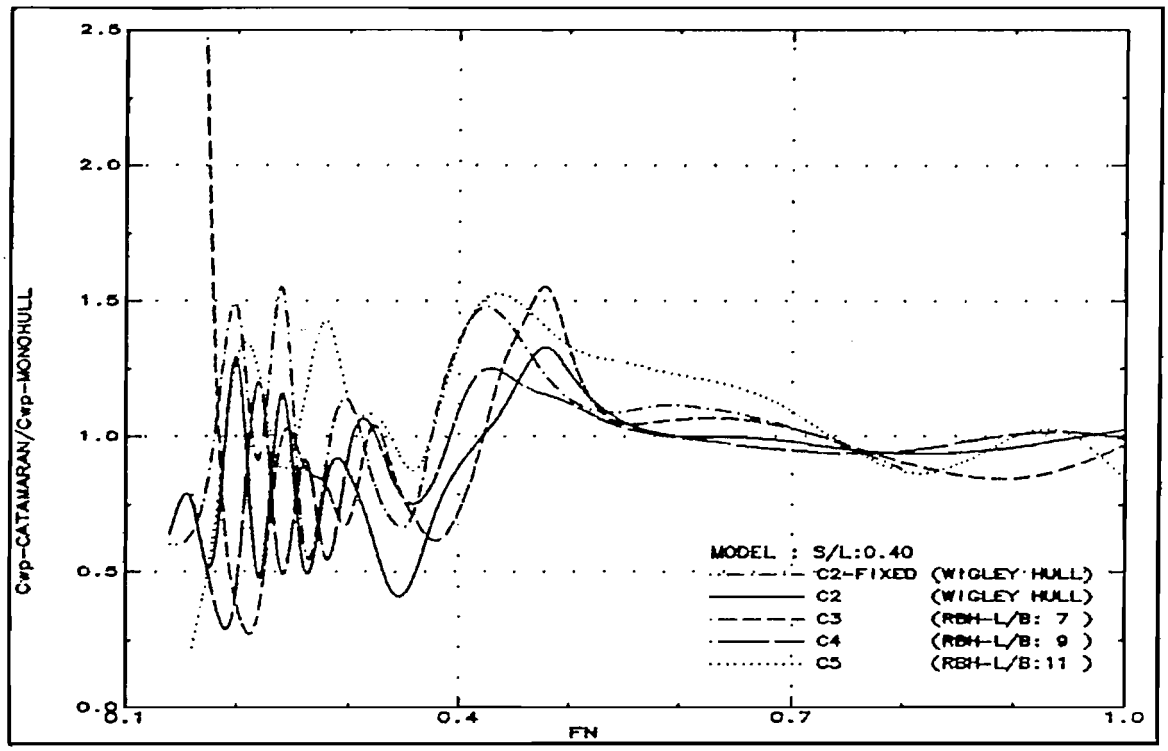

Fig.353: Wave pattern resistance interference ratio, μ, comparison (S/L:Ø.4)

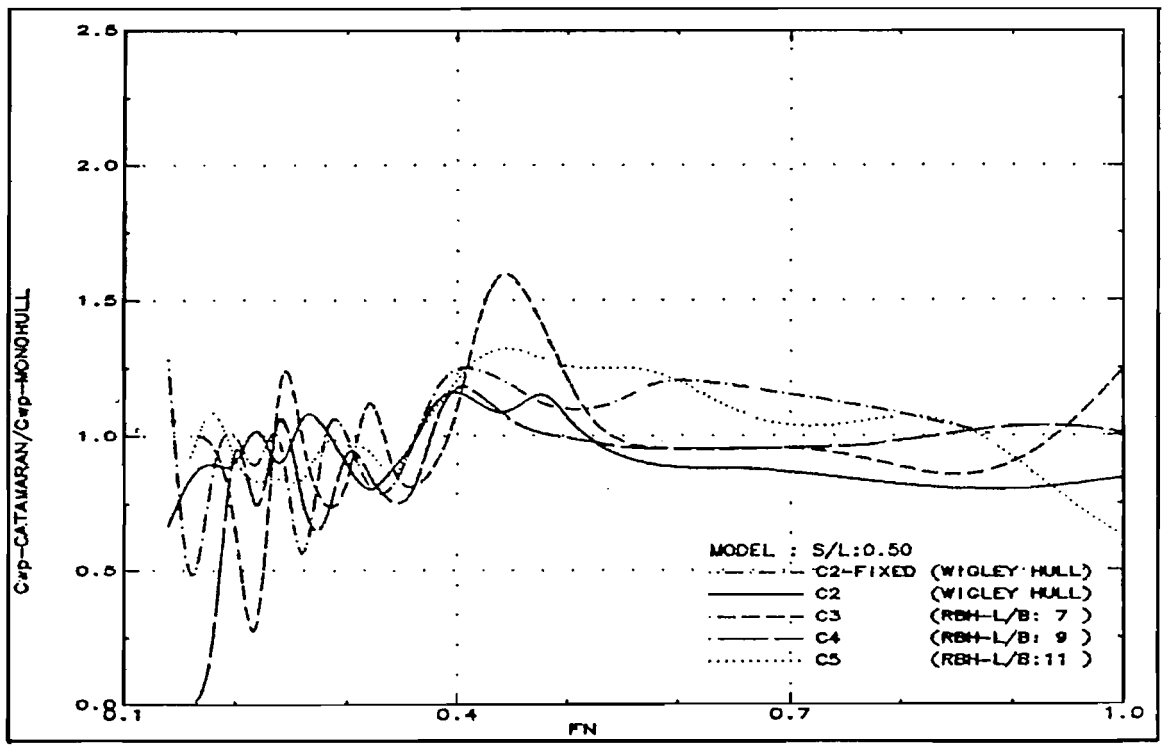

Fig.354: Wave pattern resistance interference ratio, μ, comparison (S/L:Ø.5)

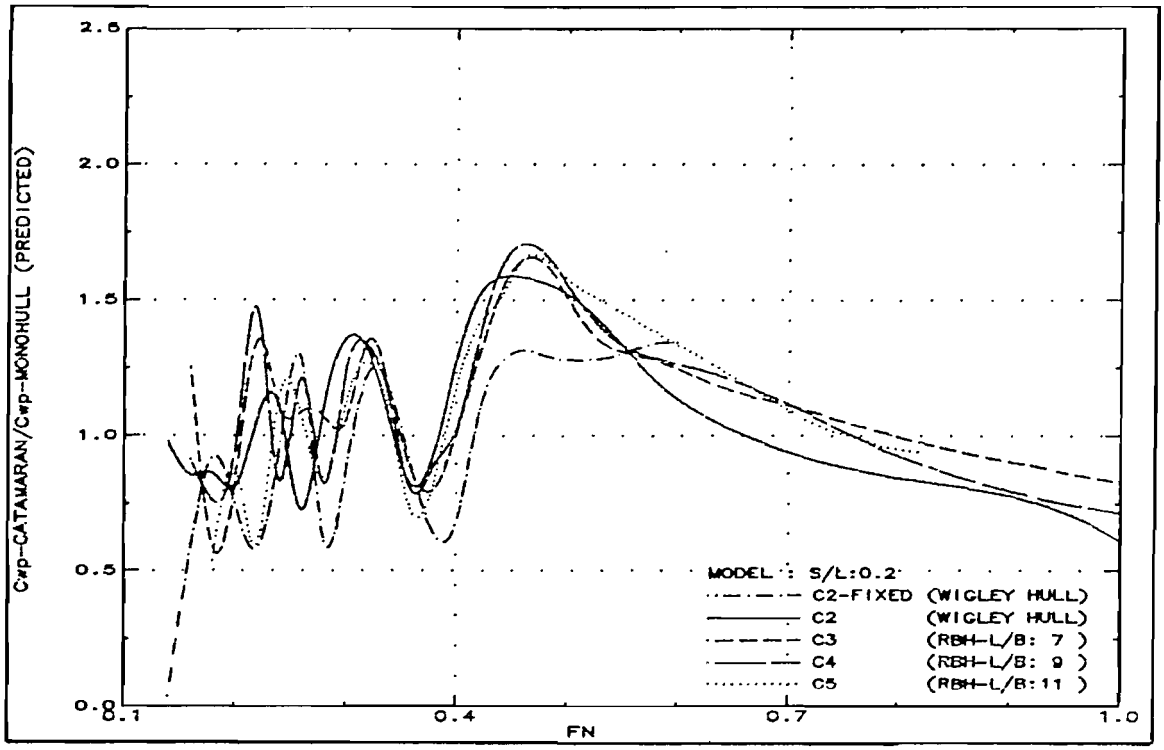

Fig.355: Wave pattern resistance interference ratio predicted from monohull wave pattern analysis (S/L:Ø.2)

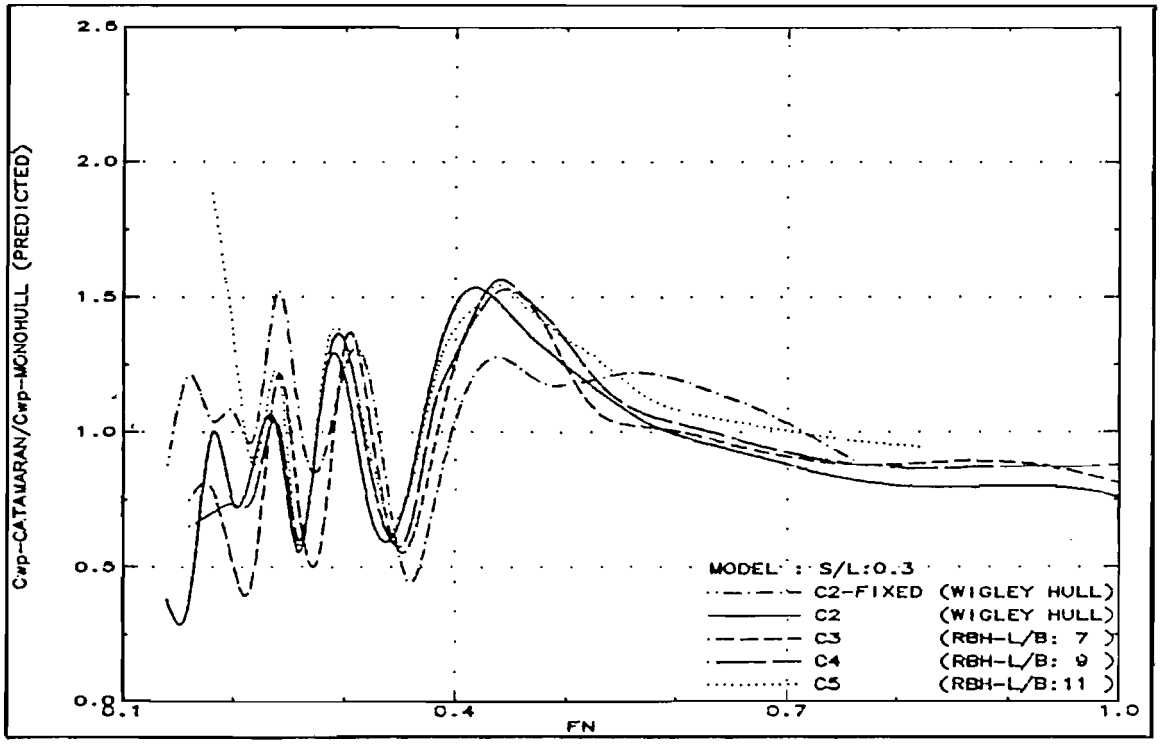

Fig.356: Wave pattern resistance interference ratio predicted from monohull wave pattern analysis (S/L:Ø.3)

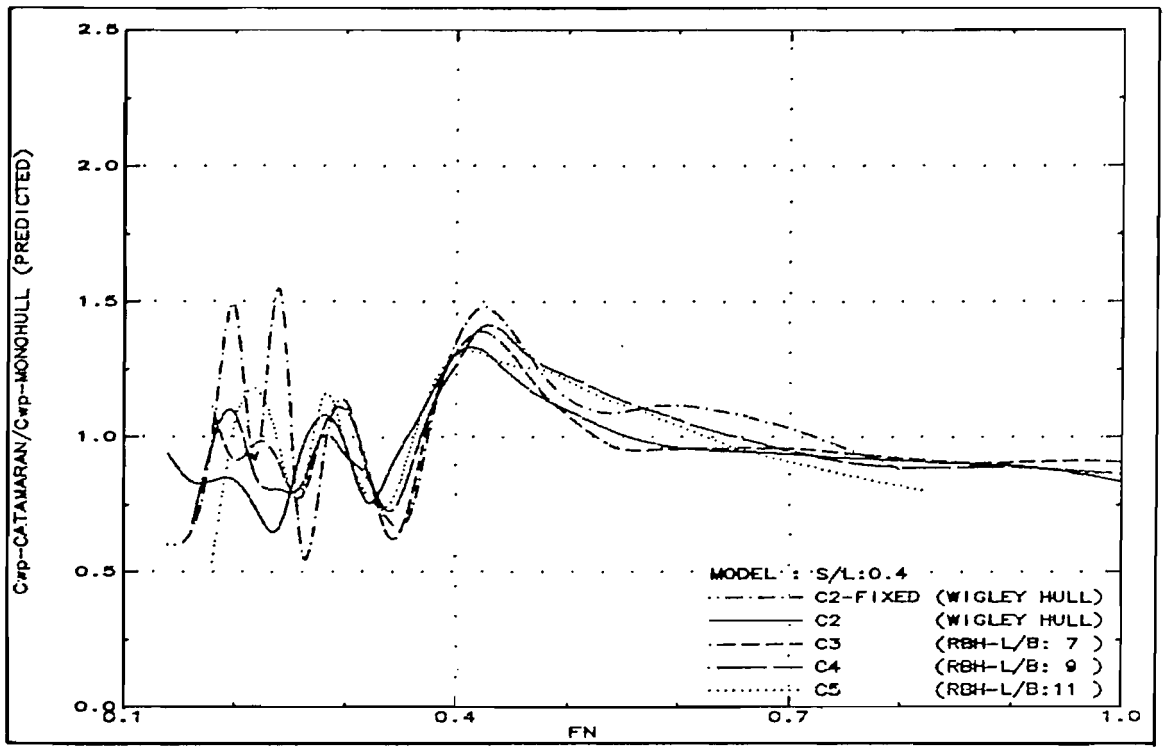

Fig.357: Wave pattern resistance interference ratio predicted from monohull wave pattern analysis (S/L:0.4)

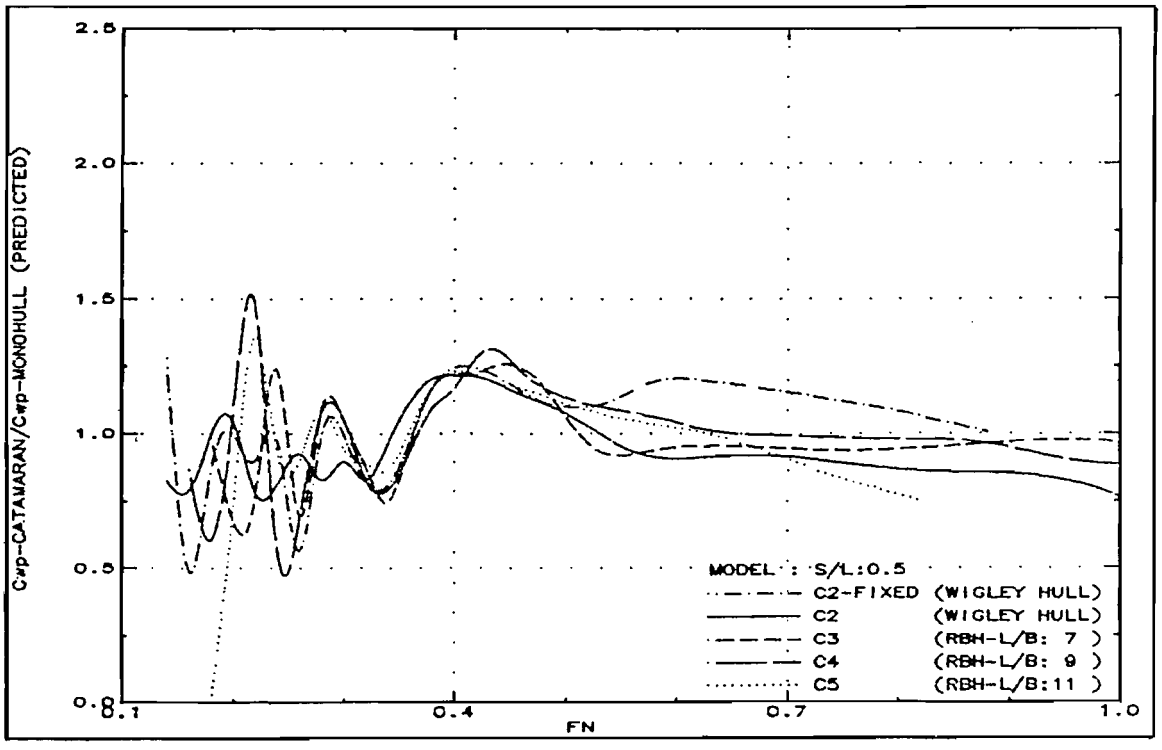

Fig.358: Wave pattern resistance interference ratio predicted from monohull wave pattern analysis (S/L:0.5)

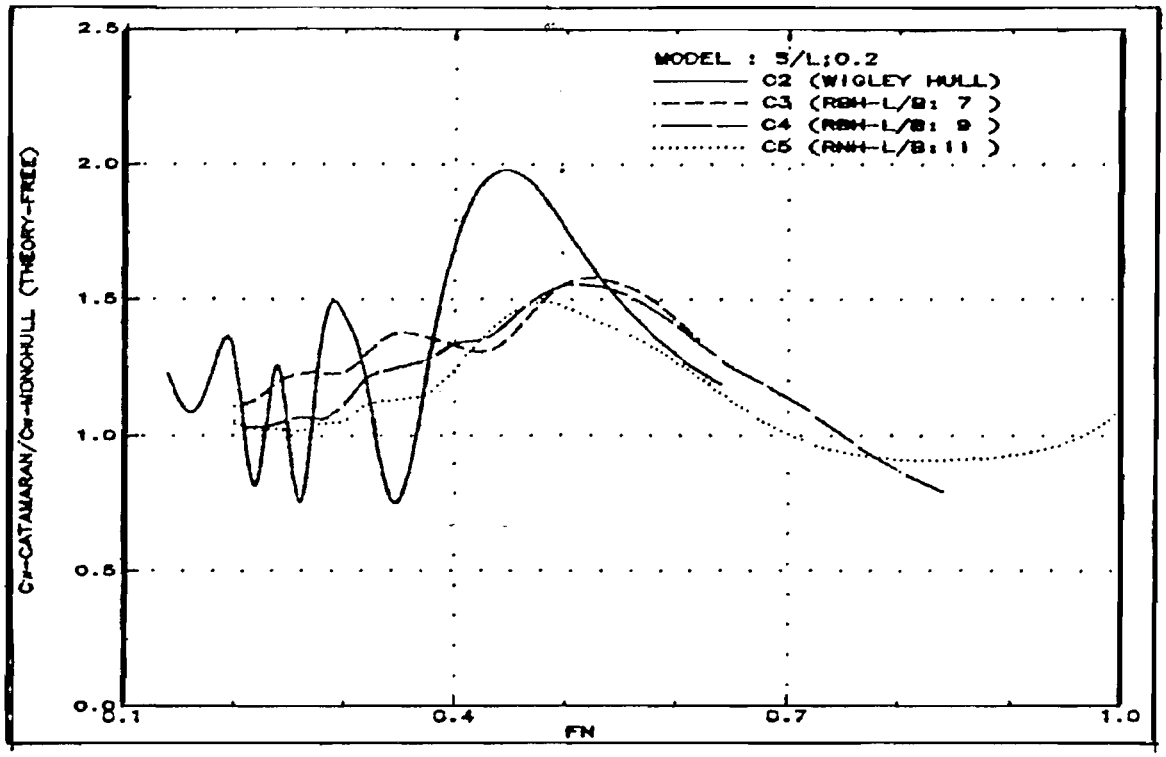

Fig.359: Theoretical wave resistance interference ratio (S/L:0.2)

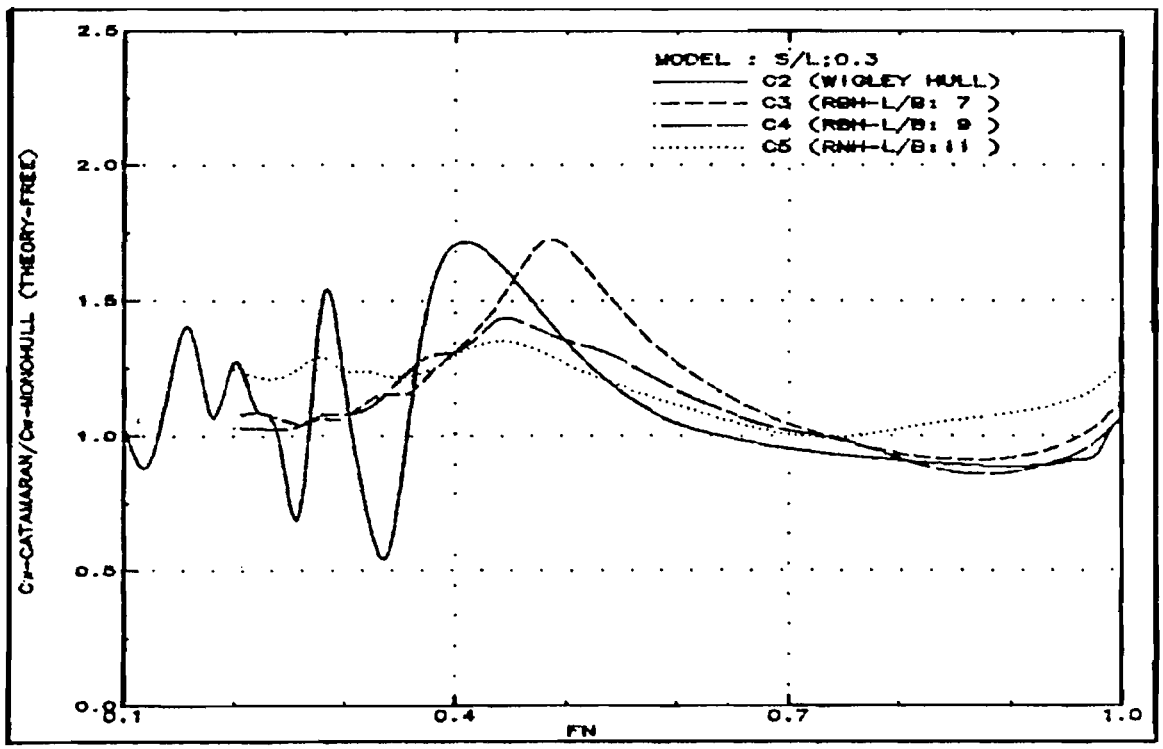

Fig.360: Theoretical wave resistance interference ratio (S/L:0.3)

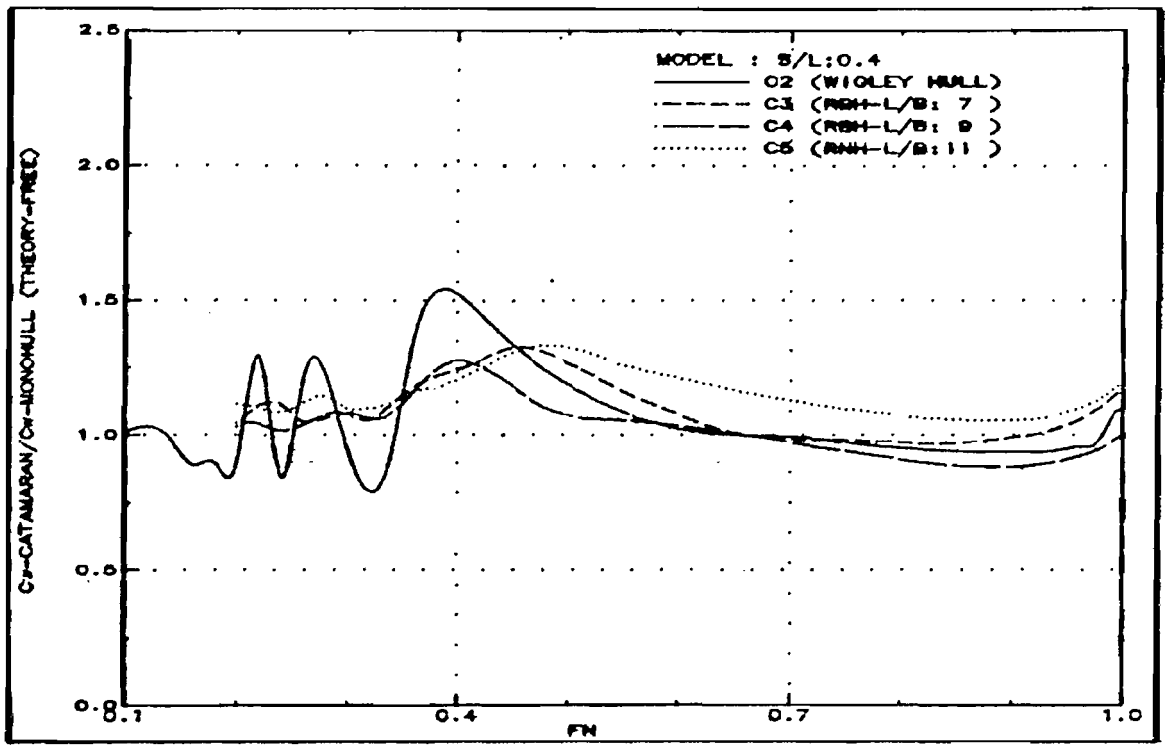

Fig.361: Theoretical wave resistance interference ratio (S/L:Ø.4)

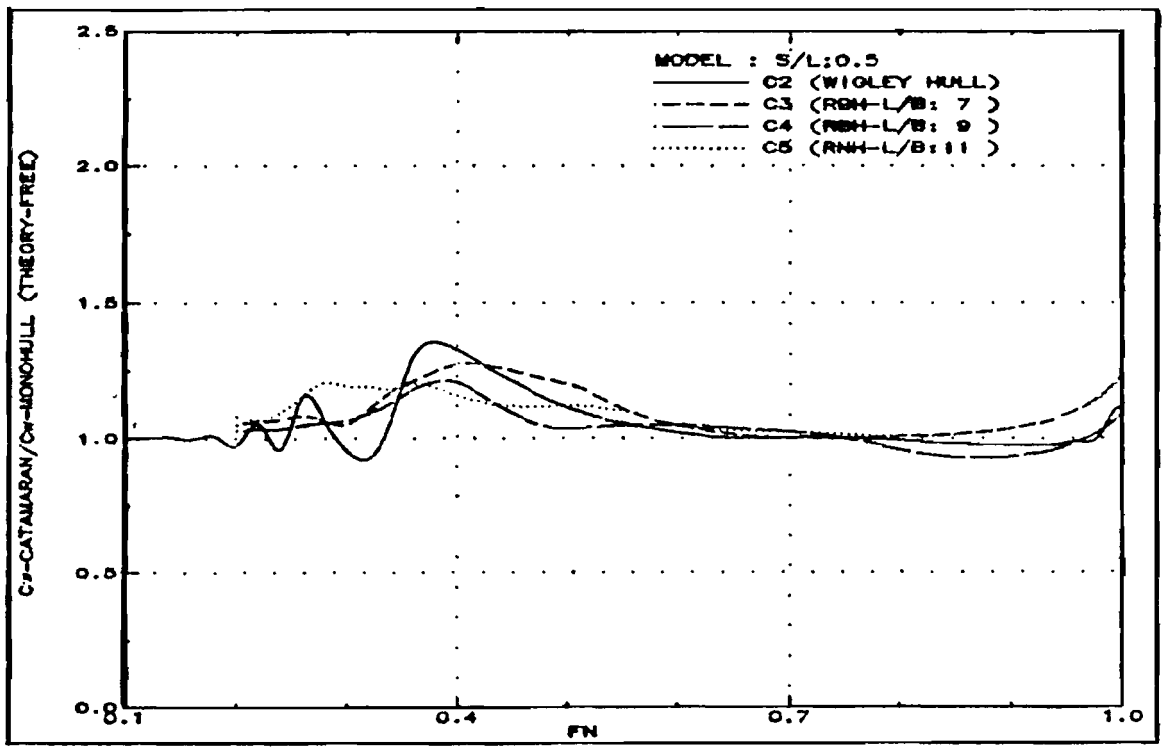

Fig.362: Theoretical wave resistance interference ratio (S/L:Ø.5)

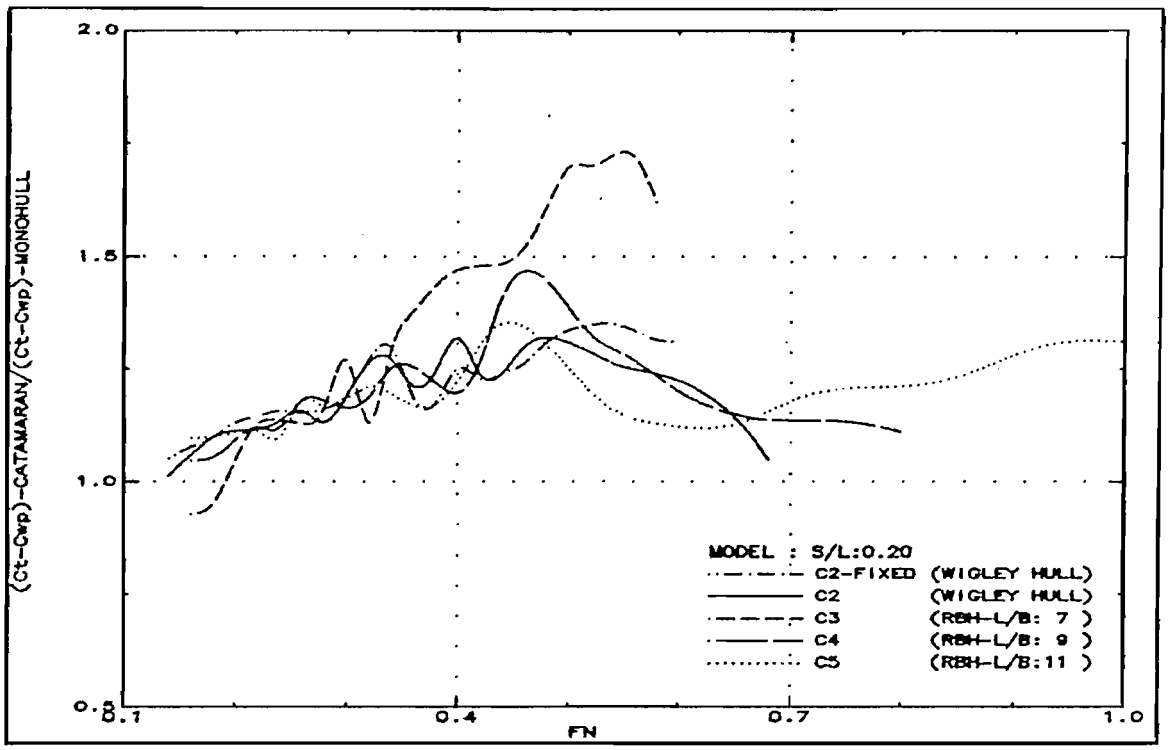

Fig.363: Total resistance minus wave pattern resistance interference ratio (S/L:Ø.2)

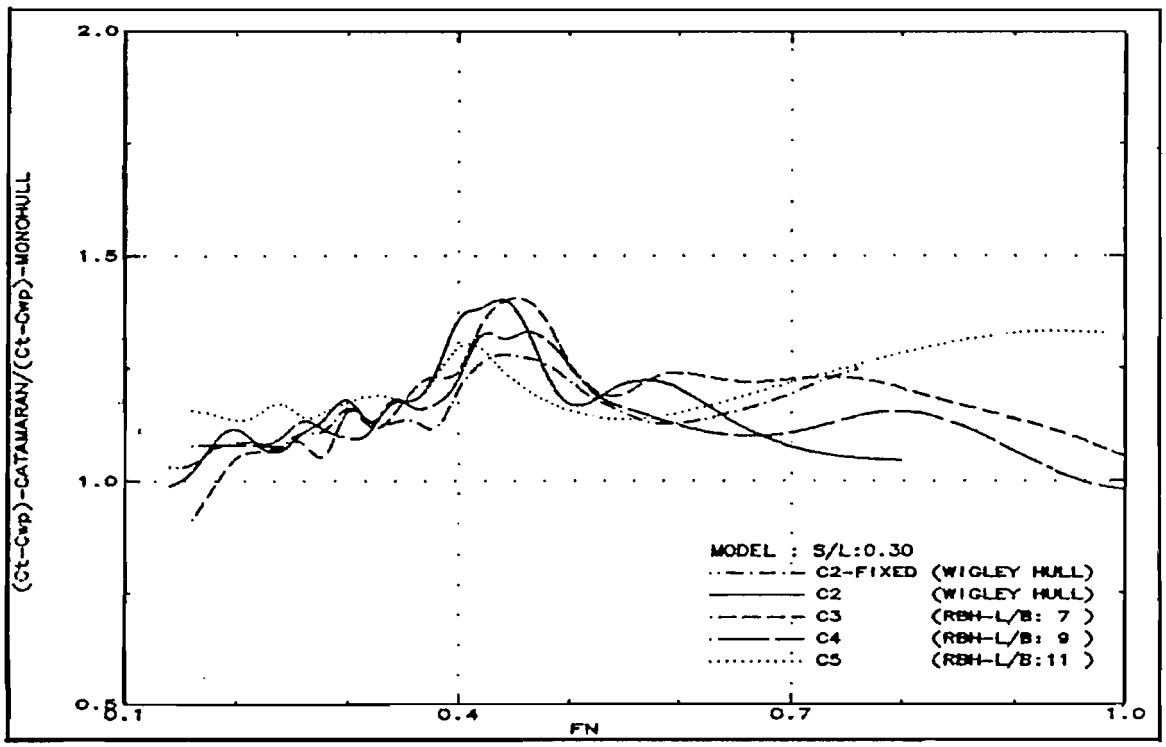

Fig.364: Total resistance minus wave pattern resistance interference ratio (S/L:Ø.3)

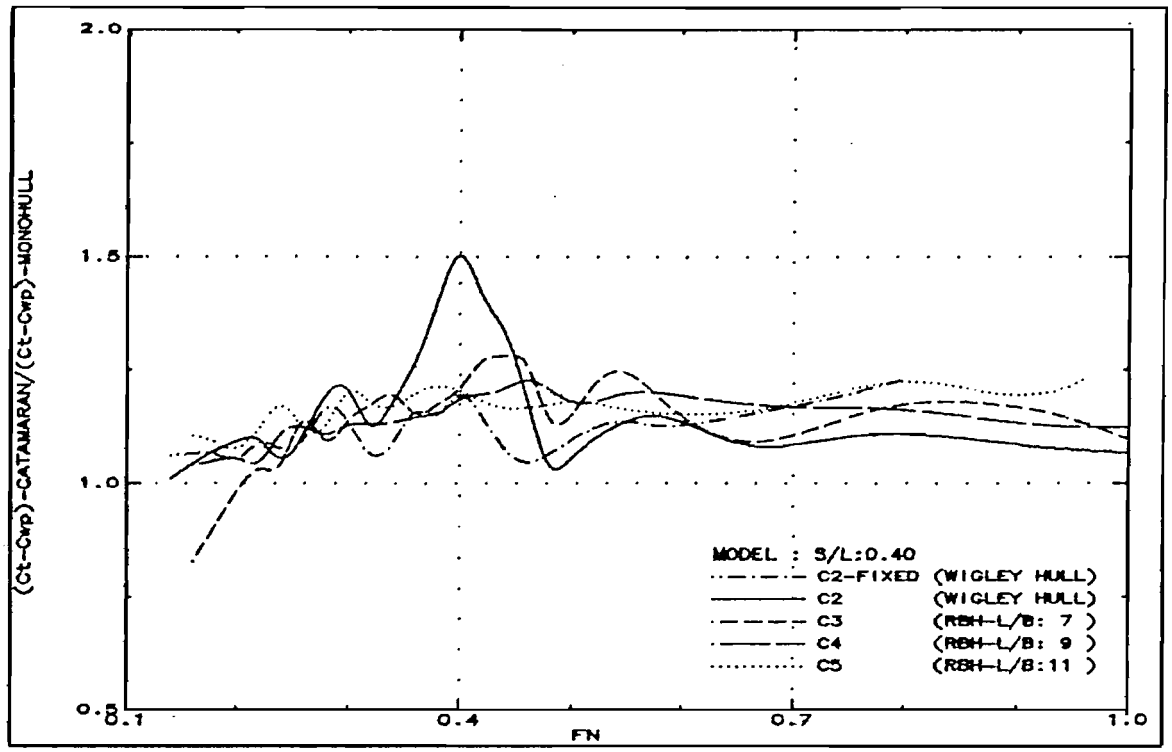

Fig.365: Total resistance minus wave pattern resistance interference ratio (S/L:Ø.4)

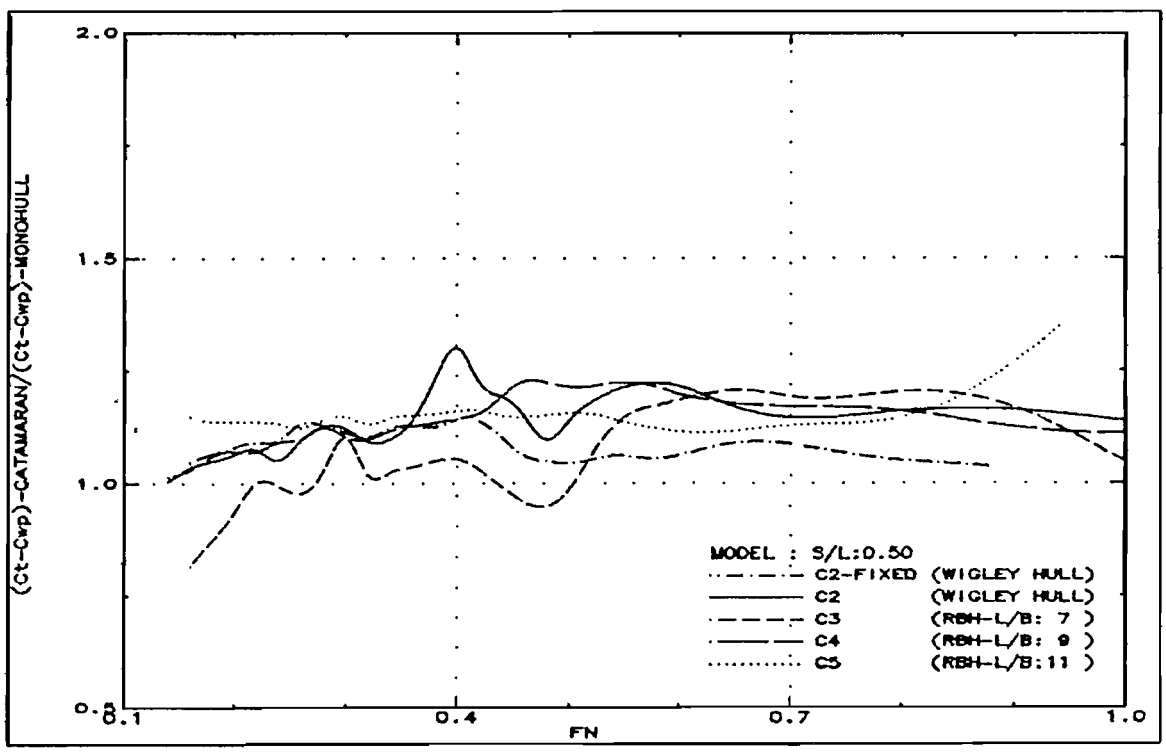

Fig.366: Total resistance minus wave pattern resistance interference ratio (S/L:Ø.5)

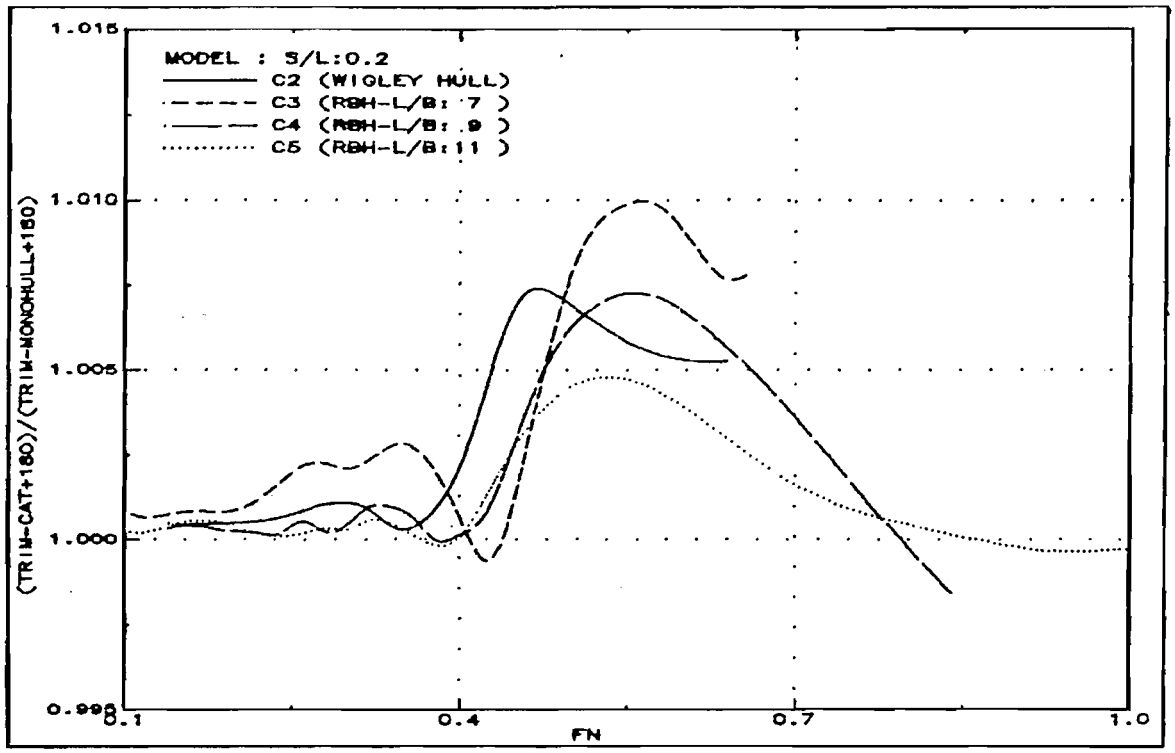

Fig.367: Running trim interference (S/L:Ø.2)

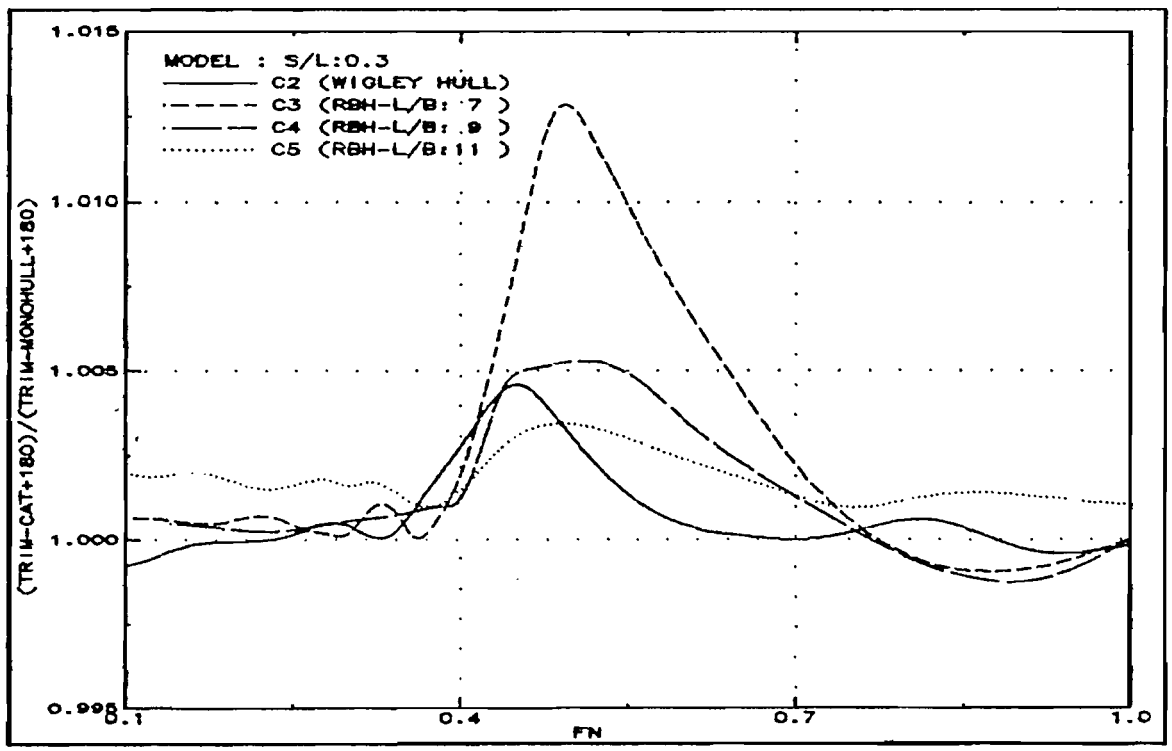

Fig.368: Running trim interference (S/L:Ø.3)

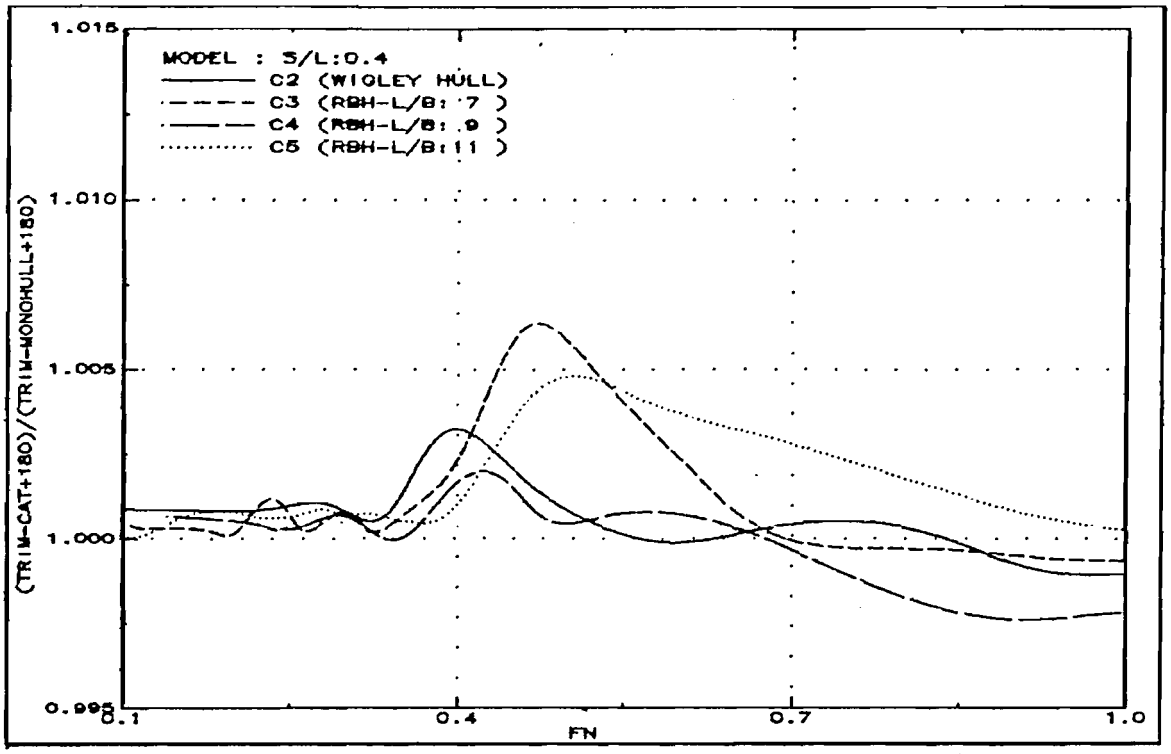

Fig.369: Running trim interference (S/L:0.4)

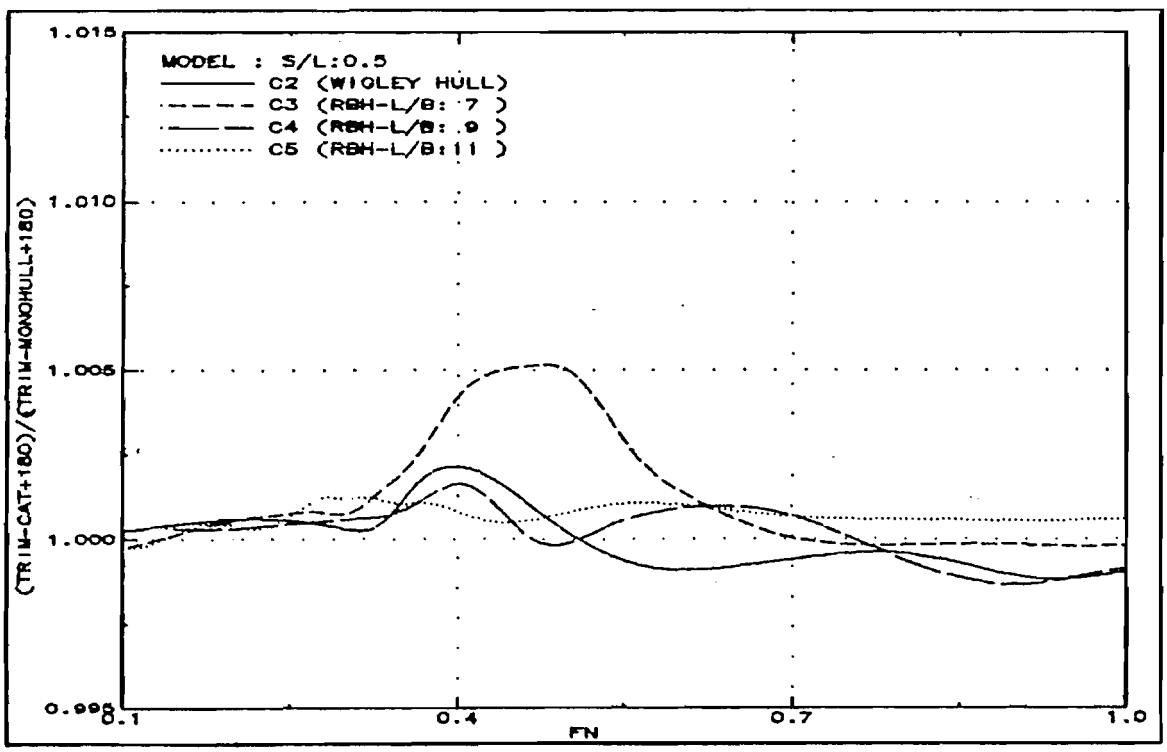

Fig.370: Running trim interference (S/L:0.5)

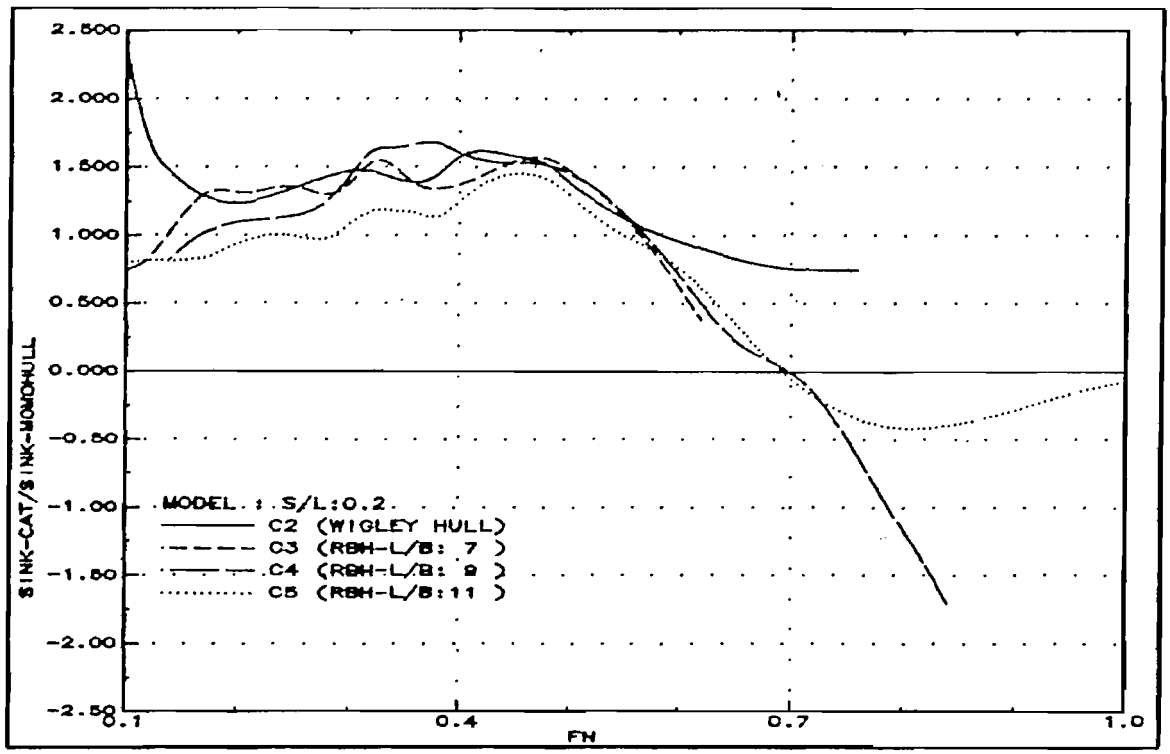

Fig.371: Sinkage interference (S/L:Ø.2)

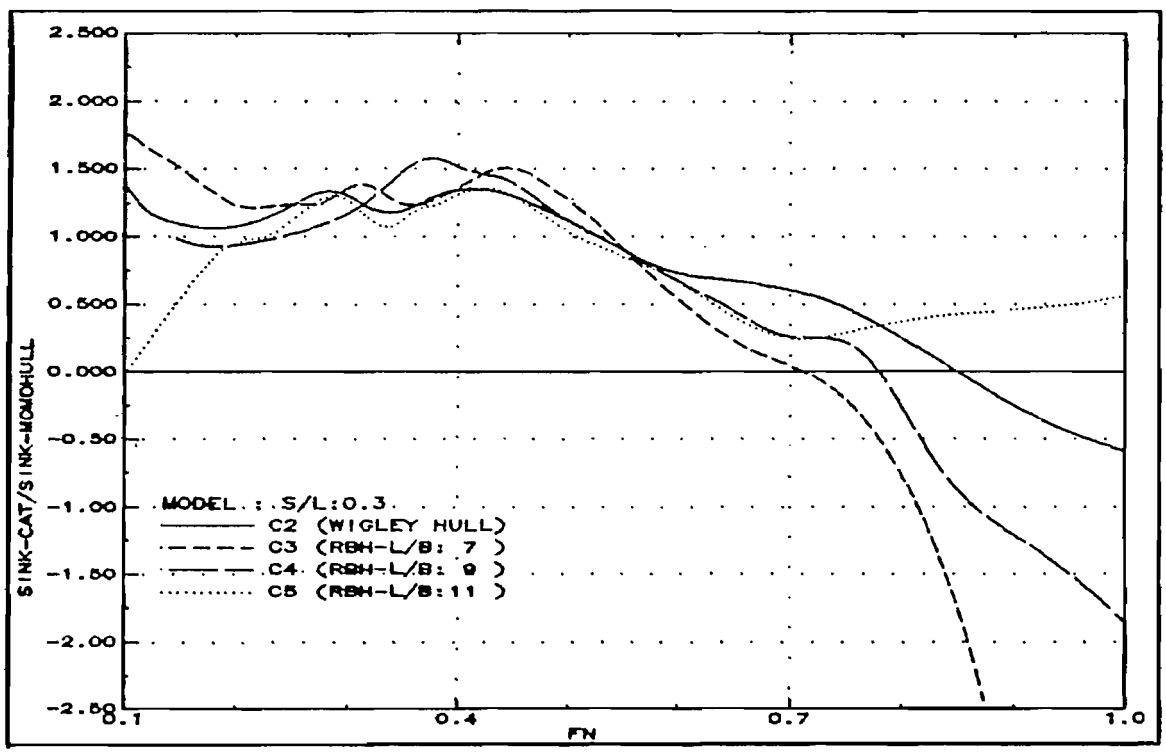

Fig.372: Sinkage interference (S/L:Ø.3)

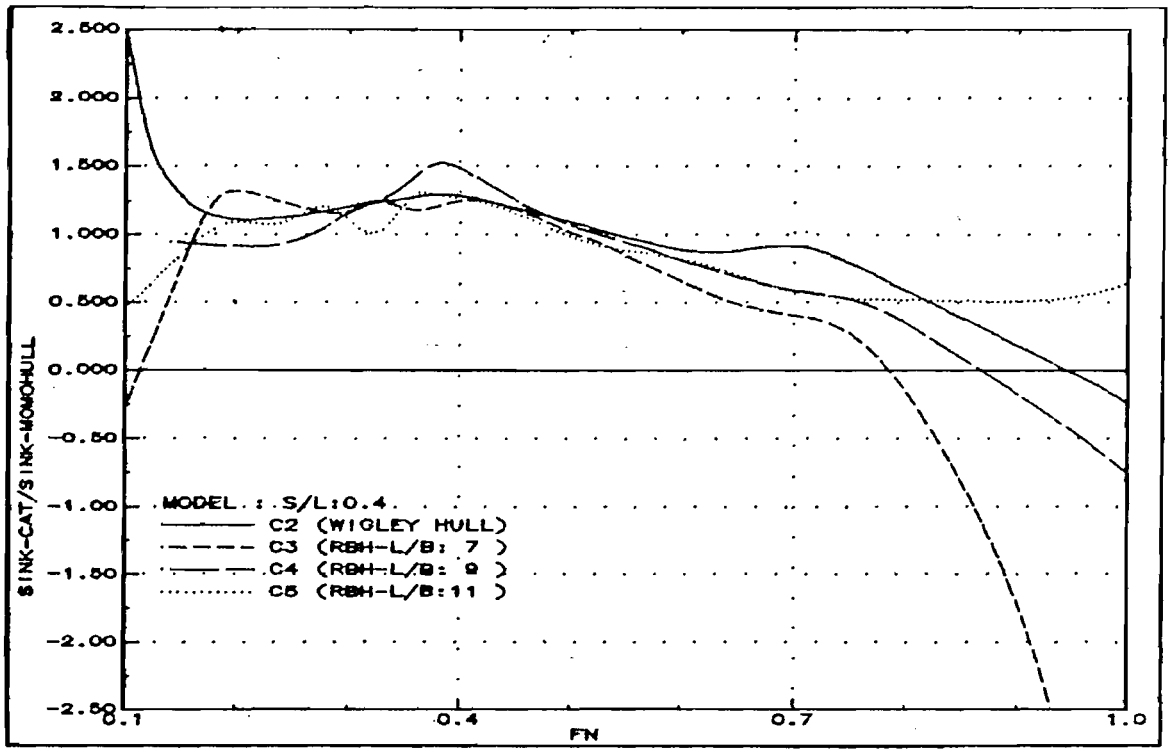

Fig.373: Sinkage interference (S/L:Ø.4)

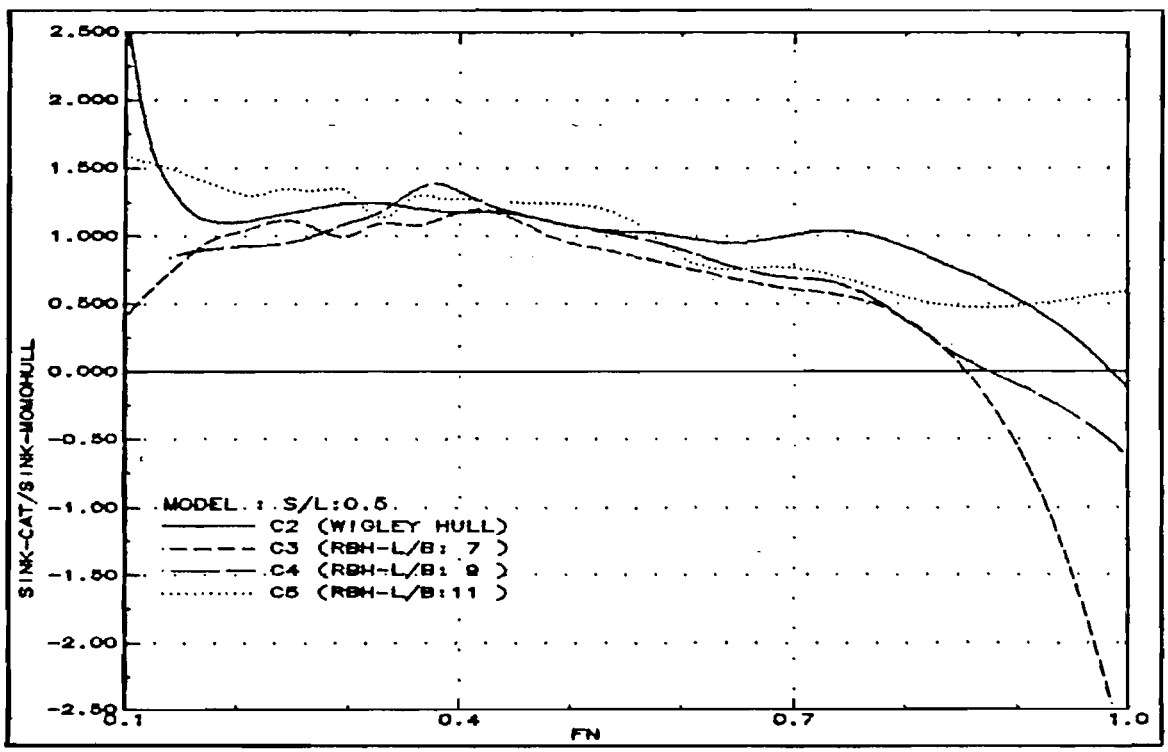

Fig.374: Sinkage interference (S/L:Ø.5)

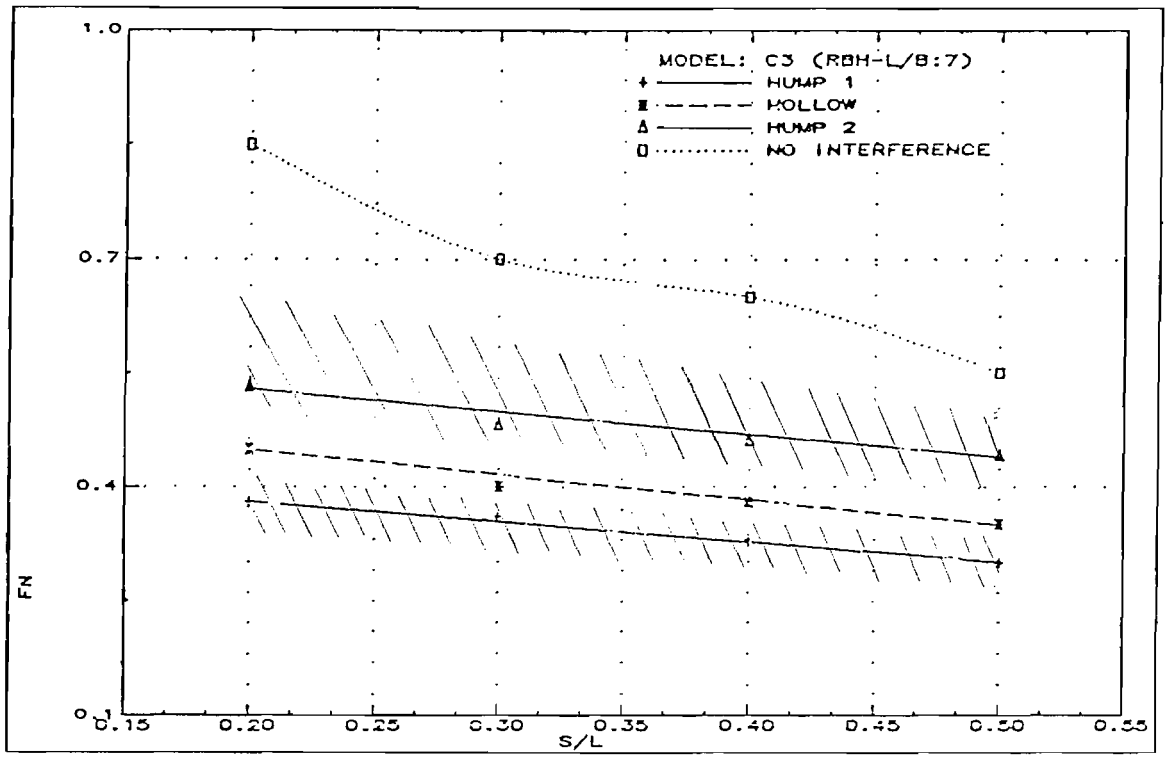

Fig.375: Positions of humps and hollows across the separation range (C3)

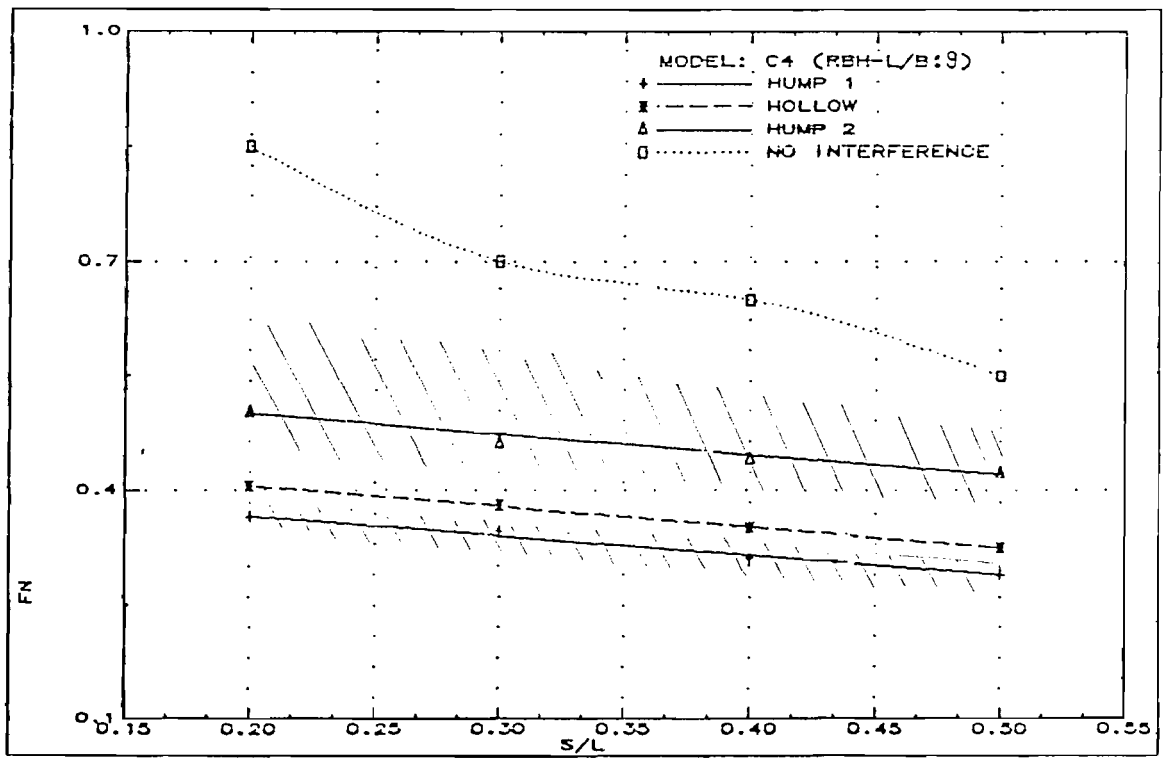

Fig.376: Positions of humps and hollows across the separation range (C4)

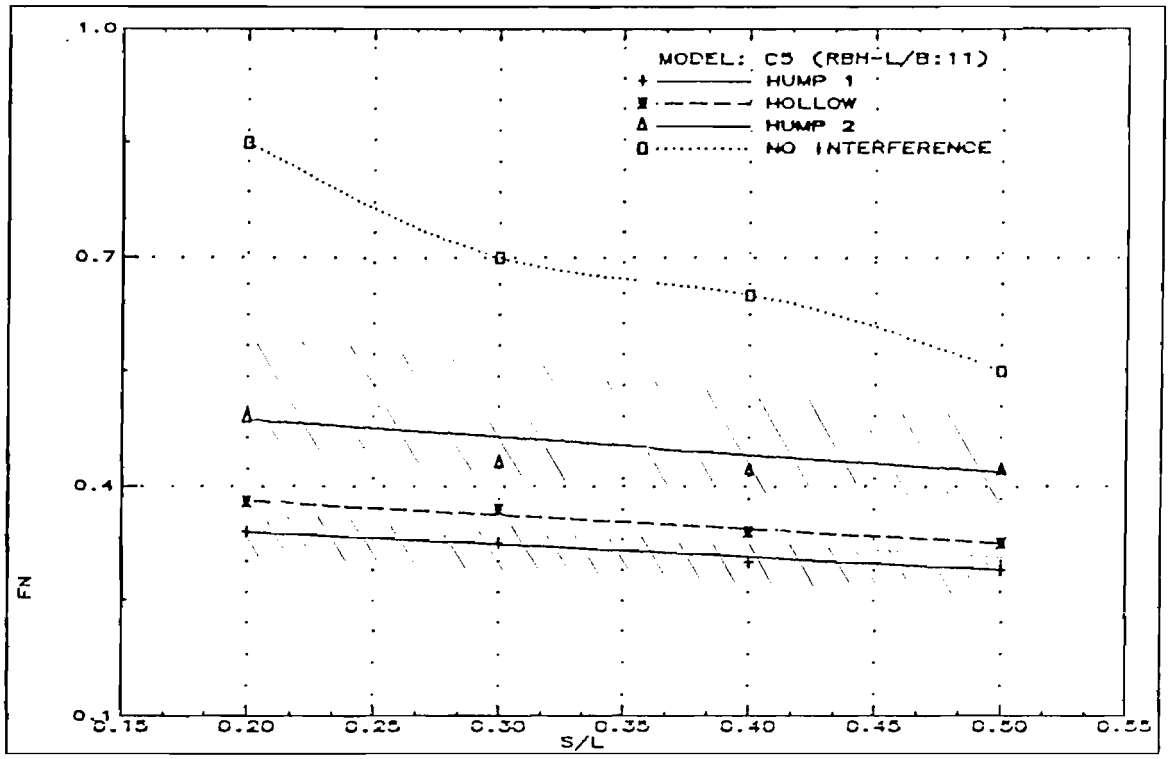

Fig.377: Positions of humps and hollows across the separation range (C5)

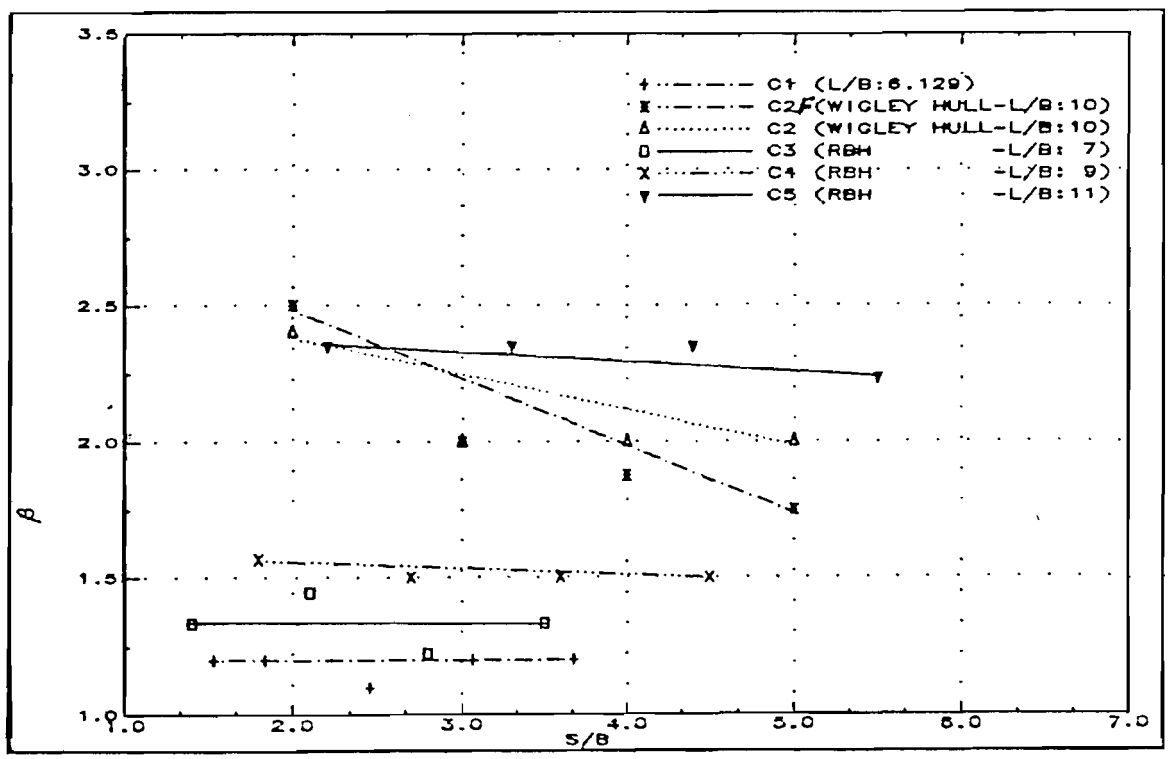

Fig.378: Viscous interference factor β across S/B

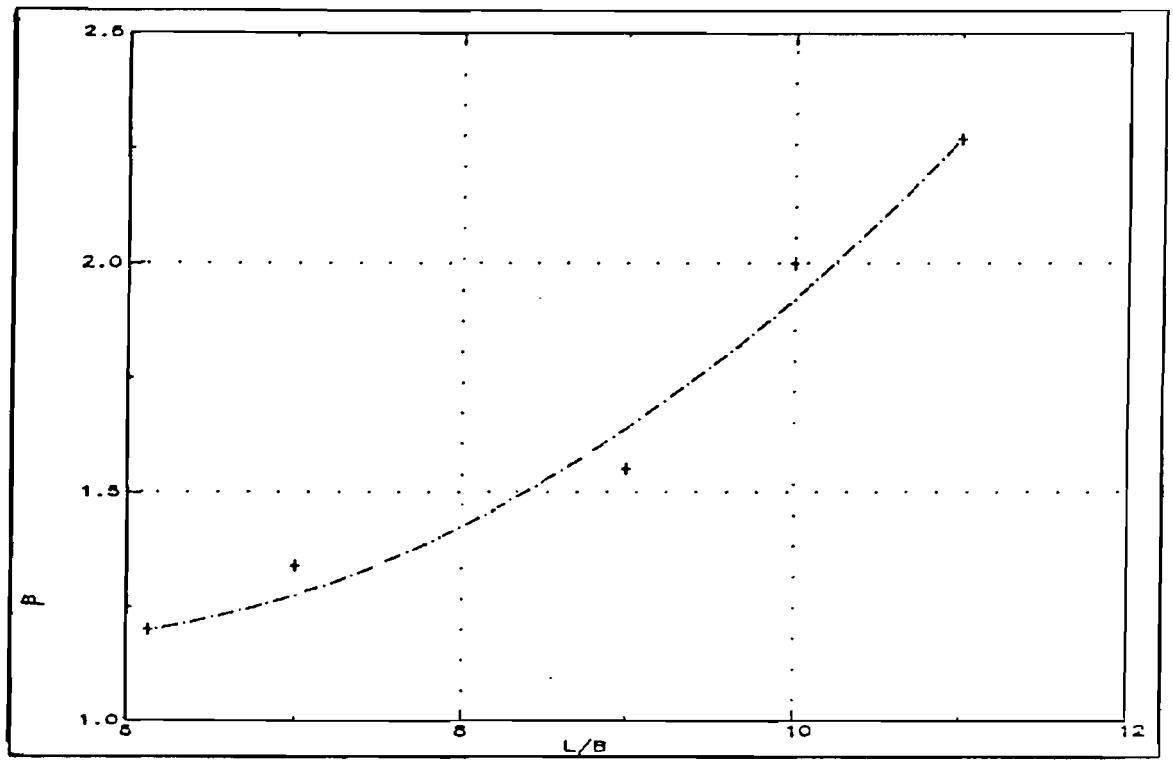

Fig.379: Viscous interference factor β across L/B (S/B:3.Ø)

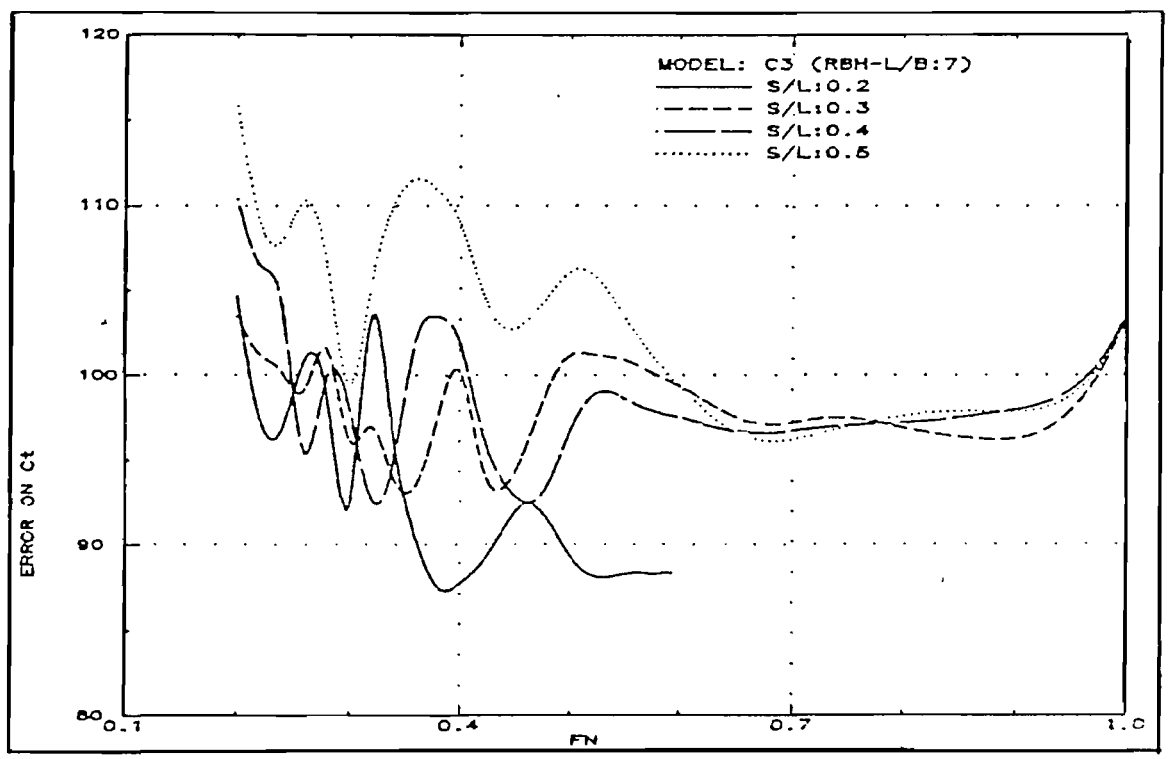

Fig.38Ø: Errors in the prediction of total resistance (C3)

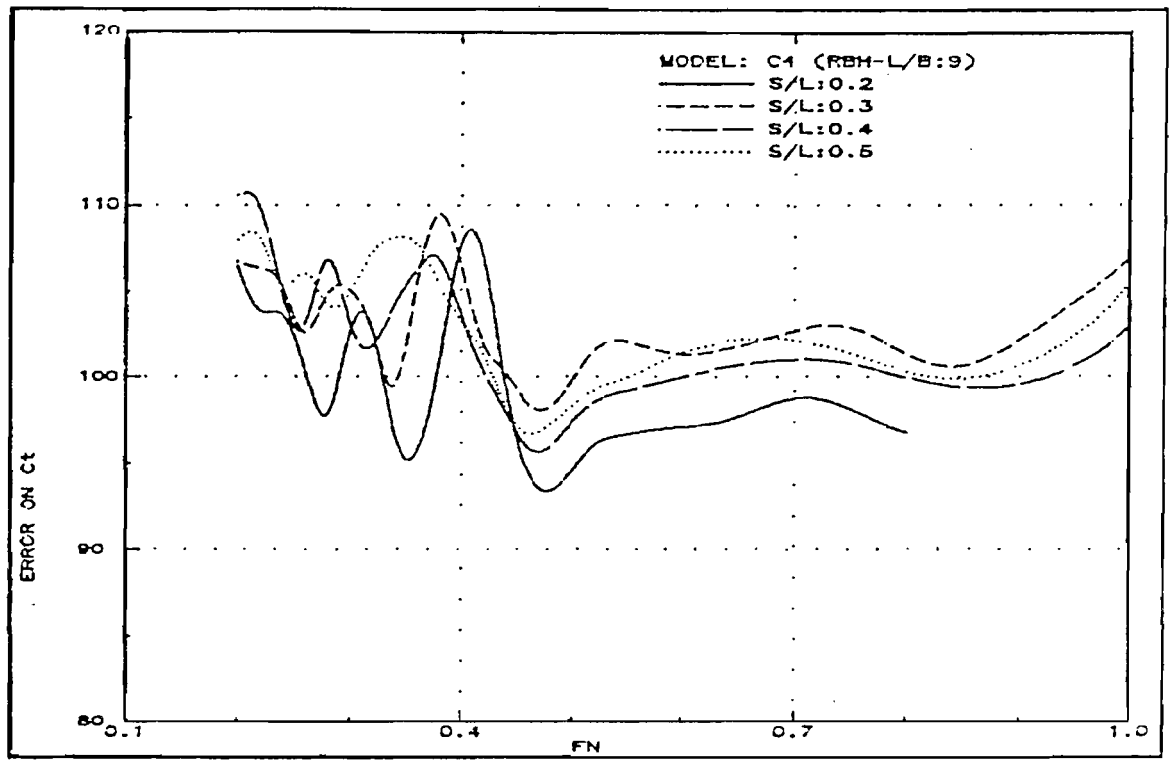

Fig.381: Errors in the prediction of total resistance (C4)

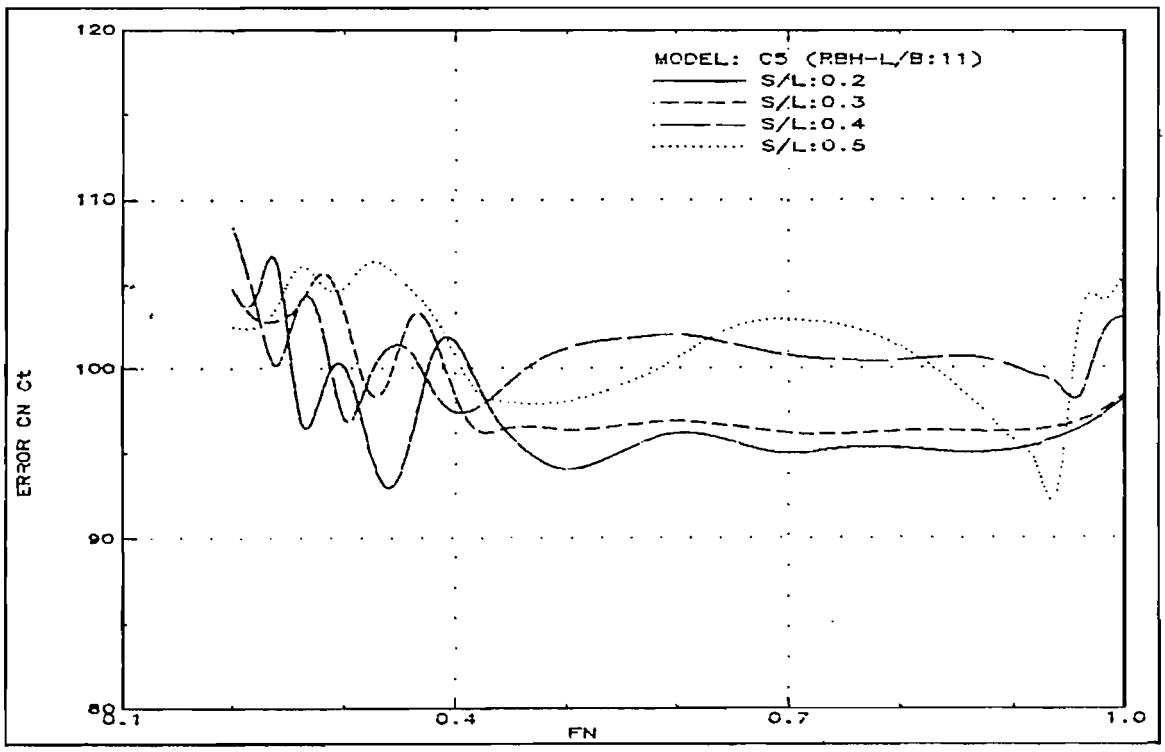

Fig.382: Errors in the prediction of total resistance (C5)

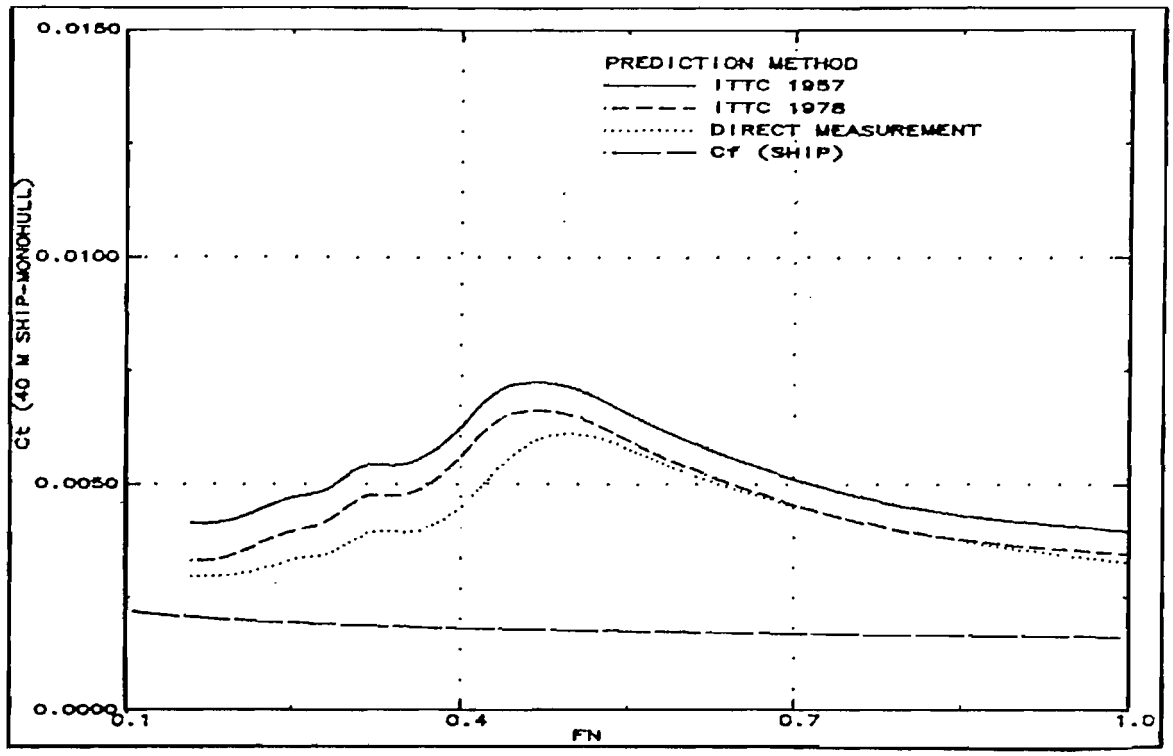

Fig.383: Prediction of full scale ship resistance by different methods (C4-Monohull)

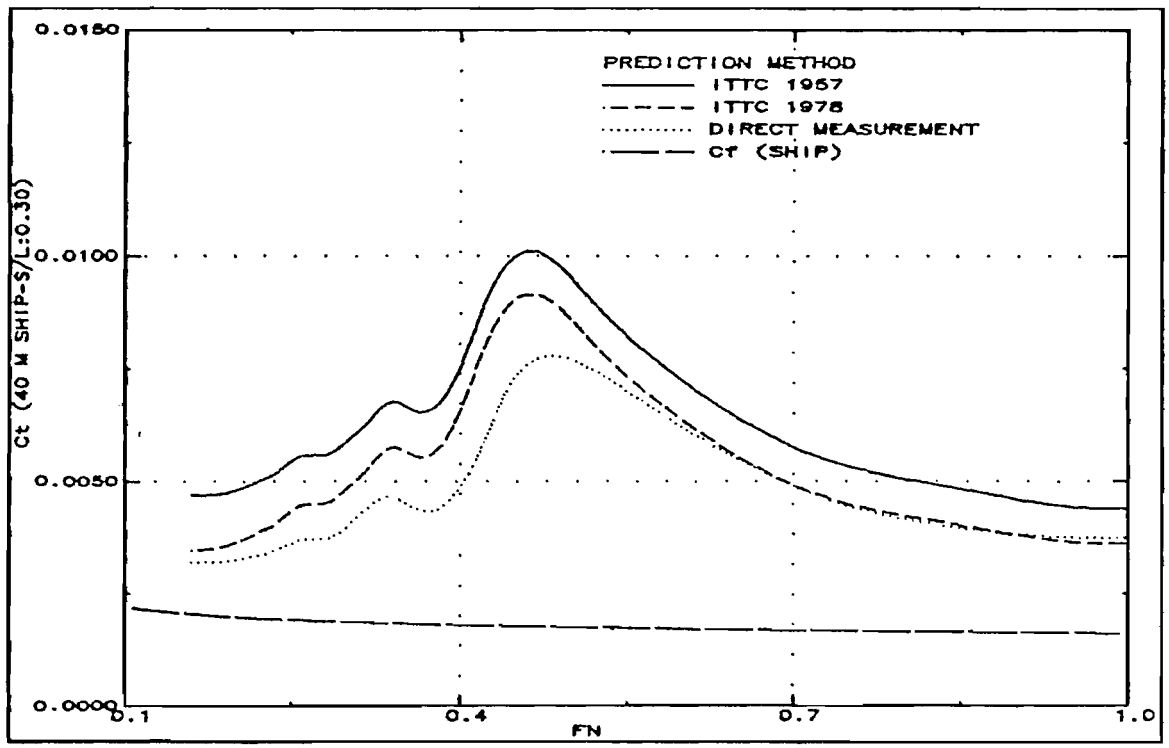

Fig.384: Prediction of full scale ship resistance by different methods (C4-S/L:0.3)

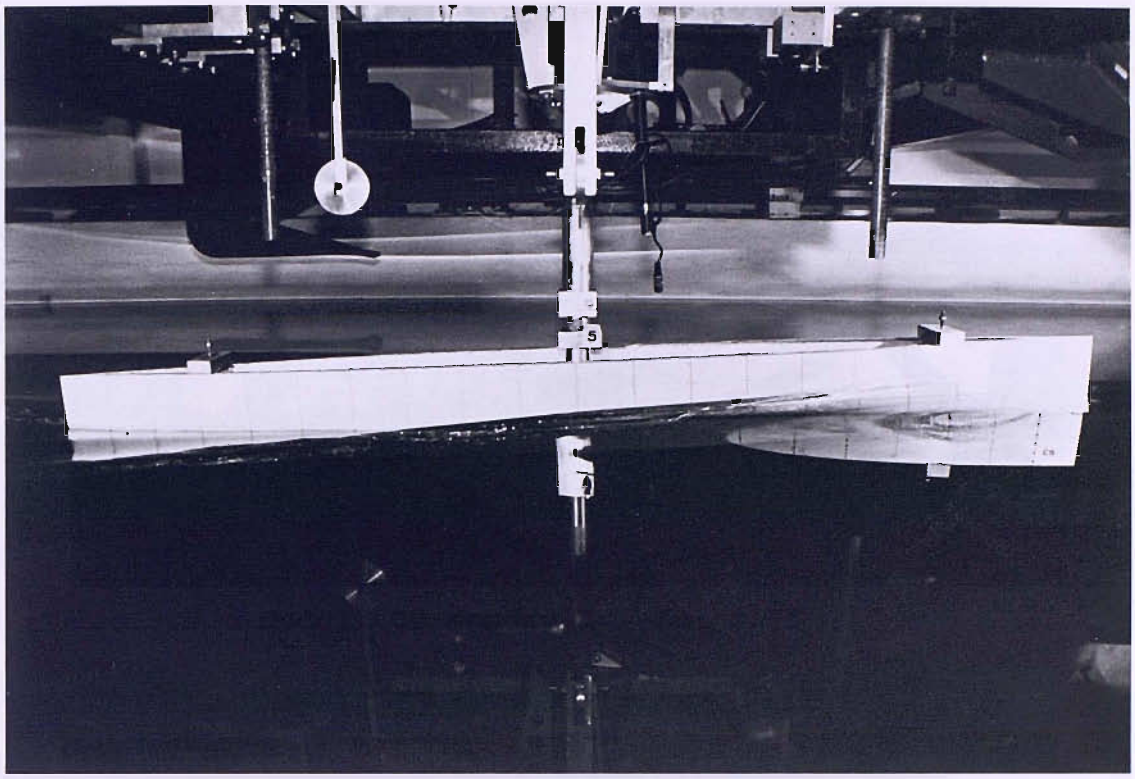

Fig.385 : Model: C2-Monohull Fn: Ø.75

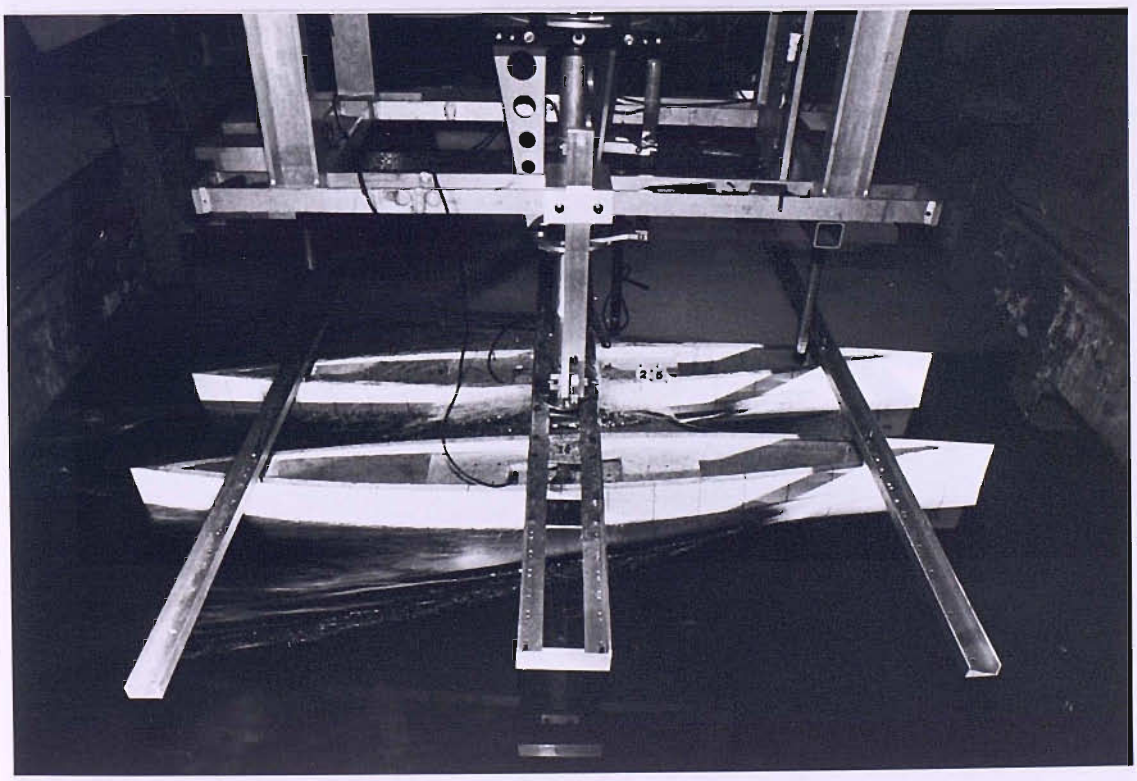

Fig.386 : Model: C2-S/L:Ø.2 Fn: Ø.75

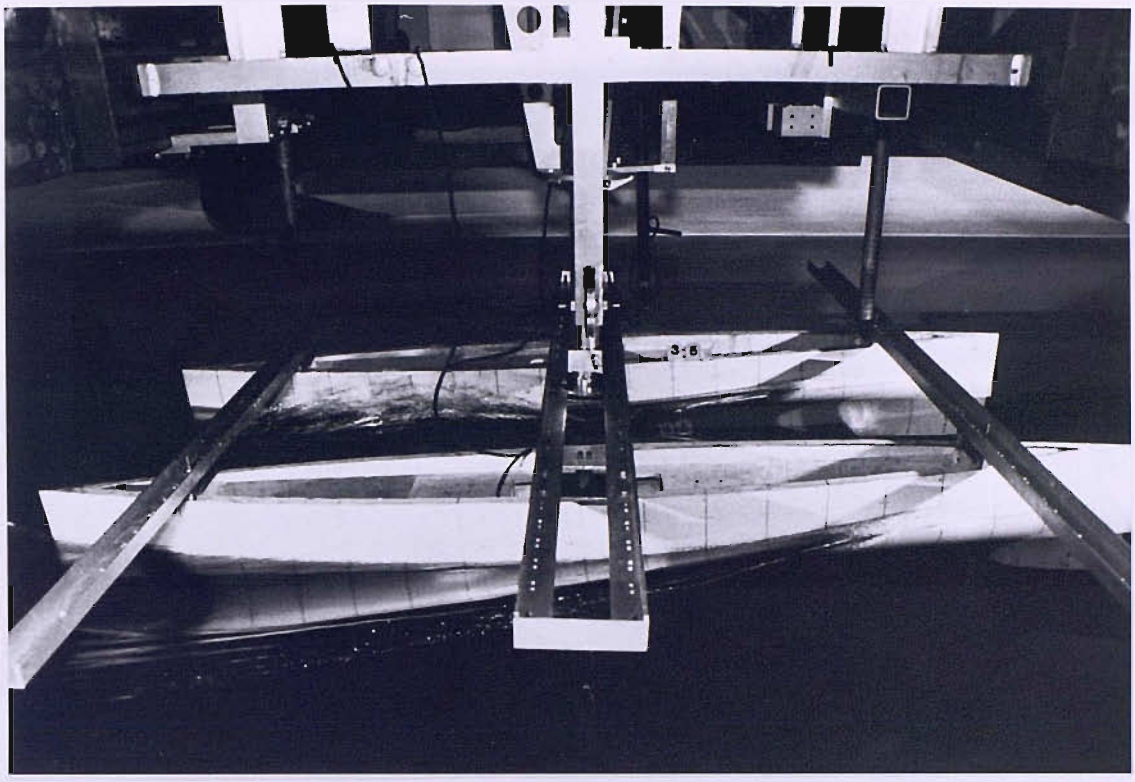

Fig.387 : Model: C2-S/L:Ø.3 Fn: Ø.75

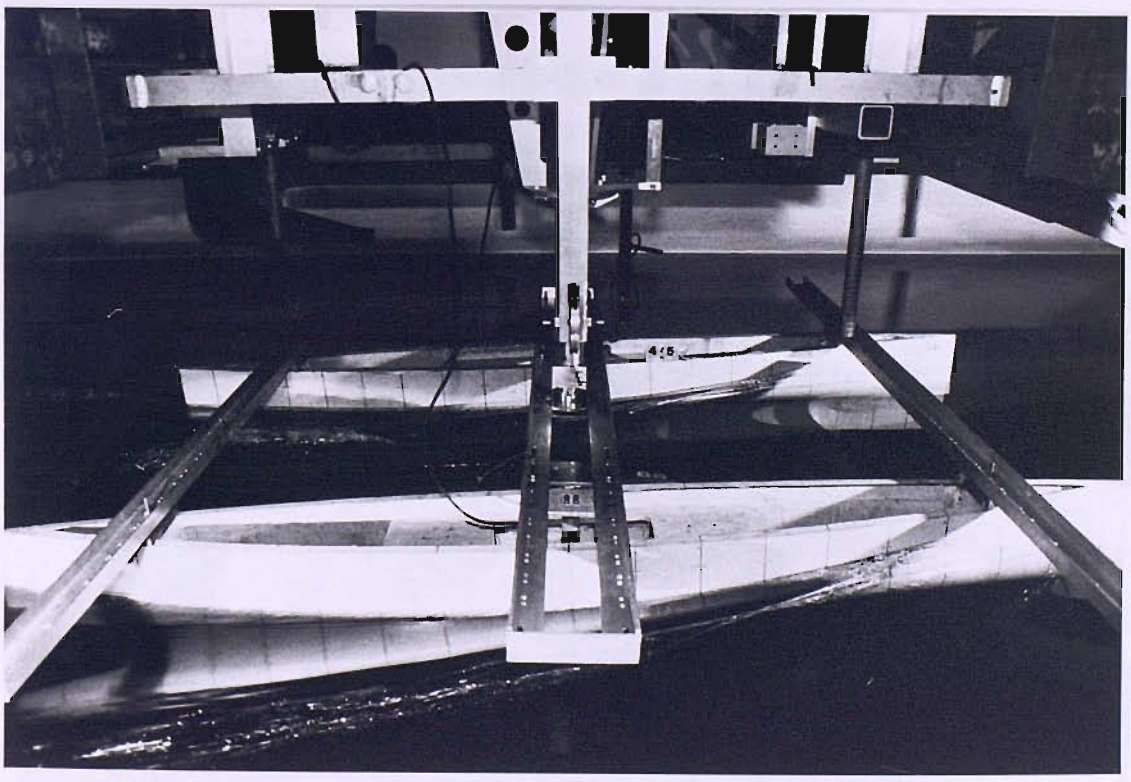

Fig.388 : Model: C2-S/L:Ø.4 Fn: Ø.75

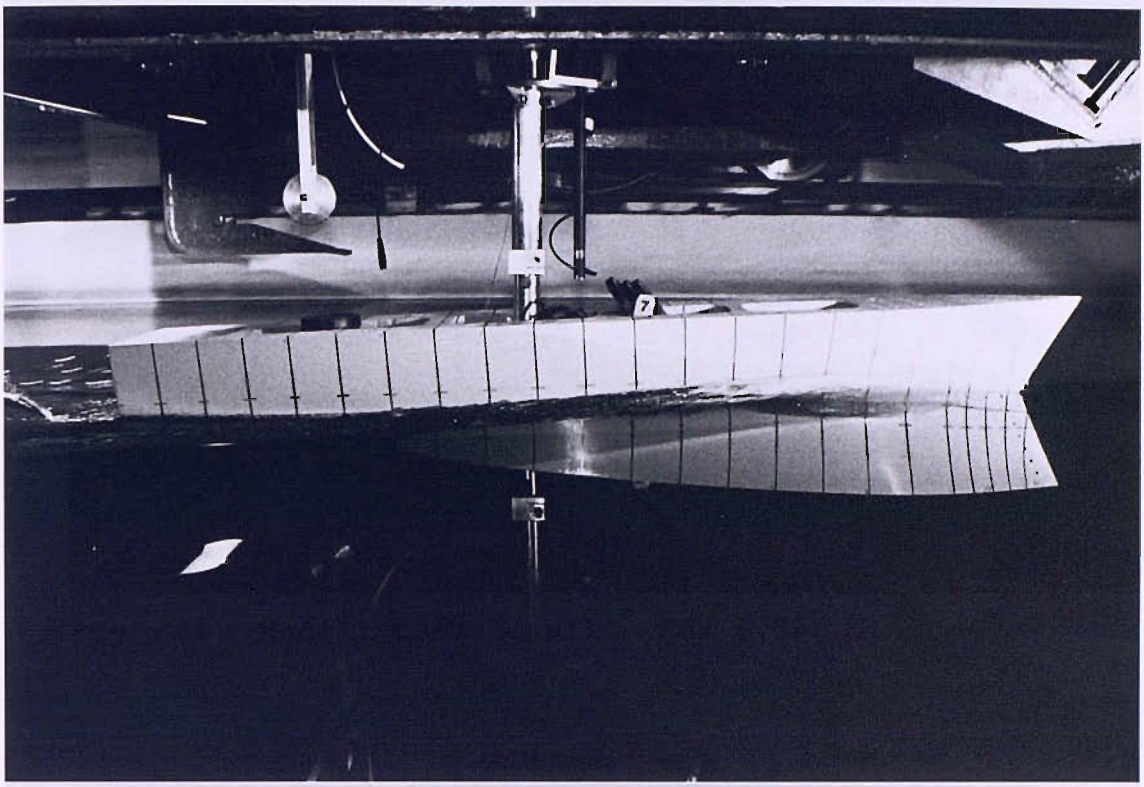

Fig. 389 : Model: C3-Monohull Fn: Ø.75

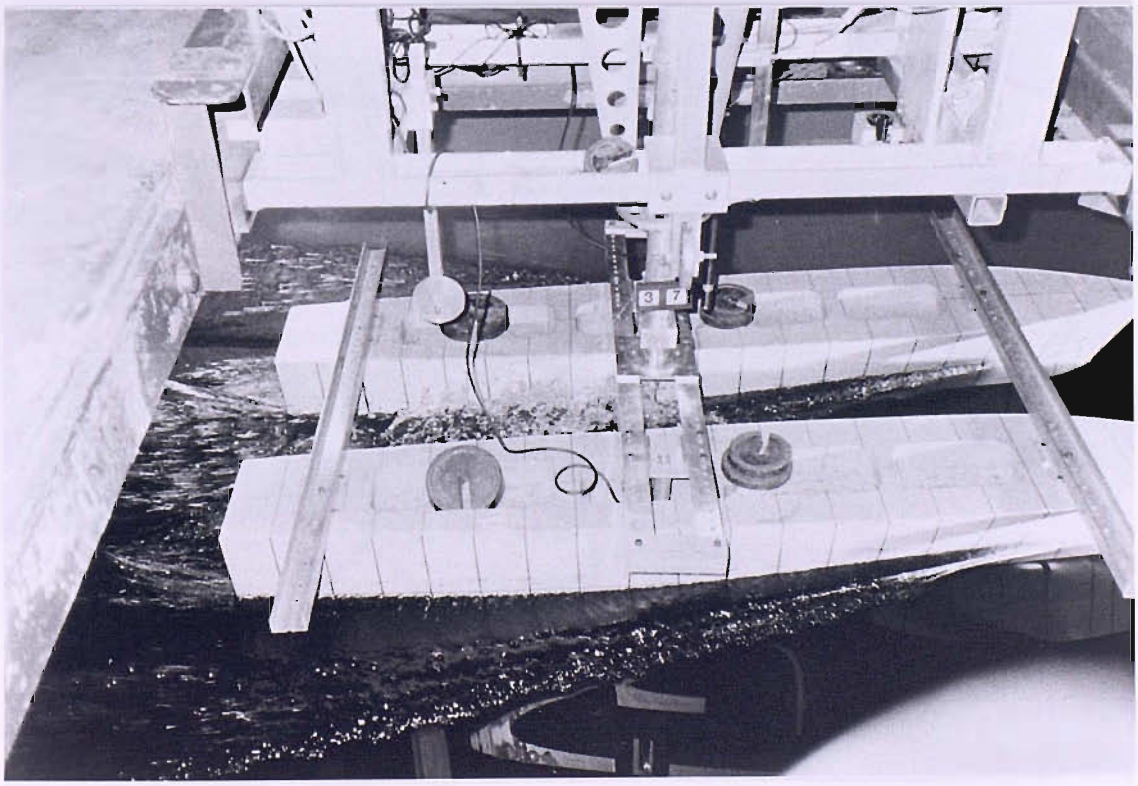

Fig.39Ø : Model: C3-S/L:Ø.3 Fn: Ø.75

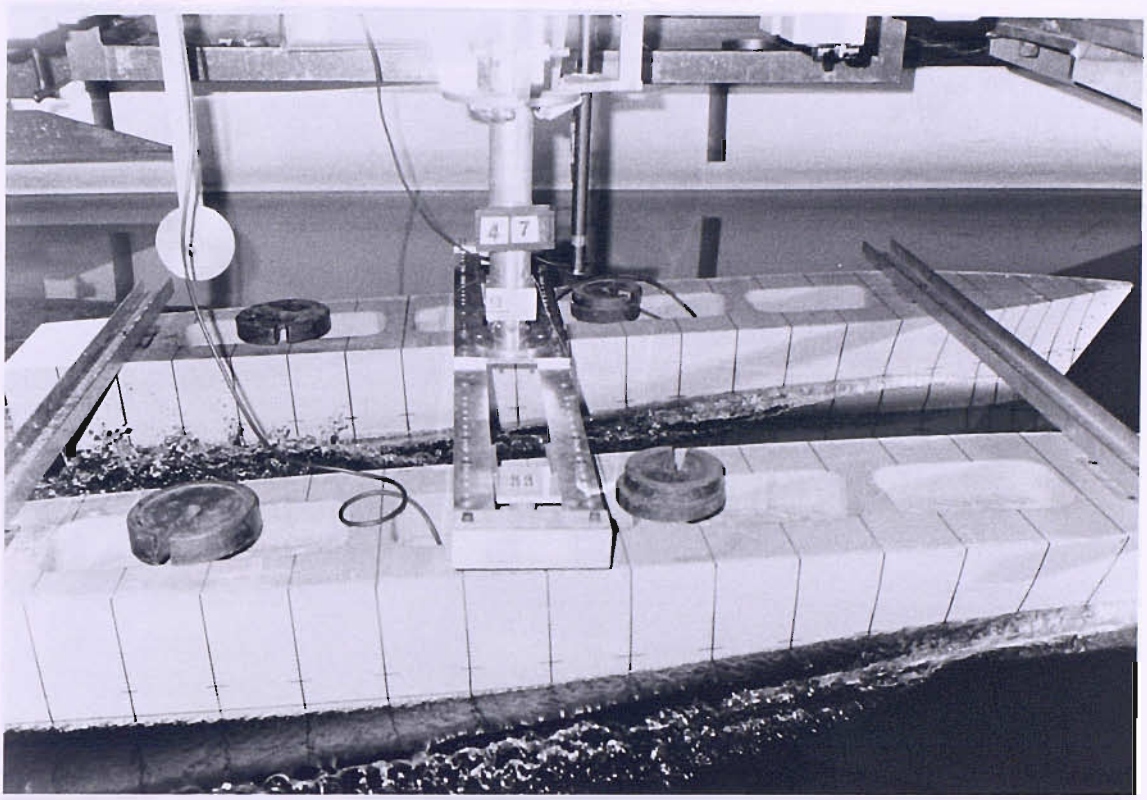

Fig.391 : Model: C3-S/L:0.4 Fn: 0.75

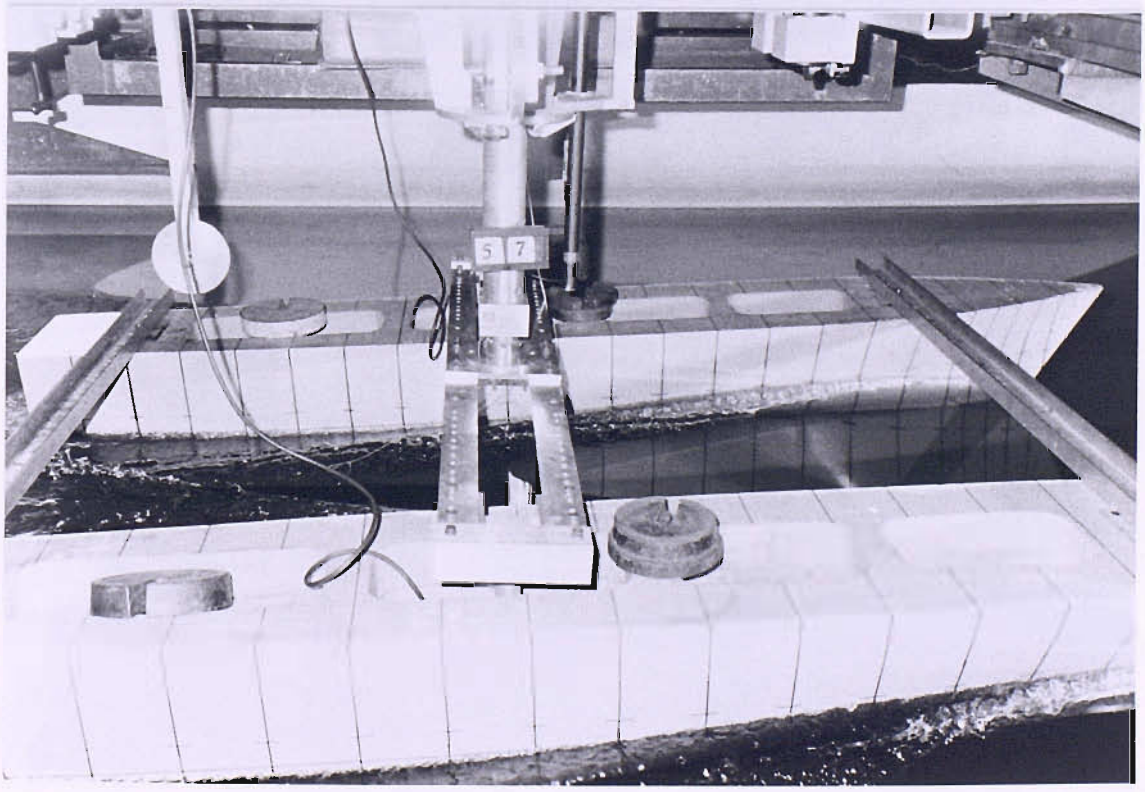

Fig.392 : Model: C3-S/L:0.5 Fn: 0.75

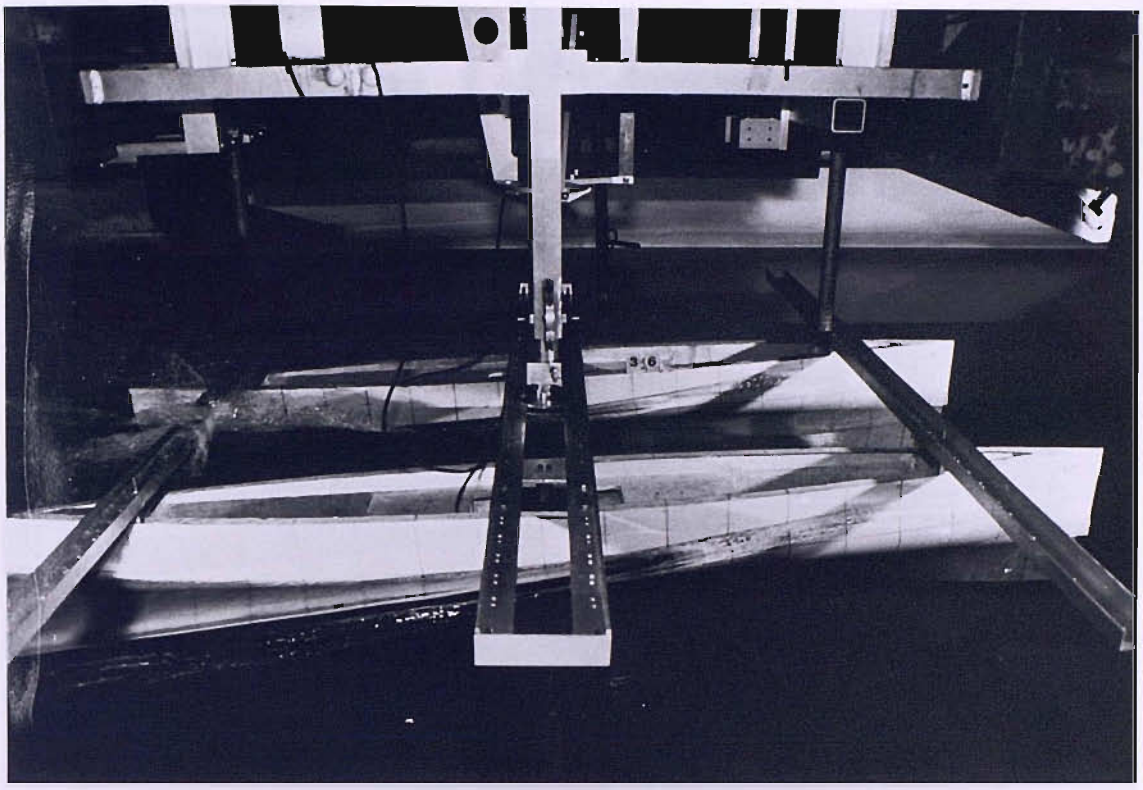

Fig.393 : Model: C2-S/L:0.3 Fn: 0.90

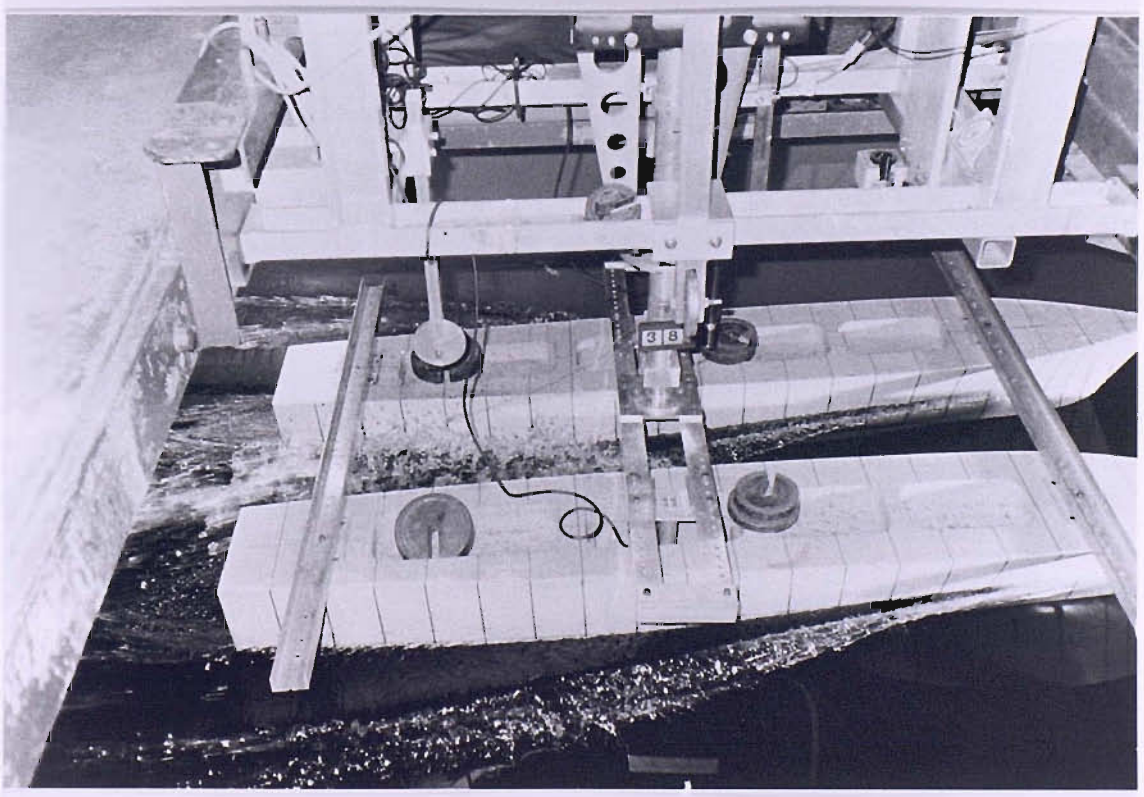

Fig. 394 : Model: C3-S/L:0.3 Fn: 1.0

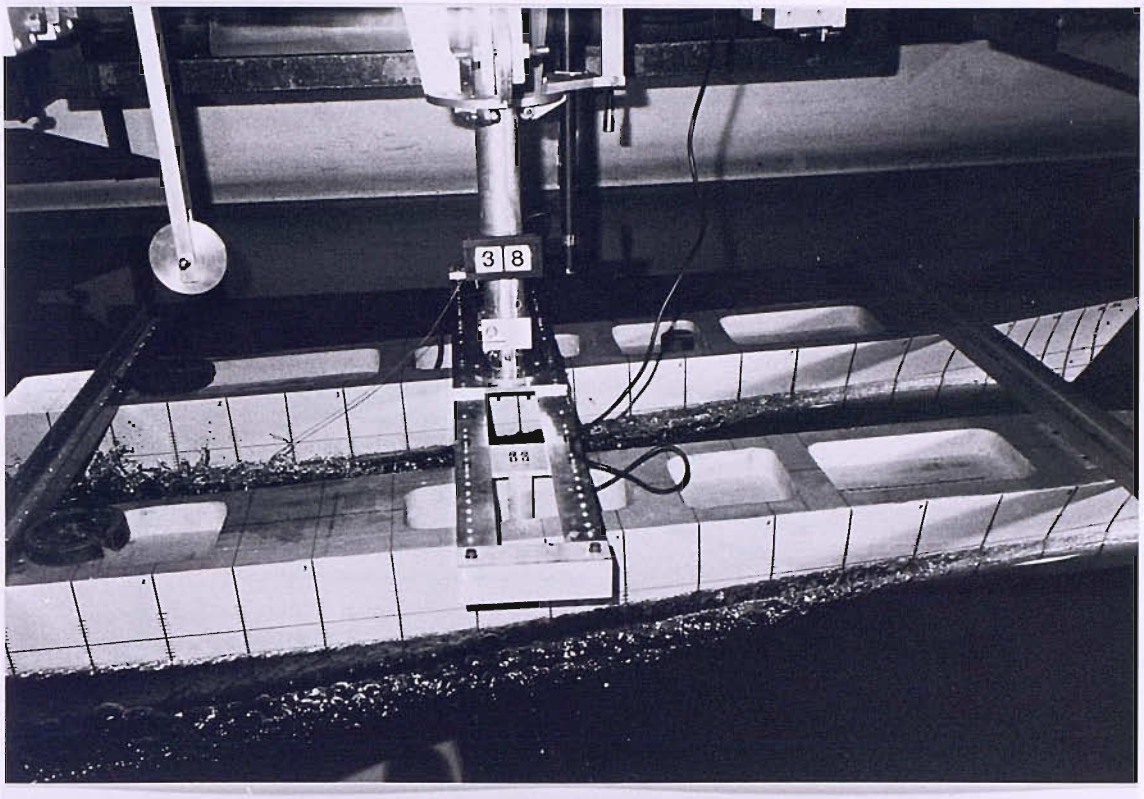

Fig. 395 : Model: C4-S/L:0.3 Fn: 1.0

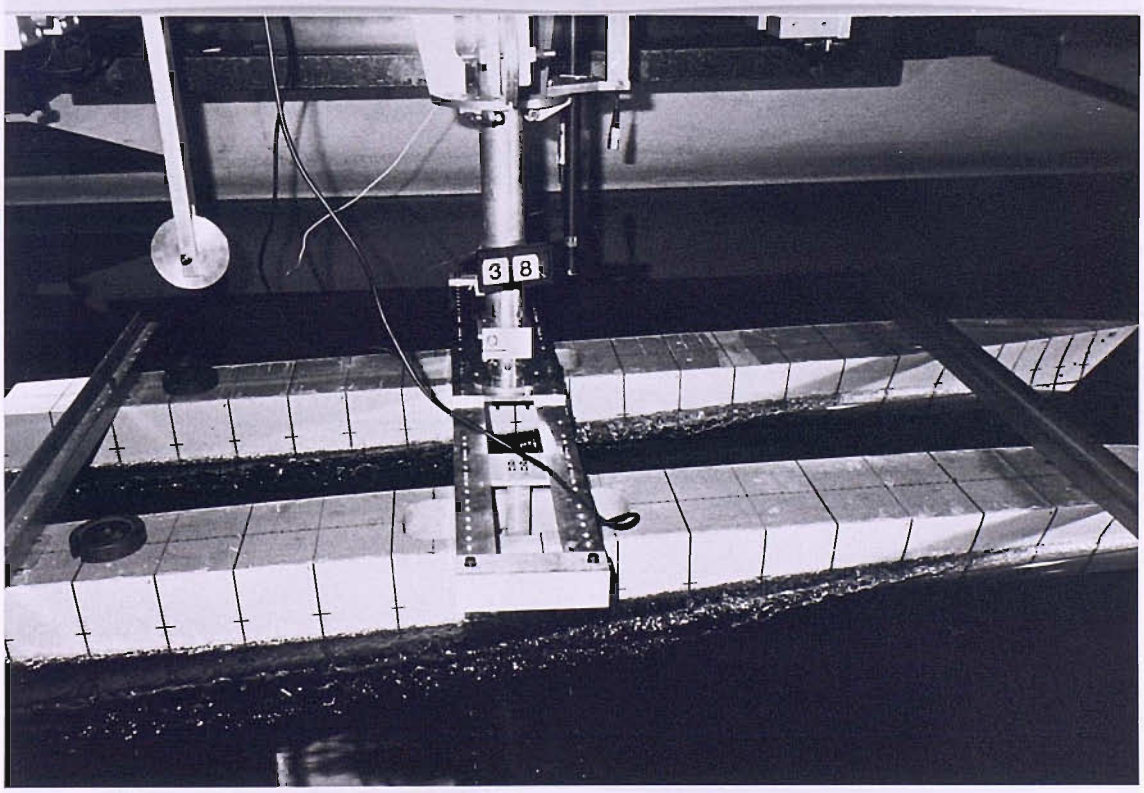

Fig. 396 : Model: C5-S/L:0.3 Fn: 1.0

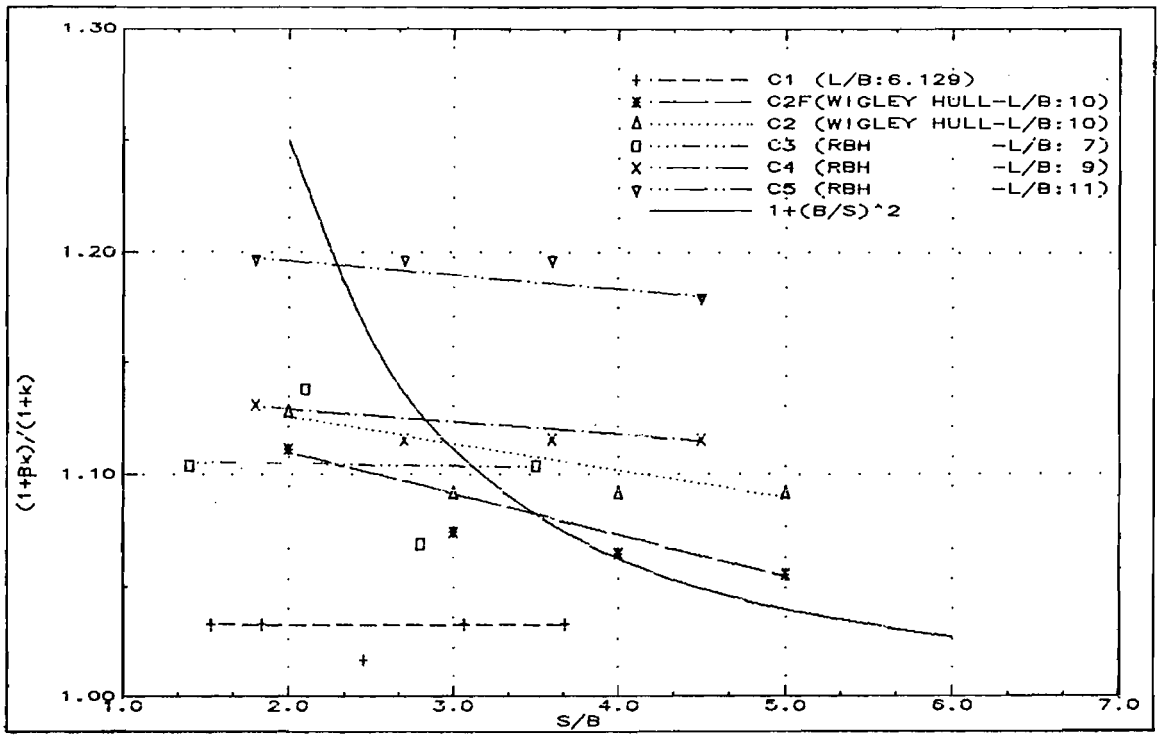

Fig.397: Comparison of viscous interference with 1+(B/S)^2

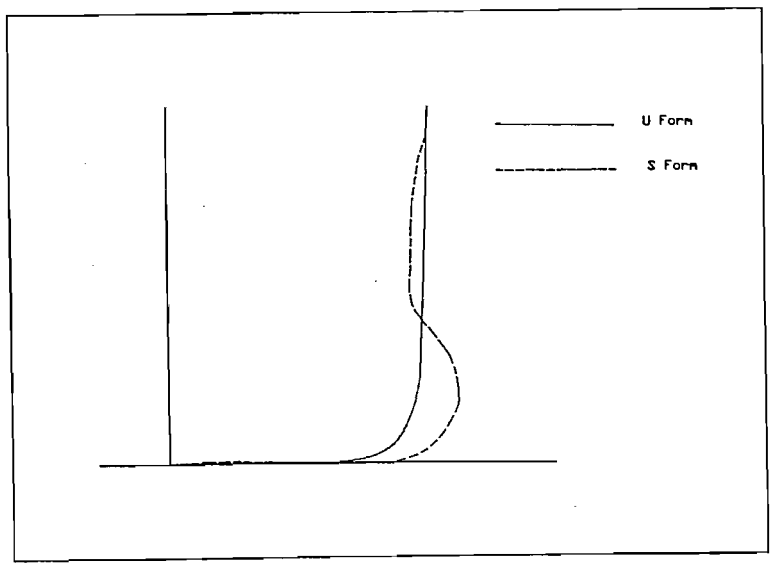

Fig.398: U and S hull Forms

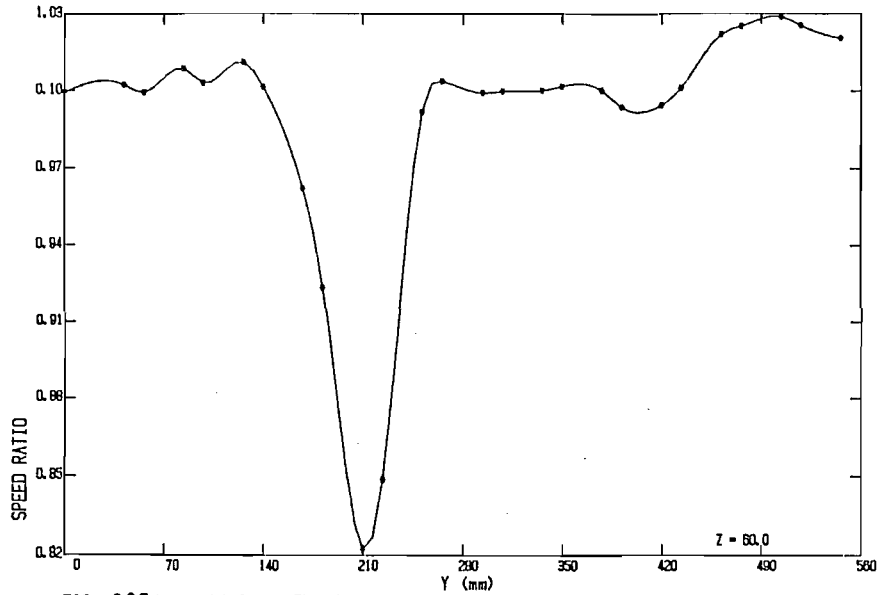

FIG ; 399 SPEED RATIO DISTRIBUTION

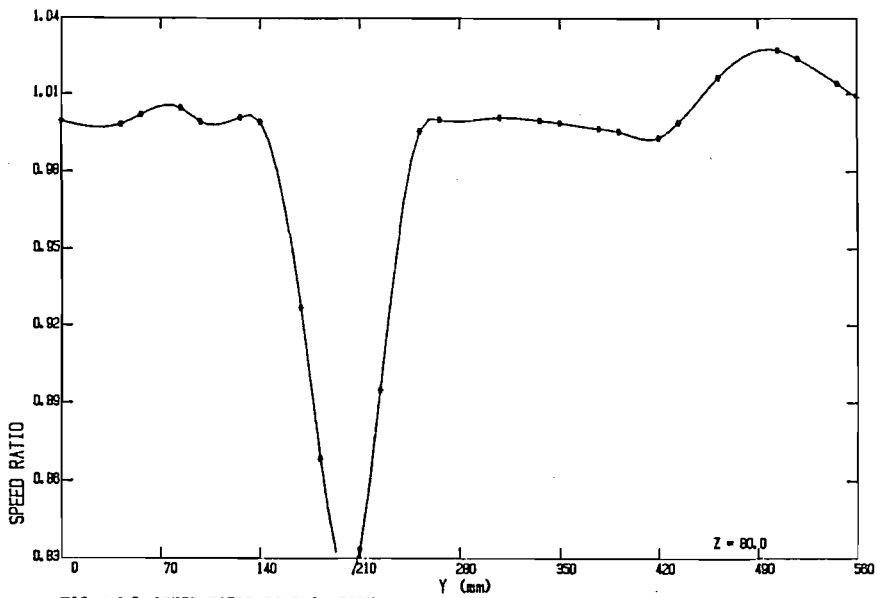

FIG 400 : SPEED RATIO DISTRIBUTION

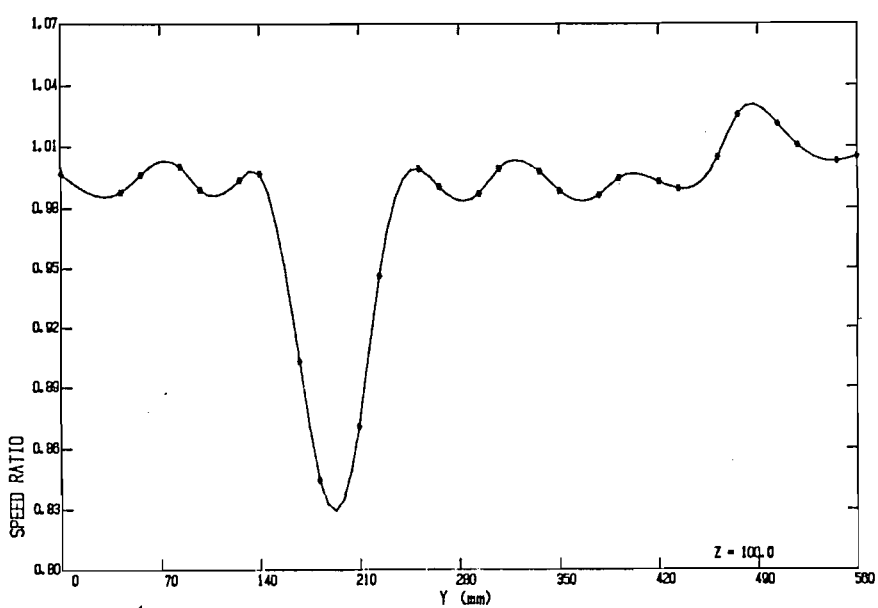

FIG 401 : SPEED RATIO DISTRIBUTION